Influence of centrosome amplification on the response to chemotherapy in epithelial ovarian cancer

Giulia Fantozzi

PSL UNIVERSITÉ PARIS

THÈSE DE DOCTORAT
DE L'UNIVERSITÉ PSL

Préparée à l'Institut Curie, Laboratoire Basto (UMR144)

Influence of centrosome amplification on the response to chemotherapy in epithelial ovarian cancer

Influence de l'amplification des centrosomes sur la réponse à la chimiothérapie dans le cancer de l'ovaire

Soutenue par
Giulia FANTOZZI
Le 10 novembre 2023

Ecole doctorale n° 515
Complexité du Vivant

Spécialité
Biologie cellulaire

Composition du jury :

Juliette, AZIMZADEH PhD, Institut Jacques Monod	*Président* *Rapporteur*
Stefano, SANTAGUIDA PhD, European Institute of Oncology, Milan, Italy	*Rapporteur*
Clara, NAHMIAS PhD, Institut Gustave Roussy	*Examinateur*
Maria, ALMONACID PhD, Collège de France	*Examinateur*
Frances, EDWARDS PhD, Institut Curie	*Co-encadrant*
Renata, BASTO PhD, Institut Curie	*Directeur de thèse*

institutCurie | PSL

Thesis outlines

This manuscript resumes experimental findings about how centrosome amplification influences the response to chemotherapy in epithelial ovarian cancer. The work was carried out during my three years of thesis in the laboratory of Renata Basto at the Institut Curie in Paris, France at the Cell Biology Unit (UMR144). I started my work in November 2020 and I luckily was able to continue the work despite the sanitary crisis, which affected us all.

The Introduction, Discussion, and Perspectives sections all center on the two main topics, the centrosome and ovarian cancer, trying to offer a comprehensive perspective of the literature, considering the new data disclosed within this document.
Material and Methods include all the techniques used for the experimental strategy, data analysis, images acquisition and processing.
The Results section describes and analyze in detail the data obtained during the PhD. My work is part of a wider project to which many people participated. The outcome of the complete project is included as *Annex* (Edwards et al., 2023).

Epithelial Ovarian Cancer (EOC) remains one leading cause of death from cancer in woman. First-line treatment involves debulking surgery followed by chemotherapy treatment, represented by a combination of paclitaxel and carboplatin. However, relapse is frequent. The centrosome is the major microtubule organizing centre in proliferating animal cells and contributes to cell division, migration, and invasion. Centrosome amplification, the presence of more than two centrosomes per cell, is often observed in cancer cell lines, including EOC. Centrosome amplification is suggested to contribute to oncogenesis via chromosome mis-segregation which generates aneuploidy.

In *Results – Section 1* I investigated if centrosome status can influence the response to chemotherapy. The experiments were conducted in EOC cell lines inducible for Polo-like kinase4 (PLK4), the main regulator of centrosome duplication cycle, to generate centrosome amplification. Surprisingly, I have found through proliferation and viability assays that centrosome amplification favours cell death in response to chemotherapy.

The hypothesis that centrosomes amplification can potentiate the response to chemotherapy was confirmed via live-imaging approaches *(Results – Section 2)*. Moreover,

this approach allowed me to investigate the mechanisms responsible for the increase in cell death in presence of extra centrosomes and chemotherapy. By correlating cell fate with behaviors along mitosis and interphase, I discovered that centrosome amplification potentiates the response to combined chemotherapy by inducing multipolar divisions. Surprisingly, increased response to carboplatin in presence of extra centrosomes resulted to be independent from induction of mitotic errors.

In *Results - Section 3* a further detailed characterization of cell cycle is presented. Via live imaging and flow cytometry approaches, I observed cell cycle arrest or cell death occurring in S/G2 phase in the second generation, in response to carboplatin.

At this point, I wanted to investigate other hypothesis on how centrosome amplification can represent a stress for cancer cells, sensitizing them to cell death. Thus, I wondered whether centrosome amplification could promote the induction of DNA damage in presence of carboplatin *(Results - Section 4)*. I quantified DNA damage by immunofluorescence approaches using an antibody against γ-H2AX, which detects DNA double-strand breaks. I found that although carboplatin increased DNA damage as expected, it had a similar effect on cells independent of centrosome amplification. Similarly, DNA repair, quantified with markers of homologous recombination (RAD51, FANCD2) and non-homologous end joining (53BP1), did not increase in cells with centrosome amplification.

Finally, I determined whether the higher levels of chromosome mis-segregation observed in OVCAR8 cells with centrosome amplification correlated with higher levels of aneuploidy *(Results - Section 5)*. I first analyzed the number of micronuclei, known to result from chromosome mis-segregation. However, although the number of micronuclei was present in the vast majority of OVCAR8 cells, this proportion was not increased in cells with centrosome amplification. Results from single-cell DNA sequencing in collaboration with Floris Foijer (U. Groningen, Netherlands) showed that OVCAR8 cells have a high level of aneuploidy, but that this level was not increased by centrosome amplification. This suggests that centrosome amplification does not sensitizes cells to death via increased aneuploidy in EOC cells.

Thus, extra centrosomes seem to alter how cells respond to stress, independently of the type of stress induced by chemotherapy. This work will contribute to elucidate the role of centrosome amplification in EOC and how they can affect chemotherapy treatment.

Aknowledgements

Thanks to the Foundation for Medical Research, the National League Against Cancer for having funded my thesis project. Thanks to the Institut Curie, the UMR144, the ED Complexité du vivant and the PSL for the supervision of my PhD work. Thank you to all the people of the administration, the UMR144 preparation laboratory, the microscopy and flow cytometry platforms, ADIC association for helping me and allowing me to do this PhD under the best possible conditions.

Thank you to all my collaborators and all the people who contributed with their work and enriching discussions: the lab of Floris Foijer, Pierre Gönczy, Stephen Taylor, Alexis Barr, Adrian Saurin and my thesis committee Molla Herman Anahi, Paul Conduit and Marc-Henri Stern. Thanks to the reviewers Juliette Azimzadeh and Stefano Santaguida for their work and time in reviewing this manuscript. Thank you to all other members of the PhD jury for examining and discussing my work Maria Almonacid, Clara Nahmias and Paul Conduit.

Thanks to all the lab members, current and past, for the good and collaborative scientific environment they created to work within. It was a real pleasure to have the opportunity to learn from very talented people. Thanks to my collogues of the ovarian cancer project Frances, Oumou and Anthony for supporting each other all long.

Thank you to Renata, for sharing all the insights of the scientific world and investing an incredible amount of time in forming PHD students in her lab. Thank you for the opportunity to go to congress and meet people inside the scientific community. Your attention to details and search for innovation always reassured me in the quality of the work and training I chose to invest in.

Thanks to Frances for forming me, helping, discussing from the very first day of my master-two internship to the end of the PhD, being always available. Thank you for always being transparent as a person and understanding. I am not sure you always realize how brilliant you are. I always felt very lucky to have the chance to learn from you in a critical time of formation as is the one of the PhD.

Thank you to Manon, my PhD buddy, with whom I shared all the moments of this path. The constant discussions, scientific and not, and the reciprocal support have been fundamental. Your enthusiasm and the personality tests really brighten up lab days for everyone.
Thanks to Riham for the sincere conversations we could share. We are still even at playing UNO! I kept the score…
Thanks to Anthony, which lucky had the bench next to my desk so I could feel his aura of positive attitude. Thanks for not just making my life way easier in the lab but also for making sure I also enjoyed and felt good in this, once new, city.
Thank you to Federica that even if she shared a smaller part of this journey with me has been very important in bringing new perspectives about the scientific world. Thank you for being such a trustworthy person.
Thank you to Margot, my introvert buddy, who made me feel very understood and at ease in my way of being.

Thanks to Quentin for always being Quentin, so kind and thoughtful. I think you know the snacks I prefer better than anyone else.
Thank you to Oumou, for her smile and her attitude in the lab.
Thank you to Simon, for always being patient and taking time to answer my questions, even when they were not clear neither to me.
Thank you to Vero, for always showing her incredible passion for science and sharing her knoledge.

Thank you to my dad for giving me the curiosity for the world, scientific and not. Thank you to my mum, for reminding me that people and life are much more.
Thank you to my sister, without whom I would have never find the strength to get through this journey as myself.
Thank you to my brother, for always giving me different perspectives in life, more enjoyable usually.

Thank you to all my friends, because only them knows how much they had to listen and support me in this journey. Thank you to Martina and Michele for being my “family contacts” when I started my PhD in full COVID sanitary crisis. Thank you to Alfredo, because of its fundamental support and sincerity in all Dixit matches. Thank you to Chiara Pelliccia, the glue of our expat group, the and the philosophers for helping me evading sometimes.

Thank you to my friends of a lifetime Francesca, Laura, Alice, Giada, Agni and Cri to make everything so much better and for getting through life together even when we live in different nations.

Thank you to Edwige Delattre and Sliman to be the first happiest good morning at the entry of the Institut Curie.
Thank you to the incredible people of the second floor Neda, Etienne, Reda, Clarisse and Carlos for always being ready to have a laugh.
Thank you to Angela Taddei and Anne-Sophie Godfroy for the course “Raising awareness on History, Epistemology and Ethics of Science” which created an incredible environment where to slow down time and think about science and its impact in the outside world.
Thank you to Celine for all our chats in Italian.
Thank you to Agata, Clara, Marine and Edward for having shared part of the journey, making it definitely more enjoyable.

Thank you to Giulia Grigi and all her collogues whose help and support was essential all along this journey.

Thank you to all the internet pages and memes about PhD humor.

Finally, thanks to me for all the hard work and the choices made.

Table of contents

List of abbreviations

A-EJ	alternative end joining
ADP	Adenosine diphosphate
AMP	Adenosine monophosphate
ATP	Adenosine triphosphate
AU	arbitrary units
BER	base excision repair
CCC	Clear cell carcinoma
CIN	chromosome instability
CKI	cyclin dependent kinase inhibitor
CNR	centrosome nucleus ratio
CRISPR	Clustered regularly interspaced short palindromic repeats
DBD	DNA binding
DDR	DNA damage response
DMSO	dimethylsulfoxide
DNA	deoxyribonucleic acid
DSB	double-strand break
EC	endometroid carcinoma
EJ	end joining
EM	electron microscopy
EMA	european medecines agency
EOC	epithelial obvarian cancer
ER	endoplasmic reticulum
FDA	food and drug administration
FIGO	international federation of gynecology and obstetrics
GDP	guanosine diphosphate
HGSC	high grade serous carcinoma
HGSOC	high grade serous ovarian carcinoma
HR	homologous recombination
HRD	homologous recombination deficient
HRP	homologous recombination proficient
IC50	half maximal inhibitory concentration
IF	immunofluorescence
KO	knock out
LGSC	low grade serous carcinoma
MAP	microtubule associated protein
MC	mucinous carcinoma
MMR	mismatch repair
MOMP	mitochondria outer membrane permeabilisation
MSI	microsatellite instability
MT	microtubule
MTOC	microtubule organising center
NAD	nicotinamide adenine dinucleotide
NCI	national cancer institute
NER	nucleotide excision repair
NHEJ	non homologous end-joining

OE	over expression
PCM	peri centriolar material
PFS	progression free survival
PLK4	polo like kinase 4
ROS	reactive oxygen species
SAC	spindle assembly checkpoint
SAS6	spindle assembly abnormal protein 6 homolog
SCKS	microcephaly and seckel syndrome
SDSA	synthesis dependent strand annealing
SSB	single strand break
TCGA	the cancer genome atlas
USDA	united states department of agriculture
UV	ultraviolet
WHO	world health organisation

Chapter 1 – Introduction

1. The cell cycle

1. The cell cycle

1.1 Cell cycle phases

The cell cycle is a universal process through which cells duplicate, serving as the foundation for growth and development of all living organisms. Cell cycle progression is tightly regulated and leads the cell through a series of ordered events culminating in mitosis, when the cell divides giving birth to two daughter cells with same genome (Matthews et al., 2021). The time between two mitosis, during which the cell prepares to divide, it is called interphase (Figure 1). The aim of interphase is to duplicate the cell content, both cytoplasm and DNA, in order to prepare cell division. In healthy proliferating animal cells, interphase is composed of three phases: G1 or gap1, when the cell increases it size and it produces resources needed for the following phases (Figure 1). Then, there is the synthesis stage or S-phase when DNA is replicated. Before mitosis (M-phase) cells undergo a second gap phase (G2) during which they prepare to divide by synthetizing and activating complexes required for mitosis. During G1, cells can also stop proliferating and enter a quiescent state - G0 (Figure 1). G0 is a reversible exit from cell cycle that can be activated in mammalian cells in response to environmental changes such as depletion of nutrition or growth factors, changes in cell adhesion and increased cell density (Coller et al., 2006; Zetterberg dan Larsson, 1985).

Once the DNA and other cellular contents are duplicated, the cell is ready to divide to create two genetically identical cells. Mitosis has been well characterized (Mitchison dan Salmon, 2001; Satzinger, 2008b). In prophase, chromosomes condense becoming visible while the nuclear envelope breaks down. The two centrosomes move towards opposite poles, while actively nucleating microtubules. In prometaphase, mitotic spindle microtubules attach the chromosomes at a specialized structure called kinetochore, which assembles on centromeres. Then, the cell progress into “metaphase” when chromosomes align on a metaphase plate. Each sister chromatid of each chromosome is attached to microtubule bundles from opposite poles of the mitotic spindle. . Once all chromosomes are properly attached, the cell proceeds into anaphase, when the sister chromatids are separated and pulled toward opposite poles. After chromatid separation, the cell divides into two daughter cells through the process of cytokinesis. In animal cells, during cytokinesis a cleavage furrow forms a constriction which

separates the cytoplasm of the two daughter cells. During this phase chromosomes decondense and the nuclear envelope is reformed. Thus, a new cell cycle can be initiated.

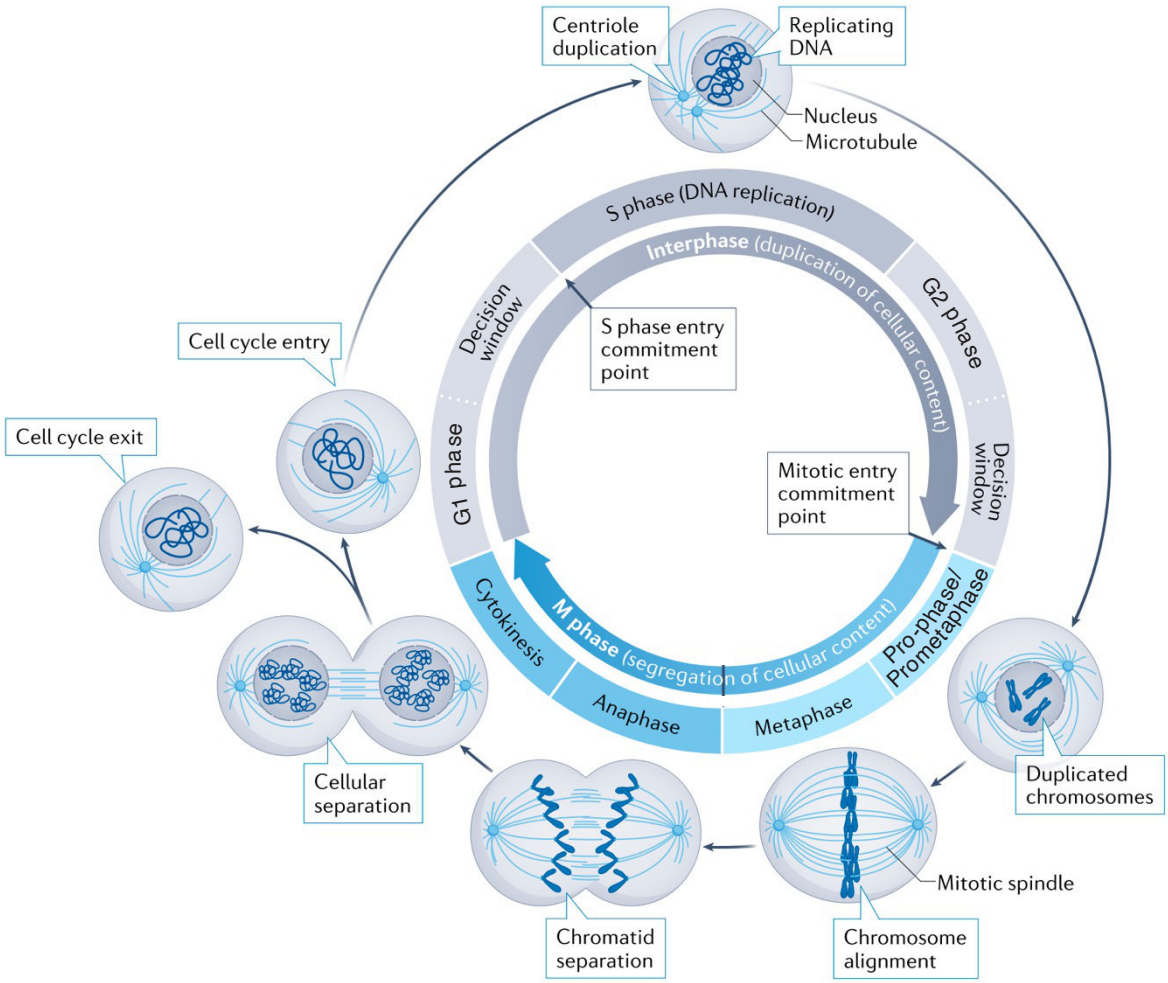

Figure 1: The cell cycle. Schematic representation of the ordered phases of the eukaryotic cell cycle. During interphase, cellular content is duplicated. It is composed by two gap phases (G1- and G2-phases), separated by a DNA replication phase (S-phase). Transition from one phase to another is tightly regulated during a decision window time. During G1-phase, cells can temporarily exit the cell cycle and enter into a quiescent state (G0-phase). The purpose of mitosis (M-phase) is to segregate the replicated DNA into two daughter cells. Mitosis starts with prophase and prometaphase, with chromosome condensation (dark blue), nuclear envelope breakdown and microtubule nucleation from the centrosomes (light-blue). Then, in metaphase the mitotic spindle aligns chromosomes in a plate at the equator of the cell. Chromatid separation and segregation occurs in anaphase, followed by cellular separation into two daughter cells during cytokinesis. Figure modified from (Matthews et al., 2021).

1.2 Cell cycle control

Cell cycle progression is regulated by the activity of Cyclin dependent kinases (CDKs) and these are regulated by phosphorylation, dephosphorylation and proteolysis (Besson et al., 2008; Malumbres & Barbacid, 2005.; Nurse, 2000) (Figure 2). Additionally, CDK inhibitors (CKIs) negatively regulate CDKs and they are classified into two families: INK4 family and Cip/Kip family (Cánepa et al., 2007; Chim et al., 2006). Among them, the most important factors for cell cycle regulation are P21, P16 and P27. In particular, P21 activation leads to G1 cell cycle arrest and its expression is tightly controlled by p53 (Koutsodontis et al., 2001; Levine, 2010). P53, encoded by the TP53 gene, is the main tumor suppressor and it is mutated in more than a half of human tumors. The p53 protein is a transcription factor which binds DNA activating genes involved in a variety of responses, such as DNA damage repair, cell cycle arrest and cell death (Boutelle&Attardi, 2021). Further details regarding p53 will be provided below.

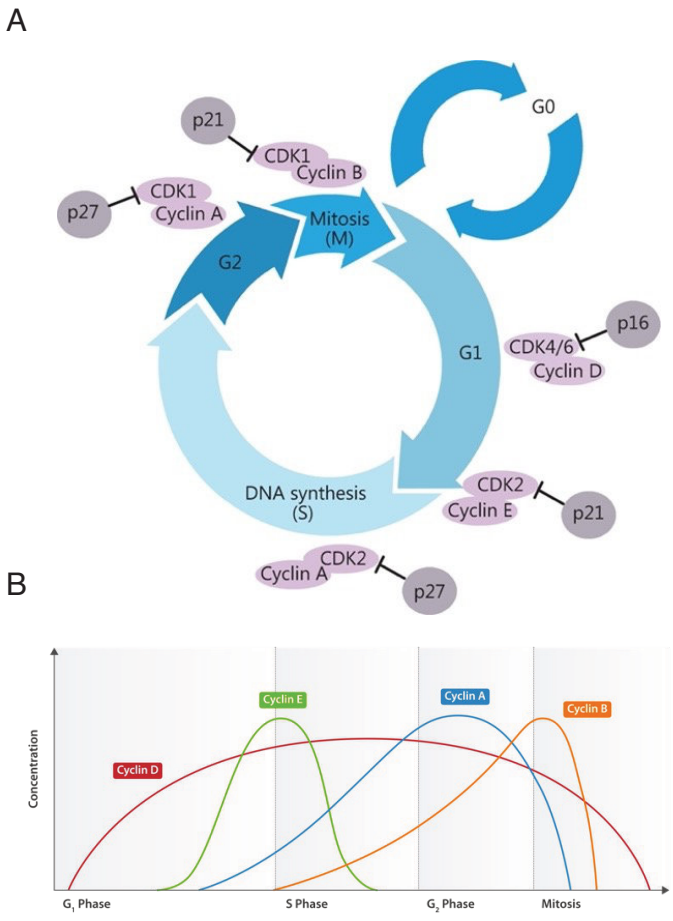

Figure 2: Cell cycle progression and its regulatory proteins. (A) Schematic view of different phases of cell cycle and corresponding Cyclin proteins and CDKs. (B) Oscillations of different Cyclins throughout cell cycle drive entry and exit from cell cycle phases. Figure from (Jingwen et al., 2017).

The CDK family belongs to a well-conserved family of serine/threonine protein kinases. Specific CDKs are activated in specific cell cycle phases by binding to their partner cyclins. Unlike CDKs, cyclins are not always present during the whole cell cycle, but their transcription and degradation is coupled to different phases (Evans et al., 1983; Murray et al., 1989; Murray & Kirschner, 1989). CDK- Cyclin complexes play a central role in regulating cell cycle progression. According to the classical cell cycle model, cyclin D levels gradually increase during G1 in response to mitogenic stimuli (Baldin et al., 1993) (Figure 2).

D-type cyclins bind to CDK4/6, generating complexes that are stabilized by p21 or p27. Subsequently, the CyclinD-CDK4/6 complexes localize into the nucleus, where they initiate the phosphorylation the of retinoblastoma (RB) protein (Kato et al., 1993; Narasimha et al., 2014). RB is a key regulator of G1 and an inhibitor of E2F, a transcription factor with essential functions in cell cycle progression. (Baldin et al., 1993). E2F target genes comprises Cyclin E, for example. As levels of Cyclin E increase in late G1, CDK2 becomes activated (Ohtsubo et al., 1995) (Figure 2). Cyclin E-CDK2 activity generates a positive feedback loop which results in increased activity of cyclin E-CDK2. CDK2 increased activity results in RB hyperphosphorylation and inactivation. Thus, E2F inactivation is released resulting in increased transcription of downstream genes and allowing the initiation of replication (S-phase entry). Progression through S phase is assured by increased levels of cyclin A which also form a complex with CDK2 (Pagano et al., 1992; Pines&Hunter, 1989). After S-phase completion, the accumulation of cyclin A/B -CDK1 activity drives mitotic entry (Guadagno dan Newport, 1996) (Figure 2). Additionally, CDK1 collaborates with various other kinases, including Polo-like kinases and Aurora, in facilitating the transition from the G2 to M-phase, thereby actively contributing to the progression of mitosis during cell division (Barr dan Gergely, 2007). Finally, the degradation of Cyclin A and B after ubiquitination by the anaphase-promoting complex cyclosome (APC/C), induces mitotic exit allowing initiation of G1 (Peters, 2006).

1.3 Mitotic exit

Mitotic exit, terminating a full cell cycle is highly regulated. In particular, proteolysis plays an essential role. At the core of mitotic exit regulation resides the activity of APC/C, which is a 1.5-MDa anaphase (Peters, 2006). APC/C is an E3 ubiquitin ligase, which transfers Ubiquitin a 8.5KD protein into substrates to mark them for degradation. The covalent modification of a protein by

ubiquitin is called ubiquitination and it is the starting point for one of the main degradation processes: the ubiquitin–proteasome system (UPS) (Tai dan Schuman, 2008). The UPS involves the proteosome, responsible for protein degradation and several ubiquitin ligases and de-ubiquitinating enzymes. The APC/C can only ubiquitylate substrates with the help of three cofactors: the ubiquitin-activating (E1) enzyme, a ubiquitin-conjugating (E2) enzyme and a co-activator protein. E1 enzymes activate ubiquitin and transfer it to an E2 enzyme. APC/C in collaboration with the E2 enzymes UBCH5 and UBCH10 transfer the activated ubiquitin to the target proteins (Aristarkhov et al., 1996; Harper et al., 2002). Noteworthy examples of substrates that are targeted by APC/C and induce mitosis include the mitotic-specific Aurora kinases, PLK1, cyclins A and B among many others (Rape et al., 2006; Lindon dan Pines, 2004; Littlepage dan Ruderman, 2002).

During prometaphase the APC/C is kept inactive until all microtubules are correctly attached (Rieder et al., 1995). The correct attachment of spindle microtubules to kinetochores is monitored by a control system: the spindle assembly checkpoint (SAC) (Musacchio & Salmon, 2007; Varetti et al., 2011). The ability of the SAC to monitor the correct attachment of microtubules is still under debate. The two main hypothesis currently propose that the SAC senses the attachment of microtubules at the surface of kinetochores or alternatively, the tension generated from kinetochore attachment (Figure 3) (Etemad et al., 2015; Nicklas, 1997; Nicklas et al., 1995; Waters et al., 1998).

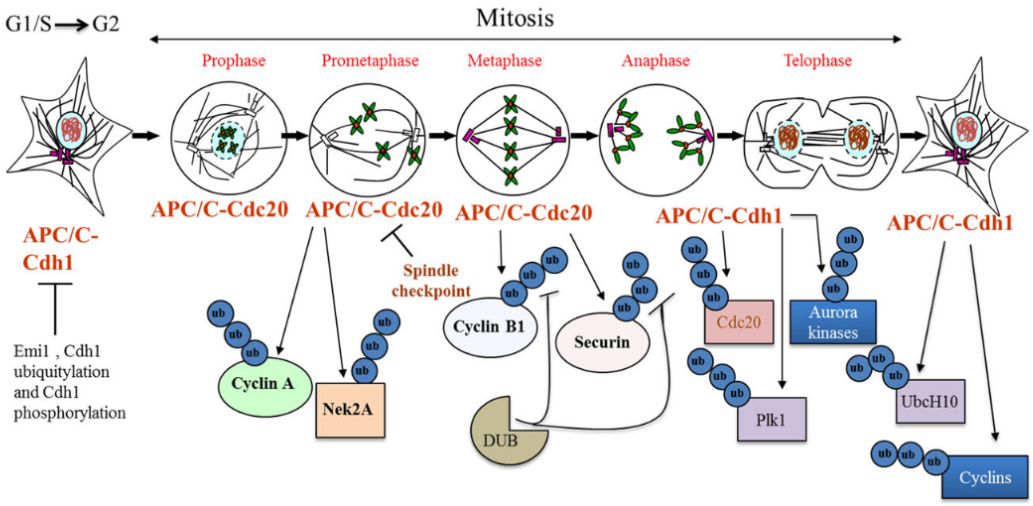

Figure 3: APC/C activation at mitotic exit. APC/C activity results in the ubiquitylation of proteins, marking their degradation at specific times **a**nd driving progression of the cell cycle. Substrates in early M-Phase are ubiquitylated

by APC/C bound to Cdc20 while APC/C-Cdh1 is activate during anaphase. Mitotic exit requires the degradation of mitotic exit inhibitors such as Cyclin A, Cyclin B and Securin. APC/C activity is suppressed by the SAC. At the G1-S transition, APC/C-Cdh1 is inactivated. From (Sivakumar dan Gorbsky, 2015).

In case of errors in chromosome attachment, the SAC is maintained in an active state and so the progression to anaphase is blocked. Unattached kinetochores accumulate the mitotic-arrest deficient 2 (Mad2), BubR1 and Bub3 proteins (De Antoni et al., 2005; Hoyt et al., 1991; Li & Murray, 1991; Sudakin et al., 2001). Once all chromosomes are attached to spindle microtubules and the SAC is satisfied, APC/C becomes activated. APC/C activation is strictly regulated and depends on two main co-activators: Cell Division Cycle 20 (Cdc20) and Cdh1 (Dube et al., 2005; Hwang et al., 1998; Kim et al., 1998; Kraft et al., 2005; Pfleger et al., 2001).

1.4 Mitotic errors

Even if mechanisms to prevent mitotic errors exist, chromosome mis-segregation can still occur. Certain types of errors can be undetected by the SAC or mutations of SAC encoding genes can decrease the strength of the checkpoint. Lagging chromosomes and misaligned chromosomes are two examples of mitotic errors poorly detected by the SAC. Lagging chromosomes are chromosomes that lag behind during anaphase. Lagging chromosomes can be the results of merotelic attachments (Cimini et al., 2001; Climini et al., 2002; Gregan et al., 2007). Merotelic attachment occurs when a given kinetochore is attached by microtubules emanating from opposite poles (Cimini et al., 2003b). During anaphase, the position of the merotelic kinetochore and chromosome relies on microtubule bundle sizes. A significantly thicker bundle directs the kinetochore toward that pole, while similar-sized bundles lead to kinetochore lag at the spindle equator (Salmon et al., 2005; Cimini et al., 2004a). Even if undetected by the SAC, lagging chromosomes can be corrected during anaphase. Midzone-localized Aurora A and B have recently been showed to be implicated in the process of lagging chromosome correction at anaphase (Sen et al., 2021).

Lagging chromosomes can be successfully incorporated in the main nucleus of one of the two daughter cells, with 50% of the cases being segregated in the wrong daughter cell and so generating aneuploidy (see following paragraph). Otherwise, the lagging chromosome can remain excluded from the main nucleus. In this case they can generate discreet structures called

micronuclei (Cimini et al., 2003b) (Figure 4). Further, lagging chromosomes can also remain trapped in the cleavage furrow and suffer DNA damage (Janssen et al., 2011).

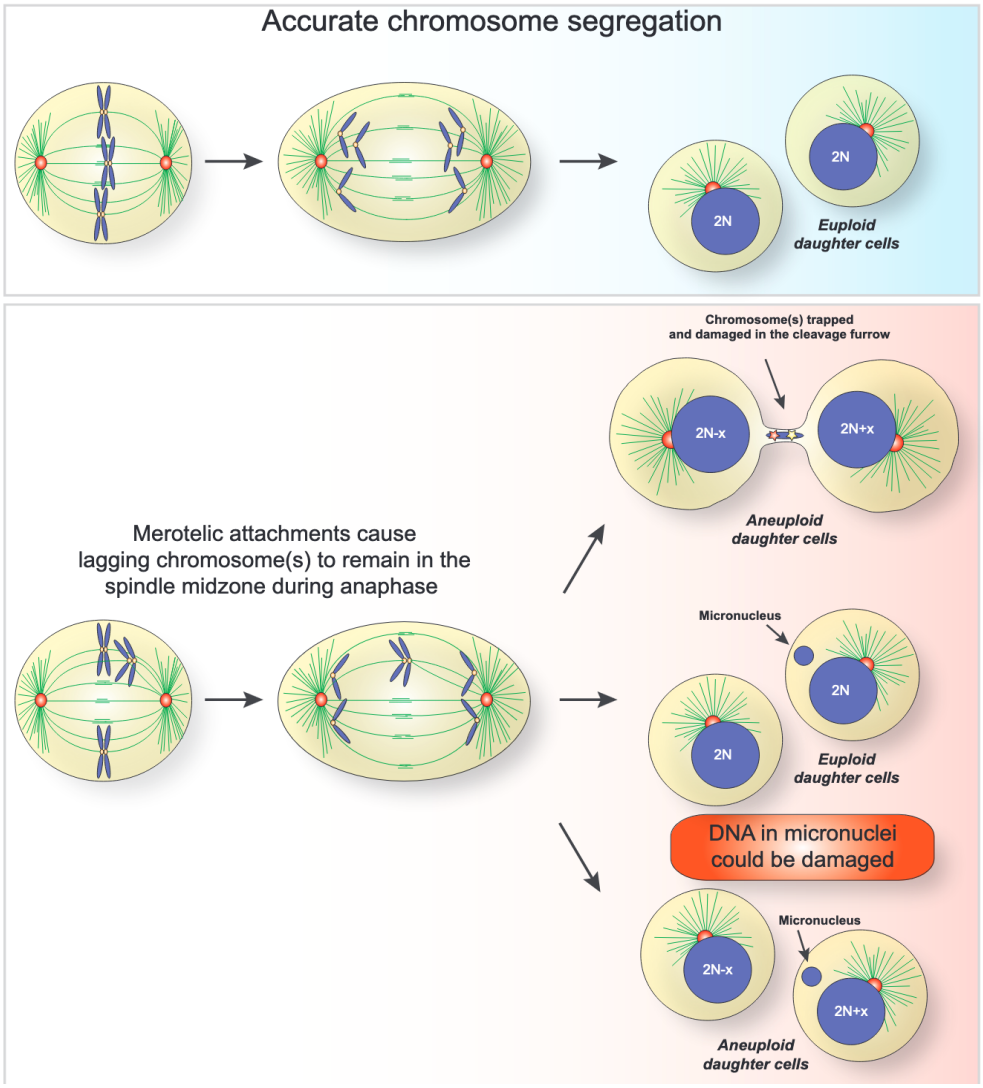

Figure 4: Mitotic errors leading to aneuploidy progeny. On top cells divide normally and two euploid identical daughter cells are formed. On the bottom, merotelic attachments can lead to chromosome trapped in the cleavage furrow, which can even be the source of DNA damage. Lagging chromosomes can be maintained outside the main nucleus in daughter cells, forming the a micronuclei. From (Santaguida dan Amon, 2015).

Acentric chromosomes are another type of mitotic error not detected by the SAC. Acentric chromosomes are fragments of chromosomes that lack the centromere, which is essential for kinetochore assembly (Williams et al., 1998). Importantly, acentric chromosomes may not exclusively originate during mitosis; instead, they can emerge from DNA double-strand breaks that can happen at various cell cycle stages (Warecki dan Sullivan, 2020). As lagging

chromosomes, acentric chromosomes remain undetected by the SAC and can be incorporated in the main nucleus of one of the daughter cells or give rise to micronuclei (Royou et al., 2010).

Another type of mitotic errors are chromosome bridges. Chromosome bridges refer to the presence of chromatin material that stretch between the dividing masses of chromosomes during the anaphase stage of cell division (Gisselsson, 2008). Although they become noticeable during mitosis, the underlying cause of chromosome bridges can be traced back to events occurring during interphase. Chromosome bridges can arise from under-replicated DNA or unresolved DNA damage (Chan et al., 2009). In human cells, chromatin bridges can result from chromosome fusion, occurring as a consequence of telomere attrition (Maciejowski et al., 2015). Chromatin bridges can be resolved at anaphase by the TREX1 nuclease or can persist mitosis (Pampalona et al., 2016).

Finally, multipolar mitosis occurs when the chromatin is segregated into more than two sets of chromosomes, giving origin to two or more daughter cells with an unbalanced DNA content. The progeny deriving from this kind of division frequently die or arrest in the following interphase (Brinkley, 2001; Ganem et al., 2009; Kwon et al., 2008b). Multipolar divisions can occur in the presence of centrosome amplification, the presence of more than two centrosomes per cell, a condition observed in cancer cell lines (Ganem et al., 2009; Harris, 2008; Leber et al., 2010a; Marteil et al., 2018; Kwon et al., 2008b).

1.5 Cytokinesis: success or failure

Cytokinesis starts with the determination of furrow position and the assembly of the contractile ring which moves inward before culminating in abscission of cytoplasm and generation of two daughter cells (Figure 5). The contractile ring is a rich actin and myosin structure (Schroeder, 1968; 1970). Actin can participate in different protein-protein interaction, and in vertebrate cells can be found both in a monomeric (G-actin) or filamentous form (F-actin) (Chen et al., 2017; Kabsch et al., 1990). Myosin II is a hexameric protein consisting of two heavy chains, two essential light chains and two regulatory light chains (Rahmani et al., 2021). Myosin-II is the essential motor for cytokinesis in animal cell and localizes at the contractile ring (Fenix et al., 2016; Wang et al., 2019). An essential controller of cytokinesis is the Rho GTPase, which was the initial regulatory protein factor identified as having a role in contractile ring assembly (Mabuchi et al., 1993; Kishi et al., 1993). To assemble the contractile the cell first needs to reorganize the

actin cytoskeleton (regulated by RhoA, profilins, and formins), followed by ingression of the furrow mediated by Myosin II (Piekny et al., 2005). The attachment of these mechanical-force generators to the membrane, facilitated by scaffold proteins Anillin and Septins is also important for the constriction process (Maddox et al., 2007).

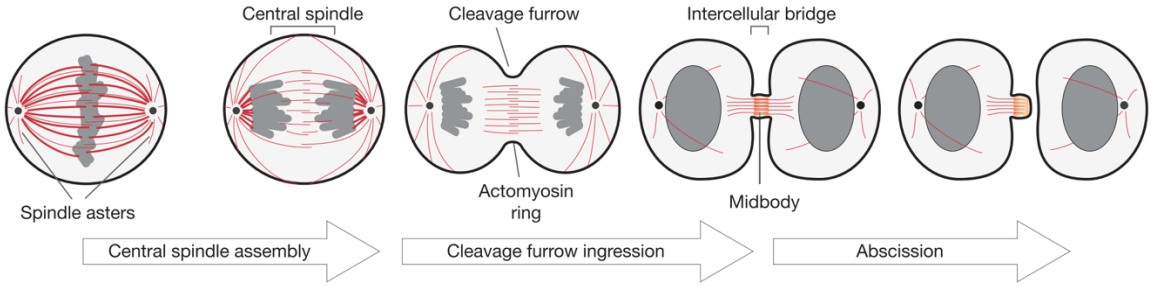

Figure 5: Overview of cytokinesis in animal cells. A schematic representation showing the reorganization of an animal cell as it advances through distinct stages of cytokinesis. Microtubules are highlighted in red, chromosomes are depicted in grey and centrosomes in black. Figure from (Fededa dan Gerlich, 2012).

The final stage of cytokinesis in animal cell is abscission of the midbody structure, densely populated by microtubules and trafficking proteins (Figure 5) (Carlton dan Martin-Serrano, 2007; Morita et al., 2007).Direct disruption of any of the components involved in cytokinesis may inhibit furrow ingression leading to failed cell division(Normand dan King, 2010). Formation of chromatin bridges is an example of an obstacle encountered by the cleavage furrow, representing a major cause of cytokinesis failure. Mitotic slippage occurs when the cell exit mitosis without dividing resulting in a daughter cell with altered ploidy (Lok et al., 2020). During a prolonged mitotic arrest, the cell can die or perform mitotic slippage. The decision between these two fates seems to be decided by the competition of two mechanisms (Gascoigne dan Taylor, 2008a). The first one involves triggering pathways that lead to cell death, while the other centers around the protection of cyclin B1 from degradation. These two mechanisms appear to have distinct thresholds and the eventual outcome depends on which threshold is bypassed first. Hence, if the levels of cyclin B1 drop beneath the threshold required for exiting mitosis, slippage occurs whereas if the threshold for cell death is surpassed first, the cell undergoes death during mitosis. After mitotic slippage cell can undergo different fates such as cell cycle arrest, cell death during interphase or even cell cycle progression. The factors that dictate the choice between these different outcomes following slippage are still unknown.

1.6 Micronuclei

Micronuclei are small nuclei-like structures containing DNA surrounded by a nuclear envelope which failed to be reincorporated in to the main nucleus after mitosis. Even if micronuclei were already observed more than 50 years ago (Kato & Sandberg, 1968), recent work promoted our knowledge on their origin and on the consequences of exiting mitosis with this type of structures. Through the combination of live imaging to track mis-segregated chromosomes and single-cell sequencing techniques, it has been shown that micronuclei can generate chromothripsis (Crasta et al., 2012; Zhang et al., 2015). Chromothripsis is a complex series of rearrangements in DNA resulting from the fragmentation and abnormal stitching of DNA sequences (Stephens et al., 2011; Cortamp et al., 2020; Shoshani et al., 2021). The DNA trapped in the micronucleus does not replicate correctly, resulting in DNA damage and chromosome fragmentation (Liu et al., 2018). Interesting in the subsequent mitosis, the micronuclei DNA can be incorporated in the main nucleus (Agustinus et al., 2023; Lin et al., 2023; Tang et al., 2022; Trivedi et al., 2022). Furthermore, the fragmentation of DNA trapped in the micronucleus has been suggested to occur as a consequence of a fragile nuclear envelope, which may expose DNA to the action of nucleases present in the cytoplam (Tang et al., 2022). Recently, it has been shown that fragmented DNA in the micronucleus can be maintained together to the action of Cip2A-TOPBP1 (Lin et al., 2023; Trivedi et al., 2022).

1.7 Aneuploidy

Aneuploidy is currently identified as numerical aberration of whole chromosomes or chromosome arms (Taylor et al., 2018a). It is associated with cancer, birth defects (as for trisomy 21) and organism unviability (Gordon et al., 2012; Torres et al., 2008). Defects in chromatin cohesion, supernumerary centrosomes and chromosome mis-segregation can all lead to the generation of aneuploid karyotypes (Cimini et al., 2001; Bakhoum et al., 2009; Ganem et al., 2009; Silkworth et al., 2009). Different mechanisms can lead to chromosome mis-segregation, as previously described. A compromised SAC can lead to aneuploidy, however SAC genes mutations are very rare in human cancer (Cahill et al., 1999; Haruki et al., 2001; Myrie et al., 2000; Kops et al., 2005). Because some mitotic defects can undergo undetected by SAC, as for merotelic attachments, most of the tumors are characterized by high levels of chromosome instability (CIN). Whereas aneuploidy refers to an altered state of the karyotype, the increased

frequency of mitotic errors is referred as CIN (Gordon et al., 2012). Aneuploidy and CIN mutually drive each other in cancer (Passerini et al., 2016; Garribba et al., 2023).

One of the main consequences of aneuploidy is an imbalanced number of genes when compared to the euploid karyotype (Santaguida dan Amon, 2015). This may generate altered gene expression leading to defects in protein complex stoichiometry and proteotoxicity (Figure 6). Altered gene expression, even if not being a universal response, has been detected in aneuploid yeasts, plants and mammalian cells (Dephoure et al., 2014; Kahlem et al., 2004; Kurnit, 1979; Mao et al., 2003; Pavelka et al., 2010; Stingele et al., 2012).

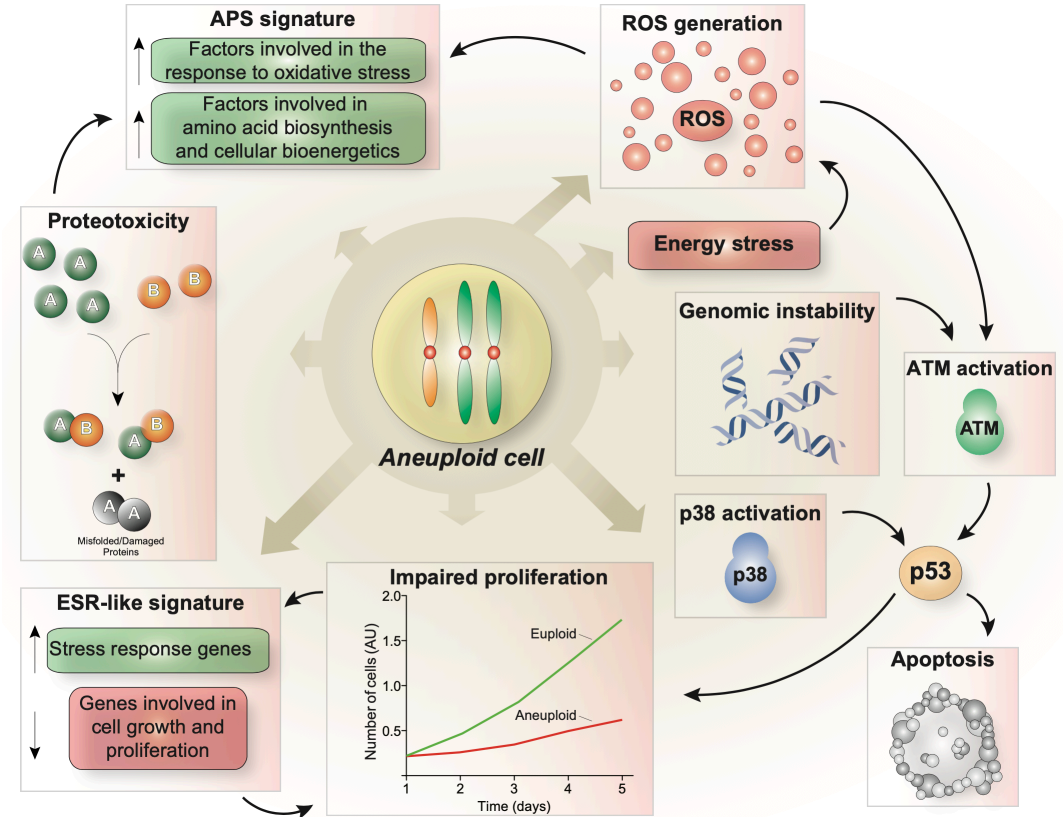

Figure 6: Aneuploidy impairs several cellular processes. Aneuploid cells show a variety of altered functions that culminate with proliferation defects and the generation of DNA damage leading to genomic instability. From (Santaguida dan Amon, 2015)

In particular, proteomic analysis in budding yeast has shown that the presence of a single extra chromosome would increase gene expression in ~ 80% of the genes present in an extra copy (Dephoure et al., 2014; Pavelka et al., 2010). Therefore, the changes in dosage of many

genes and proteins cause a series of different stresses, referred as aneuploid-associated stresses (Figure 6). Protein misfolding, activation of stress response pathways and altered metabolic landscape are shared features of aneuploid cells (Oromendia & Amon, 2014; Santaguida & Amon, 2015; Williams et al., 2008). The main consequence of these increased levels of stress is a decrease in fitness due to an extended cell cycle and in particular, lengthening of G1 and S-phases. The ability of aneuploidy to increase the extension of G1 resulting in slow proliferation rates was discovered by studies performed in yeast (Torres et al., 2007; Thorburn et al., 2013; Niwa et al., 2006).The same consequences have been reported in mammalian cells (Burds et al., 2005; Thompson & Compton, 2010). This decrease in proliferation was thought to be mainly due to p53 activation (Burds et al., 2005; Li et al., 2010; Schvartzman et al., 2011; Thompson & Compton, 2010). Upon physiological conditions, p53 levels are low, but they increase in responses to a variety of stresses, such as DNA damage, oncogene activation, hypoxia, nutrient deprivation (Prieur et al., 2011; Lim et al., 2021) but also centrosome amplification (Fukasawa et al., 1996b). However, recent studies that compare different cell lines and culture conditions show that in some cases the mitotic arrest was completely/partially independent from P53 activation (Santaguida et al., 2017; Narkar et al., 2021). These data suggest that other mechanisms may be responsible for the induction of decreased proliferation in an aneuploid conditions.

1.8 Activation of an inflammatory response due to aneuploidy and micronuclei

Single-cell sequencing analysis of aneuploid arrested cells and genomic analysis conducted on primary tumor and breast adenocarcinoma showed that cells with complex karyotypes generate an immune-response (Santaguida et al., 2017; Bakhoum et al., 2018). In particular, isolated aneuploid arrested cells obtained by 24 hours Reversine treatment to inhibit the checkpoint protein MPS1, showed senescent associated and pro-inflammatory signals (Santaguida et al., 2017). Furthermore, activation of the cyclic GMP– AMP synthase (cGAS)–stimulator of interferon genes (STING) pathway was also described. In mammalian cells, the cGAS-STING pathway is a stress-response pathway evolved as a way to detect foreign DNA (Figure 7) (Cohen et al., 2019; Morehouse et al., 2020). Its activation is often detected in human cells as a consequence of micronuclei (MacKenzie et al., 2017; Harding et al., 2017b).

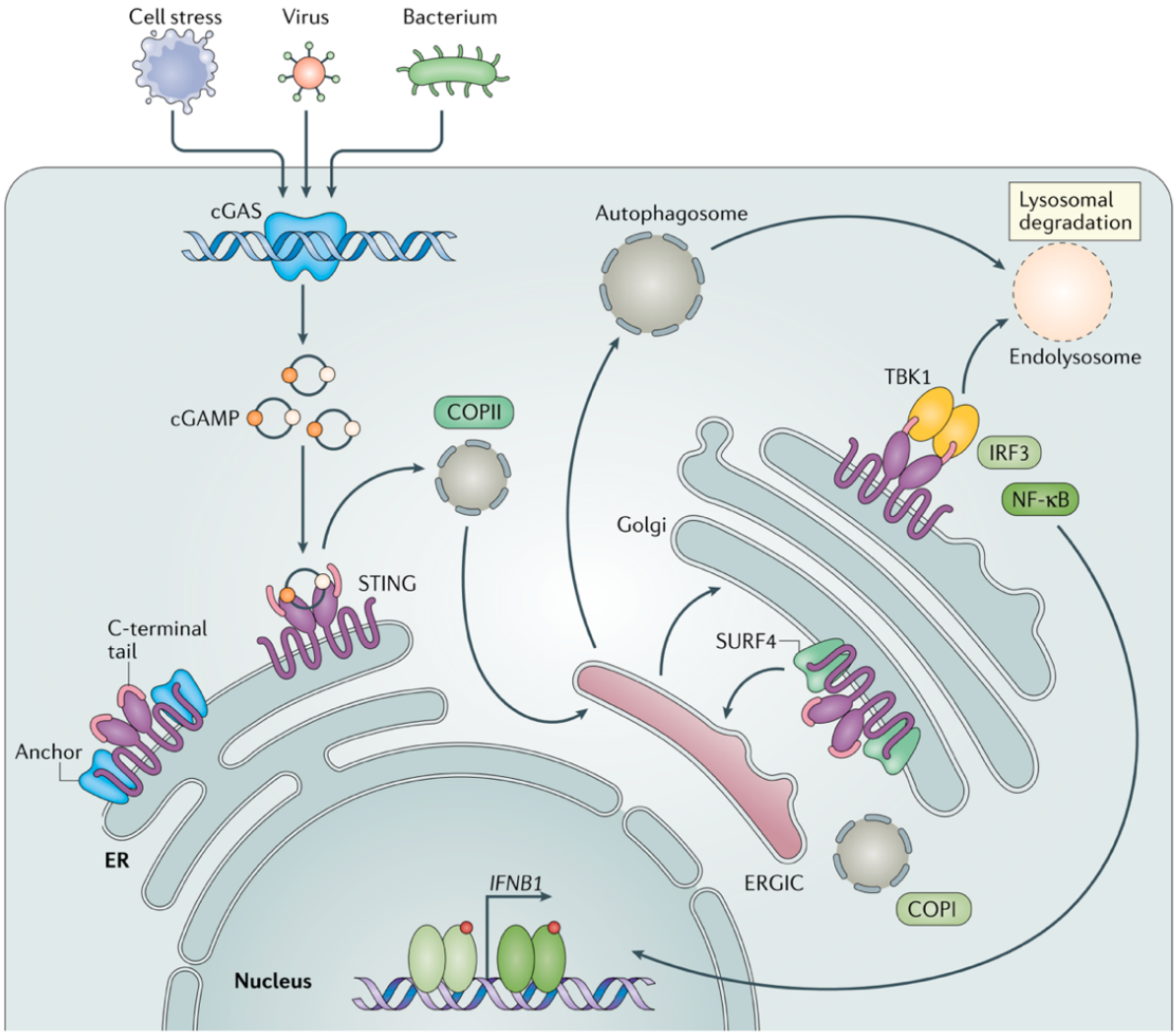

Figure 7: Overview of the cGAS-STING signaling pathway. Schematic representation of the cGAS-STING pathway. The pathway is activated upon binding to cytosolic double-stranded DNA from cGAS and culminate with the activation of an immunoinflammatory response. Figure modified from (Decout et al., 2021).

The binding of cGAS to double-stranded cytosolic DNA activates its catalytic activity and leads to the production of 2'3' cyclic GMP–AMP (cGAMP), a second messenger molecule and potent agonist of STING (Ablasser et al., 2013; Diner et al., 2013; Gao et al., 2013; X. Zhang et al., 2013). STING is a membrane protein localized to the endoplasmic reticulum which upon binding to cGAMP undergoes oligomerization and conformational changes (Ablasser et al., 2013). These changes trigger downstream responses resulting in the activation of several genes such as type I interferon, pro-apoptotic genes, chemokines and the NF-kB pathway (Decout et al., 2021; Motwani et al., 2019). All these genes are involved in different processes of the immune and inflammatory responses. The sustained

inflammation induced by CIN in tumors has been shown to induce the formation of metastasis (Bakhoum et al., 2018).

.

2. The centrosome

2. The centrosome

Centrosomes are membrane less organelles formed by two orthogonally organized centrioles surrounded by a dense mass of protein, the pericentriolar material (PCM), located in the cytoplasm (Conduit et al., 2015). Within a centriole pair, mother and daughter centrioles can be distinguished as they exhibit variations in age, structure and potential to nucleate cilia (Anderson, 1972; Graser et al., 2007; Tanos et al., 2013; Vorobjev & Chentsov, 1982). Centrosomes undergo a duplication cycle, tightly regulated throughout the cell cycle (Nigg et al., 2014; Nigg dan Holland, 2018; Conduit et al., 2015). Described for the first time in 1876 by Theodor Boveri and Eduard Van Beneden (Boveri, 1887), centrosome structure started to be elucidated along the XX century. This is still ongoing thanks to techniques such as cryo-Electron microscopy tomography and expansion microscopy. Evolutionary-genomic studies suggest that centrosomes are present in the last eukaryotic common ancestor. Interestingly, centrosomes were lost in some evolutionary branches, like in higher plants (Carvalho-Santos et al., 2010). This conservation among different species is tightly associated with its function as a basal body for the nucleation of cilia and flagella (Azimzadeh, 2014).

In proliferating animal cells, the centrosome acts as the main microtubule organizing center (MTOC) (Bornens, 2002). Besides its role in facilitating the accuracy of chromosome segregation and organization of the mitotic spindle, the centrosome influence cell motility, shape and polarity (Bettencourt-Dias & Glover, 2007; Bornens, 2012).

A more detailed description of centrosome structure, centrosome associated proteins and duplication cycle will be provided in the following sections. Finally, centrosome function will be described with particular attention given to its role in mitosis.

2.1 Centrosome structure

The centriole structure has been investigated first by electron microscopy, followed by confocal and super resolution microscopy (Anderson, 1972; Kuriyama dan Borisy, 1981; Vorobjev dan Chentsov, 1982). Together with imaging approaches, structural studies and i*n vitro* reconstitution approaches have pushed forward our understanding of the structure of centrioles and the PCM (Kitagawa et al., 2011; Van Breugel et al., 2011). In humans, each

centriole is a barrel- like structure, of ~450nm in height and ~250 nm of diameter. It is formed by a nine-fold symmetrical structure, organized in triplets of microtubules which become doublets toward the distal end (Figure 8). Microtubules are polymers formed by 13 aligned protofilaments, organized in a tube-shape manner, each one composed by α- and β- tubulin heterodimers. Development of techniques as high sensitivity mass spectrometry together with the sequencing and annotation of several genomes has allowed the identification of more than 100 different centriolar proteins (Andersen et al., 2003; Keller et al., 2005).

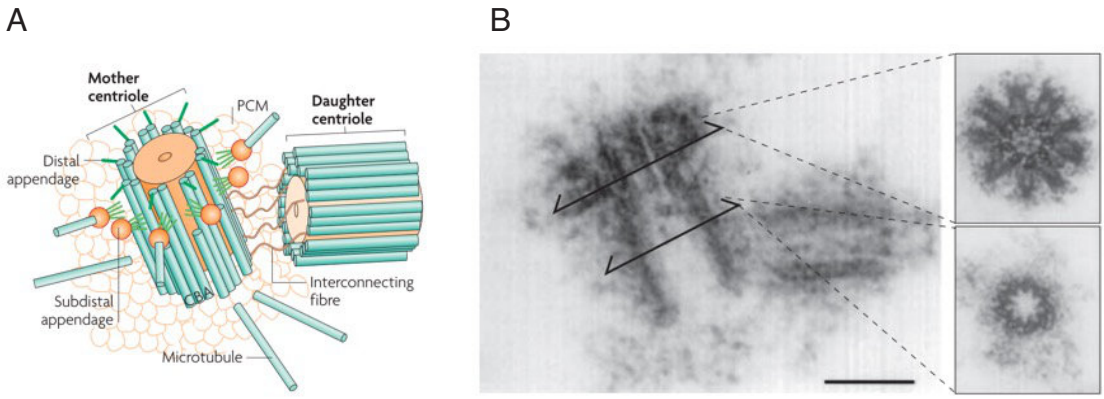

Figure 8: Centrosome structure (A) Schematic view of the centrosome. The centrosome is formed by two centrioles surrounded by pericentriolar matrix. It is the main Microtubule Organizing Center (MTOC) in proliferating animal cells. The centriole is formed by an inner tube surrounded by triplets of microtubules, called A, B, C from the more internal tubule to the more external one. The mother centriole is recognizable by the presence of distal and subdistal appendages at the distal end. The daughter centriole is orthogonally oriented in respect to the mother centriole to which it is connected through interconnecting fibers. (B) Electron micrograph of the centrosome. The top inset indicates a cross-section of the distal mother centriole. The bottom inset indicates a cross-section of the proximal part of the centriole. Scale bar: 0.2 µm. Image adapted from (Bettencourt-Dias & Glover, 2007).

According to the presence of different elements along the main axis, three regions can be distinguished: proximal, central and distal (LeGuennec et al., 2021). In the proximal region, at the center of the barrel, a cartwheel structure is present (Figure 8). The cartwheel it is formed by an inner tube, from which nine spokes protrude towards the surrounding microtubules (Klena et al., 2020) where Spindle Assembly abnormal protein 6 (SAS-6), is one of the main component (Banterle et al., 2021; Kitagawa et al., 2011). At the top of each

spoke a pinhead can be found, composed by centrosomal P4.1-associated protein (CPAP- also known as SAS-4), Centrosomal Protein 135 (Cep135) and SCL/TAL1 (STIL) interrupting locus, also known as SIL. The pinhead and the A-C linker connect the inner tube with the microtubules and the triplet base. (Guichard et al., 2013; Yu Chih Lin et al., 2013).

The central region has been well characterized in *Chlamydomonas* and *Paramecium*. In these model systems, cryo-electron tomography studies have revealed an helical inner scaffold adjacent to microtubules (Li et al., 2012; Le Guennec et al., 2020). Counterparts of some of the components have been also found in human centrioles, such as FAM161 Centrosomal Protein A (FAM161A), Proteome Of Centriole Protein 1B (POC1B), Protein Of Centriole 5 (POC5), Centrin-2 and WD Repeat-Containing Protein 90 (WDR90) (Ibrahim et al., 2009; Greenan et al., 2018).

Finally, the distal region can be distinguished in the mother centriole by the presence of the proximal and distant appendages. These appendages protrude into the cytoplasm and appear as a bundle of fibers which ends in a bulb (Bowler et al., 2019; Chong et al., 2020). Besides their known functions in centriole- membrane docking and ciliogenesis (Schmidt et al., 2012; Tanos et al., 2013; Ye et al., 2014), the distal appendages have recently been shown to be involved in the activation of a signaling pathway- the PIDDosome pathway (described below**)** (Tinel dan Tschopp, 2004; Fava et al., 2017; Burigotto et al., 2021; Evans et al., 2021)**.**

The other component of the centrosome, the PCM, was believed to be an amorphous mass of proteins without much organization. However, this view has changed after studies using super resolution microscopy performed both in *D. melanogaster* and cultured vertebrate cells. In interphase, the PCM seems to assume a concentric toroidal distribution of discrete diameter organized around the mother centriole. These distinct radial layers are organized mainly by Pericentrin (PCNT) or Pericentrin like protein (Plp) in flies, which represents one of the major PCM component. Pericentrin is a large coiled-coil protein involved in centrosome maturation across metazoans, which forms fibrils responsible from the compartmentalization other PCM proteins (Fu & Glover, 2012; Lawo et al., 2012; Mennella et al., 2014). The levels of PCM recruited around centrioles dramatically at mitotic entry in most animal cells.

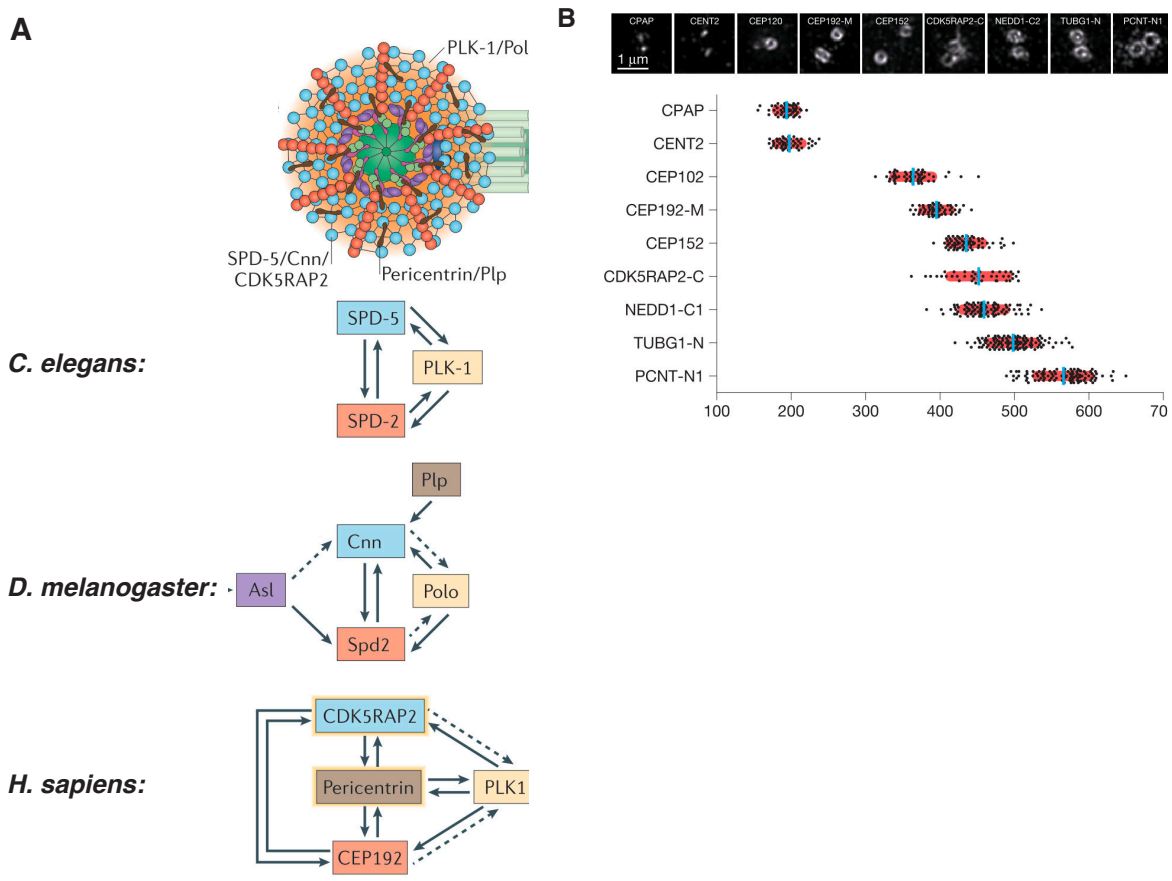

Figure 9. PCM maturation and organization. (A) Schematic drawing of PCM organization and PCM maturation in different model organisms. Image modified from (Conduit et al., 2015). (B) 3D-SIM micrographs of interphase centrosomes labelled with antibodies for the indicated PCM proteins in Hela cells. Quantification of outer toroid/ring diameters (nm) of the indicated centriole or PCM proteins which helped to identify the PCM layered organization. Image modified from (Lawo et al., 2012).

This will increase microtubule nucleation capacity, which is fundamental in mitosis for the generation of the mitotic spindle (Dobbelaere et al., 2008; Lee & Rhee, 2011; Woodruff et al., 2014). The presence of a scaffold guiding this process has been hypothesized and now started to be described in both flies and *C. elegans*. Assembly of this scaffold seems to be guided by spindle-defective protein 2 (SPD2) (Giansanti et al., 2008; Kemp et al., 2004; Pelletier et al., 2004) and by the phosphorylation of centrosomin (CNN) or spindle-defective protein 5 (SPD5) by, respectively, Polo/ PLK-1 depending on the animal model (Figure 9). (Conduit et al., 2010, 2014; Hamill et al., 2002; Megraw et al., 1999; Sunkel & Glover, 1988; Woodruff et al., 2015) CEP192/SPD2 can be found in two distinct regions- one at the centriole wall and one localized within the PCM. In addition, the

centriolar component Sas-4 has been shown to be an important player for PCM assembly in flies, favoring the recruitment of other proteins such as Asterless (Asl), Cnn and Plp (Gopalakrishnan et al., 2012, 2011).

It remains uncertain whether the mitotic PCM scaffold is present within vertebrate cells. If such a scaffold exists, it raises questions about whether the CDK5 regulatory subunit-associated protein 2 (CDK5RAP2) and CEP192, orthologs of Cnn and SPD-2 respectively, are responsible for driving the assembly of such a scaffold. CDK5RAP2 and CEP192 are the main proteins involved in PCM maturation in human cells (Choi et al., 2010; Fong et al., 2008). Importantly, in cultured vertebrate cells, the serine/threonine-protein kinase Polo-like kinase 1 (PLK1) phosphorylates Pericentrin which drives the recruitment of other PCM proteins (Haren et al., 2009; Lee & Rhee, 2011). Among those proteins we find γ-tubulin, a highly conserved protein among eukaryotes which is essential for microtubule nucleation and centrosome function (Joshi et al., 1992). To nucleate microtubules, different γ- tubulin subunits associate in a ring complex, called the γ- gamma-tubulin ring complex (γ-TuRCs) (Moritz et al., 2000; Wiese & Zheng, 2000; Zheng et al., 1995). Both CDK5RAP2 and Pericentrin play a central role in recruiting γ-TuRCs to the PCM, whereas CEP192 achieves this by interacting with the adaptor protein NEDD1 (Fong et al., 2008; Gomez-Ferreria et al., 2012; Zimmerman et al., 2004). Finally, CEP192 seems to be an important activator of Aurora- A, mediating the reciprocal activation of Aurora-A and PLK1 (Meng et al., 2015; Terada et al., 2003). Even if ultrastructure of the PCM has been studied, several questions remain such as the kinetics of individual components and the possible contribution of different Pericentrin isoforms and splicing variants.

2.2 The centrosome duplication cycle and its regulation

2.2.1 The centrosome duplication cycle and assembly

The centrosome is duplicated during the cell cycle. The use of electron microscopy approaches allowed the identification of four consecutive steps in mammalian cells: centriole disengagement, centriole duplication, centrosome maturation and centrosome separation (Alvey, 1985; Conduit et al., 2015; Kuriyama & Borisy, 1981; Robbins et al.,1967; Vorobjev & Chentsov, 1982). I will first provide an overview of the main steps of centrosome

duplication cycle, followed by a more detailed description of the proteins regulating this process.

At mitotic exit, one centrosome containing two centrioles, perpendicularly arranged can be identified. The older centriole, the mother centriole, can be distinguished by the presence of appendages in mammalian cells, as previously mentioned. Between the end of mitosis and early G1, the tight orthogonal configuration gets weaker, a process referred to as "centriole disengagement" (Tsou dan Stearns, 2006). In human cells centriole disengagement occurs in a PLK1 dependent manner (Tsou et al., 2009). Although still highly debatable, it has been shown that Separase mediated cohesin cleavage can contribute to centriole disengagement, in addition to sister chromatid separation (Schöckel et al., 2011).

During S phase, centriole duplication takes place. First, the new cartwheel is formed perpendicularly to the proximal site of each parental-centriole seeding procentriole assembly (Dzhindzhev et al., 2014; Ohta et al., 2014). Then, microtubule triplets are incorporated (Matsuura et al., 2004; Kitagawa et al., 2011). The two procentrioles, assembled at orthogonal positions of the parental centrioles keep elongating during S and G2 phases, originating two mature centrioles of similar size (Lange dan Gull, 1995). Moreover, the younger-parental centriole acquires appendages (Huang et al., 2017) and so it will become a mother. Before entering M-phase, the connection between the two centrosomes is cut, allowing their separation to form the opposite poles of the mitotic spindle (Mayor et al., 2000).

2.2.2 Regulation of the centrosome duplication cycle

Centrosomes must replicate only once per cell cycle (cell cycle control) and only a single centriole must be formed next to the parental centriole (Nigg, 2007; Nigg dan Holland, 2018). Thus, a tight control on the duplication cycle is present in most cells. The knowledge about centrosome duplication cycle and the proteins involved comes mainly from groundbreaking discoveries in the animal model *Caenorhabditis elegans (C. elegans)* after genome wide screens performed around 25 years ago. Different approaches allowed to correlate protein function with the different steps of centriole duplication (Figure 10) (Dammermann et al., 2004; Delattre et al., 2006; Kemp et al., 2004; Kitagawa et al., 2009; Leidel et al., 2005; Leidel & Gönczy, 2003; O'Connell et al., 2001; Pelletier et al., 2004, 2006).

In *C. elegans*, centriole assembly starts with the recruitment of kinase zygote defective 1 (ZYG-1) on the mother centriole, mediated by SPD-2 (Pelletier et al., 2004; Kitagawa et al., 2009; O'Connell et al., 2001a; Kemp et al., 2004).

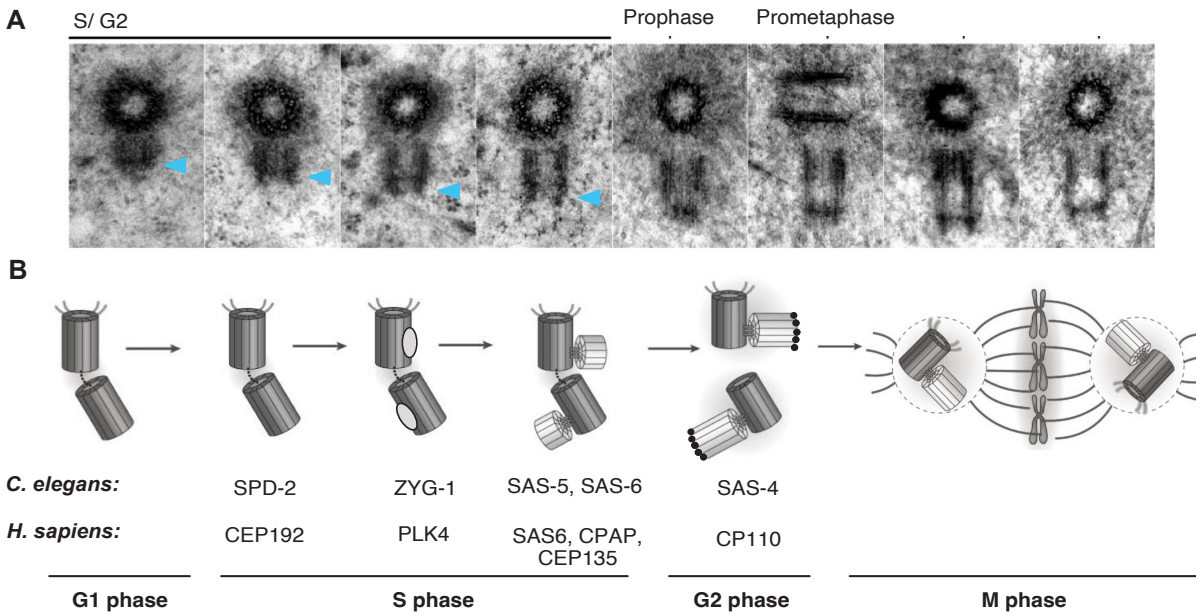

Figure 10: The centrosome duplication cycle (A) Electron microscopy images showing elongation of the daughter centriole (light blue arrow-heads) during G1/S- phases in HeLa cells. Image modified from (Shukla et al., 2015). (B) Schematic representation of the centrosome duplication cycle during different phases of cell cycle. Procentrioles and daughter centrioles are shown in light gray. The main proteins involved in centriole duplication during S- Phase in *C. elegans and* humans are reported below. Figure modified from (Bettencourt-Dias dan Glover, 2007).

Procentriole assembly is then mediated by recruitment of SAS-5 and SAS-6 and it terminated by the loading of SAS-4 at the edge of the novel-formed centriole (Kirkham et al., 2003; Zheng et al., 2014; Leidel dan Gönczy, 2003; Delattre et al., 2004; Leidel et al., 2005; Dammermann et al., 2004). Great advancements in the field have been made with the identification of the main counterparts also in *Chlamydomonas, Drosophila,* mice and human cells either through screens or by homology search of the *C. elegans* proteins (Bettencourt-Dias et al., 2005; Blachon et al., 2008; Dzhindzhev et al., 2014; Habedanck et al., 2005; Ohta et al., 2014; Sonnen et al., 2012; Strnad, et al., 2007).

In humans, Polo Like Kinase 4 (PLK4) has been identified as the main regulator of the centriole duplication cycle (Bettencourt-Dias et al., 2005; Habedanck et al., 2005). Its recruitment on the parental centriole occurs during S phase and it depends on CEP152 and

CEP192 (Kim et al., 2013; Sonnen et al., 2013; Blachon et al., 2008; Hatch et al., 2010). This step is indispensable to initiate centriole assembly. When PLK4 is over-expressed, extra centrosomes are formed, while lower PLK4 levels result in centriole duplication defects (Wong et al., 2015; Basto et al., 2008b; Coelho et al., 2015; Levine et al., 2017; Bettencourt-Dias et al., 2005). PLK4 undergoes an autoregulation process (Holland et al., 2010). Indeed, PLK4 can trigger its autophosphorylation, which will activate the recruitment of $SCF^{\beta TrCP}$ complexes triggering ubiquitin-dependent proteolysis and so its degradation (Cunha-Ferreira et al., 2009, 2013; Guderian et al., 2010; Holland et al., 2010, 2012; Yamamoto & Kitagawa, 2019). Thanks to timely PLK4 degradation the capacity to generate extra centrosomes is prevented. In human cells, it has been proposed that the tethering between the two centrioles established in S and G2 phase is responsible for preventing further duplication events (Tsou dan Stearns, 2006). The loss of centriole engagement during G1, this allows the initiation of centriole duplication cycle. When PLK4 is associated with the mother centriole, it recruits STIL, the SAS-5 homologue. STIL phosphorylation by PLK4 allows the recruitment of SAS-6, which will form the cartwheel (Dzhindzhev et al., 2014; Ohta et al., 2014; Strnad, et al., 2007). These proteins, with the help of cCEP135, recruit SAS-4/CPAP contributing to the assembly of centriolar microtubules at the new procentriole (Kohlmaier et al., 2009; Lin et al., 2013a; Tang et al., 2009, 2011). Procentrioles continue to elongate during G2 phase and when the right size is reached, centriolar coiled coil protein 110 (CP110) will localize at the tip of the centriole, blocking elongation. Indeed, its depletion has been shown to promote centriole elongation (Kohlmaier et al., 2009; Schmidt et al., 2009).

2.3 Centrosome functions

During interphase, centrosomes are required to organize the microtubule network and function as molecular platforms for the nucleation of cilia and flagella (Karsenti et al. 1984; Kellogg et al. 1994; Ishikawa and Marshall 2011). Moreover, the centrosome has been shown to colocalize with proteins involved in various processes such as DNA damage signaling (Mullee dan Morrison, 2015) cell cycle progression (Matsumoto dan Maller, 2004; Hinchcliffe et al., 1999), mitotic entry (Hirota et al., 2003; Atherton-Fessler et al., 2017; Alfa et al., 1990) and the PIDDosome pathway (described below) (Burigotto et al., 2021; Evans

et al., 2021; Fava et al., 2017). Thus, a role of the centrosome as a docking station for protein complexes has been proposed. However, this hypothesis emerges from observation of colocalization of the centrosomes with proteins involved in those process, while an actual interaction has not been demonstrated up to date. For the purpose of this work, cilia and flagella will not be discussed further and the focus of this section will be on the role of centrosome in mitosis.

In mitosis, chromosome separation is ensured by the bipolar mitotic spindle, which is formed by different population of microtubules. The expansion of PCM before mitosis, ensures an increase in microtubule nucleation capacity allowing the assembly of the mitotic spindle, as described in paragraph 2.1. Microtubules exist in a steady state equilibrium where assembly and disassembly occur at the two extremities, classified *plus* and *minus* ends. The polarity is defined by the rate of polymerization of the two microtubules sides. The plus end is more dynamic and polymerization is more important at this extremity (Akhmanova & Steinmetz, 2008, 2015; Howard & Hyman, 2007; Mitchison & Kirschner, 1984; Nehlig et al., 2017; Velot et al., 2015). The process of assembly and disassembly is guanosine-5'-triphosphate (GTP) dependent, it is promoted by magnesium ions, while inhibited by calcium ions (Desai dan Mitchison, 1997; Carlier dan Pantaloni, 1981; Brouhard dan Rice, 2018). Temperature also strongly affects this process. In the mitotic spindle, the minus ends of microtubules are oriented towards the centrosome, whereas plus ends towards the cortex or the metaphase plate. The spindle comprises different types of microtubules (Figure 11): kinetochore microtubules that attach the chromosomes to the spindle pole, astral microtubules, which radiate out from the poles and contact the cell cortex and interpolar microtubules, which maintain the bipolarity of this structure (Prosser dan Pelletier, 2017).

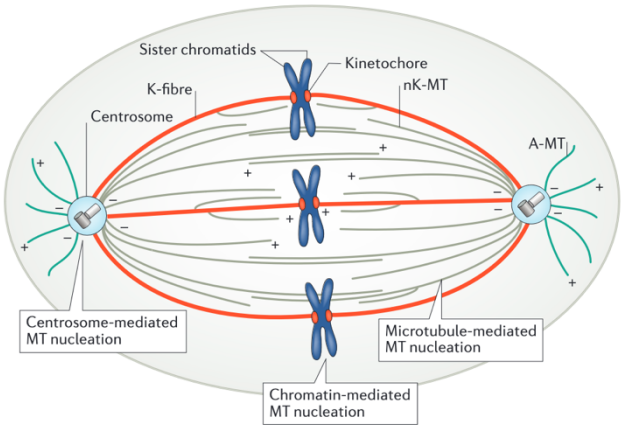

Figure 11: The mitotic spindle. Astral microtubules (A-MT) are nucleated from the centrosome towards the cortex. Kinetochore fibers comprise many microtubules and contact the kinetochores. Microtubule minus ends are localized towards the centrosomes and plus ends towards the chromosomes and cell cortex (Prosser dan Pelletier, 2017).

Because the centrosome has been described for many years as the main microtubule organizing center of proliferating animal cell (McIntosh et al., 2002), it has been considered for long time to be indispensable for the formation of bipolar spindles and accurate chromosome segregation. However, several studies demonstrated that bipolar spindle formation and correct chromosome segregation can occur even in absence of centrosomes (Heald et al., 1996; Khodjakov et al., 2000; Basto et al., 2006; Azimzadeh et al., 2012; Azimzadeh, 2014; Sanchez, Ariana D; Feldman, 2015). Indeed, microtubules can be generated and organized by others MTOCs, such as chromatin and the kinetochores (Lüders et al., 2006), preexisting microtubules (Sánchez-Huertas dan Lüders, 2015; Brinkley, 1985) and even the Golgi apparatus (Chabin-Brion et al., 2001; Mukherjee et al., 2020), Moreover, plants and female oocytes from almost all animals also have no centrosomes (Yubuki dan Leander, 2013; Azimzadeh, 2014). Thus, the question if centrosomes have an indispensable role in mitosis has been investigated for long. It has been proposed that centrosomes could actually increase the fidelity in chromosome segregation in certain cell types (Sir et al., 2013; Wong et al., 2015). However, the frequency of mitotic errors appears to be low in a variety other setting including *Drosophila*, mouse and non-transformed human cells (Basto et al., 2006; Bazzi & Anderson, 2014; Wong et al., 2015). On the other hand, an emerging view suggests centrosomes to be important in regulating the time of specific cell cycle transitions (Silkworth et al., 2012; Hornick et al., 2011). Indeed, it was demonstrated both in invertebrate and vertebrate animal models that cells lacking centrosomes have a prolonged prometaphase/metaphase (Basto et al., 2006; Pfaff et al., 2007). While in invertebrates this has no major consequence, in vertebrates this leads to the activation of the mitotic stop watch pathway (see below). This suggests that cell without

centrosome take more time to organize the mitotic spindle.

At the same as the PCM undergoes maturation, centrosomes need to separate to opposite sides of the cell to assemble a bipolar spindle. At the beginning of mitosis, NIMA-related kinase 2 (Nek2) is activated and phosphorylates nucleosome assembly protein (C-Nap1), located on the proximal end of the parental centriole (Fry, 2015). C-Nap1 detaches from the centriole, causing the loss of the connection between the two centrosomes, allowing their separation (Mardin et al., 2010). The timing of centrosome separation is important as it has been proposed that delayed centrosome separation may favor abnormal kinetochore- microtubule attachments (Silkworth dan Cimini, 2012).

Furthermore, centrosomes regulate the position and orientation of mitotic spindle via the astral microtubule that they nucleate (Siller dan Doe, 2009). Astral microtubules interact with cell cortex through dynein which uses centrosomes as anchor to exert its force and regulating spindle orientation (Basto et al., 2006; Bazzi & Anderson, 2014; Morin & Bellaïche, 2011).

2.4 Centrosome abnormalities in cancer

All processes in which centrosomes take part can be potentially disrupted by structural and/or numerical centrosome defects. More than a century ago, Theodore Boveri was the first to propose that centrosome number defects can cause cancer (Harris, 2008). Boveri's hypothesis was based on his di-spermic experiments performed in sea-urchin eggs, which contained multiple centrosomes. Eggs with extra centrosomes performed multipolar divisions and chromosome mis-segregation, resulting in three or more daughter cells with aneuploid karyotypes. These observations provided the bases for the association between centrosome amplification (the presence of more than two centrosomes in a cell), chromosomal segregation abnormalities (aneuploidy) and cancer: "*Nuclear defects, such as I have described in sea urchins, are the result of multipolar mitoses. Since abnormalities of this sort are not infrequently found in malignant tumors, it is reasonable to suppose that there is some connection between them and the origin of tumors"* (Harris, 2008) **(**Figure 12).

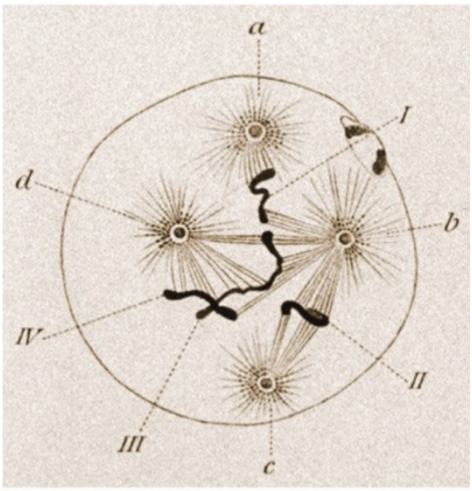

Figure 12: Multipolarity in sea urchin eggs. Drawing by T.Boveri illustrating the abnormal presence of 4 centrosomes forming a multipolar spindle in Sea Urchin embryos. From (Satzinger, 2008a).

The idea that centrosome amplification caused errors in chromosome segregation during mitosis, which promote tumor establishment or progression, had important contributions from his contemporaneous colleague David von Hansemann (Hansemann, 1890). *Von Hansemann,* while observing tumor histology, noted that abnormal mitosis were common in cancer cells. However, the potential role of centrosomes and mitotic abnormalities in cancer has been underestimated for several years by the scientific community. It was only in the late 1990s that this concept returned to light and re-examined (Brinkley & Goepfert, 1998; Fukasawa et al., 1996; Lingle et al., 1998; Lingle & Salisbury, 1999a, 1999b; Salisbury, 2001). In 1996, the observation that loss of tumor suppressor p53 was associated with centrosome amplification, brought new interest for the role of centrosomes abnormalities and mitotic defects in cancer (Fukasawa et al., 1996b), even if this remains an area of debate. The characterization of human breast carcinomas and healthy breast tissue revealed that structural and numerical centrosome abnormalities are characteristic of cancer cells *in situ* (Lingle & Salisbury, 1999a, 1999b). In the following years, centrosome structural and numerical defects have been detected in several cancer cell lines of different origins (Marteil et al., 2018). Centrosome amplification in particular has been observed *in situ* in patients tumor samples (Goundiam & Basto, 2021; Morretton et al., 2022; Wang et al., 2019). Moreover induction of centrosome amplification has been demonstrated to be a tumor-initiating event in animal models such as *Drosophila and* mice (Basto et al., 2008; Coelho et al., 2015; Levine et al., 2017; Serçin et al., 2016).

In the next sections an overview of centrosome defects will be provided, with particular interest in centrosome amplification and their consequences.

2.4.1 Structural abnormalities

Centrosome structural defects can be subdivided into two categories: defects in centriolar structure or in PCM structure. However, this category has been harder to investigate compared to defects in centrosome number due to the small size of this organelle (~0.2–0.5 µm long). Time consuming techniques as high-resolution microscopy and electron microscopy are required to characterize centrosome structure. Two different studies have described a direct connection between defects in centrosome structure and cancer. In the first one, through an analysis of the NCI-60 panel of human cancer cell lines originating from diverse tissues, centriole over-elongation emerged as a recurrent feature (Marteil et al., 2018). This centriole over-elongation can generate supernumerary centrosomes though both centriole fragmentation and ectopic procentriole nucleation. Interesting, centriole over-elongation was obtained via the overexpression of CPAP/SAS-4 in cancer cell lines and this also caused centriole fragmentation (Marteil et al., 2018). However, the possible mis-regulation of other genes involved in centriole nucleation is hypothesized as at the origin of this kind of defects in cancer (Guo et al., 2007; Lingle et al., 1998). In the second study, structural centrosome aberrations, induced by overexpression of Ninein-like protein (NLP), resulted in selective budding of mitotic cells from 3Dimentional (3D) epithelial spheres. This invasive behavior reflects the acquisition of two distinct properties: cytoskeleton reorganization and increased stiffness, which results in the displacement of mitotic cells away from the spheres (Ganier et al., 2018). NLP has been detected to be frequently overexpressed in human cancers, ovarian cancer included and to confer resistance to paclitaxel in breast cancer (Shao et al., 2010; Yu et al., 2009; Qu et al., 2008; Zhao et al., 2012).

Finally increased PCM size has also been categorized as a structural defect, frequently observed in cancer cell lines (D'Assoro et al., 2002). However, since the work mentioned above (Marteil et al., 2018) suggested that centriole elongation can lead to centrosome fragmentation, it is possible that a clear distinction between structural and numerical defects cannot be made. This issue may be overcome using more resolutive techniques to classify centrosomal defects.

2.4.2 Numerical abnormalities: centrosome loss

Centriolar loss has been observed several times independently in eukaryotes during evolution (Yubuki dan Leander, 2013; Azimzadeh, 2014; Azimzadeh et al., 2012). Centrosomes are naturally absent in higher plants and in most animal female oocytes. Moreover, removal of centrosomes has been shown to not disrupt the capacity of *Drosophila* flies to develop into adults (Basto et al., 2006). *Drosophila* larvae were able to develop normally, even if adults died because of lack of cilia in sensory neurons. This study show that centrioles are essential for development of centrosomes, cilia and flagella but not for most aspects of *Drosophila* development. In the planarian *Schmidtea mediterranea* it has been shown that centrioles are only necessary to sustain cilia assembly but not for processes related with cell proliferation (Azimzadeh et al., 2012). In this study, it was shown that after depletion by RNAi interference technology of centriole-biogenesis homologous proteins in *Planaria*, body movement was impaired due to lack of cilia. However, the animal depleted for centriole components was still able to regenerate tissues in a similar way to that of wild type individuals. In mouse, it has been shown that Sas4-null mutants *(Sas4$^{-/-}$)* embryos lack centrioles and die at mid-gestation with elevated levels of p53 and increased apoptotic cell death (Bazzi dan Anderson, 2014). Further, p53 was found to activated as a consequence of prolonged prometaphase in absence of centrioles but defects in spindle organization, chromosome segregation defects DNA damage were not found. Co-depletion of SAS-4 and p53 could rescue cell death and prolonged embryo viability to later developmental stages.

In human cells, lack of centrosomes did not correlate with mitotic defects but cell cycle arrest was noticed in non-transformed cells such as RPE-1 cells (Lambrus et al., 2016; Wong et al., 2015; Meitinger et al., 2016)). With the aim of identifying proteins involved in cell cycle arrest screens have been made using either RPE-1 PLK4 knock out (KO) cells or Centrinone treatment. Centrinone is a PLK4 inhibitor that has been widely used to inhibit the centriole duplication cycle (Wong et al., 2015). These screens have identified the 53BP1-USP28-p53 axis(Lambrus et al., 2016) and Tripartite Motif Containing 37 (TRIM37) as proteins promoting p53 activation and cell cycle arrest (Figure 13) (Meitinger et al., 2020; Yeow et al., 2020).

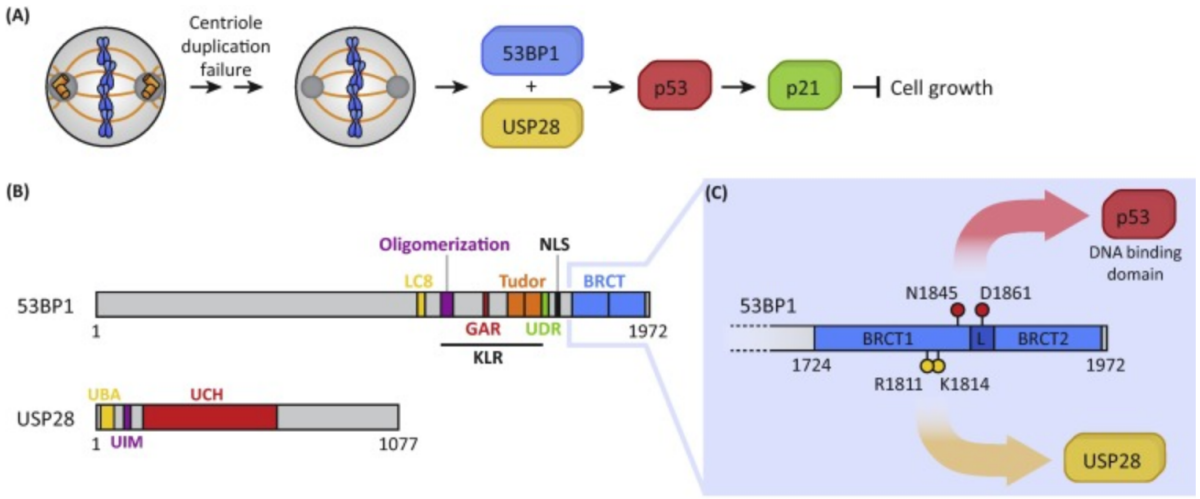

Figure 13: p53 and p21 mediated cell cycle arrest in response to centrosome loss. (A) Defects in centriole duplication are translated in the expression of USP28 and 53BP1**,** which activate p53 and p21 inducing cell cycle arrest. (B) Schematic drawings of the structure of 53BP1 and USP28 depicting their main functional and interaction domains. From (Lambrus dan Holland, 2017).

Ubiquitin-Specific-Processing Protease 2 (USP28) is a deubiquitinase initially identified as a binding partner of the DNA damage signaling protein 53BP1 (Lambrus et al., 2016). TRIM37 is a E3 ubiquitin-protein ligase required to prevent centriole reduplication (Kallijärvi et al., 2005; Balestra et al., 2013). Interestingly, a likely activating factor of these pathways is the extended mitotic timing of cells without extra centrosomes (Figure 13). Indeed, prolonged mitosis by nocodazole treatment was sufficient to trigger p53 activation and cell cycle arrest (Lambrus et al., 2016; Uetake & Sluder, 2010) All together, these results lead to the concept of mitotic stop watch where cells “measure” the time spend in mitosis. In particular, a prometaphase longer than 90min appears responsible for activating the stop watch and trigger p53 depend cell cycle arrest (Uetake dan Sluder, 2010b). This mechanism was later shown to be responsible for cell cycle arrest during late mouse development (Phan et al., 2021; Allais dan FitzHarris, 2022). Both USP28 and p53 interact with 53BP1 through the tandem C-terminal BRCT (BRCA1 C Terminus) repeats (Knobel et al., 2014; Joo et al., 2002). However, the exact mechanism of recruitment of these proteins in the stopwatch mechanism remain to be investigated.

Even if centrosome loss has been observed *in vivo* in human tumors, such as prostate cancer (Wang et al., 2020) and epithelial ovarian cancers (Morretton et al., 2022) (Figure 14) , it remains to be understood if there is any advantage related with this

condition. In has been proposed that centrosome loss in prostate cancer increased CIN (Wang et al., 2020). However, this is not the case for ovarian cancer (unpublished results Basto lab).

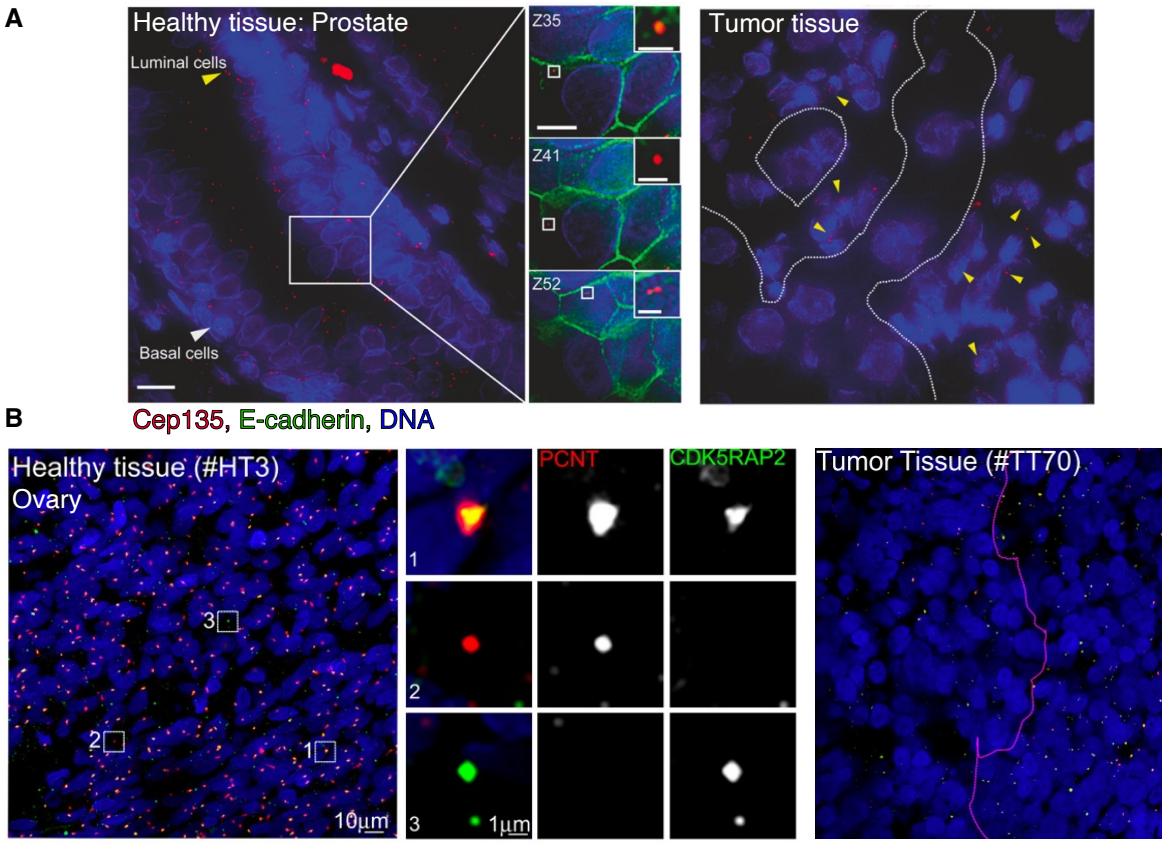

Figure 14: Centrosome loss in human cancers (A) Immunofluorescence microscopy images of human prostate and the corresponding centrosome status in healthy tissues (left) and cancer (right). Antibodies were used against the centrosome protein CEP135 and plasma membrane protein E-cadherin. DNA in blue. Examples of centrosomes in healthy tissues are highlighted in the white square box. The dotted white line identify regions without centrosomes whereas yellow arrows indicates centrosomes in prostate tumors. Scale, 10 µm. Image modified from (Wang et al., 2020). (B) Confocal microscopy images of healthy ovarian tissue (left) and epithelial ovarian tumors (right) labeled with antibodies against centrosomal proteins Pericentrin and CDKRAP2. DNA is shown in blue. The magenta line identifies regions without centrosomes in tumors. Image modified from (Morretton et al., 2022).

Interestingly, neuroblastoma and breast cancer cells containing TRIM37 amplification have been shown to be particularly vulnerable to the inhibition of PLK4 and so centrosome loss (Yeow et al., 2020; Meitinger et al., 2020). In these cancer types, as well

as in others displaying amplification of the TRIM37 gene region, the inhibition of PLK4 represents a promising approach for specifically inducing mitotic failure.

2.4.3 Numerical abnormalities: centrosome amplification

Centrosome amplification, the presence of more than two centrosomes in a cell, is the most studied centrosomal alteration in cancer. This feature has been found in a variety of cultured cancer cell types such as breast, prostate, colon, ovarian, pancreatic, multiple myeloma, non-Hodgkin's and Hodgkin's lymphomas, acute and chronic myeloid leukemia (Krämer et al., 2005; Marteil et al., 2018). Moreover, centrosome amplification has also been detected *in situ* in both solid and hematological malignancies (Chan et al., 2011).

Cells can acquire more than two centrosomes by different mechanisms. First, deregulation of centrosome duplication cycle (see paragraphs 1.2.3 - 1.2.4), which may rely on PLK4. In this case centrosome amplification would derive from the mother centriole making more daughter centrioles. Over-expression of PLK4 has been shown to lead to centrosome amplification (Bettencourt-Dias et al., 2005; Habedanck et al., 2005; Kleylein-Sohn et al., 2007; Peel et al., 2007; Basto et al., 2008). Deregulation of PLK4 activity can derive from alteration in its expression levels or alteration of its autophosphorylation-regulating process or its proteolysis by the ubiquitin system. Another centriole duplication, whose over-expression can result in centrosome amplification is SAS-6 (Leidel et al., 2005; Kitagawa et al., 2011; Strnad et al., 2007). However, even if used experimentally as a way to induce amplification, there is little evidence that these proteins are over- expressed in cancers (Goundiam dan Basto, 2021). It is possible that defects in ubiquitination or activity nevertheless leads to stabilization of these factors. Moreover, overexpression of certain PCM components and PCM fragmentation can also lead to the formation of acentriolar centrosomes (Schatten & Schatten, 1986; Loncarek et al., 2008). Centrosome amplification can also result from a cell inheriting many centrosomes, for example through mitotic slippage or cytokinesis failure. Centrosome amplification can indeed be found in tetraploid cells (Ganem et al., 2007).

The difficulty to study centrosome amplification and its consequences results mostly from the complication to uncouple from whole genome duplication or polyploidy. For this reason, the identification of PLK4 over- expression has become a useful tool to

obtain centriole duplication in a single cell cycle (Bettencourt-Dias et al., 2005; Habedanck et al., 2005). Later on, induction of mild levels of overexpression of PLK4 in *Drosophila* (Basto et al., 2008; Gambarotto et al., 2019) and mice (Coelho et al., 2015; Serçin et al., 2016; Levine et al., 2017) allowed the study of induction of centrosome amplification in animal models too.

2.4.3.1 Consequences in mitosis

Centrosome amplification represents an obstacle for bipolarity during mitosis. A problem with lack of bipolarity is the failure in segregating a diploid genome into two daughter cells and so the generation of aneuploidy progeny, frequently not viable (Kwon et al., 2008; Godinho and Pellman, 2014) . Increased CIN is suggested to be the mechanism through which centrosome amplification favor cancer progression (Basto et al., 2008 b; Coelho et al., 2015; Serçin et al., 2016; Levine et al., 2017). However, the exact process through which centrosome amplification favor CIN has remained obscure for a long time. Centrosome amplification can lead to multipolar mitosis (Ganem et al., 2009b; Harris, 2008; Kwon et al., 2008; Leber et al., 2010; Sabino et al., 2015). However, multipolar mitosis can be catastrophic and cause cell death or arrest in the following interphase (Brinkley, 2001; Ganem et al., 2009; Kwon et al., 2008a). These levels of lethality seemed incompatible with cancer cells proliferation. Cancer cells have indeed evolved mechanisms to avoid multipolarity in the presence of centrosome amplification such as centrosome clustering.

Centrosome clustering is the best characterized mechanism used by cancer cells with extra centrosomes. Centrosome clustering describes the gradual grouping of extra centrosomes into two poles during mitosis to assemble a bipolar spindle and avoid multipolarity. This mechanism was initially described to occur both in interphase and in mitosis in the mouse neuroblastoma N1E-115 cell line more than 40 years ago (Brinkley et al., 1981; Ring et al., 1982). More recently, further characterization of this process has been performed in other studies (Basto et al., 2008; Godinho & Pellman, 2014; Krämer et al., 2011; Kwon et al., 2008; Marthiens et al., 2012; Quintyne et al., 2005). Proteins responsible for centrosome clustering have started to be identified (Figure 15) (Kwon et al., 2008; Leber et al., 2010).

Most proteins involved in this process belong are microtubule-associated proteins (MAPs), the spindle assembly checkpoint and regulators of acto-myosin contractility (Kwon et al., 2008). MAPS and mitotic motor proteins exerts different types of forces on microtubules originating from centrosomes and chromosomes, which leads to clustering (Loughlin et al., 2011, 2010; Burbank et al., 2007) (Figure 15).

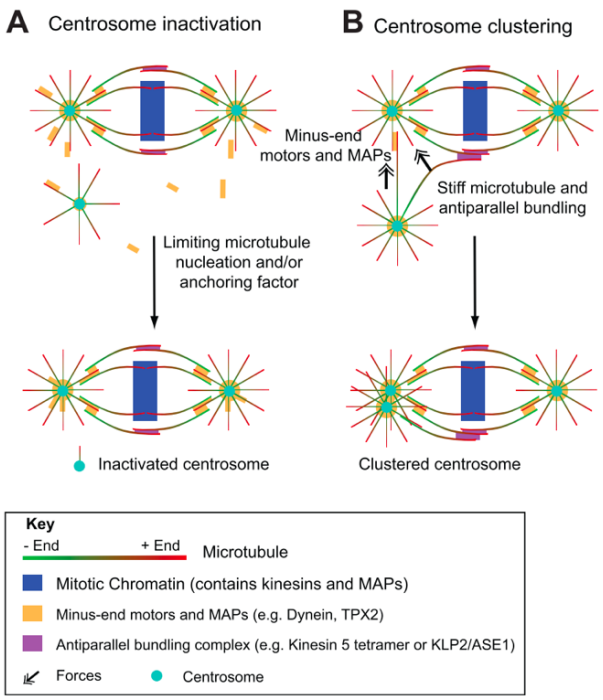

Figure 15: Mechanisms involved in bipolar spindle assembly in the presence of extra centrosomes Schematic representation of mechanisms of centrosome inactivation (A) and centrosome clustering (B). Image modified from (Marthiens et al., 2012).

Further, the minus-end director motors kinesin HSET, a KIf14 member plays an essential role in this process (Kwon et al., 2008; Basto et al., 2008; Rhys et al., 2018). More recently, it has been shown that clustering involves two steps (Rhys et al., 2018). In the initial step, a search-and-capture mechanism, marked by the gradual motion of centrosomes was noticed. Subsequently, in the second phase, termed the motorized phase, centrosomes engage in fast directional movement which appears to be HSET mediated.

Importantly, inter centrosome distance plays a direct role in promoting clustering. Dynein and the nuclear mitotic associated protein (NuMA) also participate in this process (Quintyne et al., 2005). Interestingly, inhibitors of centrosome clustering have been developed and are currently tested in clinical trials (Navarro-Serer et al., 2019; Konotop et al., 2016; Kawamura et al., 2013; Watts et al., 2013; Galimberti et al., 2011). Although centrosome clustering seems to be a general mechanism used by cells to survive

centrosome amplification, the efficiency of clustering can be very variable in transformed cultured cells (Ganem et al., 2009; Quintyne et al., 2005). The reason behind this variability remains an unresolved question.

Other mechanisms such as centrosome inactivation or elimination have also been described in cells with centrosome amplification. Centrosome inactivation is associated with the loss or decrease of microtubule nucleation capacity and thus MTOC function. To be inactivated, centrosomes face a gradual reduction in PCM levels. The event of centrosome inactivation takes place exclusively during mitosis. Indeed, centrosomes transient regain the capacity to nucleate microtubules has been observed following inactivation at mitotic exit (Basto et al., 2008). However, centrosome inactivation has only been described in *Drosophila* neuroblasts and it remain to be investigated whether this mechanism contributes to bipolar spindle formation in cancer cells.

It is important to mention at this point to mention that certain cells loose centrosomes as part of programed process. Centrosome elimination occurs in almost all animal female oocytes, as cells are to ensure that the fertilized zygote maintain the appropriate number of centrioles brought by the sperm (Dae dan Roy, 2006; Manandhar et al., 2005; Pimenta-Marques et al., 2016; Nakashima dan Kato, 2001; Sluder et al., 1989; Szollosi et al., 1972; Gruss, 2018). Certain mechanisms leading to centrosome elimination have been described such as PCM reduction (Kushner et al., 2014) and centriole fragmentation or exclusion from the cell concomitant to polar body extrusion (Karki et al., 2017). In principle, these mechanisms can also occur in cancer cells to eliminate the presence of extra centrosomes. Interestingly, it has been recently shown that asymmetric clustering of extra centrosomes in tetraploid cells conditions the evolution of these cells by reducing centrosome numbers (Baudoin et al., 2020).

Because multipolarity must occur at low frequency in cancer cells with extra centrosomes, other mechanisms have been investigated for how CIN can generated in these conditions. In 2009 it was proposed by two independent groups that centrosome amplification induces CIN by favoring merotelic attachments (Ganem et al., 2009; Silkworth et al., 2009) (Figure 16). Through live-imaging approaches these studies showed that cells with extra centrosomes, even if managing to cluster centrosomes into two poles, they pass

through an intermediate stage of transient-multipolarity. During this step, the formation of merotelic attachments is favored (Cimini et al., 2001; Silkworth et al., 2009).

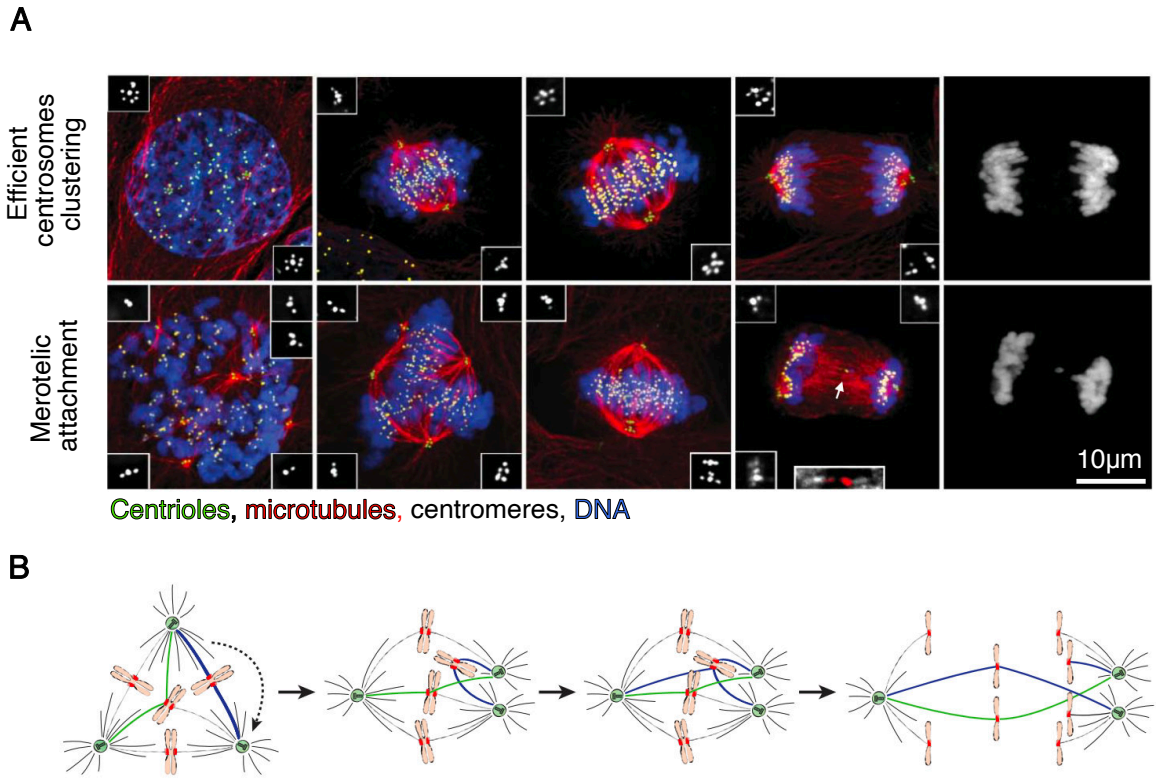

Figure 16: Centrosome amplification favor chromosomal instability (CIN) by promoting merotelic attachment (A) Stills from images acquired with spinning disc confocal microscope of U2OS osteosarcoma cell line inducible for PLK4 overexpression. Cells were incubated for 15 hours with 1uM doxycycline to induce centrosome amplification (centrioles shown in the inset in white). In the upper panel, efficient centrosome clustering into a bipolar spindle is shown. In the lower panel, a cell going through transient multipolar spindle is shown, resulting in the generation of merotelic attachment and lagging chromosome in anaphase. The white arrow indicates a lagging chromosome. (B) Schematic representation of centrosome amplification promoting merotelic attachment (blue microtubules). Unresolved merotelic attachment can give rise to lagging chromosomes at anaphase and thus they promote CIN. Figure modified from (Ganem et al., 2009).

2.4.3.2 Consequences in interphase

Centrosome play an important role in maintaining the organization of the interphase microtubule array. Thus, the possibility that centrosome amplification can affect other aspects than the ploidy, as for cell shape, polarity or mobility has to be considered. Centrosome amplification has been reported to be associated with advanced tumor stage

in breast cancer and several other tumor types (Chan, 2011; D'Assoro et al., 2002). Thus, it was hypothesized that centrosome amplification could favor cell invasion capacity of cancer cells. In the last 10 years, it has been demonstrated that centrosome amplification can indeed favor cell invasion capacity both in a cell-autonomous and non-cell-autonomous manner (Adams et al., 2021; Arnandis et al., 2018; Godinho et al., 2014). PLK4 over-expression in 3D human mammary epithelial cells was sufficient to induce features of migratory cells- such as cell protrusions. These features seem to be derived from an increased capacity to nucleate microtubules in presence of extra centrosomes, which was also described in other studies (Lingle et al., 1998, 2002). This increased microtubule nucleation capacity resulted in increased Rac Family Small GTPase 1 (Rac1) activity, which disrupts cell–cell adhesion and promotes invasion (Godinho et al., 2014). Indeed, both microtubule polymerization and depolymerization have been shown to lead to different Rho GTPases activation, involved in cell migration (Van Horck et al., 2001; Lozano et al., 2003). Moreover, centrosome amplification was shown to favor non-cell-autonomous invasion capacity by promoting the production of reactive oxygen species (ROS). ROS are derivatives of molecular oxygen, as hydrogen peroxide (H_2O_2) and the superoxide anion radical ($O_2^{\cdot -}$), which leads to oxidative stress (Sies dan Jones, 2020). Furthermore, it is important to mention that increased microtubule nucleation capacity induced through centrosome amplification has the potential to affect many other processes as focal adhesion assembly, transport and organization of cytoplasmic organelles as the Golgi apparatus, the endoplasmic reticule and mitochondria (Gonçalves et al., 2010; Lozano et al., 2003; Monteiro et al., 2023; Rodrigues-Ferreira et al., 2019; Tang & Marshall, 2012; Zmuda & Rivas, 1998).

2.4.3.3 Centrosome amplification and p53 activation

Centrosome amplification appears detrimental, as supported by previous research demonstrating that newly formed tetraploid cells naturally eliminate excess centrosomes during continuous passaging in culture (Ganem et al., 2009; Silkworth et al., 2009; Baudoin et al., 2020). The presence of extra centrosomes, indeed has been shown to elicit a durable p53-dependent proliferative arrest in non-transformed human cells (Holland et al., 2012). Activation of p53 in interphase, when extra centrosomes are present, seems

to be independent from the stopwatch mechanism activated by centrosome loss in non-transformed cell lines. Indeed, knockout of 53BP1 or USP28 in RPE1 cells did not rescue the cell cycle arrest caused by supernumerary centrosomes (Lambrus et al., 2016). Thus, even if both centrosome loss and centrosome amplification activate p53, the pathways leading to its activation appear to be independent.

Recently, the presence of centrosome amplification has been linked to p53 stabilization by the PIDDOsome pathway (Fava et al., 2017; Evans et al., 2021; Burigotto et al., 2021) (Figure 17). Activation of this pathway seems to depend on the presence of multiple mother centrioles containing distal centriolar appendages. In particular, this mechanism relies on Ankyrin Repeat Domain 2 (ANKR2) binding and priming the P53-Induced Death Domain Protein 1 (PIDD1) protein , which localizes on distal centriolar appendages (Evans et al., 2021). Upon priming, PIDD1 is released and it can bind to other PIDDOsome components: caspase and RIP adaptor with death domain (CRADD) and Caspase-2, the most conserved protease among the caspase family (Nematollahi et al., 2015; Park et al., 2007; Tinel dan Tschopp, 2004). Cleavage of Caspase-2 and subsequent activation leads to cleavage of MDM2. MDM2 is an E3 ubiquitin-protein ligase that mediates ubiquitination of p53, leading to its degradation by the proteasome. MDM2 cleavage results thus in p53 stabilization and activation of downstream genes involved in cell cycle arrest such as p21 or in cell death (Burigotto et al., 2021; Fava et al., 2017).

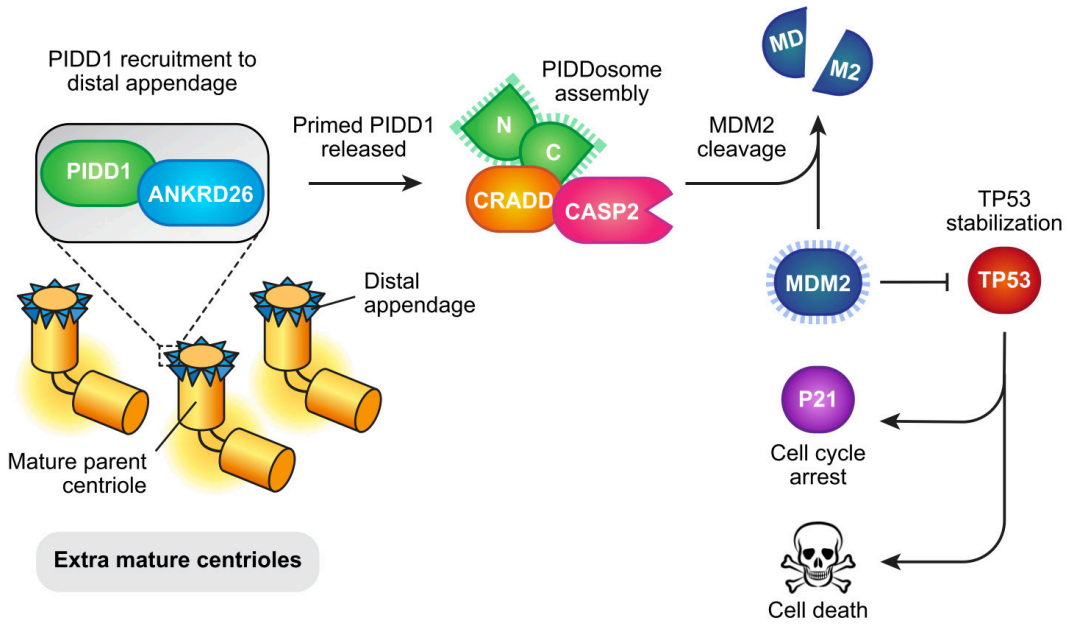

Figure 17: The PIDDosome pathway Schematic representation of the proteins involved in the PIDDosome pathway which is activated in the cell by the presence of extra centrosomes. It results in activation of p53 and consequent cell cycle arrest, mediated by p21, or cell death. Figure modified from (Evans et al., 2021).

Mutations in p53 which results in lack of protein expression or the expression of a non-functional protein in cancer cells generate a permissive environment for cells to survive even if centrosomes are amplified. Indeed, experiments which shown generation of squamous cell carcinomas upon PLK4 overexpression in mice were performed in a p53 null context (Serçin et al., 2016). In alignment with this relationship, in Barrett's esophagus, a condition linked to an increased susceptibility to esophageal cancer, centrosome amplification was identified to be concomitant with the loss of p53 during the process of malignant transformation (Lopes et al., 2018). Thus, maintenance of centrosome amplification in cancer cells and most likely in human cancers, while allowing proliferation, seems strictly dependent on p53 dysregulation p53. It remains unclear if centrosome amplification can trigger tumor formation in the absence of direct effects on the p53 and which mutated p53 forms allows the survival of cells with centrosome amplification.

Other ways through which centrosome amplification has been linked to activation of p53 are by favoring CIN, formation of micronuclei and consequently cGAS/STING pathway activation and extended mitotic timing (Harding et al., 2017a; Bakhoum dan Cantley, 2018; MacKenzie et al., 2017).

2.4.3.4 Apoptosis

An alternative antitumor activity of p53, besides triggering p21-mediated cell cycle arrest is related with cell death by apoptosis. Apoptosis is a type of regulated cell death highly conserved among animal species (Carneiro & El-Deiry, 2020; Elmore, 2007). Regulated cell death is defined as a form of cell death that results from the activation of one or more signal transduction modules, and hence can be pharmacologically or genetically modulated (Galluzzi et al., 2018). A great contribution in the description of this pathway was performed by *Robert Horvitz and Ellis R.E*., whose studies in *C. elegans* were awarded with the Nobel Prize in Physiology or Medicine in 2002 (Ellis dan Horvitz, 1986; Ellis et al., 1991).

Apoptosis can be triggered in cells through both intrinsic and extrinsic pathways. Intrinsic apoptosis can be activated by perturbations of the extracellular or intracellular microenvironment and it is characterized by mitochondrial outer membrane permeabilization (MOMP) (Figure 18) (Galluzzi et al., 2016; Kalkavan dan Green, 2017; Roos et al., 2016; Czabotar et al., 2014). MOMP is a process which results in the release of cytochrome C from mitochondria into the cytoplasm (Galluzzi et al., 2016; Kalkavan dan Green, 2017; Garrido et al., 2006). Cytochrome C is a protein normally located in the mitochondrial intermembrane space, it functions as an electron shuttle between complex III and IV of the respiratory chain. Cytochrome C activity is necessary for life and disruption of unique somatic Cytochrome C gene causes embryonic lethality (Li et al., 2000). Extrinsic apoptosis is activated by extracellular perturbations which are detected by plasma membrane receptors (Hymowitz et al., 1999; Itoh et al., 1991; Pan et al., 1997; Schneider et al., 1997; Wu et al., 1997). Intrinsic and extrinsic apoptotic pathways ultimately come together to control the activation of caspases (Chang & Yang, 2000; McIlwain et al., 2013), which are a family of cysteine proteases. Their activity results in the proteolysis of thousands of cellular proteins, membrane blebbing and cleavage of chromosomal DNA by endonucleases. Among them, caspase 3 is considered the main player in the execution of cell death. For the purpose of this study, I will focus on the intrinsic apoptotic pathway.

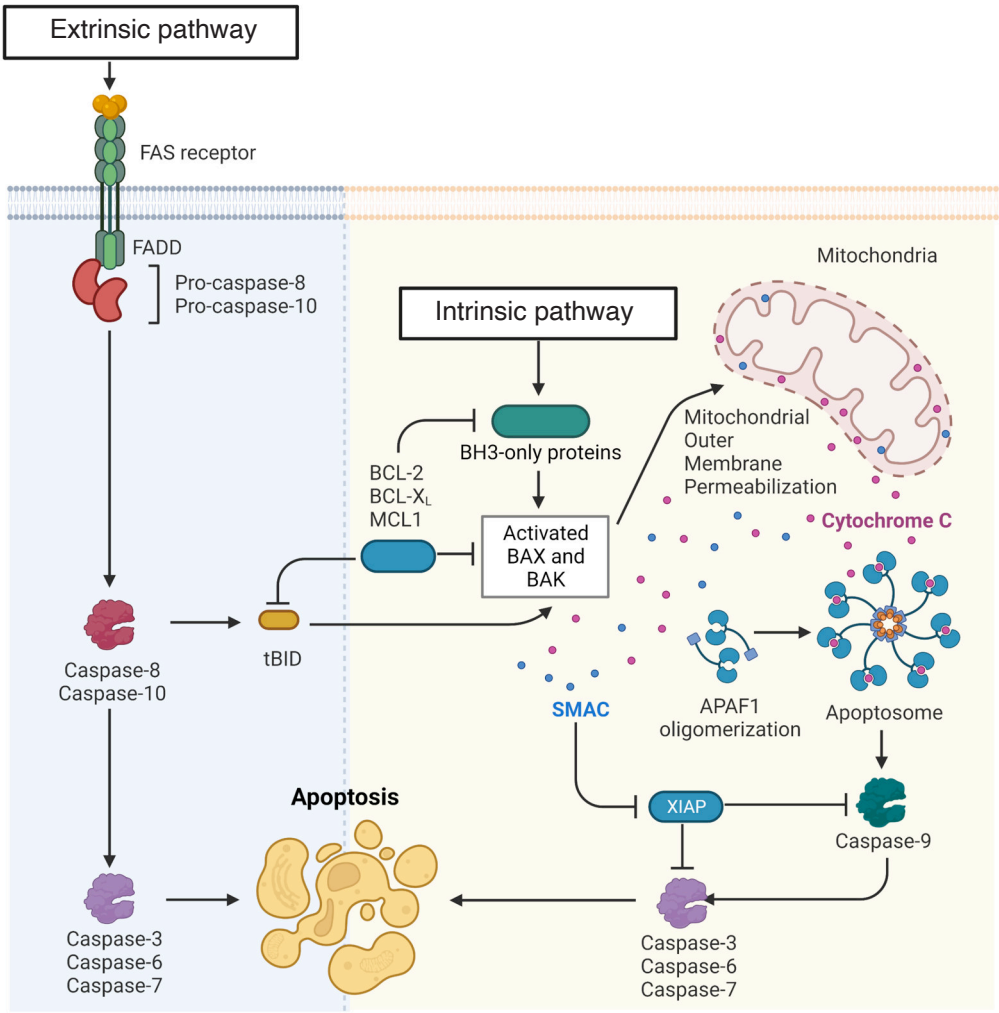

Figure 18: Overview of apoptosis signaling pathway Schematic representation of the extrinsic and intrinsic apoptotic pathways. The main proteins involved in the two pathways are shown. Both extrinsic and intrinsic pathways culminate with the activation of effector caspase 3, caspase 6 and caspase 7. Image modified from https://bpsbioscience.com/screeningprofilingservices/apoptosis?protein_family=apoptosis.

In mammalian cells, activation of the intrinsic apoptotic pathway is regulated by a threshold mechanism where anti-apoptotic and pro-apoptotic signals compete for MOMP and subsequent release of cytochrome C (Figure 18) (Czabotar et al., 2014; Kalkavan dan Green, 2017; Roos et al., 2016). These anti- and pro- apoptotic signals belong to the B-cell lymphoma-2 (BCL-2) protein family which regulate MOMP (Youle dan Strasser, 2008; Czabotar et al., 2014; Kalkavan dan Green, 2017). The BCL-2 gene was discovered at the t(14;18) chromosome translocation breakpoint in B-cell follicular lymphomas (Tsujimoto et al., 1984). The BCL-2 family comprises different categories of

proteins: first, pro-apoptotic proteins which permeabilize mitochondria, represented by BCL2 Associated X Protein (BAX) and BCL-2 Homologous Antagonist/Killer (BAK) (Figure 18) (Kim et al., 2009; Cheng et al., 2001; Zha et al., 1996). Then, there are anti-apoptotic proteins (pro-survival) which suppress MOMP. The main ones of this category are B-cell lymphoma-extra-large (*Bcl-xL),* B-cell lymphoma-2 (BCL-2) and Myeloid Cell Leukemia Sequence 1 (MCL-1) (Czabotar et al., 2014).

Finally, there are BH3-only proteins which regulates the activity of the other components of this family in response to damage signals. Among them we find BH3-Interacting Domain Death Agonist (Bid), BCL-2 Interacting Mediator of cell death (BIM), p53 Up-Regulated Modulator Of Apoptosis (PUMA), BCL-2 Associated Agonist Of Cell Death (BAD) and Phorbol-12-myristate-13-acetate-induced protein 1 (Noxa) (Kim et al., 2009; Kuwana et al., 2002; Letai et al., 2002; Nakano & Vousden, 2001; Kun Wang et al., 1996). Certain BH3-only proteins (such as BID, BIM, and PUMA) directly activate BAX and BAK, while others referred to as sensitizers (like BAD or NOXA) solely attach to anti-apoptotic BCL-2 proteins. BCL-2 proteins constantly shuttle between the cytosol and mitochondria in healthy cells. However, upon damage signaling the shuttling is altered and pro apoptotic proteins are recruited on the outer membrane. They can be regulated both by increase in transcription, which is normally regulated by p53 (Toshiyuki dan Reed, 1995; King et al., 2022). The dynamic exchange of BCL-2 proteins between mitochondria and cytosol which regulate MOMP, is referred as mitochondrial priming. Once cytochrome C is released, it binds to APAF1 in an ATP-dependent process, which binds pro-caspase 9 on its side. As a consequence, Pro-caspase 9 is cleaved and it activates caspase 3 (Ledgerwood dan Morison, 2009).

Elevated expression levels of pro-apoptotic BCL-2 proteins can enhance the impact of cytotoxic agents in both cancer and normal cells. For this reason, several inhibitors of BCL-2 proteins have been developed and are currently undergoing preclinical or clinical trial in different tumor types, including ovarian cancer. Those inhibitors differ in several parameters in terms of specificity. WEHI-539 is an example of BCL-xL specific inhibitor which is now being tested in preclinical studies for ovarian cancer, breast cancer, chondrosarchoma and osteosarcoma (Lessene et al., 2013).

Venetoclax is an inhibitor of BCL-2 (Wei et al., 2019; Roberts et al., 2019, 2016; Souers et al., 2013), whereas A1210477 selectively inhibits MCL-1 (Leverson et al., 2015).

3. Ovarian cancer

3. Ovarian cancer

3.1 Incidence and classification

Ovarian cancer is a group of malignancies that accounts every year for ~200000 death and more than 300000 new cases worldwide (*Ovarian Cancer Statistics | World Cancer Research Fund International*, 2020). It is the eight more lethal form of cancer in women and it represents the first cause of death among gynecological diseases (Huang et al., 2022; Siegel et al., 2022).

This pathology is highly heterogeneous, and it is currently classified according to cell of origin in: epithelial, sex-cord stromal, germ cell and mixed type. Because 90% of those tumors have epithelial origin, ovarian cancer tumor can be classified into two wide subgroups: epithelial and non- epithelial (Matulonis et al., 2016; Vaughan et al., 2011). According to the fifth edition of the World Health Organization (WHO) in 2020, on the Classification of Female Genital Tumors (Höhn et al., 2021), ovarian epithelial neoplasms accounts for five principal types: high-grade serous carcinoma (HGSC), low-grade serous carcinoma (LGSC), endometrioid carcinoma (EC), clear cell carcinoma (CCC) and mucinous carcinoma (MC) (Figure 19).

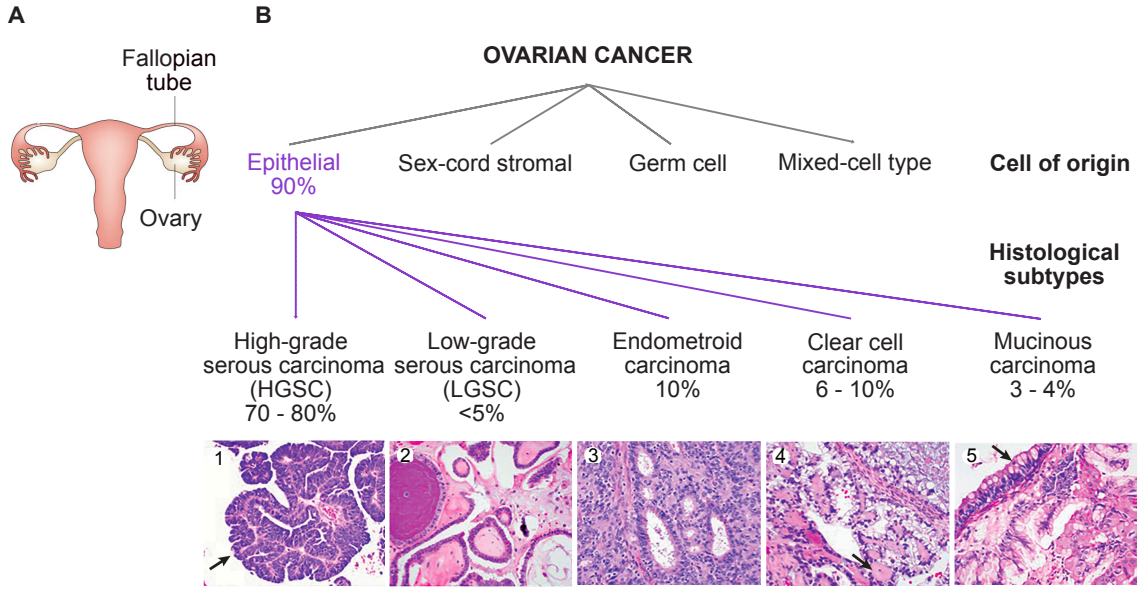

Figure 19: Classification of ovarian cancer (A) Schematic representation of the female reproductive system with indication of the sites of origin of the tumor. Image modified from (Vaughan et al., 2011). (B) Scheme of the classification of ovarian cancer types according to cell of origin (first line). In the second line, epithelial

ovarian cancer histological subtypes according to the fifth edition (2020) of the World Health Organization (WHO) Classification of Female Genital Tumors. For each subtype, histologic appearance (hematoxylin and eosin) images are shown from (Matulonis et al., 2016). Arrow in section A indicate papillary architecture, recurrent in HGSOC; arrow in section 5 indicate mucin-filled tumor cells in MC. Image modified from (Rojas et al., 2016).

This classification reflects different sites of origin but also molecular characteristics. Different tumor subtypes can be diagnosed via immune- histochemical markers and histotype-specific oncogenic alterations. Another classification provides the classification of tumor grade, which gives an indication about tumor proliferation characteristics and so how fast the tumor will grow and spread through metastasis. Low grade tumors are well differentiated tumors with low probability to spread, while high grade tumors are poorly differentiated, have high metastatic potential and show high mitotic indexes, indicative of being highly proliferative (Ahmed et al., 2010; De Leo et al., 2021; Köbel & Kang, 2022; Singer et al., 2003).

Serous tumors are the most common ones, accounting for ~70% of epithelial ovarian cancers (EOCs) and they can originate both from ovary, fallopian tubes or peritoneum (Kindelberger et al., 2007). Previous classifications tended to group HGSCs and LGSCs in a unique category and, within this category, the distinction of different grades. However, the classification according to "grade" has been considered mis-leading in EOCs because it suggested HGSCs to be later stages of LGSC (Kurman, 2013; Kurman & Shih, 2011). Recent advances in clinicopathologic and molecular characterization of EOCs suggests that LGSC and HGSC are not follow up stages of the same disease but rather that they arise from different patterns of genomic variations with different prognostic implications (Köbel dan Kang, 2022; De Leo et al., 2021). In particular, it has been shown a distinction between low-grade tumors harboring mutations in the Mitogen-activated protein kinases (MAPK) pathway (KRAS, BRAF, NRAS and others) versus high-grade serous carcinomas now ubiquitously characterized by TP53 mutations (Ahmed, et al., 2010; Singer et al., 2003).

Another method to classify ovarian cancers is according to the stage. The stage takes into account parameters as the spreading area of the tumor. According to the International Federation of Gyneacological Oncologists (FIGO) four main stages can be identified in ovarian cancer: I) the tumor is limited to the ovary/fallopian tubes; II) the tumor has spread into the

pelvis; III) the tumor has spread into the abdomen and/or the lymph nodes at the back of the abdomen (called retroperitoneal lymph nodes) and IV) it has invaded more distant organs (Prat, 2014). Unfortunately, the large majority of patients (approximately 58%) is diagnosed at advanced stages (III or IV) and this contributes to unfavorable outcomes, as indicated by a 5- year survival rate of 27% for stage III and only 13% for stage IV ovarian cancer (Siegel et al., 2022; Menon et al., 2021). Late detection is indeed one of the main reasons for the high lethality of ovarian cancer together with frequent relapse after chemotherapy.

3.2 Genomic characterization of epithelial ovarian cancer

3.2.1 High-grade Serous Carcinoma (HGSC)

HGSCs are the most common and aggressive among ovarian cancers. Alone, they are responsible for 70-80% of ovarian cancer deaths and they are associated with poor prognosis and relapse after chemotherapy (Kurman, 2013; Lisio et al., 2019a). HGSOC is a highly morphologically heterogeneous disease. *S*ubtype classification based on transcriptomic data and mRNA signatures have been proposed (Bell et al., 2011; Tothill et al., 2008).

Interestingly, oncogenic signatures across human cancers have classified ovarian cancers as C-class tumors, defined as tumors with Somatic Copy Number Alterations (SCNA), which are different from M-types tumor are characterized mostly by point mutations (Figure 20) (Ciriello et al., 2013b). Among them, HGSC are the ones showing the highest correlation coefficient to this class. However, certain point mutations are recurrent.

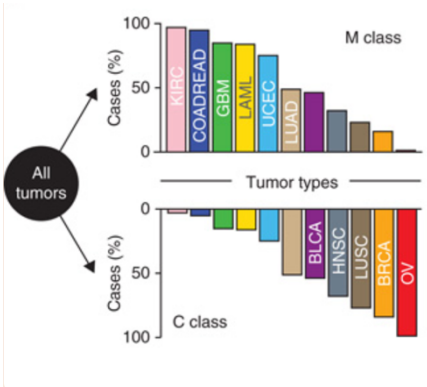

Figure 20: human tumor classification. Analysis of pan-cancer data identifies tow type sof cancer. OV-ovarian cancer. From (Ciriello et al., 2013b).

The second main feature of HGSOC is mutations in p53, which affect ~96% of the patients (Ahmed, et al., 2010; Taylor et al., 2018). p53 disruption has been proposed as an important mechanism enabling the propagation of CIN, both *in vitro* and *in vivo*, using mouse

cancer models (Bronder et al., 2021). Moreover, it has been shown that almost 50% of ovarian cancers tumors have mutations in genes encoding components of the Homologous Recombination pathway (HR). Mutations in BRCA1 and BRCA2, two genes essential in DNA repair through HR, have been described either as somatic or germline mutations in 22% of the patients (Walsh et al., 2010; Alsop et al., 2012). Interestingly, in 11% of the tumors where BRCA1 or BRCA2 are not mutated, their promoter is silenced by hypermetilation (Kondrashova et al., 2018). The most common focal amplifications encoded CCNE1 (Cyclin E) MYC, which have been detected to be highly amplified in more than 20% of tumors (Bell et al., 2011). Tumors with mutations in any of the HR genes are defined as HR deficient (HRD), while tumors without these mutations are considered to be HR proficient (HRP). More recently, expression signatures have been analyzed at the level of RNA single cell sequencing data both in tumors and in ovarian cancer cell line (Bell et al., 2011; Nelson et al., 2020)s. According to gene expression, HGSOC have been classified in different subtypes: differentiated, immune reactive, mesenchymal or proliferative (Bell et al., 2011).

In a recent study, the contribution of frequent HGSOC mutations has been addressed using an immortalized primary ovarian cell. With genome editing via CRISPR/Cas9, mutations in TP53 and BRCA1 were introduced. Further, Myc was over- expressed (Bronder et al., 2021). Interestingly, it has been suggested that the absence of TP53 alone was sufficient to generate (or allow the establishment of) chromosomal instability (CIN).

3.2.2 Low-Grade Serous Carcinoma (LGSC)

LGSC accounts for < 5% of epithelial ovarian cancer cases. They are usually detected at advanced stage (De Leo et al., 2021). LGSCs are not linked to BRCA gene mutations and do not display chromosomal instability. Genomic analyses have revealed that this type of tumor is characterized by mutations in the MAP kinase pathway, a signaling pathway involved in regulation of several processes such as cell proliferation, differentiation, migration and stress responses (Singer et al., 2003; Cheasley et al., 2021). The main genes of this pathway which are frequently mutated in LGSC are the Kirsten Rat Sarcoma Viral Proto-Oncogene (KRAS) (30% of LGSCs), the serine/threonine protein kinase BRAF (30%) and the Neuroblastoma RAS (%) Viral Oncogene Homolog (NRAS).

3.2.3 Endometroid Carcinoma (EC)

The molecular composition of ovarian endometrioid carcinoma generally mirrors that of its equivalent in the endometrium and represent 10% of epithelial ovarian cancers (Parra-Herran et al., 2017). Just as The Cancer Genome Atlas (TCGA) has delineated molecular subtypes for endometrial endometrioid carcinoma, a comparable classification defining four molecular cohorts for ovarian endometrioid carcinoma has been postulated: “ultra mutated” due to POLE exonuclease domain mutations (~5%), “hy- permutated” due to mismatch repair deficiency (MMRd)/microsatellite instability (MSI) (~13%), “TP53-mutated” (9–13%), and “no specific molecular profile” (NSMP; 69–73%) (Cybulska et al., 2019). Furthermore, other common alterations identified in endometroid carcinoma are somatic mutations of CTNNB1, the gene encoding for β-catenin, which occurs in 38-50% of cases, AT-rich interactive domain 1A gene (ARID1A) (30%) and phosphatidylinositol 3-kinase (PI3K) pathway (40%) (Herman Chui et al., 2021; Fernandez et al., 2020; Shrestha et al., 2021; Sieh et al., 2013). Mutations in Phosphatase And Tensin Homolog PTEN are also common, occurring in ~20% of the patients (Hollis et al., 2020).

3.2.4 Clear Cell Carcinoma (CCC)

Among epithelial ovarian cancers, 6-10% are classified as clear cell carcinomas (CCCs) and are most often low-stage, representing 25% of all FIGO stage I and II (Prat, 2014). They originate from endometriosis. Differing from HGSCs clear cell carcinomas (CCCs) are not linked to BRCA mutations, chromosomal instability and TP53 mutations (Chui et al., 2014). In contrast to endometrioid carcinoma, alterations involving CTNNB1 (β-catenin) and microsatellite instability (MSI) are infrequent in CCCs. These tumors are heterogeneous in regard of molecular abnormalities and the most frequent mutations have been detected in PIK3CA (30-40%), ARID1A (50%), PTEN (5-20%) and telomerase reverse transcriptase (TERT) promotor (~16%) (Wu et al., 2014; Iida et al., 2021). PIK3CA and ARID1A mutations often coexist in CCCs. Clinical trials suggest the use of immune therapy and checkpoint inhibitors to specifically target CCCs (Lin et al., 2020; Sue-A-Quan et al., 2021; Khalique et al., 2021).

3.2.5 Mucinous Carcinomas (MCs)

Mucinous carcinomas (MCs) represent 3-4% of epithelial ovarian cancers and their site of origin is unknown (Höhn et al., 2021). Early stages copy number losses of Cyclin Dependent Kinase Inhibitor 2A (CDKN2A) and KRAS are frequent, respectively detected in 76% and 64% of the cases (McAlpine et al., 2009). Moreover, HER-2 define amplification has been shown in 26% of the cases (Cheasley et al., 2019). Additional p53 mutations (64%) and copy number alterations are associated to MC progression (McAlpine et al., 2009).

3.3 Therapeutic treatment of ovarian cancer

Before 1950 the only two options for treating ovarian cancer were surgery and radiotherapy (Stewart et al., 2019; Bowtell et al., 2015; Matulonis et al., 2016). Medicine and clinical research have come a long way since then, with current therapy for ovarian cancer including surgical debulking to reduce tumor size and subsequent chemotherapy treatment (Lheureux et al., 2019).

Chemotherapy is a type of anticancer drug treatment which aims to kill cancer cells. However, because total selectivity in targeting only cancer cells is not achieved, chemotherapy usually shows important toxic side effects. Important efforts have and are currently taken to try to reduce side effects and increase target specificity. The first drugs approved for treating ovarian cancer were platinum-based drugs, such as cisplatin which was later substituted with the less toxic carboplatin (Calvert et al., 2016). To improve the outcome of platin-based drugs, different combinations of chemotherapy were tested (Omura et al., 1986; Piccart et al., 2000; McGuire et al., 1996a; du Bois et al., 2003). In 1996, a report of randomized phase III trial showed that the combination of platinum compounds and Paclitaxel, an antimitotic drug, delivered good results in advanced ovarian cancer (Vasey et al., 2004; McGuire et al., 1996a; McGuire, 1989). Nowadays, the combination of carboplatin and paclitaxel still represents the first-line chemotherapy for advanced stages of ovarian cancer with 75% of the patients showing initial sensitivity to this combination (Lheureux et al., 2019).However, chemotherapy-resistance arises in 80-90% of the patients, within 15 months from starting the treatment (Gronlund et al., 2001). In the last ten years, PARP inhibitors entered the clinic as a new therapeutic strategy that seems to be effective in patients after they developed resistance to platinum-based strategy (Bryant et al., 2005a; Farmer et al., 2005; Lord dan Ashworth, 2017). In particular it is very successful against HRD tumors (Farmer et al., 2005; Bryant et al., 2005a). Moreover, specific treatments according

to EOC subtypes are under investigation. For example, validation of treatments for LGSC as CDK4/6 inhibitors or MEK inhibitors, selective inhibitors for the MAPK pathway, are under validation in preclinical models and clinical trials (Sieh et al., 2013; Llaurado Fernandez et al., 2020; Shrestha et al., 2021; Chui et al., 2021). Furthermore, potential molecular target therapies for endometroid carcinoma, which are currently under investigations are mTOR inhibitors and immune checkpoint inhibitors (Musacchio et al., 2020; Roncolato et al., 2019). Finally, advanced MC stages often shows resistance to platinum-taxane chemotherapy with no therapeutic options are available (McAlpine et al., 2009). For individuals diagnosed with MC exhibiting HER2 amplification and overexpression, the administration of trastuzumab, a monoclonal antibody used in antitumor immunotherapy, represent treatment alternatives (McAlpine et al., 2009).

In the following sections, I will describe first how aneuploidy can influence chemotherapy and then the detailed mechanisms of action of carboplatin, paclitaxel and PARP inhibitors.

3.4 Aneuploidy in cancer and chemotherapy

Aneuploidy has been detected in ~90% of solid tumors and 50% of hematopoietic tumors (Beroukhim et al., 2010; Mitelman Database 2023), shoiwng that gain or loss of at least a whole chromosome or chromosome arm is the most common alteration in cancer. Both aneuploidy and CIN have been mostly associated with poor prognosis in cancer patients (Bakhoum dan Cantley, 2018; Jamal-Hanjani et al., 2017; Turajlic et al., 2018). Studies in mouse and human embryonic stem cells have shown that the presence of a single extra chromosome can confer a selective growth advantage to cancer cells (Liu et al., 1997; Ben-David dan Benvenisty, 2012; Zhang et al., 2016; Ben-David et al., 2014). Moreover, analysis of cancer genomes revealed that aneuploidy can be translated by loss of tumor suppressor genes or gain of oncogenes. These genetic events contribute to the formation of distinct clonal aneuploid karyotypes associated with particular types of cancer (Davoli et al., 2013). Importantly, analysis of 12 different tumor types from 5255 distinct samples and the clinical outcome of patients after immune checkpoint blockade highlighted a correlation between reduced immunotherapy response and high levels of aneuploidy (Davoli et al., 2017).

The possible roles of aneuploidy and CIN in promoting tumorigenesis and tumor progression is still under debate. The detrimental effects on viability and proliferation

observed in yeast (Torres et al., 2007), mouse and human cells (Stingele et al., 2012; Williams et al., 2008) contrast with the expected advantages in tumors. It is proposed that aneuploidy and CIN promote or inhibit tumor progression according to its frequency, cell and tissue of origin (Weaver et al., 2007; Sotillo et al., 2007a) . In a simplified view low levels of chromosome mis-segregation seems to favor karyotypes which promote tumorigenesis, while high rates leads to cell death and so tumor suppression (Chin et al., 1999; Girish et al., 2023; Greenberg et al., 1999; Rowald et al., 2016; Rutledge et al., 2016b; Silk et al., 2013; Sotillo et al., 2010; Yona et al., 2012).

Aneuploidy and CIN have also been shown to favor resistance to chemotherapy (Ben-David et al., 2017; Rutledge et al., 2016). For a long time research has mainly focused as sources of chemoresistance on gene mutations (genetic theory), and alterations of gene functions (epigenetic theory). However, resistance to chemotherapy arise at higher rates compared to the rates of genetic and epigenetic mutations (Goldie, 2001). Moreover, the ability to acquire multidrug resistance cannot be explained by single gene mutations (Duesberg et al., 2001). It is in this context that a more important role of whole karyotype alterations in driving resistance was hypothesized (Duesberg et al., 2007). Two main hypotheses have been proposed to explain how aneuploidy can drive chemoresistance. The first hypothesis states that it is the change in copy number of specific genes that lead to drug resistance (Santaguida dan Amon, 2015; Santaguida et al., 2017; Torres et al., 2007; Stingele et al., 2012c; Pavelka et al., 2010). According to this model, both aneuploidy and CIN will initially contribute to tumor heterogeneity. The addition of a given chemotherapy drug, besides killing cancer cells, may also induces a selective pressure. In unfavorable conditions, only cells with specific gene combinations that allow adaptation to the new environment can survive. The cells displaying a “winner karyotype” will be resistant to the drug and will constitute the large part of tumor cell population after the treatment 2021)(Ippolito et al., 2021; Lukow et al., 2021). Within this view, aneuploidy is seen as favoring tumor progression by generating different karyotypes in a short time window. Observations describing recurrent gain or loss of specific chromosomes in a given cancer type after chemotherapy support this hypothesis (Cohen-Sharir et al., 2020.; Rutledge et al., 2016). The second hypothesis emerges from the fact that a universal aneuploid karyotype providing resistance against a specific drug has not been found. This hypothesis proposes that aneuploidy may drive chemoresistance through a general effect of aneuploidy rather than a particular karyotype. As previously

mentioned, aneuploid cells show G1 lengthening or arrest (Kops et al., 2004; Santaguida et al., 2017; Sheltzer et al., 2017; Stingele et al., 2012; Tang et al., 2011; Torres et al., 2007; Williams et al., 2008). If the chemotherapy agent acts outside G1, affecting for example DNA replication during S-Phase or mitosis like the large majority of chemotherapeutic drugs or inhibitors (Replogle et al., 2020), these drugs will not be effective.

3.5 Carboplatin

Carboplatin is used together with paclitaxel in the clinic as a standard of care to treat ovarian cancer patients (Armstrong et al., 2006; McGuire et al., 1996; Ozols et al., 2003). Carboplatin is a member of the widely employed platinum-based chemotherapeutic group. The pioneer of this group, cisplatin, was discovered by chance by *B. Rosenberg* while investigating the impact of an electric field on *Escherichia coli* bacteria and cell growth (Rosenberg et al., 1965). It was noted an interesting side effect on bacteria: cell division was inhibited without interference with cell growth. Later, he understood that this effect was due to release of platinum ions by the electrodes. This revelation led him to test if platinum- based compounds possess anti-tumor properties in mice (Rosenberg et al., 1969b). *In vivo* further tests were performed at the Chester Beatty Institute in London and clinical tests taken by the US National Cancer Institute (NCI). Subsequentially, cisplatin earned approval from the U.S. Food and Drug Administration (FDA) for treating testicular and bladder cancer in 1978 (Kelland, 2007). However, cisplatin treatments were accompanied with important side effects such as myelosuppression, peripheral neuropathy, renal toxicity and hepatic dysfunction. Consequently, a new generation of platinum-based pharmaceuticals has been developed (Wilkinson et al., 1978). Among them, carboplatin (Figure 21) emerged as the most successful option due to its diminished chemical reactivity, rarely resulting in nephrotoxicity and peripheral neuropathy. The major toxicity and dose limiting factors are myelosuppression, specifically neutropenia and thrombocytopenia. As a result, Carboplatin obtained FDA approval for ovarian cancer treatment in 1989 and gradually began to replace cisplatin (Aabo et al., 1998). The chemical structure of cisplatin and carboplatin is very similar, as for their mechanisms of action and effects on DNA (Wilkinson et al., 1978). Both in cisplatin and carboplatin, a platinum anion is bonded to two ammonium groups. However, chlorine atoms of cisplatin are substituted by a cyclobutane- dicarboxyl residue in carboplatin.

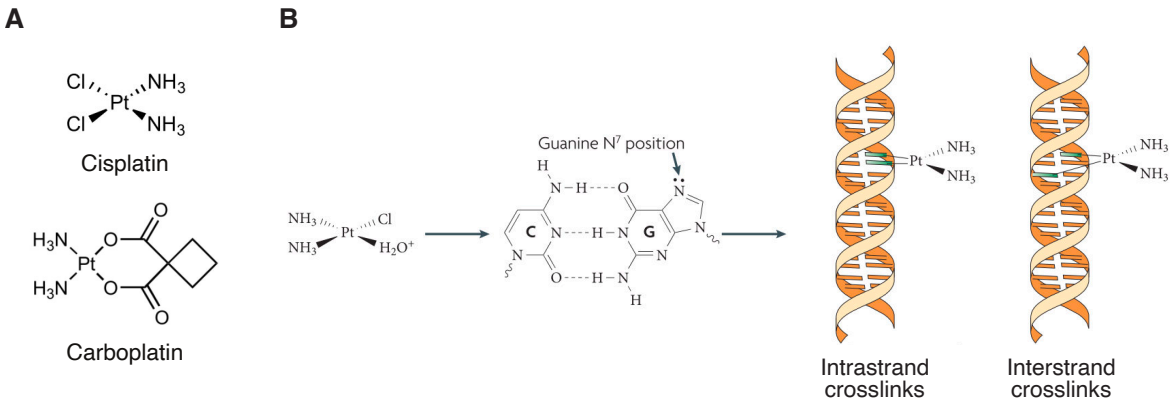

Figure 21: Cisplatin and carboplatin DNA forming intrastrand or interstrand crosslinks (A) 2D schematic representation of the chemical structure of cisplatin and carboplatin. Aqua activated carboplatin can enter the nucleus and preferentially bind to the nitrogen on position 7 of guanine occurs. Consequent binding to the adjacent guanine on the same or opposite strand, result in formation of intrastrand or interstrand crosslink respectively. Image modified from (Kelland, 2007).

Due to this substitution, carboplatin exhibits reduced reactivity and slower DNA binding kinetics, leading to a substantial reduction in cisplatin's side effects, excluding myelosppression, which still remains a dose-limiting factor (Eastman, 1986).

Carboplatin is administered through intravenous infusion or via intraperitoneal injections to patients (Armstrong et al., 2006b; Katsumata et al., 2009) and a significant portion of it is eliminated via renal excretion, with a half-life (t1/2) in the bloodstream of approximately 2 hours. Carboplatin uptake in the cell was first thought to occurs via passive diffusion, however different studies suggest the implication of active transporters such as CTR1 (Holzer et al., 2004; Ishida et al., 2002; Howell et al., 2010). The uptake of platinum based compounds is influenced by factors like the concentrations of sodium and potassium ions, pH levels, and the presence of reducing agents (Howell et al., 2010).

Because carboplatin acts mainly *via* induction of DNA damage (Figure 21), I will now introduce DNA damage and DNA damage repair pathways along the cell cycle. A more detailed description of carboplatin mechanism of action and resistance will follow.

3.5.1 DNA damage

The accurate replication and maintain of DNA integrity is fundamental for the cell to transmit correct genetic information to its progeny and, more widely, for organism

viability. However, cells are continuously exposed to different sources of DNA damage. Two main categories of DNA damage exist based on its origin: endogenous and exogenous. The main source of endogenous DNA damage is represented by Reactive Oxigen Species (ROS). ROS derive from oxygen and are typically formed during electron transport chain or redox (Sies dan Jones, 2020). Other endogenous DNA damage can be generated during replication due to the action of DNA polymerases with lower fidelity rate (Loeb dan Monnat, 2008), spontaneous base deamination or formation of abasic sites. Base deamination occurs when DNA bases lose their exocyclic amine group because of spontaneous hydrolysis, nitrosative stress or activities of cellular deaminase enzymes (Lindahl, 1993). Formation of abasic site sites can result from cleavage of the N-glycosylic bond between the nitrogenous base and the deoxyribose sugar in DNA, due to spontaneous hydrolyzation or cleavage by a DNA glycosylase (Thompson dan Cortez, 2020). On the other hand, exogenous DNA damage can be generated by external factors of environmental, physical or chemical nature which acts on DNA. Examples include ultraviolet (UV) and ionizing radiation, chemotherapy drugs as alkylating agents and crosslinking agents (Lomax et al., 2013; Rastogi et al., 2010; Fu et al., 2012; Noll et al., 2006).

The existence of many different mechanisms as source of DNA damage leads to the generation of different types of DNA damage. DNA damage frequently appears as single-strand breaks (SSBs) and double-strand breaks (DSBs). DSBs occur when two single-stranded nicks appear on opposite DNA strands very close to each other, usually around 10–20 base pairs apart (Khanna dan Jackson, 2001). Other types of DNA damage are DNA crosslinks, which are generated by platinum-based compounds.

In order to maintain genome integrity and tolerable levels of DNA damage which would not induce cell death, cells have developed different mechanisms to monitor and repair DNA. The ensemble of these mechanisms is referred to as DNA damage response (DDR). In eukaryotic cells, DDR signaling pathways evolves different signaling sensors, transducers and effectors (Zhou&Elledge,2000). The sensors are proteins that directly recognized aberrant DNA structures and activate the downstream kinases of the DDR. DNA damage-associated histone modifications are important in providing DNA repair factors access to damaged DNA. An early cellular response to DSBs is the rapid phosphorylation of the histone variant H2AX, which occurs on Ser-139 in mammalian

cells (Mah et al., 2010). The DDR transducers include a series of protein kinases and mediators that facilitate phosphorylation and signaling of the DDR network. In mammalian cells, the ATM (ataxia-telangiectasia mutated), ATR (ATM- and Rad3-Related) kinases are the main and most upstream DDR transducers (Maréchal dan Zou, 2013; Jazayeri et al., 2006).

The activation of DDR pathway is coordinated to the cell cycle progression via DNA damage checkpoints. DNA damage checkpoints are triggered by DSBs during the interphase of the cell cycle in G1, intra S or G2/M phase(Chao et al., 2017; Zhou dan Elledge, 2000). DSBs detected in G1 trigger the activation of ATM, which, in turn, phosphorylates and activates CHK2. CHK2 then phosphorylates and inactivates cdc25A, preventing it from removing the inhibitory phosphate on CDK2 (Stark dan Taylor, 2004; Maity et al., 1994). On the other hand, the replication stress checkpoint is activated during S-phase when single-stranded DNA is detected. It relies on the checkpoint protein kinases ATR and CHK1(Stark dan Taylor, 2004; Maity et al., 1994). The G2/M DNA damage checkpoint plays a crucial role in preventing cells from progressing into mitosis (M-phase) when their genomic DNA is damaged(de Gooijer et al., 2017; Stark dan Taylor, 2004). Transition from G2 to M phase is controlled mainly by the activity of the Cyclin B-cdc2 (CDK1) complex. Upon detection of DNA damage, ATM and CHK1 are activated, with CHK1 phosphorylating and inactivating CDC25, which prevents activation of cdc2. Moreover other kinases as Wee1 and Myelin Transcription Factor 1 (Myt1) contribute to keep cdc2 inactive until DNA damage is repaired (Ghelli et al., 2020). Finally, the effects of DDR pathway are involved in various essential cell activities that maintain genomic stability, like DNA replication, repair, and controlling the cell cycle (Marechal 2013).

Because carboplatin mainly acts via formation of DSB, I will focus mainly on repair of DSBs since they are the most frequent type of lesion and the more subjected to cell cycle regulation.

3.5.2 DNA damage repair pathways along the cell cycle

The main mechanisms involved in the repair of DSBs in eukaryotic cells are Homologous Recombination (HR) and non-homologous end-joining (NHEJ) pathways. HR uses the DNA template of the undamaged sister chromatid to copy the DNA sequence at the site of DNA damage (West, 2003). On the contrary, NHEJ pathway facilitates modification

and ligation of the two DNA ends present at the DSB (Ahnesorg et al., 2006).

The main category of DNA repair pathways in G1 is represented by End joining pathways (EJ). Indeed, during this phase the high-level chromatin compaction and the absence of sister chromatin does not favor HR. Contrary to HR, EJ is active during the whole interphase, and both pathways are inhibited in mitosis. EJ pathways are subdivided into the non-homologous end-joining pathway (NHEJ) and a group of less well characterized alternative end joining (A-EJ) (Chang et al., 2017). NHEJ is the predominant mechanism to repair DSBs in G1 and early S phase (Figure 22). This pathway is dependent on DNA ligase IV and the Ku heterodimer, whose subunits ku70/80 are ATP-dependent helicase (Rathmell dan Chu, 1994; Verhaegh et al., 1995; Getts dan Stamato, 1994). The initial step in NHEJ is the recognition and binding of the Ku heterodimer to the DSB. Ku serves as a scaffold to recruit the core NHEJ machinery to DNA DSBs (Mari et al., 2006). DNA end processing, which requires polymerase activity can be initiated, rendering them compatible for ligation. Recruitments of heterodimers of XRCC4 (X-Ray Repair Cross Complementing 4) and XLF (XRCC4-like factor), forms a scaffold around the break site on DNA, helping to keep together the DNA strands. The vicinity of the two DNA ends allows the recruitment of DNA ligase IV, which will ligate DNA ends together (Chang et al., 2017; Davis & Chen, 2013).

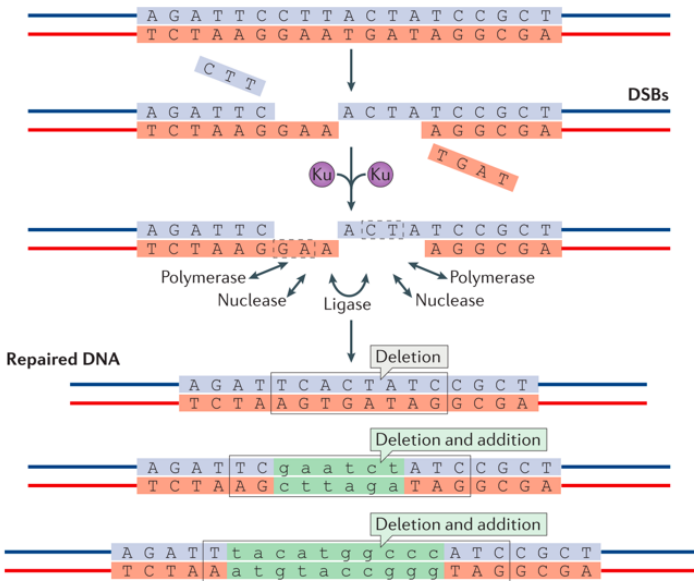

Figure 22: Overview of Non-homologous DNA end joining pathway. Schematic representation of DNA DSBs and their repair by NHEJ. First, the Ku70/80 heterodimer binds to DSBs favoring the following recruitment of NHEJ polymerase, nuclease and ligase complexes. . The process is believed to be more error-prone than HR and can result in diverse DNA sequences at the repair junction. Image modified from (Chang et al., 2017)

Because of the direct juxtaposition of DNA ends, NHEJ pathways is considered to be more error prone than HR, due to its template independent nature in the process of repair (Mao et al., 2008). Besides NHEJ pathways, other mechanisms of DNA repair are active in G1. For example, nucleotide excision repair pathway (NER) plays an important role in G1 to remove pyrimidine dimers which are caused by UVs (Sancar et al., 2004). Other pathways of DNA repair which are active during the whole cell cycle and that does not seem to be cell-cycle regulated according to current knowledge, are the base-excision repair pathway (BER) and the transcription-coupled repair (Krokan dan Bjørås, 2013; Wyatt et al., 2013a).

During S phase, presence of crosslinks can impair the progress of DNA replication generating replication stress and DSBs. Replication stress can be defined as a wide range of errors which can occurs during DNA synthesis as nucleotide misincorporation, slippage of repetitive sequences, accumulation of nicks and gaps or fork collapse at DNA breaks (Branzei dan Foiani, 2005). DSBs are mainly repaired by NHEJ pathway during early S-phase, while HR is the main repair pathway in late S-phase and G2 (Sartori et al., 2007a; Pylayeva-Gupta dan Kelsey C. Martin Mhatre V. Ho, 2012). Indeed, several studies suggest that HR activation and S-phase entry are uncoupled events and that HR is suppressed in early S-phase (Karanam et al., 2012; Rothkamm et al., 2003). In the Takata et al. study of *1998,* for example, it has been shown that NHEJ-defective ΔKu70 avian DT40 cells were highly sensitive to ionizing radiation in G1 and early S phase, indicating a deficiency in their repair capacity in the absence of the NHEJ pathway.

However, as cells proceed into S-phase they become more and more resistant (Takata et al., 1998). The HR activation in late S-phase is probably due to the fact that in early S-phase only a small fraction of the total DNA is already replicated and so can serve as a template for repair. Moreover several studies show that as cells progressed through S-phase, the increase loading of cohesin favors sister chromatid cohesion, thus promoting activation of HR (Karanam et al., 2012; Rothkamm et al., 2003). Indeed, recruitment of cohesion at DSB sites has been shown to occur both in budding yeast and mammalian cells and to favor HR (Kim et al., 2002).

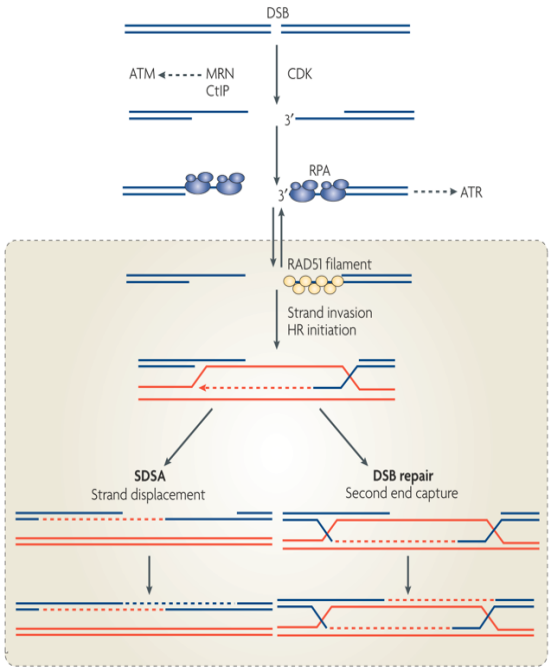

Figure 23: Repair of DSBs by Homologous Recombination Schematic representation of the main steps of HR. After the recognition of a DNA DSB by the MRN complex, DNA damage is signaled. 3' single strand DNA is formed by activity of endonucleases and it is coated by RPA proteins. Then, RPA is replaced by RAD51 which allow strand invasion. After synthesis of the annealed filament, this structure is resolved by SDSA or by resolution of Hollyday junctions. Image modified from (Branzei et al., 2008)

The repair of DNA damage in late S-phase and G2 by HR (Aylon et al., 2004) is highly conserved and it is non-mutagenic (Wyman et al., 2004). As mentioned above, its low error rate is due to the use of sister chromatids as template of DNA repair. The importance of this repair pathway is also shown by the fact that it is frequently defective in cancers, mainly because of mutations in two of the main genes of the pathway like BRCA1 and BRCA2. During HR, DNA damage is recognized by proteins of the Mre11-Rad50-Nbs1 (MRN) complex (Figure 23). The MRN complex recruits and activates ATM initiating the DNA damage response (Dinkelmann et al., 2009; Xie et al., 2009; Rass et al., 2009; Taylor et al., 2010). Then, ATM recruits and phosphorylates the members of MRN complex and others endonucleases (Linding et al., 2007; Matsuoka et al., 2007). Through the activity of these endonucleases, 5'DNA strand is degraded, resulting in a 3'-single-stranded DNA end. This is the first of the three main steps of HR, also referred as "presynaptic stage". The second step, "synaptic stage" consists in the coating of the filaments by replication protein A (RPA), which will activate ATR signaling. During the third step, which is called "postsynaptic stage", RPA is replaced by RAD51, a recombinase, in a BRCA1 and BRCA2 dependent manner. The presence of RAD51 allows DNA strand invasion and the formation of a D-loop, which can be extended by DNA synthesis, using the paired DNA filament as a template (Krajewska et al., 2015; Heyer, 2008).

The resolution of these structures can occur in mainly two ways: via synthesis dependent strand annealing (SDSA), where the invading strand is displaced after DNA synthesis and annealed with the second end. In this case, disengagement is mediated by a DNA helicase such as Srs2 in yeast (Ghelli Luserna Di Rorà et al., 2020). This process produces a localized conversion without crossover (non-crossover) and can be repeated several times to complete the repair of a DSB. Alternatively, an intermediate step can occur where Holliday junctions are formed. Holliday junctions are four-way DNA junctions which were first described in 1964 by *Robin Holliday* (Holliday, 1964). These junctions are resolved in three different ways. The first one involves the BTR complex composed of helicase Bloom Syndrome Protein (BLM), Topoisomerase III and RMI1/2. The BTR complex will generate non-cross products (Sung dan Klein, 2006). The other two mechanisms use nucleases and generate either non-crossovers or crossovers. In the first case a complex of SLX1/4-MUS81-EME1 (SLX-MUS complex) is used , while in the second one only the just GEN1 nuclease(Chan dan West, 2014; Wyatt et al., 2013b; Sarbajna et al., 2014). Since the sister chromatid is used as a template, it is important that the two sister chromatids are close to one another. The linkage is established by cohesin, which connects the sister chromatids from S phase until anaphase, when they separate. Indeed, it has been shown that mutations affecting the cohesion complex are defective in repair of DSBs (Ström et al., 2004; Sjögren dan Nasmyth, 2001).

3.5.3 Regulation of DNA repair choice along the cell cycle

Different mechanisms have been identified that regulate the choice of the DNA repair pathway and coordinate it with cell cycle. The main one, is controlled by the activity of CDKs that regulates the switch between NHEJ in favor of HR during S phase, by favoring end resection (Figure 24). DNA End resection is a biochemical process where 5'-3' degradation occurs, leaving a long 3' single stranded DNA. DNA end resection while favoring HR, it simultaneously inhibits NHEJ. Since three of the main DNA repair pathways diverge at the step of end resection, it has been suggested that end resection represents a key point in the repair mechanism choice. The extension of DNA end degradation differentiates between occurrence of HR or NHEJ. Indeed, end resection is distinguished into two phases: the "end-clipping" phase is the initial step where the DNA is degraded by MRE11 and Ctlp nucleases (Quennet et al., 2011; Sartori et al., 2007). At

this stage only a small number of base pair are processed: up to 20 Bp in mammalian cells. The short DNA ends produced by end clipping phase will allow NHEJ. The DNA extremity can be further degraded in a second phase called “extensive resection” by different exonucleases, including CtIP and EXO1 (Eid et al., 2010; Tomimatsu et al., 2012, 2014).

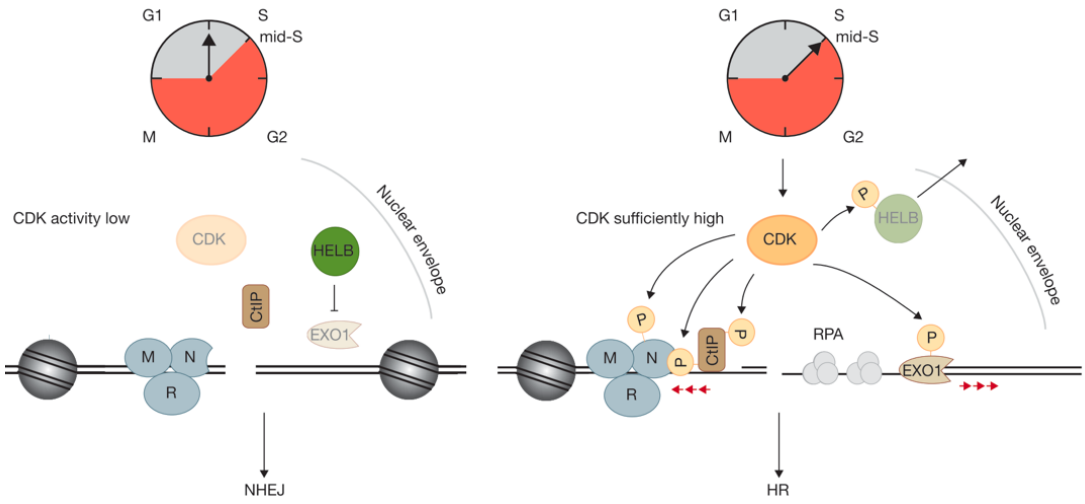

Figure 24: CDK activity regulates end resection influencing the choice of DNA repair pathway Schematic representation of the switch between NHEJ and HR during S-phase mediated by CDKs. CDK activity progressively increases during S- phase, triggering enough phosphorylation of CtIP, HELB and EXO1 to stimulate resection and HR. Image modified from (Hustedt dan Durocher, 2017).

Different mechanisms have been identified that regulate the choice of the DNA repair pathway and coordinate it with cell cycle. The main one, is controlled by the activity of CDKs that regulates the switch between NHEJ in favor of HR during S phase, by favoring end resection. DNA End resection is a biochemical process where 5’-3’ degradation occurs, leaving a long 3’ single stranded DNA. DNA end resection while favoring HR, it simultaneously inhibits NHEJ. Since three of the main DNA repair pathways diverge at the step of end resection, it has been suggested that end resection represents a key point in the repair mechanism choice. The extension of DNA end degradation differentiates between occurrence of HR or NHEJ. Indeed, end resection is distinguished into two phases: the “end-clipping” phase is the initial step where the DNA is degraded by MRE11 and Ctlp nucleases (Quennet et al., 2011; Sartori et al., 2007). At this stage only a small

number of base pair are processed: up to 20 Bp in mammalian cells. The short DNA ends produced by end clipping phase will allow NHEJ. The DNA extremity can be further degraded in a second phase called “extensive resection” by different exonucleases, including CtlP and EXO1 (Eid et al., 2010; Tomimatsu et al., 2012, 2014). This will result in the generation of long ssDNA ends, committing to the HR pathway (Ceccaldi et al., 2016). The DNA end resection is promoted by CDK activity through the phosphorylation of several substrates. Thus, the cell cycle phase plays a crucial role in the pathway choice. The importance of DNA end processing in DSB repair pathway choice and the essential role of CDK activity in activating end resection was first described in budding yeast (Bennett et al., 2013; Ira et al., 2004; Frank-Vaillant dan Marcand, 2002). It was shown that CDK1 phosphorylates the CtlP homologue Sae2 on Ser267 residue in mid S-phase. This stimulates MRE11 activity promoting end resection and so, HR. Moreover, CDK1 activity would also stimulate Fun30 activity, to antagonize Rad9 which is the 53Bp1 orthologue and it is an inhibitor of the process of end resection(Chen et al., 2016). The role of CDK activity in regulating end resection, which influences the choice of DNA damage repair pathway according to cell cycle stage, has been shown to be conserved across species from yeast to human cells (Jazayeri et al., 2006). In particular, in mammalian cells during G1/early S-phase, CDK activity is low, thus Ctlp remains inactive and 53BP1 and Rif1 proteins are recruited to DSBs. This results in blocking DNA end resection and therefore the NHEJ pathway is favored (Panier dan Boulton, 2014). During late S- and G2 phases, an increase in CDK activity takes place, resulting in phosphorylation of several substrates including the MRN complex and Ctlp, favoring end resection and so HR (Yun dan Hiom, 2009). Moreover, CDK-dependent phosphorylation of EXO1- definition and what it does also favors end resection in response to DNA damage during late S/G2. At the same time, impairment of EXO1 phosphorylation diminishes resection and HR, while it shifts the balance towards NHEJ (Tomimatsu et al., 2014).

Other factors contribute to the choice of repair pathway to be used namely the balance between BRCA1 and 53BP1. It has been described that BRCA1 and 53BP1 act as antagonists and their balance is crucial for the shift between HR and NHEJ pathways. More precisely, during G1 phase, as already described, ATM signaling results in the recruitment of 53BP1 to damaged chromatin sites. 53BP1 allows the recruitment of RIF1 and, together, they block DNA end resection (Chapman et al., 2013; Escribano-Díaz et

al., 2013). On the contrary, during S-G2 phases, the phosphorylation of Ctlp promotes its interaction with BRCA1 and chromatin at the damaged sites, preventing the association of 53BP1-RIF1 at the same time. Interesting, increased BRCA1 activity promotes the action of several phosphatases that dephosphorylate 53BP1 and release RIF1, inhibiting NHEJ pathway and favoring HR (Isono et al., 2017).

3.5.4 Mechanism of action of carboplatin

Both cisplatin and carboplatin share the same mechanism of action (Knox, 1986; Kasparkova et al., 2003) and more attention has been given to describe in detail cisplatin (87987 results on pubmed against 20525 of carboplatin). Once localized inside the cell, these molecules lose their oxalate ions, which is substituted by two water molecules (Fichtinger-Schepman et al., 1985). In this way it becomes positively charged and can interact with nucleophilic molecules such as DNA, RNA and proteins. Carboplatin binds preferential DNA and this occurs independently of the cell cycle phase. The cytotoxicity of cisplatin and carboplatin derive primarily from interaction with the N7 atoms of the imidazole rings in guanine which serve as binding sites for DNA (Eastman, 1987; Davies et al., 2000). During this interaction, crosslinks are formed with a preference for intrastrand crosslinks resulting in the distortion of the DNA double helix (Kelland, 1993; Pinto dan Lippard, 1985; Szefler et al., 2021).

DNA crosslinks can result in inhibition of both replication and transcription processes and their resolution leads to formation of DNA DSBs (Räschle et al., 2008; Siddik, 2003b). DNA adducts and DSBs are then recognized by proteins involved in DNA damage signaling as the MRN complex but also MutS Homolog 2 (hMSH2) involved in mismatch repair, non-histone chromosomal high-mobility groups 1 and 2 proteins (HMG1 and HMG 2) and the transcriptional factor “TATA-binding protein” (TBP) (Vichi et al., 1997; Huangt et al., 1994; Chaney dan Vaisman, 1999; Wang et al., 2023; Treiber et al., 1994; Cohen et al., 2000). These DNA damage recognition proteins will activate downstream players resulting in activation of p53 as a main target (Basu & Krishnamurthy, 2010; Kelland, 1993; Siddik, 2003). However, since the p53 gene is frequently mutated in cancer, other mechanisms have been described such as the activation of p73 and the Mitogen-activated protein kinase (MAPK) pathway in response to cisplatin (Gong et al., 1999; Losa et al., 2003; Mandic et al., 2002, Tsai et al., 2003).

This lead to the activation of one of the DNA damage checkpoints, resulting in G2/M arrest (Dasari dan Bernard Tchounwou, 2014; Shapiro dan Harper, 1999; Moens et al., 2021). Eventually, the high levels of DNA damage lead to activation of cell death via apoptosis or necroptosis (Nuñez et al., 1998; Kischkel et al., 1995; Meng et al., 2016).

3.5.5 Resistance to carboplatin in ovarian cancer

Even if 80% of EOC patients respond initially to carboplatin, almost 80% of those responding cases will recur with resistant disease (Damia dan Broggini, 2019). Platinum compound resistance is a multifactorial process which relies on different mechanisms, still to be fully elucidated. Regarding inability to reach the target DNA, the main data available come from *in vitro* experiments which indicate that decrease in drug uptake rather than increase in its extrusion is one of the leading causes of relapse. For example, in resistant EOCs, decreased expression of the copper transporter CTR-1 has been described (Sørensen et al., 2016; Öhrvik et al., 2013; Kishimoto et al., 2017; Li et al., 2017; Ishida et al., 2010). However, modulation of proteins involved with carboplatin extrusion has also been detected, mainly of ATPase copper transporting alpha and beta (ATP7A and ATP7B) families (Li et al., 2017). Modification of intracellular proteins with the capacity to bind and capture platinum ions also decrease carboplatin access to DNA. These species are rich in amino acids containing Sulphur such as cysteine and methionine and the negative charge of Sulphur can inactivate this type of compounds. Reduced glutathione levels, which can react with carboplatin in a non-enzymatic manner or mediated by glutathione-S- transferase (GST) were find to be significantly higher in cells derived from resistant epithelial ovarian cancer tumors (Okuno et al., 2003; Hagrman et al., 2003; Okuno et al., 2003). Metallothioneins, characterized by their abundance of cysteine residues and their affinity for binding metal ions, have also be found to be elevated in resistant cells. These molecules function similarly to GST by contributing to the promotion of carboplatin resistance (Hagrman et al., 2003).

Finally, an altered expression of pro-survival or anti-survival proteins has been described as one of the main mechanisms of carboplatin resistance in EOCs (Mansouri et al., 2002; Dai et al., 2017; Beale et al., 2000). Besides, modulation of apoptotic gene expression, can be achieved by the removal of carboplatin-DNA crosslinks before the apoptosis program is triggered. Indeed, some components of the NER pathway, as

Excision Repair Cross-Complementation Group 1 (ERCC1) and ERCC1/XFP complexes, have been shown to be overexpressed in EOC after cisplatin exposure, resulting in an hyperactivation of this pathway (Reed, 1998).

3.6 Paclitaxel

Paclitaxel, a tetracyclic diterpenoid, was originally derived from the bark of the Pacific Yew tree, *Taxus brevifolia* (Wani et al., 1971). This compound was discovered during an expedition funded by the National Cancer Institute (NCI) and the U.S. Department of Agriculture (USDA) aimed at uncovering novel antineoplastic agents. The active principle was subsequently isolated, and its structural elucidation was documented in 1971 under the name Taxol, later revised to Paclitaxel (Wani et al., 1971). But it is the same year, following the identification of its antineoplastic properties, Paclitaxel was approved as a therapeutic intervention for breast and ovarian cancer in 1992. It is the first discovered member of the taxane family, which nowadays also includes docetaxel and cabazitaxel (Vasey et al., 2004; Vestergaard Madsen et al., 2020). Paclitaxel is usually given to patients *via* intravenous administration. Because of the high hydrophobic nature of this molecule, currently the main strategies to deliver paclitaxel is via the use of nanoparticles, liposomes and polymeric micelle (Ma dan Mumper, 2013; Peetla et al., 2013). Paclitaxel exhibits strong affinity for intact microtubules and its binding site is primarily located at the N-terminal of the β-tubulin subunit (Sharma et al., 2013b).

3.6.1 Mechanism of action of paclitaxel

The mechanism of action was initially elucidated by Peter B. Schiff and Susan B. Horwitz in 1979 through *in vitro* studies (Shiff & Horwitz, 1979). They observed that cell division was completely inhibited in HeLa cells after incubation for 4 hours with 0,25μM of paclitaxel. Moreover, they reported that paclitaxel promoted microtubule assembly by decreasing the lag time required for the process and that microtubules were more resistant to depolymerization by cold (4 °C) and $CaCl_2$ (4nM). This work showed that paclitaxel promotes microtubule assembly and protects them from depolymerization. In 1980, the same group described that paclitaxel induced a late G2/ M arrest in both HeLa cells after a 18 hour incubation using 0,25μM of paclitaxel and mouse fibroblasts after 22 hour incubation with 10

μM of paclitaxel (Schiff & Horwitz, 1980). Later, paclitaxel was shown to induce mitotic arrest in animal tumor models and in other Consequently, the destabilizing effects caused by GTP hydrolysis are counteracted, leading to enhanced microtubule stability (Klein dan Lehmann, 2021). cells culture (Figure 25) (Fuchs & R.K, 1978.; Jordan & Wilson, 2004; Li & Murray, 1991; Milas et al., 1995). Cell cycle arrest during M phase results from the activation of the SAC due to a decrease in microtubule dynamics, leading to decrease kinetochore tension and consequent maintenance of SAC in an active state (Waters et al., 1998a). Prolonged mitotic arrest can result in death in mitosis or either mitotic slippage, depending on a threshold competing mechanism (Gascoigne dan Taylor, 2009).

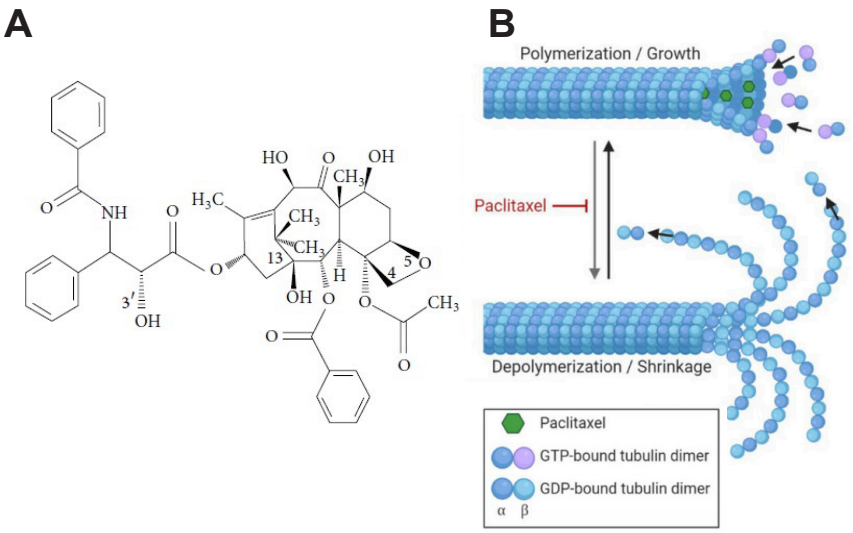

Figure 25: Paclitaxel is a microtubule stabilizing agent. (A) 2D representation of the chemical structure of paclitaxel. Image from (Kampan et al., 2015). B) Paclitaxel enhances the stability of microtubules by interfering with their dynamics. Tubulin dimers bound to GTP are added to the growing ends of microtubules forming a stabilizing cap composed of GTP-bound tubulin. However, as GTP is hydrolyzed to GDP within the tubulin dimers, a conformational change occurs, leading to the destabilization of the microtubule lattice. This destabilization results in the depolymerization of microtubules as the protective GTP-tubulin cap is lost. Paclitaxel disrupts this process, by binding to β-tubulin and preventing the depolymerization of microtubules, from (Klein dan Lehmann, 2021).

The impact of paclitaxel in cancer cell death has been assumed to be solely explained by prolonged mitotic arrest. However, recent work using lower paclitaxel concentrations that better mimic the doses administrated to patients at the nanomolar range (Zasadil et al., 2014a; Weaver, 2014a), showed a different scenario. Indeed, multipolar divisions followed by cytokinesis failure were noticed in breast cancer cells and breast cancer tissue biopsies after

chemotherapy treatment. Importantly, as expected daughter cells died by apoptosis most likely due to their aneuploid content. Together, these results show that paclitaxel can impact cancer viability either through mitotic arrest or through multipolar divisions which leads to aneuploidy.

3.6.2 Resistance to paclitaxel in ovarian cancer

Resistance mechanisms for paclitaxel have been described over the last years, including increased drug efflux, alteration of survival pathways, metabolic reprogramming, apoptosis evasion and altered tubulin expression (Kampan et al., 2015). Sherman- Baust et al. in 2011 analyzed a series of ovarian cancer cell lines resistant to different drugs, such as paclitaxel and cisplatin. In the cohort of paclitaxel resistant patients, 337 genes were found significantly altered in terms of expression levels (Sherman-Baust et al., 2011). The altered gene expression genes were involved in different pathways such as oxidative stress, glycolysis, glutathione metabolism and leukocyte trans endothelial migration. Moreover, several ribosomal genes and translation factors involved in mRNA and protein synthesis showed also modified expression. Besides, reduction in the accumulation of paclitaxel inside tumor cells seems to be explained by increased efflux rate, due to the overexpression of P-glycoprotein, a membrane transporter of the ATP-binding cassette family (ABC) (Mechetner et al., 1998; Johnatty et al., 2013).

The capacity of cancer cells to endure extended mitosis induced by taxanes through a process known as mitotic slippage stands as a significant mechanism of resistance. Ability to endure prolonged mitosis by disruption of SAC proteins or modulation of cell death pathways, as overexpression of BCL2 family proteins, has been observed in OC patients (Sloss et al., 2016; Etemadmoghadam et al., 2009; Wertz et al., 2011; Rodrigues-Ferreira et al., 2020). Another major mechanism of paclitaxel resistance involves modification in tubulin concentration, expression or alteration of tubulin isotypes, referred as Class III β-tubulin(Mozzetti et al., 2005; Kavallaris et al., 1997). Furthermore, microtubule dynamic disruption has also been detected in paclitaxel-resistant cells (Orr et al., 2003). In particular hypoxic adaptation, which is the ability of the tumor to survive and continue to grow in the presence of low oxygen levels, has been shown (McEvoy et al., 2015; Huang et al., 2010). Hypoxia leads to activation of pro-inflammatory transcriptions factors such as STAT3 and NF-kB which control genes

involved in cell survival, angiogenesis, proliferation and metastasis (Aggarwal et al., 2009; Duan et al., 2006).

3.7 PARP inhibitors

Because 75% of EOC patients become resistant to the treatment of combined paclitaxel and carboplatin, the search for alternative treatments has continued. In the last 23 years PARP inhibitors emerged as a new efficient therapeutic alternative (Pilié et al., 2019; Banerjee dan Lord, 2020; White et al., 2000; Farmer et al., 2005; Bryant et al., 2005b). PARP enzymes are a family of proteins involved in detection and repair of DNA damage (Rouleau et al., 2010). The first demonstration that PARP inhibition disrupts DNA repair *in vitro* goes back to 1980 (Durkacz et al., 1980). From the beginning of the 2000, PARP inhibitors have been developed starting with AG014699 (Rucaparib) (White et al., 2000). The importance of PARP inhibitors as a new therapeutic strategies emerged in 2005, when two independent groups showed synthetic of PARP inhibitors in BRCA1/2-deficient cancer cells and xenographs (Bryant et al., 2005; Farmer et al., 2005). Then, in 2008 Olaparib was developed (Menear et al., 2008). In 2009 the antitumor activity of Olaparib was shown for the first time in a clinical study with patients carrying BRCA1/2 mutations (Fong et al., 2009). In 2014 Olaparib was the first PARP inhibitor to be approved by the European Medicines Agency (EMA) and FDA for the treatment of advanced stage, EOCs with BRCA mutations (Kim et al., 2015; Kaufman et al., 2015; Ledermann et al., 2012, 2014). During the following three years, Niraparib and Rucaparib were also approved as maintenance therapy for HGSOC independently from the BRCA1/2 status (Kristeleit et al., 2016; Mirza et al., 2016; Swisher et al., 2017).

PARP inhibitors are typically administered to patients orally in the form of tablets or capsules. Despite the progress, ~ 70% of the women diagnosed with advanced stage of EOC relapse within 3 years, with recurrent EOC remaining incurable. In 2008 phase III of SOLO1 trial was conducted in 391 women diagnosed with advanced stage EOC BRCA1/2-mutated (Moore et al., 2018). The trial revealed that using Olaparib as a first-line maintenance therapy led to an improvement of approximately 36 months in Progression-Free Survival (PFS) compared to a placebo. Because of this result, Olaparib was approved in the same year by the FDA and EMA as first-line maintenance therapy for women with BRCA1/2-mutated advanced-stage EOC. Many questions remain to be

answered, as if also women with wild type BRCA1/2 can benefit of first- line PARP inhibitors. Moreover the efficiency of PARP inhibitors in the context of BRCA1/2 methylations or reversed mutation are also started to be investigated (Kondrashova et al., 2018; Lord dan Ashworth, 2013). However, PARP inhibitors remain the greatest advanced in the treatment for EOC patients in the last 20 years.

3.7.1 Mechanism of action of PARP inhibitors

PARP inhibitors specifically target the PARP enzymes, which belong to a family of 17 nuclear proteins in humans. PARP inhibitors are particularly efficient in HRD tumors since they provide an alternative mechanism of DNA repair (Bryant et al., 2005a; Farmer et al., 2005; Fong et al., 2009; Kaufman et al., 2015; Ledermann et al., 2012, 2014).

PARP enzymes are responsible for a post-translational modification called PARylation, which involves the transfer of poly(ADP-ribose) (pADPr) units from NAD+ to target proteins (Tao et al., 2009; Altmeyer et al., 2009). These enzymes are recruited and activated by DNA breaks, either single-stranded or double-stranded (Figure 26) (Hassa dan Hottiger, 2008; Gradwohl et al., 1990). The most abundant and characterized member is PARP1, composed of three domains: the N-terminal domain with zinc-finger motifs for DNA break binding, the C-terminal catalytic domain responsible for PARylation, and the central domain where auto-modification occurs (Shizuta et al., 1986; Tao et al., 2008; Langelier et al., 2008; Altmeyer et al., 2009). The effect of PARylation includes chromatin relaxation due to its negative charge facilitating the recruitment of to the DNA break site, involved in a variety of processes such as gene transcription, replication, and repair (Rouleau et al., 2010).

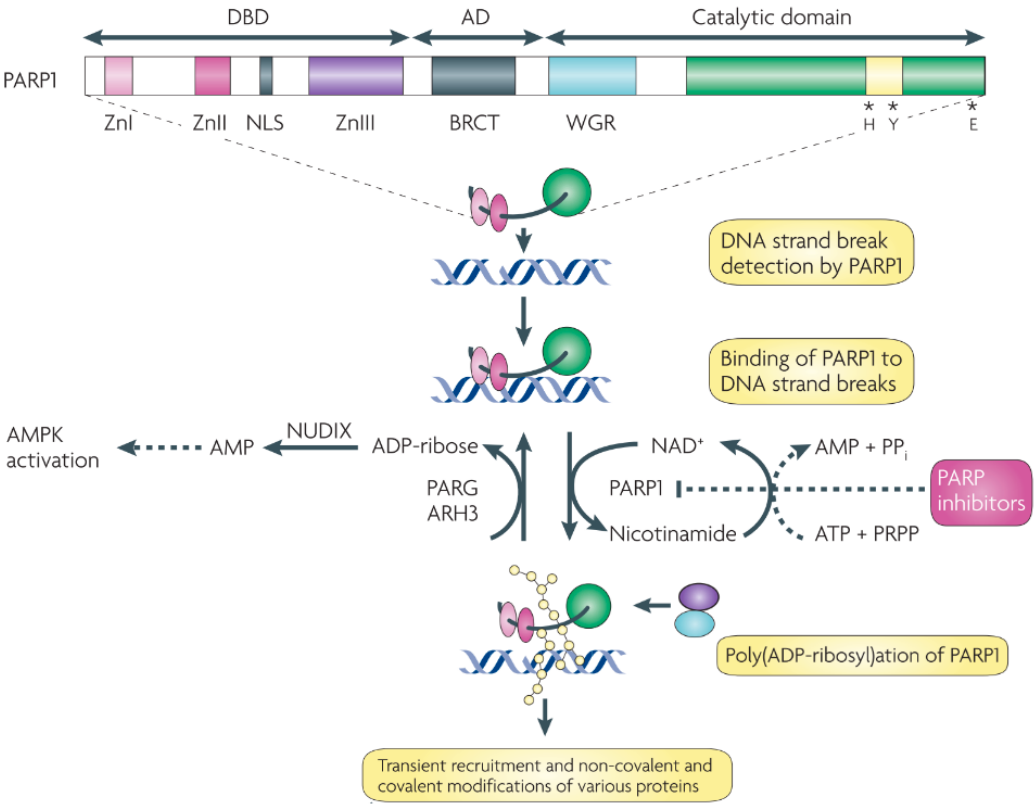

Figure 26: Structure and mechanism of PARP1 enzyme. Schematic representation of PARP1 gene structure. DNA-binding (DBD), automodification (AD) and catalytic domains are shown. PARP1 binding to DNA damage, initiatiate PARylation process which will start the recruitment and modification of proteins involved in different DNA repair pathways. PARP inhibitors prevent the synthesis of pADPr and hinder subsequent downstream repair processes. Figure modified from (Rouleau et al., 2010)

Once PARylation is complete, PARPs dissociate from DNA break sites, assisted by molecules like Poly(ADP-ribose) glycohydrolase (PARG) and ADP-ribosylhydrolase 3 (ARH3) (Oka et al., 2006; Meyer-Ficca et al., 2004). PARP inhibitors compete with NAD+ at the enzyme binding site and can also trap PARP on DNA, causing further DNA damage. In the absence of HR, PARP1 and 2 play vital roles in base excision repair and restoring replicative forks arrested at damage sites. Inhibiting PARP leads to unresolved DNA damage accumulation and subsequent cell death.

3.7.2 Resistance to PARP inhibitors in ovarian cancer

PARP inhibitors often lead to a favorable initial response in ovarian cancers, but most patients eventually develop resistance to these compounds, leading to a recurrence of the disease. Mechanism of resistance to PARP inhibitors have now started to be

characterize, with three main categories being identified via genomic analysis of tumor biopsis (Dias et al., 2021; Pilié et al., 2019). First, resistance can arise as a consequence of restoration of HR repair activity, which can occur through direct or indirect mechanisms. Direct mechanisms include reversion mutation to restore the wild-type form of the genes. In EOC it has been observed in BRCA1/2 and RAD51, the main components of HR pathway, but also in other genes such as HSP90 which can prevent the degradation of certain BRCA1 variants (Quigley et al., 2017; Kondrashova et al., 2017; Goodall et al., 2017; Johnson et al., 2013). Further, reverse mutations have been described in ~20-25% of PARP-inhibitors resistant patients (Domchek, 2017). Moreover, epigenetic changes also account as direct mechanism, as for demethylation of HR genes promoters and their consequent activation (Ter Brugge et al., 2016). Among the indirect mechanisms to restore HR, alteration of signaling that leads to increased activity and/or expression of the HR complexes has also been described (Quigley et al., 2017; Kondrashova et al., 2017; Goodall et al., 2017).

The second main mechanism of PARP resistance is represented by mitigation of replication stress. This occurs mostly by the restoration of fork stability, though mechanisms of replication fork protection and decreased proliferation. When BRCA1/2 are not present, the unregulated removal of stalled forks without protection by MRE11 can cause the collapse of these forks, contributing to genomic instability. In tumors resistant to PARP inhibitors, loss of myeloid/lymphoid or mixed-lineage leukemia 3 and 4 (MLL3, MLL4), Enhancer Of Zeste Homolog 2 EZH2, PAX Interacting protein (PTIP) has been observed with the resulting reduction in the recruitment of MRE11 to stalled forks (Quigley et al., 2017; Kondrashova et al., 2017; Goodall et al., 2017). Furthermore, SKOV3 cells shows increased reliability on ATR-CHK1 pathway for DNA repair (Murai et al., 2016). Therefore, the combination of PARP-inhibitors with ATR-inhibitors has started to be investigated as a strategy to overcome PARP-resistance (Kim et al., 2017, 2020; Murai et al., 2018, 2016).

Finally, alteration related to the drug and/or its target is also a common mechanism of resistance. For example, mutation in PARP1 protein itself, loss of poly(ADP- ribose) glycohydrolase (PARG) or epithelial-to-mesenchymal transition signatures have been observed in PARP resistant tumors (Gogola et al., 2018; Pettitt et al., 2013, 2018). Moreover, upregulation of drug efflux transporters as ABCB1, also

known as P-glycoprotein, has been described. ABCB1 belongs to ATP-biding cassette (ABC) transporters and ABCB1 induced resistance was initially observed in BRCA1/2 deficient mice models which developed spontaneous mammary tumors (Rottenberg et al., 2008; Jaspers et al., 2015). Then, ABCB1 upregulation have also been reported in chemo resistant EOCs (Patch et al., 2015).

To counteract PARP inhibitors resistance, a new class of inhibitors targeting Poly(ADP-ribose) glycohydrolase (PARG) is now under investigation(Pillay et al., 2021). PARG plays a crucial role in reversing PARylation by cleaving the poly(ADP-ribose) chains from target proteins, limiting the duration of this process (Min et al., 2010; Singatulina et al., 2019). The development of the first selective PARG inhibitor, PDD00017273, has open the way to pre-clinical investigations of this class of drugs potential in targeting cancer cells (Pillay et al., 2021; Jain et al., 2019; Pillay et al., 2019; Gravells et al., 2017, 2018).

4. Background to the project

4. Background to the project

Even though centrosome numerical abnormalities are well characterized in cancer cell lines, they have not been widely investigated *in situ* tumors. Few studies about centrosome status in prostate, breast and hepatocellular carcinoma exist, however centrosome detection is often performed only with one marker (Wang et al., 2020; Lingle et al., 2002; Nakajima et al., 2004). For this reason, the Basto lab in a previous study investigated centrosome number alteration in epithelial ovarian tumors. The cohort characterized in this study comprised 100 patients with epithelial ovarian cancer (EOC) and 19 healthy tissues (Morretton et al., 2022). These were categorized as healthy tissues (corresponding to healthy ovaries from prophylactic oophorectomy or hysterectomy) or tumor tissues, including a mix of serous (90%), endometrioid (3%), mucinous (4%), and clear cell carcinoma (3%).

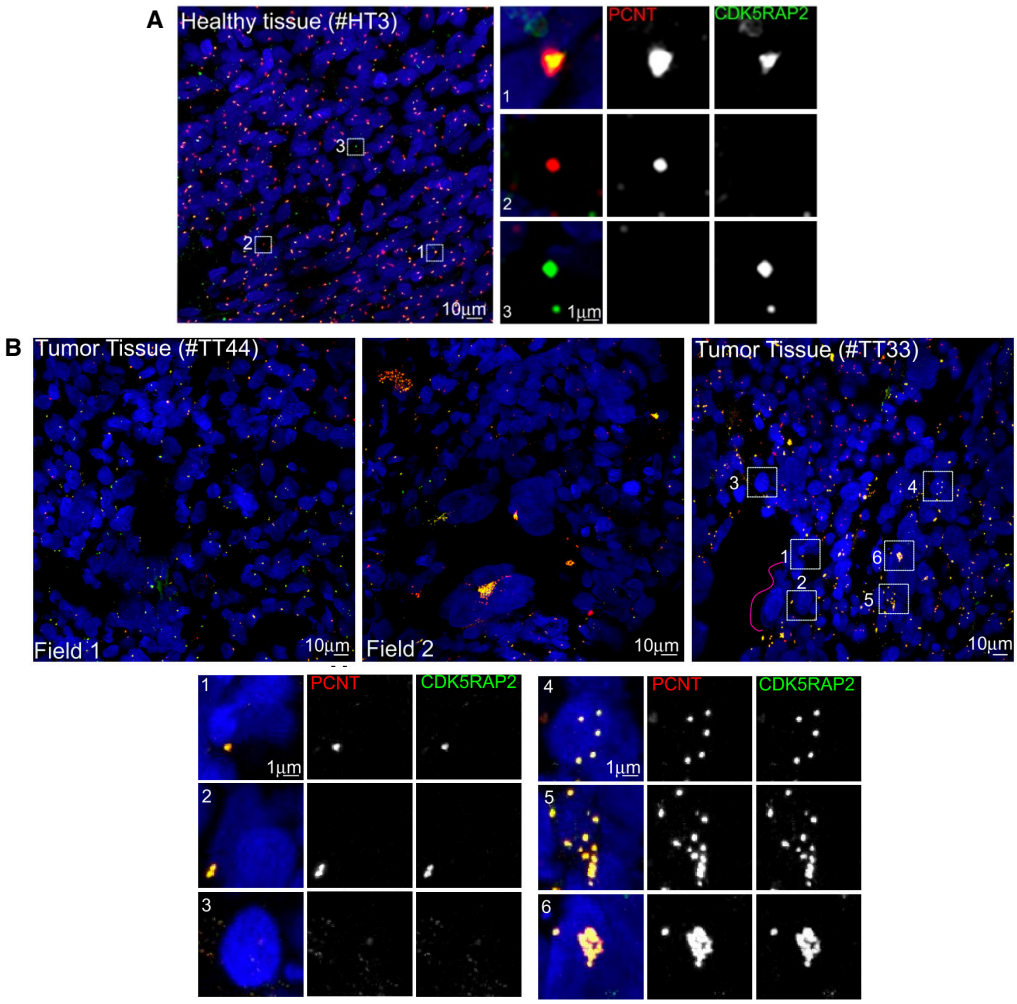

Figure 27: Centrosome amplification in EOC Confocal microscopy images of healthy ovarian tissue (A) and epithelial ovarian tumors (B) labeled with antibodies against centrosomal proteins PCNT and CDKRAP2. DNA is shown in blue. (B) Representative images of two different fields of the same tumor. The white-dashed squares represent the regions shown in higher magnifications in insets below. Image modified from (Morretton et al., 2022).

All tumors were treatment-naive, obtained after surgery without previous neo-adjuvant chemotherapy. Tissue sections were obtained from the pathology department of Institut Curie. Frozen tissues were sliced and labeled for pericentrin (PCNT) and CDK5RAP2. Images were acquired via confocal microscopy. In healthy tissue it was observed the presence of one centrosome per nucleus, which agrees with the fact that adult epithelial ovarian tissue is not a highly proliferative tissue type. On the contrary, highly heterogeneous centrosome number and tissue aspect was observed in tumor tissues (Figure 27).

To better evaluate the centrosome number, the centrosome to nucleus ratio (CNR) was defined (Edwards et al., 2023). This ratio is determined by dividing the number of detected centrosomes within a given field by the number of nuclei. The average CNR across 10 fields for each patient was determined. In healthy tissues, the CNR was around 1.02±0.02, indicating an average presence of one centrosome per cell. In tumor tissues however, the average CNR was 1.43±0.04, with a range spanning from 0.61 to 2.55. Notably, only 9% of tumors exhibited a CNR exceeding 2, suggesting low levels of centrosome amplification—defined as the presence of more than 2 centrosomes per cell. However, a significant 89% of tumors showed a CNR surpassing the mean CNR observed in healthy tissues.

Chapter 2 – Material and methods

During my thesis, I investigated the impact of centrosome amplification on the response to chemotherapy in epithelial ovarian cancers. The cellular biology research aimed to determine whether and how centrosome amplification contributes to enhanced cell death in response to first-line chemotherapy currently used in the clinic for epithelial ovarian cancer patients, as combination of carboplatin and paclitaxel. With this purpose a combination of single cell live imaging and classical cell biology experiments such as flowcytometry and immunohistochemistry were used. All the presented data has been replicated in 2 to 3 biological replicates. Previous clinical work performed by Basto lab aiming to identify if centrosome numbers can influence clinical parameter in a EOC patient cohort represent the basis for this work.

1 Cell culture and generation of stable human cell lines

1.1 Cell lines and cell culture

OVCAR8

OVCAR8 cells were obtained from the laboratory of F. Mechta-Grigoriou (Stress and Cancer Laboratory, Institut Curie, PSL Research University, France). The OVCAR8 cell line was originally generated from epithelial tissues of a patient with EOC refractory to carboplatin (Godwin et al., 1992; Schilder et al., 1990). Spectral karyotype (SKY) and genomic analysis have revealed an hyperdiploid-define karyotype in this cell line (Roschke et al., 2002). Although articular gene mutations have not been detected for BRCA1 and BRCA2, gene variants for both genes and heterozygous BRCA1 methylation have been detected in several studies, when assessed by quantitative qRT-PCR and genomic analysis (Kondrashova et al., 2018; Stordal et al., 2013). In the same study of Kondrashova et al., OVCAR8 cell lines showed resistance to both platinum and PARPi agents *in vitro* and the ability to form RAD51 foci, suggesting a competent HR pathway, at least a certain extent.

In OVCAR8 cells, the p53 gene is mutated, which results in the alternative splicing of exon 5. Additionally, there is a deletion of six amino acids within the DNA binding domain of the p53 protein (O'Connor et al., 1997). Finally, OVCAR-8 cells appear to be competent for the mismatch repair pathway (Roschke et al., 2002; Taverna et al., 2000; Umar et al., 1994).

COV504

The COV504 cell line cells was obtained from the laboratory of F. Mechta-Grigoriou. It was originated from an epithelial serous carcinoma and it shows a near tetraploid karyotype (van den Berg-Bakker et al., 1993). TP53 has been reported to have a deletion in COV504 cell line, which results in protein mutation and reduction of the function (Beaufort et al., 2014).

SKOV3

SKOV3 (American Type Culture Collection, ATCC#HTB-77) cell lines used in this study were purchased from ATCC (LGC Promochem Sarl). It is an ovarian cancer cell line originated from ascites- define (Hills et al., 1989). Previous studies revealed a near-tetraploid karyotype in this cell line (Roschke et al., 2002). Mutations in BRCA1 and BRCA2 genes have been described in SKOV3 cells, however BRCA2 variants have been detected (Stordal et al., 2013). p53 has been reported to be mutated, with a 179 H/R mutation that is supposed to destabilize p53 (Cho et al., 1994; O'Connor et al., 1997). Finally, SKOV3 cells have been described to be defective in nucleotide mismatch recognition and repair (Roschke et al., 2002; Taverna et al., 2000; Umar et al., 1994).

For the three cell lines, cell cultures underwent authentication by short tandem repeat analysis (powerplex16 HS kit, Promega #DC2101) and were routinely checked for mycoplasma (PlasmoTest Mycoplasma detection kit, InvivoGen, #rep-pt1). All cell lines were cultured at 37°C with 5% CO2 in DMEM/F12 media (ThermoFisher Scientific #31331028) supplemented with 10% Tetracyclin-free Fetal Bovine Serum (Dutscher #500101L), 100 µg/ml streptomycin and 100U/ml penicillin (ThermoFisher Scientific #15140122).

1.2 Establishment of cell lines

Inducible PLK4 over-expression, inducible SAS-6 and ΔKEN-SAS-6 over-expression and stable expression of H2B-RFP, PCNAmiRFP, RNFmiRFP, MDC1miRFP were established by lentiviral infection. Viruses were produced in HEK cells using Lipofectamine 2000 (ThermoFisher Scientific #11668019) to co-transfect lentiviral constructs with pMD2.G and psPAX2 plasmids. Viral particles were collected in the supernatant 48h after transfection, filtered and used to infect cell during 24h. Cells were then FACS sorted selecting GFP expression for inducible PLK4 over-expression and RFP expression for H2B-RFP. Otherwise, cells were selected using

Blasticidin at 5 µg/ml for PCNA expression. For cell line expressing both inducible PLK4 over-expression and FUCCI, cells were first selected with 7,5 µg/ml of Blasticidine for inducible PLK4 overexpression, then they were FACS sorted for FUCCI. The concentration of Blasticidin used in the OVCAR8 cell line was determined by concentration kill-curve (Fatma Gomaa, Zhuhong Li, Roberto Docampo, Peter Girguis, Virginia Edgcomb 2018. G418 Kill curve protocol dx.doi.org/10.17504/protocols.io.sh4eb8w). The list of plasmids used in this study is available in Table 1.

1.3 Drug treatment

For the induction of centrosome amplification, cells were treated to doxycycline (1 µg/ml) during 72h and DMSO (diluent control, 1/10000) was used as a control. If cells were subsequently subjected to another drug treatment, they were detached and reseeded without the addition of doxycycline to the PLK4OE population and left to attach for 8h. Drug treatments were then carried out for 72h at the indicated IC50 concentrations for carboplatin and paclitaxel. All chemicals are listed in table 3.

2 Cell proliferation and viability trypan blue assays

For proliferation and viability assays after 72 hours treatment for centrosome amplification (Doxycycline/DMSO 1 µg/ml) and 72 hours chemotherapy treatment, cells were plated at 100000 cells/well in 6-well plates. Cells were then detached, resuspended in 500uL medium, and live/dead cells were counted using a Beckman Coulter Vi-Cell cell counter.

3 Immunohistochemistry and imaging

3.1 Immunofluorescence

Cells were plated on 18mm glass coverslips in 6 or 12-well plates. Cells were fixed for 3min at -20 °C in ice- cold methanol for centrosomes staining, or for 10min in 4%PFA at room-temperature for centrosomes staining in OVCAR8 FUCCI cell line or at 4°C for DNA damage and DNA damage repair staining. Cells were washed 3 times in PBST (PBS + 0,1% Triton X-100), with 5min between one wash and the following one and incubated in PBST + BSA 0,5%

for 30min at room temperature. Cells were then incubated for 1h in primary antibodies diluted in PBST + BSA 0,5%, washed 3 times in PBST, incubated for 30min in secondary antibodies diluted in PBST + BSA 0,5% and washed 3 times in PBST. Cells were then stained for DNA using 3 µg/ml DAPI diluted in PBST + BSA 0,5%, washed 3 times in PBS and mounted with mounting medium (1.25% n-propyl gallate, 75% glycerol, in H2O). Antibodies used are listed in Table 5.

3.2 Immunofluorescence imaging and quantification

Immunofluorescence images were acquired with a sCMOS camera (Flash 4.0 V2, Hamamatsu) on a widefield microscope (DM6B, Leica systems), with a 63x objective (63x HCX PL APO 1.40-0.60 Oil from Leica), using Metamorph software (Metamorph 7.10.1 software; Molecular Devices, SCR 002368). Z-stacks were acquired automatically at a z-distance of 0,3 µm. Centrosome numbers and micronuclei were scored manually. Centrosomes were counted only when colocalization of two centrosomal markers was observed. DNA damage and DNA damage repair markers intensity or foci number were determined on Z-projections of images, using a custom Python script to run the h_maxima function from the skimage.morphology.extrema module. For using the macro, nuclear area was selected manually. Nuclei partially out of the field were excluded. Nuclei with coverage lower to 1000 pixels were also excluded, as considered to be micronuclei. Masks of the nuclei were generated. Then, the macro was run on nuclei masks and the Z-projection images of the marker to analyze, each marker analyzed separately (Figure 1). Images are presented as maximum intensity projections generated with ImageJ software (SCR 002285, version 2.1.0/1.53c).

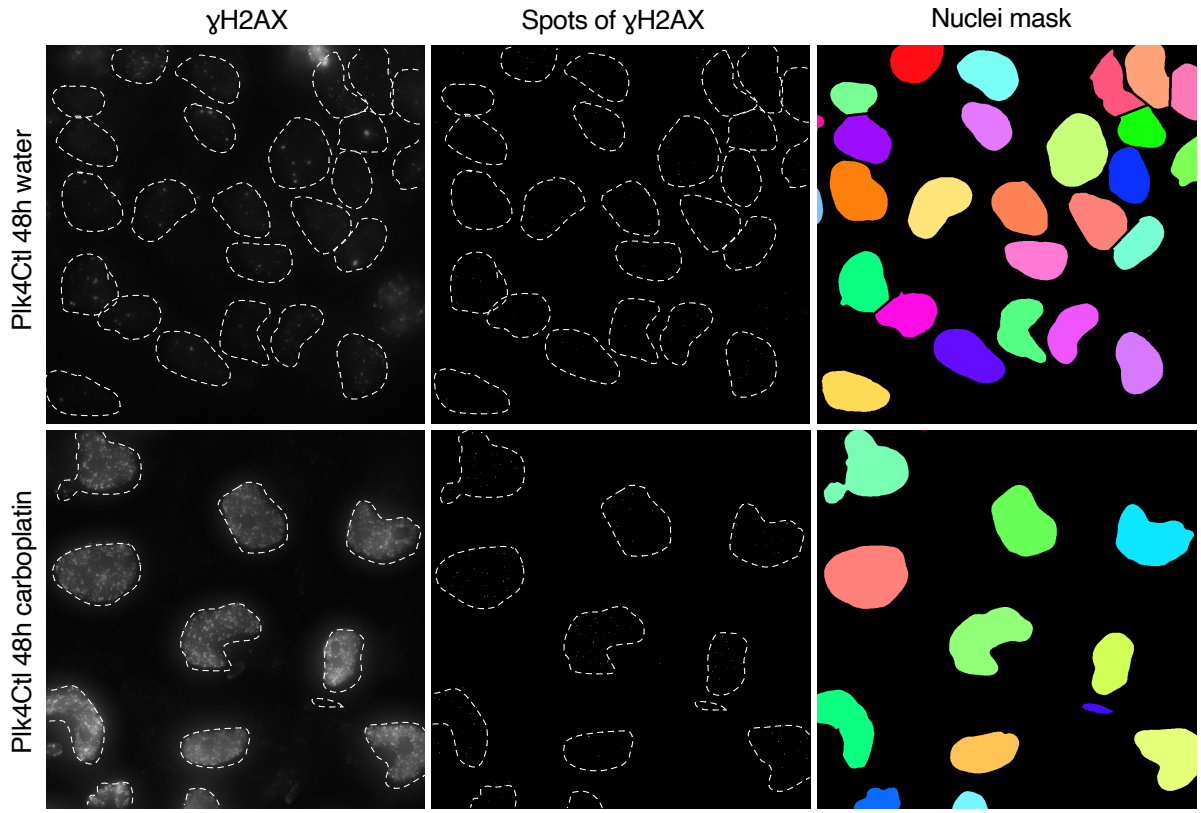

Figure 1: DNA damage macro. Representative images of different steps realized for analysis of DNA damage markers and DNA damage repair. OVCAR8 cells with antibodies directed against γ-H2AX are shown as an example, in the first column. In the second column, the foci detected via the macro and in the third column the area of the nuclei selected.

4 Live imaging and analysis

I used the same strategy to realize OVCAR8 FUCCI movies and OVCAR8 H2B-RFP PCNAmiRFP movies. For live-imaging of chemotherapy responses, cells were plated on Ibidi µ-Slide 8 Well slides (Clinisciences, #80806-G500). Cells subjected to chemotherapy and those left untreated from both PLK4Ctl and PLK4OE populations were imaged concurrently within the same experimental setup. Imaging was performed with a 20x objective (CFI Plan Apo LBDA 20x 0,75/1 mm CCo 0,17) with an EMCCD camera (Evolve, Photometrics) on an inverted microscope (Inverted Ti-E Nikon) equipped with a spinning disk (CSU-X1 Yokogawa), a stage-top temperature and CO2 incubator (Tokai Hit) and integrated in Metamorph software. In each well, 4-10 distinct positions were captured at 10-minute intervals over a span of 72 hours. For imaging, a single slice was captured in the brightfield channel, whereas 10 slices per Z-stack were obtained in the H2B-RFP channel or in the mKO2-Cdt1(30-120) and mAzami-

Green-Gem1(1-110) channels for the FUCCI cells or in the miRFP (LAMP1-emiRFP670) for PCNA cells. Movie analysis was performed on movies OVCAR8 H2B-RFP carboplatin, OVCAR8 H2B-RFP combination of carboplatin and paclitaxel, OVCAR8 FUCCI and OVCAR8 H2B-RFP PCNAmiRFP. Analysis was performed for each of the four conditions (with or without centrosome amplification, with or without chemotherpy), for two replicates. Time-lapse movies were then analyzed manually using a custom Fiji macro to record a list of events. 15 lineages were analyzed in controls and 100 for conditions with chemotherapy. The lineages were tracked over multiple generations. Lineage analysis consists in counting for each starting cell, the number of cells adopting different fates. Generation analysis consists in determining the percentage of a generation that will adopt the different fates. Mitosis and fate correlation involves assessing the percentage of cells that assume distinct fates, depending on the behavior of the mother cell during mitosis. Moreover, for OVCAR8 FUCCI and OVCAR8 H2B-RFP PCNAmiRFP passage through cell cycle phases was annotated and length of each phase was calculated and correlated to fate. Events were registered via a package containing:

-a DATA folder: containing CSV files, which contains all your events in the form of a list.
-The EventSorter.py python script: custom Python script to generate excel data files and single-cell profiles -a Results folder: containing excel files
-a ROI folder: containing ROI.zip files generated by manual annotation through Fiji
-The SetUpFile.tx: containing instructions for analysis
Once events recorded, I run the custom Python script to generate excel data files and single-cell profiles. Examples of the file generated and analyzed are shown in Figure 2. The File1 (Figure 2A) allowed me to generate single cells graphs. The File2 (Figure 2B) was used for analysis via pivot-tables of different parameters shown in graphs of each movie. Stills from time-lapses are presented as maximum intensity projections generated with ImageJ software (SCR 002285, version 2.0.0-rc-69/1.52p).

A

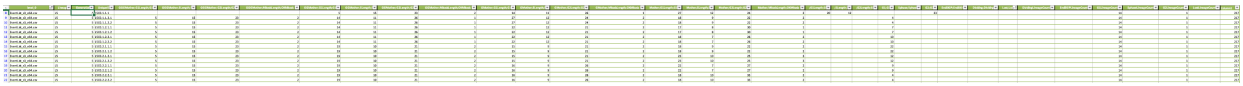

B

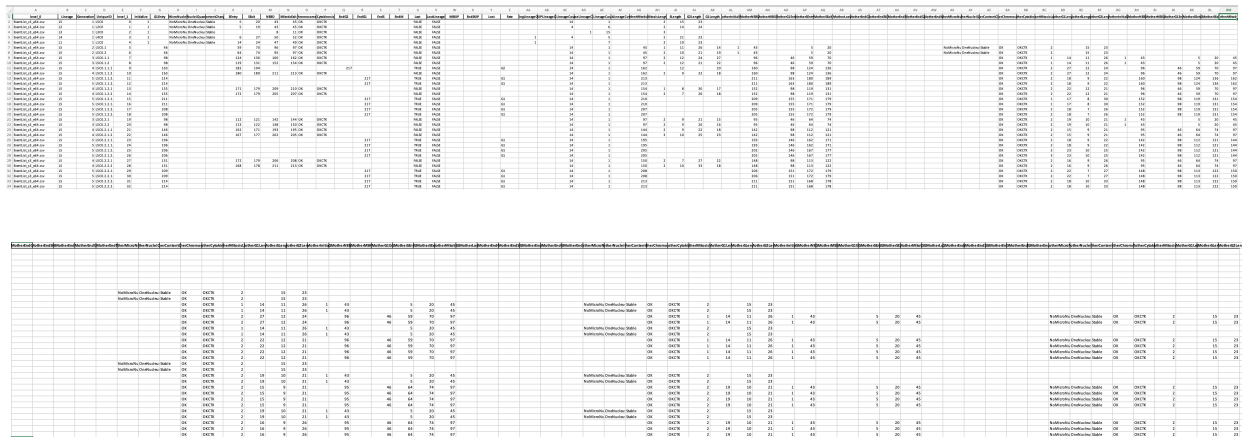

Figure 2: Live-imaging data analysis Examples of the excel files generated from the customed Python script, in OVCAR8 FUCCI cell line. Data for only one cell lineage are shown. (A) File1, used for single cell profile graphs and (B) file2, used to extract information to generate other graphs of the analysis.

5 Molecular biology

Plasmid design was performed using the SnapGene software. Construction and assembly of the plasmid was performed through Gibson assembly (https://international.neb.com/applications/cloning-and-synthetic-biology/dna-assembly-and-cloning/nebuilder-hifi-dna-assembly). Fragment to be assembled in the final plasmid were amplified by PCR and PCR products were analyzed through gel electrophoresis on regular agarose to confirm successful amplification. Primers used are enlisted in Table 2 and plasmids in Table 1. After confirmation of the expected size, the DNA fragments were run on a new gel and they were excised from the agarose gel using a scalpel under UV light, and DNA was then extracted from the gel fragments using the QIAquick Gel Extraction Kit (28704, QUIAGEN) following the manufacturer's instructions. The concentration of DNA after elution was determined using a NanoDropTM One/OneC Microvolume UV-Vis Spectrophotometer (Thermo Fisher Scientific, MA). Subsequently, the DNA fragments were assembled using the NEBuilder HiFi DNA Assembly Master Mix (NEB #E2621, New England BioLabs Inc., MA) following the manufacturer's guidelines (Table 4). This assembly reaction was carried out at 50°C for 1 hour. Plasmid transformation was performed in NEB 5-alpha Competent *E. coli* (High Efficiency, NEB #C2987, New England Biolabs). Colonies were collected and purified by

Miniprep (17106, QUIAGEN). The sequence of the plasmid was verified first using restriction enzyme profile, then 2-3 positive clone were chosen and the construct was sent to Eurofins Genomics for Sanger Sequencing. Once verified the correct sequence of the plasmid, bacterial culture of the correct colonies was expanded overnight at 37°C, in shaking incubator at 200RPM. The plasmid was then collected and purified by Maxiprep (12362, QUIAGEN). Following assembly, competent cells were transformed and expanded as previously outlined. The process just described was carried out for the generation of the following plasmids:

- **PCNAmiRFP plasmid** miRFP was cloned from pLAMP1-emiRFP670 (Addgene), PCNA chromobody cloned from pCCC-TagRFP (Chromotech) and pLX303 (Addgene) was used as empty lentiviral backbone.
- For **GFP substitution** with blasticidin resistance gene in Lenti Tet-ON Myc-hPLK4 plasmid (Gift from Andrew Holland), Blasticidin was obtained from pcDNA3-eGFP-NLS-RNF168 (Addgene).
- For **RNF168miRFP**, since pcDNA3-eGFP-NLS-RNF168 plasmid, it is not lentiviral I will insert the gene I am interested (RNF168) into PCNA-emiRFP plasmid I previously generated, which will be the main vector. Indeed, PCNA plasmid is lentiviral and allow for antibiotic selection in mammalian cells.
- For **MDC1miRFP,** MDC1 original plasmid pLenti CMV/TO GFP-MDC1 (779-2) was coupled to fluorophore GFP, which is already present in the cell line I am using coupled to PLK4. Thus I replaced GFP with miRFP gene, which I took from PCNA-emiRFP plasmid I previously generated.
- For **SAS-6OE:** I substituted SAS6 gene from pENTR Age HsSAS-6 ST with PLK4 gene in 340-Lenti Tet-ON Myc-hPlk4, because pENTR Age HsSAS-6 ST is not a lentiviral plasmid.
- For **ΔKEN-SAS-6:** The KEN box is a domain of 3 aminoacids in the C terminal portion of the protein, target for degradation (KEN motif: aaggaaaat). The C terminal portion, I is a target for degradation which occurs during mitosis starting at anaphase, by 26S proteasome. The protein later reappears in S phase. ΔKEN-SAS6 results from the mutation of 3 amino acids K589A, E590A, N591A which has been reported to increase centrosome amplification upon overexpression(Strnad et al., 2007). The mutation was induced in the SAS6 lentiviral plasmid I previously generated, by Q5® Site-Directed Mutagenesis Kit (New England Biolabs,

https://international.neb.com/products/e0554-q5-site-directed-mutagenesis-kit#Product%20Information). The primers for the substitution were generated via https://nebasechanger.neb.com/, as depicted in the following image:

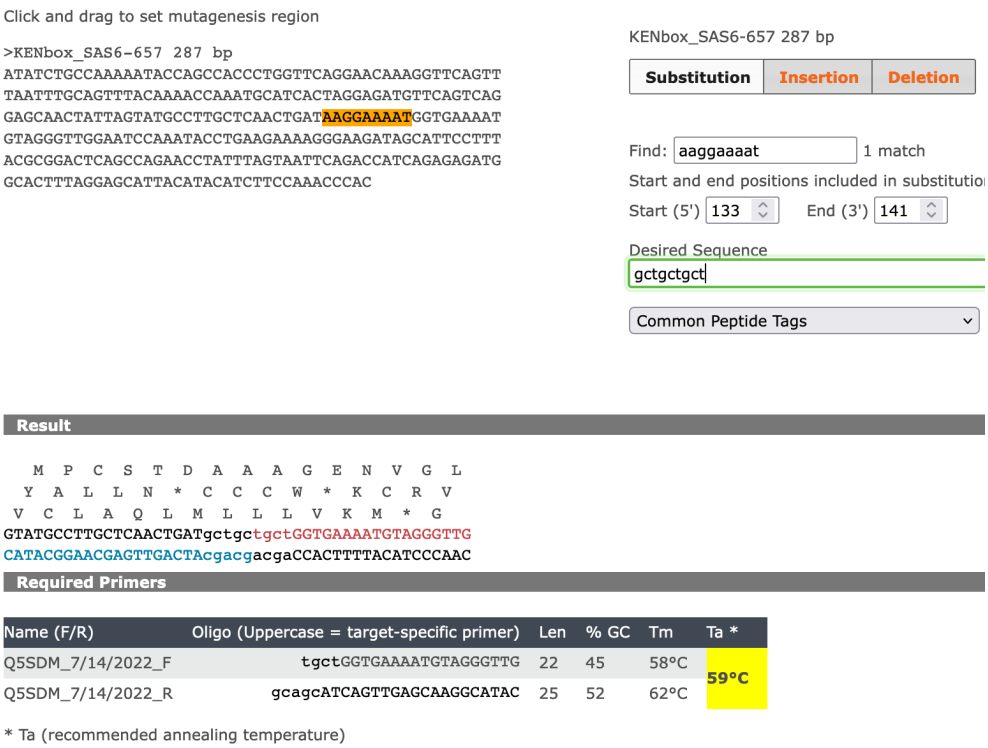

6 Flow cytometry for cell cycle profiling

For the analyzis of cell cycle profile by flow cytometry, OVCAR8 cells inducible for PLK4OE were treated with doxycycline(1 µg/ml) or DMSO (diluent control, 1/10000) for 72h. Then, cells were replated in two different 6 wells plates (20000 cells/well), one per condition and incubated in 136 µM carboplatin or water (3 wells per condition) for 48 and 72 hours. Cells were detached by treatment with trypsin (Fisher scientific) and pooled for every condition in a single tube. Cells were immediately washed in PBS, fixed in 2 ml 70% ethanol and stored at −20 °C overnight. Afterwards, cells were washed in PBS and staining buffer (BD Pharmingen 554656).

For cell cycle analysis, DNA content was visualized by incubating the cells with 2 µg/ml Hoescht 33342 (Sigma Aldrich 94403) in staining buffer for 15 min at room temperature. Flow

cytometry analysis was done using LSRII (BD Biosciences), by analyzing 10,000 cells per condition. Data were then analyzed with FlowJo 10.6.0 software (Tree Star).

7 Cell preparation for single-cell whole genome sequencing

Cells were treated with DMSO (1/10000), doxycycline (1µg/mL) or AZ3146 (1µM) for 72h. Cells were then frozen in freezing medium (10% DMSO, 40% FBS in DMEM-F12) in 1ml cryotubes (10^6 cells/ml, volume of 1ml) and preserved at -80°C.

8 Statistical analysis

Statistical analyses were conducted using GraphPad Prism software. The specific tests used are indicated in the corresponding figure legends. Information regarding the number of cells analyzed and the number of replicates can be found either directly on the figures or provided within the associated figure legends.

Table1: List of plasmids used in this study.

Plasmid	Origin
Lenti Tet-ON Myc-hPLK4	Gift from Andrew Holland (Department of Molecular Biology and Genetics, Johns Hopkins University School of Medicine, Baltimore, MD, 21205; A.J.H., Johns Hopkins University School of Medicine, 615A PCTB, 725 North Wolfe Street, Baltimore)
-IRIS-Neo-H2B-RFP	Gift from Daniele Facchinetti (Institut Curie, PSL Research University, CNRS, UMR144 Paris, France)
pBOB-EF1-FastFUCCI-Puro	Addgene plasmid 86849, gift from Kevin Brindle (Department of Biochemistry, University of Cambridge, Cambridge, UK) and Duncan Jodrell (Addenbrooke's Hospital, Cambridge University Hospitals NHS Foundation Trust, Cambridge, CB2 0RE, UK)
LAMP1 (Lysosome Membrane) labeling with near-infrared fluorescent protein emiRFP670 (enhanced miRFP670)	Addgene plasmid 136570, gift from Vladislav Verkhusha (Department of Anatomy and Structural Biology, Albert Einstein College of Medicine, Bronx, New York, USA)
pLX303 empty lentiviral backbone	Addgene plasmid 25897, gift from David Root (Broad Institute of MIT and Harvard, 7 Cambridge Center, Cambridge, MA 02142, USA.)
pCCC-TagRFP	Chromotech, https://www.chromotech.com/
pcDNA3-eGFP-NLS-RNF168	Addgene plasmid 133977, gift from Daniel Durocher (Department of Molecular Genetics, University of Toronto, Toronto, Ontario, Canada)
pLenti CMV/TO GFP-MDC1 (779-2)	Addgene plasmid 26285, gift from Eric Campeau (University of Massachusetts Medical School, 364 Plantation Street, Worcester, MA 01605, USA)
pENTR Age HsSAS-6 ST	Addgene plasmid 46382, gift from Pierre Gonczy (Swiss Institute for Experimental Cancer Research (ISREC), School of Life Sciences, Swiss Federal Institute of Technology (EPFL), CH-1015 Lausanne, Switzerland)

Table2: List of oligonucleotides used for Gibson assembly in this study.

List of oligonucleotides (5' to 3')
PCNAmiRFP
FORWARD: TACCAAACGACGAGCGTGACACCACGATGC
REVERSE: ATCGTGGTGTCACGCTCGTCGTTTGGTATGG
FORWARD:CACTAAACCagctctgcttatatagacctcc
REVERSE: gcagagctGGTTTAGTGAAC
FORWARD:agaggttgattatcgataagcttg
REVERSE: gcttatcgataatcaacctctggattacaaaatt
GFP→ blasticidin substitution
FORWARD:CCAGTTACTTCGTAGAAATCCAGCAGATCG
REVERSE: GGATTTCTACGAAGTAACTGGTGAATAAGGTCC
FORWARD:aaaggcttggccatGGTTGTGGCCATATTATCATCG
REVERSE: ATATGGCCACAACCatggccaagcctttg
FORWARD:ccgctgccctcccacacataaccagagggcagcaattc
REVERSE: ggttatgtgtgggagggcagcggccgcgtcg
FORWARD:GATTTATCAGCAATAAACCAGCCAGCCGGAAGG
REVERSE: CGGCCCTTCCGGCTGGCTGGTTTATTGCTG
RNF168miRFP
FORWARD: TACCAAACGACGAGCGTGACACCACGATGC
REVERSE: ATCGTGGTGTCACGCTCGTCGTTTGGTATGG
FORWARD: ATCTCCGGCCAGAAGCTTaggtggaggaggttctgg
REVERSE: ctAAGCTTCTGGCCGGAGATCTGAGTCC
FORWARD: gcttgagagcggcgcgggacccaag
REVERSE: ccgcttcttcttgggtcccgcgccgctctcaagcgc
FORWARD: ccgcttcttcttgggtcccgcgccgctctcaagcgc
REVERSE: tcgcggccgcttactttgtgcatctctgaaacatctgaaaaac
MDC1miRFP
REVERSE: ccgccatggtggcGGTGGCGACCGGTAGCG
FORWARD: GGTCGCCACCgccaccatggcggaaggctc
REVERSE: AGTCCGGCCGGAgctctcaagcgcggtgatcc
FORWARD:gcttgagagcTCCGGCCGGACTCAGATCTCG
REVERSE: CGCCCTGAGTTCTTTCTTCCACATATCTTC
FORWARD:TGGAAGAAAGAACTCAGGGCGTTAGAAAGG
SAS6OE
FORWARD: cgataccggtccaccgccgccaccatgagcc
REVERSE: cagcacttggctcatggtggcggcggtggacc
FORWARD: gggcagttaccaaacagttaaatcgataagc
REVERSE: ctcccaagcttatcgatttaactgtttggtaac
FORWARD: ggtacccgggtcgagtaggcgttgatcagatgctgc
REVERSE: gcagctgcttatatgcagcatctgatcaacgcctactcg
FORWARD: GATTTATCAGCAATAAACCAGCCAGCCGGAAGG
REVERSE: CGGCCCTTCCGGCTGGCTGGTTTATTGCTG
∆KEN-SAS6

FORWARD:tgctGGTGAAAATGTAGGGTTG
REVERSE: gcagcATCAGTTGAGCAAGGCATAC

Table3: List of chemicals used in this study.

Chemical	Origin	Stock dilution
Doxycyline	Sigma-Aldrich D3447	10 mg/mL in DMSO
Puromycine dichlorhydrate	ThermoFisher Scientific A1113803	10 mg/mL in 20mM HEPES
Blasticidine	Sigma-Aldrich SBR00022-1ML	10 mg/mL in 20mM HEPES
Carboplatin	Selleck chemicals S1215	10mM in Water
Paclitaxel	Sigma-Aldrich T7402	10mM in DMSO
AZ3146	Selleck chemicals S2731	10mM in DMSO
DMSO	ThermoFisher Scientific 022914.M1	

Table 4: HiFi DNA Assembly reaction protocol

	Recommended Amount of Fragments Used for Assembly		
	2–3 Fragment Assembly*	4–6 Fragment Assembly**	NEBuilder Positive Control†
Recommended DNA Molar Ratio	vector:insert = 1:2	vector:insert = 1:1	
Total Amount of Fragments	0.03–0.2 pmols* X µl	0.2–0.5 pmols** X µl	10 µl
NEBuilder HiFi DNA Assembly Master Mix	10 µl	10 µl	10 µl
Deionized H_2O	10-X µl	10-X µl	0
Total Volume	20 µl††	20 µl††	20 µl

* Optimized cloning efficiency is 50–100 ng of vector with 2-fold excess of each insert. Use 5-fold molar excess of any insert(s) less than 200 bp. Total volume of unpurified PCR fragments in the assembly reaction should not exceed 20%. To achieve optimal assembly efficiency, design 15-20 bp overlap regions between each fragment.

** To achieve optimal assembly efficiency, design 20-30 bp overlap regions between each fragment with equimolarity of all fragments (suggested: 0.05 pmol each).

† Control reagents are provided for 5 experiments.

†† If greater numbers of fragments are assembled, increase the volume of the reaction, and use additional NEBuilder HiFi DNA Assembly Master Mix.

(Table from: https://international.neb.com/protocols/2014/11/26/nebuilder-hifi-dna-assembly-reaction-protocol)

Table5: List of antibodies used in this study.

Antibody	Source	Species	Working dilution
CEP192	Home-made (Vargas-Hurtado et al., 2019; Gemble et al., 2022)	Guinea pig	1/1000
Pericentrin	ab4448	Rabbit	1/1000
ß-Catenin	Sigma C2206	Rabbit	1/200
γ-H2AX (S139)	Abcam 22551	Mouse	1/500
Rad51	Abcam 133534	Rabbit	1/500
53BP1	Millipoare MAB3802	Mouse	1/250
FANCD2	Novus Biologicals 100-182	Rabbit	1/250
anti-guinea pig IgG (H+L) Highly Cross-Adsorbed Secondary Antibody, Alexa Fluor 647	ThermoFisher Scientific A-21450	Goat	1/250
anti-rabbit IgG (H+L) Highly Cross-Adsorbed Secondary Antibody, Alexa Fluor 488	ThermoFisher Scientific A-11034	Goat	1/250
HRP-coupled anti-mouse	Jackson ImmunoResearch 115-035-003	Goat	1/250
anti-Rat IgG (H+L) Cross-Adsorbed Secondary Antibody, Alexa Fluor 633	Thermo Fisher Scientific A21094	Goat	1/250
anti-Mouse IgG (H+L) Highly Cross-Adsorbed Secondary Antibody, Alexa Fluor 546	Thermo Fisher Scientific A-11030	Goat	1/250

.

Chapter 3 – Results

Results – Section 1

1 - Centrosome amplification favors cell death in response to chemotherapy in epithelial ovarian cancer cell lines

1.1 Centrosome amplification reduces proliferation but does not affect viability in epithelial ovarian cancer cell lines

To study the influence of centrosome amplification on the response to paclitaxel and carboplatin in epithelial ovarian cancer we chose an *in vitro* system. Three epithelial ovarian cancer cell lines were selected: OVCAR8, COV504 and SKOV3 (details for cell lines are provided in material and methods). Centrosome amplification is defined as the presence of more than two centrosomes per cell. Inducible centrosome amplification was achieved by lentiviral infection with a Polo Like Kinase 4 (PLK4) transgene under the control of a doxycycline inducible promotor (see material and methods). PLK4 is the kinase which plays the major role in the centrosome duplication cycle (Habedanck et al., 2005; Bettencourt-Dias et al., 2005).

I first verified the capacity of each cell line to present centrosome amplification upon PLK4 overexpression. To do so, cells were incubated with doxycycline or DMSO as a control at a concentration of 10 μg/ml for 72 hours (scheme in Figure 1.1A). Then, cells were fixed and labelled for centrosome markers using antibodies against the Centrosomal protein 192 (CEP192) and Pericentrin. DAPI was used to visualize DNA. Images were acquired at epifluorescence microscope and centrosome number per cell was quantified manually (Figure 1.1B). Starting with the OVCAR8 cell line, in control cells (DMSO) only 4% of the cells showed centrosome amplification (Figure 1.1C). This suggests that in OVCAR8 cells, a low level of centrosome amplification is present. In contrast, 80% of the cells showed centrosome amplification after PLK4 overexpression. High number of centrosomes were detected per cell: ~10% had 5 or 6 centrosomes per cell, ~ 15% had from 7 to 10 centrosomes and ~8% had between 11 and 20 centrosomes. This means that PLK4 overexpression is a suitable tool to induce centrosome amplification in the OVCAR8 cell line. The same strategy was applied to COV504 and SKOV3 cell lines. COV504 and SKOV3 showed respectively basal levels of centrosome amplification of 6% and 4% (Figure 1.1C). Thus, centrosome amplification is infrequent in all the three cell lines. Upon PLK4 overexpression centrosome amplification was present in 90% of COV504 cells and in 70% in SKOV cells. Most cells showed high levels of centrosome amplification. In COV504 cells, ~28% had between 11 and 20 centrosomes per

cell and ~30% had between 7 and 10 centrosomes. In SKOV3 cells centrosome number per cell was between 11 and 20 in ~10% of cells, between 7 and 10 in ~15% of cells and 5 or 6 in ~12% of the cells. This means that centrosome amplification can be induced in the majority of cells upon PLK4 overexpression also in COV504 and SKOV3 cell lines.

Figure 1.1

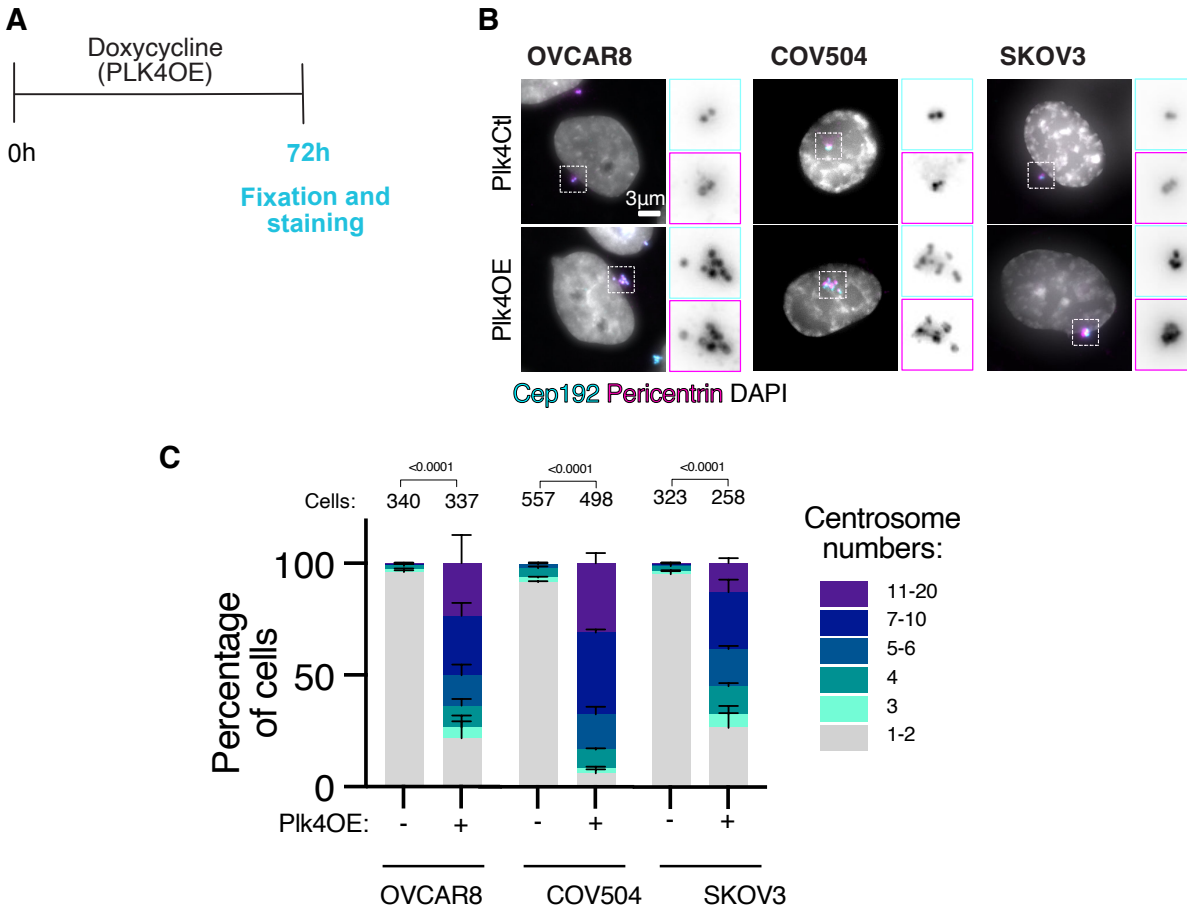

Figure 1.1: PLK4OE induces centrosome amplification in Epithelial Ovarian Cancer (EOC) cell lines

(A)Schematic representation of the experimental workflow for fixed immunofluorescence imaging. Cells were incubated in 10 µg/ml of doxycycline or DMSO, as a control, for 72 hours. (B) Representative images of cells labeled with antibodies against centrosomal proteins CEP192 (Cyan) and pericentrin (magenta). DNA is shown in gray. The three epithelial ovarian cancer cell lines are shown: OVCAR8, COV504 and SKOV3 for the two conditions PLK4 control (upper panel) and PLK4 overexpression (lower panel). Insets displaying zoom of the centrosomes are shown on the right of each image, with color-coded border according to the antibody used. (C) Graph bar showing the average and standard error of the mean (SEM) of the proportion of cells according to centrosome number as indicated for each cell line. Numbers on the top of each graph represent the number of cells analyzed per condition. Three independent experiments for each cell line. Statistical test: Fisher's exact test comparing the number of cells with more than 2 centrosomes.

Cancer cells can survive with centrosome amplification by frequently mutated TP53 gene (Fukasawa et al., 1996a) and by mechanisms of centrosome clustering (Kwon et al., 2008a) (for further details see introduction 2.4.3.1 and 2.4.3.3 chapters). To verify that cells can survive and proliferate with centrosome amplification in our system, I verified how centrosome amplification affects proliferation and viability in the three cell lines described above. Cell proliferation is the process that results in an increased number of cells through time. Cell viability is defined as the number of viable cells in respect to the whole cell population. Cells were treated with 10 μg/ml concentration of doxycycline or DMSO as a control for 72 hours. After induction of centrosome amplification proliferation and viability as assessed at 24, 48 and 72 hours using trypan blue assays. Trypan blue is a die which penetrates and labels exclusively cells where membrane integrity has been compromised and so it is used as an indicator of dead cells (Strober, 2015) (Figure 1.2A).

I first focused on OVCAR8 cell line. As expected, control cells grew exponentially through time, with the number of viable cells reaching 2,8 x 10^5 at 24 hours; 6 x 10^5 at 48 hours and 1,3 x 10^6 at 72 hours (Figure 1.2B). This indicates that OVCAR8 cells proliferate exponentially. Then, I focused on conditions with centrosome amplification. PLK4OE cells showed exponential growth reaching 9,5 x 10^5 cells after 72 hours (Figure 1.2B). These results indicate that the OVCAR8 cell line can sustain proliferation in the presence of centrosome amplification. Importantly, the number of cells in conditions of centrosome amplification was significantly reduced compared to the control at 72 hours. This suggests that centrosome amplification represents a break to cell proliferation.

To verify if the decrease in cell proliferation is not due to an increase in cell death, I characterized cell viability. 97% of control cells were alive and the viability remained constant through the 72 hours (Figure 1.2C). This was also the case in cells with centrosome amplification. Since differences in cell viability were not detected between cells with or without extra centrosomes I concluded that centrosome amplification does not induce cell death in OVCAR8 cell lines.

The same experiments were performed in COV504 and SKOV3 cell lines. Both cell lines showed exponential growth in control cells, with the number of viable cells produced after 72hours reaching 9,8 x 10^5 and 4,8 x 10^5 in COV504 and SKOV3 cells respectively (Figure 1.2A,B). After induction of centrosome amplification, exponential cell growth is maintained with mean cell numbers at 72 hours equal to 6,8 x 10^5 for COV504 and equal to 3,7 x 10^5 for

SKOV3 cells. However, if we compare to control cells, proliferation is decreased when extra centrosomes are present in both cell lines. Thus, we can conclude that centrosome amplification decreases proliferation in all three ovarian cancer cell lines.

I then focused on the analysis of viability (Figure 1.2C). In control conditions the levels of cell death were very low, with viability around 95% in COV504, 96% in SKOV3 cells, at the three time points analyzed. Thus, COV504 and SKOV3 have low basal cell death. Cells with centrosome amplification displayed consistent viability around 96% for COV504 and 95% for SKOV3, over a period of 72 hours (Figure 1.2C). Differences in viability were not observed between cells with or without extra centrosomes. These findings indicate that centrosome amplification does not trigger cell death in either COV504 or SKOV3 cell lines. In conclusion, COV504 and SKOV3 cell lines tolerate centrosome amplification.

Figure 1.2

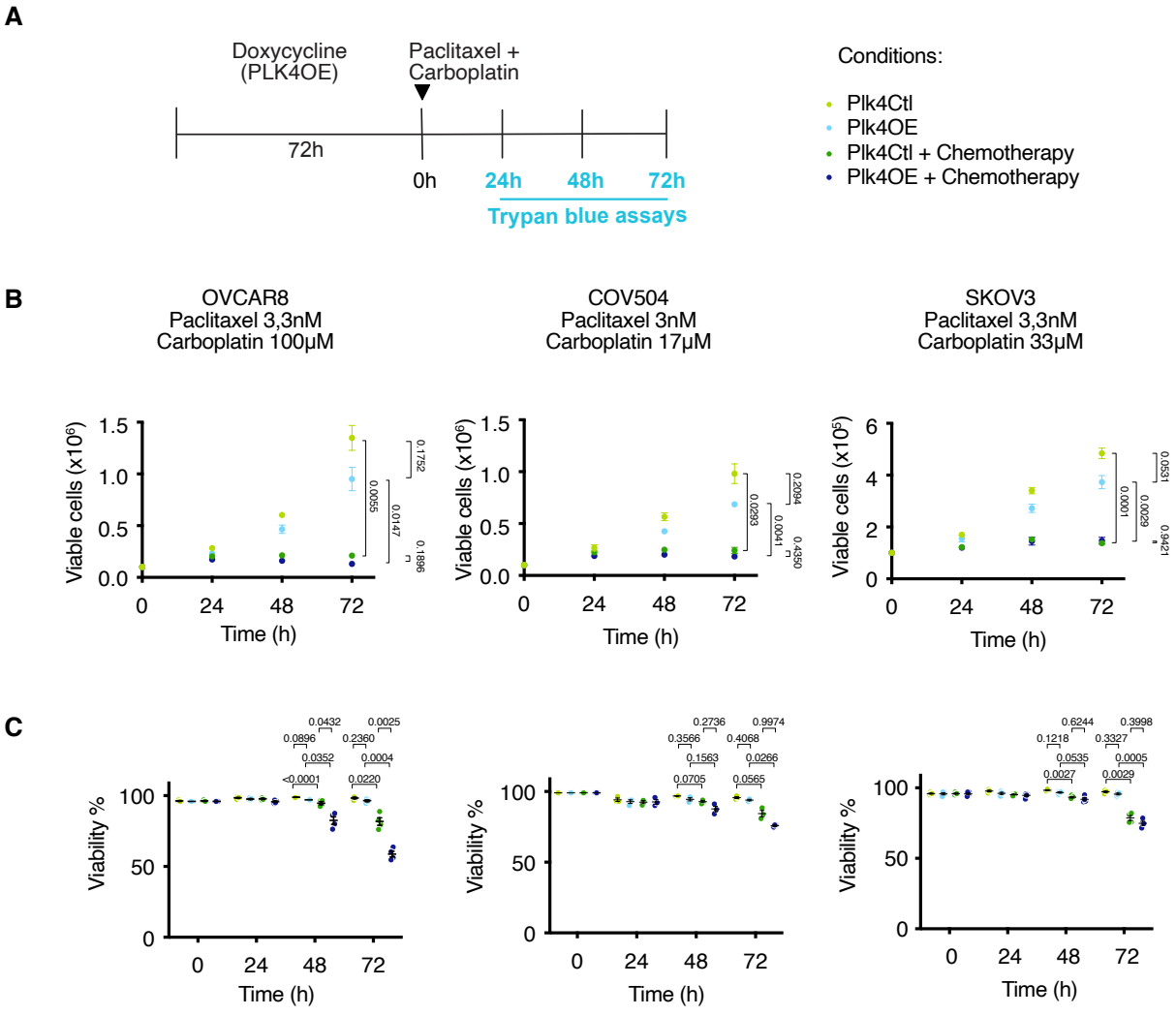

Figure 1.2: Centrosome amplification favors the response to combined paclitaxel and carboplatin in EOC cell lines

(A) Schematic representation of the experimental workflow for proliferation and viability assays. After incubation for 72 hours in 10 μg/ml of doxycycline or DMSO, cells were treated with a combination of paclitaxel and carboplatin and the respective controls (DMSO and water) at the indicated IC50 concentrations. IC50 was determined via the MTT dose-response viability assays, for PLK4Ctl OVCAR8, COV504 and SKOV3. Proliferation and viability were assessed through Trypan Blue assays, after 24, 48 and 72 hours in the four indicated conditions, in each cell line. (B) Number of viable cells (Trypan Blue negative cells) counted for PLK4Ctl and PLK4OE OVCAR8 (Left), COV504 (Middle) and SKOV3 (Right) over time. The four different conditions are indicated by the color code. The presented values represent the average and SEM derived from the average of three technical replicates. Statistical test: two-way Anova, performed on means. (C) Percentage of viable cells (Trypan Blue negative cells) counted for the same conditions as described in panel B. The presented values represent the mean and SEM derived from averaging three technical replicates. Statistical test: two-way ANOVA with Sidak's multiple comparison test.

Overall, these results indicate that centrosome amplification can affect proliferation but not viability in epithelial ovarian cancer cell lines. Thus, the cell system exploited in this study is suitable to investigate the effect of centrosome amplification in the response to chemotherapy in epithelial ovarian cancer cell lines.

1.2 Centrosome amplification favors cell death in response to combined paclitaxel and carboplatin in epithelial ovarian cancer cell lines

Currently, the first line of chemotherapy for ovarian cancer patients is the a combination of two drugs: paclitaxel and carboplatin (Ozols et al., 2003b). Paclitaxel stabilizes microtubules while carboplatin forms DNA crosslinks (Kelland, 2007; Yang dan Horwitz, 2017). Chemotherapy was used at the half maximal inhibitory concentration (IC50), to allow the comparison of its effect between different cell lines. The values of IC50 were previously determined by my collegue Oumou Goundiam (Transfert department Institut Curie,Paris) for all the drugs either in combination or in single use and for all cell lines via MTT assays. MTT assays informs on cell proliferation, viability and cytotoxicity based on the measure of cellular metabolic activity (Meerloo, 2011). Therefore, I used the same strategy described in the previous paragraph, where I started by inducing centrosome amplification for 72 hours. Afterwards, I incubated cells with the combination of paclitaxel and carboplatin and the respective dilution controls (DMSO and water). I then evaluated proliferation and viability

using trypan blue assays for each condition with or without extra centrosomes and with or without combined chemotherapy after 24, 48 and 72 hours (Figure 1.2A).

Proliferation and viability of the cell lines in the presence of extra centrosomes was described in the previous paragraph, thus I will now focus only on the two conditions with chemotherapy. In the OVCAR8 cell line without centrosome amplification, the combination of 3,3nM of paclitaxel and 100 µM of carboplatin initially didn't impair proliferation. Indeed, doubling of the cell population in the first 24h passing from 1 x 10^5 to 2 x 10^5 was noticed similar to untreated cells. However, an increase in cell number was not detected anymore at 48 and 72 hours (Figure 1.2B). As expected upon chemotherapy exposure, cell proliferation was highly reduced compared to controls. These data suggest a cytostatic effect in the response to chemotherapy. A cytostatic effect occurs when a substance stops or slows cell proliferation. Next I characterized the cells with centrosome amplification exposed to combined chemotherapy and also observed an initial increase in cell number from 1 x 10^5 to 2 x 10^5, which then remains constant similar to cells without centrosome amplification (Figure 1.2B). However, no significant difference was observed between conditions with or without extra centrosomes in the presence of chemotherapy. Thus, I conclude that in OVCAR8 cells, proliferation is decreased in the presence of carboplatin and paclitaxel, independently of centrosome amplification.

At this point I wanted to know if this reduction in proliferation is also due to a reduction in viability. Thus, I focused on the percentage of viable cells through time (Figure 1.2C). In chemotherapy conditions, viability at 0, 24 and 48 hours is equal to 95 - 96% in OVCAR8 cells. This suggests that chemotherapy does not induce cell death in the first 48 hours. Indeed, a significant difference compared to controls was not observed. In contrast, after 72 hours, the levels of viability reached values of ~82%. Compared to control cells, a significant reduction in the percentage of viable cells was observed (Figure 1.2C). These data indicate that combined chemotherapy induces cell death between 48 and 72 hours, which results in a reduction in the overall cell population. Then I focused on conditions with both centrosome amplification and combined chemotherapy. After 48 hours, viability was around 83% of the whole cell population. Thus, the number of viable cells was decreased compared to controls. The decrease was much greater after 72 hours, reaching values of ~59%. Viability was therefore further decreased in the population of cells with centrosome amplification

exposed to paclitaxel and carboplatin. These results show that centrosome amplification favors the response to chemotherapy in OVCAR8 cells.

To test these results in other ovarian cancer cell lines, I studied proliferation and viability in COV504 and SKOV3 exposed to combined chemotherapy (Figure 1.2B-C). The concentrations of chemotherapy used for COV504 were 3nM of paclitaxel and 17µM of carboplatin, and in SKOV3 3,3nM of paclitaxel and 33µM of carboplatin. A slight increase in cell number was observed in the first 24 hours, both for COV504 and SKOV3 cells (Figure 1.2B). However, no increase in the number of viable cells was observed afterwards, with the cell population reaching 2,1 x 10^5 cells for COV504 and 1,3 x 10^5 cells for SKOV3 at 72 hours. Interestingly, differences in cell proliferation were not detected in conditions with chemotherapy with or without centrosome amplification. Based on these findings, I concluded that the combination of carboplatin and paclitaxel reduces proliferation in COV504 and SKOV3 cell line, independently from centrosome status.

Next, I investigated how the combination of paclitaxel and carboplatin and centrosome amplification modulate cell death (Figure 1.2C). After 72 hours of chemotherapy, 84% of COV504 cells were still alive when in the presence of combined chemotherapy, against 76% when chemotherapy was combined with extra centrosomes. Thus, I conclude that centrosome amplification enhances cell death in response to combined chemotherapy in the COV504 cell line. Viability of SKOV3 cells was around 78% after 72 hours, showing a significant decrease when compared to controls. However, viability in conditions with centrosome amplification and combined chemotherapy was of 75%, showing no significant difference when compared to conditions with chemotherapy alone. This indicates that centrosome amplification does not favor cell death in SKOV3 cell line in response to combined chemotherapy.

Overall, these data indicate that centrosome amplification can favor the response to combined carboplatin and paclitaxel in certain epithelial ovarian cancer cell lines, while it has no such effect in others.

1.3 Centrosome amplification favors cell death in response to individual paclitaxel in epithelial ovarian cancer cell lines

The results described above have shown that centrosome amplification can favor the response to combined paclitaxel and carboplatin in OVCAR8 and COV504 cell lines by

increasing cell death. Then, I wanted to investigate if centrosome amplification shows a synergistic effect with the two drugs when administrated separately.

I repeated the protocol described in the previous paragraph for paclitaxel using DMSO for dilution control (Figure 1.3A). In OVCAR8 a concentration of 5nM of paclitaxel, which corresponds to the IC50, resulted in generation of 6,7 x 10^5 cells after 72 hours (Figure 1.3B) compared to 1,3 x 10^6 cells in controls, showing that proliferation was reduced by almost half. This indicates that paclitaxel reduces proliferation in the OVCAR8 cell line. Combination of centrosome amplification and paclitaxel resulted also in a mean equal to 3,4 x 10^5 cells generated after 72 hours. This indicates a decrease of proliferation of more than a half compared to OVCAR8 controls. Finally, I did not aborve a significant difference between cells with or without extra centrosomes in the presence of paclitaxel was not noticed.

Figure 1.3

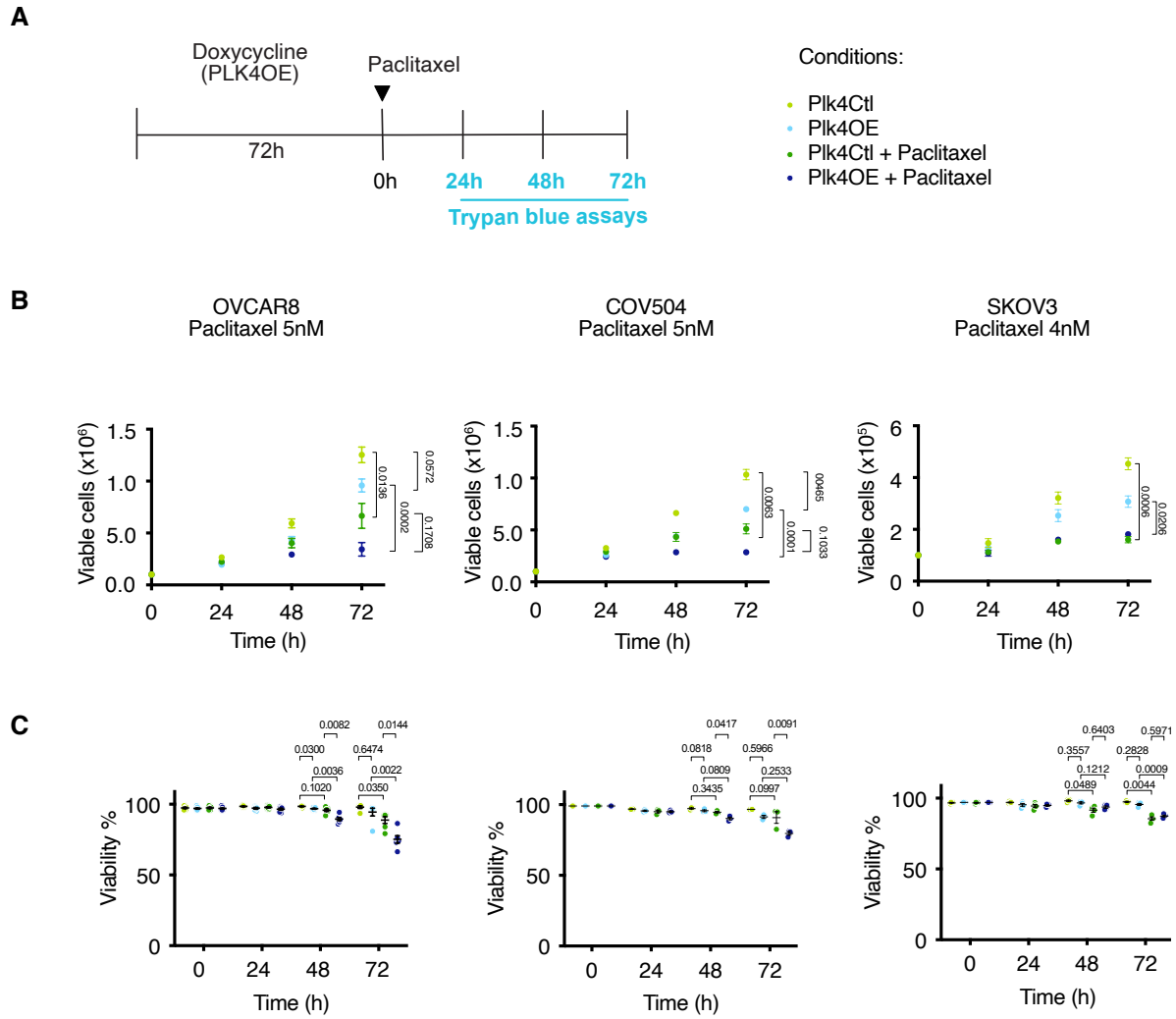

Figure 1.3: Centrosome amplification favors the response to paclitaxel in EOC cell lines

(A) Schematic representation of the experimental workflow for proliferation and viability assays. After incubation for 72 hours in in 10 μg/ml of doxycycline or DMSO, cells were treated with paclitaxel or DMSO as a control, at the indicated IC50 concentrations. IC50 was determined via MTT dose-response viability assays, for PLK4Ctl OVCAR8, COV504 and SKOV3. Proliferation and viability were assessed through Trypan Blue assays, after 24, 48 and 72 hours in the four indicated conditions, in each cell line. (B) Number of viable cells (Trypan Blue negative cells) counted for PLK4Ctl and PLK4OE OVCAR8 (Left), COV504 (Middle) and SKOV3 (Right) over time. The four different conditions are indicated by the color code. The presented values represent the mean and SEM derived from the average of three technical replicates. Statistical test: two-way Anova, performed on means. (C) Percentage of viable cells (Trypan Blue negative cells) counted for the same conditions as described in panel B. The presented values represent the mean and SEM derived from averaging three technical replicates. Statistical test: two-way ANOVA with Sidak's multiple comparison test.

To understand whether centrosome amplification affects cell death in response to paclitaxel, I focused on viability (Figure 1.3C). In cells without centrosome amplification, the presence of paclitaxel, 89% of the cells were viable after 72 hours, while in control cells this value was close to 98%. This result shows that paclitaxel alone induces cell death in OVCAR8 cells. Importantly, viability was further decreased to 75% in cells with centrosome amplification. Together, these results show that centrosome amplification can increase the levels of cell death due to paclitaxel treatment in OVCAR8 cells.

To further test the hypothesis that centrosome amplification can increase the effect of paclitaxel in epithelial ovarian cancer cells, I used the other two cell lines, COV504 and SKOV3. COV504 cells gradually grew over time, transitioning from 1 x 10^5 cells at time 0, to 5,1 x 10^5 cells at 72 hours in the presence of 5nM of paclitaxel, which represents a reduction in proliferation when compared to controls (Figure 1.3B). When combined with centrosome amplification, lower proliferation levels were noticed, as only 2,9 x 10^5 cells were produced after 72 hours. I concluded that paclitaxel reduces the proliferation of COV504 in the presence of centrosome amplification. I next investigated whether this treatment impacted cell death. After 72h of paclitaxel treatment, 91% of the cells were alive showing that in this cell line, paclitaxel does not lead to high levels of cell death. Importantly, the 3 independent experiments showed variable results: 95%, 82 % and 94% (Figure 1.3C). Interestingly however, the combination of paclitaxel with centrosome amplification induced a significant reduction in viability compared to cells without centrosome amplification. Thus, centrosome amplification favors cell death in response to paclitaxel in the COV504 cell line.

Finally, I analyzed proliferation and viability in response to paclitaxel and centrosome amplification in the SKOV3 cell line. Over time, the cell population showed a small increase from 1 x 10^5 cells at the start of the experiment, to 5.1 x 10^5 cells at 72 hours when treated with 4nM of paclitaxel (Figure 1.3B). This indicates that the cells are still capable of proliferating in the presence of paclitaxel. However, when comparing these results to the control group, where the final population size reached 4,5 x 10^6 cells, a reduction in proliferation due to paclitaxel became evident. On the contrary, no difference in the levels of proliferation was observed when comparing paclitaxel conditions with or without extra centrosomes. Therefore, paclitaxel slows down proliferation in the SKOV3 cell line as well.

Finally, I investigated how centrosome amplification can affect cell death in the SKOV3 cell line. After 72 hours of incubation with paclitaxel, 86% of the cells survived while in control cell viability was equal to 96% (Figure 1.3C). Thus, as expected, paclitaxel induces cell death in SKOV3 cell line. When paclitaxel was combined with centrosome amplification, cell viability was around 87%. Comparing paclitaxel conditions, no difference in the levels of cell viability was noticed depending on centrosome status in SKOV3 cell line. Thus, centrosome amplification does not increase levels of cell death induced by paclitaxel in SKOV3 cell lines.

Overall, these data show that centrosome amplification increases cell death induced by paclitaxel in OVCAR8 and COV504 cell lines, but not in SKOV3 cells.

1.4 Centrosome amplification favors cell death in response to carboplatin in epithelial ovarian cancer cell lines

The results described above show that centrosome amplification favors the response to both paclitaxel and to combined chemotherapy in OVCAR8 and COV504 cell lines. I next investigated if centrosome amplification can synergize also with carboplatin in inducing cell death. Thus, I repeated the protocol described in the previous paragraphs using carboplatin and water as dilution control (Figure 1.4A).

Figure 1.4

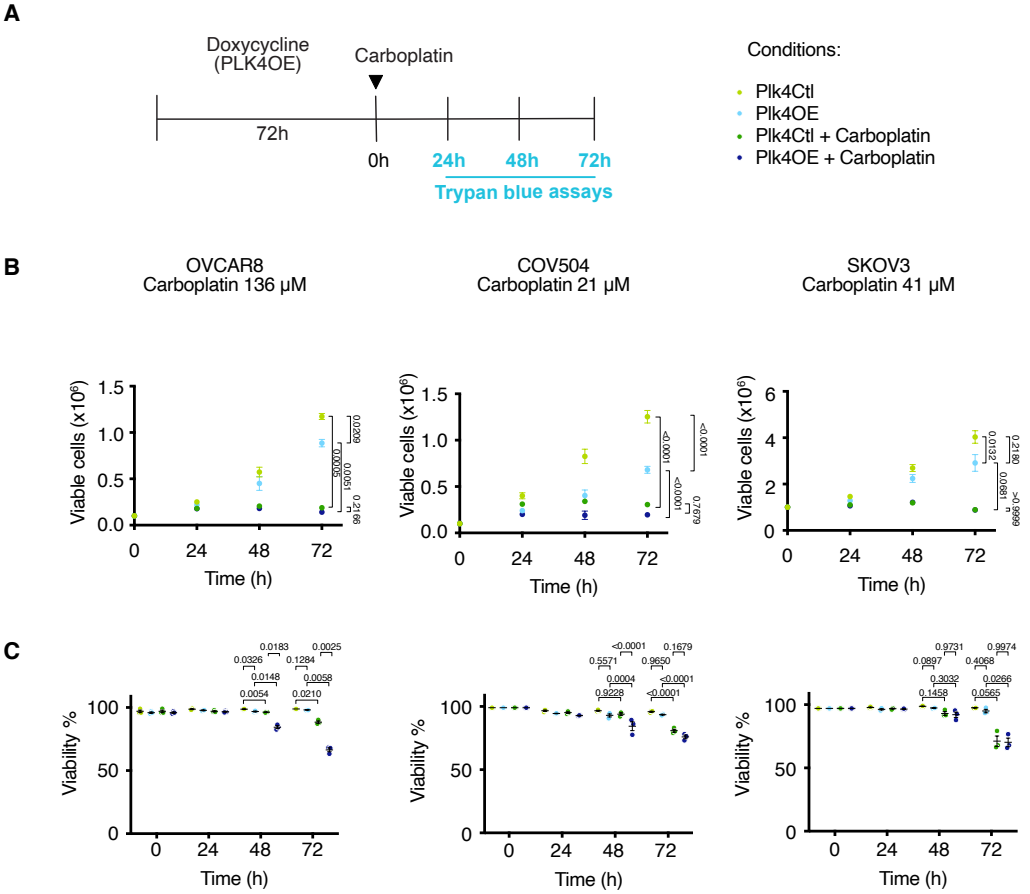

Figure 1.4: Centrosome amplification favors the response to carboplatin in EOC cell lines

(A) Schematic representation of the experimental workflow for proliferation and viability assays. After incubation for 72 hours in in 1 µM of doxycycline or DMSO, cells were treated with carboplatin or water as a control, at the indicated IC50 concentrations. IC50 was determined via MTT dose-response viability assays, for PLK4Ctl OVCAR8, COV504 and SKOV3. Proliferation and viability were assessed through Trypan Blue assays, after 24, 48 and 72 hours in the four indicated conditions, in each cell line. (B) Number of viable cells (Trypan Blue negative cells) counted for PLK4Ctl and PLK4OE OVCAR8 (Left), COV504 (Middle) and SKOV3 (Right) over time. The four different conditions are indicated by the color code. The presented values represent the mean and SEM derived from the average of three technical replicates. Statistical test: two-way Anova, performed on means. (C) Percentage of viable cells (Trypan Blue negative cells) counted for the same conditions as described in panel B. The presented values represent the mean and SEM derived from averaging three technical replicates. Statistical test: two-way ANOVA with Sidak's multiple comparison test.

In OVCAR8 cells, I used the IC50 concentration of 136 µM of carboplatin. After an initial increase in the number of cells after 24 hours, cell numbers remained constant - 1,8 x 10^5 through the remaining time. Compared to OVCAR8 controls, where the proliferation leads to 1,2 x 10^6 cells, I noticed a great reduction in cell proliferation in response to carboplatin.

(Figure 1.4B). This suggests a cytostatic effect of carboplatin. Cytostatic effects occurs when a drug induces slow down or an arrest in proliferation (Kubara et al., 2012; Swift dan Golsteyn, 2016), which has been already been reported in the literature for carboplatin (Siddik, 2003). When I characterized the condition with both centrosome amplification and carboplatin, I found that proliferation was reduced, reaching values of 1,8 x 10^5 both at 48 and 72 hours. However, a significant difference with carboplatin in the presence of extra centrosomes was not noticed. Thus, carboplatin reduces proliferation in OVAR8 cell lines and this is not influenced by centrosome numbers. Then I focused on how carboplatin affects cell viability depending on the centrosome status in the OVCAR8 cell line (Figure 1.4C). Viability in response to carboplatin after 48 hours did not show differences when compared to controls. This suggests that carboplatin does not induce high cell death levels in the first 48 hours. On the contrary, viability was reduced to 88% after 72 hours. These results indicate that carboplatin induces cell death in OVCAR8. Moreover, these data suggests that carboplatin

induction of cell death mostly occurs between 48 and 72 hours. I will thus focus on the effect of carboplatin at 72 hours, since the effect of carboplatin reaches its maximum. Combination of centrosome amplification and carboplatin resulted in a reduction of viability to 70%. Cell viability was therefore significantly reduced when carboplatin was combined with centrosome amplification. I conclude that centrosome amplification favors cell death in response to carboplatin in OVCAR8 cells.

I next characterized COV504 and SKOV3. In COV504, like in OVCAR8 cells, a cytostatic effect of carboplatin was noticed. Comparing to control cells, where cell proliferation leads to the generation of 1,2 x 10^6 cells after 72 hours, a reduction in proliferation to almost a half was detected in response to carboplatin (Figure 1.4B). These data suggest that carboplatin reduces proliferation in COV504 cells. In conditions where carboplatin was combined to extra centrosomes, 2 x 10^5 cells were generated after 72 hours, but a significant difference was not detected when comparing cell proliferation in response to carboplatin depending on the centrosome status. Thus, carboplatin reduces cell proliferation in COV504 cell line, independently of the number of centrosomes.

Then I wanted to investigate if carboplatin and centrosome amplification modulate cell death in COV504 cells. At 48 hours, 94% of the cells were alive and a reduction to 80% after 72 hours was observed (Figure 1.4C). In control cells, viability remained constant through time. I conclude that COV504 cells are sensitive to carboplatin, reaching its maximum

effect at 72 hours. Combination of centrosome amplification and carboplatin resulted in 76% of viability after 72 hours. Although the difference with cells without centrosome amplification was not significant, the same tendency as in OVCAR8 to increase cell death in response to carboplatin in presence of supernumerary centrosomes, was observed in COV504. Thus, centrosome amplification seems to sensitize COV504 to carboplatin, even if into a smaller extent compared to OVCAR8 cells.

In SKOV3 cells, a decrease in cell number induced in the presence of carboplatin was noticed over time. The number of cells went from $1,3 \times 10^5$ at 48 hours and to $9,4 \times 10^4$ at 72 hours, indicating a cytostatic effect of carboplatin in the SKOV3 cell lines (Figure 1.4B). However, cell proliferation was not impacted when carboplatin was combined with centrosome amplification. Therefore, carboplatin reduces cell proliferation in the SKOV3 cell line independently of centrosomes number.

Related to cell death, after 48 hours, 92% of the cells were still alive, but it decreased to 66% after 72 hours. In the control group, cell viability remained constant over time, with mean values close to 98%. These findings show that the SKOV3 cell line is sensitive to carboplatin and secondly, that the maximum effect of carboplatin is observed after 72 hours. Importantly, when centrosome amplification was combined with carboplatin, a significant difference was not observed. Therefore, I concluded that centrosome amplification does not favor cell death in response to carboplatin in SKOV3 cells.

1.5 Section 1 conclusion: centrosome amplification enhances cell death in response to chemotherapy in some but not all ovarian cancer cell lines.

Together, my results from the proliferation and viability assays in response to chemotherapy show the following. Centrosome amplification favours cell death in response to carboplatin, paclitaxel and their combination in OVCAR8. This increased cell death only leads to a mild decrease in cell proliferation, most likely because of the dominating cytostatic effect of these drugs.

This effect of centrosome amplification on cell death in response to chemotherapy seems to depend on the cell type studied. For COV504, the sensitization to paclitaxel in presence of supernumerary centrosomes is also observed, and also for carboplatin but to a lesser extent. For SKOV3 however, I detected no effect of centrosome amplification on cell proliferation or viability, irrespective of the chemotherapy applied.

Results – Section 2

2 - Centrosome amplification improves the response to chemotherapy both dependently and independently of mitotic defects

2.1 Live imaging approaches show that centrosome amplification favours cell death in response to combined chemotherapy in OVCAR8 cells

I wanted to verify the hypothesis that centrosome amplification favours the response to carboplatin and paclitaxel in epithelial ovarian cancer cell lines. Moreover, I was interested in investigating the mechanisms responsible for increased cell death in the presence of centrosome amplification and the combination of paclitaxel and carboplatin. Taking into consideration the results obtained previously, we decided to focus on the characterization of two out of the three cell lines initially selected: OVCAR8 and SKOV3. OVCAR8 cells were chosen because they showed the best response to chemotherapy when extra centrosomes were present in proliferation and viability assays. SKOV3 cells, on the other hand did not show an improved response and so they were used as a point of comparison.

We chose to use live imaging approaches following the set up depicted in Figure 2.1A. Epithelial ovarian cancer cell lines have been transfected to stably express H2B-RFP, which allows to visualize the nucleus in interphase and chromosomes during mitosis. Centrosome amplification was induced for 72 hours as before. Cells were incubated with a combination of paclitaxel and carboplatin or of DMSO and water as a control for 72 hours. During this incubation time with chemotherapy, cells were filmed for 72 hours using a spinning disc microscope. Images were acquired every 10 minutes. Importantly, the four different conditions were filmed at the same time and two replicates were realized by Frances Edwards, a post doc in the lab. To analyse the movies, I used a pipeline also developed by Frances Edwards and a macro installed in ImageJ. This pipeline allowed me to track single cells through different generations, recording their behaviour in mitosis and interphase and correlating it with cellular fate.

Figure 2.1

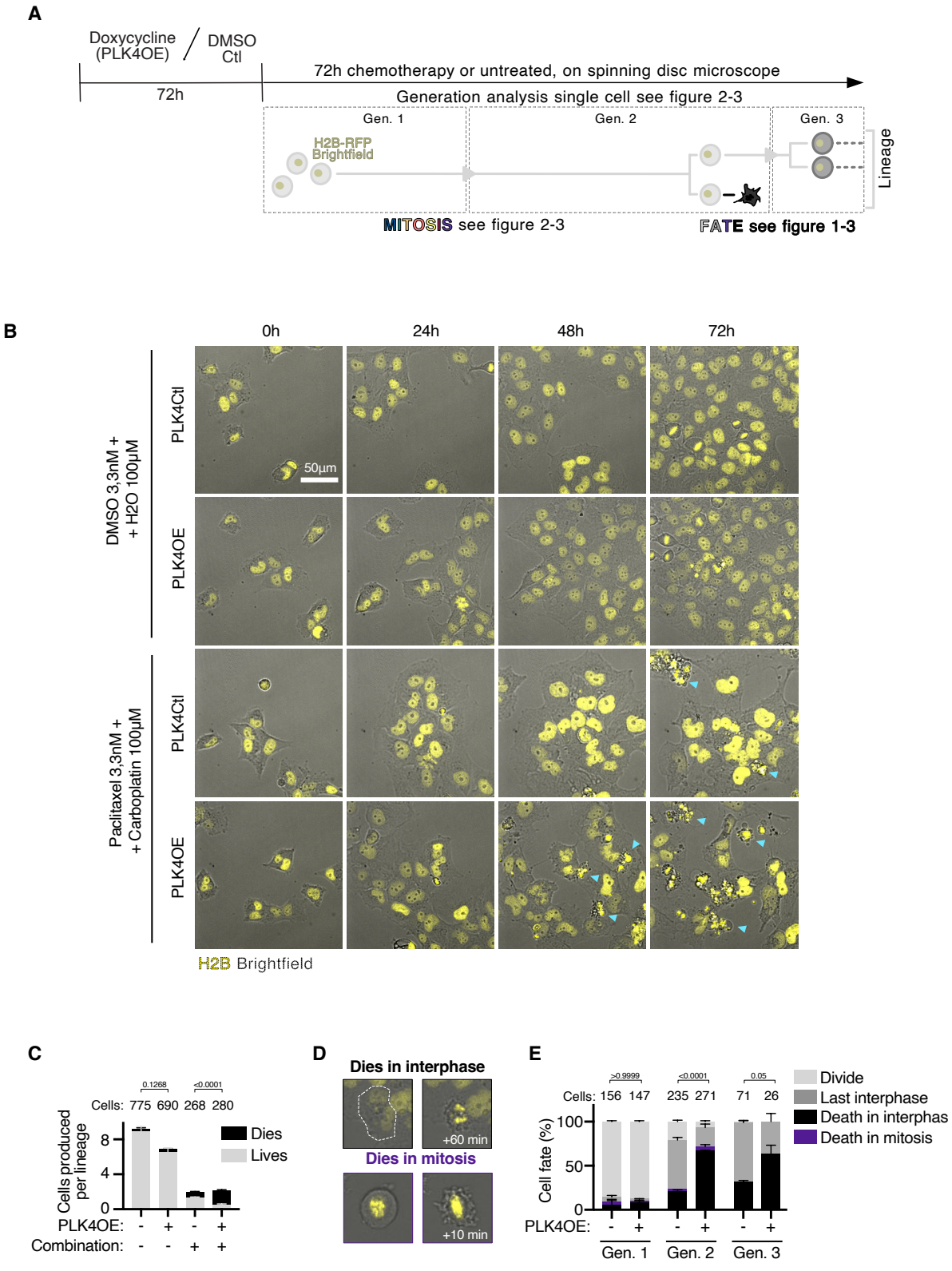

Figure 2.1: Centrosome amplification favors cell death in response to paclitaxel and carboplatin, during the interphase of the 2nd cell generation

(A) Single-cell live-imaging workflow performed with a spinning disc microscope. The lineages were tracked over multiple generations. Lineage analysis consists in counting for each starting cell, the number of cells adopting different fates. Generation analysis consists in determining the percentage of a generation that will adopt the different fates. Mitosis and fate correlation involves assessing the percentage of cells that assume distinct fates, depending on the behavior of the mother cell during mitosis. (B) Representative stills from live images of OVCAR8-H2B cells. The same field for each condition is shown throughout time progression, at 0, 24, 48 and 72 hours of chemotherapy treatment. Each line of the panel corresponds to a different condition, from top to bottom: PLK4Ctl and PLKOE in chemotherapy control conditions (DMSO plus water); PLK4Ctl and PLKOE in combined chemotherapy (paclitaxel 3,3nM plus carboplatin 100μM). Light-blue arrow heads indicate dead cells. (C) Bar graphs showing the average and SEM of the percentages of cells undergoing indicated fates in the legend. Numbers on the top of each graph represent the number of cells analyzed per condition from two independent experiments. Statistical tests: Fisher's exact test on the number of cell death events (pooling death in interphase and death in mitosis). (D) Representative stills from live imaging of cell fates are shown. DNA from a single cell is highlighted by the dashed white line. (E) Bar graphs showing the average and SEM of the percentage of cells undergoing indicated fates, listed in the figure legend, according to the cell generation. Numbers on the top of each graph represent the number of cells analyzed per condition from two independent experiments. Statistical tests: Fisher's exact test on the number of cell death events (pooling death in interphase and death in mitosis).

From a starting cell, I recorded the behaviour of each daughter through the whole movie duration. Each mother cell defines, with its full progeny, a lineage. An overview of cell behavior is showed in Figures 2.1B and C and 2.3A and B, where every line represents a single cell progressing through the cell cycle. First, I will describe the results relative to the combination of paclitaxel and carboplatin in presence of centrosome amplification, in OVCAR8 and SKOV3 cell lines. Then, I will present the results for carboplatin alone in presence of centrosome amplification.

Initially I wanted to confirm the results from proliferation and viability assays (Results - Section 1). Thus, I focused on proliferation, assessed as the number of cells produced per lineage after 72 hours. In OVCAR8 control cells, a single cell produced a mean of 9 daughter cells after 72 hours (Figure 2.1B upper panels, 2.1C and 2.2B). Moreover, a very low rate of cell death was associated with these cells (Figure 2.1C). This indicates that the filming conditions are not phototoxic for the cells. In the presence of centrosome amplification each mother cell produced a mean of 7 daughters over 72 hours. Also in this case, very low levels of cell death were detected and a significant increase in cell death was not noticed when

comparing these two conditions. These data confirm that centrosome amplification is not sufficient to induce cell death in OVCAR8 cells.

Then, I analysed the effect of combined chemotherapy according to centrosome numbers. After 72 hours, only a mean of two cells was produced from a starting mother cell (Figure 2.1B, bottom panels, - 2.1C). Moreover, cell death was associated with the response to combined chemotherapy, as expected from the proliferation and viability assays. Finally, a mean of 2 cells was generated from a mother cell in the presence of centrosome amplification and combined chemotherapy. Importantly, a significant increase in the levels of cell death was observed when extra centrosomes were present (Figure 2.1C). In conclusion, these results reinforce the initial hypothesis that centrosome amplification favours the response to combined chemotherapy in epithelial ovarian cancer cells. Moreover, these findings confirm results previously obtained via proliferation and viability assays.

To better understand how centrosome amplification affects cell death in response to the combination of paclitaxel and carboplatin, I characterized the fate of each cell according to the generation. The relative quantifications are depicted in Figure 2.1D-E. The fates I characterized comprised: cell division, cell surviving without dividing and cell death. I distinguished cell death according to the phase of the cell cycle, namely if it took place during interphase or mitosis. In response to combined chemotherapy, 86% of cells divided during the first generation. Levels of cell death occurring both in interphase and in mitosis were very low, respectively of 5% and 4%. In contrast, only 20% of the cells divided in the second generation and an even lower percentage in the third generation. Indeed, 55% of cells were maintained during interphase in the second generation. The frequency of cell death in response to combined chemotherapy was 33% in the second generation. Therefore, the impact of combined chemotherapy is observed primarily in the second generation of cells, with cells being arrested or delayed in interphase as the most frequent behaviour.

In conditions of centrosome amplification and combined chemotherapy, I observed 87% of the cells dividing during the first generation (Figure 2.1E). Very little cell death occurred during either interphase or mitosis with rates of 8% and 2%, respectively. In contrast, in the second generation, only 6% of cells divided and cellular division was undetected in the third generation. 23% of the cells were delayed in interphase, while 67% of the cells died in interphase. In the presence of combined chemotherapy, cell death was significantly increased when extra centrosomes were present. This effect only occurred

during the second and third generations. In conclusion, most of the cells divide only once in response to combined chemotherapy independently from their centrosomes status, underlining again the strong cytostatic effect observed in the proliferation and viability assays. Moreover, the combination of paclitaxel and carboplatin induces two fates not seen in control cells in the second and third cell generation: cell cycle arrest or death in interphase. Importantly, centrosome amplification appears to shift the rates between these two fates towards cell death.

2.2 Centrosome amplification induces slight mis-segregation errors during mitosis

Both combined chemotherapy and centrosome amplification have the potential to affect mitosis (Ganem et al., 2009; Scribano et al., 2021; Siddik, 2003a). I characterized different behaviours observed during cell division in the time lapse movies. I focused on the first mitosis because, as shown in the previous paragraph, only a single mitosis occurred in conditions of combined chemotherapy and centrosome amplification in the majority of OVCAR8 cells. Examples of different mitotic behaviours are depicted in Figure 2.2A. Mitosis with no mis-segregation errors were considered when the chromosomes separated into two sets without any DNA structure being present between the two poles. Considering mitotic defects, I distinguished chromatin bridges, lagging chromosomes and misaligned chromosomes. Chromatin bridges were annotated when thin threads of chromatin were detected during anaphase (Chan et al., 2009b). Lagging chromosomes when one or more delayed chromosome masses were noticed between the two main chromosome masses at anaphase (Cimini et al., 2004b; Thompson dan Compton, 2011). Chromosome misalignment was observed as chromosomes separate from the metaphase plate, and observed in a polar position during anaphase. These three behaviours were not always easy to identify and distinguish because of the imaging and time resolution used. Thus, I classified lagging chromosomes and chromatin bridges in the “slight mis-segregated” category.

Figure 2.2

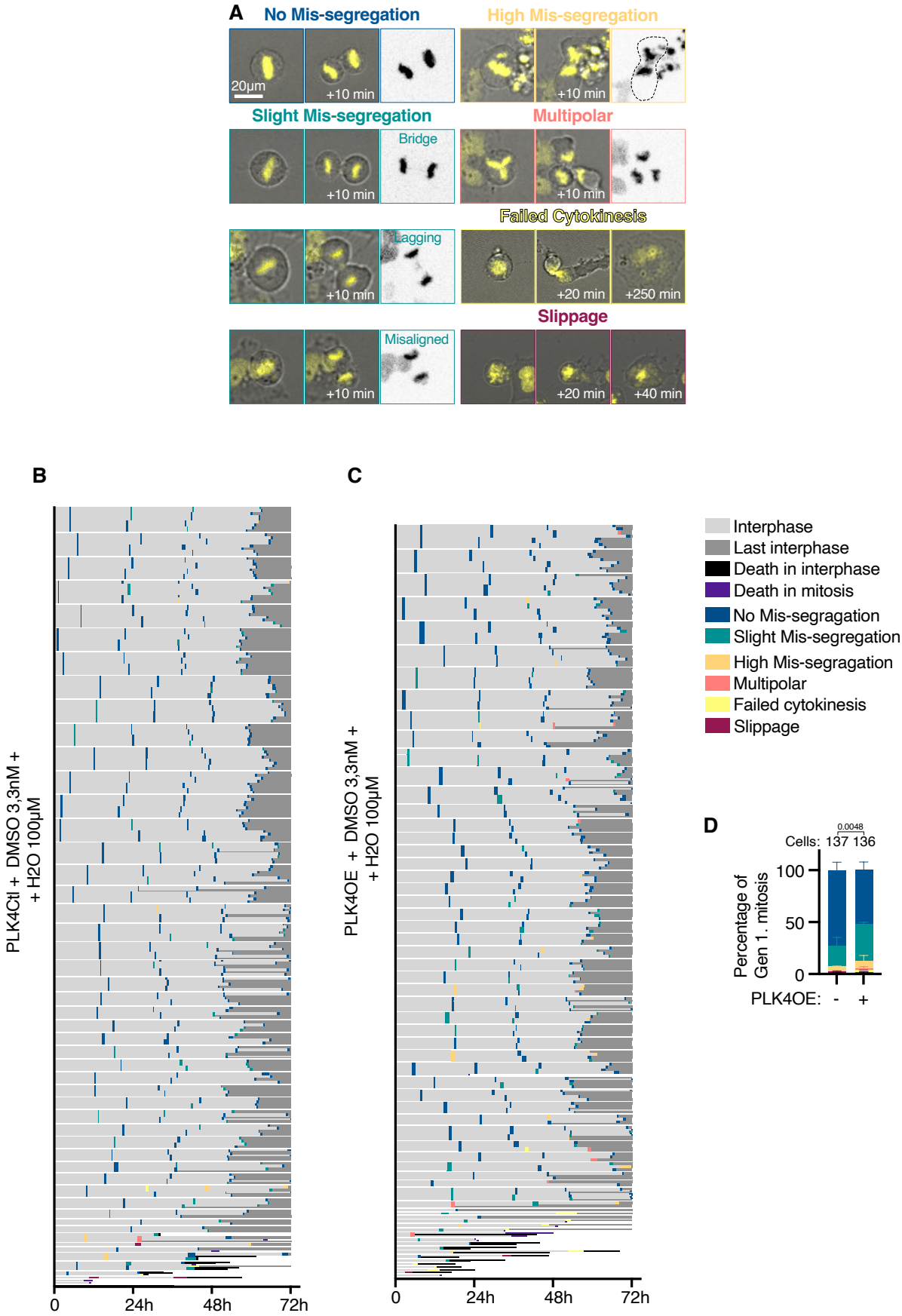
A
No Mis-segregation
High Mis-segregation
20µm
+10 min
+10 min
Slight Mis-segregation
Multipolar
Bridge
+10 min
+10 min
Failed Cytokinesis
Lagging
+10 min
+20 min
+250 min
Slippage
Misaligned
+10 min
+20 min
+40 min
B
PLK4Ctl + DMSO 3.3nM + + H2O 100µM
0
24h
48h
72h
C
PLK4OE + DMSO 3.3nM + + H2O 100µM
0
24h
48h
72h
Interphase
Last interphase
Death in interphase
Death in mitosis
No Mis-segragation
Slight Mis-segregation
High Mis-segragation
Multipolar
Failed cytokinesis
Slippage
D
0.0048
Cells: 137 136
Percentage of Gen 1. mitosis
100
50
0
PLK4OE: - +

Figure 2.2: Mitotic phenotypes characterization in OVCAR8 cells

(A) Representative stills from live imaging of mitotic behaviors in OVCAR8-H2B cells. Images are shown with the color-coded legends used in the subsequent panels. Chromatin from H2B-RFP signal is shown in yellow. Black and white panels highlight chromatin (in black) at anaphase in the different conditions. (B– C) Single cell profiles of PLK4Ctl (B) and PLK4OE (C) untreated cells. Each line represents the life of a cell throughout the 72 hours movie. Color coding of mitosis and fates refers to categories defined in panel A with legend reported beside. (D) Average and SEM of the percentages of mitotic phenotypes (legend above) observed in the first mitosis for each cell. from two independent experiments. Statistical test: Fisher's exact test on the number of Slight mis-segregation events.

On the other hand, I used the "High mis-segregation" to classify cells where a large fraction of chromosomes failed to align during metaphase, resulting in the presence of undefined chromosome masses at anaphase making it hard ot establish the contributions of chromatin bridges, lagging chromosomes and/or misaligned chromosomes. Divisions were categorized as "Multipolar" when more than two sets of chromosomes at anaphase were observed , giving origin to two or more daughter cells (Silkworth et al., 2009). Moreover, we also considered cytokinesis failure, when anaphase occurred but the cytoplasm failed to separate into two daughter cells and mitotic slippage, defined as mitotic entry followed by mitotic exit and DNA decondensation before anaphase, with consequently generation of one single cell.

In control cells, 77% of mitosis showed no errors in chromosome segregation, while 15% of mitosis presented slight mis-segregation events (Figure 2.2B-D), suggesting that control OVCAR8 present a considerable level of chromosome instability (CIN). In cells with centrosome amplification, the frequency of slight mis-segregation was increased to 38% (Figure 2.2C-D) and consequently, error-free mitosis were decreased to 48%. High mis-segregation errors or multipolar events remained infrequent. This suggests that OVCAR8 cells, in the presence of extra centrosomes, can undergo bipolar mitosis, probably through mechanisms of centrosome clustering. However, as expected from previous studies, I observe increased CIN most likely associated with the establishment of syntelic or merotelic attachments(Basto et al., 2008; Silkworth et al., 2009; Ganem et al., 2009). I conclude that centrosome amplification does indeed increase CIN compared to control OVCAR8, but not to high levels owing to efficient centrosome clustering mechanisms.

2.3 Centrosome amplification favors cell death in response to combined chemotherapy by inducing multipolar divisions

I next analyzed the effect of combined chemotherapy in OVCAR8 cells and found that 40% of the cells had error- free mitosis (Figure 2.3A, C). Slight or high mis-segregation events represented respectively 21% and 22% of all mitosis, whereas multipolar divisions were restricted to only 6% of the cells. Other types of mitotic defects were rare. Compared to controls, I observed an increase in the global levels of mitotic errors, as expected from the combination of paclitaxel and carboplatin. The correlation between the type of mitosis and cell fate are shown in figure 3.2C. 7% of cells died even if undergoing mitosis without segregation defects, while 10% of the cells that died showed slight mis-segregation events. As expected, cell divisions with major chromosome segregation defects were associated with higher rates of cell death: 38% after high mis-segregated mitosis and 47% after multipolar mitosis.

Importantly, however the frequency of abnormal mitotic behaviors changed in the presence of extra centrosomes (Figure 2.3B, C). Error-free mitosis only represented 15%, slight mis-segregated mitosis 14% and high mis-segregated 13%. Remarkably, 47% of mitosis were multipolar. The frequency of multipolar divisions was significantly increased when combined chemotherapy and centrosome amplification were present compared to combined chemotherapy alone. This suggests that in presence of combined chemotherapy, OVCAR8 lose their capacity to cluster supernumerary centrosomes. Moreover, 80% of the progeny of multipolar divisions died in the following interphase in conditions with extra centrosomes. This therefore shows that enhanced cell death is observed in response to chemotherapy in presence of supernumerary s=centrosomes, because of the occurrence of lethal multipolar divisions.

Interestingly however, levels of cell death were also higher following other types of mitotic errors, in the presence of centrosome amplification. 35% in the category of slight mis-segregation errors and 68% after high mis-segregated mitosis died compared to 10% and 38% in cells without centrosome amplification. Surprisingly, following mitosis with no errors, 43% of the cells also died if centrosome amplification was present resulting in a significant increase in levels of cell death compared to combined chemotherapy alone.

Overall, these data indicate that combined paclitaxel and carboplatin mostly induce cell death via abnormal mitosis. However, in presence of centrosome amplification, cell death

is enhanced both via an increased proportion of lethal multipolar divisions, but also by a mitosis independent susceptibility to cell death.

Figure 2.3

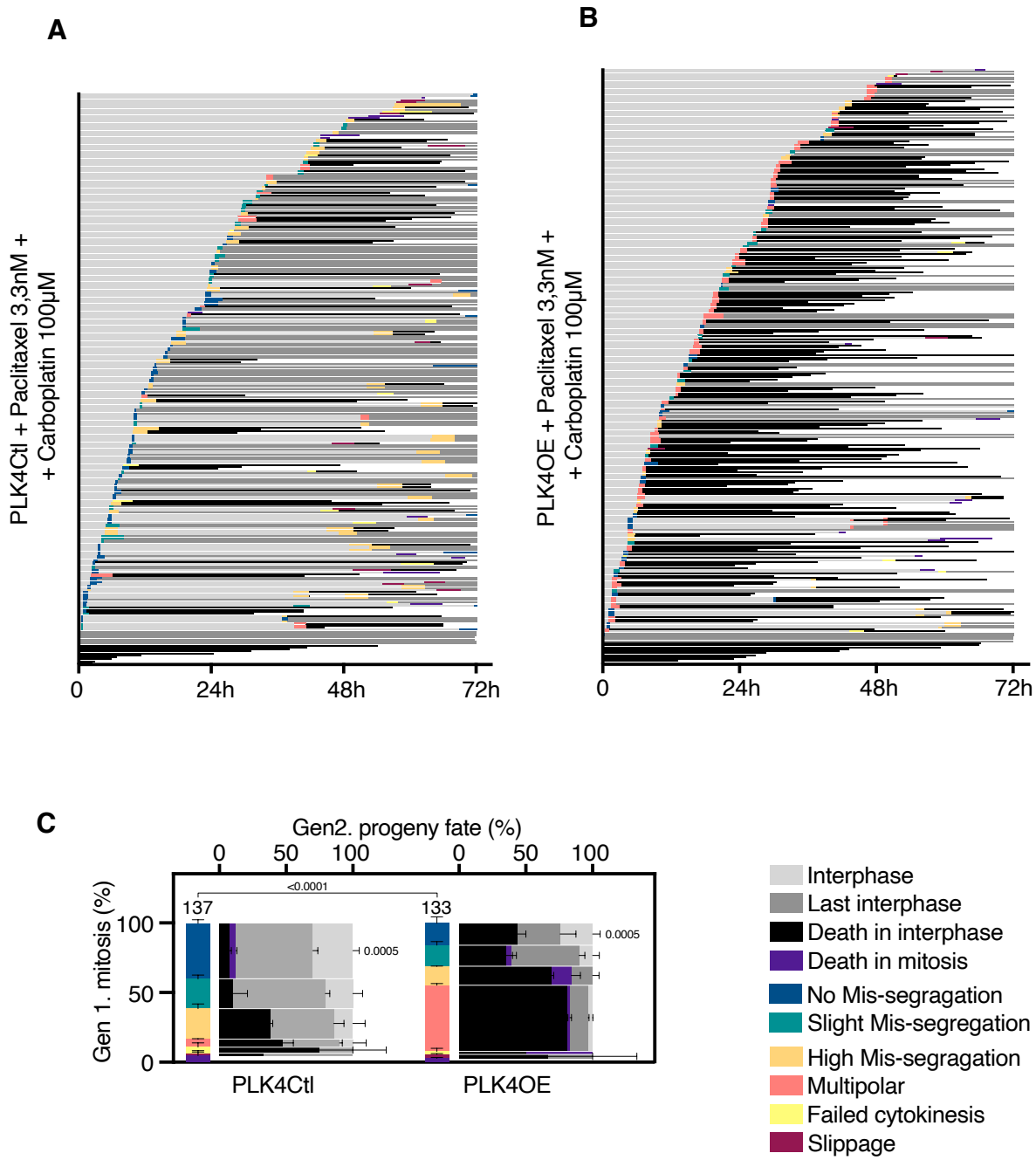

Figure 2.3: Centrosome amplification induces increased cell death due to the generation of multipolar mitosis in response to combined chemotherapy

(A) Single cell profiles of PLK4Ctl (A) and PLK4OE (B) undergoing Carboplatin + Paclitaxel exposure at the indicated concentrations. Each line represents the life of a cell throughout the 72 hours movie. Color coding of mitosis and fates are listed in the legend below, same figure. Cells are ordered, from bottom to top,

according to increasing time of first mitotic entry, defined as the time of Nuclear Envelope Breakdown (NEB). (C) Vertical axis: Bar graphs showing the average and SEM of the percentages of mitotic phenotypes of the first cell generation according to the accompanying legend. 137 and 133 cell divisions were analyzed for PLK4Ctrl and PLK4OE OVCAR8 cells, respectively from two independent experiments. Statistical test: Fisher's exact test on the number of multipolar divisions. Horizontal axis: Bar graphs showing the average and SEM of the percentages of cells undergoing the indicated cell fates according to the mitotic behavior of the mother cells, with bar width depending on the proportion of cells displaying a given mitotic phenotype. Two independent experiments, statistical test: Fisher's exact test on the number of No mis-segregation progeny (progeny of blue mitosis) dying in mitosis and interphase.

2.4 Centrosome amplification does not favour cell death or multipolar divisions in response to carboplatin and paclitaxel in the SKOV3 cell line

SKOV3, one of the epithelial ovarian cancer cell line initially selected, did not show increased response to carboplatin and paclitaxel in the presence of centrosome amplification in proliferation and viability assays (Results – Section 1). I characterized the behaviour of SKOV3 cell lines by live imaging approaches as described above for OVCAR8 cells. I used SKOV3 cells stably expressing H2B-RFP to visualize chromatin. Live imaging was analysed for four conditions, with centrosome amplification, the combination of carboplatin and paclitaxel and the respective controls as described in paragraph 2.1 (Figure 2.1 A).

SKOV3 control cells produced on average 5 daughter cells per mother cell within the 72-hour timeframe (Figure 2.4 A, upper panel, -B), showing reduced proliferation compared to OVCAR8 cells. A decrease in the number of daughter cells was noticed in the presence of centrosome amplification with an average of 3 daughters over the same period of time. Very low levels of cell death were detected in both conditions. In the presence of combined chemotherapy, the number of cells generated was even lower, but this did not change when extra centrosomes were present (Figure 2.4A, bottom panels, - B). Furthermore, as expected, increased cell death was observed in response to combined chemotherapy but without a significant increase when extra centrosomes were present. Therefore, both centrosome amplification and combined chemotherapy, reduce cell proliferation. Combined chemotherapy induces cell death independently from the centrosome status in SKOV3 cells.

Figure 2.4

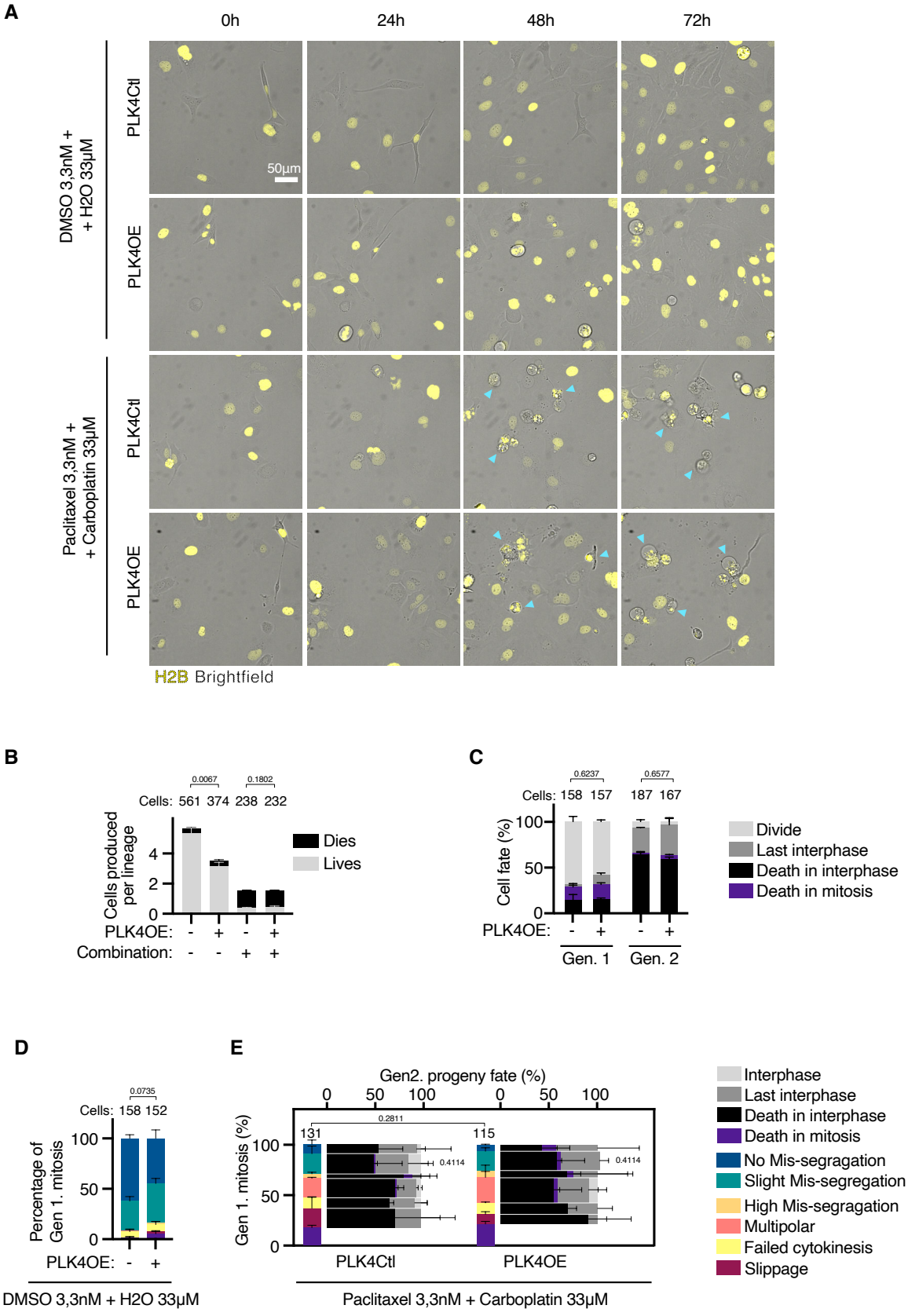

Figure 2.4: The presence of extra centrosomes does not promote cell death in response to carboplatin and paclitaxel in the SKOV3 cell line

(A) Representative stills from time-lapse movies of SKOV3-H2B. The same field for each condition is shown throughout time progression, at 0, 24, 48 and 72 hours of chemotherapy treatment. Each line of the panel corresponds to a different condition, from top to bottom: PLK4Ctl and PLKOE in chemotherapy control conditions (DMSO plus water); PLK4Ctl and PLKOE in combined chemotherapy (paclitaxel 3,3nM plus carboplatin 3,3μM). Light-blue arrow heads indicate dead cells. (B) Bar graphs showing the average and SEM of the percentages of cells undergoing indicated fates in the legend. Numbers on the top of each graph represent the number of cells analyzed per condition from two independent experiments. Statistical tests: Fisher's exact test on the number of cell death events (pooling death in interphase and death in mitosis). (C) Bar graphs showing the average and SEM of the percentages of cells undergoing indicated fates as indicated, according to cell generation. Numbers on the top of each graph represent the number of cells analyzed per condition from two independent experiments, statistical tests: Fisher's exact test on the number of cell death events (pooling death in interphase and death in mitosis). (D) Average and SEM of the percentages of mitotic phenotypes (legend besides panel E) observed in the first mitosis for each cell from two independent experiments. Statistical test: Fisher's exact test on the number of Slight mis-segregation events. (E) Vertical axis: Bar graphs showing the average and SEM of the percentages of mitotic phenotypes of the first cell generation as indicated. 131 and 115 cell divisions were analyzed for PLK4Ctrl and PLK4OE SKOV3 cells, respectively from two independent experiments. Statistical test: Fisher's exact test on the number of multipolar divisions. Horizontal axis: Bar graphs showing the average and SEM of the percentages of cells undergoing indicated fates, according to the mitotic behavior of mother cells, with bar width depending on the proportion of cells displaying a given mitotic phenotype, from two independent experiments. Statistical test: Fisher's exact test on the number of No mis-segregation progeny (progeny of blue mitosis) dying in mitosis and interphase.

To better characterize the SKOV3 response to paclitaxel and carboplatin, I investigated levels of cell death, occurring in interphase or in mitosis, according to the cell generation. In response to combined chemotherapy, 69% of the cells divided during the first generation (Figure 2.4C). The levels of cell death, whether occurring in interphase or mitosis, were 14% and 15% respectively. Conversely, in the second generation, 28% of cells were in their final interphase and 64% of cells died during this interphase. These data indicate that cell death in response to combined chemotherapy represents the major fate of SKOV3 cells, occurring in the second generation. When extra centrosomes were present, 58% of the cells divided during the first generation (Figure 2.4C). Cell death was detected during either interphase or mitosis, with rates of 15% and 16% respectively. In contrast, in the second generation approximately 33% of cells were in their final interphase, while 59% of cells died. Significant differences in the levels of cell death were not detected in either the first or in the second generation according to centrosome number. All together, these results validate the findings

obtained from previous proliferation and viability assays, confirming that centrosome amplification does not favour the response to carboplatin and paclitaxel in SKOV3 cells. The effect of combined chemotherapy achieves its maximum during the second cell generation also in SKOV3 cells. However, differently from what I observed in OVCAR8 cells, the most frequent effect of chemotherapy in SKOV3 cells is cell death occurring during the second generation and this independently from extra centrosomes.

I also investigated the mitotic behaviour of SKOV3 cells by analysing the behaviour of chromosomes during their first division. To classify mitotic defects, I used the same classification described previously or OVCAR8 (Figure 2.2A). In the control group, 62% of mitosis exhibited error-free chromosome segregation, while 29% of mitosis showed slight mis-segregation events (Figure 2.4D). The frequency of higher levels of chromosome mis-segregation or mitotic failure was rare, representing only 9% of the overall mitosis. In the presence of centrosome amplification, 45% of the cells showed error-free mitosis and 39% slight mis-segregation errors. Moreover, multipolar divisions were not detected, suggesting that SKOV3 can efficiently cluster supernumerary centrosomes. Considering mitotic defects in the presence of chemotherapy, slight or high mis-segregation events occurred in 20% and 6% of the cells respectively, while multipolar divisions represented 19% of divisions and only 9% showed error-free mitosis (Figure 2.4E). Moreover, errors in mitotic exit were also detected, with 11% of the cells undergoing cytokinesis failure, 19% mitotic slippage and 18% showing death in mitosis. The correlation between the type of mitosis and cell fate is depicted in Figure 2.4E. Surprisingly and unlike in OVCAR8, there was little association between the type of mitosis and the following cell fate. Indeed, in absence of mitotic errors, 55% of cells died, while 73% died after multipolar divisions.

The combination of centrosome amplification and chemotherapy resulted in 6% of the cells showing lack of mitotic errors, 19% showed slight mis-segregation errors and 7% high levels of mis-segregation. Multipolar divisions represented 25 % of all mitosis. Remarkably, an increase in the levels of multipolar divisions was not detected according to centrosome number, which is different from the results obtained for OVCAR8 cells. Considering the cells that failed to exit mitosis, I noticed that 11% failed cytokinesis, 10% showed mitotic slippage while 21% died during mitosis. In terms of cell fate, 43% of the cells showing error-free mitosis, 50% showing slight mis-segregation defects, 69% with high mis-segregation errors

and 55% displaying multipolar configurations died in the following interphase, showing no striking differences compared to cells without centrosome amplification.

I therefore concluded that multiple differences define the response to chemotherapy in SKOV3 compared to OVCAR8, explaining why centrosome amplification doesn't have the same effect on this response. First, cell death rather than cell cycle arrest is the main response to chemotherapy in absence of centrosome amplification. Second, this cell death seems largely unrelated to the behaviours observed during mitosis suggesting that CIN isn't what is driving cell death in SKOV3. Finally, these data show that centrosome amplification does not promote multipolar divisions in response to paclitaxel and carboplatin in the SKOV3 cell line.

2.5 Centrosome amplification favors cell death in interphase in response to carboplatin alone

The results described above show that centrosome amplification promotes the response to combined chemotherapy by increasing the frequency of multipolar divisions. I next investigated the effect of each separate drug on cells with centrosome amplification. Paclitaxel has been suggested to induce multipolar divisions at the clinical relevant doses of 80 mg/m^2 in breast cancer patients (Scribano et al., 2021). Moreover, multipolar divisions induced by paclitaxel have been shown to be exacerbated in presence of extra centrosome in epithelial ovarian cancer cell lines (Edwards et al., 2023) explaining the increase in multipolar divisions I observed in response to combined chemotherapy. I therefore chose to focus next on the influence of centrosome amplification on the response to carboplatin. Proliferation and viability assays indeed showed that centrosome amplification favors cell death in response to carboplatin. I was therefore interested in observing if this is because of more multipolar divisions, or if it is independent of mitosis as observed for the response to combined chemotherapy.

I used the same strategy as described above. I started by validating the findings obtained from the proliferation and viability assays mentioned in chapter I for carboplatin, by performing live-imaging approaches. After a period of 72 hours, I observed that on average, only two cells were produced from a single mother cell in the presence of carboplatin (Figure 2.5A and 2.6A). Notably, a significant decrease in proliferation was evident when comparing the response to carboplatin with control cells. Furthermore, when both centrosome amplification and carboplatin were present, the mean number of cells produced from a single

mother cell was restricted to two cells. The presence of extra centrosomes was linked to a significant increased in cell death (Figure 2.5A-B). Thus, centrosome amplification favors cell death in response to carboplatin in the OVCAR8 cell line, confirming results from proliferation and viability assays.

Figure 2.5

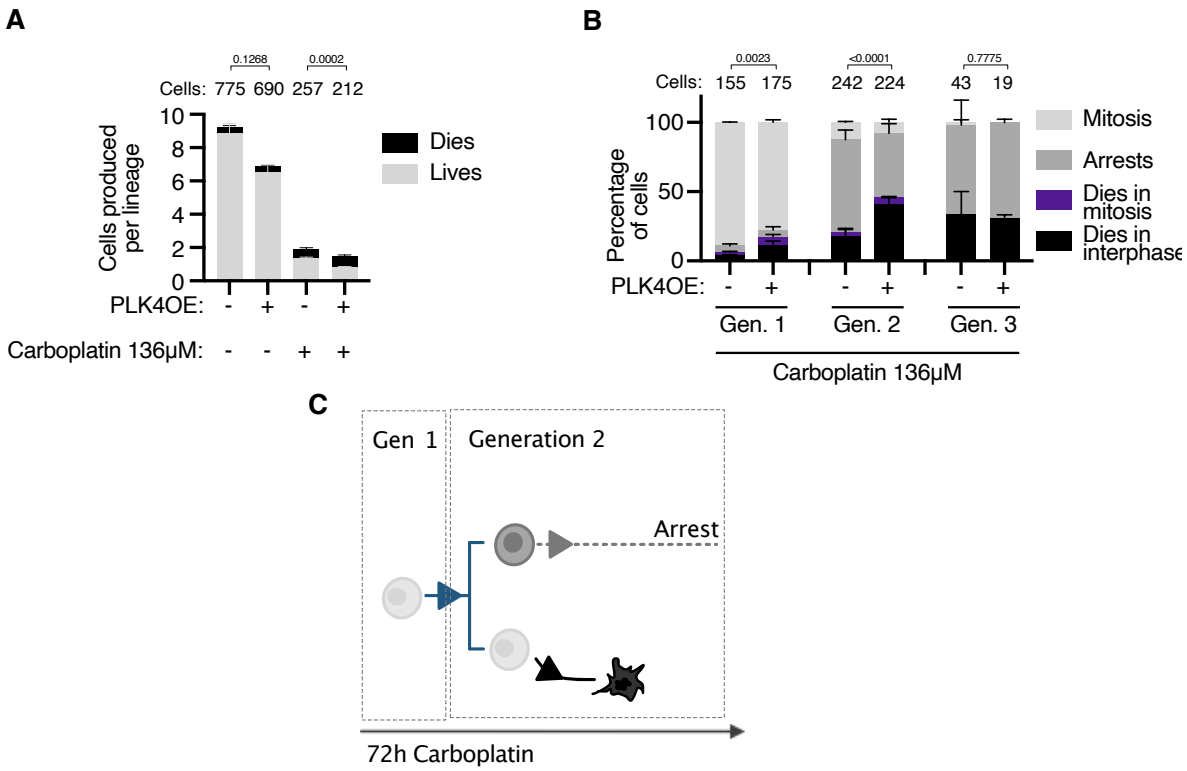

Figure 2.5: Centrosome amplification shifts cell fate towards death in response to carboplatin

(A) Bar graphs showing the average and SEM of the percentages of cells undergoing indicated fates in the legend. PLK4Ctl and PLK4OE OVCAR8 H2B-RFP cells were treated with 136µM of carboplatin or water as a control during the recording. Numbers on the top of each graph represent the number of cells analyzed per condition from two independent experiment. , Statistical test: Fisher's exact test on the number of cell death events (pooling death in interphase and death in mitosis). (B) Bar graphs showing the average and SEM of the percentages of cells undergoing indicated fates, according to cell generation. Numbers on the top of each graph represent the number of cells analyzed per condition, from two independent experiments. Statistical test: Fisher's exact test on the number of cell death events (pooling death in interphase and death in mitosis). (C) Schematic representation of the behavior of OVCAR8 cells observed in response to 136 µM of carboplatin during the 72 hour treatment.

To gain a better understanding of how centrosome amplification influences cell death in response to carboplatin, I analyzed the cell fate according to generation. The results are

shown in Figure 2.5B. Upon exposure to carboplatin, 89% of cells underwent one division during the first generation. The frequency of cell death, both in interphase and mitosis, was very low. In contrast, only 12% of cells divided during the second generation, while 67% were arrested in interphase. Notably, during the second generation, 17% of the cells died, indicating that the strongest effect of carboplatin occurs in the second generation, primarily through cell cycle arrest and cell death in interphase. These observations suggest that the majority of cells divide only once during the 72-hour period.

The analysis of the combination of centrosome amplification and carboplatin showed that 77% of the cells divided during the first generation. Very limited cell death occurred during both interphase and mitosis. However, in the second generation, only 8% of the cells divided, while 45% remained arrested in interphase. Interestingly, cell death increased as 40% of the cells died during interphase. This indicates that centrosome amplification favors cell death in response to carboplatin during the second-cell generation while in interphase. In conclusion, carboplatin induces two main cell fates: death in interphase or cell cycle arrest (Figure 2.5C). Importantly, centrosome amplification shifts the balance between these two fates towards cell death.

2.6 Centrosome amplification promotes the response to carboplatin independently from mitotic errors

Carboplatin induces DNA-crosslinks which can impair the process of DNA replication, resulting in DNA double strand breaks (Unger et al., 2009). If a cell enters mitosis with unrepaired DNA, this can give rise to errors in chromosome segregation, with chromatin bridges being the most frequent mitotic consequence described in the literature (Wilhelm et al., 2014).

I analyzed the first mitosis because, as just shown, the majority of the cells undergo only one mitosis during the 72 hours filmed period. In cells treated with carboplatin, 44% of mitosis did not show any errors (Figure 2.6A and 2.6C). Slight or high levels of mis segregation events represented 21% each, of all cell divisions. Other types of mitotic defects were rare. Importantly, an increase in the overall levels of mitotic errors compared to the control group was observed in response to carboplatin. The correlation between the type of mitosis and cell fate is shown in Figure 2.6A and 2.6C. Cell death occurred mainly because of high mis-segregated mitosis with rates reaching 37%. In contrast, 4% of the cells that had an error-free mitosis died and 11% of those presenting slight mis-segregated mitosis. Thus, “high mis-

segregation" mitosis was the most frequent category of mitotic errors in OVCAR8 cells after treatment with carboplatin.

Figure 2.6

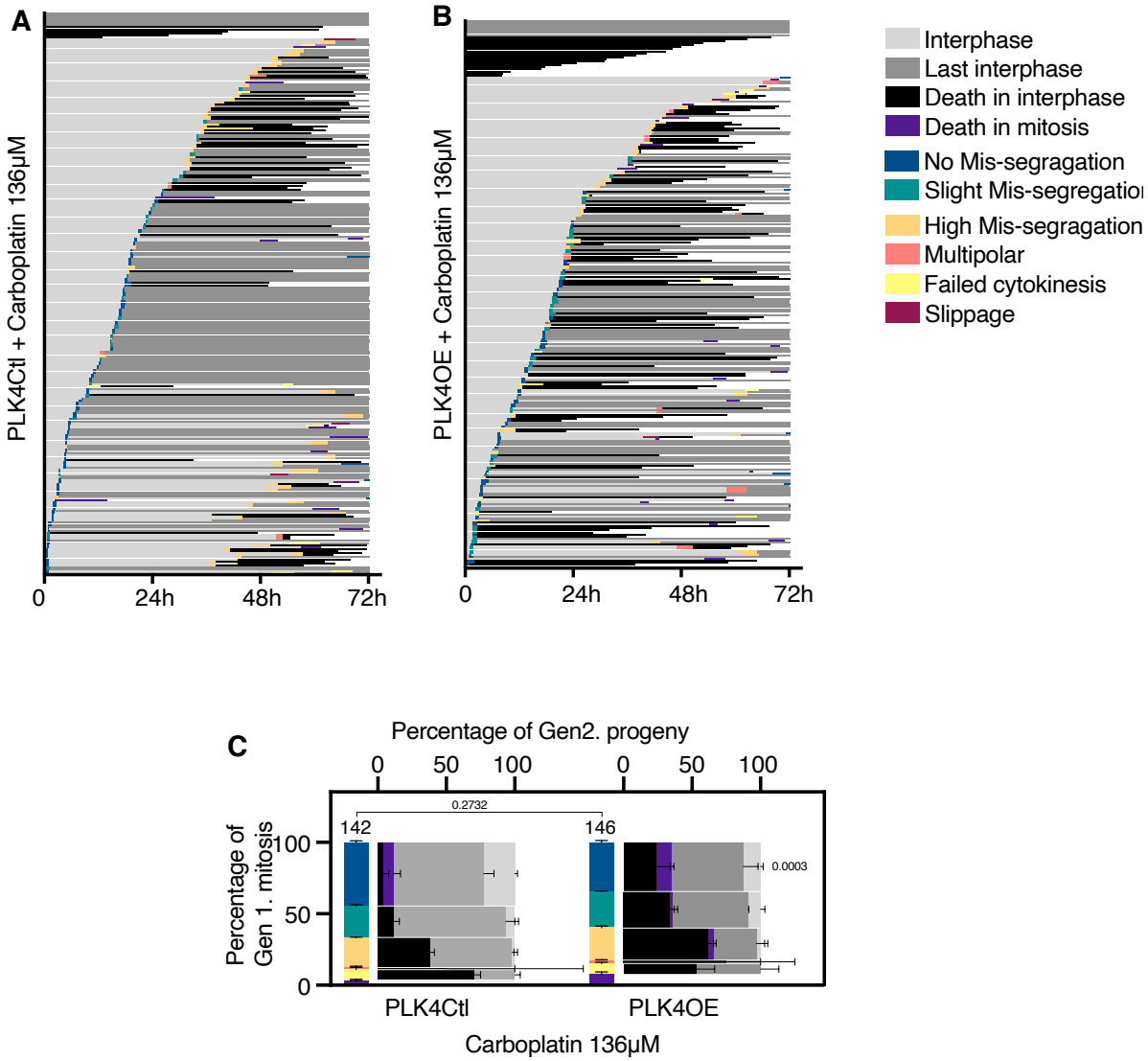

Figure 2.6: Centrosome amplification influences the response to carboplatin independently of mitotic errors

(A– B) Single cell profiles of PLK4Ctl (A) and PLK4OE (B) undergoing Carboplatin exposure. Color coding of mitosis and fates legends in panel besides. Each line represents the behavior of a cell throughout the 72 hour time-lapse. (C) Vertical axis: Bar graphs showing the average and SEM of the percentages of mitotic phenotypes according to the legends above. 142 and 146 cell divisions were analyzed from two independent experiments. Statistical test: Statistical test: Fisher's exact test on the number of No mis-segregation progeny (progeny of blue mitosis) dying in mitosis and interphase. Horizontal axis: Bar graphs showing the averages and SEM of the percentages of cells undergoing indicated fates, according to the mitotic behavior of the mother cell, with the bar width depending on the proportion of cells. Data from two independent

experiments. Statistical test: Fisher's exact test on the number of No mis-segregation progeny (progeny of blue mitosis) dying in mitosis and interphase.

I previously showed that centrosome amplification induces higher levels of cell death in response to combined paclitaxel and carboplatin, relying on an increase in multipolar divisions, but also via a cell death susceptibility independent of mitosis (Figure 2.3). Thus, I wanted to investigate if centrosome amplification favors the response to carboplatin by enhancing specific mitotic errors (Figure 2.6A -C). In the presence of extra centrosomes, the main mitotic phenotypes detected were: error free mitosis- 34%, slight mis-segregation errors- 25% and high mis- segregation errors-22%. Interestingly, multipolar divisions were only found in 2% of the mitotic cells. Moreover, a significant difference in the frequency of mitotic errors was not detected when compared to cells treated with carboplatin. However, the levels of cell death were higher when extra centrosomes were present, independently of the type of division (Figure 2.6C): 23% after error-free mitosis, 34% after slight mis-segregation errors and 61% after high mis- segregation errors. Thus, while carboplatin induces cell death mostly after a catastrophic mitosis, this is not the case when carboplatin is combined to extra centrosomes.

Overall, these results indicate that centrosome amplification does not rely on induction of multipolar divisions to favor the response to carboplatin, as when carboplatin is combined with paclitaxel. In conclusion, centrosome amplification favors the response to carboplatin independently from mitotic errors.

2.7 Both centrosome amplification and carboplatin can affect interphase and mitotic length

Altered cell cycle length- interphase or mitosis- can affect proliferation and in certain occasions even lead to cell death (Malumbres dan Barbacid, 2009, 2001; Massagué, 2004). The centrosome has been described to colocalize with several proteins involved in cell cycle control, such as cyclin B- CDK1, cyclin E- CDK2 and others (Jackman et al., 2003; Lin et al., 2022). Moreover, my previous results from proliferation and viability assay and movies, showed a decrease in proliferation due to centrosome amplification and chemotherapy. I next investigated if centrosome amplification or any of the chemotherapy treatments used above influence cell cycle timing.

Figure 2.7

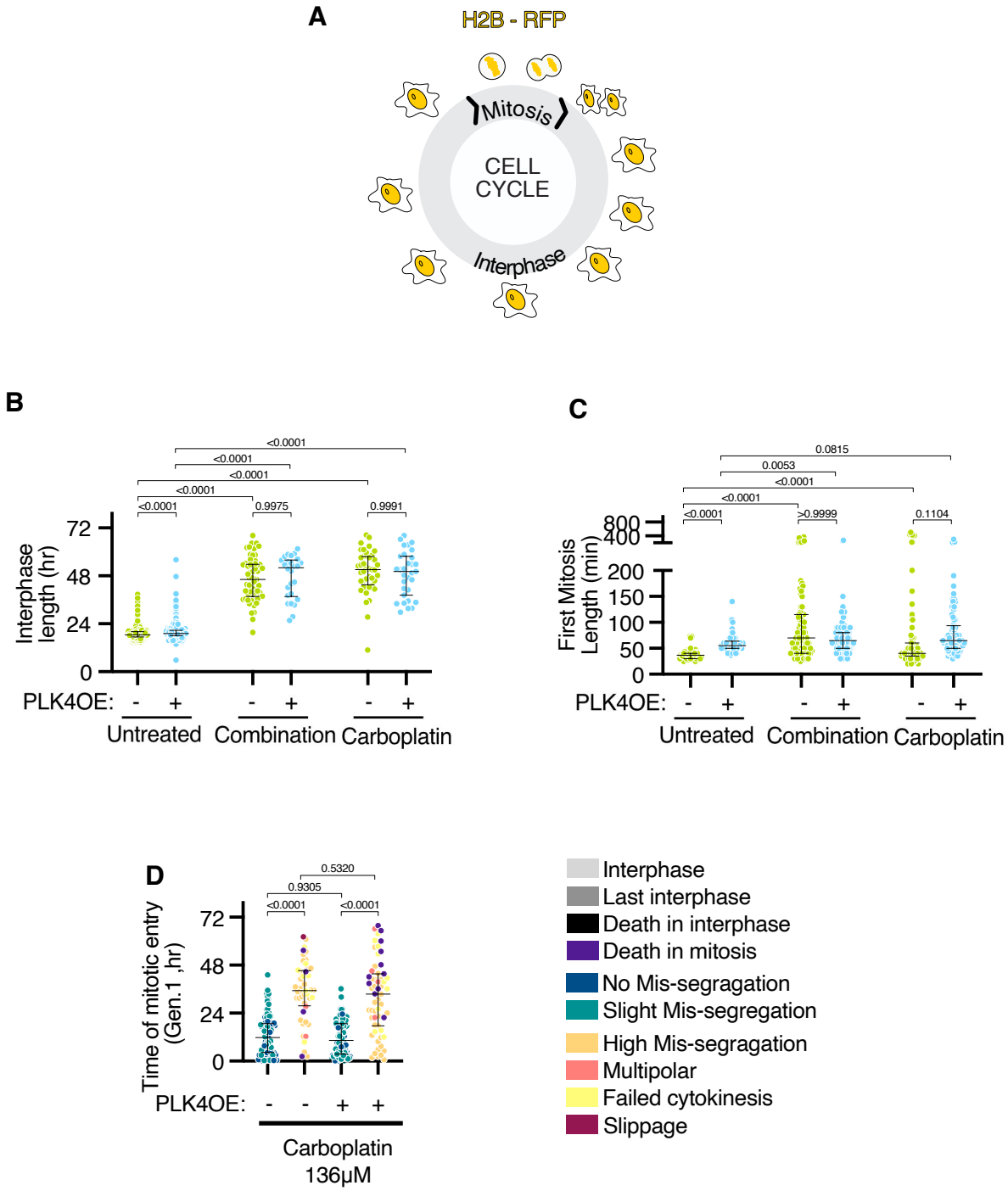

Figure 2.7: Both interphase and mitotic length are increased in response to combined chemotherapy and centrosome amplification

(A) Schematic representation of H2B signal appearance through interphase and mitosis (B– C) Scatter dot plots of interphase length (B) and first mitosis length (C), with median and interquartile range. Data from two independent experiments were pooled for combined treatment and Carboplatin treatment and data from the 4 corresponding control experiments were pooled for untreated conditions. For interphase length, a minimum of 26 cells was analyzed, and for mitosis length a minimum of 133 cells was analyzed. Statistical

tests: Kruskal-Wallis with Dunn's multiple comparisons tests. (D) Scatter dot plot graphs showing time of mitotic entry with median and interquartile range. Cells were classified depending on mitotic phenotypes with color-code defined in the legend. Two independent experiments with a minimum of 48 mitosis analyzed per category. Statistical tests: Kruskal-Wallis with Dunn's multiple comparisons tests.

Control cells spent a mean of 18h30 minutes in interphase and ~37 minutes in mitosis (Figure 2.7B, C). When extra centrosomes were present both interphase and mitotic length were significantly extended, with a mean of respectively 19 hours and 55 minutes. Thus, centrosome amplification seems to increase cell cycle length, affecting both interphase and mitosis.

In response to the combination of paclitaxel and carboplatin, cells spent 46 hours in interphase and 70 minutes in mitosis. A significant difference according to the centrosome status was not observed in addition to combined chemotherapy. In cells exposed to carboplatin alone, interphase was extended to 51 hours while mitosis took around 40 minutes. Again, extra centrosomes did not induce a significant increase in interphase when carboplatin was present: 50 hours. However, a tendency to extended mitosis remained: 65 minutes. I concluded that carboplatin alone or in combination with paclitaxel leads to an extended interphase and mitotic length, but that centrosome amplification doesn't have a significant additional consequence on cell cycle lengthening.

Finally, I wanted to investigate how mitotic entry time correlates with errors in mitosis in the presence of carboplatin (Figure 2.7D). Cells showing lack of mitotic errors or slight mis-segregation errors entered and exited mitosis mostly within the first 24 hours, with a mean equal to 11h 45 minutes for control cells and 10h20 minutes for cells with centrosome amplification. In contrast, cells showing high mis-segregation errors or mitotic failure, entered mitosis later at around 35h20 minutes (without extra centrosomes) and 33h20 minutes (with centrosome amplification). This difference in behavior depending on timing of first mitosis entry suggests an influence of the cell cycle on the effect of carboplatin. Indeed, one explanation could be that cells which received carboplatin earlier in the cell cycle – G1 or early S- and therefore enter mitosis later, have higher frequency of mitotic errors.

In conclusion, both centrosome amplification and carboplatin can impact cell cycle progression in OVCAR8 cells. Given that the response to carboplatin seems to have a strong

dependency on cell cycle stage, I decided to investigate further the relationship between centrosome amplification and cell cycle progression, in relation to the carboplatin response.

2.8 Section 2 conclusion: centrosome amplification enhances cell death in response to chemotherapy via multiple mechanisms.

Together, my results from the live imaging assays in response to chemotherapy show the following. Centrosome amplification is associated with a slight increase in CIN in OVCAR8 which already presents a considerable level of CIN. In response to combined chemotherapy, centrosome amplification favours cell death both by increasing lethal multipolar divisions, but also by favouring cell death independently of mitotic behaviours. In response to carboplatin, centrosome amplification also favours cell death, however without increasing multipolarity. This effect seems to be independent of mitosis behaviours. The live-imaging also shows links between centrosome amplification, carboplatin response, and cell cycle progression so I decided to study this more in the next section.

Results – Section 3

3 - Influence of carboplatin and centrosome amplification on the cell cycle of OVCAR8 cells

3.1 Centrosome amplification reduces cell proliferation by increasing cell cycle length

Results from proliferation assays and from time-lapse movies showed that both centrosome amplification and carboplatin can reduce cell proliferation (Results – Sections 1-2). To investigate if reduced proliferation in the presence of extra centrosomes is due to a cell cycle dysregulation, I chose to use a live imaging approach. I generated a PLK4OE inducible OVCAR8 cell line stably expressing H2B coupled to RFP fluorophore and to Proliferating Cell Nuclear Antigen (PCNA) coupled to emiRFP. PCNA is loaded on DNA during S phase, allowing the visualization of DNA replication phase. Indeed, PCNA is a cofactor of DNA polymerase-δ and it has a major role in DNA replication by increasing the processivity of leading strand synthesis (Bravo et al., 1987; Tan et al., 1986). The behavior of H2B-RFP and PCNA signal through cell cycle is outlined in Figure 3.1.1 B-C.

Figure 3.1.1

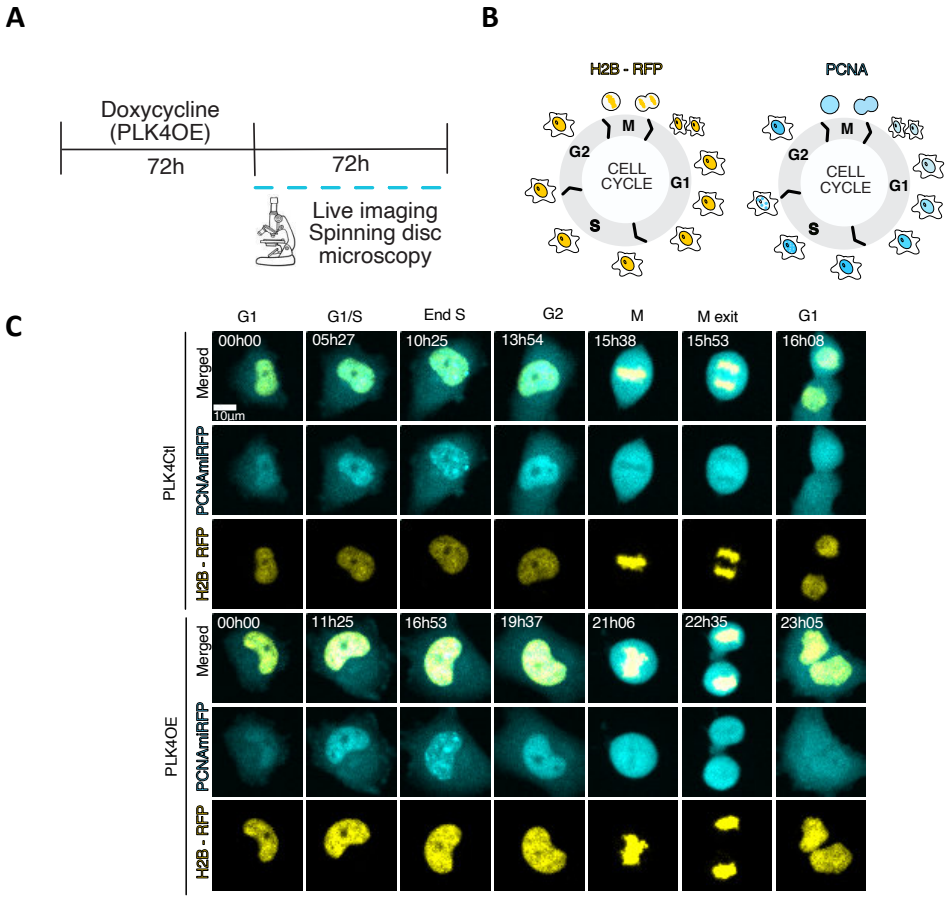

Figure 3.1.1: Generation of OVCAR8 H2B-RFP PCNAmiRFP cell line to study cell cycle length

(A) Schematic representation of the experimental workflow. (B) Schematic representation of H2B-RFP and PCNAmiRFP signals throughout the cell cycle. PCNAmiRFP protein which is loaded on DNA during replication phase (S-phase) appears as a dotting signal marking the end of S-phase. (C) Stills images from time-lapse movies showing H2B-RFP and PCNAmiRFP behaviour through different phases of the cell cycle. Merged and separated channels are shown for PLK4Ctl and PLK4OE. Phases of the cell cycle are indicated above in the panels.

According to the literature, beginning of DNA replication is detectable by appearance of small PCNA foci (Burgess et al., 2012). Unfortunately, I could not distinguish entry in S phase because I could not detect clear formation of small foci. Impairment of PCNA signal can be due to the fact that PCNA is also involved in DNA repair. Indeed, PCNA accumulates at damaged regions, and it is involved in several forms of DNA repair, including Nucleotide Excision Repair pathway (NER)(Essers et al., 2005). Thus, the signal of PCNA is probably disturbed by basal levels of DNA damage present in OVCAR8 cells. On the other end, appearance of big foci clearly marked the exit from S phase (Figure 3.1.1B-C). Thus, even if I was not able to distinguish G1 from S phase, OVCAR8 H2B-RFP PCNAmiRFP cell line still allows me to distinguish clearly cells in G1/S, G2 and M phase.

Progression through cell cycle of single cells was annotated through 72h, for both the conditions with and without centrosome amplification. To record cell behavior, I used a pipeline developed by Frances Edwards, a post-doc in the lab. An overview of cell behavior is showed in figure 3.1.2A, where every row represents a single cell progressing through cell cycle. From the quantification of ~170 cells per condition, I noticed that cell death did not occur in OVCAR8 cells control (Figure 3.1.2A-B). Expectedly, very few cells underwent cell death when PLK4 was over-expressed. This observation confirms that OVCAR8 cells can proliferate despite the presence of extra centrosomes.

Figure 3.1.2

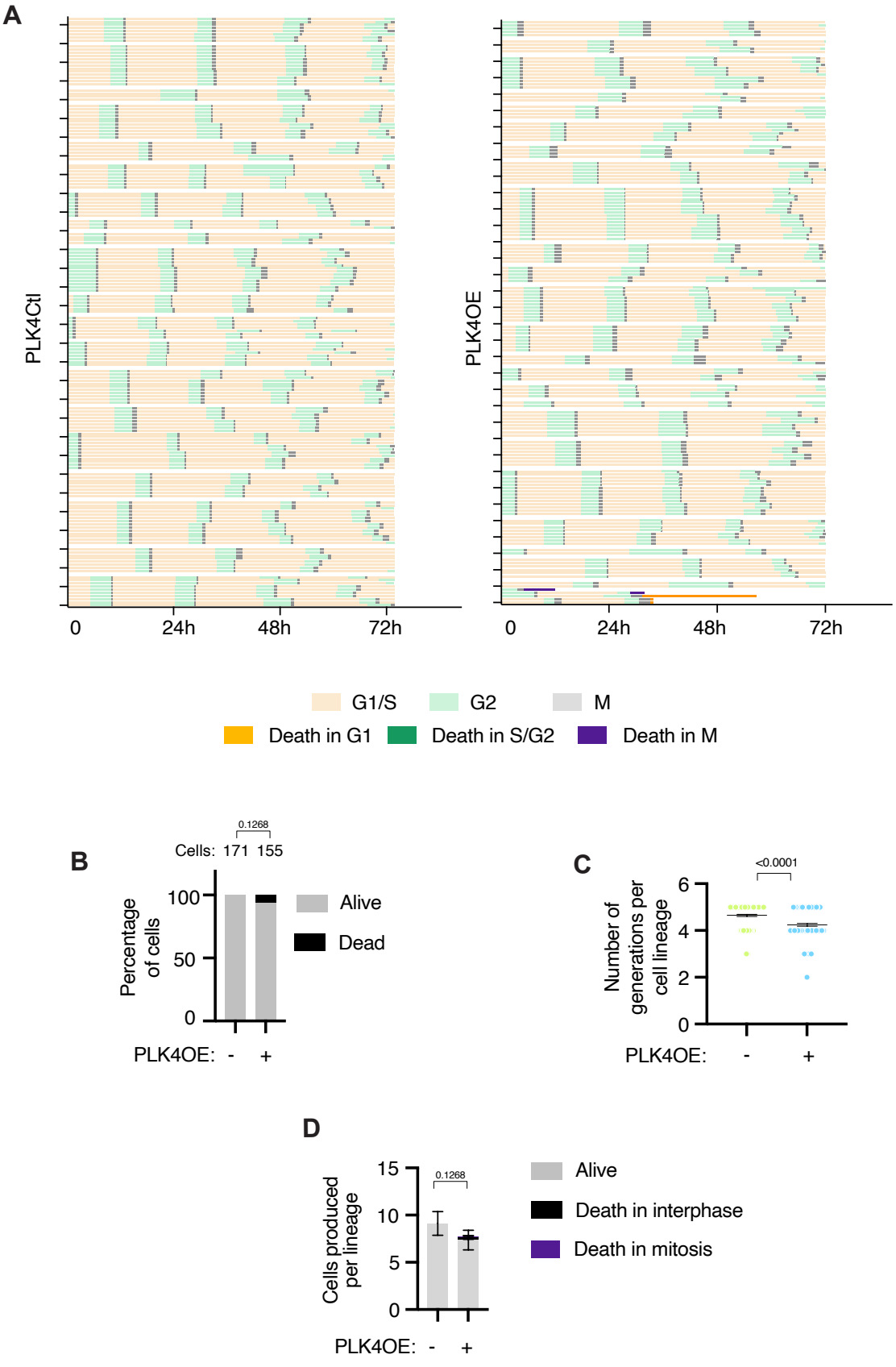

Figure 3.1.2: Centrosome amplification slows down cell cycle progression

(A) Single cell profiles of OVCAR8 H2B-RFP PCNAmiRFP PLK4Ctl and PLK4OE cells. Each row represents the single cell through the 72 hour time-lapse recording. Times in G1, S/G2 and mitosis, as well as death in each of these phases are color- coded as indicated. (B) Bar graphs showing the averages of the percentages of cells undergoing indicated fates. Numbers on the top of each graph represent the number of cells analyzed per condition from two independent experiments. Statistical tests: Fisher's exact test on the number of cell death events (pooling death in interphase and death in mitosis). (C) Scatter dot plot showing the number of generations reached per cell lineage along the 72 hours movie with median and interquartile range. Two independent experiments with a minimum of 10 cell lineages analyzed per category. Statistical tests: Welch's test. (D) Bar graphs showing the average and SEM of the number of cells produced per lineage, adopting the indicated fates. A minimum of 15 lineages were analyzed from two independent experiments. Statistical tests: Fisher's exact test on the number of cell death events (pooling death in interphase and in mitosis).

In control condition, cells could perform on average 5 mitosis during the 72 hours period (Figure 3.1.2C), which shows that cell cycle length is around 20 hours for OVCAR8 cells. In contrast, in conditions where extra centrosomes were present, cells performed a mean of 4 mitosis. This indicates an increase in cell cycle length in cells with extra centrosomes. To investigate if this increase in cell cycle duration is sufficient to decrease cell proliferation, I quantified the number of cells produced per lineage (Figure 3.1.2D). Indeed, in controls each initial cell was able to produce a mean of 9 cells during the 72 hours period. However, cells with extra centrosomes produced a mean of 7 cells in the same period of time. These data confirm the decrease in proliferation detected in proliferation/ viability assays in the presence of extra centrosomes showed in Results Sections 1, and using live-imaging of H@B-RFP expressing cells in Results Section 2. Thus, I concluded that centrosome amplification can reduce cell proliferation by increasing cell cycle length in ovarian cancer cells.

To understand which phase of the cell cycle is affected by centrosome amplification, I analyzed the duration of the G1/S, G2 and M phase separately (Figure 3.1.3A- D). OVCAR8 cells had a mean of G1/S duration of 15,32 hours, which correspond to 77% of the overall cell cycle length. Thus, G1 and S-phase account for the longest cell cycle phases as expected. Surprisingly, cells with extra centrosomes have a significant longer G1/S phase, with a mean of 17,34 hours. Thus, centrosome amplification seems to extend G1/S phase for around 2 hours in the OVCAR8 H2B-RFP PCNAmiRFP cell line. Concerning the G2 phase, OVCAR8 control cells spend on average 3,92 hours in G2, corresponding to around 20% of total cell cycle

duration in G2. Cells with centrosome amplification had also a slightly significant increase in the time spent in G2 (4,93 hours). The observed cell cycle lengthening therefore seems to affect all phases of the cell cycle.

Figure 3.1.3

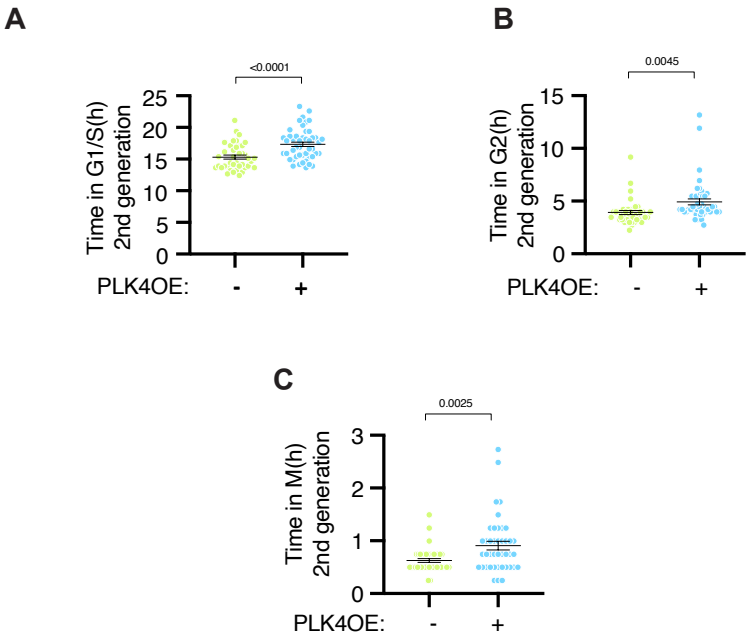

D

Duration (h):	G1/S	G2	M	Total
PLK4Ctl	15,32	3,92	0,63	19,87
PLK4OE	17,34	4,93	0,91	23,18

E

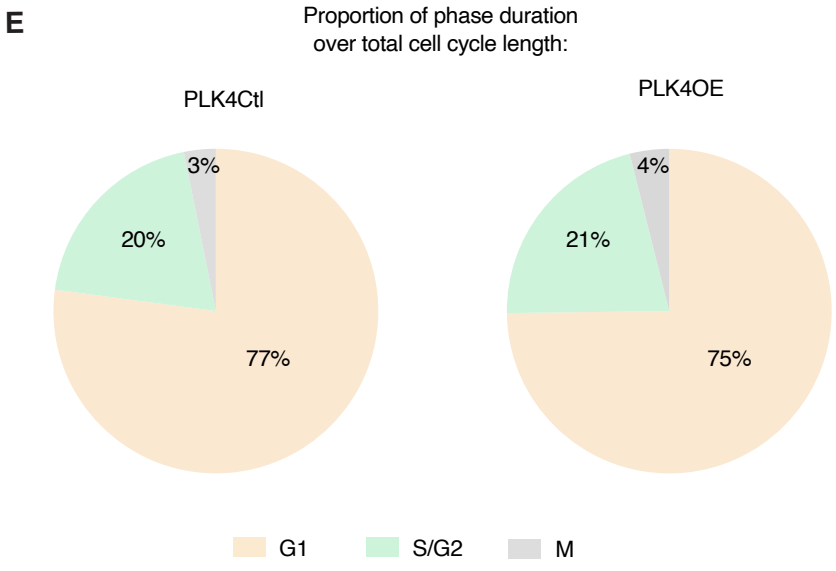

Figure 3.1.3: Centrosome amplification induces an increase in both interphase and mitotic duration
(A– C) Scatter dot plots of cell cycle analysis of OVCAR8 H2B-RFP PCNAmiRFP in their second generation. For each graph, PLK4Ctl and PLK4OE conditions are shown with mean and SEM. Two independent experiments with a minimum of 10 lineages analyzed per category. Statistical tests: Kruskal-Wallis. (D) Table reporting the average duration of different cell cycle phases. (E) Circle chart showing the proportion of each cell cycle phase compared to the overall cell cycle length. Only cells in the second generation were considered. A minimum of 15 lineages were analyzed from two independent experiments.

Finally, I calculated the time cells spent in mitosis. I took into account the time point before nuclear envelope breakdown to the timepoint before anaphase onset. Controls cells spend in mitosis a mean of 0,63 hours, which corresponds to 38 minutes (Figure 3.1.3 C, D). As expected, and as observed in the H2B-RFP expressing cells, cells with extra centrosomes tend to spend a significantly higher amount of time in mitosis, with a mean of 55 minutes. Consequently, cells with extra centrosomes spend almost 20 minutes longer in mitosis. Increased mitotic length for cells with centrosome amplification was already described in the literature (Basto et al., 2008; Kwon et al., 2008; Yang et al., 2008).

Altogether, these data suggest that centrosome amplification reduces cell proliferation by increasing cell cycle length. Both an increase in mitosis and in interphase duration contributes to the cell cycle elongation in presence of extra centrosomes in OVCAR8 H2B-RFP PCNAmiRFP cell line.

3.2 Carboplatin has a cytostatic effect and arrests cells in S/G2 phase

I next investigated how carboplatin affects cell cycle progression. Unfortunately, I could not use H2B-RFP PCNAmiRFP cells because PCNA behavior was altered in carboplatin treated cells. Indeed, PCNA signals were diffuse in the nucleus throughout the movie in the presence of carboplatin. Lack of PCNA foci appearance was most likely due to the high levels of DNA damage induced by the drug. Thus, I chose a different approach: I sorted the OVCAR8 cells according to cell cycle phase *via* flow cytometry. Using this method, every cell is assigned to the corresponding cell cycle phase based on the DNA content. Another advantage of this method is to analyze a great number of cells in a relatively small amount of time.

I incubated cells in doxycycline or DMSO as control for 72 hours, to induce centrosome amplification. Then, I added carboplatin or water as a control. I analyzed cells by flow cytometry after 48 hours and 72 hours incubation in carboplatin (Figure 3.2). As expected,

most control cells at 48h were in G1 (Figure 3.2B, upper panel). G2 cells can be identified according to double the amount of DNA compared to the G1 population. Cells with intermediate DNA content were considered to be in S-phase. These data revealed that S-phase was the shorter phase in the control OVCAR8 H2B-RFP PCNA-emiRFP cells. Significant differences were not detected in cells after 72 hours (Figure 3.2B, lower panel). In cells with centrosome amplification, differences in cell cycle distribution were not evident. The lack of difference in cells in G1 between cells with extra centrosomes and control can be due to the fact that flow cytometry is not sensitive enough to discriminate between cell cycle length differences of just a few hours. Additionally, the cytometry data only provides the relative length of the different phases. As my live-imaging approach showed that centrosome amplification increases cell cycle length globally without affecting a specific cell-cycle phase, I did not necessarily expect to observe different profiles dependent on centrosome status.

Figure 3.2

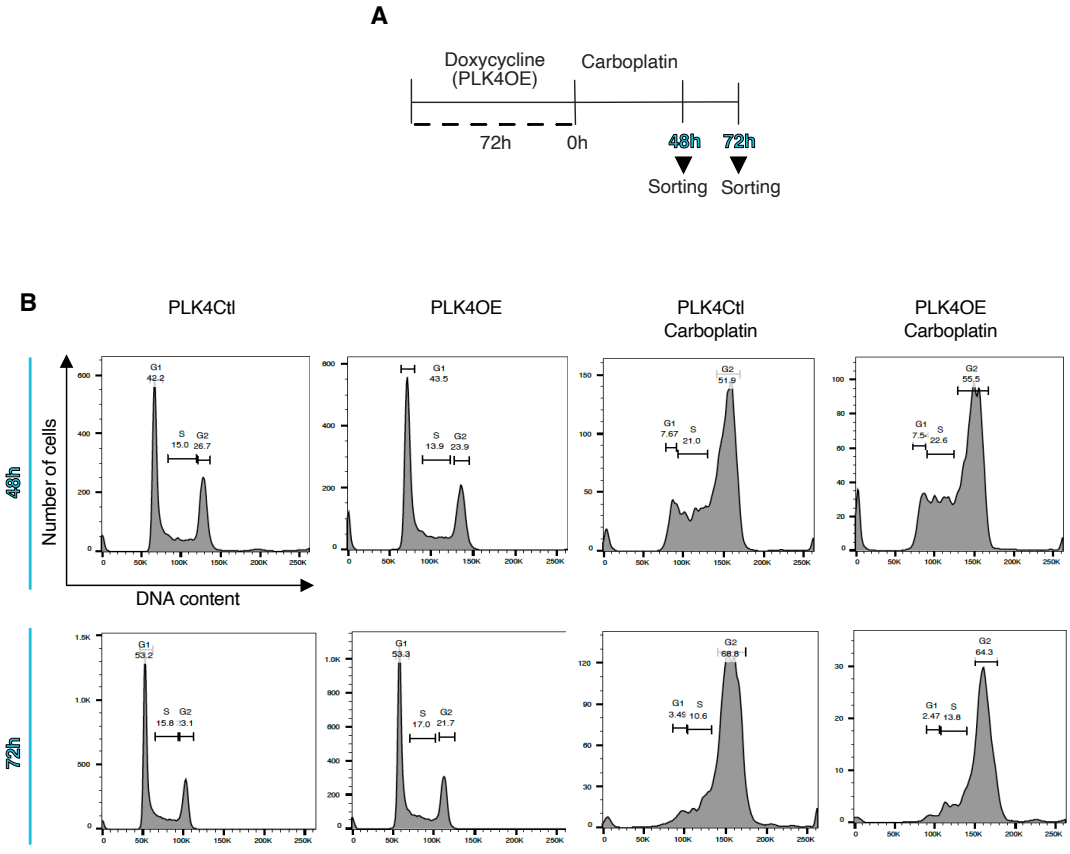

Figure 3.2: Carboplatin induces cell cycle arrest in S/G2 phase

(A) Schematic representation of the experimental workflow. (B) Cell cycle profiles determined by FACS. The graphs illustrate the number of cells (y axes) in the different phases of the cell cycle, determined based on

DNA content (X axes). Cell cycle phase and percentage of cells in each phase are reported on top of the corresponding peak of profiles. Three technical replicates were performed.

I then studied the effects of carboplatin. At 48 hours, only a small proportion of cells appears to be in G1 (Figure 3.2B, upper panel). Most cells have accumulated in S and G2 phase. After 72 hours, almost all cells accumulated in a single peak in S/G2 phase, while the G1 population appeared very reduced (Figure 3.2B, lower panel). This suggests that carboplatin treatment induces a cell cycle arrest in S/G2 phase. These data confirmed the movies results showed in Results - Section 2. I currently cannot conclude if the G1/early S population presented at 48h, undergoes apoptosis or if cells have simply progressed to late S/ G2 phase. A cytostatic effect of carboplatin has already been described in other studies (Siddik, 2003a). In this experimental set up, cells arrest in S/G2 phase, suggesting that OVCAR8 carboplatin treated cells, activate the G2 checkpoint, but they are probably deficient for the G1 checkpoint. Interestingly, analysis of cells with both centrosome amplification and carboplatin, reveal no differences in cell cycle profiles, when compared to carboplatin only treated cells. In conclusion, carboplatin arrests OVCAR8 cells in S/G2 phase.

3.3 Carboplatin has both a cytostatic and a cytotoxic effect occurring in S/G2 phase

I wanted to characterize in which phase of the cell cycle cell death occurs in response to carboplatin and whether this is influenced by the presence of extra centrosomes. Because live- imaging approaches allow to assess cellular fate together with cell cycle progression, I generated an OVCAR8 cell line expressing the FUCCI system (Sakaue-Sawano et al., 2008). The FUCCI system allows to follow cell cycle progression, by the appearance of an RFP signal coupled to Chromatin Licensing And DNA Replication Factor 1 (Cdt1) in G1 phase and GFP signal coupled to Geminin in S/G2 phases (Figure 3.3.1A). Compared with the H2B-RFP PCNAmiRFP reporters, the FUCCI system offers the advantage of allowing to distinguish G1 phase, and of avoiding interference of DNA damage response with the cell cycle progression signals. Because PLK4 was coupled to GFP fluorophore in the original OVCAR8 cell line, I replaced the GFP with an antibiotic resistance gene for blasticidin (see methods). Antibiotic resistance allows to select the cells containing the PLK4 over-expression transgene and avoid overlap of GFP signal (Figure 3.3.1B).

Figure 3.3.1

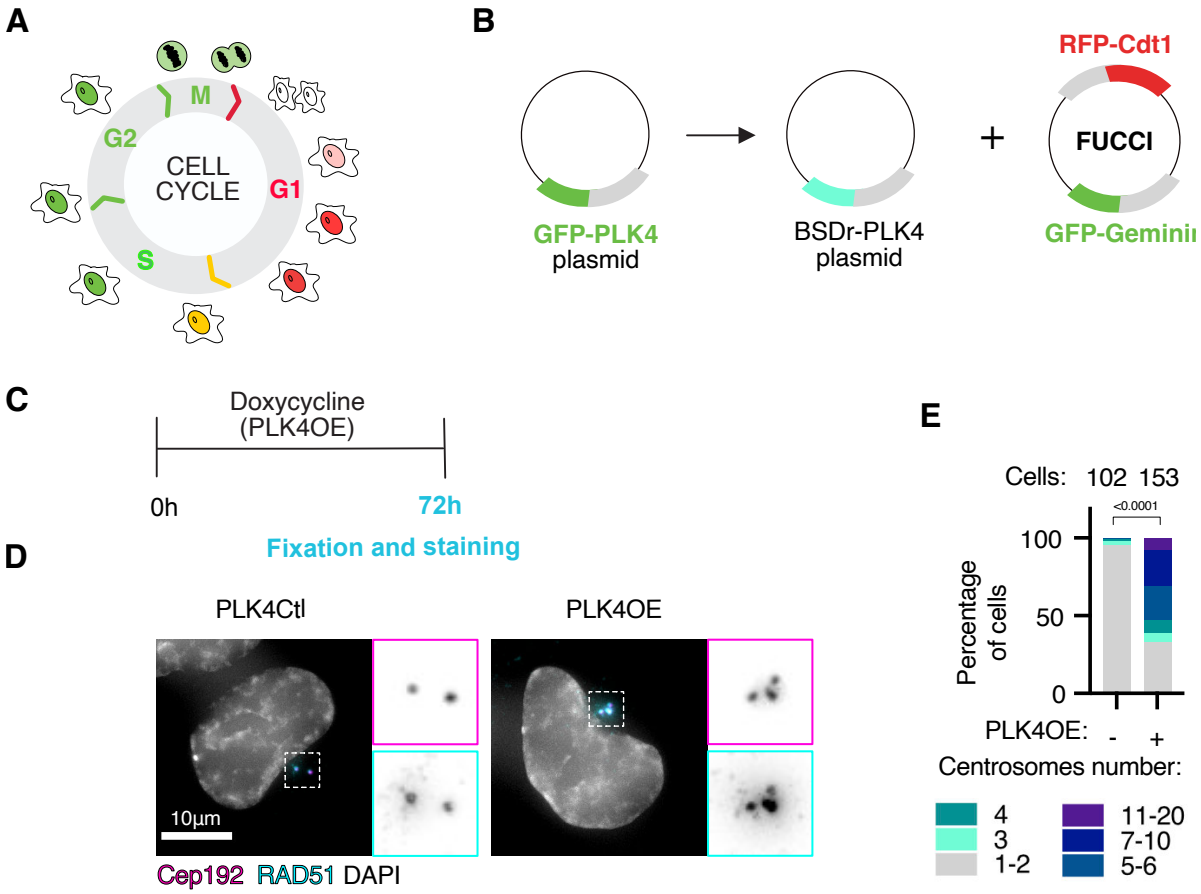

Figure 3.3.1: Generation and characterization of OVCAR8 FUCCI cell line

(A) Schematic representation of the FUCCI system across the cell cycle. (B) Schematic representation of molecular biology strategy used to substitute GFP in PLK4 plasmid with an antibiotic resistance gene for Blasticidin. (C) Schematic representation of the experimental workflow for fixed immunofluorescence imaging. (D) Representative images of cells labeled with antibodies against CEP192 (Cyan) and Pericentrin (magenta). DNA is shown in gray. Two conditions PLK4 control (upper panel) andPLK4 overexpression (lower panel) are shown. Inset displaying zoom of the centrosomes are shown on the right of each image, with color-coded border according to the antibody used. (E) Graph bar showing the SEM of centrosome numbers. Numbers on the top of each graph represent the number of cells analyzed per condition from two independent experiments for each cell line. Statistical test: Fisher's exact test comparing the number of cells with more than 2 centrosomes.

I first confirmed the capacity of the newly generated OVCAR8 FUCCI cell line to amplify centrosomes. I used a fixed imaging approach, as performed in the original OVCAR8 cell line (Figure 3.3.1C-E). To do so, I induced centrosome amplification through incubation with doxycycline as before. After 72 hours I fixed and stained cells with the centrosome markers

CEP192 and Pericentrin. Centrosome amplification was detected in 67% of the cells and the majority of cells showed either 5- 6 centrosomes (22%) or 7-10 centrosomes (23%). Cells with 3, 4 or more than 10 centrosomes were also observed but less frequently (~8% each). The levels of centrosome amplification were comparable to the ones induced in the original OVCAR8 cell line. Thus, the OVCAR8 FUCCI cell line can be used to study effects of centrosome amplification and carboplatin on the cell cycle.

I proceeded to investigate the cell cycle using live imaging approaches of the OVCAR8 FUCCI cell line. After overexpression of PLK4 over 72 hours, cells were incubated with carboplatin and filmed at spinning disc microscope for the following 72 hours (Figure 3.3.2A-C). Importantly, the four conditions with or without centrosome amplification and carboplatin were filmed at the same time. To ensure clarity, I will first describe results relative to centrosomes amplification, followed by results for carboplatin and combination of the two conditions.

The progression of cells through the cell cycle was annotated using a modified version of the pipeline described in the Results - Section 2.1. An example of cell behavior throughout cell cycle is shown in figures 3.3.2B and C. I first wanted to verify the increase in cell cycle length induced by centrosome amplification. To avoid taking into account any perturbation due to the filming conditions, I focused the analysis on the phase length of the second generation of cells (Figure 3.3.2 D-G). Controls cells show a G1 mean duration of 6,84 hours and S/G2 mean duration equal to 12,53 hours. Surprisingly, an increase in time spent in interphase was not detected in the OVCAR8 FUCCI cell line when PLK4 was over-expressed. In control cells, the cell cycle length was globally 1 hour longer in the OVCAR8 FUCCI cell line compared to the OVCAR8 cell lines expressing H2B-RFP and the PCNA chromobody. Whether this can be linked to the different PLK4 over-expression transgene, expression of the FUCCI system, or the selection of cells during cell line establishment remains undetermined at this point. Nevertheless this suggests that cell cycle progression is already altered in the OVCAR8 FUCCI cells compared to the ones used previously, and in this context centrosome amplification seems not to have the same effect on cell-cycle progression. Regarding mitosis

Figure 3.3.2

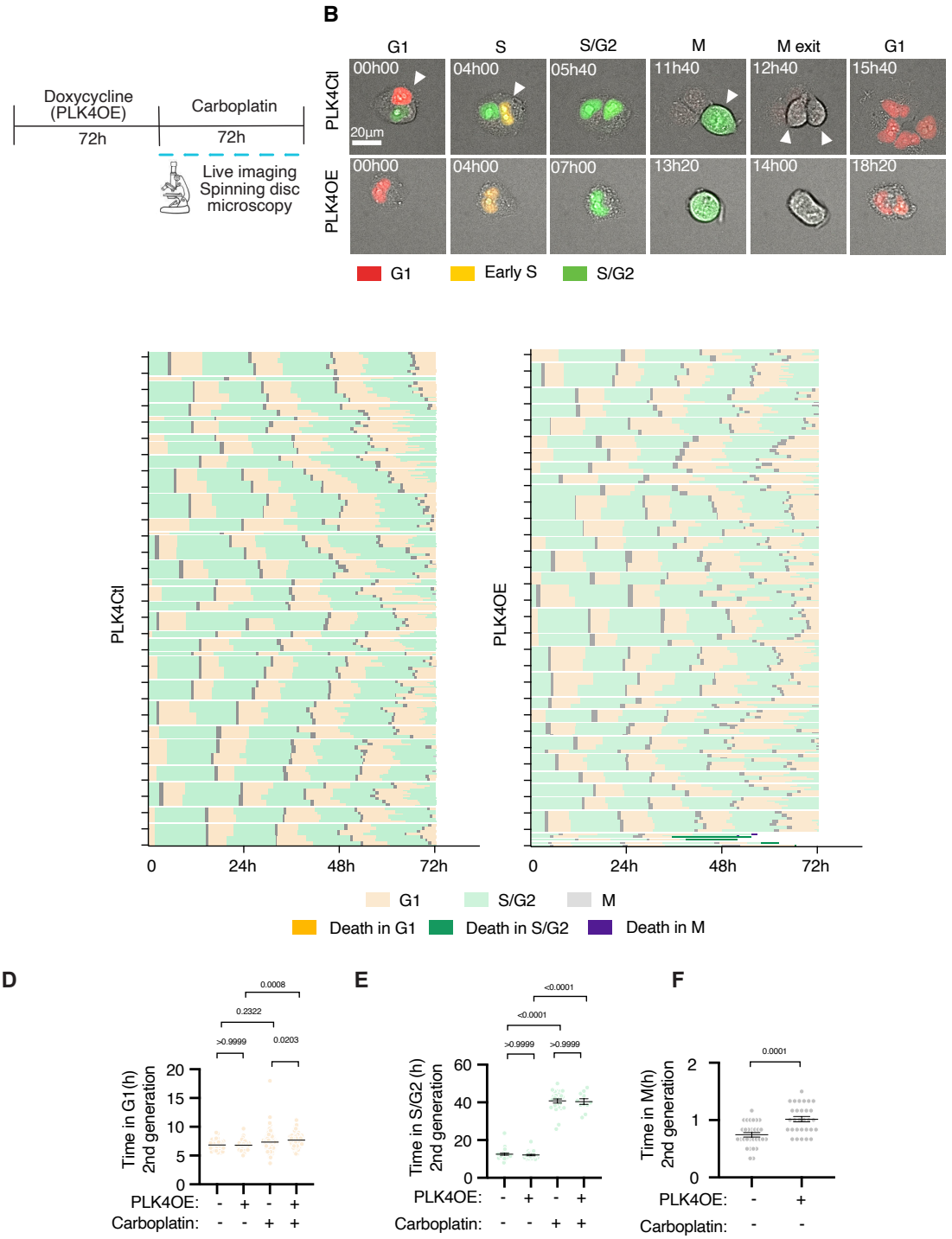

G

Duration (h):	G1	S/G2	M	Total
PLK4Ctl	6,84	12,53	0,74	20,11
PLK4OE	6,81	12,10	1,02	19,93

Figure 3.3.2 : Centrosome amplification and carboplatin influence cell cycle length

(A) Single-cell live-imaging workflow using a spinning disc microscope. (B) Representative stills from time-lapse movies along the cell cycle. Arrows/arrowheads indicate the indicated cell cycle phase (legend on top). (C) Single cell profiles from live-imaging analysis. Each row represents the lprogression of a single cells through the 72 hours of time lapse recording. Time in G1, S/G2 and mitosis, as well as death in each of these phases are color-coded as indicated in the legend below. (D-F) Scatter dot plots showing the time spent in each cell cycle. For each graph, all conditions are shown with mean and SEM. Two independent experiments with a minimum of 15 lineages were analyzed forPLK4Ctl cells and 100 lineages for PLK4OE cells. Statistical test: Kruskal-Wallis. (G) Table reporting the average duration of each cell cycle phase.

however, I found that in control cells mitosis lasted on average 44 minutes. In contrast, in cells with extra centrosomes, mitosis took on average 61 minutes. These results confirm that centrosome amplification increases mitotic duration.

Then, I focused on the effects of carboplatin. I wanted to know in which phase of the cell cycle cell death in response to carboplatin takes place (Figure 3.3.3). Cells in carboplatin spend a mean of 7h in G1, independently of the centrosome status (Figure 3.3.2D). Carboplatin did not induce an increase in G1 length when compared to control untreated cells. However, cells spend a mean of 40 hours in S/G2 in response to carboplatin, which is represents extended timing when compared to control cells. This observation confirms the results obtained by flow cytometry showing that OVCAR8 cells arrested in S/G2 phase in response to carboplatin treatment. Interestingly, cell death occurred almost exclusively in S/G2 phase in both conditions of carboplatin alone or in combination with extra centrosomes (Figure 3.3.3 A-C). These results suggest activation of the G2 checkpoint as a possible mechanism which discriminates between arrest or cell death. Moreover, I found that cell death can occur both at the beginning or at the end of this last S/G2 interphase in response to carboplatin (Figure 3.3.3D). The same happens for carboplatin in combination with extra centrosomes. Thus, cell death seems to occur in response to carboplatin in S/G2 phase, independently from the time spent in this phase.

Figure 3.3.3

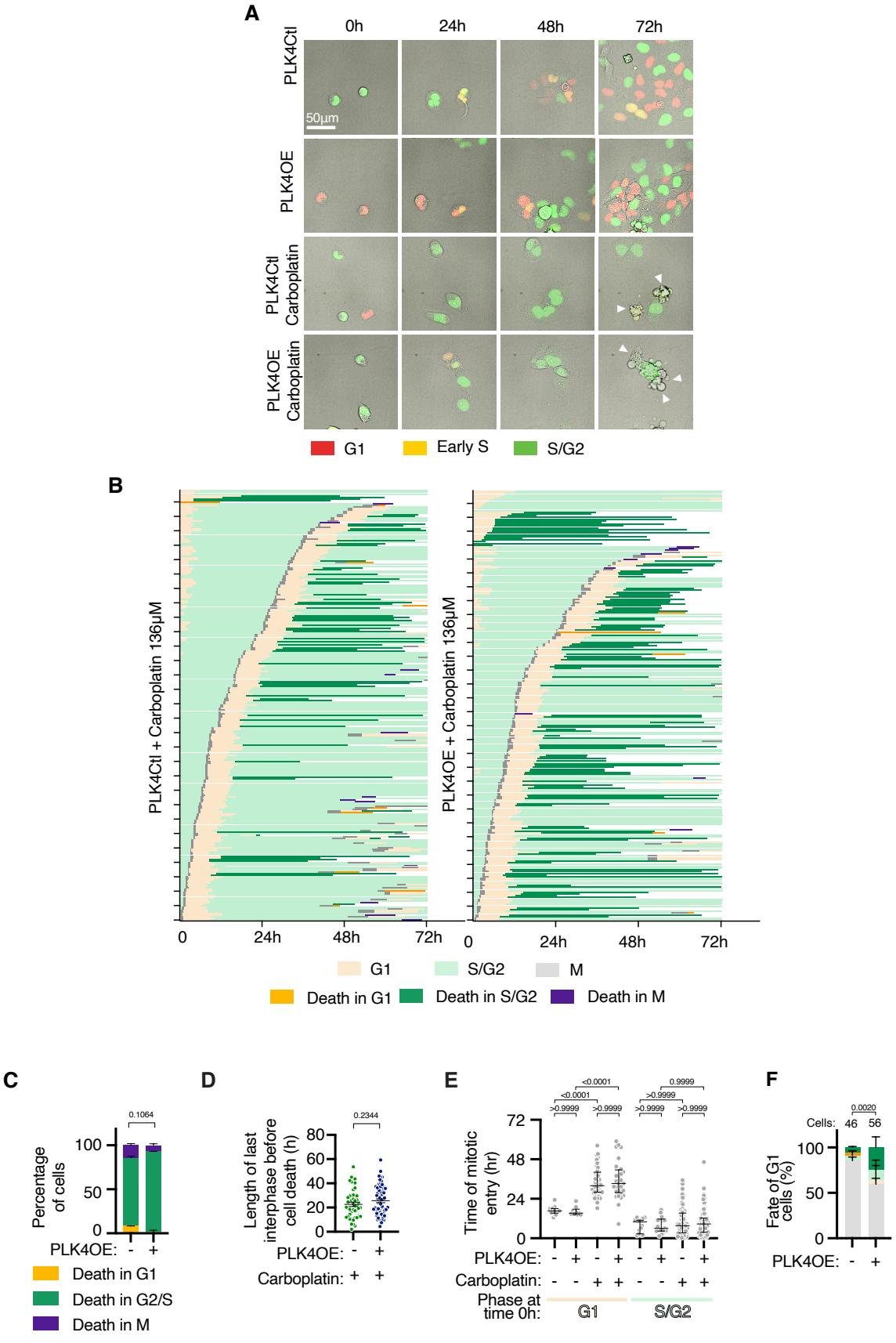
A
0h
24h
48h
72h
PLK4Ctl
PLK4OE
PLK4Ctl Carboplatin
PLK4OE Carboplatin
50µm
G1
Early S
S/G2
B
PLK4Ctl + Carboplatin 136µM
PLK4OE + Carboplatin 136µM
0
24h
48h
72h
G1
S/G2
M
Death in G1
Death in S/G2
Death in M
C
Percentage of cells
0.1064
PLK4OE: - +
Death in G1
Death in G2/S
Death in M
D
Length of last interphase before cell death (h)
0.2344
PLK4OE: - +
Carboplatin: + +
E
Time of mitotic entry (hr)
<0.0001
0.9999
PLK4OE: - + - + - + - +
Carboplatin: - - + + - - + +
Phase at time 0h: G1 S/G2
F
Fate of G1 cells (%)
0.0020
Cells: 46 56
PLK4OE: - +

Figure 3.3.3: Carboplatin induces cell cycle arrest or cell death during S/G2 phase

(A) Representative stills from time-lapse movies of OVCAR8-FUCCI cells described in the previous figure legend. The same field for each condition is shown throughout time progression at 0, 24, 48 and 72 hours of chemotherapy. Arrowheads highlight events of cell death. (B) Single cell profiles from live-imaging analysis. Each row represents the progression of a given cell through the 72 hours of time lapse recording. Time in G1, S/G2 and mitosis, as well as death in each of these phases are color-coded as indicated in the legend below. Cells are ordered, from bottom to top, according to increasing time of mitotic entry, defined as the time of Nuclear Envelope Breakdown. (C) Bar graphs showing the mean and SEM on the percentages of cell death events occurring in the indicated cell-cycle phases from two independent experiments. Statistical test: Fisher's exact test on number of death events occurring in S/G2. (D) Scatter dot-plot representing the length of the last interphase before death occurring in interphase from two independent experiments with a minimum of 10 time points analyzed per category. Statistical test: Mann-Whitney test. (E) Scatter dot plots of the time of mitotic entry depending on cell-cycle phase at the start of the movie, with median and interquartile range from two independent experiments with a minimum of 10 time cell lineages analyzed per category. Statistical tests: Kruskal-Wallis with Dunn's multiple comparisons tests. (F) Bar graphs showing the average and SEM on the percentage of cells adopting the indicated fates (legends in panel B) from two independent experiments. Statistical test: Fischer's exact.

Finally, I correlated mitotic entry timing of a given cell with the corresponding cell cycle phase of this cell at the beginning of the movie (Figure 3.3.3E and F). Control cells entered mitosis after 17 hours, if they were initially in G1 at the start of the movie and after ~27 hours if they were in S/G2. Differences due to the presence of extra centrosomes were not noticed.

Thus, the presence of extra centrosomes does not delay mitotic entry in this cell line. Carboplatin treated cells entered mitosis after a mean of 35 hours if they received carboplatin in G1. Instead, if at the beginning of the movie cells were in S/G2 they entered mitosis with a mean of 10 hours. The same tendency is seen for cells with carboplatin and centrosome amplification. Interestingly, if I compared cells in carboplatin with controls, I noticed that mitotic entry was delayed for more than 15 hours in carboplatin treated cells which were initially in G1. On the contrary, if cells were initially in G2 a delay in mitotic entry time was not observed. These data suggest that cells that are in G1 at the onset of carboplatin exposure undergo replication stress which, most likely activates the G2 checkpoint, delaying mitotic entry. However, the delay is probably not sufficient to arrest cells, and most likely they can enter mitosis with unrepaired DNA damage, driving high levels of chromosome mis-

segregation as observed (Results - Section 2). Together, these observations indicate that carboplatin induces cell death or arrest in S/G2.

3.4 Section 3 conclusion: centrosome amplification does not strongly modify the cell cycle response to carboplatin.

To study if centrosome amplification enhances cell death by modifying the cell cycle response to carboplatin, I used different approaches to study the cell cycle: a PCNA chromobody and FUCCI reporters for live imaging, and cytometry. In some cases I observed a slight effect of centrosome amplification on cell cycle progression, without specifically disrupting any cell cycle phase. However in response to carboplatin, the cell cycle was perturbed similarly with and without centrosome amplification: cells mainly arrest in S/G2, and this is also the phase when cell death occurs. It is therefore unlikely that centrosome amplification favours cell death by modifying the cell cycle response to carboplatin.

Results – Section 4

4 - Centrosome amplification does not modulate the DNA damage response during carboplatin treatment

4.1 Centrosome amplification does not favor induction of DNA damage in response to carboplatin

The cytotoxic effect of carboplatin is mainly due to the generation of DNA crosslinks, which occurs when platinum interacts with purine bases (adenine and guanine) in the DNA double strand helix (Eastman, 1987). DNA crosslinks impair replication leading to double strand breaks, which are recognized by proteins from the DNA damage signaling cascade, leading to activation of DNA damage repair, cell cycle arrest or apoptosis (Siddik et al., 2003). Centrosomes have been involved in regulation of the DNA damage response via recruitment of proteins involved in signaling and repair(Mullee dan Morrison, 2015). I was therefore interested in studying if the DNA damage response was modified in presence of centrosome amplification to explain the increase in cell death I observed (Results - Sections 1 and 2).

I investigated whether centrosome amplification can increase DNA damage levels or favor the DNA damage response after carboplatin treatment. I chose a fixed imaging approach, where centrosome amplification was induced for 72h in the OVCAR8 cell line. This was followed by carboplatin treatment. Cells were fixed, labelled for DNA damage and imaged at an epifluorescence microscope at 0h, 24h and 48 hours. after chemotherapy treatment as showed in (Figure 4.1A). I did not perform the experiment at 72h because at this time point, a large proportion of cells has died by apoptosis. Antibodies against γ–H2AX were chosen as a DNA double-strand break marker. γ–H2AX results from the phosphorylation of the histone variant H2AX, which occurs on Ser-139 in mammalian cells (Mah et al., 2010). Phosphorylation of H2AX resulting in γ–H2AX recruitment occurs at the level of double strand breaks at early steps of the DNA damage response (Sedelnikova et al., 2002; Maréchal dan Zou, 2013). Thus, the detection of γ– H2AX by antibodies allows me to reveal presence of DNA damage.

In control conditions, γ– H2AX foci were always detected (Fig. 4.1B-E) and the number of foci per nucleus could vary substantially (Figure 4.1D). In control cells, a mean of 19 foci per nucleus was detected. This means that OVCAR8 cells as many other cancer cell lines have basal levels of DNA damage. In the presence of centrosome amplification, I observed a mean

of 22 foci per nucleus at the starting time point, suggesting that no major differences in γ–H2AX recruitment were detected between cells with centrosome amplification and in control cells. Interestingly, the mean value of γ– H2AX foci remained constant at all the time points analyzed in these two conditions, indicating that centrosome amplification is not responsible for induction of additional DNA damage.

Figure 4.1

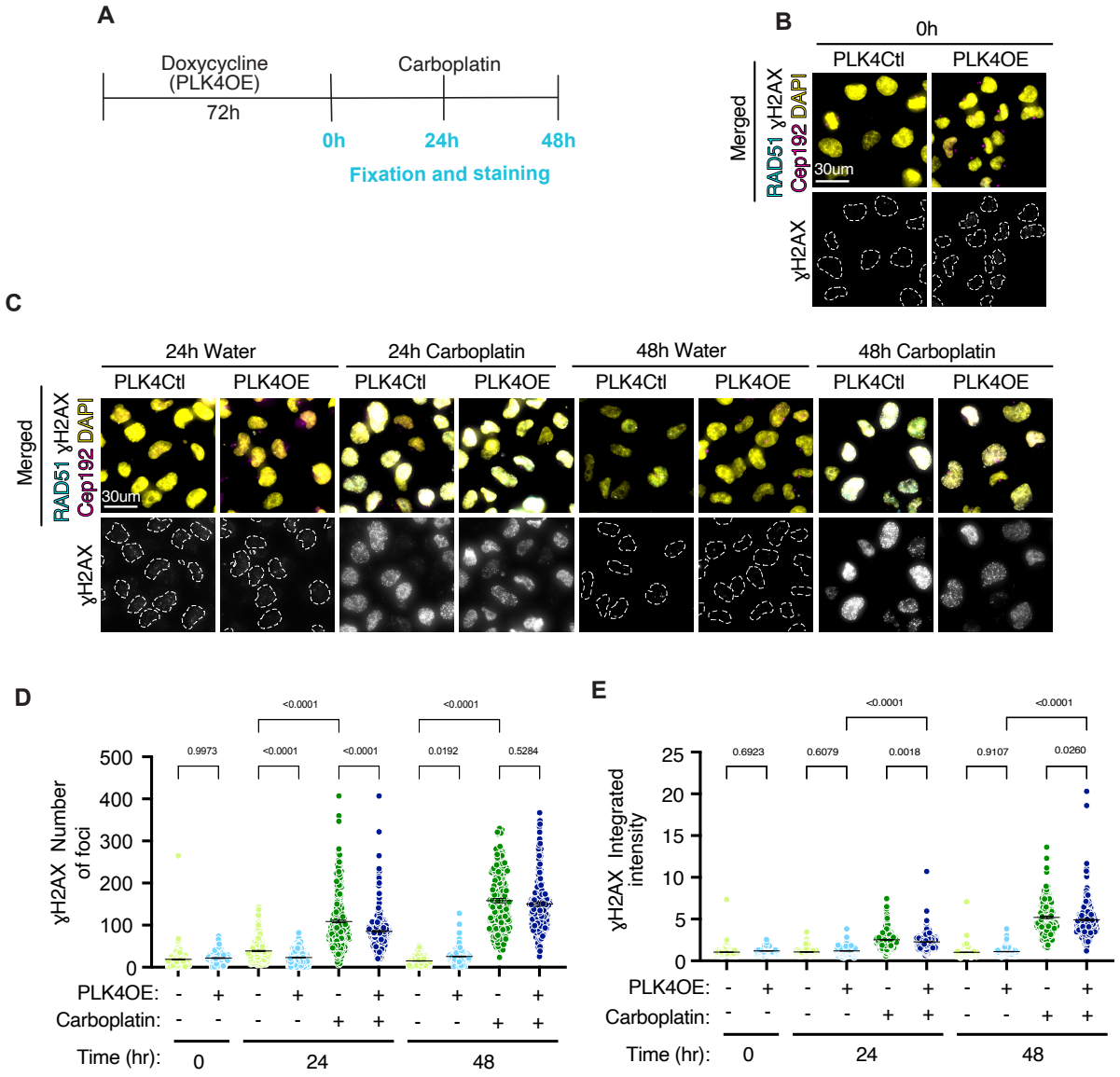

Figure 4.1: Centrosome amplification does not rely on DNA damage to favor carboplatin response

(A) Schematic representation of the experimental set up. (B) Representative images of OVCAR8 cells after 72 hours of incubation in 1μM of doxycycline (PLK4OE) or DMSO (PLK4Ctl), which correspond to time "0" of chemotherapy treatment. Immunofluorescence staining were performed with antibodies directed against γ-H2AX (DNA damage) in gray, Cep192 (centrosome marker) in magenta and RAD51 in cyan. DNA is shown in

yellow. Merged image of the four channels are shown in the top panel. The bottom panel represent γ-H2AX alone. The nuclear area is highlighted by white dashed lines in conditions where it is difficult to identify nuclei due to low levels of DNA damage. (C) Representative images of PLK4Ctrl or PLK4OE OVCAR8 cells after 24 and 48 hours of carboplatin (or water treatment, as a control. Immunofluorescence staining were performed with antibodies directed against γ-H2AX (DNA damage) in gray, Cep192 (centrosome marker) in magenta and RAD51 in cyan. DNA is shown in yellow. Merged image of the four channels are shown in the top panel. Bottom panel represent γ-H2AX alone. The dashed lines highlight the border of each nucleus. (D – E) Scatter dot graph showing the number of foci (D) or corresponding values of integrated intensity (E) for γ-H2AX per nucleus in the different conditions described above after 0, 24 and 48 hours of water or carboplatin incubation. Individual values and SEM for more than 200 cells *per* replicate, *per* three independent experiments are reported for each condition. Data for integrated intensity of γ-H2AX were normalized by the average of untreated PLK4Ctl cells at 24 hours. Statistical test: ANOVA with Sidak's multiple comparison tests.

In contrast, the number of γ–H2AX foci were strongly increased after carboplatin treatment. This indicates an accumulation of DNA damage, in agreement with platinum based chemotherapeutic drugs mode of action described in literature (Rosenberg et al., 1969a; Jamieson dan Lippard, 1999). Because of the high density of foci in the carboplatin condition, distinguishing and counting single foci was sometimes not feasible. Thus I plotted the integrated intensity of γ–H2AX signal per nucleus (Figure 4.1E). The levels of γ–H2AX were more than doubled after 24 hours, shifting from a mean of 1,06 to 2,52 arbitrary units (AU) of fluorescence integrated intensity. An even greater increase in γ–H2AX levels was observed after 48 hours, resulting in a mean of 5,21. These results show that the accumulation of DNA double-strand breaks increases through time in the presence of carboplatin. Finally, when centrosome amplification and carboplatin were both present, a mean of 2,26 at 24 hours and of 4,91 at 48 hours was detected for γ–H2AX integrated intensity. Comparing conditions with both carboplatin and centrosome amplification to carboplatin alone, I did not detect differences in terms of γ–H2AX recruitment. Therefore, centrosome amplification does not favor formation of DNA damage in the presence of carboplatin.

4.2 Centrosome amplification does not alter capacity of DNA damage repair

Another possibility is that cells with extra centrosomes have an altered capacity to repair DNA damage. To test this hypothesis, I characterized the main DNA damage repair pathways which could be activated in response to carboplatin crosslinks and DNA damage: Homologous Recombination (HR) and Non homologous End- Joining pathway (NHEJP) (See introduction chapter 3.5.2 and 3.5.3). Because current knowledge about proficiency of OVCAR8 for HR is not clear, I decided to study both HR and NHEJ pathways (Kondrashova et al., 2018). The main players of these pathways which were detected through antibodies were: RAD51 (RAD51), Fanconi Anemia Complementation Group D2 (FANCD2) and Tumor Protein P53 Binding Protein 1 (53BP1). RAD51 and FANCD2 are major players of HR (Baumann dan West, 1998; Li dan Heyer, 2008), whereas 53BP1 belongs to the NHEJ pathway (Bothmer et al., 2011).

Cells were submitted to centrosome amplification *via* incubation with doxycycline for 72h. This treatment was followed by incubation in carboplatin. As for γ-H2AX experiments, cells were fixed and stained at 0h, 24 and 48 hours after carboplatin treatment. Analysis of seven hundred cells per condition revealed that RAD51, FANCD2 and 53BP1 levels were very low in untreated OVCAR8 cells, with means ~1,00 for the integrated intensity of the three markers (Figure 4.2A-E). Indeed, nuclei with no foci were frequent. These quantifications suggest that the basal level of DNA damage in the cells (Figure 4.1) don't induce a stron DNA damage response. Conditions with centrosome amplification showed a mean integrated intensity of ~1,00 for the three proteins tested, at 0, 24 and 48 hours. Thus, no difference in the recruitment of RAD51, FANCD2 nor 53BP1 was observed in presence of centrosome amplification. These observations indicate that centrosome amplification does not influence DNA repair pathways in OVCAR8 cells at the basal levels.

Then, I focused on conditions treated with carboplatin (Figure 4.2). The levels of recruitment of RAD51 were slightly increased in response to carboplatin with a mean integrated intensity of 1,4 at 24h and of 1,90 at 48 hours. However, the overall levels of RAD51 were very low compared to the levels of DNA damage which were ~4 times higher (Figure 4.2C).

Figure 4.2

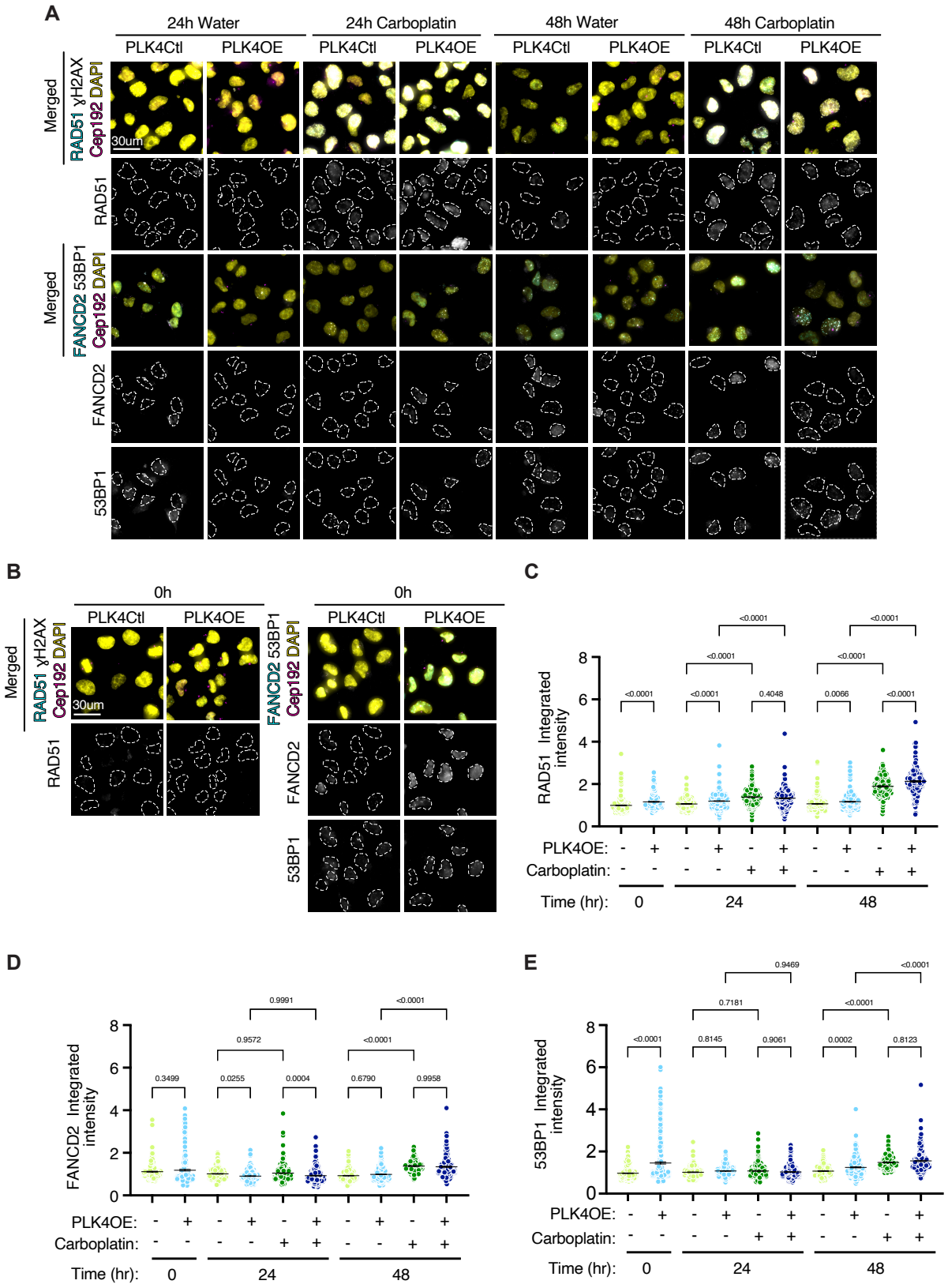

Figure 4.2: Centrosome amplification does not modify DNA damage repair capacity in OVCAR8 cells

(A- B) Representative images of OVCAR8 cells. Top panels shows merged signals from RAD51 in cyan, and Cep192 (in magenta) and γ-H2AX (in gray). DNA is shown in yellow. In the panel below, RAD51 is shown separately. The nuclear area is highlighted by white dashed lines in conditions where it is difficult to identify nuclei. In second merged panels, FANCD2 (in cyan,) 53BP1 (in gray) and Cep192 (in magenta) are shown. DAPI is shown in yellow. Below, l FANCD2 and 53BP1 are shown separately. Nuclear area is highlighted by white dashed lines. (C- E) Dot graphs showing the corresponding values of integrated intensity for RAD51, FANCD2 and 53BP1as indicated. Values for more than 200 cells *per* replicate, from three independent experiments are reported for each condition. Data for integrated intensity of the three markers were normalized by the average of untreated PLK4Ctl cells at 24 hours of the respective marker. Statistical test: ANOVA with Sidak's multiple comparison tests.

Similarly, higher FANCD2 and 53BP1 recruitment was noticed in the presence of carboplatin but their overall levels were very low compared to the observed increase in DNA damage (Figure 4.2D-E). These results suggest that a low level of DNA damage repair is activated in response to carboplatin in OVCAR8 cells. Lastly, a slight increase in RAD51 levels was detected at 48h in carboplatin when combined with extra centrosomes (Figure 4.2C). However, it is important to mention that in general RAD51 signals were extremely low and so it may preclude this comparison. FANCD2 and 53BP1 integrated intensity values were not significantly increased in cells with extra centrosomes (Figure 4.2D-E). Therefore, I think it is safe to conclude that centrosome amplification does not alter DNA repair in OVCAR8 cells. Overall, these findings demonstrate that centrosome amplification does not potentiate the response to carboplatin through altering DNA damage levels or DNA damage repair.

4.3 Section 4 conclusion: centrosome amplification does not strongly modify the DNA damage response to carboplatin.

By using IF, I tested if there is a difference in the DNA damage response to carboplatin in presence of centrosome amplification. I saw no differences in the levels of double strand break reporter γ–H2AX, and no difference in the levels of 3 different DNA repair proteins: Rad51, 53BP1 and FANCD2. Therefore I conclude that centrosome amplification doesn't lead to more death because of a different DNA damage response.

Results – Section 5

5 – Consequences of centrosome amplification on chromosomal instability and aneuploidy

Centrosome amplification is associated with CIN, and indeed I observed by live-imaging that there is more chromosome mis-segregation in OVCAR8 with centrosome amplification. This can lead to aneuploidy and could generate stress that might make cells more sensitive to die. I was therefore interested in defining aneuploidy levels in OVCAR8 cells depending on the centrosome status.

5.1 Centrosome amplification does not favor micronucleation in OVCAR8 cells

Mis-segregated chromosomes can generate micronuclei, which are a source of CIN for the cell in the following mitosis (Zhang et al., 2015; Trivedi et al., 2022). I characterized the number of micronuclei in OVCAR8 cells according to centrosome status (Figure 5.1). I incubated cells for 72 hours with 10 µg/ml doxycycline or DMSO to induce centrosome amplification. Then, I fixed and stained the cells with the DNA die DAPI and an antibody that recognizes the centrosome marker CEP192 (Figure 5.1A). I quantified the number of cells containing micronuclei. The number of micronuclei per cell varied. Cells with 1 to 3 micronuclei were frequent but cells with more than 10 micronuclei were also observed. Interestingly, a significant difference in micronuclei number was not observed according to the centrosome status as 4% of the cells in control and 7% in cells with centrosome amplification presented micronuclei (Figure 5.1B-C).

Figure 5.1

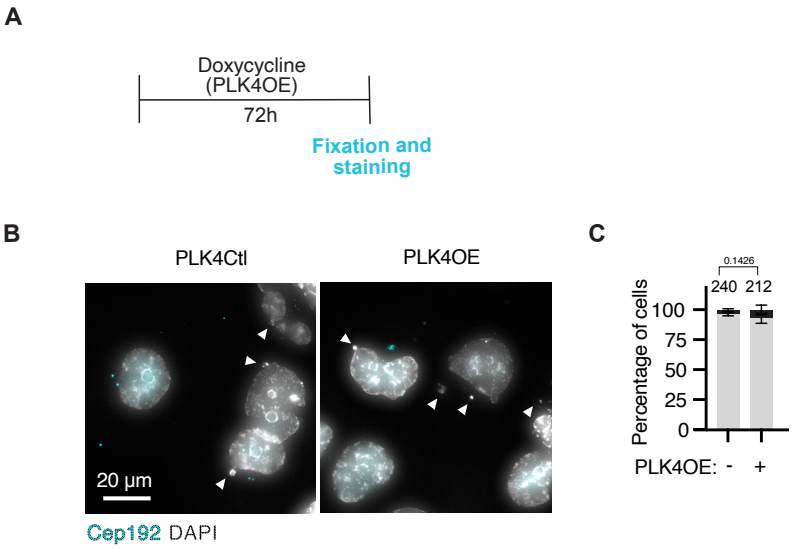

Figure 5.1: Centrosome amplification does not increase the frequency of micronuclei in OVCAR8 cells

(A) Schematic representation of the experimental workflow for fixed immunofluorescence imaging. (B) Representative images of OVCAR8 cells labeled with antibodies against CEP192 (Cyan). DNA is shown in gray. White arrow-head indicate micronuclei. (C) Graph bar showing the mean and SEM of cells with micronuclei. Data are the average of two biological replicates. Numbers on top of the bars represent the number of cells analyzed. Statistical test: Fisher's exact test on number of cells with at list one micronucleus.

5.2 Centrosome amplification does not increase aneuploidy in OVCAR8 cell

Despite not inducing high levels of multinucleation, we nevertheless observe an increase in CIN in presence of centrosome amplification using live-imaging approaches (Results Section 2.2). We therefore can still not exclude that this increase in the basal level of CIN contributes to favouring cell death in response to carboplatin by increasing aneuploidy. To directly test whether centrosome amplification can favor aneuploidy, I treated cells with 10 μg/ml doxycycline or DMSO as a control for 72 hours (Figure 5.2). The MPS1 inhibitor AZ3146 (MPS1i) was used as positive control at 1μM to induce CIN. G1 cells were FACS sorted for the 3 conditions, followed by DNA single cell sequencing and bioinformatic analysis which were performed by the laboratory of Floris Foijer (European Research Institute for the Biology of Ageing, University of Groningen, University Medical Center Groningen, Groningen, The Netherlands). To evaluate the extent of karyotype alterations, heterogeneity and aneuploidy scores were calculated as the divergence from the expected ploidy state (expected ploidy = 2N in our case, which correspond to an aneuploid score equal 0,000). As expected, high divergence from diploid state was noticed in the OVCAR8 cell line control, with aneuploidy score of 0,734 and heterogeneity score of 0,119. Indeed, the OVCAR8 karyotype is defined as hyper diploid in the literature and in general, ovarian cancers are characterized by copy number alterations. (Roschke et al., 2002). In particular, monosomy of chromosome X, 3-somy of chromosomes 5, 13, 14 and 20 and 4-somy of chromosome 8 was observed. Moreover, deletions were detected in every chromosome. As expected, in the positive control with MPS1i, aneuploidy score was slightly increased from 0,734 to 0,757 and heterogeneity score was doubled (0,283). Monosomy of chromosome X, 3-somy of chromosomes 5, 13,14 and 20 and 4-somy of chromosome 8 were maintained. OVCAR8 cells with centrosome amplification displayed an aneuploidy score of 0,747 and a heterogeneity score of 0,137. Neither the aneuploidy or heterogeneity scores show a strong deviation in presence of centrosome amplification, compared to the scores observed in the DMSO control.

Figure 5.2

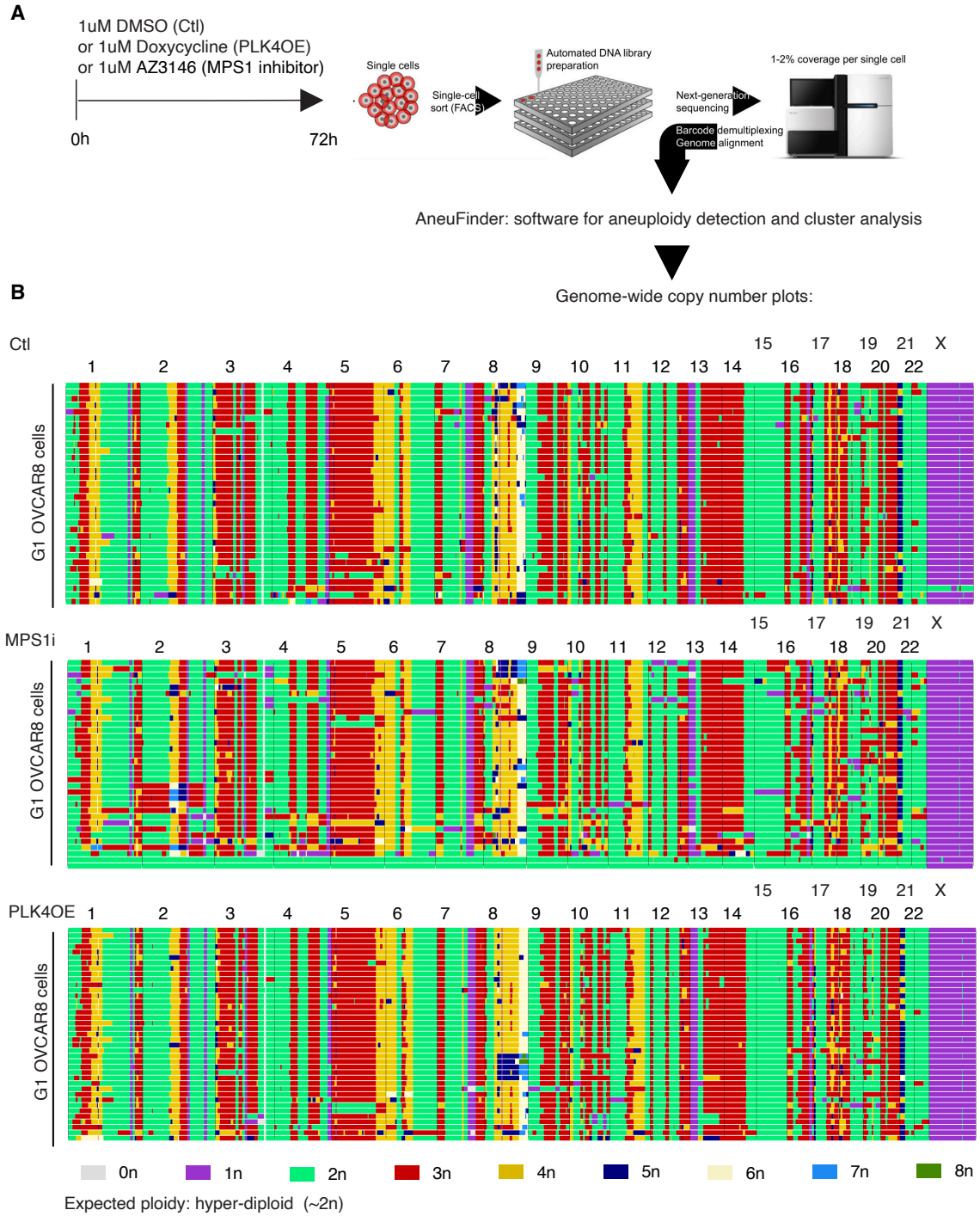

C

Sample:	Expected ploidy	Aneuploidy	Heterogeneity
Ctl	2n	0,734	0,119
MPS1i	2n	0,757	0, 283
PLK4COE	2n	0,747	0,137

Figure 5.2: Centrosome amplification does not favor the generation of aneuploidy in OVCAR8 cells

(A) Schematic representation of the workflow for DNA single cell sequencing. Image modified from (Bakker et al., 2016). (B) Genome-wide copy number profile of G1 OVCAR8 cells for each of the three conditions

indicated. Each row represents a cell with chromosomes plotted as chromosomes. On top, the respective chromosome number is indicated. Copy number states are depicted in different colors. Cells are clustered based on the similarity of their copy number profile. (C) Table reporting values for each condition of the expected ploidy levels, aneuploidy and heterogeneity scores. The extent of aneuploidy is measured as the divergence of a given chromosome from the normal euploid state. At the cell population level, heterogeneity is measured as the number of cells with a distinct copy number profile within the population. More details are provided in material and methods chapter.

In conclusion, these findings indicate that centrosome amplification does not lead to a significant increase in the occurrence of aneuploidy in OVCAR8 cells, making it unlikely that this contributes to enhancing cell death in response to chemotherapy.

5.3 Section 5 conclusion: centrosome amplification does not increase aneuploidy in OVCAR8

I used different methods to study if centrosome amplification increases aneuploidy in OVCAR8 which already presents considerable CIN. I observed that centrosome amplification does not increase the proportion of cells with micronuclei. Using single-cell whole-genome sequencing in collaboration with the team of Floris Foijer, I observed that the aneuploidy and heterogeneity scores for OVCAR8 are not strongly increased in presence of centrosome amplification.

Chapter 4 - Discussion

Centrosome amplification and chemotherapy

Centrosome amplification is viewed as a detrimental condition in healthy cells, whereas its role in cancer has been hypothesized to favor response to chemotherapy by promoting overall levels of CIN and aneuploidy (Basto et al., 2008a; Coelho et al., 2015; Raff dan Basto, 2017; Serçin et al., 2016; Ganem et al., 2009). Furthermore, centrosome amplification has been associated with favoring cell invasion by affecting cellular homeostasis (Arnandis et al., 2018; Godinho et al., 2014). Centrosome amplification has been detected in several types of cancer cell lines, EOC included (Marteil et al., 2018), and *in vivo* in EOC tumors (Morretton et al., 2022). However, the role of centrosome amplification on the response to chemotherapy has mostly been analyzed according to its role against antimitotic drugs, and their capacity to inhibit centrosome clustering and thus multipolarity (Weaver, 2014b; Zasadil et al., 2014b). On the contrary, how centrosome amplification influence DNA damage inducing agents, the other class of drugs currently used as first-line chemotherapy to treat EOC patients (Ozols et al., 2003a), has received less attention.

During my PhD I showed how centrosome amplification can counter-intuitively favor the response to chemotherapy in EOC cell lines. Moreover, I showed that centrosome amplification favors the response to the combination of paclitaxel and carboplatin through the induction of a particular mitotic phenotype: multipolar divisions. On the contrary, centrosome amplification favored the response to carboplatin treatment alone. My work contributed to rule out the influence of certain mechanisms currently described in the literature. In fact, even if centrosome amplification represents a form of stress for the cell, their effect when combined with carboplatin does not result from increased mitotic errors, or DNA damage, defects in DNA damage repair, neither from increased frequencies of aneuploidy or CIN.

As previously mentioned centrosome amplification has been associated to favor tumor progression. My results indicate that centrosome amplification favors the response to carboplatin and paclitaxel, both individually or in combination, in two out of the three EOC cell lines: OVCAR8 and COV504. Differences in the response to chemotherapy in SKOV3 compared to the two other cell lines, might be explained by several factors. Differences in genetic background can impact the response to chemotherapy. In particular it has been shown that cells display both intra-line and interline variation to taxanes (Gascoigne dan

Taylor, 2008b). These observations add complexity to identify different cell behaviors in the analyzed cell lines. Another factor that may influence the response to chemotherapy and centrosome amplification related with cell identity and its origin. The SKOV3 cell line was derived from ascite cultures (representing metastatic capacity), whereas OVCAR8 and COV504 were derived from the ovary epithelium. Further, it is important to take into account that HGSOCs which represents 80% of EOC, are characterized by high levels of chromosome copy number alterations and so wide-spread genetic differences(Kurman, 2013; Lisio et al., 2019b; Ciriello et al., 2013a), which may contribute to the response of centrosome amplification and chemotherapy. These may be translated in changes in copy number or expression of genes related DNA repair, cell cycle regulation and progression or stress responses to name a few.

Among them, an important difference which could influence the response to chemotherapy concerns TP53 status (Boutelle dan Attardi, 2021). TP53 has been described to be mutated in all the three cell lines used in the study, even if the mutations reported differ in each cell line (O'Connor et al., 1997; Cho et al., 1994; Beaufort et al., 2014). Indeed, these mutations results in the expression of different p53 protein variants and absence of p53 expression in the SKOV3 cell line, as shown though western blots performed by my colleague Frances Edward(Edwards et al., 2023). Even if p53 is expressed and can be phosphorylated on Serin15, which is an event important for its stabilization, it is interesting to note that OVCAR8 cells proliferate in these conditions. Further, this also shows that this mutant isoform does not respond to centrosome amplification. Indeed, centrosome amplification has been shown to induce a p53 dependent cell cycle arrest in human cells (Holland et al., 2012b). It would be interesting to investigate which p53 mutant isoforms are permissive for cell proliferation in the presence of extra centrosomes. This could be achieved by inducing centrosome amplification in a large group of cancer cell lines while characterizing TP53 and p53 isoforms through DNA sequencing and protein expression levels. Moreover, analysis of the whole genome and transcriptome in the different EOC cell lines, via DNA and RNA single cell sequencing would provide useful information to this comparison.

Impact of chemotherapy in EOC cell lines

Paclitaxel it is an antimitotic agent, which binds and stabilize microtubules (Sharma et al., 2013a; Zasadil et al., 2014b). On the other hand carboplatin belongs to platinum based drugs which induce DNA damage (Kelland, 1993; Pinto dan Lippard, 1985; Szefler et al., 2021). Through live-imaging, I showed that centrosome amplification favors the response to combined chemotherapy mainly by favoring multipolar divisions. Increased multipolar divisions are more likely the results of paclitaxel disrupting the clustering process in cell with extra centrosomes. Indeed, paclitaxel has been previously shown to induce multipolar divisions as a mechanism of action, at the clinical relevant doses (Zasadil et al., 2014b). Moreover, this phenotype has been shown to be exacerbated by presence of centrosome amplification in breast cancer cell lines (Scribano et al., 2021). Besides multipolar divisions, recent findings suggests also a role for taxanes in the modification of the tumor microenvironment and immune response as a mechanism to drive apoptosis *in vivo* (Vennin et al., 2023; Volk-Draper et al., 2014). Interestingly, in the SKOV3 cell line I detected high levels of multipolar divisions already in control cells (without PLK4 over-expression) in response to combined chemotherapy. This increased sensitivity may partially explain the lack of effect in cell death levels according to centrosome status. However, it remains to be explained the lack of effect in terms of paclitaxel sensitivity. Differences in centrosome clustering capacity do not seem a likely explanation because comparable clustering was noticed in the three cell lines used in this study. Indeed, even if slight differences in clustering were detected, this did not result in significant differences in the frequency of multipolar divisions. Another possibility is that OVCAR8 cells may have already developed some degree of resistance to paclitaxel whereas this is not the case for SKOV3 cells. Nevertheless, this explanation does not see likely since according to data found in the literature, these cells have been solely described as carboplatin resistant, since they were derived from one patient with EOC refractory to carboplatin treatment (Godwin et al., 1992; Schilder et al., 1990).

The impact of centrosome number during carboplatin remains much less explored. Carboplatin forms DNA crosslinks, which cause replication stress and DNA damage (Kelland, 2007; Flchtlnger-schepman et al., 1995). This can lead to the generation of DNA bridges during mitosis (Chan et al., 2009b). Centrosome amplification could in principle impact the geometry of mitosis contributing to clustering efficiency. Unexpectedly, our data suggests that

centrosome favors carboplatin response independently of mitotic errors. Indeed, both normally dividing cells or in cells presenting mitotic defects, cell death was enhanced in response to carboplatin when extra centrosomes were present. It is important to mention that I could not exclude other types of mitotic errors, which remained undetected through the live-imaging approaches used in this study. In this respect, would be important to characterize ultrafine bridges, which can be investigated via imaging of PICH and BLM proteins.

The main principle of action of Carboplatin results from the generation of DNA damage, in particular generation of double strand breaks (Kelland, 2007). Centrosomal proteins have been described to colocalize with several proteins involved in DNA damage signaling pathways, even if a direct link with of activation of DNA damage response has not been established (Mullee dan Morrison, 2015). My results show however, that an increase in double strand breaks was not detected in OVCAR8 cells in the presence of extra centrosomes, and with without carboplatin. Because DNA damage can lead to further errors during chromosome segregation, it is of highly importance for the cell to detect and repair DNA damage before mitosis. Non-homologous end joining (NHEJ) and homologous recombination (HR) are the main repair pathways in response to double strand breaks. These pathways are regulated in a cell cycle dependent manner (West, 2003; Ahnesorg et al., 2006; Bennett et al., 2013; Frank-Vaillant dan Marcand, 2002; Ira et al., 2004). My results indicate that the recruitment of proteins involved in NHEJ pathways is not enhanced when extra centrosomes are present. Levels of HR recruitment were slightly higher in the presence of extra centrosomes. However, the overall levels of proteins involved in DNA damage repair pathway remained very low in OVCAR8 cells and do not appear to be sufficient to justify the difference in cell death observed in response to carboplatin and centrosome amplification. Overall, these results suggest low DNA damage capacity repair, which is often observed in ovarian cancer cells and patients (Alsop et al., 2012; Walsh et al., 2010; Kondrashova et al., 2018; Bell et al., 2011; Nelson et al., 2020).

Altogether, these results show that centrosome amplification does not favor the response to carboplatin by increasing the levels of DNA damage or decreasing the capacity to undergo DNA repair. Even if other repair pathways may be involved like nucleotide excision repair (NER- which is involved in the removal of crosslinks) (Sancar et al., 2004), we excluded this possibility by analyzing the main DNA damage effectors. Immunoblots performed by

Frances Edwards showed indeed comparable levels of p53 and CHK1 between control an treated cells (Edwards et al., 2023). To understand if this enhanced effect of centrosome amplification can be applied to DNA damage inducing agents in general, it would be interesting to test other DNA damaging agents in cells with centrosome amplification.

Cell cycle

The presence of centrosome amplification decreases proliferation rate without impacting cell death levels. Moreover, centrosomes have been described to colocalize with cell cycle markers (Mullee dan Morrison, 2015). In particular, centrosome amplification has been reported to increase mitotic duration because it takes more time to satisfy the SAC(Ganem et al., 2009; Basto et al., 2008; Kwon et al., 2008).My data confirmed that centrosome amplification influence cell cycle duration by increasing mitotic duration. We hypothesized that this increase in mitotic duration could participate in favoring cell death in the presence of carboplatin, reasonably by activating the mitotic stopwatch pathway. The Stopwatch mechanism relies on the activation of 53BP1-USP28-p53 to activate apoptosis (Lambrus dan Holland, 2017; Uetake dan Sluder, 2010a). This hypothesis did not see likely because the increased mitotic length of ~40 minutes induced by centrosome amplification is inferior to what has been described in the literature to induce cell death (Uetake dan Sluder, 2010a). Nevertheless, this hypothesis was tested by my colleague Frances Edwards(Edwards et al., 2023), using a strategy where cells were treated with either MPS1 inhibitor or with CENP-E inhibitors to modulate mitotic duration (Bennett et al., 2015; Bolomsky et al., 2020). MPS1 is a member of the SAC and CENPE is a plus-end directed kinesin-7 motor protein, required for chromosome alignment during mitosis (Weaver et al., 2003). But even if mitotic duration was altered with these drugs, an increase in apoptosis was not noticed in OVCAR-8 cells. These data, lead us to refute the possibility of centrosome amplification favoring response to carboplatin by altering mitotic duration. On the contrary I could not conclude about the contribution of centrosome on interphase duration, because it appeared to be lineage dependent. Indeed, in OVCAR8 cells with centrosome amplification an increased interphase lengthening in the lineage expressing H2B-RFP PCNAmiRFP was seen, which was not confirmed in the FUCCI expressing cell line. To further address this question and detect possible differences, it would be important to film cells with a lower time resolution.

I also tested whether extending G1 phase by treating cells with CDK4/6 inhibitors Palbociclib or Abemacicli, could contribute to OVCAR-8 cell death with extra centrosomes. However, preliminary data (not presented here) showed no effect of these drugs on the OVCAR8 cell cycle. This is probably explained by the fact that *CCNE1, Cyclin E gene, has been described be amplified (Au-yeung et al., 2018). It is therefore tempting to speculate that increased levels of cyclin E may represent the underlying OVCAR8 resistance to CDK4/6 inhibition.*

Carboplatin is described to bind DNA and form crosslinks all along the cell cycle (Kelland, 2007). However, to display its effect in inducing DNA damage it is thought that cells have to pass through S-Phase to replicate their DNA. My results show that carboplatin, besides inducing cell death, induces cell cycle length extension or arrest in S/G2 phase. This coincides with what has been described in literature for most cell lines (Siddik, 2003b). Moreover, cells which received carboplatin in S/G2 phase tend to perform at least one mitosis before arresting in the following S/G2 phase. In contrast, cells were exposed to carboplatin early in the cell cycle during G1, frequently arrested or died without undergoing mitosis. This, further suggests that cells have to pass through S-Phase, at least once, for observing the effect of carboplatin. It is reasonable to hypothesize that the arrest occurs as a consequence of checkpoint activation, for cells to prevent entry in mitosis in order to amplify the extent of damage. We do not know what is the contribution of p21/p53 in this arrest even if both proteins are expressed. An interesting question is how can mutated p53 allow cells with extra centrosomes to proliferate even if it induces arrest in the presence of carboplatin and DNA damage.

Chromosome segregation errors

Chromosome mis-segregation can generate micronuclei and aneuploidy progeny, which are a source of chromosome instability (CIN) in daughter cells (Zhang et al., 2015; Trivedi et al., 2022). Increased CIN is suggested to be one of the mechanism through which centrosome amplification favor cancer progression (Coelho et al., 2015; Levine et al., 2017; Serçin et al., 2016). Centrosome amplification favors CIN by promoting merotelic attachment (Ganem et al., 2009; Cimini et al., 2003a). Even if CIN levels can be positive for cancer progression, high levels can also be detrimental (Chin et al., 1999a; Girish et al., 2023;

Greenberg et al., 1999a; Rowald et al., 2016; Rutledge et al., 2016b; Silk et al., 2013; Sotillo et al., 2007b; Yona et al., 2012). We tested the possibility that centrosome amplification favors the response to chemotherapy by favoring CIN. However, our data suggest that centrosome amplification contribution to CIN is very small. Thus, even if centrosome can induce CIN it does not seems sufficient to explain the difference detected in terms of cell death in response to carboplatin. Increased CIN can also favor aneuploidy (Garribba et al., 2023; Passerini et al., 2016). However, our data indicates that it is not the case. This maybe due to the fact that OVCAR8 cells have already a highly heterogeneous karyotype. It would be interesting to test how centrosome amplification affect karyotype by DNA single cell sequencing or FISH techniques in different cancers cell lines, in response to centrosome amplification. In particular cancer cell lines with a less heterogeneous karyotype and a more stable genome.

Main conclusions and future directions

The results obtained during my PhD show that centrosome amplification represents a stress factor which can enhance the response to paclitaxel and carboplatin via different mechanisms, not fully understood. The possibility that centrosome amplification represents an additional stress is supported by findings describing centrosome amplification resulting in Reactive Oxygen Species increase favoring invasive behaviors in both a cell-and non-cell autonomous manner (Arnandis et al., 2018). To understand the extension of centrosome amplification in favoring response to chemotherapy, it would be interesting to test if centrosome amplification can induce increase cell death also in cells naturally having extra centrosomes and in other cancer cell lines or cancer types. Moreover, studies in patient tissues would also provide valuable information. To help such studies, developing methods to automatically screen and count centrosomes, which seems reachable with future improvement of artificial intelligence would be very important. Identification of centrosome amplification as a vulnerability of cancer cells in response to chemotherapy, instead of only favoring cancer progression add more complexity to this centrosome number alterations.

A limitation of this study is related with the fact that we used the over-expression of PLK4. I tried to overcome this limitation by inducing centrosome amplification through a different strategy. I generated OVCAR8 cell lines inducible for the over-expression of SAS-6 or its mutated form ΔKEN-SAS-6 , which stabilizes this protein and can induce centrosome

amplification (Strnad et al., 2007; Leidel et al., 2005). However, this strategy only generated very low levels of centrosome amplification.

Altogether, my research contributes to the understanding of the role played by centrosome amplification in EOC cells. Moreover, it shows that presence of extra centrosomes favors the response to different types of chemotherapy in an unexpected way, in EOC cells. This work contribute to highlight the interest of further investigation of the role of centrosome amplification also *in vivo* and in other tumor types.

Chapter 5 - Bibliography

Aabo, K., M. Adams, P. Adnitt, D.S. Alberts, A. Athanazziou, V. Barley, D.R. Bell, U. Bianchi, G. Bolis, M.F. Brady, H.S. Brodovsky, H. Bruckner, M. Buyse, R. Canetta, V. Chylak, C.J. Cohen, N. Colombo, P.F. Conte, D. Crowther, J.H. Edmonson, C. Gennatas, E. Gilbey, M. Gore, D. Guthrie, S.B. Kaye, A.H. Laing, F. Landoni, R.C. Leonard, C. Lewis, P.Y. Liu, C. Mangioni, S. Marsoni, H. Meerpohl, G.A. Omura, M.K.B. Parmar, J. Pater, S. Pecorelli, M. Presti, W. Sauerbrei, D. V. Skarlos, R. V. Smalley, H.J. Solomon, L.A. Stewart, J.F.G. Sturgeon, M.H.N. Tattersall, J.T. Wharton, W.W. Ten Bokkel Huinink, M. Tomirotti, W. Torri, C. Trope, M.M. Turbow, J.B. Vermorken, M.J. Webb, D.W. Wilbur, C.J. Williams, E. Wiltshaw, dan B.Y. Yeap. 1998. Chemotherapy in advanced ovarian cancer: Four systematic meta-analyses of individual patient data from 37 randomized trials. *Br. J. Cancer*. 78:1479–1487. doi:10.1038/bjc.1998.710.

Ablasser, A., M. Goldeck, T. Cavlar, T. Deimling, G. Witte, I. Röhl, K.P. Hopfner, J. Ludwig, dan V. Hornung. 2013. CGAS produces a 2’-5’-linked cyclic dinucleotide second messenger that activates STING. *Nature*. 498:380–384. doi:10.1038/nature12306.

Adams, S.D., J. Csere, G. D’angelo, E.P. Carter, M. Romao, T. Arnandis, M. Dodel, H.M. Kocher, R. Grose, G. Raposo, F. Mardakheh, dan S.A. Godinho. 2021. Centrosome amplification mediates small extracellular vesicle secretion via lysosome disruption. *Curr. Biol.* 31:1403-1416.e7. doi:10.1016/j.cub.2021.01.028.

Aggarwal, B.B., R. V. Vijayalekshmi, dan B. Sung. 2009. Targeting inflammatory pathways for prevention and therapy of cancer: short-term friend, long-term foe. *Clin. Cancer Res.* 15:425–430. doi:10.1158/1078-0432.CCR-08-0149.

Agustinus, A.S., D. Al-rawi, B. Dameracharla, R. Raviram, B.S.C.L. Jones, S. Stransky, L. Scipioni, J. Luebeck, M. Di Bona, D. Norkunaite, R.M. Myers, M. Duran, dan S. Choi. 2023. Epigenetic dysregulation from chromosomal transit in micronuclei. doi:10.1038/s41586-023-06084-7.

Ahmed, A.A., D. Etemadmoghadam, J. Temple, A.G. Lynch, M. Riad, R. Sharma, C. Stewart, S. Fereday, C. Caldas, A. deFazio, D. Bowtell, dan J.D. Brenton. 2010a. Driver mutations in TP53 are ubiquitous in high grade serous carcinoma of the ovary. *J. Pathol.* 221:49–56. doi:10.1002/path.2696.

Ahmed, A.A., D. Etemadmoghadam, J. Temple, A.G. Lynch, M. Riad, R. Sharma, C. Stewart, S. Fereday, C. Caldas, A. DeFazio, D. Bowtell, dan J.D. Brenton. 2010b. Driver mutations in

TP53 are ubiquitous in high grade serous carcinoma of the ovary. *J. Pathol.* 221:49–56. doi:10.1002/path.2696.

Ahmed, A.A., D. Etemadmoghadam, J. Temple, A.G. Lynch, M. Riad, R. Sharma, C. Stewart, S. Fereday, C. Caldas, A. DeFazio, D. Bowtell, dan J.D. Brenton. 2010c. Driver mutations in TP53 are ubiquitous in high grade serous carcinoma of the ovary. *J. Pathol.* 221:49–56. doi:10.1002/path.2696.

Ahnesorg, P., P. Smith, dan S.P. Jackson. 2006. XLF interacts with the XRCC4-DNA ligase IV complex to promote DNA nonhomologous end-joining. *Cell*. 124:301–313. doi:10.1016/J.CELL.2005.12.031.

Akhmanova, A., dan M.O. Steinmetz. 2008. Tracking the ends: a dynamic protein network controls the fate of microtubule tips. *Nat. Rev. Mol. Cell Biol.* 9:309–322. doi:10.1038/NRM2369.

Akhmanova, A., dan M.O. Steinmetz. 2015. Control of microtubule organization and dynamics: two ends in the limelight. *Nat. Rev. Mol. Cell Biol. 2015 1612*. 16:711–726. doi:10.1038/nrm4084.

Alfa, C.E., B. Ducommun, D. Beach, dan J.S. Hyams. 1990. Distinct nuclear and spindle pole body populations of cyclin–cdc2 in fission yeast. *Nat. 1990 3476294*. 347:680–682. doi:10.1038/347680a0.

Allais, A., dan G. FitzHarris. 2022. Absence of a robust mitotic timer mechanism in early preimplantation mouse embryos leads to chromosome instability. *Dev.* 149. doi:10.1242/dev.200391.

Alsop, K., S. Fereday, C. Meldrum, A. DeFazio, C. Emmanuel, J. George, A. Dobrovic, M.J. Birrer, P.M. Webb, C. Stewart, M. Friedlander, S. Fox, D. Bowtell, dan G. Mitchell. 2012. BRCA Mutation Frequency and Patterns of Treatment Response in BRCA Mutation–Positive Women With Ovarian Cancer: A Report From the Australian Ovarian Cancer Study Group. *J. Clin. Oncol.* 30:2654. doi:10.1200/JCO.2011.39.8545.

Altmeyer, M., S. Messner, P.O. Hassa, M. Fey, dan M.O. Hottiger. 2009. Molecular mechanism of poly(ADP-ribosyl)ation by PARP1 and identification of lysine residues as ADP-ribose acceptor sites. *Nucleic Acids Res.* 37:3723–3738. doi:10.1093/NAR/GKP229.

Alvey, P.L. 1985. AN INVESTIGATION OF THE CENTRIOLE CYCLE USING 3T3 AND CHO CELLS. 78. 147–162 pp.

Andersen, J.S., C.J. Wilkinson, T. Mayor, P. Mortensen, E.A. Nigg, dan M. Mann. 2003.

Proteomic characterization of the human centrosome by protein correlation profiling. *Nature*. 426:570–574. doi:10.1038/nature02166.

Anderson, R.G.W. 1972. The three-dimensional structure of the basal body from the rhesus monkey oviduct. *J. Cell Biol.* 54:246–265. doi:10.1083/jcb.54.2.246.

De Antoni, A., C.G. Pearson, D. Cimini, J.C. Canman, V. Sala, L. Nezi, M. Mapelli, L. Sironi, M. Faretta, E.D. Salmon, dan A. Musacchio. 2005. The Mad1/Mad2 complex as a template for Mad2 activation in the spindle assembly checkpoint. *Curr. Biol.* 15:214–225. doi:10.1016/J.CUB.2005.01.038.

Aristarkhov, A., E. Eytan, A. Moghe, A. Admon, A. Hershko, dan J. V. Ruderman. 1996. E2-C, a cyclin-selective ubiquitin carrier protein required for the destruction of mitotic cyclins. *Proc. Natl. Acad. Sci. U. S. A.* 93:4294–4299. doi:10.1073/PNAS.93.9.4294.

Armstrong, D.K., B. Bundy, L. Wenzel, H.Q. Huang, R. Baergen, S. Lele, L.J. Copeland, J.L. Walker, dan R.A. Burger. 2006a. Intraperitoneal Cisplatin and Paclitaxel in Ovarian Cancer. *N. Engl. J. Med.* 354:34–43. doi:10.1056/NEJMoa052985.

Armstrong, D.K., B. Bundy, L. Wenzel, H.Q. Huang, R. Baergen, S. Lele, L.J. Copeland, J.L. Walker, dan R.A. Burger. 2006b. Intraperitoneal Cisplatin and Paclitaxel in Ovarian Cancer. *N. Engl. J. Med.* 354:34–43. doi:10.1056/NEJMoa052985.

Arnandis, T., P. Monteiro, S.D. Adams, V.L. Bridgeman, V. Rajeeve, E. Gadaleta, J. Marzec, C. Chelala, I. Malanchi, P.R. Cutillas, dan S.A. Godinho. 2018. Oxidative Stress in Cells with Extra Centrosomes Drives Non-Cell-Autonomous Invasion. *Dev. Cell*. 47:409-424.e9. doi:10.1016/j.devcel.2018.10.026.

Atherton-Fessler, S., F. Liu, B. Gabrielli, M.S. Lee, C.Y. Peng, dan H. Piwnica-Worms. 2017. Cell cycle regulation of the p34cdc2 inhibitory kinases. *https://doi.org/10.1091/mbc.5.9.989*. 5:989–1001. doi:10.1091/MBC.5.9.989.

Au-yeung, G., F. Lang, W.J. Azar, C. Mitchell, K.E. Jarman, K. Lackovic, D. Aziz, C. Cullinane, R.B. Pearson, D. Rischin, A.M. Karst, R. Drapkin, P. Maccallum, C. Centre, E. Melbourne, P. Maccallum, C. Centre, E. Melbourne, P. Maccallum, C. Centre, E. Melbourne, O. Cancer, C. Centre, dan N. South. 2018. HHS Public Access. 23:1862–1874. doi:10.1158/1078-0432.CCR-16-0620.Selective.

Aylon, Y., B. Liefshitz, dan M. Kupiec. 2004. The CDK regulates repair of double-strand breaks by homologous recombination during the cell cycle. *EMBO J.* 23:4868–4875. doi:10.1038/SJ.EMBOJ.7600469.

Azimzadeh, J. 2014. Exploring the evolutionary history of centrosomes. *Philos. Trans. R. Soc. B Biol. Sci.* 369:20130453. doi:10.1098/rstb.2013.0453.

Azimzadeh, J., M. Lie Wong, D. Miller Downhour, A. Sánchez Alvarado, dan W.F. Marshall. 2012. Centrosome Loss in the Evolution of Planarians. *Science (80-.).* 335:461–463. doi:10.1126/science.1214457.

Bakhoum, S.F., dan L.C. Cantley. 2018. The Multifaceted Role of Chromosomal Instability in Cancer and Its Microenvironment. *Cell*. 174:1347–1360. doi:10.1016/j.cell.2018.08.027.

Bakhoum, S.F., G. Genovese, dan D.A. Compton. 2009. Deviant Kinetochore Microtubule Dynamics Underlie Chromosomal Instability. *Curr. Biol.* 19:1937–1942. doi:10.1016/j.cub.2009.09.055.

Bakhoum, S.F., B. Ngo, A.M. Laughney, J.A. Cavallo, C.J. Murphy, P. Ly, P. Shah, R.K. Sriram, T.B.K. Watkins, N.K. Taunk, M. Duran, C. Pauli, C. Shaw, K. Chadalavada, V.K. Rajasekhar, G. Genovese, S. Venkatesan, N.J. Birkbak, N. McGranahan, M. Lundquist, Q. LaPlant, J.H. Healey, O. Elemento, C.H. Chung, N.Y. Lee, M. Imielenski, G. Nanjangud, D. Pe'er, D.W. Cleveland, S.N. Powell, J. Lammerding, C. Swanton, dan L.C. Cantley. 2018. Chromosomal instability drives metastasis through a cytosolic DNA response. *Nature*. 553:467–472. doi:10.1038/nature25432.

Bakker, B., A. Taudt, M.E. Belderbos, D. Porubsky, D.C.J. Spierings, T. V. de Jong, N. Halsema, H.G. Kazemier, K. Hoekstra-Wakker, A. Bradley, E.S.J.M. de Bont, A. van den Berg, V. Guryev, P.M. Lansdorp, M. Colomé-Tatché, dan F. Foijer. 2016. Single-cell sequencing reveals karyotype heterogeneity in murine and human malignancies. *Genome Biol.* 17:1–15. doi:10.1186/s13059-016-0971-7.

Baldin, V., J. Lukas, M.J. Marcote, M. Pagano, dan G. Draetta. 1993. Cyclin D1 is a nuclear protein required for cell cycle progression in G1. *Genes Dev.* 7:812–821. doi:10.1101/GAD.7.5.812.

Balestra, F.R., P. Strnad, I. Flückiger, dan P. Gönczy. 2013. Discovering regulators of centriole biogenesis through siRNA-based functional genomics in human cells. *Dev. Cell*. 25:555–571. doi:10.1016/J.DEVCEL.2013.05.016.

Banerjee, S.N., dan C.J. Lord. 2020. First-line PARP inhibition in ovarian cancer — standard of care for all? *Nat. Rev. Clin. Oncol.* 17:136–137. doi:10.1038/s41571-020-0335-9.

Banterle, N., A.P. Nievergelt, S. de Buhr, G.N. Hatzopoulos, C. Brillard, S. Andany, T. Hübscher, F.A. Sorgenfrei, U.S. Schwarz, F. Gräter, G.E. Fantner, dan P. Gönczy. 2021.

Kinetic and structural roles for the surface in guiding SAS-6 self-assembly to direct centriole architecture. *Nat. Commun.* 12. doi:10.1038/s41467-021-26329-1.

Barr, A.R., dan F. Gergely. 2007. Aurora-A: the maker and breaker of spindle poles. *J. Cell Sci.* 120:2987–2996. doi:10.1242/JCS.013136.

Basto, R., K. Brunk, dan T. Vinadogrova. 2008a. Centrosome amplification can initiate tumorigenesis in flies. *Chemtracts*. 21:111–113. doi:10.1016/j.cell.2008.05.039.Centrosome.

Basto, R., K. Brunk, T. Vinadogrova, N. Peel, A. Franz, A. Khodjakov, dan J.W. Raff. 2008b. Centrosome amplification can initiate tumorigenesis in flies. *Cell*. 133:1032–1042. doi:10.1016/j.cell.2008.05.039.

Basto, R., J. Lau, T. Vinogradova, A. Gardiol, C.G. Woods, A. Khodjakov, dan J.W. Raff. 2006a. Flies without Centrioles. *Cell*. 125:1375–1386. doi:10.1016/j.cell.2006.05.025.

Basto, R., J. Lau, T. Vinogradova, A. Gardiol, C.G. Woods, A. Khodjakov, dan J.W. Raff. 2006b. Flies without Centrioles. *Cell*. 125:1375–1386. doi:10.1016/j.cell.2006.05.025.

Basu, A., dan S. Krishnamurthy. 2010. Cellular responses to cisplatin-induced DNA damage. *J. Nucleic Acids*. 2010. doi:10.4061/2010/201367.

Baudoin, N.C., J.M. Nicholson, K. Soto, O. Martin, J. Chen, dan D. Cimini. 2020. Asymmetric clustering of centrosomes defines the early evolution of tetraploid cells. *Elife*. 9. doi:10.7554/eLife.54565.

Baumann, P., dan S.C. West. 1998. Role of the human RAD51 protein in homologous recombination and double-stranded-break repair. *Trends Biochem. Sci.* 23:247–251. doi:10.1016/S0968-0004(98)01232-8.

Bazzi, H., dan K. V. Anderson. 2014. Acentriolar mitosis activates a p53-dependent apoptosis pathway in the mouse embryo. *Proc. Natl. Acad. Sci. U. S. A.* 111:E1491–E1500. doi:10.1073/pnas.1400568111.

Beale, P.J., P. Rogers, F. Boxall, S.Y. Sharp, dan L.R. Kelland. 2000. BCL-2 family protein expression and platinum drug resistance in ovarian carcinoma. *Br. J. Cancer*. 82:436–440. doi:10.1054/bjoc.1999.0939.

Beaufort, C.M., J.C.A. Helmijr, A.M. Piskorz, M. Hoogstraat, K. Ruigrok-Ritstier, N. Besselink, M. Murtaza, W.F.J. Van IJcken, A.A.J. Heine, M. Smid, M.J. Koudijs, J.D. Brenton, E.M.J.J. Berns, dan J. Helleman. 2014. Ovarian Cancer Cell Line Panel (OCCP): Clinical Importance of In Vitro Morphological Subtypes. *PLoS One*. 9:e103988.

doi:10.1371/JOURNAL.PONE.0103988.

Bell, D., A. Berchuck, M. Birrer, J. Chien, D.W. Cramer, F. Dao, R. Dhir, P. Disaia, H. Gabra, P. Glenn, A.K. Godwin, J. Gross, L. Hartmann, M. Huang, D.G. Huntsman, M. Iacocca, M. Imielinski, S. Kalloger, B.Y. Karlan, D.A. Levine, G.B. Mills, C. Morrison, D. Mutch, N. Olvera, S. Orsulic, K. Park, N. Petrelli, B. Rabeno, J.S. Rader, B.I. Sikic, K. Smith-Mccune, A.K. Sood, D. Bowtell, R. Penny, J.R. Testa, K. Chang, H.H. Dinh, J.A. Drummond, G. Fowler, P. Gunaratne, A.C. Hawes, C.L. Kovar, L.R. Lewis, M.B. Morgan, I.F. Newsham, J. Santibanez, J.G. Reid, L.R. Trevino, Y.Q. Wu, M. Wang, D.M. Muzny, D.A. Wheeler, R.A. Gibbs, G. Getz, M.S. Lawrence, K. Cibulskis, A.Y. Sivachenko, C. Sougnez, D. Voet, J. Wilkinson, T. Bloom, K. Ardlie, T. Fennell, J. Baldwin, S. Gabriel, E.S. Lander, L. Ding, R.S. Fulton, D.C. Koboldt, M.D. McLellan, T. Wylie, J. Walker, M. O'Laughlin, D.J. Dooling, L. Fulton, R. Abbott, N.D. Dees, Q. Zhang, C. Kandoth, M. Wendl, W. Schierding, D. Shen, C.C. Harris, H. Schmidt, J. Kalicki, K.D. Delehaunty, C.C. Fronick, R. Demeter, L. Cook, J.W. Wallis, L. Lin, V.J. Magrini, J.S. Hodges, J.M. Eldred, S.M. Smith, C.S. Pohl, F. Vandin, B.J. Raphael, et al. 2011. Integrated genomic analyses of ovarian carcinoma. *Nature*. 474:609–615. doi:10.1038/nature10166.

Ben-David, U., G. Arad, U. Weissbein, B. Mandefro, A. Maimon, T. Golan-Lev, K. Narwani, A.T. Clark, P.W. Andrews, N. Benvenisty, dan J. Carlos Biancotti. 2014. Aneuploidy induces profound changes in gene expression, proliferation and tumorigenicity of human pluripotent stem cells. *Nat. Commun.* 5:1–11. doi:10.1038/ncomms5825.

Ben-David, U., dan N. Benvenisty. 2012. High prevalence of evolutionarily conserved and species-specific genomic aberrations in mouse pluripotent stem cells. *Stem Cells*. 30:612–622. doi:10.1002/stem.1057.

Ben-David, U., G. Ha, Y.Y. Tseng, N.F. Greenwald, C. Oh, J. Shih, J.M. McFarland, B. Wong, J.S. Boehm, R. Beroukhim, dan T.R. Golub. 2017. Patient-derived xenografts undergo mouse-specific tumor evolution. *Nat. Genet.* 49:1567–1575. doi:10.1038/ng.3967.

Bennett, A., B. Bechi, A. Tighe, S. Thompson, D.J. Procter, dan S.S. Taylor. 2015. Cenp-E inhibitor GSK923295: Novel synthetic route and use as a tool to generate aneuploidy. *Oncotarget*. 6:20921–20932. doi:10.18632/oncotarget.4879.

Bennett, G., M. Papamichos-Chronakis, dan C.L. Peterson. 2013. DNA repair choice defines a common pathway for recruitment of chromatin regulators. *Nat. Commun. 2013 41*. 4:1–10. doi:10.1038/ncomms3084.

Beroukhim, R., C.H. Mermel, D. Porter, G. Wei, S. Raychaudhuri, J. Donovan, J. Barretina, J.S. Boehm, J. Dobson, M. Urashima, K.T. McHenry, R.M. Pinchback, A.H. Ligon, Y.J. Cho, L. Haery, H. Greulich, M. Reich, W. Winckler, M.S. Lawrence, B.A. Weir, K.E. Tanaka, D.Y. Chiang, A.J. Bass, A. Loo, C. Hoffman, J. Prensner, T. Liefeld, Q. Gao, D. Yecies, S. Signoretti, E. Maher, F.J. Kaye, H. Sasaki, J.E. Tepper, J.A. Fletcher, J. Tabernero, J. Baselga, M.S. Tsao, F. Demichelis, M.A. Rubin, P.A. Janne, M.J. Daly, C. Nucera, R.L. Levine, B.L. Ebert, S. Gabrie, A.K. Rustgi, C.R. Antonescu, M. Ladanyi, A. Letai, L.A. Garraway, M. Loda, D.G. Beer, L.D. True, A. Okamoto, S.L. Pomeroy, S. Singer, T.R. Golub, E.S. Lander, G. Getz, W.R. Sellers, dan M. Meyerson. 2010. The landscape of somatic copy-number alteration across human cancers. *Nat. 2010 4637283*. 463:899–905. doi:10.1038/nature08822.

Besson, A., S.F. Dowdy, dan J.M. Roberts. Developmental Cell Review CDK Inhibitors: Cell Cycle Regulators and Beyond. doi:10.1016/j.devcel.2008.01.013.

Besson, A., S.F. Dowdy, dan J.M. Roberts. 2008. CDK Inhibitors: Cell Cycle Regulators and Beyond. *Dev. Cell*. 14:159–169. doi:10.1016/J.DEVCEL.2008.01.013.

Bettencourt-Dias, M., dan D.M. Glover. 2007. Centrosome biogenesis and function: Centrosomics brings new understanding. *Nat. Rev. Mol. Cell Biol.* 8:451–463. doi:10.1038/nrm2180.

Bettencourt-Dias, M., A. Rodrigues-Martins, L. Carpenter, M. Riparbelli, L. Lehmann, M.K. Gatt, N. Carmo, F. Balloux, G. Callaini, dan D.M. Glover. 2005. SAK/PLK4 is required for centriole duplication and flagella development. *Curr. Biol.* 15:2199–2207. doi:10.1016/j.cub.2005.11.042.

Blachon, S., J. Gopalakrishnan, Y. Omori, A. Polyanovsky, A. Church, D. Nicastro, J. Malicki, dan T. Avidor-Reiss. 2008. Drosophila asterless and vertebrate Cep152 are orthologs essential for centriole duplication. *Genetics*. 180:2081–2094. doi:10.1534/genetics.108.095141.

du Bois, A., H.J. Lück, W. Meier, H.P. Adams, V. Möbus, S. Costa, T. Bauknecht, B. Richter, M. Warm, W. Schröder, S. Olbricht, U. Nitz, C. Jackisch, G. Emons, U. Wagner, W. Kuhn, J. Pfisterer, K. von Maillot, W. Lange, D. Berg, E. Schlicht, H. Peterseim, D. Elling, T. Öney, V. Zimmermann, K. Renziehausen, G. Rohrmann, H.J. Bach, H. Müller, W. Jäger, H. Mickan, R.H. Ackermann, K. Wernicke, P.J. Czygan, J. Schulze-Tollert, H.J. Becker, J. Nast, P. Kramb, M. Kröner, E. Petru, M. Carstensen, W. Müller, H.H. Zippel, J. Hilfrich,

W. Herchenhein, M. Mesrogli, A. Schneider, G. Deutsch, F.K. Klöck, W. Maurer, S. Sünter, A. Göppinger, R. Strigl, R. Schuhmann, K. Kühndel, D. Fischer, C. Leißner, F. Peters, W. Niedner, K.H. Peschke, T. Silz, D. Schwörer, W. Meinerz, D. Kramer, P. Richter, D.F. Steichele, P. Krieger, M. Lange, T. Beck, K. Friese, D. Rother, L. Heilmann, J. Dietel, E. Petri, J. Meyer-Grohbrügge, V. Jovanovic, K. Robke, E. Merkle, G. Göretzlehner, J.P. Hanker, C. Karg, W. Burkert, A. Grüneberger, dan S. Flachsenberg. 2003. A randomized clinical trial of cisplatin/paclitaxel versus carboplatin/paclitaxel as first-line treatment of ovarian cancer. *J. Natl. Cancer Inst.* 95:1320–1330. doi:10.1093/jnci/djg036.

Bolomsky, A., M. Vogler, M.C. Köse, C.A. Heckman, G. Ehx, H. Ludwig, dan J. Caers. 2020. MCL-1 inhibitors, fast-lane development of a new class of anti-cancer agents. *J. Hematol. Oncol.* 13:1–19. doi:10.1186/s13045-020-01007-9.

Bornens, M. 2002. Centrosome composition and microtubule anchoring mechanisms. *Curr. Opin. Cell Biol.* 14:25–34. doi:10.1016/S0955-0674(01)00290-3.

Bornens, M. 2012. The centrosome in cells and organisms. *Science (80-.).* 335:422–426. doi:10.1126/science.1209037.

Bothmer, A., D.F. Robbiani, M. Di Virgilio, S.F. Bunting, I.A. Klein, N. Feldhahn, J. Barlow, H.T. Chen, D. Bosque, E. Callen, A. Nussenzweig, dan M.C. Nussenzweig. 2011. Regulation of DNA end joining, resection, and immunoglobulin class switch recombination by 53BP1. *Mol. Cell*. 42:319–329. doi:10.1016/J.MOLCEL.2011.03.019.

Boutelle, A.M., dan L.D. Attardi. 2021. p53 and Tumor Suppression: It Takes a Network. *Trends Cell Biol.* 31:298–310. doi:10.1016/J.TCB.2020.12.011.

Boveri, T. 1887. Ueber den Antheil des Spermatozoon an der Teilung des Eies. *Sitzungsber. Ges. Morph. Physiol. Munchen*. 151–164.

Bowler, M., D. Kong, S. Sun, R. Nanjundappa, L. Evans, V. Farmer, A. Holland, M.R. Mahjoub, H. Sui, dan J. Loncarek. 2019. High-resolution characterization of centriole distal appendage morphology and dynamics by correlative STORM and electron microscopy. *Nat. Commun.* 10. doi:10.1038/s41467-018-08216-4.

Bowtell, D.D., S. Böhm, A.A. Ahmed, P.J. Aspuria, R.C. Bast, V. Beral, J.S. Berek, M.J. Birrer, S. Blagden, M.A. Bookman, J.D. Brenton, K.B. Chiappinelli, F.C. Martins, G. Coukos, R. Drapkin, R. Edmondson, C. Fotopoulou, H. Gabra, J. Galon, C. Gourley, V. Heong, D.G. Huntsman, M. Iwanicki, B.Y. Karlan, A. Kaye, E. Lengyel, D.A. Levine, K.H. Lu, I.A.

McNeish, U. Menon, S.A. Narod, B.H. Nelson, K.P. Nephew, P. Pharoah, D.J. Powell, P. Ramos, I.L. Romero, C.L. Scott, A.K. Sood, E.A. Stronach, dan F.R. Balkwill. 2015. Rethinking ovarian cancer II: reducing mortality from high-grade serous ovarian cancer. *Nat. Rev. Cancer 2015 1511*. 15:668–679. doi:10.1038/nrc4019.

Branzei, D., dan M. Foiani. 2005. The DNA damage response during DNA replication. *Curr. Opin. Cell Biol.* 17:568–575. doi:10.1016/J.CEB.2005.09.003.

Bravo, R., R. Frank, P.A. Blundell, dan H. Macdonald-Bravo. 1987. Cyclin/PCNA is the auxiliary protein of DNA polymerase-δ. *Nat. 1987 3266112*. 326:515–517. doi:10.1038/326515a0.

Van Breugel, M., M. Hirono, A. Andreeva, H.A. Yanagisawa, S. Yamaguchi, Y. Nakazawa, N. Morgner, M. Petrovich, I.O. Ebong, C. V. Robinson, C.M. Johnson, D. Veprintsev, dan B. Zuber. 2011. Structures of SAS-6 suggest its organization in centrioles. *Science (80-.).* 331:1196–1199. doi:10.1126/science.1199325.

Brinkley, B. 1985. Microtubule Organizing Center. *Annu. Rev. Cell Dev. Biol.* 1:145–172. doi:10.1146/annurev.cellbio.1.1.145.

Brinkley, B.R. 2001. Managing the centrosome numbers game: From chaos to stability in cancer cell division. *Trends Cell Biol.* 11:18–21. doi:10.1016/S0962-8924(00)01872-9.

Brinkley, B.R., S.M. Cox, D.A. Pepper, S. Wible, S.L. Brenner, dan R.L. Pardue. 1981. Enhanced Reader.pdf. *Nature*. 388:1–14.

Brinkley, B.R., dan T.M. Goepfert. 1998. Supernumerary centrosomes and cancer: Boveri's hypothesis resurrected. *Cell Motil. Cytoskeleton*. 41:281–288. doi:10.1002/(SICI)1097-0169(1998)41:4<281::AID-CM1>3.0.CO;2-C.

Bronder, D., A. Tighe, D. Wangsa, D. Zong, T.J. Meyer, R. Wardenaar, P. Minshall, D. Hirsch, K. Heselmeyer-Haddad, L. Nelson, D. Spierings, J.C. McGrail, M. Cam, A. Nussenzweig, F. Foijer, T. Ried, dan S.S. Taylor. 2021. TP53 loss initiates chromosomal instability in fallopian tube epithelial cells. *DMM Dis. Model. Mech.* 14. doi:10.1242/dmm.049001.

Brouhard, G.J., dan L.M. Rice. 2018. Microtubule dynamics: An interplay of biochemistry and mechanics. *Nat. Rev. Mol. Cell Biol.* 19:451–463. doi:10.1038/s41580-018-0009-y.

Ter Brugge, P., P. Kristel, E. Van Der Burg, U. Boon, M. De Maaker, E. Lips, L. Mulder, J. De Ruiter, C. Moutinho, H. Gevensleben, E. Marangoni, I. Majewski, K. Jozwiak, W. Kloosterman, M. Van Roosmalen, K. Duran, F. Hogervorst, N. Turner, M. Esteller, E. Cuppen, J. Wesseling, dan J. Jonkers. 2016. Mechanisms of Therapy Resistance in

Patient-Derived Xenograft Models of BRCA1-Deficient Breast Cancer. *J. Natl. Cancer Inst.* 108. doi:10.1093/JNCI/DJW148.

Bryant, H.E., N. Schultz, H.D. Thomas, K.M. Parker, D. Flower, E. Lopez, S. Kyle, M. Meuth, N.J. Curtin, dan T. Helleday. 2005a. Specific killing of BRCA2-deficient tumours with inhibitors of poly(ADP-ribose) polymerase.[erratum appears in Nature. 2007 May 17;447(7142):346]. *Nature*. 434:913–917.

Bryant, H.E., N. Schultz, H.D. Thomas, K.M. Parker, D. Flower, E. Lopez, S. Kyle, M. Meuth, N.J. Curtin, dan T. Helleday. 2005b. Specific killing of BRCA2-deficient tumours with inhibitors of poly(ADP-ribose) polymerase. *Nature*. 434:913–917. doi:10.1038/nature03443.

Burbank, K.S., T.J. Mitchison, dan D.S. Fisher. 2007. Slide-and-Cluster Models for Spindle Assembly. *Curr. Biol.* 17:1373–1383. doi:10.1016/J.CUB.2007.07.058.

Burds, A.A., A.S. Lutum, dan P.K. Sorger. 2005. Generating chromosome instability through the simultaneous deletion of Mad2 and p53. *Proc. Natl. Acad. Sci. U. S. A.* 102:11296–11301. doi:10.1073/pnas.0505053102.

Burgess, A., T. Lorca, dan A. Castro. 2012. Quantitative Live Imaging of Endogenous DNA Replication in Mammalian Cells. *PLoS One*. 7:45726. doi:10.1371/JOURNAL.PONE.0045726.

Burigotto, M., A. Mattivi, D. Migliorati, G. Magnani, C. Valentini, M. Roccuzzo, M. Offterdinger, M. Pizzato, A. Schmidt, A. Villunger, S. Maffini, dan L.L. Fava. 2021. Centriolar distal appendages activate the centrosome-PIDDosome-p53 signalling axis via ANKRD26. *EMBO J.* 40:1–22. doi:10.15252/embj.2020104844.

Cahill, D.P., L.T. Da Costa, E.B. Carson-Walter, K.W. Kinzler, B. Vogelstein, dan C. Lengauer. 1999. Characterization of MAD2B and other mitotic spindle checkpoint genes. *Genomics*. 58:181–187. doi:10.1006/geno.1999.5831.

Calvert, A.H., D.R. Newell, L.A. Gumbrell, S. O'Reilly, M. Burnell, F.E. Boxall, Z.H. Siddik, I.R. Judson, M.E. Gore, dan E. Wiltshaw. 2016. Carboplatin dosage: prospective evaluation of a simple formula based on renal function. *https://doi.org/10.1200/JCO.1989.7.11.1748*. 7:1748–1756. doi:10.1200/JCO.1989.7.11.1748.

Cánepa, E.T., M.E. Scassa, J.M. Ceruti, M.C. Marazita, A.L. Carcagno, P.F. Sirkin, dan M.F. Ogara. 2007. INK4 proteins, a family of mammalian CDK inhibitors with novel biological

functions. *IUBMB Life*. 59:419–426. doi:10.1080/15216540701488358.

Carlier, M.F., dan D. Pantaloni. 1981. Kinetic Analysis of Guanosine 5'-Triphosphate Hydrolysis Associated with Tubulin Polymerization. *Biochemistry*. 20:1918–1924. doi:10.1021/bi00510a030.

Carlton, J.G., dan J. Martin-Serrano. 2007. Parallels between cytokinesis and retroviral budding: A role for the ESCRT machinery. *Science (80-.).* 316:1908–1912. doi:10.1126/SCIENCE.1143422/SUPPL_FILE/CARLTON.SOM.PDF.

Carneiro, B.A., dan W.S. El-Deiry. 2020. Targeting apoptosis in cancer therapy. *Nat. Rev. Clin. Oncol.* 17:395–417. doi:10.1038/s41571-020-0341-y.

Carvalho-Santos, Z., P. Machado, P. Branco, F. Tavares-Cadete, A. Rodrigues-Martins, J.B. Pereira-Leal, dan M. Bettencourt-Dias. 2010. Stepwise evolution of the centriole-assembly pathway. *J. Cell Sci.* 123:1414–1426. doi:10.1242/jcs.064931.

Ceccaldi, R., B. Rondinelli, dan A.D. D'Andrea. 2016. Repair Pathway Choices and Consequences at the Double-Strand Break. *Trends Cell Biol.* 26:52–64. doi:10.1016/j.tcb.2015.07.009.

Chabin-Brion, K., J. Marceiller, F. Perez, C. Settegrana, A. Drechou, G. Durand, dan C. Poüs. 2001. The Golgi complex is a microtubule-organizing organelle. *Mol. Biol. Cell*. 12:2047–2060. doi:10.1091/mbc.12.7.2047.

Chan, Jason Yongsheng (Medical Resident, Ministry of Health Holdings, S. 2011. A Clinical Overview of Centrosome Amplification in Human Cancers. *Int. J. Biol. Sci.* 7:1122–1144.

Chan, J.Y. 2011. A Clinical Overview of Centrosome Amplification in Human Cancers. *Int. J. Biol. Sci.* 7:1122. doi:10.7150/IJBS.7.1122.

Chan, K.L., T. Palmai-Pallag, S. Ying, dan I.D. Hickson. 2009a. Replication stress induces sister-chromatid bridging at fragile site loci in mitosis. *Nat. Cell Biol.* 11:753–760. doi:10.1038/NCB1882.

Chan, K.L., T. Palmai-Pallag, S. Ying, dan I.D. Hickson. 2009b. Replication stress induces sister-chromatid bridging at fragile site loci in mitosis. *Nat. Cell Biol.* 11:753–760. doi:10.1038/NCB1882.

Chan, Y.W., dan S.C. West. 2014. Spatial control of the GEN1 Holliday junction resolvase ensures genome stability. *Nat. Commun. 2014 51*. 5:1–11. doi:10.1038/ncomms5844.

Chaney, S.G., dan A. Vaisman. 1999. Specificity of platinum-DNA adduct repair. *J. Inorg. Biochem.* 77:71–81. doi:10.1016/S0162-0134(99)00149-X.

Chang, H.H.Y., N.R. Pannunzio, N. Adachi, dan M.R. Lieber. 2017. Non-homologous DNA end joining and alternative pathways to double-strand break repair. *Nat. Rev. Mol. Cell Biol.* 18:495–506. doi:10.1038/nrm.2017.48.

Chang, H.Y., dan X. Yang. 2000. Proteases for cell suicide: functions and regulation of caspases. *Microbiol. Mol. Biol. Rev.* 64:821–846. doi:10.1128/MMBR.64.4.821-846.2000.

Chao, H.X., C.E. Poovey, A.A. Privette, G.D. Grant, H.Y. Chao, J.G. Cook, dan J.E. Purvis Correspondence. 2017. Orchestration of DNA Damage Checkpoint Dynamics across the Human Cell Cycle. *Cell Syst.* 5:445-459.e5. doi:10.1016/j.cels.2017.09.015.

Chapman, J.R., P. Barral, J.B. Vannier, V. Borel, M. Steger, A. Tomas-Loba, A.A. Sartori, I.R. Adams, F.D. Batista, dan S.J. Boulton. 2013. RIF1 is essential for 53BP1-dependent nonhomologous end joining and suppression of DNA double-strand break resection. *Mol. Cell*. 49:858–871. doi:10.1016/J.MOLCEL.2013.01.002.

Cheasley, D., A. Nigam, M. Zethoven, S. Hunter, D. Etemadmoghadam, T. Semple, P. Allan, M.S. Carey, M.L. Fernandez, A. Dawson, M. Köbel, D.G. Huntsman, C. Le Page, A.M. Mes-Masson, D. Provencher, N. Hacker, Y. Gao, D. Bowtell, A. deFazio, K.L. Gorringe, dan I.G. Campbell. 2021. Genomic analysis of low-grade serous ovarian carcinoma to identify key drivers and therapeutic vulnerabilities. *J. Pathol.* 253:41–54. doi:10.1002/PATH.5545.

Cheasley, D., M.J. Wakefield, G.L. Ryland, P.E. Allan, K. Alsop, K.C. Amarasinghe, S. Ananda, M.S. Anglesio, G. Au-Yeung, M. Böhm, D.D.L. Bowtell, A. Brand, G. Chenevix-Trench, M. Christie, Y.E. Chiew, M. Churchman, A. DeFazio, R. Demeo, R. Dudley, N. Fairweather, C.G. Fedele, S. Fereday, S.B. Fox, C.B. Gilks, C. Gourley, N.F. Hacker, A.M. Hadley, J. Hendley, G.Y. Ho, S. Hughes, D.G. Hunstman, S.M. Hunter, T.W. Jobling, K.R. Kalli, S.H. Kaufmann, C.J. Kennedy, M. Köbel, C. Le Page, J. Li, R. Lupat, O.M. McNally, J.N. McAlpine, A.M. Mes-Masson, L. Mileshkin, D.M. Provencher, J. Pyman, K. Rahimi, S.M. Rowley, C. Salazar, G. Samimi, H. Saunders, T. Semple, R. Sharma, A.J. Sharpe, A.N. Stephens, N. Thio, M.C. Torres, N. Traficante, Z. Xing, M. Zethoven, Y.C. Antill, C.L. Scott, I.G. Campbell, dan K.L. Gorringe. 2019. The molecular origin and taxonomy of mucinous ovarian carcinoma. *Nat. Commun. 2019 101*. 10:1–11. doi:10.1038/s41467-019-11862-x.

Chen, A., P.D. Arora, C.A. McCulloch, dan A. Wilde. 2017. Cytokinesis requires localized β-

actin filament production by an actin isoform specific nucleator. *Nat. Commun.* 8. doi:10.1038/s41467-017-01231-x.

Chen, X., H. Niu, Y. Yu, J. Wang, S. Zhu, J. Zhou, A. Papusha, D. Cui, X. Pan, Y. Kwon, P. Sung, dan G. Ira. 2016. Enrichment of Cdk1-cyclins at DNA double-strand breaks stimulates Fun30 phosphorylation and DNA end resection. *Nucleic Acids Res.* 44:2742–2753. doi:10.1093/NAR/GKV1544.

Cheng, E.H.Y., M.C. Wei, S. Weiler, R.A. Flavell, T.W. Mak, T. Lindsten, dan S.J. Korsmeyer. 2001. BCL-2, BCL-X(L) sequester BH3 domain-only molecules preventing BAX- and BAK-mediated mitochondrial apoptosis. *Mol. Cell*. 8:705–711. doi:10.1016/S1097-2765(01)00320-3.

Chim, C.S., T.K. Fung, F. Wong, J.S. Lau, M. Law, dan R. Liang. 2006. Methylation of INK4 and CIP/KIP families of cyclin-dependent kinase inhibitor in chronic lymphocytic leukaemia in Chinese patients. *J Clin Pathol*. 59:921–926. doi:10.1136/jcp.2005.035089.

Chin, L., S.E. Artandi, Q. Shen, A. Tam, S.L. Lee, G.J. Gottlieb, C.W. Greider, dan R.A. DePinho. 1999a. p53 deficiency rescues the adverse effects of telomere loss and cooperates with telomere dysfunction to accelerate carcinogenesis. *Cell*. 97:527–538. doi:10.1016/S0092-8674(00)80762-X.

Chin, L., S.E. Artandi, Q. Shen, A. Tam, S.L. Lee, G.J. Gottlieb, C.W. Greider, dan R.A. DePinho. 1999b. p53 deficiency rescues the adverse effects of telomere loss and cooperates with telomere dysfunction to accelerate carcinogenesis. *Cell*. 97:527–538. doi:10.1016/S0092-8674(00)80762-X.

Cho, Y., S. Gorina, P.D. Jeffrey, dan N.P. Pavletich. 1994. Crystal structure of a p53 tumor suppressor-DNA complex: understanding tumorigenic mutations. *Science*. 265:346–355. doi:10.1126/SCIENCE.8023157.

Choi, Y.K., P. Liu, S.K. Sze, C. Dai, dan R.Z. Qi. 2010. CDK5RAP2 stimulates microtubule nucleation by the γ-tubulin ring complex. *J. Cell Biol.* 191:1089–1095. doi:10.1083/jcb.201007030.

Chong, W.M., W.J. Wang, C.H. Lo, T.Y. Chiu, T.J. Chang, Y.P. Liu, B. Tanos, G. Mazo, M.F.B. Tsou, W.N. Jane, T.T. Yang, dan J.C. Liao. 2020. Super-resolution microscopy reveals coupling between mammalian centriole subdistal appendages and distal appendages. *Elife*. 9. doi:10.7554/eLife.53580.

Chui, M.H., J.C. Chang, Y. Zhang, A. Zehir, A.M. Schram, J. Konner, A.E. Drilon, A.D.C. Paula,

B. Weigelt, dan R.N. Grisham. 2021. Spectrum of BRAF Mutations and Gene Rearrangements in Ovarian Serous Carcinoma. *https://doi.org/10.1200/PO.21.00055*. 1480–1492. doi:10.1200/PO.21.00055.

Chui, M.H., P. Ryan, J. Radigan, S.E. Ferguson, A. Pollett, M. Aronson, K. Semotiuk, S. Holter, K. Sy, J.S. Kwon, A. Soma, N. Singh, S. Gallinger, P. Shaw, J. Arseneau, W.D. Foulkes, C.B. Gilks, dan B.A. Clarke. 2014. The histomorphology of lynch syndrome-associated ovarian carcinomas: Toward a subtype-specific screening strategy. *Am. J. Surg. Pathol.* 38:1173–1181. doi:10.1097/PAS.0000000000000298.

Cimini, D., L.A. Cameron, dan E.D. Salmon. 2004a. Anaphase Spindle Mechanics Prevent Mis-Segregation of Merotelically Oriented Chromosomes of kinetochores and spindle poles). We identified pro-metaphase/metaphase cells possessing one or more merotelic kinetochores by taking a through-focus image. *Curr. Biol.* 14:2149–2155. doi:10.1016/j.

Cimini, D., L.A. Cameron, dan E.D. Salmon. 2004b. Anaphase Spindle Mechanics Prevent Mis-Segregation of Merotelically Oriented Chromosomes. *Curr. Biol.* 14:2149–2155. doi:10.1016/J.CUB.2004.11.029.

Cimini, D., B. Howell, P. Maddox, A. Khodjakov, F. Degrassi, dan E.D. Salmon. 2001. Merotelic kinetochore orientation is a major mechanism of aneuploidy in mitotic mammalian tissue cells. *J. Cell Biol.* 152:517–527. doi:10.1083/JCB.153.3.517/VIDEO-1.

Cimini, D., B. Moree, J.C. Canman, dan E.D. Salmon. 2003a. Merotelic kinetochore orientation occurs frequently during early mitosis in mammalian tissue cells and error correction is achieved by two different mechanisms. *J. Cell Sci.* 116:4213–4225. doi:10.1242/JCS.00716.

Cimini, D., B. Moree, J.C. Canman, dan E.D. Salmon. 2003b. Merotelic kinetochore orientation occurs frequently during early mitosis in mammalian tissue cells and error correction is achieved by two different mechanisms. *J. Cell Sci.* 116:4213–4225. doi:10.1242/JCS.00716.

Ciriello, G., M.L. Miller, B.A. Aksoy, Y. Senbabaoglu, N. Schultz, dan C. Sander. 2013a. Emerging landscape of oncogenic signatures across human cancers. *Nat. Genet.* 45:1127–1133. doi:10.1038/ng.2762.

Ciriello, G., M.L. Miller, B.A. Aksoy, Y. Senbabaoglu, N. Schultz, dan C. Sander. 2013b. Emerging landscape of oncogenic signatures across human cancers. *Nat. Genet.*

45:1127–1133. doi:10.1038/ng.2762.

Climini, D., D. Fioravanti, E.D. Salmon, dan F. Degrassi. 2002. Merotelic kinetochore orientation versus chromosome mono-orientation in the origin of lagging chromosomes in human primary cells. *J. Cell Sci.* 115:507–515. doi:10.1242/JCS.115.3.507.

Coelho, P.A., L. Bury, M.N. Shahbazi, K. Liakath-Ali, P.H. Tate, S. Wormald, C.J. Hindley, M. Huch, J. Archer, W.C. Skarnes, M. Zernicka-Goetz, dan D.M. Glover. 2015. Over-expression of Plk4 induces centrosome amplification, loss of primary cilia and associated tissue hyperplasia in the mouse. *Open Biol.* 5. doi:10.1098/rsob.150209.

Cohen-Sharir, Y., J.M. Mcfarland, M. Abdusamad, C. Marquis, H. Tang, M.R. Ippolito, S. V Bernhard, K. Laue, H.L.H. Malaby, A. Jones, M. Kazachkova, N. Lyons, A. Nagaraja, A.J. Bass, R. Beroukhim, S. Santaguida, J. Stumpff, T.R. Golub, Z. Storchova, dan U. Ben-David. Selective vulnerability of aneuploid human cancer cells to inhibition of the spindle assembly checkpoint. doi:10.1101/2020.06.18.159038.

Cohen, D., S. Melamed, A. Millman, G. Shulman, Y. Oppenheimer-Shaanan, A. Kacen, S. Doron, G. Amitai, dan R. Sorek. 2019. Cyclic GMP–AMP signalling protects bacteria against viral infection. *Nature*. 574:691–695. doi:10.1038/s41586-019-1605-5.

Cohen, S.M., E.R. Jamieson, dan S.J. Lippard. 2000. Enhanced binding of the TATA-binding protein to TATA boxes containing flanking cisplatin 1,2-cross-links. *Biochemistry*. 39:8259–8265. doi:10.1021/bi0004495.

Coller, H.A., L. Sang, dan J.M. Roberts. 2006. A new description of cellular quiescence. *PLoS Biol.* 4:0329–0349. doi:10.1371/JOURNAL.PBIO.0040083.

Conduit, P.T., K. Brunk, J. Dobbelaere, C.I. Dix, E.P. Lucas, dan J.W. Raff. 2010. Centrioles regulate centrosome size by controlling the rate of Cnn incorporation into the PCM. *Curr. Biol.* 20:2178–2186. doi:10.1016/j.cub.2010.11.011.

Conduit, P.T., J.H. Richens, A. Wainman, J. Holder, C.C. Vicente, M.B. Pratt, C.I. Dix, Z.A. Novak, I.M. Dobbie, L. Schermelleh, dan J.W. Raff. 2014. A molecular mechanism of mitotic centrosome assembly in Drosophila. *Elife*. 3:1–23. doi:10.7554/ELIFE.03399.

Conduit, P.T., A. Wainman, dan J.W. Raff. 2015. Centrosome function and assembly in animal cells. *Nat. Rev. Mol. Cell Biol.* 16:611–624. doi:10.1038/nrm4062.

Cortamp, I., J. June-Koo Lee, R. Xi, D. Jain, Y.L. Jung, L. Yang, D. Gordenin, L.J. Klimczak, C.-Z. Zhang, D.S. Pellman, K.C. Akdemir, E.G. Alvarez, A. Baez-Ortega, R. Beroukhim, P.C.

Boutros, D.D. L Bowtell, B. Brors, K.H. Burns, P.J. Campbell, K. Chan, K. Chen, A. Dueso-Barroso, A.J. Dunford, P.A. Edwards, X. Estivill, D. Etemadmoghadam, L. Feuerbach, J. Lynn Fink, M. Frenkel-Morgenstern, D.W. Garsed, M. Gerstein, D.A. Gordenin, D. Haan, J.E. Haber, J.M. Hess, B. Hutter, M. Imielinski, D.T. W Jones, Y. Seok Ju, M.D. Kazanov, Y. Koh, J.O. Korbel, K. Kumar, E. Alice Lee, Y. Li, A.G. Lynch, G. Macintyre, F. Markowetz, igo Martincorena, A. Martinez-Fundichely, S. Miyano, H. Nakagawa, F.C. P Navarro, S. Ossowski, P.J. Park, J. V Pearson, M. Puiggramp, K. Rippe, N.D. Roberts, S.A. Roberts, B. Rodriguez-Martin, S.E. Schumacher, R. Scully, M. Shackleton, N. Sidiropoulos, L. Sieverling, C. Stewart, D. Torrents, J.M. C Tubio, I. Villasante, N. Waddell, J.A. Wala, J. Weischenfeldt, X. Yao, S.-S. Yoon, J. Zamora, L.A. Aaltonen, F. Abascal, A. Abeshouse, H. Aburatani, D.J. Adams, N. Agrawal, K. Soo Ahn, S.-M. Ahn, H. Aikata, R. Akbani, H. Al-Ahmadie, S.T. Al-Sedairy, F. Al-Shahrour, M. Alawi, M. Albert, K. Aldape, L.B. Alexandrov, A. Ally, K. Alsop, F. Amary, S.B. Amin, B. Aminou, et al. 2020. Comprehensive analysis of chromothripsis in 2,658 human cancers using whole-genome sequencing. *Nat. Genet. 2020 523*. 52:331–341. doi:10.1038/s41588-019-0576-7.

Crasta, K., N.J. Ganem, R. Dagher, A.B. Lantermann, E. V. Ivanova, Y. Pan, L. Nezi, A. Protopopov, D. Chowdhury, dan D. Pellman. 2012. DNA breaks and chromosome pulverization from errors in mitosis. *Nature*. 482:53–58. doi:10.1038/nature10802.

Cuella-Martin, R., C. Oliveira, H.E. Lockstone, S. Snellenberg, N. Grolmusova, dan J.R. Chapman. 2016. 53BP1 Integrates DNA Repair and p53-Dependent Cell Fate Decisions via Distinct Mechanisms. *Mol. Cell*. 64:51–64. doi:10.1016/j.molcel.2016.08.002.

Cunha-Ferreira, I., I. Bento, A. Pimenta-Marques, S.C. Jana, M. Lince-Faria, P. Duarte, J. Borrego-Pinto, S. Gilberto, T. Amado, D. Brito, A. Rodrigues-Martins, J. Debski, N. Dzhindzhev, dan M. Bettencourt-Dias. 2013. Regulation of autophosphorylation controls PLK4 self-destruction and centriole number. *Curr. Biol.* 23:2245–2254. doi:10.1016/j.cub.2013.09.037.

Cunha-Ferreira, I., A. Rodrigues-Martins, I. Bento, M. Riparbelli, W. Zhang, E. Laue, G. Callaini, D.M. Glover, dan M. Bettencourt-Dias. 2009. The SCF/Slimb Ubiquitin Ligase Limits Centrosome Amplification through Degradation of SAK/PLK4. *Curr. Biol.* 19:43–49. doi:10.1016/j.cub.2008.11.037.

Cybulska, P., A.D.C. Paula, J. Tseng, M.M. Leitao, A. Bashashati, D.G. Huntsman, T.M.

Nazeran, C. Aghajanian, N.R. Abu-Rustum, D.F. DeLair, S.P. Shah, dan B. Weigelt. 2019. Molecular profiling and molecular classification of endometrioid ovarian carcinomas. *Gynecol. Oncol.* 154:516–523. doi:10.1016/J.YGYNO.2019.07.012.

Czabotar, P.E., G. Lessene, A. Strasser, dan J.M. Adams. 2014. Control of apoptosis by the BCL-2 protein family: implications for physiology and therapy. *Nat. Rev. Mol. Cell Biol.* 15:49–63. doi:10.1038/NRM3722.

D'Assoro, A.B., S.L. Barrett, C. Folk, V.C. Negron, K. Boeneman, R. Busby, C. Whitehead, F. Stivala, W.L. Lingle, dan J.L. Salisbury. 2002. Amplified centrosomes in breast cancer: A potential indicator of tumor aggressiveness. *Breast Cancer Res. Treat.* 75:25–34. doi:10.1023/A:1016550619925.

Dae, Y.K., dan R. Roy. 2006. Cell cycle regulators control centrosome elimination during oogenesis in Caenorhabditis elegans. *J. Cell Biol.* 174:751–757. doi:10.1083/jcb.200512160.

Dai, Y., S. Jin, X. Li, dan D. Wang. 2017. The involvement of Bcl-2 family proteins in AKT-regulated cell survival in cisplatin resistant epithelial ovarian cancer. *Oncotarget*. 8:1354–1368. doi:10.18632/oncotarget.13817.

Damia, G., dan M. Broggini. 2019. Platinum resistance in ovarian cancer: Role of DNA repair. *Cancers (Basel).* 11. doi:10.3390/cancers11010119.

Dammermann, A., T. Müller-Reichert, L. Pelletier, B. Habermann, A. Desai, dan K. Oegema. 2004. Centriole Assembly Requires Both Centriolar and Pericentriolar Material Proteins. *Dev. Cell*. 7:815–829. doi:10.1016/J.DEVCEL.2004.10.015.

Dasari, S., dan P. Bernard Tchounwou. 2014. Cisplatin in cancer therapy: Molecular mechanisms of action. *Eur. J. Pharmacol.* 740:364–378. doi:10.1016/j.ejphar.2014.07.025.

Davies, M.S., S.J. Berners-Price, dan T.W. Hambley. 2000. Rates of platination of -AG- and -GA- containing double-stranded oligonucleotides: Effect of chloride concentration. *J. Inorg. Biochem.* 79:167–172. doi:10.1016/S0162-0134(99)00180-4.

Davis, A.J., dan D.J. Chen. DNA double strand break repair via non-homologous end-joining. doi:10.3978/j.issn.2218-676X.2013.04.02.

Davoli, T., H. Uno, E.C. Wooten, dan S.J. Elledge. 2017. Tumor aneuploidy correlates with markers of immune evasion and with reduced response to immunotherapy. *Science (80-.).* 355. doi:10.1126/science.aaf8399.

Davoli, T., A.W. Xu, K.E. Mengwasser, L.M. Sack, J.C. Yoon, P.J. Park, dan S.J. Elledge. 2013. Cumulative Haploinsufficiency and Triplosensitivity Drive Aneuploidy Patterns and Shape the Cancer Genome. *Cell*. 155:948–962. doi:10.1016/j.cell.2013.10.011.

Decout, A., J.D. Katz, S. Venkatraman, dan A. Ablasser. 2021. The cGAS–STING pathway as a therapeutic target in inflammatory diseases. *Nat. Rev. Immunol.* 21:548–569. doi:10.1038/s41577-021-00524-z.

Delattre, M., C. Canard, dan P. Gönczy. 2006. Sequential Protein Recruitment in C. elegans Centriole Formation. *Curr. Biol.* 16:1844–1849. doi:10.1016/J.CUB.2006.07.059.

Delattre, M., S. Leidel, K. Wani, K. Baumer, J. Bamat, H. Schnabel, R. Feichtinger, R. Schnabel, dan P. Gönczy. 2004. Centriolar SAS-5 is required for centrosome duplication in C. elegans. *Nat. Cell Biol. 2004 67*. 6:656–664. doi:10.1038/ncb1146.

Dephoure, N., S. Hwang, C. O'Sullivan, S.E. Dodgson, S.P. Gygi, A. Amon, dan E.M. Torres. 2014. Quantitative proteomic analysis reveals posttranslational responses to aneuploidy in yeast. *Elife*. 3:1–27. doi:10.7554/eLife.03023.

Desai, A., dan T. Mitchison. 1997. Microtubule Polymerization. *Annu. Rev. Cell Dev. Biol*. 13:83–117.

Dias, M.P., S.C. Moser, S. Ganesan, dan J. Jonkers. 2021. Understanding and overcoming resistance to PARP inhibitors in cancer therapy. *Nat. Rev. Clin. Oncol.* 18:773–791. doi:10.1038/s41571-021-00532-x.

Diner, E.J., D.L. Burdette, S.C. Wilson, K.M. Monroe, C.A. Kellenberger, M. Hyodo, Y. Hayakawa, M.C. Hammond, dan R.E. Vance. 2013. The Innate Immune DNA Sensor cGAS Produces a Noncanonical Cyclic Dinucleotide that Activates Human STING. *Cell Rep.* 3:1355–1361. doi:10.1016/j.celrep.2013.05.009.

Dinkelmann, M., E. Spehalski, T. Stoneham, J. Buis, Y. Wu, J.M. Sekiguchi, dan D.O. Ferguson. 2009. Multiple functions of MRN in end-joining pathways during isotype class switching. *Nat. Struct. Mol. Biol.* 16:808–813. doi:10.1038/NSMB.1639.

Dobbelaere, J., F. Josué, S. Suijkerbuijk, B. Baum, N. Tapon, dan J. Raff. 2008. A genome-wide RNAi screen to dissect centriole duplication and centrosome maturation in Drosophila. *PLoS Biol.* 6:1975–1990. doi:10.1371/journal.pbio.0060224.

Domchek, S.M. 2017. Reversion Mutations with Clinical Use of PARP Inhibitors: Many Genes, Many Versions. *Cancer Discov.* 7:937–939. doi:10.1158/2159-8290.CD-17-0734.

Duan, Z., R. Foster, D.A. Bell, J. Mahoney, K. Wolak, A. Vaidya, C. Hampel, H. Lee, dan M. V.

Seiden. 2006. Signal transducers and activators of transcription 3 pathway activation in drug-resistant ovarian cancer. *Clin. Cancer Res.* 12:5055–5063. doi:10.1158/1078-0432.CCR-06-0861.

Dube, P., F. Herzog, C. Gieffers, B. Sander, D. Riedel, S.A. Müller, A. Engel, J.M. Peters, dan H. Stark. 2005. Localization of the coactivator Cdh1 and the cullin subunit Apc2 in a cryo-electron microscopy model of vertebrate APC/C. *Mol. Cell*. 20:867–879. doi:10.1016/J.MOLCEL.2005.11.008.

Duesberg, P., R. Li, R. Sachs, A. Fabarius, M.B. Upender, dan R. Hehlmann. 2007. Cancer drug resistance: The central role of the karyotype. *Drug Resist. Updat.* 10:51–58. doi:10.1016/j.drup.2007.02.003.

Duesberg, P., R. Stindl, dan R. Hehlmann. 2001. Origin of multidrug resistance in cells with and without multidrug resistance genes: Chromosome reassortments catalyzed by aneuploidy. *Proc. Natl. Acad. Sci. U. S. A.* 98:11283–11288. doi:10.1073/pnas.201398998.

Durkacz, B.W., O. Omidiji, D.A. Gray, dan S. Shall. 1980. (ADP-ribose)n participates in DNA excision repair. *Nat. 1980 2835747*. 283:593–596. doi:10.1038/283593a0.

Dzhindzhev, N.S., G. Tzolovsky, Z. Lipinszki, S. Schneider, R. Lattao, J. Fu, J. Debski, M. Dadlez, dan D.M. Glover. 2014. Plk4 phosphorylates ana2 to trigger SAS6 recruitment and procentriole formation. *Curr. Biol.* 24:2526–2532. doi:10.1016/j.cub.2014.08.061.

Eastman, A. 1986. Reevaluation of Interaction of cis-Dichloro(ethylenediamine)platinum(II) with DNA. *Biochemistry*. 25:3912–3915. doi:10.1021/bi00361a026.

Eastman, A. 1987. The formation, isolation and characterization of DNA adducts produced by anticancer platinum complexes. *Pharmacol. Ther.* 34:155–166. doi:10.1016/0163-7258(87)90009-X.

Edwards, F., G. Fantozzi, A.Y. Simon, J. Morretton, A.E. Tijhuis, R. Wardenaar, S. Foulane, S. Gemble, C.J. Diana, F. Foijer, O. Mariani, A. Vincent-salomon, S.R. Roman, X. Sastre-garau, O. Goundiam, dan R. Basto. 2023. Centrosome amplification primes for apoptosis and favors the response to chemotherapy in ovarian cancer beyond multipolar divisions. 1–58.

Eid, W., M. Steger, M. El-Shemerly, L.P. Ferretti, J. Peña-Diaz, C. König, E. Valtorta, A.A. Sartori, dan S. Ferrari. 2010. DNA end resection by CtIP and exonuclease 1 prevents genomic instability. *EMBO Rep.* 11:962–968. doi:10.1038/EMBOR.2010.157.

Ellis, H.M., dan H.R. Horvitz. 1986. Genetic control of programmed cell death in the nematode C. elegans. *Cell*. 44:817–829. doi:10.1016/0092-8674(86)90004-8.

Ellis, R.E., J. Yuan, dan H.R. Horvitz. 1991. Mechanisms and functions of cell death. *Annu. Rev. Cell Biol.* 7:663–698. doi:10.1146/ANNUREV.CB.07.110191.003311.

Elmore, S. Apoptosis: A Review of Programmed Cell Death.

Escribano-Díaz, C., A. Orthwein, A. Fradet-Turcotte, M. Xing, J.T.F. Young, J. Tkáč, M.A. Cook, A.P. Rosebrock, M. Munro, M.D. Canny, D. Xu, dan D. Durocher. 2013. A cell cycle-dependent regulatory circuit composed of 53BP1-RIF1 and BRCA1-CtIP controls DNA repair pathway choice. *Mol. Cell*. 49:872–883. doi:10.1016/J.MOLCEL.2013.01.001.

Essers, J., A.F. Theil, C. Baldeyron, W.A. van Cappellen, A.B. Houtsmuller, R. Kanaar, dan W. Vermeulen. 2005. Nuclear Dynamics of PCNA in DNA Replication and Repair. *Mol. Cell. Biol.* 25:9350–9359. doi:10.1128/mcb.25.21.9350-9359.2005.

Etemad, B., T.E.F. Kuijt, dan G.J.P.L. Kops. 2015. Kinetochore–microtubule attachment is sufficient to satisfy the human spindle assembly checkpoint. *Nat. Commun. 2015 61*. 6:1–8. doi:10.1038/ncomms9987.

Etemadmoghadam, D., A. Defazio, R. Beroukhim, C. Mermel, J. George, G. Getz, R. Tothiil, A. Okamoto, M.B. Raeder, P. Harnett, S. Lade, L.A. Akslen, A. V. Tinker, B. Locandro, K. Aisop, Y.E. Chiew, N. Traficante, S. Fereday, D. Johnson, S. Fox, W. Sellers, M. Urashima, H.B. Salvesen, M. Meyerson, dan D. Bowtell. 2009. Integrated genome-wide DMA copy number and expression analysis identifies distinct mechanisms of primary chemoresistance in ovarian carcinomas. *Clin. Cancer Res.* 15:1417–1427. doi:10.1158/1078-0432.CCR-08-1564.

Evans, L.T., T. Anglen, P. Scott, K. Lukasik, J. Loncarek, dan A.J. Holland. 2021. ANKRD26 recruits PIDD1 to centriolar distal appendages to activate the PIDDosome following centrosome amplification. *EMBO J.* 40:1–18. doi:10.15252/embj.2020105106.

Evans, T., E.T. Rosenthal, J. Youngblom, D. Distel, dan T. Hunt. 1983. Cyclin: A protein specified by maternal mRNA in sea urchin eggs that is destroyed at each cleavage division. *Cell*. 33:389–396. doi:10.1016/0092-8674(83)90420-8.

Farmer, H., N. McCabe, C.J. Lord, A.N.J. Tutt, D.A. Johnson, T.B. Richardson, M. Santarosa, K.J. Dillon, I. Hickson, C. Knights, N.M.B. Martin, S.P. Jackson, G.C.M. Smith, dan A. Ashworth. 2005. Targeting the DNA repair defect in BRCA mutant cells as a therapeutic strategy. *Nature*. 434:917–921. doi:10.1038/nature03445.

Fava, L.L., F. Schuler, V. Sladky, M.D. Haschka, C. Soratroi, L. Eiterer, E. Demetz, G. Weiss, S. Geley, E.A. Nigg, dan A. Villunger. 2017. The PIDDosome activates p53 in response to supernumerary centrosomes. *Genes Dev.* 31:34–45. doi:10.1101/gad.289728.116.

Fededa, J.P., dan D.W. Gerlich. 2012. Molecular control of animal cell cytokinesis. *Nat. Cell Biol.* 14:440–447. doi:10.1038/ncb2482.

Fenix, A.M., N. Taneja, C.A. Buttler, J. Lewis, S.B. Van Engelenburg, R. Ohi, dan D.T. Burnette. 2016. Expansion and concatenation of nonmuscle myosin IIA filaments drive cellular contractile system formation during interphase and mitosis. *Mol. Biol. Cell*. 27:1465–1478. doi:10.1091/MBC.E15-10-0725/ASSET/IMAGES/LARGE/MBC-27-1465-G006.JPEG.

Fichtinger-Schepman, A.M.J., P.H.M. Lohman, J.L. van der Veer, J.H.J. den Hartog, dan J. Reedijk. 1985. Adducts of the Antitumor Drug cis-Diamminedichloroplatinum(II) with DNA: Formation, Identification, and Quantitation. *Biochemistry*. 24:707–713. doi:10.1021/bi00324a025.

Flchtlnger-schepman, A.M.J., H.C.M. Van Dijk-knijnenburg, S.D. Van Der Velde-visser, F. Berends, dan R.A. Baan. 1995. Cisplatin- and carboplatin-DNA adducts: Is pt-ag the cytotoxic lesion? *Carcinogenesis*. 16:2447–2453. doi:10.1093/carcin/16.10.2447.

Fong, K.W., Y.K. Choi, J.B. Rattner, dan R.Z. Qi. 2008a. CDK5RAP2 is a pericentriolar protein that functions in centrosomal attachment of the γ-tubulin ring complex. *Mol. Biol. Cell*. 19:115–125. doi:10.1091/mbc.E07-04-0371.

Fong, K.W., Y.K. Choi, J.B. Rattner, dan R.Z. Qi. 2008b. CDK5RAP2 is a pericentriolar protein that functions in centrosomal attachment of the γ-tubulin ring complex. *Mol. Biol. Cell*. 19:115–125. doi:10.1091/mbc.E07-04-0371.

Fong, P.C., D.S. Boss, T.A. Yap, A. Tutt, P. Wu, M. Mergui-Roelvink, P. Mortimer, H. Swaisland, A. Lau, M.J. O'Connor, A. Ashworth, J. Carmichael, S.B. Kaye, J.H.M. Schellens, dan J.S. de Bono. 2009. Inhibition of Poly(ADP-Ribose) Polymerase in Tumors from BRCA Mutation Carriers . *N. Engl. J. Med.* 361:123–134. doi:10.1056/NEJMOA0900212/SUPPL_FILE/NEJM_FONG_123SA1.PDF.

Frank-Vaillant, M., dan S. Marcand. 2002. Transient stability of DNA ends allows nonhomologous end joining to precede homologous recombination. *Mol. Cell*. 10:1189–1199. doi:10.1016/S1097-2765(02)00705-0.

Fry, A.M. 2015. Solving the centriole disengagement puzzle. *Nat. Cell Biol.* 17:3–5. doi:10.1038/ncb3087.

Fu, D., J.A. Calvo, dan L.D. Samson. 2012. Balancing repair and tolerance of DNA damage caused by alkylating agents. *Nat. Rev. Cancer*. 12:104–120. doi:10.1038/NRC3185.

Fu, J., dan D.M. Glover. 2012. Structured illumination of the interface between centriole and peri-centriolar material. *Open Biol.* 2. doi:10.1098/RSOB.120104.

Fuchs, D.A., dan J. R.K. Cytologic evidence that taxol, an antineoplastic agent from Taxus brevifolia, acts as a mitotic spindle poison - PubMed.

Fukasawa, K., T. Choi, R. Kuriyama, S. Rulong, dan G.F. Vande Woude. 1996a. Abnormal centrosome amplification in the absence of p53. *Science (80-.).* 271:1744–1747. doi:10.1126/science.271.5256.1744.

Fukasawa, K., T. Choi, R. Kuriyama, S. Rulong, dan G.F. Vande Woude. 1996b. Abnormal Centrosome Amplification in the Absence of p53. *Science (80-.).* 271:1744–1747. doi:10.1126/science.271.5256.1744.

Galimberti, F., S.L. Thompson, S. Ravi, D.A. Compton, dan E. Dmitrovsky. 2011. Anaphase Catastrophe is a Target for Cancer Therapy. *Clin. Cancer Res.* 17:1218. doi:10.1158/1078-0432.CCR-10-1178.

Galluzzi, L., O. Kepp, dan G. Kroemer. 2016. Mitochondrial regulation of cell death: a phylogenetically conserved control. *Microb. cell (Graz, Austria)*. 3:101–108. doi:10.15698/MIC2016.03.483.

Galluzzi, L., I. Vitale, S.A. Aaronson, J.M. Abrams, D. Adam, P. Agostinis, E.S. Alnemri, L. Altucci, I. Amelio, D.W. Andrews, M. Annicchiarico-Petruzzelli, A. V. Antonov, E. Arama, E.H. Baehrecke, N.A. Barlev, N.G. Bazan, F. Bernassola, M.J.M. Bertrand, K. Bianchi, M. V. Blagosklonny, K. Blomgren, C. Borner, P. Boya, C. Brenner, M. Campanella, E. Candi, D. Carmona-Gutierrez, F. Cecconi, F.K.M. Chan, N.S. Chandel, E.H. Cheng, J.E. Chipuk, J.A. Cidlowski, A. Ciechanover, G.M. Cohen, M. Conrad, J.R. Cubillos-Ruiz, P.E. Czabotar, V. D'Angiolella, T.M. Dawson, V.L. Dawson, V. De Laurenzi, R. De Maria, K.M. Debatin, R.J. Deberardinis, M. Deshmukh, N. Di Daniele, F. Di Virgilio, V.M. Dixit, S.J. Dixon, C.S. Duckett, B.D. Dynlacht, W.S. El-Deiry, J.W. Elrod, G.M. Fimia, S. Fulda, A.J. García-Sáez, A.D. Garg, C. Garrido, E. Gavathiotis, P. Golstein, E. Gottlieb, D.R. Green, L.A. Greene, H. Gronemeyer, A. Gross, G. Hajnoczky, J.M. Hardwick, I.S. Harris, M.O. Hengartner, C. Hetz, H. Ichijo, M. Jäättelä, B. Joseph, P.J. Jost, P.P. Juin, W.J. Kaiser, M. Karin, T. Kaufmann, O. Kepp, A. Kimchi, R.N. Kitsis, D.J. Klionsky, R.A. Knight, S. Kumar, S.W. Lee, J.J. Lemasters, B. Levine, A. Linkermann, S.A. Lipton, R.A. Lockshin, C. López-Otín, S.W.

Lowe, T. Luedde, E. Lugli, M. MacFarlane, F. Madeo, M. Malewicz, et al. 2018. Molecular mechanisms of cell death: recommendations of the Nomenclature Committee on Cell Death 2018. *Cell Death Differ. 2018 253*. 25:486–541. doi:10.1038/s41418-017-0012-4.

Gambarotto, D., C. Pennetier, J.M. Ryniawec, D.W. Buster, D. Gogendeau, A. Goupil, M. Nano, A. Simon, D. Blanc, V. Racine, Y. Kimata, G.C. Rogers, dan R. Basto. 2019. Plk4 Regulates Centriole Asymmetry and Spindle Orientation in Neural Stem Cells. *Dev. Cell*. 50:11-24.e10. doi:10.1016/J.DEVCEL.2019.04.036.

Ganem, N.J., S.A. Godinho, dan D. Pellman. 2009. A mechanism linking extra centrosomes to chromosomal instability. *Nature*. 460:278–282. doi:10.1038/nature08136.

Ganem, N.J., Z. Storchova, dan D. Pellman. 2007. Tetraploidy, aneuploidy and cancer. *Curr. Opin. Genet. Dev.* 17:157–162. doi:10.1016/J.GDE.2007.02.011.

Ganier, O., D. Schnerch, P. Oertle, R.Y. Lim, M. Plodinec, dan E.A. Nigg. 2018. Structural centrosome aberrations promote non-cell-autonomous invasiveness. *EMBO J.* 37:1–19. doi:10.15252/embj.201798576.

Gao, P., M. Ascano, Y. Wu, W. Barchet, B.L. Gaffney, T. Zillinger, A.A. Serganov, Y. Liu, R.A. Jones, G. Hartmann, T. Tuschl, dan D.J. Patel. 2013. Cyclic [G(2’,5’)pA(3’,5’)p] is the metazoan second messenger produced by DNA-activated cyclic GMP-AMP synthase. *Cell*. 153:1094–1107. doi:10.1016/j.cell.2013.04.046.

Garribba, L., G. De Feudis, V. Martis, M. Galli, M. Dumont, Y. Eliezer, R. Wardenaar, M.R. Ippolito, D.R. Iyer, A.E. Tijhuis, D.C.J. Spierings, M. Schubert, S. Taglietti, C. Soriani, S. Gemble, R. Basto, N. Rhind, F. Foijer, U. Ben-David, D. Fachinetti, Y. Doksani, dan S. Santaguida. 2023. Short-term molecular consequences of chromosome mis-segregation for genome stability. *Nat. Commun.* 14. doi:10.1038/s41467-023-37095-7.

Garrido, C., L. Galluzzi, M. Brunet, P.E. Puig, C. Didelot, dan G. Kroemer. 2006. Mechanisms of cytochrome c release from mitochondria. *Cell Death Differ.* 13:1423–1433. doi:10.1038/sj.cdd.4401950.

Gascoigne, K.E., dan S.S. Taylor. 2008a. Cancer Cells Display Profound Intra- and Interline Variation following Prolonged Exposure to Antimitotic Drugs. *Cancer Cell*. 14:111–122. doi:10.1016/j.ccr.2008.07.002.

Gascoigne, K.E., dan S.S. Taylor. 2008b. Cancer Cells Display Profound Intra- and Interline Variation following Prolonged Exposure to Antimitotic Drugs. *Cancer Cell*. 14:111–122.

doi:10.1016/j.ccr.2008.07.002.

Gascoigne, K.E., dan S.S. Taylor. 2009. How do anti-mitotic drugs kill cancer cells? *J. Cell Sci.* 122:2579–2585. doi:10.1242/jcs.039719.

Gemble, S., R. Wardenaar, K. Keuper, N. Srivastava, M. Nano, A.-S. Macé, A.E. Tijhuis, S.V. Bernhard, D.C.J. Spierings, A. Simon, O. Goundiam, H. Hochegger, M. Piel, F. Foijer, Z. Storchová, dan R. Basto. 2022. Genetic instability from a single S phase after whole-genome duplication. *Nature*. 604:146–151. doi:10.1038/s41586-022-04578-4.

Getts, R.C., dan T.D. Stamato. 1994. Absence of a Ku-like DNA end binding activity in the xrs double-strand DNA repair-deficient mutant. *J. Biol. Chem.* 269:15981–15984. doi:10.1016/S0021-9258(17)33960-1.

Ghelli Luserna Di Rorà, A., C. Cerchione, G. Martinelli, dan G. Simonetti. 2020. A WEE1 family business: regulation of mitosis, cancer progression, and therapeutic target. *J. Hematol. Oncol. 2020 131*. 13:1–17. doi:10.1186/S13045-020-00959-2.

Giansanti, M.G., E. Bucciarelli, S. Bonaccorsi, dan M. Gatti. 2008. Drosophila SPD-2 Is an Essential Centriole Component Required for PCM Recruitment and Astral-Microtubule Nucleation. *Curr. Biol.* 18:303–309. doi:10.1016/j.cub.2008.01.058.

Girish, V., A.A. Lakhani, S.L. Thompson, C.M. Scaduto, L.M. Brown, R.A. Hagenson, E.L. Sausville, B.E. Mendelson, P.K. Kandikuppa, D.A. Lukow, M. Lou Yuan, E.C. Stevens, S.N. Lee, K.M. Schukken, S.M. Akalu, A. Vasudevan, C. Zou, B. Salovska, W. Li, J.C. Smith, A.M. Taylor, R.A. Martienssen, Y. Liu, R. Sun, dan J.M. Sheltzer. 2023. Oncogene-like addiction to aneuploidy in human cancers. *Science*. 381. doi:10.1126/SCIENCE.ADG4521.

Gisselsson, D. 2008. Classification of chromosome segregation errors in cancer. *Chromosoma*. 117:511–519. doi:10.1007/S00412-008-0169-1/FIGURES/2.

Godinho, S.A., dan D. Pellman. 2014. Causes and consequences of centrosome abnormalities in cancer. *Philos. Trans. R. Soc. B Biol. Sci.* 369. doi:10.1098/rstb.2013.0467.

Godinho, S.A., R. Picone, M. Burute, R. Dagher, Y. Su, C.T. Leung, K. Polyak, J.S. Brugge, M. Théry, dan D. Pellman. 2014. Oncogene-like induction of cellular invasion from centrosome amplification. *Nature*. 510:167–171. doi:10.1038/nature13277.

Godwin, A.K., A. Meister, P.J. O'Dwyer, C.S. Huang, T.C. Hamilton, dan M.E. Anderson. 1992. High resistance to cisplatin in human ovarian cancer cell lines is associated with marked

increase of glutathione synthesis. *Proc. Natl. Acad. Sci. U. S. A.* 89:3070–3074. doi:10.1073/PNAS.89.7.3070.

Gogola, E., A.A. Duarte, J.R. de Ruiter, W.W. Wiegant, J.A. Schmid, R. de Bruijn, D.I. James, S. Guerrero Llobet, D.J. Vis, S. Annunziato, B. van den Broek, M. Barazas, A. Kersbergen, M. van de Ven, M. Tarsounas, D.J. Ogilvie, M. van Vugt, L.F.A. Wessels, J. Bartkova, I. Gromova, M. Andújar-Sánchez, J. Bartek, M. Lopes, H. van Attikum, P. Borst, J. Jonkers, dan S. Rottenberg. 2018. Selective Loss of PARG Restores PARylation and Counteracts PARP Inhibitor-Mediated Synthetic Lethality. *Cancer Cell*. 33:1078-1093.e12. doi:10.1016/J.CCELL.2018.05.008.

Goldie, J.H. 2001. Drug resistance in cancer: A perspective. *Cancer Metastasis Rev.* 20:63–68. doi:10.1023/A:1013164609041.

Gomez-Ferreria, M.A., M. Bashkurov, A.O. Helbig, B. Larsen, T. Pawson, A.C. Gingras, dan L. Pelletier. 2012. Novel NEDD1 phosphorylation sites regulate γ-tubulin binding and mitotic spindle assembly. *J. Cell Sci.* 125:3745–3751. doi:10.1242/jcs.105130.

Gonçalves, J., S. Nolasco, R. Nascimento, M.L. Fanarraga, J.C. Zabala, dan H. Soares. 2010. TBCCD1, a new centrosomal protein, is required for centrosome and Golgi apparatus positioning. *EMBO Rep.* 11:194–200. doi:10.1038/EMBOR.2010.5.

Gong, J.G., A. Costanzo, H.Q. Yang, G. Mellno, W.G. Kaelin, M. Levrero, dan J.Y.J. Wang. 1999. The tyrosine kinase c-Abl regulates p73 in apoptotic response to cisplatin-induced DNA damage. *Nature*. 399:806–809. doi:10.1038/21690.

Goodall, J., J. Mateo, W. Yuan, H. Mossop, N. Porta, S. Miranda, R. Perez-Lopez, D. Dolling, D.R. Robinson, S. Sandhu, G. Fowler, B. Ebbs, P. Flohr, G. Seed, D.N. Rodrigues, G. Boysen, C. Bertan, M. Atkin, M. Clarke, M. Crespo, I. Figueiredo, R. Riisnaes, S. Sumanasuriya, P. Rescigno, Z. Zafeiriou, A. Sharp, N. Tunariu, D. Bianchini, A. Gillman, C.J. Lord, E. Hall, A.M. Chinnaiyan, S. Carreira, dan J.S. De Bono. 2017. Circulating Cell-Free DNA to Guide Prostate Cancer Treatment with PARP Inhibition. *Cancer Discov.* 7:1006–1017. doi:10.1158/2159-8290.CD-17-0261.

de Gooijer, M.C., A. van den Top, I. Bockaj, J.H. Beijnen, T. Würdinger, dan O. van Tellingen. 2017. The G2 checkpoint—a node-based molecular switch. *FEBS Open Bio*. 7:439. doi:10.1002/2211-5463.12206.

Gopalakrishnan, J., Y.C. Frederick Chim, A. Ha, M.L. Basiri, D.A. Lerit, N.M. Rusan, dan T. Avidor-Reiss. 2012. Tubulin nucleotide status controls Sas-4-dependent pericentriolar

material recruitment. *Nat. Cell Biol.* 14:865–873. doi:10.1038/ncb2527.

Gopalakrishnan, J., V. Mennella, S. Blachon, B. Zhai, A.H. Smith, T.L. Megraw, D. Nicastro, S.P. Gygi, D.A. Agard, dan T. Avidor-Reiss. 2011. Sas-4 provides a scaffold for cytoplasmic complexes and tethers them in a centrosome. *Nat. Commun.* 2:1–11. doi:10.1038/ncomms1367.

Gordon, D.J., B. Resio, dan D. Pellman. 2012a. Causes and consequences of aneuploidy in cancer. *Nat. Rev. Genet.* 13:189–203. doi:10.1038/nrg3123.

Gordon, D.J., B. Resio, dan D. Pellman. 2012b. Causes and consequences of aneuploidy in cancer. *Nat. Rev. Genet.* 13:189–203. doi:10.1038/nrg3123.

Goundiam, O., dan R. Basto. 2021. Centrosomes in disease: how the same music can sound so different? *Curr. Opin. Struct. Biol.* 66:74–82. doi:10.1016/j.sbi.2020.09.011.

Gradwohl, G., J. Menissier De Murcia, M. Molinete, F. Simonin, M. Koken, J.H.J. Hoeijmakers, dan G. De Murcia. 1990. The second zinc-finger domain of poly(ADP-ribose) polymerase determines specificity for single-stranded breaks in DNA. *Proc. Natl. Acad. Sci. U. S. A.* 87:2990. doi:10.1073/PNAS.87.8.2990.

Graser, S., Y.D. Stierhof, S.B. Lavoie, O.S. Gassner, S. Lamla, M. Le Clech, dan E.A. Nigg. 2007. Cep164, a novel centriole appendage protein required for primary cilium formation. *J. Cell Biol.* 179:321–330. doi:10.1083/jcb.200707181.

Gravells, P., E. Grant, K.M. Smith, D.I. James, dan H.E. Bryant. 2017. Specific killing of DNA damage-response deficient cells with inhibitors of poly(ADP-ribose) glycohydrolase. *DNA Repair (Amst).* 52:81–91. doi:10.1016/J.DNAREP.2017.02.010.

Gravells, P., J. Neale, E. Grant, A. Nathubhai, K.M. Smith, D.I. James, dan H.E. Bryant. 2018. Radiosensitization with an inhibitor of poly(ADP-ribose) glycohydrolase: A comparison with the PARP1/2/3 inhibitor olaparib. *DNA Repair (Amst).* 61:25–36. doi:10.1016/J.DNAREP.2017.11.004.

Greenan, G.A., B. Keszthelyi, R.D. Vale, dan D.A. Agard. 2018. Insights into centriole geometry revealed by cryotomography of doublet and triplet centrioles. *Elife*. 7. doi:10.7554/eLife.36851.

Greenberg, R.A., L. Chin, A. Femino, L. Kee-Ho, G.J. Gottlieb, R.H. Singer, C.W. Greider, dan R.A. DePinho. 1999a. Short dysfunctional telomeres impair tumorigenesis in the INK4a(Δ2/3) cancer-prone mouse. *Cell*. 97:515–525. doi:10.1016/S0092-8674(00)80761-8.

Greenberg, R.A., L. Chin, A. Femino, L. Kee-Ho, G.J. Gottlieb, R.H. Singer, C.W. Greider, dan R.A. DePinho. 1999b. Short dysfunctional telomeres impair tumorigenesis in the INK4a(Δ2/3) cancer-prone mouse. *Cell*. 97:515–525. doi:10.1016/S0092-8674(00)80761-8.

Gregan, J., C.G. Riedel, A.L.L. Pidoux, Y. Katou, C. Rumpf, A. Schleiffer, S.E. Kearsey, K. Shirahige, R.C. Allshire, dan K. Nasmyth. 2007. The Kinetochore Proteins Pcs1 and Mde4 and Heterochromatin Are Required to Prevent Merotelic Orientation. *Curr. Biol.* 17:1190–1200. doi:10.1016/j.cub.2007.06.044.

Gronlund, B., C. Hogdall, H.H. Hansen, dan S.A. Engelholm. 2001. Results of reinduction therapy with paclitaxel and carboplatin in recurrent epithelial ovarian cancer. *Gynecol. Oncol.* 83:128–134. doi:10.1006/GYNO.2001.6364.

Gruss, O.J. 2018. Animal female meiosis: The challenges of eliminating centrosomes. *Cells*. 7. doi:10.3390/cells7070073.

Guadagno, T.M., dan J.W. Newport. 1996. Cdk2 kinase is required for entry into mitosis as a positive regulator of Cdc2-cyclin B kinase activity. *Cell*. 84:73–82. doi:10.1016/S0092-8674(00)80994-0.

Guderian, G., J. Westendorf, A. Uldschmid, dan E.A. Nigg. 2010. Plk4 trans-autophosphorylation regulates centriole number by controlling βTrCP-mediated degradation. *J. Cell Sci.* 123:2163–2169. doi:10.1242/jcs.068502.

Le Guennec, M., N. Klena, D. Gambarotto, M.H. Laporte, A.M. Tassin, H. van den Hoek, P.S. Erdmann, M. Schaffer, L. Kovacik, S. Borgers, K.N. Goldie, H. Stahlberg, M. Bornens, J. Azimzadeh, B.D. Engel, V. Hamel, dan P. Guichard. 2020. A helical inner scaffold provides a structural basis for centriole cohesion. *Sci. Adv.* 6:4137–4151. doi:10.1126/sciadv.aaz4137.

Guichard, P., V. Hachet, N. Majubu, A. Neves, D. Demurtas, N. Olieric, I. Fluckiger, A. Yamada, K. Kihara, Y. Nishida, S. Moriya, M.O. Steinmetz, Y. Hongoh, dan P. Gönczy. 2013. Native architecture of the centriole proximal region reveals features underlying its 9-fold radial symmetry. *Curr. Biol.* 23:1620–1628. doi:10.1016/j.cub.2013.06.061.

Guo, H. qin, M. Gao, J. Ma, T. Xiao, L. lin Zhao, Y. Gao, dan Q. jing Pan. 2007. Analysis of the cellular centrosome in fine-needle aspirations of the breast. *Breast Cancer Res.* 9:1–7. doi:10.1186/bcr1752.

Habedanck, R., Y.-D. Stierhof, C.J. Wilkinson, dan E.A. Nigg. 2005. The Polo kinase Plk4

functions in centriole duplication. *Nat. Cell Biol.* 7:1140–1146. doi:10.1038/ncb1320.

Hagrman, D., J. Goodisman, J.C. Dabrowiak, dan A.K. Souid. 2003. Kinetic study on the reaction of cisplatin with metallothionein. *Drug Metab. Dispos.* 31:916–923. doi:10.1124/dmd.31.7.916.

Hamill, D.R., A.F. Severson, J.C. Carter, dan B. Bowerman. 2002. Centrosome maturation and mitotic spindle assembly in C. elegans require SPD-5, a protein with multiple coiled-coil domains. *Dev. Cell*. 3:673–684. doi:10.1016/S1534-5807(02)00327-1.

Hansemann, D. 1890. Ueber asymmetrische Zelltheilung in Epithelkrebsen und deren biologische Bedeutung. *Arch. für Pathol. Anat. und Physiol. und für Klin. Med.* 119:299–326. doi:10.1007/BF01882039/METRICS.

Harding, S.M., J.L. Benci, J. Irianto, D.E. Discher, A.J. Minn, dan R.A. Greenberg. 2017a. Mitotic progression following DNA damage enables pattern recognition within micronuclei. *Nature*. 548:466–470. doi:10.1038/nature23470.

Harding, S.M., J.L. Benci, J. Irianto, D.E. Discher, A.J. Minn, dan R.A. Greenberg. 2017b. Mitotic progression following DNA damage enables pattern recognition within micronuclei. *Nature*. 548:466–470. doi:10.1038/nature23470.

Haren, L., T. Stearns, dan J. Lüders. 2009. Plk1-Dependent Recruitment of γ-Tubulin Complexes to Mitotic Centrosomes Involves Multiple PCM Components. *PLoS One*. 4:e5976. doi:10.1371/journal.pone.0005976.

Harris, H. 2008. Concerning the origin of malignant tumours by Theodor Boveri. Translated and annotated by Henry Harris. Preface. *J. Cell Sci.* 121 Suppl:1–62.

Haruki, N., H. Saito, T. Harano, S. Nomoto, T. Takahashi, H. Osada, Y. Fujii, dan T. Takahashi. 2001. Molecular analysis of the mitotic checkpoint genes BUB1, BUBR1 and BUB3 in human lung cancers. *Cancer Lett.* 162:201–205. doi:10.1016/S0304-3835(00)00675-3.

Hassa, P.O., dan M.O. Hottiger. 2008. The diverse biological roles of mammalian PARPS, a small but powerful family of poly-ADP-ribose polymerases. *Front. Biosci.* 13:3046–3082. doi:10.2741/2909.

Hatch, E.M., A. Kulukian, A.J. Holland, D.W. Cleveland, dan T. Stearns. 2010. Cep152 interacts with Plk4 and is required for centriole duplication. *J. Cell Biol.* 191:721–729. doi:10.1083/jcb.201006049.

Heald, R., R. Tournebize, T. Blank, R. Sandaltzopoulos, P. Becker, A. Hyman, dan E. Karsenti. 1996. Self-organization of microtubules into bipolar spindles around artificial

chromosomes in Xenopus egg extracts. *Nature*. 382:420–425. doi:10.1038/382420a0.

Hinchcliffe, E.H., C. Li, E.A. Thompson, J.L. Maller, dan G. Sluder. 1999. Requirement of Cdk2-Cyclin E Activity for Repeated Centrosome Reproduction in Xenopus Egg Extracts. *Science (80-.).* 283:851–854. doi:10.1126/SCIENCE.283.5403.851.

Hirota, T., N. Kunitoku, T. Sasayama, T. Marumoto, D. Zhang, M. Nitta, K. Hatakeyama, dan H. Saya. 2003. Aurora-A and an Interacting Activator, the LIM Protein Ajuba, Are Required for Mitotic Commitment in Human Cells. *Cell*. 114:585–598. doi:10.1016/S0092-8674(03)00642-1.

Höhn, A.K., C.E. Brambs, G.G.R. Hiller, D. May, E. Schmoeckel, dan L.C. Horn. 2021. 2020 WHO Classification of Female Genital Tumors. *Geburtshilfe Frauenheilkd.* 81:1145–1153. doi:10.1055/a-1545-4279.

Holland, A.J., D. Fachinetti, Q. Zhu, M. Bauer, I.M. Verma, E.A. Nigg, dan D.W. Cleveland. 2012a. The autoregulated instability of Polo-like kinase 4 limits centrosome duplication to once per cell cycle. *Genes Dev.* 26:2684–2689. doi:10.1101/gad.207027.112.

Holland, A.J., D. Fachinetti, Q. Zhu, M. Bauer, I.M. Verma, E.A. Nigg, dan D.W. Cleveland. 2012b. The autoregulated instability of Polo-like kinase 4 limits centrosome duplication to once per cell cycle. *Genes Dev.* 26:2684–2689. doi:10.1101/gad.207027.112.

Holland, A.J., W. Lan, S. Niessen, H. Hoover, dan D.W. Cleveland. 2010a. Polo-like kinase 4 kinase activity limits centrosome overduplication by autoregulating its own stability. *J. Cell Biol.* 188:191–198. doi:10.1083/jcb.200911102.

Holland, A.J., W. Lan, S. Niessen, H. Hoover, dan D.W. Cleveland. 2010b. Polo-like kinase 4 kinase activity limits centrosome overduplication by autoregulating its own stability. *J. Cell Biol.* 188:191–198. doi:10.1083/jcb.200911102.

Holland, A.J., W. Lan, S. Niessen, H. Hoover, dan D.W. Cleveland. 2010c. Polo-like kinase 4 kinase activity limits centrosome overduplication by autoregulating its own stability. *J. Cell Biol.* 188:191–198. doi:10.1083/jcb.200911102.

Holliday, R. 1964. THE INDUCTION OF MITOTIC RECOMBINATION BY MITOMYCIN C IN USTILAGO AND SACCHAROMYCES. *Genetics*. 50:323–335. doi:10.1093/GENETICS/50.3.323.

Hollis, R.L., J.P. Thomson, B. Stanley, M. Churchman, A.M. Meynert, T. Rye, C. Bartos, Y. Iida, I. Croy, M. Mackean, F. Nussey, A. Okamoto, C.A. Semple, C. Gourley, dan C.S. Herrington. 2020. Molecular stratification of endometrioid ovarian carcinoma predicts

clinical outcome. *Nat. Commun. 2020 111*. 11:1–10. doi:10.1038/s41467-020-18819-5.

Holzer, A.K., G. Samimi, K. Katano, W. Naerdemann, X. Lin, R. Safaei, dan S.B. Howell. 2004. The copper influx transporter human copper transport protein 1 regulates the uptake of cisplatin in human ovarian carcinoma cells. *Mol. Pharmacol.* 66:817–823. doi:10.1124/mol.104.001198.

Van Horck, F.P.G., M.R. Ahmadian, L.C. Haeusler, W.H. Moolenaar, dan O. Kranenburg. 2001. Characterization of p190RhoGEF, a RhoA-specific guanine nucleotide exchange factor that interacts with microtubules. *J. Biol. Chem.* 276:4948–4956. doi:10.1074/JBC.M003839200.

Hornick, J.E., C.C. Mader, E.K. Tribble, C.C. Bagne, K.T. Vaughan, S.L. Shaw, dan E.H. Hinchcliffe. 2011. Amphiastral mitotic spindle assembly in vertebrate cells lacking centrosomes. *Curr. Biol.* 21:598–605. doi:10.1016/j.cub.2011.02.049.

Howard, J., dan A.A. Hyman. 2007. Microtubule polymerases and depolymerases. *Curr. Opin. Cell Biol.* 19:31–35. doi:10.1016/J.CEB.2006.12.009.

Howell, S.B., R. Safaei, C.A. Larson, dan M.J. Sailor. 2010. Copper transporters and the cellular pharmacology of the platinum-containing cancer drugs. *Mol. Pharmacol.* 77:887–894. doi:10.1124/mol.109.063172.

Hoyt, M.A., L. Totis, dan B.T. Roberts. 1991. S. cerevisiae genes required for cell cycle arrest in response to loss of microtubule function. *Cell*. 66:507–517. doi:10.1016/0092-8674(81)90014-3.

Huang, J., W.C. Chan, C.H. Ngai, V. Lok, L. Zhang, D.E. Lucero-Prisno, W. Xu, Z.J. Zheng, E. Elcarte, M. Withers, dan M.C.S. Wong. 2022. Worldwide Burden, Risk Factors, and Temporal Trends of Ovarian Cancer: A Global Study. *Cancers (Basel).* 14:1–12. doi:10.3390/cancers14092230.

Huang, L., Q. Ao, Q. Zhang, X. Yang, H. Xing, F. Li, G. Chen, J. Zhou, S. Wang, G. Xu, L. Meng, Y. Lu, dan D. Ma. 2010. Hypoxia induced paclitaxel resistance in human ovarian cancers via hypoxia-inducible factor 1alpha. *J. Cancer Res. Clin. Oncol.* 136:447–456. doi:10.1007/S00432-009-0675-4.

Huang, N., Y. Xia, D. Zhang, S. Wang, Y. Bao, R. He, J. Teng, dan J. Chen. 2017. Hierarchical assembly of centriole subdistal appendages via centrosome binding proteins CCDC120 and CCDC68. *Nat. Commun. 2017 81*. 8:1–14. doi:10.1038/ncomms15057.

Huangt, J.-C., D.B. Zamblet, J.T. Reardont, S.J. Lippard, dan A. Sancart. 1994. HMG-domain

proteins specifically inhibit the repair of the major DNA adduct of the anticancer drug cisplatin by human excision nuclease (ccthrapy/DNA repair/xeroderma pgmentosum). 91. 10394–10398 pp.

Hustedt, N., dan D. Durocher. 2017. The control of DNA repair by the cell cycle. *Nat. Cell Biol.* 19:1–9. doi:10.1038/ncb3452.

Hwang, L.H., L.F. Lau, D.L. Smith, C.A. Mistrot, K.G. Hardwick, E.S. Hwang, A. Amon, dan A.W. Murray. 1998. Budding yeast Cdc20: a target of the spindle checkpoint. *Science*. 279:1041–1044. doi:10.1126/SCIENCE.279.5353.1041.

Hymowitz, S.G., H.W. Christinger, G. Fuh, M. Ultsch, M. O'Connell, R.F. Kelley, A. Ashkenazi, dan A.M. De Vos. 1999. Triggering cell death: the crystal structure of Apo2L/TRAIL in a complex with death receptor 5. *Mol. Cell*. 4:563–571. doi:10.1016/S1097-2765(00)80207-5.

Ibrahim, R., C. Messaoudi, F.J. Chichon, C. Celati, dan S. Marco. 2009. Electron tomography study of isolated human centrioles. *Microsc. Res. Tech.* 72:42–48. doi:10.1002/jemt.20637.

Iida, Y., A. Okamoto, R.L. Hollis, C. Gourley, dan C.S. Herrington. 2021. Clear cell carcinoma of the ovary: a clinical and molecular perspective. *Int. J. Gynecol. Cancer*. 31:605–616. doi:10.1136/IJGC-2020-001656.

Ippolito, M.R., V. Martis, S. Martin, A.E. Tijhuis, C. Hong, R. Wardenaar, M. Dumont, J. Zerbib, D.C.J. Spierings, D. Fachinetti, U. Ben-David, F. Foijer, dan S. Santaguida. 2021. Gene copy-number changes and chromosomal instability induced by aneuploidy confer resistance to chemotherapy. *Dev. Cell*. 1–15. doi:10.1016/j.devcel.2021.07.006.

Ira, G., A. Pellicioll, A. Balijja, X. Wang, S. Florani, W. Carotenuto, G. Liberi, D. Bressan, L. Wan, N.M. Hollingsworth, J.E. Haber, dan M. Folani. 2004. DNA end resection, homologous recombination and DNA damage checkpoint activation require CDK1. *Nat. 2004 4317011*. 431:1011–1017. doi:10.1038/nature02964.

Ishida, S., J. Lee, D.J. Thiele, dan I. Herskowitz. 2002. Uptake of the anticancer drug cisplatin mediated by the copper transporter Ctr1 in yeast and mammals. *Proc. Natl. Acad. Sci. U. S. A.* 99:14298–14302. doi:10.1073/pnas.162491399.

Ishida, S., F. McCormick, K. Smith-McCune, dan D. Hanahan. 2010. Enhancing Tumor-Specific Uptake of the Anticancer Drug Cisplatin with a Copper Chelator. *Cancer Cell*. 17:574–583. doi:10.1016/j.ccr.2010.04.011.

Isono, M., A. Niimi, T. Oike, Y. Hagiwara, H. Sato, R. Sekine, Y. Yoshida, S.Y. Isobe, C. Obuse, R. Nishi, E. Petricci, S. Nakada, T. Nakano, dan A. Shibata. 2017. BRCA1 Directs the Repair Pathway to Homologous Recombination by Promoting 53BP1 Dephosphorylation. *Cell Rep.* 18:520–532. doi:10.1016/j.celrep.2016.12.042.

Itoh, N., S. Yonehara, A. Ishii, M. Yonehara, S.I. Mizushima, M. Sameshima, A. Hase, Y. Seto, dan S. Nagata. 1991. The polypeptide encoded by the cDNA for human cell surface antigen Fas can mediate apoptosis. *Cell*. 66:233–243. doi:10.1016/0092-8674(91)90614-5.

Jackman, M., C. Lindon, E.A. Niggt, dan J. Pines. 2003. Active cyclin B1-Cdk1 first appears on centrosomes in prophase. *Nat. Cell Biol.* 5:143–148. doi:10.1038/ncb918.

Jain, A., L.C. Agostini, G.A. McCarthy, S.N. Chand, A.J. Ramirez, A. Nevler, J. Cozzitorto, C.W. Schultz, C.Y. Lowder, K.M. Smith, I.D. Waddell, M. Raitses-Gurevich, C. Stossel, Y.G. Gorman, D. Atias, C.J. Yeo, J.M. Winter, K.P. Olive, T. Golan, M.J. Pishvaian, D. Ogilvie, D.I. James, A.M. Jordan, dan J.R. Brody. 2019. Poly (ADP) ribose glycohydrolase can be effectively targeted in pancreatic cancer. *Cancer Res.* 79:4491–4502. doi:10.1158/0008-5472.CAN-18-3645/653605/AM/POLY-ADP-RIBOSE-GLYCOHYDROLASE-CAN-BE-EFFECTIVELY.

Jamal-Hanjani, M., G.A. Wilson, N. McGranahan, N.J. Birkbak, T.B.K. Watkins, S. Veeriah, S. Shafi, D.H. Johnson, R. Mitter, R. Rosenthal, M. Salm, S. Horswell, M. Escudero, N. Matthews, A. Rowan, T. Chambers, D.A. Moore, S. Turajlic, H. Xu, S.-M. Lee, M.D. Forster, T. Ahmad, C.T. Hiley, C. Abbosh, M. Falzon, E. Borg, T. Marafioti, D. Lawrence, M. Hayward, S. Kolvekar, N. Panagiotopoulos, S.M. Janes, R. Thakrar, A. Ahmed, F. Blackhall, Y. Summers, R. Shah, L. Joseph, A.M. Quinn, P.A. Crosbie, B. Naidu, G. Middleton, G. Langman, S. Trotter, M. Nicolson, H. Remmen, K. Kerr, M. Chetty, L. Gomersall, D.A. Fennell, A. Nakas, S. Rathinam, G. Anand, S. Khan, P. Russell, V. Ezhil, B. Ismail, M. Irvin-Sellers, V. Prakash, J.F. Lester, M. Kornaszewska, R. Attanoos, H. Adams, H. Davies, S. Dentro, P. Taniere, B. O'Sullivan, H.L. Lowe, J.A. Hartley, N. Iles, H. Bell, Y. Ngai, J.A. Shaw, J. Herrero, Z. Szallasi, R.F. Schwarz, A. Stewart, S.A. Quezada, J. Le Quesne, P. Van Loo, C. Dive, A. Hackshaw, dan C. Swanton. 2017. Tracking the Evolution of Non–Small-Cell Lung Cancer. *N. Engl. J. Med.* 376:2109–2121. doi:10.1056/nejmoa1616288.

Jamieson, E.R., dan S.J. Lippard. 1999. Structure , Recognition , and Processing of Cisplatin −

DNA Adducts.

Janssen, A., M. Van Der Burg, K. Szuhai, G.J.P.L. Kops, dan R.H. Medema. 2011. Chromosome segregation errors as a cause of DNA damage and structural chromosome aberrations. *Science*. 333:1895–1898. doi:10.1126/SCIENCE.1210214.

Jaspers, J.E., W. Sol, A. Kersbergen, A. Schlicker, C. Guyader, G. Xu, L. Wessels, P. Borst, J. Jonkers, dan S. Rottenberg. 2015. BRCA2-deficient sarcomatoid mammary tumors exhibit multidrug resistance. *Cancer Res.* 75:732–741. doi:10.1158/0008-5472.CAN-14-0839.

Jazayeri, A., J. Falck, C. Lukas, J. Bartek, G.C.M. Smith, J. Lukas, dan S.P. Jackson. 2006. ATM- and cell cycle-dependent regulation of ATR in response to DNA double-strand breaks. *Nat. Cell Biol.* 8:37–45. doi:10.1038/NCB1337.

Jingwen, B., L. Yaochen, dan Z. Guojun. 2017. Cell cycle regulation and anticancer drug discovery. *Cancer Biol. Med.* 14:348. doi:10.20892/J.ISSN.2095-3941.2017.0033.

Johnatty, S.E., J. Beesley, B. Gao, X. Chen, Y. Lu, M.H. Law, M.J. Henderson, A.J. Russell, E.L. Hedditch, C. Emmanuel, S. Fereday, P.M. Webb, E.L. Goode, R.A. Vierkant, B.L. Fridley, J.M. Cunningham, P.A. Fasching, M.W. Beckmann, A.B. Ekici, E. Hogdall, S.K. Kjaer, A. Jensen, C. Hogdall, R. Brown, J. Paul, S. Lambrechts, E. Despierre, I. Vergote, J. Lester, B.Y. Karlan, F. Heitz, A. Du Bois, P. Harter, I. Schwaab, Y. Bean, T. Pejovic, D.A. Levine, M.T. Goodman, M.E. Camey, P.J. Thompson, G. Lurie, J. Shildkraut, A. Berchuck, K.L. Terry, D.W. Cramer, M.D. Norris, M. Haber, S. MacGregor, A. DeFazio, dan G. Chenevix-Trench. 2013. ABCB1 (MDR1) polymorphisms and ovarian cancer progression and survival: a comprehensive analysis from the Ovarian Cancer Association Consortium and The Cancer Genome Atlas. *Gynecol. Oncol.* 131:8–14. doi:10.1016/J.YGYNO.2013.07.107.

Johnson, N., S.F. Johnson, W. Yao, Y.C. Li, Y.E. Choi, A.J. Bernhardy, Y. Wang, M. Capelletti, K.A. Sarosiek, L.A. Moreau, D. Chowdhury, A. Wickramanayake, M.I. Harrell, J.F. Liu, A.D. D'Andrea, A. Miron, E.M. Swisher, dan G.I. Shapiro. 2013. Stabilization of mutant BRCA1 protein confers PARP inhibitor and platinum resistance. *Proc. Natl. Acad. Sci. U. S. A.* 110:17041–17046. doi:10.1073/PNAS.1305170110.

Joo, W.S., P.D. Jeffrey, S.B. Cantor, M.S. Finnin, D.M. Livingston, dan N.P. Pavletich. 2002. Structure of the 53BP1 BRCT region bound to p53 and its comparison to the Brca1 BRCT structure. *Genes Dev.* 16:583–593. doi:10.1101/gad.959202.

Jordan, M.A., dan L. Wilson. 2004. Microtubules as a target for anticancer drugs. *Nat. Rev. Cancer*. 4:253–265. doi:10.1038/nrc1317.

Joshi, H.C., M.J. Palacios, L. McNamara, dan D.W. Cleveland. 1992. γ-Tubulin is a centrosomal protein required for cell cycle-dependent microtubule nucleation. *Nature*. 356:80–83. doi:10.1038/356080a0.

Kabsch, W., H.G. Mannherz, D. Suck, E.F. Pai, dan K.C. Holmes. 1990. Atomic structure of the actin:DNase I complex. *Nature*. 347:37–44. doi:10.1038/347037A0.

Kahlem, P., M. Sultan, R. Herwig, M. Steinfath, D. Balzereit, B. Eppens, N.G. Saran, M.T. Pletcher, S.T. South, G. Stetten, H. Lehrach, R.H. Reeves, dan M.L. Yaspo. 2004. Transcript level alterations reflect gene dosage effects across multiple tissues in a mouse model of Down syndrome. *Genome Res.* 14:1258–1267. doi:10.1101/gr.1951304.

Kalkavan, H., dan D.R. Green. 2017. MOMP, cell suicide as a BCL-2 family business. *Cell Death Differ. 2018 251*. 25:46–55. doi:10.1038/cdd.2017.179.

Kallijärvi, J., U. Lahtinen, R. Hämäläinen, M. Lipsanen-Nyman, J.J. Palvimo, dan A.E. Lehesjoki. 2005. TRIM37 defective in mulibrey nanism is a novel RING finger ubiquitin E3 ligase. *Exp. Cell Res.* 308:146–155. doi:10.1016/J.YEXCR.2005.04.001.

Kampan, N.C., M.T. Madondo, O.M. McNally, M. Quinn, dan M. Plebanski. 2015. Paclitaxel and Its Evolving Role in the Management of Ovarian Cancer. *Biomed Res. Int.* 2015. doi:10.1155/2015/413076.

Karanam, K., R. Kafri, A. Loewer, dan G. Lahav. 2012. Quantitative live cell imaging reveals a gradual shift between DNA repair mechanisms and a maximal use of HR in mid S phase. *Mol. Cell*. 47:320–329. doi:10.1016/J.MOLCEL.2012.05.052.

Karki, M., N. Keyhaninejad, dan C.B. Shuster. 2017. Precocious centriole disengagement and centrosome fragmentation induced by mitotic delay. *Nat. Commun.* 8:1–12. doi:10.1038/ncomms15803.

Kasparkova, J., V. Marini, Y. Najajreh, D. Gibson, dan V. Brabec. 2003. DNA binding mode of the cis and trans geometries of new antitumor nonclassical platinum complexes containing piperidine, piperazine, or 4-picoline ligand in cell-free media. Relations to their activity in cancer cell lines. *Biochemistry*. 42:6321–6332. doi:10.1021/bi0342315.

Kato, H., dan A.A. Sandberg. 1968. Chromosome Pulverization in Human Cells With Micronuclei<xref ref-type="fn" rid="FN2">2</xref> *JNCI J. Natl. Cancer Inst.*

40:165–179. doi:10.1093/jnci/40.1.165.

Kato, J., H. Matsushime, S.W. Hiebert, M.E. Ewen, dan C.J. Sherr. 1993. Direct binding of cyclin D to the retinoblastoma gene product (pRb) and pRb phosphorylation by the cyclin D-dependent kinase CDK4. *Genes Dev.* 7:331–342. doi:10.1101/GAD.7.3.331.

Katsumata, N., M. Yasuda, F. Takahashi, S. Isonishi, T. Jobo, D. Aoki, H. Tsuda, T. Sugiyama, S. Kodama, E. Kimura, K. Ochiai, dan K. Noda. 2009. Dose-dense paclitaxel once a week in combination with carboplatin every 3 weeks for advanced ovarian cancer: a phase 3, open-label, randomised controlled trial. *Lancet*. 374:1331–1338. doi:10.1016/S0140-6736(09)61157-0.

Kaufman, B., R. Shapira-Frommer, R.K. Schmutzler, M.W. Audeh, M. Friedlander, J. Balmaña, G. Mitchell, G. Fried, S.M. Stemmer, A. Hubert, O. Rosengarten, M. Steiner, N. Loman, K. Bowen, A. Fielding, dan S.M. Domchek. 2015. Olaparib monotherapy in patients with advanced cancer and a germline BRCA1/2 mutation. *J. Clin. Oncol.* 33:244–250. doi:10.1200/JCO.2014.56.2728.

Kavallaris, M., D.Y.S. Kuo, C.A. Burkhart, D.L. Regl, M.D. Norris, M. Haber, dan S.B. Horwitz. 1997. Taxol-resistant epithelial ovarian tumors are associated with altered expression of specific beta-tubulin isotypes. *J. Clin. Invest.* 100:1282–1293. doi:10.1172/JCI119642.

Kawamura, E., A.B. Fielding, N. Kannan, A. Balgi, C.J. Eaves, M. Roberge, S. Dedhar, E. Kawamura, A.B. Fielding, N. Kannan, A. Balgi, C.J. Eaves, M. Roberge, dan S. Dedhar. 2013. Identification of novel small molecule inhibitors of centrosome clustering in cancer cells. *Oncotarget*. 4:1763–1776. doi:10.18632/ONCOTARGET.1198.

Kelland, L. 2007. The resurgence of platinum-based cancer chemotherapy. *Nat. Rev. Cancer*. 7:573–584. doi:10.1038/nrc2167.

Kelland, L.R. 1993. New platinum antitumor complexes. *Crit. Rev. Oncol. Hematol.* 15:191–219. doi:10.1016/1040-8428(93)90042-3.

Keller, L.C., E.P. Romijn, I. Zamora, J.R. Yates, dan W.F. Marshall. 2005. Proteomic analysis of isolated Chlamydomonas centrioles reveals orthologs of ciliary-disease genes. *Curr. Biol.* 15:1090–1098. doi:10.1016/j.cub.2005.05.024.

Kemp, C.A., K.R. Kopish, P. Zipperlen, J. Ahringer, dan K.F. O'Connell. 2004. Centrosome maturation and duplication in C. elegans require the coiled-coil protein SPD-2. *Dev. Cell*. 6:511–523. doi:10.1016/S1534-5807(04)00066-8.

Khalique, S., S. Nash, D. Mansfield, J. Wampfler, A. Attygale, K. Vroobel, H. Kemp, R. Buus, H.

Cottom, I. Roxanis, T. Jones, K. von Loga, D. Begum, N. Guppy, P. Ramagiri, K. Fenwick, N. Matthews, M.J.F. Hubank, C.J. Lord, S. Haider, A. Melcher, S. Banerjee, dan R. Natrajan. 2021. Quantitative Assessment and Prognostic Associations of the Immune Landscape in Ovarian Clear Cell Carcinoma. *Cancers (Basel).* 13. doi:10.3390/CANCERS13153854.

Khanna, K.K., dan S.P. Jackson. 2001. DNA double-strand breaks: signaling, repair and the cancer connection. *Nat. Genet. 2001 273*. 27:247–254. doi:10.1038/85798.

Khodjakov, A., R.W. Cole, B.R. Oakley, dan C.L. Rieder. 2000. Centrosome-independent mitotic spindle formation in vertebrates. *Curr. Biol.* 10:59–67. doi:10.1016/S0960-9822(99)00276-6.

Kim, G., G. Ison, A.E. McKee, H. Zhang, S. Tang, T. Gwise, R. Sridhara, E. Lee, A. Tzou, R. Philip, H.J. Chiu, T.K. Ricks, T. Palmby, A.M. Russell, G. Ladouceur, E. Pfuma, H. Li, L. Zhao, Q. Liu, R. Venugopal, A. Ibrahim, dan R. Pazdur. 2015. FDA Approval Summary: Olaparib Monotherapy in Patients with Deleterious Germline BRCA-Mutated Advanced Ovarian Cancer Treated with Three or More Lines of Chemotherapy. *Clin. Cancer Res.* 21:4257–4261. doi:10.1158/1078-0432.CCR-15-0887.

Kim, H., E. George, R.L. Ragland, S. Rafail, R. Zhang, C. Krepler, M.A. Morgan, M. Herlyn, E.J. Brown, dan F. Simpkins. 2017. Targeting the ATR/CHK1 Axis with PARP Inhibition Results in Tumor Regression in BRCA-Mutant Ovarian Cancer Models. *Clin. Cancer Res.* 23:3097–3108. doi:10.1158/1078-0432.CCR-16-2273.

Kim, H., H.C. Tu, D. Ren, O. Takeuchi, J.R. Jeffers, G.P. Zambetti, J.J.D. Hsieh, dan E.H.Y. Cheng. 2009. Stepwise activation of BAX and BAK by tBID, BIM, and PUMA initiates mitochondrial apoptosis. *Mol. Cell*. 36:487–499. doi:10.1016/J.MOLCEL.2009.09.030.

Kim, H., H. Xu, E. George, D. Hallberg, S. Kumar, V. Jagannathan, S. Medvedev, Y. Kinose, K. Devins, P. Verma, K. Ly, Y. Wang, R.A. Greenberg, L. Schwartz, N. Johnson, R.B. Scharpf, G.B. Mills, R. Zhang, V.E. Velculescu, E.J. Brown, dan F. Simpkins. 2020. Combining PARP with ATR inhibition overcomes PARP inhibitor and platinum resistance in ovarian cancer models. *Nat. Commun.* 11. doi:10.1038/S41467-020-17127-2.

Kim, J.S., T.B. Krasieva, V. LaMorte, A. Malcolm, R. Taylor, dan K. Yokomori. 2002. Specific recruitment of human cohesin to laser-induced DNA damage. *J. Biol. Chem.* 277:45149–45153. doi:10.1074/JBC.M209123200.

Kim, S.H., D.P. Lin, S. Matsumoto, A. Kitazono, dan T. Matsumoto. 1998. Fission yeast Slp1:

an effector of the Mad2-dependent spindle checkpoint. *Science*. 279:1045–1047. doi:10.1126/SCIENCE.279.5353.1045.

Kim, T.S., J.E. Park, A. Shukla, S. Choi, R.N. Murugan, J.H. Lee, M. Ahn, K. Rhee, J.K. Bang, B.Y. Kim, J. Loncarek, R.L. Erikson, dan K.S. Lee. 2013. Hierarchical recruitment of Plk4 and regulation of centriole biogenesis by two centrosomal scaffolds, Cep192 and Cep152. *Proc. Natl. Acad. Sci. U. S. A.* 110:E4849. doi:10.1073/pnas.1319656110.

Kindelberger, D.W., Y. Lee, A. Miron, M.S. Hirsch, C. Feltmate, F. Medeiros, M.J. Callahan, E.O. Garner, R.W. Gordon, C. Birch, R.S. Berkowitz, M.G. Muto, dan C.P. Crum. 2007. Intraepithelial Carcinoma of the Fimbria and Pelvic Serous Carcinoma: Evidence for a Causal Relationship. *Am. J. Surg. Pathol.* 31:161–169. doi:10.1097/01.pas.0000213335.40358.47.

King, L.E., R. Rodriguez-Enriquez, R. Pedley, C.E.L. Mellor, P. Wang, E. Zindy, M.R.H. White, K. Brennan, dan A.P. Gilmore. 2022. Apoptotic priming is defined by the dynamic exchange of Bcl-2 proteins between mitochondria and cytosol. *Cell Death Differ.* 29:2262–2274. doi:10.1038/s41418-022-01013-z.

Kirkham, M., T. Müller-Reichert, K. Oegema, S. Grill, dan A.A. Hyman. 2003. SAS-4 is a C. elegans centriolar protein that controls centrosome size. *Cell*. 112:575–587. doi:10.1016/S0092-8674(03)00117-X.

Kischkel, F.C., S. Hellbardt, I. Behrmann, M. Germer, M. Pawlita, P.H. Krammer, dan M.E. Peter. 1995. Cytotoxicity-dependent APO-1 (Fas/CD95)-associated proteins form a death-inducing signaling complex (DISC) with the receptor. *EMBO J.* 14:5579–5588. doi:10.1002/j.1460-2075.1995.tb00245.x.

Kishi, K., T. Sasaki, S. Kuroda, T. Itoh, dan Y. Takai. 1993. Regulation of cytoplasmic division of Xenopus embryo by rho p21 and its inhibitory GDP/GTP exchange protein (rho GDI). *J. Cell Biol.* 120:1187–1195. doi:10.1083/JCB.120.5.1187.

Kishimoto, S., M. Yasuda, dan S. Fukushima. 2017. Changes in the expression of various transporters as influencing factors of resistance to cisplatin. *Anticancer Res.* 37:5477–5484. doi:10.21873/anticanres.11977.

Kitagawa, D., C. Busso, I. Flückiger, dan P. Gönczy. 2009. Phosphorylation of SAS-6 by ZYG-1 is critical for centriole formation in C. elegans embryos. *Dev. Cell*. 17:900–907. doi:10.1016/J.DEVCEL.2009.11.002.

Kitagawa, D., I. Vakonakis, N. Olieric, M. Hilbert, D. Keller, V. Olieric, M. Bortfeld, M.C. Erat, I.

Flückiger, P. Gönczy, dan M.O. Steinmetz. 2011. Structural basis of the 9-fold symmetry of centrioles. *Cell*. 144:364–375. doi:10.1016/j.cell.2011.01.008.

Klein, I., dan H.C. Lehmann. 2021. Pathomechanisms of Paclitaxel-Induced Peripheral Neuropathy. *Toxics 2021, Vol. 9, Page 229*. 9:229. doi:10.3390/TOXICS9100229.

Klena, N., M. Le Guennec, A. Tassin, H. van den Hoek, P.S. Erdmann, M. Schaffer, S. Geimer, G. Aeschlimann, L. Kovacik, Y. Sadian, K.N. Goldie, H. Stahlberg, B.D. Engel, V. Hamel, dan P. Guichard. 2020. Architecture of the centriole cartwheel-containing region revealed by cryo-electron tomography. *EMBO J.* 39. doi:10.15252/embj.2020106246.

Kleylein-Sohn, J., J. Westendorf, M. Le Clech, R. Habedanck, Y.D. Stierhof, dan E.A. Nigg. 2007. Plk4-induced centriole biogenesis in human cells. *Dev. Cell*. 13:190–202. doi:10.1016/J.DEVCEL.2007.07.002.

Knobel, P.A., R. Belotserkovskaya, Y. Galanty, C.K. Schmidt, S.P. Jackson, dan T.H. Stracker. 2014. USP28 Is Recruited to Sites of DNA Damage by the Tandem BRCT Domains of 53BP1 but Plays a Minor Role in Double-Strand Break Metabolism. *Mol. Cell. Biol.* 34:2062–2074. doi:10.1128/mcb.00197-14.

Köbel, M., dan E.Y. Kang. 2022. The Evolution of Ovarian Carcinoma Subclassification. *Cancers (Basel).* 14. doi:10.3390/cancers14020416.

Kohlmaier, G., J. Lončarek, X. Meng, B.F. McEwen, M.M. Mogensen, A. Spektor, B.D. Dynlacht, A. Khodjakov, dan P. Gönczy. 2009. Overly long centrioles and defective cell division upon excess of the SAS-4-related protein CPAP. *Curr. Biol.* 19:1012–1018. doi:10.1016/J.CUB.2009.05.018.

Kondrashova, O., M. Nguyen, K. Shield-Artin, A. V. Tinker, N.N.H. Teng, M.I. Harrell, M.J. Kuiper, G.Y. Ho, H. Barker, M. Jasin, R. Prakash, E.M. Kass, M.R. Sullivan, G.J. Brunette, K.A. Bernstein, R.L. Coleman, A. Floquet, M. Friedlander, G. Kichenadasse, D.M. O'Malley, A. Oza, J. Sun, L. Robillard, L. Maloney, D. Bowtell, H. Giordano, M.J. Wakefield, S.H. Kaufmann, A.D. Simmons, T.C. Harding, M. Raponi, I.A. McNeish, E.M. Swisher, K.K. Lin, dan C.L. Scott. 2017. Secondary Somatic Mutations Restoring RAD51C and RAD51D Associated with Acquired Resistance to the PARP Inhibitor Rucaparib in High-Grade Ovarian Carcinoma. *Cancer Discov.* 7:984–998. doi:10.1158/2159-8290.CD-17-0419.

Kondrashova, O., M. Topp, K. Nesic, E. Lieschke, G.Y. Ho, M.I. Harrell, G. V. Zapparoli, A. Hadley, R. Holian, E. Boehm, V. Heong, E. Sanij, R.B. Pearson, J.J. Krais, N. Johnson, O.

McNally, S. Ananda, K. Alsop, K.J. Hutt, S.H. Kaufmann, K.K. Lin, T.C. Harding, N. Traficante, G. Chenevix-Trench, A. Green, P. Webb, D. Gertig, S. Fereday, S. Moore, J. Hung, K. Harrap, T. Sadkowsky, N. Pandeya, M. Malt, A. Mellon, R. Robertson, T. Vanden Bergh, M. Jones, P. Mackenzie, J. Maidens, K. Nattress, Y.E. Chiew, A. Stenlake, H. Sullivan, B. Alexander, P. Ashover, S. Brown, T. Corrish, L. Green, L. Jackman, K. Ferguson, K. Martin, A. Martyn, B. Ranieri, J. White, V. Jayde, P. Mamers, L. Bowes, L. Galletta, D. Giles, J. Hendley, T. Schmidt, H. Shirley, C. Ball, C. Young, S. Viduka, H. Tran, S. Bilic, L. Glavinas, J. Brooks, R. Stuart-Harris, F. Kirsten, J. Rutovitz, P. Clingan, A. Glasgow, A. Proietto, S. Braye, G. Otton, J. Shannon, T. Bonaventura, J. Stewart, S. Begbie, M. Friedlander, D. Bell, S. Baron-Hay, A. Ferrier, G. Gard, D. Nevell, N. Pavlakis, S. Valmadre, B. Young, C. Camaris, R. Crouch, L. Edwards, N. Hacker, D. Marsden, G. Robertson, P. Beale, et al. 2018. Methylation of all BRCA1 copies predicts response to the PARP inhibitor rucaparib in ovarian carcinoma. *Nat. Commun.* 9. doi:10.1038/s41467-018-05564-z.

Konotop, G., E. Bausch, T. Nagai, A. Turchinovich, N. Becker, A. Benner, M. Boutros, K. Mizuno, A. Krämer, dan M.S. Raab. 2016. Pharmacological Inhibition of Centrosome Clustering by Slingshot-Mediated Cofilin Activation and Actin Cortex Destabilization. *Cancer Res.* 76:6690–6700. doi:10.1158/0008-5472.CAN-16-1144.

Kops, G.J.P.L., D.R. Foltz, dan D.W. Cleveland. 2004. Lethality to human cancer cells through massive chromosome loss by inhibition of the mitotic checkpoint. *Proc. Natl. Acad. Sci. U. S. A.* 101:8699–8704. doi:10.1073/pnas.0401142101.

Kops, G.J.P.L., B.A.A. Weaver, dan D.W. Cleveland. 2005. On the road to cancer: Aneuploidy and the mitotic checkpoint. *Nat. Rev. Cancer*. 5:773–785. doi:10.1038/nrc1714.

Koutsodontis, G., I. Tentes, P. Papakosta, A. Moustakas, dan D. Kardassis. 2001. Sp1 plays a critical role in the transcriptional activation of the human cyclin-dependent kinase inhibitor p21(WAF1/Cip1) gene by the p53 tumor suppressor protein. *J. Biol. Chem.* 276:29116–29125. doi:10.1074/JBC.M104130200.

Kraft, C., H.C. Vodermaier, S. Maurer-Stroh, F. Eisenhaber, dan J.M. Peters. 2005. The WD40 propeller domain of Cdh1 functions as a destruction box receptor for APC/C substrates. *Mol. Cell*. 18:543–553. doi:10.1016/J.MOLCEL.2005.04.023.

Krajewska, M., R.S.N. Fehrmann, E.G.E. De Vries, dan M.A.T.M. van Vugt. 2015. Regulators of homologous recombination repair as novel targets for cancer treatment. *Front.*

Genet. 6:1–15. doi:10.3389/fgene.2015.00096.

Krämer, A., B. Maier, dan J. Bartek. 2011. Centrosome clustering and chromosomal (in)stability: A matter of life and death. *Mol. Oncol.* 5:324–335. doi:10.1016/j.molonc.2011.05.003.

Krämer, A., K. Neben, dan A.D. Ho. 2005. Centrosome aberrations in hematological malignancies. *Cell Biol. Int.* 29:375–383. doi:10.1016/j.cellbi.2005.03.004.

Kristeleit, R.S., R. Shapira-Frommer, A. Oaknin, J. Balmaña, I.L. Ray-Coquard, S. Domchek, A.V. Tinker, C.M. Castro, S. Welch, A.M. Poveda, K. Bell-Mcguinn, G. Konecny, H. Giordano, L. Maloney, S. Goble, L. Rolfe, dan A. Oza. 2016. Clinical activity of the poly(ADP-ribose) polymerase (PARP) inhibitor rucaparib in patients (pts) with high-grade ovarian carcinoma (HGOC) and a BRCA mutation (BRCAmut): Analysis of pooled data from study 10 (parts 1, 2a, and 3) and ARIEL2 (parts 1 and 2). *Clin. Adv. Hematol. Oncol.* 14:11–12. doi:10.1093/annonc/mdw374.03.

Krokan, H.E., dan M. Bjørås. 2013. Base excision repair. *Cold Spring Harb. Perspect. Biol.* 5:1–22. doi:10.1101/cshperspect.a012583.

Kubara, P.M., S. Kernéis-Golsteyn, A. Studény, B.B. Lanser, L. Meijer, dan R.M. Golsteyn. 2012. Human cells enter mitosis with damaged DNA after treatment with pharmacological concentrations of genotoxic agents. *Biochem. J.* 446:373–381. doi:10.1042/BJ20120385.

Kuriyama, R., dan G.G. Borisy. 1981. Centriole Cycle in Chinese Hamster Ovary Cells as Determined by Whole-mount Electron Microscopy. 91. 814–821 pp.

Kurman, R.J. 2013. Origin and molecular pathogenesis of ovarian high-grade serous carcinoma. *Ann. Oncol.* 24. doi:10.1093/annonc/mdt463.

Kurman, R.J., dan I.M. Shih. 2011. Molecular pathogenesis and extraovarian origin of epithelial ovarian cancer - Shifting the paradigm. *Hum. Pathol.* 42:918–931. doi:10.1016/j.humpath.2011.03.003.

Kurnit, D.M. 1979. Down syndrome: Gene dosage at the transcriptional level in skin fibroblasts. *Proc. Natl. Acad. Sci. U. S. A.* 76:2372–2375. doi:10.1073/pnas.76.5.2372.

Kushner, E.J., L.S. Ferro, J.Y. Liu, J.R. Durrant, S.L. Rogers, A.C. Dudley, dan V.L. Bautch. 2014. Excess centrosomes disrupt endothelial cell migration via centrosome scattering. *J. Cell Biol.* 206:257–272. doi:10.1083/jcb.201311013.

Kuwana, T., M.R. Mackey, G. Perkins, M.H. Ellisman, M. Latterich, R. Schneiter, D.R. Green,

dan D.D. Newmeyer. 2002. Bid, Bax, and lipids cooperate to form supramolecular openings in the outer mitochondrial membrane. *Cell*. 111:331–342. doi:10.1016/S0092-8674(02)01036-X.

Kwon, M., S.A. Godinho, N.S. Chandhok, N.J. Ganem, A. Azioune, M. Thery, dan D. Pellman. 2008a. Mechanisms to suppress multipolar divisions in cancer cells with extra centrosomes. *Genes Dev.* 22:2189–2203. doi:10.1101/gad.1700908.

Kwon, M., S.A. Godinho, N.S. Chandhok, N.J. Ganem, A. Azioune, M. Thery, dan D. Pellman. 2008b. Mechanisms to suppress multipolar divisions in cancer cells with extra centrosomes. *Genes Dev.* 22:2189–2203. doi:10.1101/gad.1700908.

Lambrus, B.G., V. Daggubati, Y. Uetake, P.M. Scott, K.M. Clutario, G. Sluder, dan A.J. Holland. 2016. A USP28–53BP1–p53–p21 signaling axis arrests growth after centrosome loss or prolonged mitosis. *J. Cell Biol.* 214:143–153. doi:10.1083/JCB.201604054.

Lambrus, B.G., dan A.J. Holland. 2017. A New Mode of Mitotic Surveillance. *Trends Cell Biol.* 27:314–321. doi:10.1016/j.tcb.2017.01.004.

Lane, D., dan A. Levine. 2010. p53 Research: the past thirty years and the next thirty years. *Cold Spring Harb. Perspect. Biol.* 2. doi:10.1101/CSHPERSPECT.A000893.

Lange, B.M.H., dan K. Gull. 1995. A molecular marker for centriole maturation in the mammalian cell cycle. *J. Cell Biol.* 130:919–927. doi:10.1083/jcb.130.4.919.

Langelier, M.F., K.M. Servent, E.E. Rogers, dan J.M. Pascal. 2008. A third zinc-binding domain of human poly(ADP-ribose) polymerase-1 coordinates DNA-dependent enzyme activation. *J. Biol. Chem.* 283:4105–4114. doi:10.1074/JBC.M708558200.

Lawo, S., M. Hasegan, G.D. Gupta, dan L. Pelletier. 2012. Subdiffraction imaging of centrosomes reveals higher-order organizational features of pericentriolar material. *Nat. Cell Biol.* 14:1148–1158. doi:10.1038/ncb2591.

Leber, B., B. Maier, F. Fuchs, J. Chi, P. Riffel, S. Anderhub, L. Wagner, A.D. Ho, J.L. Salisbury, M. Boutros, dan A. Krämer. 2010a. Proteins required for centrosome clustering in cancer cells. *Sci. Transl. Med.* 2. doi:10.1126/SCITRANSLMED.3000915/SUPPL_FILE/2-33RA38_SM.PDF.

Leber, B., B. Maier, F. Fuchs, J. Chi, P. Riffel, S. Anderhub, L. Wagner, A.D. Ho, J.L. Salisbury, M. Boutros, dan A. Krämer. 2010b. Proteins required for centrosome clustering in cancer cells. *Sci. Transl. Med.* 2. doi:10.1126/SCITRANSLMED.3000915/SUPPL_FILE/2-33RA38_SM.PDF.

Ledermann, J., P. Harter, C. Gourley, M. Friedlander, I. Vergote, G. Rustin, C. Scott, W. Meier, R. Shapira-Frommer, T. Safra, D. Matei, E. Macpherson, C. Watkins, J. Carmichael, dan U. Matulonis. 2012. Olaparib maintenance therapy in platinum-sensitive relapsed ovarian cancer. *N. Engl. J. Med.* 366:1382–1392. doi:10.1056/NEJMOA1105535.

Ledermann, J., P. Harter, C. Gourley, M. Friedlander, I. Vergote, G. Rustin, C.L. Scott, W. Meier, R. Shapira-Frommer, T. Safra, D. Matei, A. Fielding, S. Spencer, B. Dougherty, M. Orr, D. Hodgson, J.C. Barrett, dan U. Matulonis. 2014. Olaparib maintenance therapy in patients with platinum-sensitive relapsed serous ovarian cancer: a preplanned retrospective analysis of outcomes by BRCA status in a randomised phase 2 trial. *Lancet. Oncol.* 15:852–861. doi:10.1016/S1470-2045(14)70228-1.

Ledgerwood, E.C., dan I.M. Morison. 2009. Targeting the apoptosome for cancer therapy. *Clin. Cancer Res.* 15:420–424. doi:10.1158/1078-0432.CCR-08-1172.

Lee, K., dan K. Rhee. 2011a. PLK1 phosphorylation of pericentrin initiates centrosome maturation at the onset of mitosis. *J. Cell Biol.* 195:1093–1101. doi:10.1083/jcb.201106093.

Lee, K., dan K. Rhee. 2011b. PLK1 phosphorylation of pericentrin initiates centrosome maturation at the onset of mitosis. *J. Cell Biol.* 195:1093–1101. doi:10.1083/jcb.201106093.

LeGuennec, M., N. Klena, G. Aeschlimann, V. Hamel, dan P. Guichard. 2021. Overview of the centriole architecture. *Curr. Opin. Struct. Biol.* 66:58–65. doi:10.1016/j.sbi.2020.09.015.

Leidel, S., M. Delattre, L. Cerutti, K. Baumer, dan P. Gönczy. 2005. SAS-6 defines a protein family required for centrosome duplication in C . elegans and in human cells. 7. doi:10.1038/ncb1220.

Leidel, S., dan P. Gönczy. 2003. SAS-4 is essential for centrosome duplication in C elegans and is recruited to daughter centrioles once per cell cycle. *Dev. Cell*. 4:431–439. doi:10.1016/S1534-5807(03)00062-5.

De Leo, A., D. Santini, C. Ceccarelli, G. Santandrea, A. Palicelli, G. Acquaviva, F. Chiarucci, F. Rosini, G. Ravegnini, A. Pession, D. Turchetti, C. Zamagni, A.M. Perrone, P. De Iaco, G. Tallini, dan D. de Biase. 2021. What Is New on Ovarian Carcinoma: Integrated Morphologic and Molecular Analysis Following the New 2020 World Health Organization Classification of Female Genital Tumors. *Diagnostics*. 11:697.

doi:10.3390/diagnostics11040697.

Lessene, G., P.E. Czabotar, B.E. Sleebs, K. Zobel, K.N. Lowes, J.M. Adams, J.B. Baell, P.M. Colman, K. Deshayes, W.J. Fairbrother, J.A. Flygare, P. Gibbons, W.J.A. Kersten, S. Kulasegaram, R.M. Moss, J.P. Parisot, B.J. Smith, I.P. Street, H. Yang, D.C.S. Huang, dan K.G. Watson. 2013. Structure-guided design of a selective BCL-XL inhibitor. *Nat. Chem. Biol. 2013 96*. 9:390–397. doi:10.1038/nchembio.1246.

Letai, A., M.C. Bassik, L.D. Walensky, M.D. Sorcinelli, S. Weiler, dan S.J. Korsmeyer. 2002. Distinct BH3 domains either sensitize or activate mitochondrial apoptosis, serving as prototype cancer therapeutics. *Cancer Cell*. 2:183–192. doi:10.1016/S1535-6108(02)00127-7.

Leverson, J.D., H. Zhang, J. Chen, S.K. Tahir, D.C. Phillips, J. Xue, P. Nimmer, S. Jin, M. Smith, Y. Xiao, P. Kovar, A. Tanaka, M. Bruncko, G.S. Sheppard, L. Wang, S. Gierke, L. Kategaya, D.J. Anderson, C. Wong, J. Eastham-Anderson, M.C. Ludlam, D. Sampath, W.J. Fairbrother, I. Wertz, S.H. Rosenberg, C. Tse, S.W. Elmore, dan A.J. Souers. 2015. Potent and selective small-molecule MCL-1 inhibitors demonstrate on-target cancer cell killing activity as single agents and in combination with ABT-263 (navitoclax). *Cell Death Dis. 2015 61*. 6:e1590–e1590. doi:10.1038/cddis.2014.561.

Levine, M.S., B. Bakker, B. Boeckx, J. Moyett, J. Lu, B. Vitre, D.C. Spierings, P.M. Lansdorp, D.W. Cleveland, D. Lambrechts, F. Foijer, dan A.J. Holland. 2017. Centrosome Amplification Is Sufficient to Promote Spontaneous Tumorigenesis in Mammals. *Dev. Cell*. 40:313-322.e5. doi:10.1016/j.devcel.2016.12.022.

Lheureux, S., M. Braunstein, dan A.M. Oza. 2019. Epithelial ovarian cancer: Evolution of management in the era of precision medicine. *CA. Cancer J. Clin.* 280–304. doi:10.3322/caac.21559.

Li, K., Y. Li, J.M. Shelton, J.A. Richardson, E. Spencer, Z.J. Chen, X. Wang, dan R.S. Williams. 2000. Cytochrome c deficiency causes embryonic lethality and attenuates stress-induced apoptosis. *Cell*. 101:389–399. doi:10.1016/S0092-8674(00)80849-1.

Li, M., X. Fang, D.J. Baker, L. Guo, X. Gao, Z. Wei, S. Han, J.M. Van Deursen, dan P. Zhang. 2010. The ATM-p53 pathway suppresses aneuploidy-induced tumorigenesis. *Proc. Natl. Acad. Sci. U. S. A.* 107:14188–14193. doi:10.1073/pnas.1005960107.

Li, R., dan A.W. Murray. 1991a. <Cell 1991 Li R.pdf>. *Cell*. 66.

Li, R., dan A.W. Murray. 1991b. Feedback control of mitosis in budding yeast. *Cell*. 66:519–

531. doi:10.1016/0092-8674(81)90015-5.

Li, S., J.J. Fernandez, W.F. Marshall, dan D.A. Agard. 2012. Three-dimensional structure of basal body triplet revealed by electron cryo-tomography. *EMBO J.* 31:552–562. doi:10.1038/emboj.2011.460.

Li, T., J. Peng, F. Zeng, K. Zhang, J. Liu, X. Li, Q. Ouyang, G. Wang, L. Wang, Z. Liu, dan Y. Liu. 2017. Association between polymorphisms in CTR1, CTR2, ATP7A, and ATP7B and platinum resistance in epithelial ovarian cancer. *Int. J. Clin. Pharmacol. Ther.* 55:774–780. doi:10.5414/CP202907.

Li, X., dan W.D. Heyer. 2008. Homologous recombination in DNA repair and DNA damage tolerance. *Cell Res.* 18:99–113. doi:10.1038/cr.2008.1.

Lim, Y., L. Dorstyn, dan S. Kumar. 2021. The p53-caspase-2 axis in the cell cycle and DNA damage response. *Exp. Mol. Med.* 53:517–527. doi:10.1038/s12276-021-00590-2.

Lin, M., S.S. Xie, dan K.Y. Chan. 2022. An updated view on the centrosome as a cell cycle regulator. *Cell Div.* 17:1–13. doi:10.1186/s13008-022-00077-0.

Lin, Y.-F., J. Espejo Valle-Inclan, A. Mazzagatti, Q. Hu, E.G. Maurais, A. Guyer, J.T. Sanders, J. Engel, G. Nguyen, D. Bronder, S.F. Bakhoum, I. Cortés-Ciriano, dan P. Ly. 2023. Mitotic clustering of pulverized chromosomes from micronuclei. doi:10.1038/s41586-023-05974-0.

Lin, Y.C., C.W. Chang, W. Bin Hsu, C.J.C. Tang, Y.N. Lin, E.J. Chou, C.T. Wu, dan T.K. Tang. 2013a. Human microcephaly protein CEP135 binds to hSAS-6 and CPAP, and is required for centriole assembly. *EMBO J.* 32:1141–1154. doi:10.1038/emboj.2013.56.

Lin, Y.C., C.W. Chang, W. Bin Hsu, C.J.C. Tang, Y.N. Lin, E.J. Chou, C.T. Wu, dan T.K. Tang. 2013b. Human microcephaly protein CEP135 binds to hSAS-6 and CPAP, and is required for centriole assembly. *EMBO J.* 32:1141–1154. doi:10.1038/emboj.2013.56.

Lin, Y.C., K.C. Wen, P.L. Sung, Y.T. Chou, P.L. Liew, L.Y. Chen, R.L. Huang, H.C. Lai, dan L. Te Chang. 2020. Complete remission of heavily treated ovarian clear cell carcinoma with ARID1A mutations after pembrolizumab and bevacizumab combination therapy: a case report. *J. Ovarian Res.* 13:1–6. doi:10.1186/S13048-020-00751-3/FIGURES/4.

Lindahl, T. 1993. Instability and decay of the primary structure of DNA. *Nat. 1993 3626422*. 362:709–715. doi:10.1038/362709a0.

Linding, R., L.J. Jensen, G.J. Ostheimer, M.A.T.M. van Vugt, C. Jørgensen, I.M. Miron, F. Diella, K. Colwill, L. Taylor, K. Elder, P. Metalnikov, V. Nguyen, A. Pasculescu, J. Jin, J.G.

Park, L.D. Samson, J.R. Woodgett, R.B.B. Russell, P. Bork, M.B. Yaffe, dan T. Pawson. 2007. Systematic discovery of in vivo phosphorylation networks. *Cell*. 129:1415–1426. doi:10.1016/J.CELL.2007.05.052.

Lindon, C., dan J. Pines. 2004. Ordered proteolysis in anaphase inactivates Plk1 to contribute to proper mitotic exit in human cells. *J. Cell Biol.* 164:233–241. doi:10.1083/JCB.200309035/VIDEO-6.

Lingle, W.L., S.L. Barrett, V.C. Negron, A.B. D'Assoro, K. Boeneman, W. Liu, C.M. Whitehead, C. Reynolds, dan J.L. Salisbury. 2002. Centrosome amplification drives chromosomal instability in breast tumor development. *Proc. Natl. Acad. Sci. U. S. A.* 99:1978–1983. doi:10.1073/pnas.032479999.

Lingle, W.L., W.H. Lutz, J.N. Ingle, N.J. Maihle, dan J.L. Salisbury. 1998. Centrosome hypertrophy in human breast tumors: Implications for genomic stability and cell polarity. *Proc. Natl. Acad. Sci. U. S. A.* 95:2950–2955. doi:10.1073/pnas.95.6.2950.

Lingle, W.L., dan J.L. Salisbury. 1999a. The role of the centrosome in the development of malignant tumors. *Curr. Top. Dev. Biol.* 49:313–329. doi:10.1016/S0070-2153(99)49015-5.

Lingle, W.L., dan J.L. Salisbury. 1999b. Altered centrosome structure is associated with abnormal mitoses in human breast tumors. *Am. J. Pathol.* 155:1941–1951. doi:10.1016/S0002-9440(10)65513-7.

Lisio, M.-A., L. Fu, A. Goyeneche, Z. Gao, dan C. Telleria. 2019a. High-Grade Serous Ovarian Cancer: Basic Sciences, Clinical and Therapeutic Standpoints. *Int. J. Mol. Sci.* 20. doi:10.3390/ijms20040952.

Lisio, M.A., L. Fu, A. Goyeneche, Z.H. Gao, dan C. Telleria. 2019b. High-grade serous ovarian cancer: Basic sciences, clinical and therapeutic standpoints. *Int. J. Mol. Sci.* 20. doi:10.3390/ijms20040952.

Littlepage, L.E., dan J. V. Ruderman. 2002. Identification of a new APC/C recognition domain, the A box, which is required for the Cdh1-dependent destruction of the kinase Aurora-A during mitotic exit. *Genes Dev.* 16:2274–2285. doi:10.1101/GAD.1007302.

Liu, S., M. Kwon, M. Mannino, N. Yang, F. Renda, A. Khodjakov, dan D. Pellman. 2018. Nuclear envelope assembly defects link mitotic errors to chromothripsis. *Nature*. 561:551–555. doi:10.1038/s41586-018-0534-z.

Liu, X., H. Wu, J. Loring, S. Hormuzdi, C.M. Disteche, P. Bornstein, dan R. Jaenisch. 1997.

Trisomy eight in ES cells is a common potential problem in gene targeting and interferes with germ line transmission. *Dev. Dyn.* 209:85–91. doi:10.1002/(SICI)1097-0177(199705)209:1<85::AID-AJA8>3.0.CO;2-T.

Llaurado Fernandez, M., A. Dawson, H. Kim, N. Lam, H. Russell, M. Bruce, M. Bittner, J. Hoenisch, S.A. Scott, A. Talhouk, D. Chiu, D. Provencher, M. Nourmoussavi, G. DiMattia, C.H. Lee, C.B. Gilks, M. Köbel, dan M.S. Carey. 2020. Hormone receptor expression and outcomes in low-grade serous ovarian carcinoma. *Gynecol. Oncol.* 157:12–20. doi:10.1016/J.YGYNO.2019.11.029.

Loeb, L.A., dan R.J. Monnat. 2008. DNA polymerases and human disease. *Nat. Rev. Genet.* 9:594–604. doi:10.1038/NRG2345.

Lok, T.M., Y. Wang, W.K. Xu, S. Xie, H.T. Ma, dan R.Y.C. Poon. 2020. Mitotic slippage is determined by p31comet and the weakening of the spindle-assembly checkpoint. *Oncogene 2020 3913*. 39:2819–2834. doi:10.1038/s41388-020-1187-6.

Lomax, M.E., L.K. Folkes, dan P. O'Neill. 2013. Biological Consequences of Radiation-induced DNA Damage: Relevance to Radiotherapy. *Clin. Oncol.* 25:578–585. doi:10.1016/J.CLON.2013.06.007.

Loncarek, J., P. Hergert, V. Magidson, dan A. Khodjakov. 2008. Control of daughter centriole formation by the pericentriolar material: Control of centriole duplication. *Nat. Cell Biol.* 10:322. doi:10.1038/NCB1694.

Lopes, C.A.M., M. Mesquita, A.I. Cunha, J. Cardoso, S. Carapeta, C. Laranjeira, A.E. Pinto, J.B. Pereira-Leal, A. Dias-Pereira, M. Bettencourt-Dias, dan P. Chaves. 2018. Centrosome amplification arises before neoplasia and increases upon p53 loss in tumorigenesis. *J. Cell Biol.* 217:2353–2363. doi:10.1083/JCB.201711191.

Lord, C.J., dan A. Ashworth. 2013. Mechanisms of resistance to therapies targeting BRCA-mutant cancers. *Nat. Med. 2013 1911*. 19:1381–1388. doi:10.1038/nm.3369.

Lord, C.J., dan A. Ashworth. 2017. PARP inhibitors: Synthetic lethality in the clinic. *Science (80-.).* 355:1152–1158. doi:10.1126/SCIENCE.AAM7344/ASSET/B1C2C000-4AAF-41D9-A934-CD4097D85A2A/ASSETS/GRAPHIC/355_1152_F2.JPEG.

Losa, J.H., C.P. Cobo, J.G. Viniegra, V.J. Sánchez-Arevalo Lobo, S. Ramón y Cajal, dan R. Sánchez-Prieto. 2003. Role of the p38 MAPK pathway in cisplatin-based therapy. *Oncogene*. 22:3998–4006. doi:10.1038/sj.onc.1206608.

Loughlin, R., R. Heald, dan F. Nédélec. 2010. A computational model predicts Xenopus

meiotic spindle organization. *J. Cell Biol.* 191:1239–1249. doi:10.1083/JCB.201006076/VIDEO-1.

Loughlin, R., J.D. Wilbur, F.J. McNally, F.J. Nédélec, dan R. Heald. 2011. Katanin Contributes to Interspecies Spindle Length Scaling in Xenopus. *Cell*. 147:1397–1407. doi:10.1016/J.CELL.2011.11.014.

Lozano, E., M. Betson, dan V.M.M. Braga. 2003. Tumor progression: Small GTPases and loss of cell-cell adhesion. *Bioessays*. 25:452–463. doi:10.1002/BIES.10262.

Lüders, J., U.K. Patel, dan T. Stearns. 2006. GCP-WD is a γ-tubulin targeting factor required for centrosomal and chromatin-mediated microtubule nucleation. *Nat. Cell Biol.* 8:137–147. doi:10.1038/ncb1349.

Lukow, D.A., E.L. Sausville, P. Suri, N.K. Chunduri, A. Wieland, J. Leu, J.C. Smith, V. Girish, A.A. Kumar, J. Kendall, Z. Wang, Z. Storchova, dan J.M. Sheltzer. 2021. Chromosomal instability accelerates the evolution of resistance to anti-cancer therapies. *Dev. Cell*. 56:2427-2439.e4. doi:10.1016/j.devcel.2021.07.009.

Ma, P., dan R.J. Mumper. 2013. Paclitaxel Nano-Delivery Systems: A Comprehensive Review. *J. Nanomed. Nanotechnol.* 4:1000164. doi:10.4172/2157-7439.1000164.

Mabuchi, I., Y. Hamaguchi, H. Fujimoto, N. Morii, M. Mishima, dan S. Narumiya. 1993. A rho-like protein is involved in the organisation of the contractile ring in dividing sand dollar eggs. *Zygote*. 1:325–331. doi:10.1017/S0967199400001659.

Maciejowski, J., Y. Li, N. Bosco, dan P.J. Campbell. 2015. Chromothripsis and Kataegis Induced by Telomere Crisis. *Cell*. 163. doi:10.1016/j.cell.2015.11.054.

MacKenzie, K.J., P. Carroll, C.A. Martin, O. Murina, A. Fluteau, D.J. Simpson, N. Olova, H. Sutcliffe, J.K. Rainger, A. Leitch, R.T. Osborn, A.P. Wheeler, M. Nowotny, N. Gilbert, T. Chandra, M.A.M. Reijns, dan A.P. Jackson. 2017. CGAS surveillance of micronuclei links genome instability to innate immunity. *Nature*. 548:461–465. doi:10.1038/nature23449.

Maddox, A.S., L. Lewellyn, A. Desai, dan K. Oegema. 2007. Anillin and the septins promote asymmetric ingression of the cytokinetic furrow. *Dev. Cell*. 12:827–835. doi:10.1016/J.DEVCEL.2007.02.018.

Mah, L.J., A. El-Osta, dan T.C. Karagiannis. 2010. γH2AX: a sensitive molecular marker of DNA damage and repair. *Leuk. 2010 244*. 24:679–686. doi:10.1038/leu.2010.6.

Maity, A., W.G. McKenna, dan R.J. Muschel. 1994. The molecular basis for cell cycle delays

following ionizing radiation: a review. *Radiother. Oncol.* 31:1–13. doi:10.1016/0167-8140(94)90408-1.

Malumbres, M., dan M. Barbacid. Mammalian cyclin-dependent kinases. doi:10.1016/j.tibs.2005.09.005.

Malumbres, M., dan M. Barbacid. 2001. To cycle or not to cycle: A critical decision in cancer. *Nat. Rev. Cancer*. 1:222–231. doi:10.1038/35106065.

Malumbres, M., dan M. Barbacid. 2009. Cell cycle, CDKs and cancer: A changing paradigm. *Nat. Rev. Cancer*. 9:153–166. doi:10.1038/nrc2602.

Manandhar, G., H. Schatten, dan P. Sutovsky. 2005. Centrosome reduction during gametogenesis and its significance. *Biol. Reprod.* 72:2–13. doi:10.1095/biolreprod.104.031245.

Mandic, A., K. Viktorsson, L. Strandberg, T. Heiden, J. Hansson, S. Linder, dan M.C. Shoshan. 2002. Calpain-Mediated Bid Cleavage and Calpain-Independent Bak Modulation: Two Separate Pathways in Cisplatin-Induced Apoptosis. *Mol. Cell. Biol.* 22:3003–3013. doi:10.1128/mcb.22.9.3003-3013.2002.

Mansouri, A., Q. Zhan, L.D. Ridgway, L. Tian, dan F.X. Claret. 2002. Cisplatin Resistance in an Ovarian Carcinoma Is Associated with a Defect in Programmed Cell Death Control Through XIAP Regulation. *In* Oncology Research. Tech Science Press. 399–404.

Mao, R., C.L. Zielke, H.R. Zielke, dan J. Pevsner. 2003. Global up-regulation of chromosome 21 gene expression in the developing Down syndrome brain. *Genomics*. 81:457–467. doi:10.1016/S0888-7543(03)00035-1.

Mao, Z., M. Bozzella, A. Seluanov, dan V. Gorbunova. 2008. DNA repair by nonhomologous end joining and homologous recombination during cell cycle in human cells. *Cell Cycle*. 7:2902. doi:10.4161/CC.7.18.6679.

Mardin, B.R., C. Lange, J.E. Baxter, T. Hardy, S.R. Scholz, A.M. Fry, dan E. Schiebel. 2010. Components of the Hippo pathway cooperate with Nek2 kinase to regulate centrosome disjunction. *Nat. Cell Biol.* 12:1166–1176. doi:10.1038/ncb2120.

Maréchal, A., dan L. Zou. 2013. DNA Damage Sensing by the ATM and ATR Kinases. *Cold Spring Harb. Perspect. Biol.* 5. doi:10.1101/CSHPERSPECT.A012716.

Mari, P.O., B.I. Florea, S.P. Persengiev, N.S. Verkaik, H.T. Brüggenwirth, M. Modesti, G. Giglia-Mari, K. Bezstarosti, J.A.A. Demmers, T.M. Luider, A.B. Houtsmuller, dan D.C. Van Gent. 2006. Dynamic assembly of end-joining complexes requires interaction between

Ku70/80 and XRCC4. *Proc. Natl. Acad. Sci. U. S. A.* 103:18597–18602. doi:10.1073/PNAS.0609061103.

Marteil, G., A. Guerrero, A.F. Vieira, B.P. De Almeida, P. Machado, S. Mendonça, M. Mesquita, B. Villarreal, I. Fonseca, M.E. Francia, K. Dores, N.P. Martins, S.C. Jana, E.M. Tranfield, N.L. Barbosa-Morais, J. Paredes, D. Pellman, S.A. Godinho, dan M. Bettencourt-Dias. 2018. Over-elongation of centrioles in cancer promotes centriole amplification and chromosome missegregation. *Nat. Commun.* 9. doi:10.1038/s41467-018-03641-x.

Marthiens, V., M. Piel, dan R. Basto. 2012a. Never tear us apart-the importance of centrosome clustering. *J. Cell Sci.* 125:3281–3292. doi:10.1242/jcs.094797.

Marthiens, V., M. Piel, dan R. Basto. 2012b. Never tear us apart - the importance of centrosome clustering. *J. Cell Sci.* 125:3281–3292. doi:10.1242/jcs.094797.

Massagué, J. 2004. G1 cell-cycle control and cancer. 432.

Matsumoto, Y., dan J.L. Maller. 2004. A centrosomal localization signal in cyclin E required for Cdk2-independent S phase entry. *Science (80-.).* 306:885–888. doi:10.1126/SCIENCE.1103544/SUPPL_FILE/MATSUMOTO-SOM.PDF.

Matsuoka, S., B.A. Ballif, A. Smogorzewska, E.R. McDonald, K.E. Hurov, J. Luo, C.E. Bakalarski, Z. Zhao, N. Solimini, Y. Lerenthal, Y. Shiloh, S.P. Gygi, dan S.J. Elledge. 2007. ATM and ATR substrate analysis reveals extensive protein networks responsive to DNA damage. *Science*. 316:1160–1166. doi:10.1126/SCIENCE.1140321.

Matsuura, K., P.A. Lefebvre, R. Kamiya, dan M. Hirono. 2004. Bld10p, a novel protein essential for basal body assembly in Chlamydomonas: Localization to the cartwheel, the first ninefold symmetrical structure appearing during assembly. *J. Cell Biol.* 165:663–671. doi:10.1083/jcb.200402022.

Matthews, H.K., C. Bertoli, dan R.A.M. de Bruin. 2021. Cell cycle control in cancer. *Nat. Rev. Mol. Cell Biol.* 0123456789. doi:10.1038/s41580-021-00404-3.

Matulonis, U.A., A.K. Sood, L. Fallowfield, B.E. Howitt, J. Sehouli, dan B.Y. Karlan. 2016. Ovarian cancer. *Nat. Rev. Dis. Prim.* 2:1–22. doi:10.1038/nrdp.2016.61.

Mayor, T., Y.D. Stierhof, K. Tanaka, A.M. Fry, dan E.A. Nigg. 2000. The centrosomal protein C-Nap1 is required for cell cycle-regulated centrosome cohesion. *J. Cell Biol.* 151:837–846. doi:10.1083/jcb.151.4.837.

McAlpine, J.N., K.C. Wiegand, R. Vang, B.M. Ronnett, A. Adamiak, M. Köbel, S.E. Kalloger,

K.D. Swenerton, D.G. Huntsman, C. Blake Gilks, dan D.M. Miller. 2009. HER2 overexpression and amplification is present in a subset of ovarian mucinous carcinomas and can be targeted with trastuzumab therapy. *BMC Cancer*. 9:1–12. doi:10.1186/1471-2407-9-433/FIGURES/5.

McEvoy, L.M., S.A. O'Toole, C.D. Spillane, C.M. Martin, M.F. Gallagher, B. Stordal, G. Blackshields, O. Sheils, dan J.J. O'Leary. 2015. Identifying novel hypoxia-associated markers of chemoresistance in ovarian cancer. *BMC Cancer*. 15:1–13. doi:10.1186/S12885-015-1539-8/FIGURES/4.

McGuire, W.P. 1989. Taxol: A Unique Antineoplastic Agent with Significant Activity in Advanced Ovarian Epithelial Neoplasms. *Ann. Intern. Med.* 111:273. doi:10.7326/0003-4819-111-4-273.

McGuire, W.P., W.J. Hoskins, M.F. Brady, P.R. Kucera, E.E. Partridge, K.Y. Look, D.L. Clarke-Pearson, dan M. Davidson. 1996a. Cyclophosphamide and Cisplatin Compared with Paclitaxel and Cisplatin in Patients with Stage III and Stage IV Ovarian Cancer. *N. Engl. J. Med.* 334:1–6. doi:10.1056/nejm199601043340101.

McGuire, W.P., W.J. Hoskins, M.F. Brady, P.R. Kucera, E.E. Partridge, K.Y. Look, D.L. Clarke-Pearson, dan M. Davidson. 1996b. Cyclophosphamide and Cisplatin Compared with Paclitaxel and Cisplatin in Patients with Stage III and Stage IV Ovarian Cancer. *N. Engl. J. Med.* 334:1–6. doi:10.1056/nejm199601043340101.

McIlwain, D.R., T. Berger, dan T.W. Mak. 2013. Caspase Functions in Cell Death and Disease. *Cold Spring Harb. Perspect. Biol.* 5:1–28. doi:10.1101/CSHPERSPECT.A008656.

McIntosh, J.R., E.L. Grishchuk, dan R.R. West. 2002. Chromosome-microtubule interactions during mitosis. *Annu. Rev. Cell Dev. Biol.* 18:193–219. doi:10.1146/annurev.cellbio.18.032002.132412.

Mechetner, E., A. Kyshtoobayeva, S. Zonis, H. Kim, R. Stroup, R. García, R. Parker, dan J. Fruehauf. 1998. Levels of multidrug resistance (MDR1) P-glycoprotein expression by human breast cancer correlate with in vitro resistance to taxol and doxorubicin. *Clin. Cancer Res.*

Megraw, T.L., K. Li, L.R. Kao, dan T.C. Kaufman. 1999. The Centrosomin protein is required for centrosome assembly and function during cleavage in Drosophila. *Development*. 126:2829–2839. doi:10.1242/dev.126.13.2829.

Meitinger, F., J. V. Anzola, M. Kaulich, A. Richardson, J.D. Stender, C. Benner, C.K. Glass, S.F.

Dowdy, A. Desai, A.K. Shiau, dan K. Oegema. 2016. 53BP1 and USP28 mediate p53 activation and G1 arrest after centrosome loss or extended mitotic duration. *J. Cell Biol.* 214:155–166. doi:10.1083/JCB.201604081.

Meitinger, F., M. Ohta, K.Y. Lee, S. Watanabe, R.L. Davis, J. V. Anzola, R. Kabeche, D.A. Jenkins, A.K. Shiau, A. Desai, dan K. Oegema. 2020. TRIM37 controls cancer-specific vulnerability to PLK4 inhibition. *Nature*. 585:440–446. doi:10.1038/S41586-020-2710-1.

Menear, K.A., C. Adcock, R. Boulter, X.L. Cockcroft, L. Copsey, A. Cranston, K.J. Dillon, J. Drzewiecki, S. Garman, S. Gomez, H. Javaid, F. Kerrigan, C. Knights, A. Lau, V.M. Loh, I.T.W. Matthews, S. Moore, M.J. O'Connor, G.C.M. Smith, dan N.M.B. Martin. 2008. 4-[3-(4-cyclopropanecarbonylpiperazine-1-carbonyl)-4-fluorobenzyl]-2H-phthalazin-1-one: a novel bioavailable inhibitor of poly(ADP-ribose) polymerase-1. *J. Med. Chem.* 51:6581–6591. doi:10.1021/JM8001263.

Meng, L., J.-E. Park, T.-S. Kim, E.H. Lee, S.-Y. Park, M. Zhou, J.K. Bang, dan K.S. Lee. 2015. Bimodal Interaction of Mammalian Polo-Like Kinase 1 and a Centrosomal Scaffold, Cep192, in the Regulation of Bipolar Spindle Formation. *Mol. Cell. Biol.* 35:2626–2640. doi:10.1128/mcb.00068-15.

Meng, M. Bin, H.H. Wang, Y.L. Cui, Z.Q. Wu, Y.Y. Shi, N.G. Zaorsky, L. Deng, Z.Y. Yuan, Y. Lu, dan P. Wang. 2016. Necroptosis in tumorigenesis, activation of anti-tumor immunity, and cancer therapy. *Oncotarget*. 7:57391–57413. doi:10.18632/oncotarget.10548.

Mennella, V., D.A. Agard, B. Huang, dan L. Pelletier. 2014. Amorphous no more: Subdiffraction view of the pericentriolar material architecture. *Trends Cell Biol.* 24:188–197. doi:10.1016/j.tcb.2013.10.001.

Menon, U., A. Gentry-Maharaj, M. Burnell, N. Singh, A. Ryan, C. Karpinskyj, G. Carlino, J. Taylor, S.K. Massingham, M. Raikou, J.K. Kalsi, R. Woolas, R. Manchanda, R. Arora, L. Casey, A. Dawnay, S. Dobbs, S. Leeson, T. Mould, M.W. Seif, A. Sharma, K. Williamson, Y. Liu, L. Fallowfield, A.J. McGuire, S. Campbell, S.J. Skates, I.J. Jacobs, dan M. Parmar. 2021. Ovarian cancer population screening and mortality after long-term follow-up in the UK Collaborative Trial of Ovarian Cancer Screening (UKCTOCS): a randomised controlled trial. *Lancet*. 397:2182–2193. doi:10.1016/S0140-6736(21)00731-5.

Meyer-Ficca, M.L., R.G. Meyer, D.L. Coyle, E.L. Jacobson, dan M.K. Jacobson. 2004. Human poly(ADP-ribose) glycohydrolase is expressed in alternative splice variants yielding isoforms that localize to different cell compartments. *Exp. Cell Res.* 297:521–532.

doi:10.1016/j.yexcr.2004.03.050.

Milas, L., N.R. Hunter, B. Kurdoglu, K.A. Mason, R.E. Meyn, L.C. Stephens, dan L.J. Peters. 1995. Kinetics of mitotic arrest and apoptosis in murine mammary and ovarian tumors treated with taxol. *Cancer Chemother. Pharmacol.* 35:297–303. doi:10.1007/BF00689448.

Min, W.K., U. Cortes, Z. Herceg, W.M. Tong, dan Z.Q. Wang. 2010. Deletion of the nuclear isoform of poly(ADP-ribose) glycohydrolase (PARG) reveals its function in DNA repair, genomic stability and tumorigenesis. *Carcinogenesis*. 31:2058–2065. doi:10.1093/CARCIN/BGQ205.

Mirza, M.R., B.J. Monk, J. Herrstedt, A.M. Oza, S. Mahner, A. Redondo, M. Fabbro, J.A. Ledermann, D. Lorusso, I. Vergote, N.E. Ben-Baruch, C. Marth, R. Mądry, R.D. Christensen, J.S. Berek, A. Dørum, A. V. Tinker, A. du Bois, A. González-Martín, P. Follana, B. Benigno, P. Rosenberg, L. Gilbert, B.J. Rimel, J. Buscema, J.P. Balser, S. Agarwal, dan U.A. Matulonis. 2016. Niraparib Maintenance Therapy in Platinum-Sensitive, Recurrent Ovarian Cancer. *N. Engl. J. Med.* 375:2154–2164. doi:10.1056/NEJMOA1611310.

Mitchison, T., dan M. Kirschner. 1984. Dynamic instability of microtubule growth. *Nat. 1984 3125991*. 312:237–242. doi:10.1038/312237a0.

Mitchison, T.J., dan E.D. Salmon. 2001. Mitosis: A history of division. *Nat. Cell Biol.* 3:17–21. doi:10.1038/35050656.

Moens, S., P. Zhao, M.F. Baietti, O. Marinelli, D. Van Haver, F. Impens, G. Floris, E. Marangoni, P. Neven, D. Annibali, A.A. Sablina, dan F. Amant. 2021. The mitotic checkpoint is a targetable vulnerability of carboplatin-resistant triple negative breast cancers. *Sci. Rep.* 11:3176. doi:10.1038/s41598-021-82780-6.

Monteiro, P., B. Yeon, S.S. Wallis, dan S.A. Godinho. 2023. Centrosome amplification fine tunes tubulin acetylation to differentially control intracellular organization. *EMBO J.* e112812. doi:10.15252/EMBJ.2022112812.

Moore, K., N. Colombo, G. Scambia, B.-G. Kim, A. Oaknin, M. Friedlander, A. Lisyanskaya, A. Floquet, A. Leary, G.S. Sonke, C. Gourley, S. Banerjee, A. Oza, A. González-Martín, C. Aghajanian, W. Bradley, C. Mathews, J. Liu, E.S. Lowe, R. Bloomfield, dan P. DiSilvestro. 2018. Maintenance Olaparib in Patients with Newly Diagnosed Advanced Ovarian Cancer. *N. Engl. J. Med.* 379:2495–2505. doi:10.1056/NEJMOA1810858.

Morehouse, B.R., A.A. Govande, A. Millman, A.F.A. Keszei, B. Lowey, G. Ofir, S. Shao, R. Sorek, dan P.J. Kranzusch. 2020. STING cyclic dinucleotide sensing originated in bacteria. *Nature*. 586:429–433. doi:10.1038/s41586-020-2719-5.

Morin, X., dan Y. Bellaïche. 2011. Mitotic Spindle Orientation in Asymmetric and Symmetric Cell Divisions during Animal Development. *Dev. Cell*. 21:102–119. doi:10.1016/j.devcel.2011.06.012.

Morita, E., V. Sandrin, H.Y. Chung, S.G. Morham, S.P. Gygi, C.K. Rodesch, dan W.I. Sundquist. 2007. Human ESCRT and ALIX proteins interact with proteins of the midbody and function in cytokinesis. *EMBO J.* 26:4215–4227. doi:10.1038/SJ.EMBOJ.7601850.

Moritz, M., M.B. Braunfeld, V. Guénebaut, J. Heuser, dan D.A. Agard. 2000. Structure of the γ-tubulin ring complex: A template for microtubule nucleation. *Nat. Cell Biol.* 2:365–370. doi:10.1038/35014058.

Morretton, J., A. Simon, J. Barbazan, T. Popova, C. Cosson, B. Mboup, P. Gestraud, G. Bataillon, Y. Kieffer, A. Mac, O. Mariani, A. Vincent-salomon, M. Stern, D. Meseure, F. Mechta-grigoriou, S.R. Roman, dan D.M. Vignjevic. 2022. A catalog of numerical centrosome defects in epithelial ovarian cancers. 1–12. doi:10.15252/emmm.202215670.

Motwani, M., S. Pesiridis, dan K.A. Fitzgerald. 2019. DNA sensing by the cGAS–STING pathway in health and disease. *Nat. Rev. Genet.* 20:657–674. doi:10.1038/s41576-019-0151-1.

Mozzetti, S., C. Ferlini, P. Concolino, F. Filippetti, G. Raspaglio, S. Prislei, D. Gallo, E. Martinelli, F.O. Ranelletti, G. Ferrandina, dan G. Scambia. 2005. Class III β-Tubulin Overexpression Is a Prominent Mechanism of Paclitaxel Resistance in Ovarian Cancer Patients. *Clin. Cancer Res.* 11:298–305. doi:10.1158/1078-0432.298.11.1.

Mukherjee, A., P.S. Brooks, F. Bernard, A. Guichet, dan P.T. Conduit. 2020. Microtubules originate asymmetrically at the somatic golgi and are guided via kinesin2 to maintain polarity within neurons. *Elife*. 9:1–33. doi:10.7554/eLife.58943.

Mullee, L.I., dan C.G. Morrison. 2015. Centrosomes in the DNA damage response—the hub outside the centre. *Chromosom. Res. 2015 241*. 24:35–51. doi:10.1007/S10577-015-9503-7.

Murai, J., Y. Feng, G.K. Yu, Y. Ru, S.W. Tang, Y. Shen, dan Y. Pommier. 2016. Resistance to PARP inhibitors by SLFN11 inactivation can be overcome by ATR inhibition. *Oncotarget*.

7:76534–76550. doi:10.18632/ONCOTARGET.12266.

Murai, J., S.W. Tang, E. Leo, S.A. Baechler, C.E. Redon, H. Zhang, M. Al Abo, V.N. Rajapakse, E. Nakamura, L.M.M. Jenkins, M.I. Aladjem, dan Y. Pommier. 2018. SLFN11 Blocks Stressed Replication Forks Independently of ATR. *Mol. Cell*. 69:371-384.e6. doi:10.1016/J.MOLCEL.2018.01.012.

Murray, A.W., dan M.W. Kirschner. 1989. Cyclin synthesis drives the early embryonic cell cycle. *Nature*. 16:9–13.

Murray, A.W., M.J. Solomon, dan M.W. Kirschner. 1989. The role of cyclin synthesis and degradation in the control of maturation promoting factor activity. *Nature*. 339:280–286. doi:10.1038/339280a0.

Musacchio, A., dan E.D. Salmon. 2007. The spindle-assembly checkpoint in space and time. *Nat. Rev. Mol. Cell Biol.* 8:379–393. doi:10.1038/nrm2163.

Musacchio, L., S.M. Boccia, G. Caruso, G. Santangelo, M. Fischetti, F. Tomao, G. Perniola, I. Palaia, L. Muzii, S. Pignata, P.B. Panici, dan V. Di Donato. 2020. Immune Checkpoint Inhibitors: A Promising Choice for Endometrial Cancer Patients? *J. Clin. Med.* 9:1–15. doi:10.3390/JCM9061721.

Myrie, K.A., M.J. Percy, J.N. Azim, C.K. Neeley, dan E.M. Petty. 2000. Mutation and expression analysis of human BUB1 and BUB1B in aneuploid breast cancer cell lines. *Cancer Lett.* 152:193–199. doi:10.1016/S0304-3835(00)00340-2.

Nakajima, T., M. Moriguchi, Y. Mitsumoto, S. Sekoguchi, T. Nishikawa, H. Takashima, T. Watanabe, T. Katagishi, H. Kimura, T. Okanoue, dan K. Kagawa. 2004. Centrosome aberration accompanied with p53 mutation can induce genetic instability in hepatocellular carcinoma. *Mod. Pathol.* 17:722–727. doi:10.1038/modpathol.3800115.

Nakano, K., dan K.H. Vousden. 2001. PUMA, a novel proapoptotic gene, is induced by p53. *Mol. Cell*. 7:683–694. doi:10.1016/S1097-2765(01)00214-3.

Nakashima, S., dan K.H. Kato. 2001. Centriole behavior during meiosis in oocytes of the sea urchin Hemicentrotus pulcherrimus. *Dev. Growth Differ.* 43:437–445. doi:10.1046/j.1440-169X.2001.00580.x.

Narasimha, A.M., M. Kaulich, G.S. Shapiro, Y.J. Choi, P. Sicinski, dan S.F. Dowdy. 2014. Cyclin D activates the Rb tumor suppressor by mono-phosphorylation. *Elife*. 3:1–21. doi:10.7554/elife.02872.

Narkar, A., B.A. Johnson, P. Bharne, P.A. Iglesias, A.J. Ewald, R. Li, A. Narkar, B.A. Johnson, P.

Bharne, J. Zhu, V. Padmanaban, dan D. Biswas. 2021. Report On the role of p53 in the cellular response to aneuploidy ll ll On the role of p53 in the cellular response to aneuploidy. *CellReports*. 34:108892. doi:10.1016/j.celrep.2021.108892.

Navarro-Serer, B., E.P. Childers, N.M. Hermance, D. Mercadante, dan A.L. Manning. 2019. Aurora A inhibition limits centrosome clustering and promotes mitotic catastrophe in cells with supernumerary centrosomes. *Oncotarget*. 10:1649. doi:10.18632/ONCOTARGET.26714.

Nehlig, A., A. Molina, S. Rodrigues-Ferreira, S. Honoré, dan C. Nahmias. 2017. Regulation of end-binding protein EB1 in the control of microtubule dynamics. *Cell. Mol. Life Sci.* 74:2381–2393. doi:10.1007/S00018-017-2476-2/METRICS.

Nelson, L., A. Tighe, A. Golder, S. Littler, B. Bakker, D. Moralli, S. Murtuza Baker, I.J. Donaldson, D.C.J. Spierings, R. Wardenaar, B. Neale, G.J. Burghel, B. Winter-Roach, R. Edmondson, A.R. Clamp, G.C. Jayson, S. Desai, C.M. Green, A. Hayes, F. Foijer, R.D. Morgan, dan S.S. Taylor. 2020. A living biobank of ovarian cancer ex vivo models reveals profound mitotic heterogeneity. *Nat. Commun. 2020 111*. 11:1–18. doi:10.1038/s41467-020-14551-2.

Nematollahi, L.A., A. Garza-Garcia, C. Bechara, D. Esposito, N. Morgner, C. V. Robinson, dan P.C. Driscoll. 2015. Flexible Stoichiometry and Asymmetry of the PIDDosome Core Complex by Heteronuclear NMR Spectroscopy and Mass Spectrometry. *J. Mol. Biol.* 427:737. doi:10.1016/J.JMB.2014.11.021.

Nicklas, R.B. 1997. How cells get the right chromosomes. *Science*. 275. doi:10.1126/SCIENCE.275.5300.632.

Nicklas, R.B., S.C. Ward, dan G.J. Gorbsky. 1995. Kinetochore chemistry is sensitive to tension and may link mitotic forces to a cell cycle checkpoint. *J. Cell Biol.* 130:929–939. doi:10.1083/JCB.130.4.929.

Nigg, E.A. 2007. Centrosome duplication: of rules and licenses. *Trends Cell Biol.* 17:215–221. doi:10.1016/j.tcb.2007.03.003.

Nigg, E.A., L. Čajánek, dan C. Arquint. 2014. The centrosome duplication cycle in health and disease. *FEBS Lett.* 588:2366–2372. doi:10.1016/j.febslet.2014.06.030.

Nigg, E.A., dan A.J. Holland. 2018. Once and only once: Mechanisms of centriole duplication and their deregulation in diseases. *Nat. Rev. Mol. Cell Biol.* 19:297–312. doi:10.1038/nrm.2017.127.

Niwa, O., Y. Tange, dan A. Kurabayashi. 2006. Growth arrest and chromosome instability in aneuploid yeast. *Yeast*. 23:937–950. doi:10.1002/YEA.1411.

Noll, D.M., T. McGregor Mason, dan P.S. Miller. 2006. Formation and repair of interstrand cross-links in DNA. *Chem. Rev.* 106:277–301. doi:10.1021/CR040478B.

Normand, G., dan R.W. King. 2010. Understanding Cytokinesis Failure. *Adv. Exp. Med. Biol.* 676:27. doi:10.1007/978-1-4419-6199-0_3.

Nuñez, G., M.A. Benedict, Y. Hu, dan N. Inohara. 1998. Caspases: The proteases of the apoptotic pathway. *Oncogene*. 17:3237–3245. doi:10.1038/sj.onc.1202581.

Nurse, P. 2000. A long twentieth century of the cell cycle and beyond. *Cell*. 100:71–78. doi:10.1016/S0092-8674(00)81684-0.

O'Connell, K.F., C. Caron, K.R. Kopish, D.D. Hurd, K.J. Kemphues, Y. Li, dan J.G. White. 2001a. The C. elegans zyg-1 gene encodes a regulator of centrosome duplication with distinct maternal and paternal roles in the embryo. *Cell*. 105:547–558. doi:10.1016/S0092-8674(01)00338-5.

O'Connell, K.F., C. Caron, K.R. Kopish, D.D. Hurd, K.J. Kemphues, Y. Li, dan J.G. White. 2001b. The C. elegans zyg-1 gene encodes a regulator of centrosome duplication with distinct maternal and paternal roles in the embryo. *Cell*. 105:547–558. doi:10.1016/S0092-8674(01)00338-5.

O'Connor, P.M., J. Jackman, I. Bae, T.G. Myers, S. Fan, M. Mutoh, D.A. Scudiero, A. Monks, E.A. Sausville, J.N. Weinstein, S. Friend, A.J. Fornace, dan K.W. Kohn. 1997. Characterization of the p53 tumor suppressor pathway in cell lines of the National Cancer Institute anticancer drug screen and correlations with the growth-inhibitory potency of 123 anticancer agents. *Cancer Res.* 57:4285–4300.

Öhrvik, H., Y. Nose, L.K. Wood, B.E. Kim, S.C. Gleber, M. Ralle, dan D.J. Thiele. 2013. Ctr2 regulates biogenesis of a cleaved form of mammalian Ctr1 metal transporter lacking the copper- And cisplatin-binding ecto-domain. *Proc. Natl. Acad. Sci. U. S. A.* 110:E4279–E4288. doi:10.1073/pnas.1311749110.

Ohta, M., T. Ashikawa, Y. Nozaki, H. Kozuka-Hata, H. Goto, M. Inagaki, M. Oyama, dan D. Kitagawa. 2014. Direct interaction of Plk4 with STIL ensures formation of a single procentriole per parental centriole. *Nat. Commun.* 5:5267. doi:10.1038/ncomms6267.

Ohtsubo, M., A.M. Theodoras, J. Schumacher, J.M. Roberts, dan M. Pagano. 1995. Human cyclin E, a nuclear protein essential for the G1-to-S phase transition. *Mol. Cell. Biol.*

15:2612–2624. doi:10.1128/MCB.15.5.2612.

Oka, S., J. Kato, dan J. Moss. 2006. Identification and characterization of a mammalian 39-kDa poly(ADP-ribose) glycohydrolase. *J. Biol. Chem.* 281:705–713. doi:10.1074/JBC.M510290200.

Okuno, S., H. Sato, K. Kuriyama-Matsumura, M. Tamba, H. Wang, S. Sohda, H. Hamada, H. Yoshikawa, T. Kondo, dan S. Bannai. 2003. Role of cystine transport in intracellular glutathione level and cisplatin resistance in human ovarian cancer cell lines. *Br. J. Cancer*. 88:951–956. doi:10.1038/sj.bjc.6600786.

Omura, G., J.A. Blessing, C.E. Ehrlich, A. Miller, E. Yordan, W.T. Creasman, dan H.D. Homesley. 1986. A randomized trial of cyclophosphamide and doxorubicin with or without cisplatin in advanced ovarian carcinoma. A gynecologic oncology group study. *Cancer*. 57:1725–1730. doi:10.1002/1097-0142(19860501)57:9<1725::AID-CNCR2820570903>3.0.CO;2-J.

Oromendia, A.B., dan A. Amon. 2014. Aneuploidy: Implications for protein homeostasis and disease. *DMM Dis. Model. Mech.* 7:15–20. doi:10.1242/dmm.013391.

Orr, G.A., P. Verdier-Pinard, H. McDaid, dan S.B. Horwitz. 2003. Mechanisms of Taxol resistance related to microtubules. *Oncogene*. 22:7280–7295. doi:10.1038/SJ.ONC.1206934.

Ovarian cancer statistics | World Cancer Research Fund International.

Ozols, R.F., B.N. Bundy, B.E. Greer, J.M. Fowler, D. Clarke-Pearson, R.A. Burger, R.S. Mannel, K. DeGeest, E.M. Hartenbach, dan R. Baergen. 2003a. Phase III Trial of Carboplatin and Paclitaxel Compared With Cisplatin and Paclitaxel in Patients With Optimally Resected Stage III Ovarian Cancer: A Gynecologic Oncology Group Study. *J. Clin. Oncol.* 21:3194–3200. doi:10.1200/JCO.2003.02.153.

Ozols, R.F., B.N. Bundy, B.E. Greer, J.M. Fowler, D. Clarke-Pearson, R.A. Burger, R.S. Mannel, K. DeGeest, E.M. Hartenbach, R. Baergen, dan D. Mackey. 2003b. Phase III trial of carboplatin and paclitaxel compared with cisplatin and paclitaxel in patients with optimally resected stage III ovarian cancer: A Gynecologic Oncology Group study. *J. Clin. Oncol.* 21:3194–3200. doi:10.1200/JCO.2003.02.153.

Ozols, R.F., B.N. Bundy, B.E. Greer, J.M. Fowler, D. Clarke-Pearson, R.A. Burger, R.S. Mannel, K. DeGeest, E.M. Hartenbach, R. Baergen, dan D. Mackey. 2003c. Phase III trial of carboplatin and paclitaxel compared with cisplatin and paclitaxel in patients with

optimally resected stage III ovarian cancer: A Gynecologic Oncology Group study. *J. Clin. Oncol.* 21:3194–3200. doi:10.1200/JCO.2003.02.153.

Pagano, M., R. Pepperkok, F. Verde, W. Ansorge, dan G. Draetta. 1992. Cyclin A is required at two points in the human cell cycle. *EMBO J.* 11:961–971. doi:10.1002/J.1460-2075.1992.TB05135.X.

Pampalona, J., E. Roscioli, W.T. Silkworth, B. Bowden, A. Genescà, L. Tusell, dan D. Cimini. 2016. Chromosome bridges maintain kinetochore-microtubule attachment throughout mitosis and rarely break during anaphase. *PLoS One*. 11. doi:10.1371/journal.pone.0147420.

Pan, G., K. O'Rourke, A.M. Chinnaiyan, R. Gentz, R. Ebner, J. Ni, dan V.M. Dixit. 1997. The receptor for the cytotoxic ligand TRAIL. *Science*. 276:111–113. doi:10.1126/SCIENCE.276.5309.111.

Panier, S., dan S.J. Boulton. 2014. Double-strand break repair: 53BP1 comes into focus. *Nat. Rev. Mol. Cell Biol.* 15:7–18. doi:10.1038/nrm3719.

Park, H.H., E. Logette, S. Raunser, S. Cuenin, T. Walz, J. Tschopp, dan H. Wu. 2007. Death Domain Assembly Mechanism Revealed by Crystal Structure of the Oligomeric PIDDosome Core Complex. *Cell*. 128:533. doi:10.1016/J.CELL.2007.01.019.

Parness, J., dan S.B. Horwitz. 1981. Taxol binds to polymerized tubulin in vitro. *J. Cell Biol.* 91:479–487.

Parra-Herran, C., J. Lerner-Ellis, B. Xu, S. Khalouei, D. Bassiouny, M. Cesari, N. Ismiil, dan S. Nofech-Mozes. 2017. Molecular-based classification algorithm for endometrial carcinoma categorizes ovarian endometrioid carcinoma into prognostically significant groups. *Mod. Pathol.* 30:1748–1759. doi:10.1038/MODPATHOL.2017.81.

Passerini, V., E. Ozeri-Galai, M.S. De Pagter, N. Donnelly, S. Schmalbrock, W.P. Kloosterman, B. Kerem, dan Z. Storchová. 2016. The presence of extra chromosomes leads to genomic instability. *Nat. Commun.* 7. doi:10.1038/ncomms10754.

Patch, A.M., E.L. Christie, D. Etemadmoghadam, D.W. Garsed, J. George, S. Fereday, K. Nones, P. Cowin, K. Alsop, P.J. Bailey, K.S. Kassahn, F. Newell, M.C.J. Quinn, S. Kazakoff, K. Quek, C. Wilhelm-Benartzi, E. Curry, H.S. Leong, A. Hamilton, L. Mileshkin, G. Au-Yeung, C. Kennedy, J. Hung, Y.E. Chiew, P. Harnett, M. Friedlander, M. Quinn, J. Pyman, S. Cordner, P. O'Brien, J. Leditschke, G. Young, K. Strachan, P. Waring, W. Azar, C. Mitchell, N. Traficante, J. Hendley, H. Thorne, M. Shackleton, D.K. Miller, G.M. Arnau,

R.W. Tothill, T.P. Holloway, T. Semple, I. Harliwong, C. Nourse, E. Nourbakhsh, S. Manning, S. Idrisoglu, T.J.C. Bruxner, A.N. Christ, B. Poudel, O. Holmes, M. Anderson, C. Leonard, A. Lonie, N. Hall, S. Wood, D.F. Taylor, Q. Xu, J. Lynn Fink, N. Waddell, R. Drapkin, E. Stronach, H. Gabra, R. Brown, A. Jewell, S.H. Nagaraj, E. Markham, P.J. Wilson, J. Ellul, O. McNally, M.A. Doyle, R. Vedururu, C. Stewart, E. Lengyel, J. V. Pearson, N. Waddell, A. Defazio, S.M. Grimmond, dan D.D.L. Bowtell. 2015. Whole-genome characterization of chemoresistant ovarian cancer. *Nature*. 521:489–494. doi:10.1038/NATURE14410.

Pavelka, N., G. Rancati, J. Zhu, W.D. Bradford, A. Saraf, L. Florens, B.W. Sanderson, G.L. Hattem, dan R. Li. 2010. Aneuploidy confers quantitative proteome changes and phenotypic variation in budding yeast. *Nature*. 468:321–325. doi:10.1038/nature09529.

Peel, N., N.R. Stevens, R. Basto, dan J.W. Raff. 2007. Article Overexpressing Centriole-Replication Proteins In Vivo Induces Centriole Overduplication and De Novo Formation. 17:834–843. doi:10.1016/j.cub.2007.04.036.

Peetla, C., S. Vijayaraghavalu, dan V. Labhasetwar. 2013. Biophysics of cell membrane lipids in cancer drug resistance: Implications for drug transport and drug delivery with nanoparticles. *Adv. Drug Deliv. Rev.* 65:1686–1698. doi:10.1016/J.ADDR.2013.09.004.

Pelletier, L., E. O'Toole, A. Schwager, A.A. Hyman, dan T. Müller-Reichert. 2006. Centriole assembly in Caenorhabditis elegans. *Nature*. 444:619–623. doi:10.1038/nature05318.

Pelletier, L., N. Özlü, E. Hannak, C. Cowan, B. Habermann, M. Ruer, T. Müller-Reichert, dan A.A. Hyman. 2004. The Caenorhabditis elegans Centrosomal Protein SPD-2 Is Required for both Pericentriolar Material Recruitment and Centriole Duplication. *Curr. Biol.* 14:863–873. doi:10.1016/J.CUB.2004.04.012.

Peters, J.M. 2006. The anaphase promoting complex/cyclosome: A machine designed to destroy. *Nat. Rev. Mol. Cell Biol.* 7:644–656. doi:10.1038/nrm1988.

Pettitt, S.J., D.B. Krastev, I. Brandsma, A. Dréan, F. Song, R. Aleksandrov, M.I. Harrell, M. Menon, R. Brough, J. Campbell, J. Frankum, M. Ranes, H.N. Pemberton, R. Rafiq, K. Fenwick, A. Swain, S. Guettler, J.M. Lee, E.M. Swisher, S. Stoynov, K. Yusa, A. Ashworth, dan C.J. Lord. 2018. Genome-wide and high-density CRISPR-Cas9 screens identify point mutations in PARP1 causing PARP inhibitor resistance. *Nat. Commun.* 9. doi:10.1038/S41467-018-03917-2.

Pettitt, S.J., F.L. Rehman, I. Bajrami, R. Brough, F. Wallberg, I. Kozarewa, K. Fenwick, I. Assiotis, L. Chen, J. Campbell, C.J. Lord, dan A. Ashworth. 2013. A Genetic Screen Using the PiggyBac Transposon in Haploid Cells Identifies Parp1 as a Mediator of Olaparib Toxicity. *PLoS One*. 8:e61520. doi:10.1371/JOURNAL.PONE.0061520.

Pfaff, K.L., C.T. Straub, K. Chiang, D.M. Bear, Y. Zhou, dan L.I. Zon. 2007. The Zebra fish cassiopeia Mutant Reveals that SIL Is Required for Mitotic Spindle Organization. *Mol. Cell. Biol.* 27:5887–5897. doi:10.1128/mcb.00175-07.

Pfleger, C.M., E. Lee, dan M.W. Kirschner. 2001. Substrate recognition by the Cdc20 and Cdh1 components of the anaphase-promoting complex. *Genes Dev.* 15:2396–2407. doi:10.1101/GAD.918201.

Phan, T.P., A.L. Maryniak, C.A. Boatwright, J. Lee, A. Atkins, A. Tijhuis, D.C. Spierings, H. Bazzi, F. Foijer, P.W. Jordan, T.H. Stracker, dan A.J. Holland. 2021. Centrosome defects cause microcephaly by activating the 53BP1-USP28-TP53 mitotic surveillance pathway. *EMBO J.* 40. doi:10.15252/EMBJ.2020106118.

Piccart, M.J., K. Bertelsen, K. James, J. Cassidy, C. Mangioni, E. Simonsen, G. Stuart, S. Kaye, I. Vergote, R. Blom, R. Grimshaw, R.J. Atkinson, K.D. Swenerton, C. Trope, M. Nardi, J. Kaern, S. Tumolo, P. Timmers, J.A. Roy, F. Lhoas, B. Lindvall, M. Bacon, A. Birt, J.E. Andersen, B. Zee, J. Paul, B. Baron, dan S. Pecorelli. 2000. Randomized intergroup trial of cisplatin-paclitaxel versus cisplatin- cyclophosphamide in women with advanced epithelial ovarian cancer: Three-year results. *J. Natl. Cancer Inst.* 92:699–708. doi:10.1093/jnci/92.9.699.

Piekny, A., M. Werner, dan M. Glotzer. 2005. Cytokinesis: Welcome to the Rho zone. *Trends Cell Biol.* 15:651–658. doi:10.1016/j.tcb.2005.10.006.

Pilié, P.G., C. Tang, G.B. Mills, dan T.A. Yap. 2019. State-of-the-art strategies for targeting the DNA damage response in cancer. *Nat. Rev. Clin. Oncol.* 16:81–104. doi:10.1038/s41571-018-0114-z.

Pillay, N., R.M. Brady, M. Dey, R.D. Morgan, dan S.S. Taylor. 2021. DNA replication stress and emerging prospects for PARG inhibitors in ovarian cancer therapy. *Prog. Biophys. Mol. Biol.* 163:160–170. doi:10.1016/j.pbiomolbio.2021.01.004.

Pillay, N., A. Tighe, L. Nelson, S. Littler, C. Coulson-Gilmer, N. Bah, A. Golder, B. Bakker, D.C.J. Spierings, D.I. James, K.M. Smith, A.M. Jordan, R.D. Morgan, D.J. Ogilvie, F. Foijer, D.A. Jackson, dan S.S. Taylor. 2019. DNA Replication Vulnerabilities Render Ovarian Cancer

Cells Sensitive to Poly(ADP-Ribose) Glycohydrolase Inhibitors. *Cancer Cell*. 35:519-533.e8. doi:10.1016/J.CCELL.2019.02.004.

Pimenta-Marques, A., I. Bento, C.A.M. Lopes, P. Duarte, S.C. Jana, dan M. Bettencourt-Dias. 2016. A mechanism for the elimination of the female gamete centrosome in Drosophila melanogaster. *Science (80-.).* 353. doi:10.1126/science.aaf4866.

Pines, J., dan T. Hunter. 1989. Isolation of a human cyclin cDNA: Evidence for cyclin mRNA and protein regulation in the cell cycle and for interaction with p34cdc2. *Cell*. 58:833–846. doi:10.1016/0092-8674(89)90936-7.

Pinto, A.L., dan S.J. Lippard. 1985. Binding of the antitumor drug cis-diamminedichloroplatinum(II) (cisplatin) to DNA. *Biochim. Biophys. Acta*. 780:167–180. doi:10.1016/0304-419X(85)90001-0.

Prat, J. 2014. Staging classification for cancer of the ovary, fallopian tube, and peritoneum. *Int. J. Gynecol. Obstet.* 124:1–5. doi:10.1016/j.ijgo.2013.10.001.

Prieur, A., E. Besnard, A. Babled, dan J.M. Lemaitre. 2011. P53 and p16INK4A independent induction of senescence by chromatin-dependent alteration of S-phase progression. *Nat. Commun.* 2. doi:10.1038/ncomms1473.

Prosser, S.L., dan L. Pelletier. 2017. Mitotic spindle assembly in animal cells: A fine balancing act. *Nat. Rev. Mol. Cell Biol.* 18:187–201. doi:10.1038/NRM.2016.162.

Pylayeva-Gupta, Y., dan J.-A.L. Kelsey C. Martin Mhatre V. Ho. 2012. 基因的改变NIH Public Access. *Bone*. 23:1–7.

Qu, D., H. Qu, M. Fu, X. Zhao, R. Liu, L. Sui, dan Q. Zhan. 2008. Increased expression of Nlp, a potential oncogene in ovarian cancer, and its implication in carcinogenesis. *Gynecol. Oncol.* 110:230–236. doi:10.1016/J.YGYNO.2008.04.015.

Quennet, V., A. Beucher, O. Barton, S. Takeda, dan M. Löbrich. 2011. CtIP and MRN promote non-homologous end-joining of etoposide-induced DNA double-strand breaks in G1. *Nucleic Acids Res.* 39:2144. doi:10.1093/NAR/GKQ1175.

Quigley, D., J.J. Alumkal, A.W. Wyatt, V. Kothari, A. Foye, P. Lloyd, R. Aggarwal, W. Kim, E. Lu, J. Schwartzman, K. Beja, M. Annala, R. Das, M. Diolaiti, C. Pritchard, G. Thomas, S. Tomlins, K. Knudsen, C.J. Lord, C. Ryan, J. Youngren, T.M. Beer, A. Ashworth, E.J. Small, dan F.Y. Feng. 2017. Analysis of Circulating Cell-Free DNA Identifies Multiclonal Heterogeneity of BRCA2 Reversion Mutations Associated with Resistance to PARP

Inhibitors. *Cancer Discov.* 7:999–1005. doi:10.1158/2159-8290.CD-17-0146.

Quintyne, N.J., J.E. Reing, D.R. Hoffelder, S.M. Gollin, dan W.S. Saunders. 2005. Spindle multipolarity is prevented by centrosomal clustering. *Science (80-.).* 307:127–129. doi:10.1126/science.1104905.

Raff, J.W., dan R. Basto. 2017. Centrosome Amplification and Cancer: A Question of Sufficiency. *Dev. Cell*. 40:217–218. doi:10.1016/j.devcel.2017.01.009.

Rahmani, H., W. Ma, Z. Hu, N. Daneshparvar, D.W. Taylor, J.A. McCammon, T.C. Irving, R.J. Edwards, dan K.A. Taylor. 2021. The myosin II coiled-coil domain atomic structure in its native environment. *Proc. Natl. Acad. Sci. U. S. A.* 118. doi:10.1073/pnas.2024151118.

Rape, M., S.K. Reddy, dan M.W. Kirschner. 2006. The processivity of multiubiquitination by the APC determines the order of substrate degradation. *Cell*. 124:89–103. doi:10.1016/J.CELL.2005.10.032.

Räschle, M., P. Knipsheer, M. Enoiu, T. Angelov, J. Sun, J.D. Griffith, T.E. Ellenberger, O.D. Schärer, dan J.C. Walter. 2008. Mechanism of Replication-Coupled DNA Interstrand Crosslink Repair. *Cell*. 134:969–980. doi:10.1016/j.cell.2008.08.030.

Rass, E., A. Grabarz, I. Plo, J. Gautier, P. Bertrand, dan B.S. Lopez. 2009. Role of Mre11 in chromosomal nonhomologous end joining in mammalian cells. *Nat. Struct. Mol. Biol.* 16:819–824. doi:10.1038/NSMB.1641.

Rastogi, R.P., Richa, A. Kumar, M.B. Tyagi, dan R.P. Sinha. 2010. Molecular Mechanisms of Ultraviolet Radiation-Induced DNA Damage and Repair. *J. Nucleic Acids*. 2010:32. doi:10.4061/2010/592980.

Rathmell, W.K., dan G. Chu. 1994. Involvement of the Ku autoantigen in the cellular response to DNA double- strand breaks. *Proc. Natl. Acad. Sci. U. S. A.* 91:7623–7627. doi:10.1073/PNAS.91.16.7623.

Reed, E. 1998. Platinum-DNA adduct, nucleotide excision repair and platinum based anti-cancer chemotherapy. *Cancer Treat. Rev.* 24:331–344. doi:10.1016/S0305-7372(98)90056-1.

Replogle, J.M., W. Zhou, A.E. Amaro, J.M. McFarland, M. Villalobos-Ortiz, J. Ryan, A. Letai, O. Yilmaz, J. Sheltzer, S.J. Lippard, U. Ben-David, dan A. Amon. 2020. Aneuploidy increases resistance to chemotherapeutics by antagonizing cell division. *Proc. Natl. Acad. Sci. U. S. A.* 117:30566–30576. doi:10.1073/pnas.2009506117.

Rhys, A.D., P. Monteiro, C. Smith, M. Vaghela, T. Arnandis, T. Kato, B. Leitinger, E. Sahai, A.

McAinsh, G. Charras, dan S.A. Godinho. 2018. Loss of E-cadherin provides tolerance to centrosome amplification in epithelial cancer cells. *J. Cell Biol.* 217:195–209. doi:10.1083/JCB.201704102/VIDEO-6.

Rieder, C.L., R.W. Cole, A. Khodjakov, dan G. Sluder. 1995. The checkpoint delaying anaphase in response to chromosome monoorientation is mediated by an inhibitory signal produced by unattached kinetochores. *J. Cell Biol.* 130:941–948. doi:10.1083/JCB.130.4.941.

Ring, D., R. Hubble, dan M. Kirschner. 1982. Mitosis in a cell with multiple centrioles. *J. Cell Biol.* 94:549–556. doi:10.1083/jcb.94.3.549.

Robbins, E., G. Jentzsch, dan A. Micali. THE CENTRIOLE CYCLE IN SYNCHRONIZED HELA CELLS.

Roberts, A.W., M.S. Davids, J.M. Pagel, B.S. Kahl, S.D. Puvvada, J.F. Gerecitano, T.J. Kipps, M.A. Anderson, J.R. Brown, L. Gressick, S. Wong, M. Dunbar, M. Zhu, M.B. Desai, E. Cerri, S. Heitner Enschede, R.A. Humerickhouse, W.G. Wierda, dan J.F. Seymour. 2016. Targeting BCL2 with Venetoclax in Relapsed Chronic Lymphocytic Leukemia. *N. Engl. J. Med.* 374:311–322. doi:10.1056/NEJMOA1513257.

Roberts, A.W., S. Ma, T.J. Kipps, S.E. Coutre, M.S. Davids, B. Eichhorst, M. Hallek, J.C. Byrd, K. Humphrey, L. Zhou, B. Chyla, J. Nielsen, J. Potluri, S.Y. Kim, M. Verdugo, S. Stilgenbauer, W.G. Wierda, dan J.F. Seymour. 2019. Efficacy of venetoclax in relapsed chronic lymphocytic leukemia is influenced by disease and response variables. *Blood*. 134:111–122. doi:10.1182/BLOOD.2018882555.

Rodrigues-Ferreira, S., H. Moindjie, M.M. Haykal, dan C. Nahmias. 2020. Predicting and Overcoming Taxane Chemoresistance. doi:10.1016/j.molmed.2020.09.007.

Rodrigues-Ferreira, S., A. Nehlig, H. Moindjie, C. Monchecourt, C. Seiler, E. Marangoni, S. Chateau-Joubert, M.E. Dujaric, N. Servant, B. Asselain, P. de Cremoux, M. Lacroix-Triki, M. Arnedos, J.Y. Pierga, F. André, dan C. Nahmias. 2019. Improving breast cancer sensitivity to paclitaxel by increasing aneuploidy. *Proc. Natl. Acad. Sci. U. S. A.* 116:23691–23697. doi:10.1073/PNAS.1910824116/SUPPL_FILE/PNAS.1910824116.SM04.AVI.

Rojas, V., K.M. Hirshfield, S. Ganesan, dan L. Rodriguez-Rodriguez. 2016. Molecular characterization of epithelial ovarian cancer: Implications for diagnosis and treatment. *Int. J. Mol. Sci.* 17. doi:10.3390/ijms17122113.

Roncolato, F., K. Lindemann, M.L. Willson, J. Martyn, dan L. Mileshkin. 2019. PI3K/AKT/mTOR inhibitors for advanced or recurrent endometrial cancer. *Cochrane database Syst. Rev.* 10. doi:10.1002/14651858.CD012160.PUB2.

Roos, W.P., A.D. Thomas, dan B. Kaina. 2016. DNA damage and the balance between survival and death in cancer biology. *Nat. Rev. Cancer*. 16:20–33. doi:10.1038/NRC.2015.2.

Roschke, A. V., K. Stover, G. Tonon, A.A. Schäffer, dan I.R. Kirsch. 2002. Stable Karyotypes in Epithelial Cancer Cell Lines Despite High Rates of Ongoing Structural and Numerical Chromosomal Instability. *Neoplasia*. 4:19. doi:10.1038/SJ.NEO.7900197.

Rosenberg, B., L. Van Camp, dan T. Krigas. 1965. Inhibition of cell division in Escherichia coli by electrolysis products from a platinum electrode [17]. *Nature*. 205:698–699. doi:10.1038/205698a0.

Rosenberg, B., L. Vancamp, J.E. Trosko, dan V.H. Mansour. 1969a. Platinum Compounds: a New Class of Potent Antitumour Agents. *Nature*. 222:385–386. doi:10.1038/222385a0.

Rosenberg, B., L. VanCamp, J.E. Trosko, dan V.H. Mansour. 1969b. Platinum compounds: A new class of potent antitumour agents [24]. *Nature*. 222:385–386. doi:10.1038/222385a0.

Rothkamm, K., I. Krüger, L.H. Thompson, dan M. Löbrich. 2003. Pathways of DNA double-strand break repair during the mammalian cell cycle. *Mol. Cell. Biol.* 23:5706–5715. doi:10.1128/MCB.23.16.5706-5715.2003.

Rottenberg, S., J.E. Jaspers, A. Kersbergen, E. Van Der Burg, A.O.H. Nygren, S.A.L. Zander, P.W.B. Derksen, M. De Bruin, J. Zevenhoven, A. Lau, R. Boulter, A. Cranston, M.J. O'Connor, N.M.B. Martin, P. Borst, dan J. Jonkers. 2008. High sensitivity of BRCA1-deficient mammary tumors to the PARP inhibitor AZD2281 alone and in combination with platinum drugs. *Proc. Natl. Acad. Sci. U. S. A.* 105:17079–17084. doi:10.1073/PNAS.0806092105.

Rouleau, M., A. Patel, M.J. Hendzel, S.H. Kaufmann, dan G.G. Poirier. 2010. PARP inhibition: PARP1 and beyond. *Nat. Rev. Cancer*. 10:293–301. doi:10.1038/nrc2812.

Rowald, K., M. Mantovan, J. Passos, C. Buccitelli, B.R. Mardin, J.O. Korbel, M. Jechlinger, dan R. Sotillo. 2016. Negative Selection and Chromosome Instability Induced by Mad2 Overexpression Delay Breast Cancer but Facilitate Oncogene-Independent Outgrowth. *Cell Rep.* 15:2679–2691. doi:10.1016/j.celrep.2016.05.048.

Royou, A., M.E. Gagou, R. Karess, dan W. Sullivan. 2010. BubR1- and Polo-Coated DNA Tethers Facilitate Poleward Segregation of Acentric Chromatids. *Cell*. 140:235–245. doi:10.1016/j.cell.2009.12.043.

Rutledge, S.D., T.A. Douglas, J.M. Nicholson, M. Vila-Casadesús, C.L. Kantzler, D. Wangsa, M. Barroso-Vilares, S.D. Kale, E. Logarinho, dan D. Cimini. 2016a. Selective advantage of trisomic human cells cultured in non-standard conditions. *Sci. Rep.* 6:1–12. doi:10.1038/srep22828.

Rutledge, S.D., T.A. Douglas, J.M. Nicholson, M. Vila-Casadesús, C.L. Kantzler, D. Wangsa, M. Barroso-Vilares, S.D. Kale, E. Logarinho, dan D. Cimini. 2016b. Selective advantage of trisomic human cells cultured in non-standard conditions. *Sci. Rep.* 6:1–12. doi:10.1038/srep22828.

Sabino, D., D. Gogendeau, D. Gambarotto, M. Nano, C. Pennetier, F. Dingli, G. Arras, D. Loew, dan R. Basto. 2015. Moesin is a major regulator of centrosome behavior in epithelial cells with extra centrosomes. *Curr. Biol.* 25:879–889. doi:10.1016/j.cub.2015.01.066.

Sakaue-Sawano, A., H. Kurokawa, T. Morimura, A. Hanyu, H. Hama, H. Osawa, S. Kashiwagi, K. Fukami, T. Miyata, H. Miyoshi, T. Imamura, M. Ogawa, H. Masai, dan A. Miyawaki. 2008. Visualizing Spatiotemporal Dynamics of Multicellular Cell-Cycle Progression. *Cell*. 132:487–498. doi:10.1016/j.cell.2007.12.033.

Salisbury, J.L. 2001. The contribution of epigenetic changes to abnormal centrosomes and genomic instability in breast cancer. *J. Mammary Gland Biol. Neoplasia*. 6:203–212. doi:10.1023/A:1011312808421.

Salmon, E.D., D. Cimini, L.A. Cameron, dan J.G. DeLuca. 2005. Merotelic kinetochores in mammalian tissue cells. *Philos. Trans. R. Soc. B Biol. Sci.* 360:553–568. doi:10.1098/RSTB.2004.1610.

Sancar, A., L.A. Lindsey-Boltz, K. Ünsal-Kaçmaz, dan S. Linn. 2004. Molecular Mechanisms of Mammalian DNA Repair and the DNA Damage Checkpoints. *http://dx.doi.org/10.1146/annurev.biochem.73.011303.073723*. 73:39–85. doi:10.1146/ANNUREV.BIOCHEM.73.011303.073723.

Sánchez-Huertas, C., dan J. Lüders. 2015. The Augmin Connection in the Geometry of Microtubule Networks. *Curr. Biol.* 25:R294–R299. doi:10.1016/j.cub.2015.02.006.

Sanchez, Ariana D; Feldman, J.L. 2015. Microtubule-organizing centers: from the

centrosome to non- centrosomal sites. *Curr Opin Cell Biol*. 40:1291–1296. doi:10.1016/j.ceb.2016.09.003.Microtubule-organizing.

Santaguida, S., dan A. Amon. 2015. Short- and long-term effects of chromosome mis-segregation and aneuploidy. *Nat. Rev. Mol. Cell Biol.* 16:473–485. doi:10.1038/nrm4025.

Santaguida, S., A. Richardson, D.R. Iyer, O. M'Saad, L. Zasadil, K.A. Knouse, Y.L. Wong, N. Rhind, A. Desai, dan A. Amon. 2017. Chromosome Mis-segregation Generates Cell-Cycle-Arrested Cells with Complex Karyotypes that Are Eliminated by the Immune System. *Dev. Cell*. 41:638-651.e5. doi:10.1016/j.devcel.2017.05.022.

Sarbajna, S., D. Davies, dan S.C. West. 2014. Roles of SLX1-SLX4, MUS81-EME1, and GEN1 in avoiding genome instability and mitotic catastrophe. *Genes Dev.* 28:1124–1136. doi:10.1101/GAD.238303.114.

Sartori, A.A., C. Lukas, J. Coates, M. Mistrik, S. Fu, J. Bartek, R. Baer, J. Lukas, dan S.P. Jackson. 2007a. Human CtIP promotes DNA end resection. *Nature*. 450:509–514. doi:10.1038/nature06337.

Sartori, A.A., C. Lukas, J. Coates, M. Mistrik, S. Fu, J. Bartek, R. Baer, J. Lukas, dan S.P. Jackson. 2007b. Human CtIP promotes DNA end resection. *Nature*. 450:509. doi:10.1038/NATURE06337.

Satzinger, H. 2008a. Theodor and Marcella Boveri: chromosomes and cytoplasm in hereditary and development. *Am. Biol. Teach.* 17:7–9. doi:10.2307/4438657.

Satzinger, H. 2008b. Theodor and Marcella Boveri: Chromosomes and cytoplasm in heredity and development. *Nat. Rev. Genet.* 9:231–238. doi:10.1038/NRG2311.

Schatten, H., dan G. Schatten. 1986. Motility and centrosomal organization during sea urchin and mouse fertilization. *Cell Motil. Cytoskeleton*. 6:163–175. doi:10.1002/CM.970060215.

Schiff, P.B., dan S.B. Horwitz. 1980a. Taxol stabilizes microtubules in mouse fibroblast cells. *Proc. Natl. Acad. Sci. U. S. A.* 77:1561–1565. doi:10.1073/pnas.77.3.1561.

Schiff, P.B., dan S.B. Horwitz. 1980b. Taxol stabilizes microtubules in mouse fibroblast cells. *Proc. Natl. Acad. Sci. U. S. A.* 77:1561–1565. doi:10.1073/pnas.77.3.1561.

Schilder, R.J., L. Hall, A. Monks, L.M. Handel, A.J. Fornace, R.F. Ozols, A.T. Fojo, dan T.C. Hamilton. 1990. Metallothionein gene expression and resistance to cisplatin in human ovarian cancer. *Int. J. cancer*. 45:416–422. doi:10.1002/IJC.2910450306.

Schmidt, K.N., S. Kuhns, A. Neuner, B. Hub, H. Zentgraf, dan G. Pereira. 2012. Cep164 mediates vesicular docking to the mother centriole during early steps of ciliogenesis. *J. Cell Biol.* 199:1083–1101. doi:10.1083/jcb.201202126.

Schmidt, T.I., J. Kleylein-Sohn, J. Westendorf, M. Le Clech, S.B. Lavoie, Y.D. Stierhof, dan E.A. Nigg. 2009. Control of Centriole Length by CPAP and CP110. *Curr. Biol.* 19:1005–1011. doi:10.1016/j.cub.2009.05.016.

Schneider, P., M. Thome, K. Burns, J.L. Bodmer, K. Hofmann, T. Kataoka, N. Holler, dan J. Tschopp. 1997. TRAIL receptors 1 (DR4) and 2 (DR5) signal FADD-dependent apoptosis and activate NF-kappaB. *Immunity*. 7:831–836. doi:10.1016/S1074-7613(00)80401-X.

Schöckel, L., M. Möckel, B. Mayer, D. Boos, dan O. Stemmann. 2011. Cleavage of cohesin rings coordinates the separation of centrioles and chromatids. *Nat. Cell Biol. 2011 138*. 13:966–972. doi:10.1038/ncb2280.

Schroeder, T.E. 1968. Cytokinesis: Filaments in the cleavage furrow. *Exp. Cell Res.* 53:272–276. doi:10.1016/0014-4827(68)90373-X.

Schroeder, T.E. 1970. The contractile ring - I. Fine structure of dividing mammalian (HeLa) cells and the effects of cytochalasin B. *Zeitschrift für Zellforsch. und Mikroskopische Anat.* 109:431–449. doi:10.1007/BF00343960/METRICS.

Schvartzman, J.M., P.H.G. Duijf, R. Sotillo, C. Coker, dan R. Benezra. 2011. Mad2 is a critical mediator of the chromosome instability observed upon Rb and p53 pathway inhibition. *Cancer Cell*. 19:701–714. doi:10.1016/j.ccr.2011.04.017.

Scribano, C.M., J. Wan, K. Esbona, J.B. Tucker, A. Lasek, A.S. Zhou, L.M. Zasadil, R. Molini, J. Fitzgerald, A.M. Lager, J.J. Laffin, K. Correia-Staudt, K.B. Wisinski, A.J. Tevaarwerk, R. O'Regan, S.M. McGregor, A.M. Fowler, R.J. Chappell, T.S. Bugni, M.E. Burkard, dan B.A. Weaver. 2021. Chromosomal instability sensitizes patient breast tumors to multipolar divisions induced by paclitaxel. *Sci. Transl. Med.* 13. doi:10.1126/scitranslmed.abd4811.

Sedelnikova, O.A., E.P. Rogakou, I.G. Panyutin, dan W.M. Bonner. 2002. Quantitative Detection of 125IdU-Induced DNA Double-Strand Breaks with γ-H2AX Antibody. *https://doi.org/10.1667/0033-7587(2002)158[0486:QDOIID]2.0.CO;2*. 158:486–492. doi:10.1667/0033-7587(2002)158.

Sen, O., J.U. Harrison, N.J. Burroughs, dan A.D. McAinsh. 2021. Kinetochore life histories reveal an Aurora-B-dependent error correction mechanism in anaphase. *Dev. Cell*. 1–18. doi:10.1016/j.devcel.2021.10.007.

Serçin, Ö., J.C. Larsimont, A.E. Karambelas, V. Marthiens, V. Moers, B. Boeckx, M. Le Mercier, D. Lambrechts, R. Basto, dan C. Blanpain. 2016. Transient PLK4 overexpression accelerates tumorigenesis in p53-deficient epidermis. *Nat. Cell Biol.* 18:100–110. doi:10.1038/ncb3270.

Shao, S., R. Liu, Y. Wang, Y. Song, L. Zuo, L. Xue, N. Lu, N. Hou, M. Wang, X. Yang, dan Q. Zhan. 2010. Centrosomal Nlp is an oncogenic protein that is gene-amplified in human tumors and causes spontaneous tumorigenesis in transgenic mice. *J. Clin. Invest.* 120. doi:10.1172/JCI39447.

Shapiro, G.I., dan J.W. Harper. 1999. Anticancer drug targets: Cell cycle and checkpoint control. *J. Clin. Invest.* 104:1645–1653. doi:10.1172/JCI9054.

Sharma, S., C. Lagisetti, B. Poliks, R.M. Coates, D.G.I. Kingston, dan S. Bane. 2013a. Dissecting the Paclitaxel-Microtubule Association: Quantitative Assessment of the 2'-OH Group. *Biochemistry*. 52:2328. doi:10.1021/BI400014T.

Sharma, S., C. Lagisetti, B. Poliks, R.M. Coates, D.G.I. Kingston, dan S. Bane. 2013b. Dissecting the Paclitaxel-Microtubule Association: Quantitative Assessment of the 2'-OH Group. *Biochemistry*. 52:2328. doi:10.1021/BI400014T.

Sheltzer, J.M., J.H. Ko, J.M. Replogle, N.C. Habibe Burgos, E.S. Chung, C.M. Meehl, N.M. Sayles, V. Passerini, Z. Storchova, dan A. Amon. 2017. Single-chromosome Gains Commonly Function as Tumor Suppressors. *Cancer Cell*. 31:240–255. doi:10.1016/j.ccell.2016.12.004.

Sherman-Baust, C.A., K.G. Becker, W.H. Wood III, Y. Zhang, dan P.J. Morin. 2011. Gene expression and pathway analysis of ovarian cancer cells selected for resistance to cisplatin, paclitaxel, or doxorubicin. *J. Ovarian Res.* 4:21. doi:10.1186/1757-2215-4-21.

Shizuta, Y., I. Kameshita, H. Ushiro, M. Matsuda, S. Suzuki, Y. Mitsuuchi, Y. Yokoyama, dan T. Kurosaki. 1986. The domain structure and the function of poly(ADP-ribose) synthetase. *Adv. Enzyme Regul.* 25:377–380. doi:10.1016/0065-2571(86)90024-5.

Shoshani, O., B. Bakker, L. De Haan, A.E. Tijhuis, Y. Wang, D.H. Kim, M. Maldonado, M.A. Demarest, J. Artates, O. Zhengyu, A. Mark, R. Wardenaar, R. Sasik, D.C.J. Spierings, B. Vitre, K. Fisch, F. Foijer, dan D.W. Cleveland. 2021. Transient genomic instability drives tumorigenesis through accelerated clonal evolution. *Genes Dev.* 35:1093–1109. doi:10.1101/gad.348319.121.

Shrestha, R., M.L. Fernandez, A. Dawson, J. Hoenisch, S. Volik, Y.Y. Lin, S. Anderson, H. Kim,

A.M. Haegert, S. Colborne, N.K.Y. Wong, B. McConeghy, R.H. Bell, S. Brahmbhatt, C.H. Lee, G.E. DiMattia, S. Le Bihan, G.B. Morin, C.C. Collins, dan M.S. Carey. 2021. Multiomics characterization of low-grade serous ovarian carcinoma identifies potential biomarkers of MEK inhibitor sensitivity and therapeutic vulnerability. *Cancer Res.* 81:1681–1694. doi:10.1158/0008-5472.CAN-20-2222/654283/AM/MULTIOMICS-CHARACTERIZATION-OF-LOW-GRADE-SEROUS.

Shukla, A., D. Kong, M. Sharma, V. Magidson, dan J. Loncarek. 2015. Plk1 relieves centriole block to reduplication by promoting daughter centriole maturation. *Nat. Commun.* 6:1–13. doi:10.1038/ncomms9077.

Siddik, Z.H. 2003a. Cisplatin: Mode of cytotoxic action and molecular basis of resistance. *Oncogene*. 22:7265–7279. doi:10.1038/sj.onc.1206933.

Siddik, Z.H. 2003b. Cisplatin: mode of cytotoxic action and molecular basis of resistance. *Oncogene*. 22:7265–7279. doi:10.1038/sj.onc.1206933.

Siddik, Z.H. 2003c. Cisplatin: Mode of cytotoxic action and molecular basis of resistance. *Oncogene*. 22:7265–7279. doi:10.1038/sj.onc.1206933.

Siegel, R.L., K.D. Miller, H.E. Fuchs, dan A. Jemal. 2022. Cancer statistics, 2022. *CA. Cancer J. Clin.* 72:7–33. doi:10.3322/caac.21708.

Sieh, W., M. Köbel, T.A. Longacre, D.D. Bowtell, A. deFazio, M.T. Goodman, E. Høgdall, S. Deen, N. Wentzensen, K.B. Moysich, J.D. Brenton, B.A. Clarke, U. Menon, C.B. Gilks, A. Kim, J. Madore, S. Fereday, J. George, L. Galletta, G. Lurie, L.R. Wilkens, M.E. Carney, P.J. Thompson, R.K. Matsuno, S.K. Kjær, A. Jensen, C. Høgdall, K.R. Kalli, B.L. Fridley, G.L. Keeney, R.A. Vierkant, J.M. Cunningham, L.A. Brinton, H.P. Yang, M.E. Sherman, M. García-Closas, J. Lissowska, K. Odunsi, C. Morrison, S. Lele, W. Bshara, L. Sucheston, M. Jimenez-Linan, K. Driver, J. Alsop, M. Mack, V. McGuire, J.H. Rothstein, B.P. Rosen, M.Q. Bernardini, H. Mackay, A. Oza, E.L. Wozniak, E. Benjamin, A. Gentry-Maharaj, S.A. Gayther, A. V. Tinker, L.M. Prentice, C. Chow, M.S. Anglesio, S.E. Johnatty, G. Chenevix-Trench, A.S. Whittemore, P.D.P. Pharoah, E.L. Goode, D.G. Huntsman, dan S.J. Ramus. 2013. Hormone-receptor expression and ovarian cancer survival: an Ovarian Tumor Tissue Analysis consortium study. *Lancet Oncol.* 14:853–862. doi:10.1016/S1470-2045(13)70253-5.

Sies, H., dan D.P. Jones. 2020. Reactive oxygen species (ROS) as pleiotropic physiological signalling agents. *Nat. Rev. Mol. Cell Biol.* 21:363–383. doi:10.1038/s41580-020-0230-3.

Silk, A.D., L.M. Zasadil, A.J. Holland, B. Vitre, D.W. Cleveland, dan B.A. Weaver. 2013. Chromosome missegregation rate predicts whether aneuploidy will promote or suppress tumors. *Proc. Natl. Acad. Sci. U. S. A.* 110:E4134. doi:10.1073/pnas.1317042110.

Silkworth, W.T., dan D. Cimini. 2012. Transient defects of mitotic spindle geometry and chromosome segregation errors. *Cell Div.* 7. doi:10.1186/1747-1028-7-19.

Silkworth, W.T., I.K. Nardi, R. Paul, A. Mogilner, dan D. Cimini. 2012. Timing of centrosome separation is important for accurate chromosome segregation. *Mol. Biol. Cell*. 23:401–411. doi:10.1091/mbc.E11-02-0095.

Silkworth, W.T., I.K. Nardi, L.M. Scholl, dan D. Cimini. 2009. Multipolar spindle pole coalescence is a major source of kinetochore mis-attachment and chromosome mis-segregation in cancer cells. *PLoS One*. 4. doi:10.1371/journal.pone.0006564.

Siller, K.H., dan C.Q. Doe. 2009. Spindle orientation during asymmetric cell division. *Nat. Cell Biol.* 11:365–374. doi:10.1038/ncb0409-365.

Singatulina, A.S., L. Hamon, M. V. Sukhanova, B. Desforges, V. Joshi, A. Bouhss, O.I. Lavrik, dan D. Pastré. 2019. PARP-1 Activation Directs FUS to DNA Damage Sites to Form PARG-Reversible Compartments Enriched in Damaged DNA. *Cell Rep.* 27:1809-1821.e5. doi:10.1016/J.CELREP.2019.04.031.

Singer, G., R. Oldt, Y. Cohen, B.G. Wang, D. Sidransky, R.J. Kurman, dan I.M. Shih. 2003. Mutations in BRAF and KRAS characterize the development of low-grade ovarian serous carcinoma. *J. Natl. Cancer Inst.* 95:484–486. doi:10.1093/jnci/95.6.484.

Sir, J.H., M. Pütz, O. Daly, C.G. Morrison, M. Dunning, J. V. Kilmartin, dan F. Gergely. 2013. Loss of centrioles causes chromosomal instability in vertebrate somatic cells. *J. Cell Biol.* 203:747–756. doi:10.1083/jcb.201309038.

Sivakumar, S., dan G.J. Gorbsky. 2015. Spatiotemporal Regulation of the Anaphase-Promoting Complex in Mitosis. *Nat. Rev. Mol. Cell Biol.* 16:82. doi:10.1038/NRM3934.

Sjögren, C., dan K. Nasmyth. 2001. Sister chromatid cohesion is required for postreplicative double-strand break repair in Saccharomyces cerevisiae. *Curr. Biol.* 11:991–995. doi:10.1016/S0960-9822(01)00271-8.

Sloss, O., C. Topham, M. Diez, S. Taylor, O. Sloss, C. Topham, M. Diez, dan S. Taylor. 2016. Mcl-1 dynamics influence mitotic slippage and death in mitosis. *Oncotarget*. 7:5176–5192. doi:10.18632/ONCOTARGET.6894.

Sluder, G., F.J. Miller, K. Lewis, E.D. Davison, dan C.L. Rieder. 1989. Centrosome inheritance in starfish zygotes: Selective loss of the maternal centrosome after fertilization. *Dev. Biol.* 131:567–579. doi:10.1016/S0012-1606(89)80027-2.

Sonnen, K.F., A.M. Gabryjonczyk, E. Anselm, E.A. Nigg, dan Y.D. Stierhof. 2013. Human cep192 and cep152 cooperate in plk4 recruitment and centriole duplication. *J. Cell Sci.* 126:3223–3233. doi:10.1242/jcs.129502.

Sørensen, B.H., C.S. Dam, S. Stürup, dan I.H. Lambert. 2016. Dual role of LRRC8A-containing transporters on cisplatin resistance in human ovarian cancer cells. *J. Inorg. Biochem.* 160:287–295. doi:10.1016/j.jinorgbio.2016.04.004.

Sotillo, R., E. Hernando, E. Díaz-Rodríguez, J. Teruya-Feldstein, C. Cordón-Cardo, S.W. Lowe, dan R. Benezra. 2007a. Mad2 Overexpression Promotes Aneuploidy and Tumorigenesis in Mice. *Cancer Cell*. 11:9–23. doi:10.1016/J.CCR.2006.10.019.

Sotillo, R., E. Hernando, E. Díaz-Rodríguez, J. Teruya-Feldstein, C. Cordón-Cardo, S.W. Lowe, dan R. Benezra. 2007b. Mad2 Overexpression Promotes Aneuploidy and Tumorigenesis in Mice. *Cancer Cell*. 11:9–23. doi:10.1016/J.CCR.2006.10.019.

Sotillo, R., J.M. Schvartzman, N.D. Socci, dan R. Benezra. 2010. Mad2-induced chromosome instability leads to lung tumour relapse after oncogene withdrawal. *Nature*. 464:436–440. doi:10.1038/nature08803.

Souers, A.J., J.D. Leverson, E.R. Boghaert, S.L. Ackler, N.D. Catron, J. Chen, B.D. Dayton, H. Ding, S.H. Enschede, W.J. Fairbrother, D.C.S. Huang, S.G. Hymowitz, S. Jin, S.L. Khaw, P.J. Kovar, L.T. Lam, J. Lee, H.L. Maecker, K.C. Marsh, K.D. Mason, M.J. Mitten, P.M. Nimmer, A. Oleksijew, C.H. Park, C.M. Park, D.C. Phillips, A.W. Roberts, D. Sampath, J.F. Seymour, M.L. Smith, G.M. Sullivan, S.K. Tahir, C. Tse, M.D. Wendt, Y. Xiao, J.C. Xue, H. Zhang, R.A. Humerickhouse, S.H. Rosenberg, dan S.W. Elmore. 2013. ABT-199, a potent and selective BCL-2 inhibitor, achieves antitumor activity while sparing platelets. *Nat. Med.* 19:202–208. doi:10.1038/NM.3048.

Stark, G.R., dan W.R. Taylor. 2004. Analyzing the G2/M checkpoint. *Methods Mol. Biol.* 280:51–82. doi:10.1385/1-59259-788-2:051.

Stephens, P.J., C.D. Greenman, B. Fu, F. Yang, G.R. Bignell, L.J. Mudie, E.D. Pleasance, K.W. Lau, D. Beare, L.A. Stebbings, S. McLaren, M.-L. Lin, D.J. McBride, I. Varela, S. Nik-Zainal, C. Leroy, M. Jia, A. Menzies, A.P. Butler, J.W. Teague, M.A. Quail, J. Burton, H. Swerdlow, N.P. Carter, L.A. Morsberger, C. Iacobuzio-Donahue, G.A. Follows, A.R.

Green, A.M. Flanagan, M.R. Stratton, P.A. Futreal, dan P.J. Campbell. 2011. Massive Genomic Rearrangement Acquired in a Single Catastrophic Event during Cancer Development. *Cell*. 144:27–40. doi:10.1016/j.cell.2010.11.055.

Stewart, C., C. Ralyea, dan S. Lockwood. 2019. Ovarian Cancer: An Integrated Review. *Semin. Oncol. Nurs.* 35:151–156. doi:10.1016/j.soncn.2019.02.001.

Stingele, S., G. Stoehr, K. Peplowska, J. Cox, M. Mann, dan Z. Storchova. 2012a. Global analysis of genome, transcriptome and proteome reveals the response to aneuploidy in human cells. *Mol. Syst. Biol.* 8:608. doi:10.1038/msb.2012.40.

Stingele, S., G. Stoehr, K. Peplowska, J. Cox, M. Mann, dan Z. Storchova. 2012b. Global analysis of genome, transcriptome and proteome reveals the response to aneuploidy in human cells. *Mol. Syst. Biol.* 8. doi:10.1038/msb.2012.40.

Stingele, S., G. Stoehr, K. Peplowska, J. Cox, M. Mann, dan Z. Storchova. 2012c. Global analysis of genome, transcriptome and proteome reveals the response to aneuploidy in human cells. *Mol. Syst. Biol.* 8. doi:10.1038/msb.2012.40.

Stingele, S., G. Stoehr, K. Peplowska, J. Cox, M. Mann, dan Z. Storchova. 2012d. Global analysis of genome, transcriptome and proteome reveals the response to aneuploidy in human cells. *Mol. Syst. Biol.* 8. doi:10.1038/msb.2012.40.

Strnad, P., S. Leidel, T. Vinogradova, U. Euteneuer, dan A. Khodjakov. 2007. Article Regulated HsSAS-6 Levels Ensure Formation of a Single Procentriole per Centriole during the Centrosome Duplication Cycle. 203–213. doi:10.1016/j.devcel.2007.07.004.

Strober, W. 2015. Trypan Blue Exclusion Test of Cell Viability. *Curr. Protoc. Immunol.* 111:A3.B.1. doi:10.1002/0471142735.IMA03BS111.

Ström, L., H.B. Lindroos, K. Shirahige, dan C. Sjögren. 2004. Postreplicative recruitment of cohesin to double-strand breaks is required for DNA repair. *Mol. Cell*. 16:1003–1015. doi:10.1016/J.MOLCEL.2004.11.026.

Sudakin, V., G.K.T. Chan, dan T.J. Yen. 2001. Checkpoint inhibition of the APC/C in HeLa cells is mediated by a complex of BUBR1, BUB3, CDC20, and MAD2. *J. Cell Biol.* 154:925. doi:10.1083/JCB.200102093.

Sue-A-Quan, R., P.G. Patel, N. Shakfa, M.P.N. Nyi, A. Afriyie-Asante, E.Y. Kang, M. Köbel, dan M. Koti. 2021. Prognostic significance of T cells, PD-L1 immune checkpoint and tumour associated macrophages in clear cell carcinoma of the ovary. *Gynecol. Oncol.* 162:421–430. doi:10.1016/J.YGYNO.2021.05.010.

Sung, P., dan H. Klein. 2006. Mechanism of homologous recombination: mediators and helicases take on regulatory functions. *Nat. Rev. Mol. Cell Biol. 2006 710*. 7:739–750. doi:10.1038/nrm2008.

Sunkel, C.E., dan D.M. Glover. 1988. polo, a mitotic mutant of Drosophila displaying abnormal spindle poles. *J. Cell Sci.* 89 (Pt 1):25–38. doi:10.1242/jcs.89.1.25.

Swift, L.H., dan R.M. Golsteyn. 2016. Cytotoxic amounts of cisplatin induce either checkpoint adaptation or apoptosis in a concentration-dependent manner in cancer cells. *Biol. Cell*. 108:127–148. doi:10.1111/boc.201500056.

Swisher, E.M., K.K. Lin, A.M. Oza, C.L. Scott, H. Giordano, J. Sun, G.E. Konecny, R.L. Coleman, A. V. Tinker, D.M. O'Malley, R.S. Kristeleit, L. Ma, K.M. Bell-McGuinn, J.D. Brenton, J.M. Cragun, A. Oaknin, I. Ray-Coquard, M.I. Harrell, E. Mann, S.H. Kaufmann, A. Floquet, A. Leary, T.C. Harding, S. Goble, L. Maloney, J. Isaacson, A.R. Allen, L. Rolfe, R. Yelensky, M. Raponi, dan I.A. McNeish. 2017. Rucaparib in relapsed, platinum-sensitive high-grade ovarian carcinoma (ARIEL2 Part 1): an international, multicentre, open-label, phase 2 trial. *Lancet. Oncol.* 18:75–87. doi:10.1016/S1470-2045(16)30559-9.

Szefler, B., P. Czeleń, dan P. Krawczyk. 2021. The affinity of carboplatin to b-vitamins and nucleobases. *Int. J. Mol. Sci.* 22. doi:10.3390/ijms22073634.

Szollosi, D., P. Calarco, dan R.P. Donahue. 1972. Absence of centrioles in the first and second meiotic spindles of mouse oocytes. *J. Cell Sci.* 11:521–541. doi:10.1242/jcs.11.2.521.

Tai, H.C., dan E.M. Schuman. 2008. Ubiquitin, the proteasome and protein degradation in neuronal function and dysfunction. *Nat. Rev. Neurosci.* 9:826–838. doi:10.1038/nrn2499.

Takata, M., M.S. Sasaki, E. Sonoda, C. Morrison, M. Hashimoto, H. Utsumi, Y. Yamaguchi-Iwai, A. Shinohara, dan S. Takeda. 1998. Homologous recombination and non-homologous end-joining pathways of DNA double-strand break repair have overlapping roles in the maintenance of chromosomal integrity in vertebrate cells. *EMBO J.* 17:5497–5508. doi:10.1093/EMBOJ/17.18.5497.

Tan, C.-K., C. Castillo, A.G. So, dan K.M. Downey. 1986. THE JOURNAL OP BIOLOGICAL CHEMISTRY An Auxiliary Protein for DNA Polymerase-6 from Fetal Calf Thymus*. 261:12310–12316.

Tang, C.J.C., R.H. Fu, K.S. Wu, W. Bin Hsu, dan T.K. Tang. 2009. CPAP is a cell-cycle regulated protein that controls centriole length. *Nat. Cell Biol.* 11:825–831. doi:10.1038/ncb1889.

Tang, C.J.C., S.Y. Lin, W. Bin Hsu, Y.N. Lin, C.T. Wu, Y.C. Lin, C.W. Chang, K.S. Wu, dan T.K. Tang. 2011a. The human microcephaly protein STIL interacts with CPAP and is required for procentriole formation. *EMBO J.* 30:4790–4804. doi:10.1038/emboj.2011.378.

Tang, N., dan W.F. Marshall. 2012. Centrosome positioning in vertebrate development. *J. Cell Sci.* 125:4951. doi:10.1242/JCS.038083.

Tang, S., E. Stokasimov, Y. Cui, dan D. Pellman. 2022. Breakage of cytoplasmic chromosomes by pathological DNA base excision repair. *Nature*. 606:930–936. doi:10.1038/s41586-022-04767-1.

Tang, Y.C., B.R. Williams, J.J. Siegel, dan A. Amon. 2011b. Identification of aneuploidy-selective antiproliferation compounds. *Cell*. 144:499–512. doi:10.1016/j.cell.2011.01.017.

Tanos, B.E., H.J. Yang, R. Soni, W.J. Wang, F.P. Macaluso, J.M. Asara, dan M.F.B. Tsou. 2013. Centriole distal appendages promote membrane docking, leading to cilia initiation. *Genes Dev.* 27:163. doi:10.1101/GAD.207043.112.

Tao, Z., P. Gao, D.W. Hoffman, dan H.W. Liu. 2008. Domain C of human poly(ADP-ribose) polymerase-1 is important for enzyme activity and contains a novel zinc-ribbon motif. *Biochemistry*. 47:5804–5813. doi:10.1021/BI800018A.

Tao, Z., P. Gao, dan H.W. Liu. 2009. Identification of the ADP-ribosylation sites in the PARP-1 automodification domain: Analysis and implications. *J. Am. Chem. Soc.* 131:14258–14260. doi:10.1021/JA906135D/SUPPL_FILE/JA906135D_SI_001.PDF.

Taylor, A.M., J. Shih, G. Ha, G.F. Gao, X. Zhang, A.C. Berger, S.E. Schumacher, C. Wang, H. Hu, J. Liu, A.J. Lazar, S.J. Caesar-Johnson, J.A. Demchok, I. Felau, M. Kasapi, M.L. Ferguson, C.M. Hutter, H.J. Sofia, R. Tarnuzzer, Z. Wang, L. Yang, J.C. Zenklusen, J. (Julia) Zhang, S. Chudamani, J. Liu, L. Lolla, R. Naresh, T. Pihl, Q. Sun, Y. Wan, Y. Wu, J. Cho, T. DeFreitas, S. Frazer, N. Gehlenborg, G. Getz, D.I. Heiman, J. Kim, M.S. Lawrence, P. Lin, S. Meier, M.S. Noble, G. Saksena, D. Voet, H. Zhang, B. Bernard, N. Chambwe, V. Dhankani, T. Knijnenburg, R. Kramer, K. Leinonen, Y. Liu, M. Miller, S. Reynolds, I. Shmulevich, V. Thorsson, W. Zhang, R. Akbani, B.M. Broom, A.M. Hegde, Z. Ju, R.S. Kanchi, A. Korkut, J. Li, H. Liang, S. Ling, W. Liu, Y. Lu, G.B. Mills, K.S. Ng, A. Rao, M. Ryan, J. Wang, J.N. Weinstein, J. Zhang, A. Abeshouse, J. Armenia, D. Chakravarty, W.K. Chatila, I. de Bruijn, J. Gao, B.E. Gross, Z.J. Heins, R. Kundra, K. La, M. Ladanyi, A. Luna, M.G. Nissan, A. Ochoa, S.M. Phillips, E. Reznik, F. Sanchez-Vega, C. Sander, N. Schultz, R. Sheridan, S.O.

Sumer, Y. Sun, B.S. Taylor, et al. 2018a. Genomic and Functional Approaches to Understanding Cancer Aneuploidy. *Cancer Cell*. 33:676-689.e3. doi:10.1016/j.ccell.2018.03.007.

Taylor, A.M., J. Shih, G. Ha, G.F. Gao, X. Zhang, A.C. Berger, S.E. Schumacher, C. Wang, H. Hu, J. Liu, A.J. Lazar, S.J. Caesar-Johnson, J.A. Demchok, I. Felau, M. Kasapi, M.L. Ferguson, C.M. Hutter, H.J. Sofia, R. Tarnuzzer, Z. Wang, L. Yang, J.C. Zenklusen, J. (Julia) Zhang, S. Chudamani, J. Liu, L. Lolla, R. Naresh, T. Pihl, Q. Sun, Y. Wan, Y. Wu, J. Cho, T. DeFreitas, S. Frazer, N. Gehlenborg, G. Getz, D.I. Heiman, J. Kim, M.S. Lawrence, P. Lin, S. Meier, M.S. Noble, G. Saksena, D. Voet, H. Zhang, B. Bernard, N. Chambwe, V. Dhankani, T. Knijnenburg, R. Kramer, K. Leinonen, Y. Liu, M. Miller, S. Reynolds, I. Shmulevich, V. Thorsson, W. Zhang, R. Akbani, B.M. Broom, A.M. Hegde, Z. Ju, R.S. Kanchi, A. Korkut, J. Li, H. Liang, S. Ling, W. Liu, Y. Lu, G.B. Mills, K.S. Ng, A. Rao, M. Ryan, J. Wang, J.N. Weinstein, J. Zhang, A. Abeshouse, J. Armenia, D. Chakravarty, W.K. Chatila, I. de Bruijn, J. Gao, B.E. Gross, Z.J. Heins, R. Kundra, K. La, M. Ladanyi, A. Luna, M.G. Nissan, A. Ochoa, S.M. Phillips, E. Reznik, F. Sanchez-Vega, C. Sander, N. Schultz, R. Sheridan, S.O. Sumer, Y. Sun, B.S. Taylor, et al. 2018b. Genomic and Functional Approaches to Understanding Cancer Aneuploidy. *Cancer Cell*. 33:676-689.e3. doi:10.1016/j.ccell.2018.03.007.

Taylor, E.M., S.M. Cecillon, A. Bonis, J. Ross Chapman, L.F. Povirk, dan H.D. Lindsay. 2010. The Mre11/Rad50/Nbs1 complex functions in resection-based DNA end joining in Xenopus laevis. *Nucleic Acids Res.* 38:441–454. doi:10.1093/NAR/GKP905.

Terada, Y., Y. Uetake, dan R. Kuriyama. 2003. Interaction of Aurora-A and centrosomin at the microtubule-nucleating site in Drosophila and mammalian cells. *J. Cell Biol.* 162:757–763. doi:10.1083/jcb.200305048.

Thompson, P.S., dan D. Cortez. 2020. New Insights into Abasic Site Repair and Tolerance. *DNA Repair (Amst).* 90:102866. doi:10.1016/J.DNAREP.2020.102866.

Thompson, S.L., dan D.A. Compton. 2010. Proliferation of aneuploid human cells is limited by a p53-dependent mechanism. *J. Cell Biol.* 188:369–381. doi:10.1083/jcb.200905057.

Thompson, S.L., dan D.A. Compton. 2011. Chromosome missegregation in human cells arises through specific types of kinetochore-microtubule attachment errors. *Proc. Natl. Acad. Sci. U. S. A.* 108:17974–17978. doi:10.1073/PNAS.1109720108/SUPPL_FILE/PNAS.201109720SI.PDF.

Thorburn, R.R., C. Gonzalez, G.A. Brar, S. Christen, T.M. Carlile, N.T. Ingolia, U. Sauer, J.S. Weissman, dan A. Amon. 2013. Aneuploid yeast strains exhibit defects in cell growth and passage through START. *Mol. Biol. Cell*. 24:1274–1289. doi:10.1091/MBC.E12-07-0520.

Tinel, A., dan J. Tschopp. 2004. The PIDDosome, a Protein Complex Implicated in Activation of Caspase-2 in Response to Genotoxic Stress. *Science (80-.).* 304:843–846. doi:10.1126/science.1095432.

Tomimatsu, N., B. Mukherjee, M. Catherine Hardebeck, M. Ilcheva, C. Vanessa Camacho, J. Louise Harris, M. Porteus, B. Llorente, K.K. u. Khanna, dan S. Burma. 2014. Phosphorylation of EXO1 by CDKs 1 and 2 regulates DNA end resection and repair pathway choice. *Nat. Commun. 2014 51*. 5:1–10. doi:10.1038/ncomms4561.

Tomimatsu, N., B. Mukherjee, K. Deland, A. Kurimasa, E. Bolderson, K.K. Khanna, dan S. Burma. 2012. Exo1 plays a major role in DNA end resection in humans and influences double-strand break repair and damage signaling decisions. *DNA Repair (Amst).* 11:441–448. doi:10.1016/J.DNAREP.2012.01.006.

Torres, E.M., T. Sokolsky, C.M. Tucker, L.Y. Chan, M. Boselli, M.J. Dunham, dan A. Amon. 2007. Effects of aneuploidy on cellular physiology and cell division in haploid yeast. *Science (80-.).* 317:916–924. doi:10.1126/science.1142210.

Torres, E.M., B.R. Williams, dan A. Amon. 2008. Aneuploidy: Cells Losing Their Balance. *Genetics*. 179:737–746. doi:10.1534/GENETICS.108.090878.

Toshiyuki, M., dan J.C. Reed. 1995. Tumor suppressor p53 is a direct transcriptional activator of the human bax gene. *Cell*. 80:293–299. doi:10.1016/0092-8674(95)90412-3.

Tothill, R.W., A. V. Tinker, J. George, R. Brown, S.B. Fox, S. Lade, D.S. Johnson, M.K. Trivett, D. Etemadmoghadam, B. Locandro, N. Traficante, S. Fereday, J.A. Hung, Y.E. Chiew, I. Haviv, D. Gertig, A. Defazio, dan D.D.L. Bowtell. 2008. Novel Molecular Subtypes of Serous and Endometrioid Ovarian Cancer Linked to Clinical Outcome. *Clin. Cancer Res.* 14:5198–5208. doi:10.1158/1078-0432.CCR-08-0196.

Treiber, D.K., X. Zhai, H.M. Jantzen, dan J.M. Essigmann. 1994. Cisplatin-DNA adducts are molecular decoys for the ribosomal RNA transcription factor hUBF (human upstream binding factor). *Proc. Natl. Acad. Sci. U. S. A.* 91:5672–5676. doi:10.1073/pnas.91.12.5672.

Trivedi, P., C.D. Steele, L.B. Alexandrov, dan D.W. Cleveland. 2022. Mitotic tethering enables

en masse inheritance of a shattered micronuclear chromosome. doi:10.1038/s41586-023-06216-z.

Tsou, M.F.B., dan T. Stearns. 2006. Mechanism limiting centrosome duplication to once per cell cycle. *Nature*. 442:947–951. doi:10.1038/nature04985.

Tsou, M.F.B., W.J. Wang, K.A. George, K. Uryu, T. Stearns, dan P. V. Jallepalli. 2009. Polo kinase and separase regulate the mitotic licensing of centriole duplication in human cells. *Dev. Cell*. 17:344–354. doi:10.1016/J.DEVCEL.2009.07.015.

Tsujimoto, Y., L.R. Finger, J. Yunis, P.C. Nowell, dan C.M. Croce. 1984. Cloning of the chromosome breakpoint of neoplastic B cells with the t(14;18) chromosome translocation. *Science*. 226:1097–1099. doi:10.1126/SCIENCE.6093263.

Turajlic, S., H. Xu, K. Litchfield, A. Rowan, T. Chambers, J.I. Lopez, D. Nicol, T. O'Brien, J. Larkin, S. Horswell, M. Stares, L. Au, M. Jamal-Hanjani, B. Challacombe, A. Chandra, S. Hazell, C. Eichler-Jonsson, A. Soultati, S. Chowdhury, S. Rudman, J. Lynch, A. Fernando, G. Stamp, E. Nye, F. Jabbar, L. Spain, S. Lall, R. Guarch, M. Falzon, I. Proctor, L. Pickering, M. Gore, T.B.K. Watkins, S. Ward, A. Stewart, R. DiNatale, M.F. Becerra, E. Reznik, J.J. Hsieh, T.A. Richmond, G.F. Mayhew, S.M. Hill, C.D. McNally, C. Jones, H. Rosenbaum, S. Stanislaw, D.L. Burgess, N.R. Alexander, dan C. Swanton. 2018. Tracking Cancer Evolution Reveals Constrained Routes to Metastases: TRACERx Renal. *Cell*. 173:581-594.e12. doi:10.1016/j.cell.2018.03.057.

Uetake, Y., dan G. Sluder. 2010a. Prolonged prometaphase blocks daughter cell proliferation despite normal completion of mitosis. *Curr. Biol.* 20:1666–1671. doi:10.1016/j.cub.2010.08.018.

Uetake, Y., dan G. Sluder. 2010b. Prolonged prometaphase blocks daughter cell proliferation despite normal completion of mitosis. *Curr. Biol.* 20:1666–1671. doi:10.1016/j.cub.2010.08.018.

Unger, F.T., H.A. Klasen, G. Tchartchian, R.L. de Wilde, dan I. Witte. 2009. DNA damage induced by cis- and carboplatin as indicator for in vitro sensitivity of ovarian carcinowma cells. *BMC Cancer*. 9:359. doi:10.1186/1471-2407-9-359/FIGURES/6.

Varetti, G., C. Guida, S. Santaguida, E. Chiroli, dan A. Musacchio. 2011. Homeostatic Control of Mitotic Arrest. *Mol. Cell*. 44:710–720. doi:10.1016/J.MOLCEL.2011.11.014.

Vargas-Hurtado, D., J.B. Brault, T. Piolot, L. Leconte, N. Da Silva, C. Pennetier, A. Baffet, V. Marthiens, dan R. Basto. 2019. Differences in Mitotic Spindle Architecture in

Mammalian Neural Stem Cells Influence Mitotic Accuracy during Brain Development. *Curr. Biol.* 29:2993-3005.e9. doi:10.1016/j.cub.2019.07.061.

Vasey, P.A., G.C. Jayson, A. Gordon, H. Gabra, R. Coleman, R. Atkinson, D. Parkin, J. Paul, A. Hay, dan S.B. Kaye. 2004. Phase III randomized trial of docetaxel-carboplatin versus paclitaxel-carboplatin as first-line chemotherpy for ovarian carcinoma. *J. Natl. Cancer Inst.* 96:1682–1691. doi:10.1093/jnci/djh323.

Vaughan, S., J.I. Coward, R.C. Bast, A. Berchuck, J.S. Berek, J.D. Brenton, G. Coukos, C.C. Crum, R. Drapkin, D. Etemadmoghadam, M. Friedlander, H. Gabra, S.B. Kaye, C.J. Lord, E. Lengyel, D.A. Levine, I.A. McNeish, U. Menon, G.B. Mills, K.P. Nephew, A.M. Oza, A.K. Sood, E.A. Stronach, H. Walczak, D.D. Bowtell, dan F.R. Balkwill. 2011. Rethinking ovarian cancer: Recommendations for improving outcomes. *Nat. Rev. Cancer*. 11:719–725. doi:10.1038/nrc3144.

Velot, L., A. Molina, S. Rodrigues-Ferreira, A. Nehlig, B.P. Bouchet, M. Morel, L. Leconte, L. Serre, I. Arnal, D. Braguer, A. Savina, S. Honore, dan C. Nahmias. 2015. Negative regulation of EB1 turnover at microtubule plus ends by interaction with microtubule-associated protein ATIP3. *Oncotarget*. 6:43557. doi:10.18632/ONCOTARGET.6196.

Vennin, C., C.M. Cattaneo, L. Bosch, S. Vegna, X. Ma, H.G.J. Damstra, M. Martinovic, E. Tsouri, M. Ilic, L. Azarang, J.R.T. van Weering, E. Pulver, A.L. Zeeman, T. Schelfhorst, J.O. Lohuis, A.C. Rios, J.F. Dekkers, L. Akkari, R. Menezes, R. Medema, S.R. Baglio, A. Akhmanova, S.C. Linn, S. Lemeer, D.M. Pegtel, E.E. Voest, dan J. van Rheenen. 2023. Taxanes trigger cancer cell killing in vivo by inducing non-canonical T cell cytotoxicity. *Cancer Cell*. 41:1170-1185.e12. doi:10.1016/j.ccell.2023.05.009.

Verhaegh, G.W.C.T., W. Jongmans, B. Morolli, G.J. Jaspers ', G.P. Van Der Schans, P.H.M. Lohman, dan M.Z. Zdzienicka. 1995. A novel type of X-ray-sensitive Chinese hamster cell mutant with radioresistant DNA synthesis and hampered DNA double-strand break repair. *DNA Repair Mutat. Res.* 337:119–129.

Vestergaard Madsen, C., P. Adimi, A. Jakobsen, dan K. Dahl Steffensen. 2020. Cabazitaxel - A Treatment Option in Recurrent Platinum-resistant Ovarian Cancer. *Anticancer Res.* 40:5255–5261. doi:10.21873/ANTICANRES.14529.

Vichi, P., F. Coin, J.P. Renaud, W. Vermeulen, J.H.J. Hoeijmakers, D. Moras, dan J.M. Egly. 1997. Cisplatin- and UV-damaged DNA lure the basal transcription factor TFIID/TBP. *EMBO J.* 16:7444–7456. doi:10.1093/emboj/16.24.7444.

Volk-Draper, L., K. Hall, C. Griggs, S. Rajput, P. Kohio, D. DeNardo, dan S. Ran. 2014. Paclitaxel therapy promotes breast cancer metastasis in a TLR4-dependent manner. *Cancer Res.* 74:5421–5434. doi:10.1158/0008-5472.CAN-14-0067.

Vorobjev, I.A., dan Y.S. Chentsov. 1982. Centrioles in the cell cycle. I. Epithelial cells. *J. Cell Biol.* 93:938–949. doi:10.1083/jcb.93.3.938.

Wade Harper, J., J.L. Burton, dan M.J. Solomon. 2002. The anaphase-promoting complex: it's not just for mitosis any more. *Genes Dev.* 16:2179–2206. doi:10.1101/GAD.1013102.

Walsh, T., M.K. Lee, S. Casadei, A.M. Thornton, S.M. Stray, C. Pennil, A.S. Nord, J.B. Mandell, E.M. Swisher, dan M.C. King. 2010. Detection of inherited mutations for breast and ovarian cancer using genomic capture and massively parallel sequencing. *Proc. Natl. Acad. Sci. U. S. A.* 107:12629. doi:10.1073/PNAS.1007983107.

Wang, C., S. Vegna, H. Jin, B. Benedict, C. Lieftink, C. Ramirez, R.L. de Oliveira, B. Morris, J. Gadiot, W. Wang, A. du Chatinier, L. Wang, D. Gao, B. Evers, G. Jin, Z. Xue, A. Schepers, F. Jochems, A.M. Sanchez, S. Mainardi, H. te Riele, R.L. Beijersbergen, W. Qin, L. Akkari, dan R. Bernards. 2019a. Inducing and exploiting vulnerabilities for the treatment of liver cancer. *Nature*. 574:268–272. doi:10.1038/s41586-019-1607-3.

Wang, K., C. Wloka, dan E. Bi. 2019b. Non-muscle Myosin-II Is Required for the Generation of a Constriction Site for Subsequent Abscission. *iScience*. 13:69–81. doi:10.1016/J.ISCI.2019.02.010.

Wang, K., X.M. Yin, D.T. Chao, C.L. Milliman, dan S.J. Korsmeyer. 1996. BID: a novel BH3 domain-only death agonist. *Genes Dev.* 10:2859–2869. doi:10.1101/GAD.10.22.2859.

Wang, L., Y. Xue, S. Yang, T. Bo, J. Xu, dan W. Wang. 2023. Mismatch Repair Protein Msh2 Is Necessary for Macronuclear Stability and Micronuclear Division in Tetrahymena thermophila. *Int. J. Mol. Sci.* 24:10559. doi:10.3390/ijms241310559.

Wang, M., R.B. Nagle, B.S. Knudsen, A.E. Cress, dan G.C. Rogers. 2020. Centrosome loss results in an unstable genome and malignant prostate tumors. *Oncogene*. 39:399–413. doi:10.1038/s41388-019-0995-z.

Wani, M.C., H.L. Taylor, M.E. Wall, P. Coggon, dan A.T. Mcphail. 1971. Plant Antitumor Agents.VI.The Isolation and Structure of Taxol, a Novel Antileukemic and Antitumor Agent from Taxus brevifolia2. *J. Am. Chem. Soc.* 93:2325–2327. doi:10.1021/ja00738a045.

Warecki, B., dan W. Sullivan. 2020. Mechanisms driving acentric chromosome transmission.

Chromosom. Res. 28:229–246. doi:10.1007/S10577-020-09636-Z.

Waters, J.C., R.-H. Chen, A.W. Murray, dan E.D. Salmon. 1998a. Localization of Mad2 to Kinetochores Depends on Microtubule Attachment, Not Tension. *J. Cell Biol.* 141:1181–1191.

Waters, J.C., R.H. Chen, A.W. Murray, dan E.D. Salmon. 1998b. Localization of Mad2 to kinetochores depends on microtubule attachment, not tension. *J. Cell Biol.* 141:1181–1191. doi:10.1083/JCB.141.5.1181.

Watts, C.A., F.M. Richards, A. Bender, P.J. Bond, O. Korb, O. Kern, M. Riddick, P. Owen, R.M. Myers, J. Raff, F. Gergely, D.I. Jodrell, dan S. V. Ley. 2013. Design, Synthesis, and Biological Evaluation of an Allosteric Inhibitor of HSET that Targets Cancer Cells with Supernumerary Centrosomes. *Chem. Biol.* 20:1399–1410. doi:10.1016/J.CHEMBIOL.2013.09.012.

Weaver, B.A. 2014a. How Taxol/paclitaxel kills cancer cells. *Mol. Biol. Cell*. 25:2677–2681. doi:morr.

Weaver, B.A. 2014b. How Taxol/paclitaxel kills cancer cells. *Mol. Biol. Cell*. 25:2677–2681. doi:10.1091/mbc.E14-04-0916.

Weaver, B.A.A., Z.Q. Bonday, F.R. Putkey, G.J.P.L. Kops, A.D. Silk, dan D.W. Cleveland. 2003. Centromere-associated protein-E is essential for the mammalian mitotic checkpoint to prevent aneuploidy due to single chromosome loss. *J. Cell Biol.* 162:551–563. doi:10.1083/JCB.200303167.

Weaver, B.A.A., A.D. Silk, C. Montagna, P. Verdier-Pinard, dan D.W. Cleveland. 2007. Aneuploidy acts both oncogenically and as a tumor suppressor. *Cancer Cell*. 11:25–36. doi:10.1016/J.CCR.2006.12.003.

Wei, A.H., S.A. Strickland, J.Z. Hou, W. Fiedler, T.L. Lin, R.B. Walter, A. Enjeti, I.S. Tiong, M. Savona, S. Lee, B. Chyla, R. Popovic, A.H. Salem, S. Agarwal, T. Xu, K.M. Fakouhi, R. Humerickhouse, W.J. Hong, J. Hayslip, dan G.J. Roboz. 2019. Venetoclax Combined With Low-Dose Cytarabine for Previously Untreated Patients With Acute Myeloid Leukemia: Results From a Phase Ib/II Study. *J. Clin. Oncol.* 37:1277–1284. doi:10.1200/JCO.18.01600.

Wertz, I.E., S. Kusam, C. Lam, T. Okamoto, W. Sandoval, D.J. Anderson, E. Helgason, J.A. Ernst, M. Eby, J. Liu, L.D. Belmont, J.S. Kaminker, K.M. O'Rourke, K. Pujara, P.B. Kohli, A.R. Johnson, M.L. Chiu, J.R. Lill, P.K. Jackson, W.J. Fairbrother, S. Seshagiri, M.J.C.

Ludlam, K.G. Leong, E.C. Dueber, H. Maecker, D.C.S. Huang, dan V.M. Dixit. 2011. Sensitivity to antitubulin chemotherapeutics is regulated by MCL1 and FBW7. *Nat. 2011 4717336*. 471:110–114. doi:10.1038/nature09779.

West, S.C. 2003. Molecular views of recombination proteins and their control. *Nat. Rev. Mol. Cell Biol. 2003 46*. 4:435–445. doi:10.1038/nrm1127.

White, A.W., R. Almassy, A.H. Calvert, N.J. Curtin, R.J. Griffin, Z. Hostomsky, K. Maegley, D.R. Newell, S. Srinivasan, dan B.T. Golding. 2000. Resistance-modifying agents. 9. Synthesis and biological properties of benzimidazole inhibitors of the DNA repair enzyme poly(ADP-ribose) polymerase. *J. Med. Chem.* 43:4084–4097. doi:10.1021/JM000950V.

Wiese, C., dan Y. Zheng. 2000. A new function for the γ-tubulin ring complex as a microtubule minus-end cap. *Nat. Cell Biol.* 2:358–364. doi:10.1038/35014051.

Wilhelm, T., I. Magdalou, A. Barascu, H. Técher, M. Debatisse, dan B.S. Lopez. 2014. Spontaneous slow replication fork progression elicits mitosis alterations in homologous recombination-deficient mammalian cells. *Proc. Natl. Acad. Sci.* 111:763–768. doi:10.1073/PNAS.1311520111.

Wilkinson, R., P.J. Cox, M. Jones, dan K.R. Harrap. 1978. Selection of potential second generation platinum compounds. *Biochimie*. 60:851–857. doi:10.1016/S0300-9084(78)80569-0.

Williams, B.C., T.D. Murphy, M.L. Goldberg, dan G.H. Karpen. 1998. Neocentromere activity of structurally acentric mini-chromosomes in Drosophila.

Williams, B.R., V.R. Prabhu, K.E. Hunter, C.M. Glazier, C.A. Whittaker, D.E. Housman, dan A. Amon. 2008a. Aneuploidy affects proliferation and spontaneous immortalization in mammalian cells. *Science (80-.).* 322:703–709. doi:10.1126/science.1160058.

Williams, B.R., V.R. Prabhu, K.E. Hunter, C.M. Glazier, C.A. Whittaker, D.E. Housman, dan A. Amon. 2008b. Aneuploidy affects proliferation and spontaneous immortalization in mammalian cells. *Science (80-.).* 322:703–709. doi:10.1126/science.1160058.

Wong, Y.L., J. V. Anzola, R.L. Davis, M. Yoon, A. Motamedi, A. Kroll, C.P. Seo, J.E. Hsia, S.K. Kim, J.W. Mitchell, B.J. Mitchell, A. Desai, T.C. Gahman, A.K. Shiau, dan K. Oegema. 2015. Reversible centriole depletion with an inhibitor of Polo-like kinase 4. *Science (80-.).* 348:1155–1160. doi:10.1126/science.aaa5111.

Woodruff, J.B., O. Wueseke, dan A.A. Hyman. Cite this article. doi:10.1098/rstb.2013.0459.

Woodruff, J.B., O. Wueseke, V. Viscardi, J. Mahamid, S.D. Ochoa, J. Bunkenborg, P.O.

Widlund, A. Pozniakovsky, E. Zanin, S. Bahmanyar, A. Zinke, S.H. Hong, M. Decker, W. Baumeister, J.S. Andersen, K. Oegema, dan A.A. Hyman. 2015. Regulated assembly of a supramolecular centrosome scaffold in vitro. *Science (80-.).* 348:808–812. doi:10.1126/science.aaa3923.

Wu, G.S., T.F. Burns, E.R. McDonald, W. Jiang, R. Meng, I.D. Krantz, G. Kao, D. Di Gan, J.Y. Zhou, R. Muschel, S.R. Hamilton, N.B. Spinner, S. Markowitz, G. Wu, dan W.S. El-Deiry. 1997. KILLER/DR5 is a DNA damage-inducible p53-regulated death receptor gene. *Nat. Genet.* 17:141–143. doi:10.1038/NG1097-141.

Wu, R.C., A. Ayhan, D. Maeda, K.R. Kim, B.A. Clarke, P. Shaw, M.H. Chui, B. Rosen, I.M. Shih, dan T.L. Wang. 2014. Frequent somatic mutations of the telomerase reverse transcriptase promoter in ovarian clear cell carcinoma but not in other major types of gynaecological malignancy. *J. Pathol.* 232:473–481. doi:10.1002/PATH.4315.

Wyatt, H.D.M., S. Sarbajna, J. Matos, dan S.C. West. 2013a. Coordinated actions of SLX1-SLX4 and MUS81-EME1 for holliday junction resolution in human cells. *Mol. Cell*. 52:234–247. doi:10.1016/j.molcel.2013.08.035.

Wyatt, H.D.M., S. Sarbajna, J. Matos, dan S.C. West. 2013b. Coordinated Actions of SLX1-SLX4 and MUS81-EME1 for Holliday Junction Resolution in Human Cells. *Mol. Cell*. 52:234–247. doi:10.1016/J.MOLCEL.2013.08.035.

Wyman, C., D. Ristic, dan R. Kanaar. 2004. Homologous recombination-mediated double-strand break repair. *DNA Repair (Amst).* 3:827–833. doi:10.1016/J.DNAREP.2004.03.037.

Xie, A., A. Kwok, dan R. Scully. 2009. Role of mammalian Mre11 in classical and alternative nonhomologous end joining. *Nat. Struct. Mol. Biol.* 16:814–818. doi:10.1038/NSMB.1640.

Yamamoto, S., dan D. Kitagawa. 2019. Self-organization of Plk4 regulates symmetry breaking in centriole duplication. *Nat. Commun.* 10:1–12. doi:10.1038/s41467-019-09847-x.

Yang, C.P.H., dan S.B. Horwitz. 2017. Taxol®: The first microtubule stabilizing agent. *Int. J. Mol. Sci.* 18. doi:10.3390/ijms18081733.

Yang, Z., J. Lončarek, A. Khodjakov, dan C.L. Rieder. 2008. Extra centrosomes and/or chromosomes prolong mitosis in human cells. *Nat. Cell Biol. 2008 106*. 10:748–751. doi:10.1038/ncb1738.

Ye, X., H. Zeng, G. Ning, J.F. Reiter, dan A. Liu. 2014. C2cd3 is critical for centriolar distal

appendage assembly and ciliary vesicle docking in mammals. *Proc. Natl. Acad. Sci. U. S. A.* 111:2164–2169. doi:10.1073/pnas.1318737111.

Yeow, Z.Y., B.G. Lambrus, R. Marlow, K.H. Zhan, M.A. Durin, L.T. Evans, P.M. Scott, T. Phan, E. Park, L.A. Ruiz, D. Moralli, E.G. Knight, L.M. Badder, D. Novo, S. Haider, C.M. Green, A.N.J. Tutt, C.J. Lord, J.R. Chapman, dan A.J. Holland. 2020. Targeting TRIM37-driven centrosome dysfunction in 17q23-amplified breast cancer. *Nature*. 585:447–452. doi:10.1038/S41586-020-2690-1.

Yona, A.H., Y.S. Manor, R.H. Herbst, G.H. Romano, A. Mitchell, M. Kupiec, Y. Pilpel, dan O. Dahan. 2012. Chromosomal duplication is a transient evolutionary solution to stress. *Proc. Natl. Acad. Sci. U. S. A.* 109:21010–21015. doi:10.1073/pnas.1211150109.

Youle, R.J., dan A. Strasser. 2008. The BCL-2 protein family: opposing activities that mediate cell death. *Nat. Rev. Mol. Cell Biol. 2008 91*. 9:47–59. doi:10.1038/nrm2308.

Yu, L., Y. Song, Q. Zhang, dan Z. Qimin. 2009. Ninein-like protein is overexpressed in head and neck squamous cell carcinoma and contributes to cancer growth and resistance to apoptosis. *Oncol. Rep.* 22:789–798. doi:10.3892/OR_00000501.

Yubuki, N., dan B.S. Leander. 2013. Evolution of microtubule organizing centers across the tree of eukaryotes. *Plant J.* 75:230–244. doi:10.1111/tpj.12145.

Yun, M.H., dan K. Hiom. 2009. CtIP-BRCA1 modulates the choice of DNA double-strand-break repair pathway throughout the cell cycle. *Nat. 2009 4597245*. 459:460–463. doi:10.1038/nature07955.

Zasadil, L.M., K.A. Andersen, D. Yeum, G.B. Rocque, L.G. Wilke, A.J. Tevaarwerk, R.T. Raines, M.E. Burkard, dan B.A. Weaver. 2014a. Cytotoxicity of paclitaxel in breast cancer is due to chromosome missegregation on multipolar spindles. *Sci. Transl. Med.* 6:229ra43. doi:10.1126/scitranslmed.3007965.

Zasadil, L.M., K.A. Andersen, D. Yeum, G.B. Rocque, L.G. Wilke, A.J. Tevaarwerk, R.T. Raines, M.E. Burkard, dan B.A. Weaver. 2014b. Cytotoxicity of paclitaxel in breast cancer is due to chromosome missegregation on multipolar spindles. *Sci. Transl. Med.* 6:229ra43. doi:10.1126/scitranslmed.3007965.

Zetterberg, A., dan O. Larsson. 1985. Kinetic analysis of regulatory events in G1 leading to proliferation or quiescence of Swiss 3T3 cells. *Proc. Natl. Acad. Sci. U. S. A.* 82:5365–5369. doi:10.1073/PNAS.82.16.5365.

Zha, H., C. Aimé-Sempé, T. Sato, dan J.C. Reed. 1996. Proapoptotic protein Bax

heterodimerizes with Bcl-2 and homodimerizes with Bax via a novel domain (BH3) distinct from BH1 and BH2. *J. Biol. Chem.* 271:7440–7444. doi:10.1074/JBC.271.13.7440.

Zhang, C.Z., A. Spektor, H. Cornils, J.M. Francis, E.K. Jackson, S. Liu, M. Meyerson, dan D. Pellman. 2015. Chromothripsis from DNA damage in micronuclei. *Nature*. 522:179–184. doi:10.1038/nature14493.

Zhang, M., L. Cheng, Y. Jia, G. Liu, C. Li, S. Song, A. Bradley, dan Y. Huang. 2016. Aneuploid embryonic stem cells exhibit impaired differentiation and increased neoplastic potential. *EMBO J.* 35:2285–2300. doi:10.15252/embj.201593103.

Zhang, X., H. Shi, J. Wu, X. Zhang, L. Sun, C. Chen, dan Z.J. Chen. 2013. Cyclic GMP-AMP containing mixed Phosphodiester linkages is an endogenous high-affinity ligand for STING. *Mol. Cell*. 51:226–235. doi:10.1016/j.molcel.2013.05.022.

Zhao, W., Y. Song, B. Xu, dan Q. Zhan. 2012. Overexpression of centrosomal protein Nlp confers breast carcinoma resistance to paclitaxel. *Cancer Biol. Ther.* 13:156–163. doi:10.4161/CBT.13.3.18697.

Zheng, X., L.M. Gooi, A. Wason, E. Gabriel, N.Z. Mehrjardi, Q. Yang, X. Zhang, A. Debec, M.L. Basiri, T. Avidor-Reiss, A. Pozniakovsky, I. Poser, T. Saric, A.A. Hyman, H. Li, dan J. Gopalakrishnan. 2014. Conserved TCP domain of Sas-4/CPAP is essential for pericentriolar material tethering during centrosome biogenesis. *Proc. Natl. Acad. Sci. U. S. A.* 111. doi:10.1073/PNAS.1317535111/-/DCSUPPLEMENTAL/SAPP.PDF.

Zheng, Y., M.L. Wong, B. Alberts, dan T. Mitchison. 1995. Nucleation of microtubule assembly by a γ-tubulin-containing ring complex. *Nature*. 378:578–583. doi:10.1038/378578a0.

Zhou, B.B.S., dan S.J. Elledge. 2000. The DNA damage response: putting checkpoints in perspective. *Nat. 2000 4086811*. 408:433–439. doi:10.1038/35044005.

Zimmerman, W.C., J. Sillibourne, J. Rosa, dan S.J. Doxsey. 2004. Mitosis-specific anchoring of γ tubulin complexes by pericentrin controls spindle organization and mitotic entry. *Mol. Biol. Cell*. 15:3642–3657. doi:10.1091/mbc.E03-11-0796.

Zmuda, J.F., dan R.J. Rivas. 1998. The Golgi Apparatus and the Centrosome Are Localized to the Sites of Newly Emerging Axons in Cerebellar Granule Neurons In Vitro. *Cell Motil. Cytoskeleton*. 41:18–38. doi:10.1002/(SICI)1097-0169(1998)41:1.

Annex

Centrosome amplification primes for apoptosis and favors the response to chemotherapy in ovarian cancer beyond multipolar divisions

Frances Edwards[1]*, Giulia Fantozzi[1], Anthony Y. Simon[1], Jean-Philippe Morretton[1], Aurelie Herbette[2], Andrea E. Tijhuis[3], Rene Wardenaar[3], Stacy Foulane[1], Simon Gemble[1], Diana C.J. Spierings[3], Floris Foijer[3], Odette Mariani[4], Anne Vincent-Salomon[4], Sergio Roman Roman[2], Xavier Sastre-Garau[4], Oumou Goundiam[2] and Renata Basto[1]*

[1]Biology of centrosomes and genetic instability, Institut Curie, PSL Research University, CNRS UMR 144, F-75005 Paris, France.

[2]Department of Translational Research, Institut Curie, PSL University, 26 rue d'Ulm, F-75248 Paris Cedex 05, France.

[3]European Research Institute for the Biology of Ageing, University of Groningen, University Medical Center Groningen, Groningen, The Netherlands.

[4]Department of pathology, Institut Curie, 26 rue d'Ulm, F-75248 Paris Cedex 05, France.

*Corresponding authors. Email: frances.edwards@curie.fr and renata.basto@curie.fr

ABSTRACT

Centrosome amplification is a feature of cancer cells associated with chromosome instability and invasiveness. Enhancing chromosome instability and subsequent cancer cell death via centrosome unclustering and multipolar divisions is an aimed-for therapeutic approach. Here we show that centrosome amplification favors responses to conventional chemotherapy independently of multipolar divisions and chromosome instability. We perform single-cell live imaging of chemotherapy responses in epithelial ovarian cancer cell lines and observe increased cell death when centrosome amplification is induced. By correlating cell fate with mitotic behaviors, we show that enhanced cell death occurs independently of chromosome instability. We identify that cells with centrosome amplification are primed for apoptosis. We show they are dependent on the apoptotic inhibitor BCL-XL, and that this is not a consequence of mitotic stresses associated with centrosome amplification. Given the multiple mechanisms that promote chemotherapy responses in cells with centrosome amplification, we assess such a relationship in an epithelial ovarian cancer patient cohort. We show that high centrosome numbers associate with improved chemotherapy responses and longer overall survival. Our work identifies apoptotic priming as a clinically relevant consequence of centrosome amplification, expanding our understanding of this pleiotropic cancer cell feature.

INTRODUCTION

Centrosomes are the major microtubule organizing centers in proliferating animal cells, whose structure and number are tightly regulated during the cell cycle *(1)*. The centrosome is duplicated during S-phase in a PLK4 kinase dependent manner and the two centrosomes contribute to the timely and functional assembly of a bipolar spindle during mitosis. In cancer cell lines, centrosome structural and numerical defects are common *(2)* and in particular centrosome amplification – more than 2 centrosomes per cell - has also been observed *in situ* in tumor samples *(3–5)*. Cells with centrosome amplification perform bipolar mitosis via centrosome clustering mechanisms during spindle assembly *(6–10)*. Centrosome amplification is nevertheless associated with chromosome instability *(11, 12)*, and increased invasive behaviors *(13–15)*. As first postulated by T. Boveri *(16)*, centrosome amplification can drive tumorigenesis *in vivo (7, 17–19)*. Defects in centrosome clustering capacity are associated with lethal multipolar divisions *(8, 11, 20)*, motivating the search for inhibitors that limit centrosome clustering and eliminate cells with centrosome amplification *(20–25)*.

The combination of Carboplatin and Paclitaxel is used as standard of care in various cancers including ovarian, breast, and lung cancer. Carboplatin induces DNA damage and Paclitaxel stabilizes microtubules leading to cell death via mitotic catastrophe which is defined as death during or following abnormal mitosis *(26, 27)*. Despite the central role of centrosomes in spindle assembly, how centrosome amplification influences the response to combined Carboplatin and Paclitaxel remains unexplored. Paclitaxel has been shown to induce multipolar divisions *(28)* and this can be favored by centrosome amplification *(29)*. The impact of centrosome amplification on the response to DNA damaging agents has however not been explored despite centrosomes regulating multiple signaling pathways that could influence chemotherapy responses *(30–34)*. Multiple consequences of centrosome amplification could therefore synergize with combined Carboplatin and Paclitaxel to induce efficient cancer cell elimination.

Here we chose to study how centrosome amplification influences the response to combined Carboplatin and Paclitaxel in the context of epithelial ovarian cancer, a disease with poor clinical outcome related to late diagnosis, and frequent relapse *(35)*. Centrosome amplification is observed in ovarian cancer cell lines, and we recently also characterized its

occurrence *in situ* in patient samples *(5)*. We use an inducible PLK4 over-expression system in ovarian cancer cell lines to induce centrosome amplification in isogenic backgrounds. We perform single-cell live-imaging of cells to assess the correlations between mitotic behaviors and cell fate during chemotherapy. We show that centrosome amplification favors the response to combined Carboplatin and Paclitaxel via multiple mechanisms. Beyond multipolar divisions associated with Paclitaxel exposure, we found that centrosome amplification also favors cell death independently of mitotic behaviors. We show that centrosome amplification, although well tolerated by ovarian cancer cells, leads to mitochondria outer membrane permeabilization priming. We assess the level of centrosome amplification in a previously characterized ovarian cancer patient cohort and observe an association between high centrosome numbers and the patient time to relapse as well as their overall survival. Together our work shows for the first time that centrosome amplification can synergize with combined chemotherapy, completing our understanding of its consequences in cancer.

RESULTS

Centrosome amplification favors cell death in response to combined Paclitaxel and Carboplatin

To study the influence of centrosome amplification on the response to Carboplatin and Paclitaxel, we used an inducible PLK4 over-expression system (PLK4OE) in the epithelial ovarian cancer cell line OVCAR8. Exposing cells to doxycycline for 72h at 1µg/mL induced centrosome amplification (more than 2 centrosomes per cell) in around 80% of cells, compared to 4% in control OVCAR8 (DMSO treated, PLK4Ctl) (Fig. S1A-B). We used MTT viability assays to determine Carboplatin and Paclitaxel IC50s over the 72h following PLK4OE induction (Fig. S1C-D). For both drugs, the IC50 was lower for PLK4OE (67µM and 3,4nM respectively) compared to PLK4Ctl (136µM and 5,1nM respectively), already suggesting that centrosome amplification sensitizes cells to these chemotherapeutic agents. We also determined working combination concentrations (100µM Carboplatin + 3,3nM Paclitaxel) that induce 60% growth inhibition in PLK4Ctl and 89% in PLK4OE (Fig. S1E).

We next used live-imaging to investigate how centrosome amplification influences the response to chemotherapy and in particular if it favors catastrophic mitosis. We used H2B-RFP expressing OVCAR8 allowing us to observe chromosome behaviors during mitosis and

chromatin compaction that occurs when cells die (Fig. 1A). We imaged cells during the 72h of exposure to 100μM Carboplatin + 3,3nM Paclitaxel and performed analysis of complete cell lineages, counting the number of cells produced per lineage (proliferation) and the fate of these cells (viability). In untreated OVCAR8 cells, PLK4OE reduced proliferation compared to PLK4Ctl, but independently of an increase in cell death (Fig. 1B). Combined chemotherapy reduced proliferation of both PLK4Ctl and PLK4OE cells and this reduction was associated with an increase in cell death (Fig. 1B) as well as cell cycle lengthening (Fig. S1F). In agreement with the MTT dose-response assays, combined chemotherapy induced a stronger reduction of viable cells produced per lineage in PLK4OE compared to PLK4Ctl, and this was associated with a higher proportion of cell death with 75% dying in PLK4OE and 33% dying in PLK4Ctl (Fig. 1B and Fig. 1E-F). By examining cell fate in consecutive generations, we observed that cell death was mainly occurring in generations 2 and 3 suggesting that passage through mitosis or extended exposure time to chemotherapy is detrimental for the progeny (Fig. 1C).

We therefore characterized the mitotic behaviors in the first generation focusing on chromosome mis-segregation (Fig. 1A). In untreated PLK4Ctl OVCAR8, we observed a significant proportion of chromosome instability with around 20% of mitosis occurring with either chromosome mis-alignment, one lagging chromosome, or one chromatin bridge (Fig. 1A black arrows and S1G and I). These behaviors, which are sometimes difficult to discriminate at the low spatio-temporal resolution used in our long-term live-imaging approach, were pooled together and considered as *Slight mis-segregation* events (Fig. 1A). These events were more frequent in PLK4OE (36%), in agreement with centrosome amplification inducing merotelic attachments *(11)*. However, the proportion of *Multipolar* divisions was negligible, suggesting these cells are competent to cluster supernumerary centrosomes (Fig. S1G-I). Importantly, combined chemotherapy induced an increase in two behaviors associated with strong chromosome mis-segregation: *Multipolar* divisions and bipolar divisions associated with multiple chromosome mis-segregation events (combinations of bridges, lagging and misaligned chromosomes – termed here *High mis-segregation*) (Fig. 1A and D vertical axis, Fig. S1G-H). Events of complete division failure – either via cytokinesis failure, mitotic slippage, or death in mitosis – were observed but remained infrequent upon combined chemotherapy (Fig. 1D vertical axis). PLK4OE cells exposed to combined chemotherapy present close to 47% of multipolar divisions compared to 6% observed in PLK4Ctl (Fig. 1D vertical axis and Fig. 1E-F). We next

focused on the fate of the progeny produced by the different cell division categories and observed that within cells completing cell division, higher levels of chromosome mis-segregation were associated with increased cell death in the progeny (Fig. 1D horizontal axis). In particular, multipolar divisions were associated with at least 50% cell death in the progeny, and the increase of these multipolar divisions in PLK4OE cells exposed to combined chemotherapy therefore contributes to the decreased viability observed in this condition. Paclitaxel has been suggested to induce multipolar spindles in cells that present centrosome amplification *(29)*, and exposing PLK4OE cells to Paclitaxel alone also induces multipolar divisions (Fig. S1J), suggesting the increased multipolarity we observe in presence of the combined chemotherapy is caused by the effect of Paclitaxel on the capacity of cells to cluster centrosomes. However, and surprisingly, we also observed that independently of the type of mitosis induced by combined chemotherapy, the proportion of cell death in the progeny was higher in PLK4OE compared to PLK4Ctl (Fig.1D, horizontal axis). This was in particular the case for the progeny of cells that do not show any chromosome mis-segregation, where 40% cell death is observed in PLK4OE compared to only 12% cell death in PLK4Ctl (Fig. 1D, horizontal axis). These results suggest that centrosome amplification favors cell death in response to combined chemotherapy independently of multipolarity and chromosome segregation errors.

Centrosome amplification favors cell death in response to Carboplatin independently of catastrophic mitosis

We were next interested in understanding why cell death is enhanced in PLK4OE in response to combined chemotherapy irrespective of mitotic behaviors. We observed that the IC50 of Carboplatin is lower for PLK4OE compared to PLK4Ctl (Fig. S1D). We therefore hypothesized that PLK4OE cells may respond differently to DNA damage induced by Carboplatin. In both cell populations, Carboplatin exposure at the IC50 determined for PLK4Ctl (136μM) induced an increase in DNA double-strand breaks, as visualized via staining for γ-H2AX, an early marker of the DNA damage response (Fig. S2H-I). γ-H2AX fluorescence intensity was similar in Plk4OE and PLK4Ctl, suggesting centrosome amplification does not increase the levels of DNA damage in response to Carboplatin. We therefore performed live-imaging to better understand how OVCAR8 cells respond to 136μM Carboplatin, and how centrosome amplification modifies this response. First focusing on the lineage analysis, we observed that Carboplatin treated cells have a reduction in proliferation compared to untreated cells, and an increase in cell death (Fig. S1F,

Fig. 2A-D) . In agreement with PLK4OE cells being more sensitive to Carboplatin, fewer viable cells were produced in Carboplatin exposed PLK4OE compared to PLK4Ctl, and this was associated with an increase in cell death with 47% in Plk4OE and 30% in PLK4Ctl (Fig. 2A-D). Similar to the combined chemotherapy, most cell death occurred in generation 2, suggesting that mitosis contributes to cell death in response to Carboplatin (Fig. 2E). We therefore focused on chromosome mis-segregation during the first mitosis. In both PLK4Ctl and PLK4OE treated with Carboplatin, the main phenotype was an increase in *High mis-segregation* divisions, and unlike in the response to combined chemotherapy, *Multipolar* divisions remained negligible (Fig. 2A-B and F). The observed increase in cell death in PLK4OE is therefore completely independent of the capacity to assemble a bipolar spindle.

Sorting single cell behaviors based on the time of first mitotic entry reveals that in PLK4Ctl, *high mis-segregation* events occur during mitosis initiated after a longer time spent in Carboplatin (Fig. 2A and G). It is then mainly the progeny from these divisions that died (Fig. 2A and F). To better understand this time-dependent-response, we analyzed the cell-cycle in response to Carboplatin using a FUCCI expressing OVCAR8 cell-line. This strategy allowed us to discriminate cells in G1 from cells in S/G2 (Fig. 2H-I and Fig. S2A-B), while still observing cell death events which occur mainly in S/G2 (Fig. S2E). First, we observed that Carboplatin induced an increase in S/G2 length, suggesting DNA damage in OVCAR8 cells activates the intra S and/or the G2/M checkpoint (Fig. S2C), while G1 length was not strongly varying in any observed condition (Fig. S2D). Next, we observed that S/G2 lengthening and subsequent delayed mitotic entry occurred mainly in cells that were in G1 at the onset of Carboplatin exposure, and therefore in cells exposed to Carboplatin for a complete S-phase (Fig. 2H and J). Despite this delay, these cells most likely entered mitosis with unrepaired damage, driving high levels of chromosome mis-segregation during mitosis and eventually leading to death of the progeny. In PLK4OE cells exposed to Carboplatin, the timing and proportions of mitotic and cell-cycle behaviors was similar to PLK4Ctl. *High mis-segregation* events occured in cells with a strong delay in mitotic entry (Fig. 2B, F and G), which concurred with cells that were in G1 at the onset of Carboplatin exposure (Fig. 2I and J). However, in PLK4OE, the association between cell death and mitotic phenotypes was different from PLK4Ctl. Indeed around 35% of cell death was observed for the progeny of cells that had *No mis-segregation* or *Slight mis-segregation* defects, in contrast with PLK4Ctl where less than 10% of these cells died (Fig. 2F, horizontal axis).

These observations therefore suggest that PLK4Ctl cells are essentially killed by catastrophic mitosis induced by high levels of DNA damage, while PLK4OE cells do not require a catastrophic mitosis to be eliminated. In agreement with cell death occurring independently of mitosis in PLK4OE, 17% cells died in the first generation compared to only 6% in PLK4Ctl (Fig. 2A-B and E). In particular, cells that were in G1 at the beginning of Carboplatin exposure and therefore can accumulate DNA damage in their first cell-cycle, were preferentially killed in PLK4OE with 25% of cells dying compared to 8% in PLK4Ctl (Fig. 2H-I and K). Our findings propose that centrosome amplification sensitizes cells to the effect of carboplatin in a single cell-cycle and independently of catastrophic mitotic behaviors.

The centrosome has previously been involved in regulating the DNA damage response via recruitment of ATR, ATM, Chk1 and Chk2 *(30, 31)*. We investigated whether centrosome amplification modifies the signaling downstream of DNA damage, explaining increased cell-death in response to Carboplatin. We detected phosphorylation and activation of Chk1 and p53 in response to Carboplatin, but no difference is observed in PLK4OE compared to PLK4Ctl cell extracts (Fig. S2F-G). In agreement with DNA damage levels and responses being unchanged by PLK4OE, we also observed no difference in the recruitment of DNA damage repair factors FANCD2, 53BP1 and Rad51 (Fig. S2H-I). Together, these observations suggest that centrosome amplification favors cell death in response to DNA damage, independently of catastrophic mitosis, but also independently of the DNA damage response.

Centrosome amplification modulates mitochondrial apoptosis independently of p53 and the PIDDosome

In order to better understand how centrosome amplification favors cell death in response to Carboplatin independently of mitotic errors, we characterized the type of cell death and the associated signaling network. We observed that Carboplatin treatment induced apoptosis characterized by Caspase-3 cleavage (Fig. 3A-B), as well as cells becoming positive for Annexin-V by flow cytometry, which was completely suppressed by the pan-caspase inhibitor Q-VD-Oph (Fig. 3C). PLK4OE induces both a premature cleavage of Caspase-3 (t=48h compared to t=72h in PLK4Ctl), as well as an increase in the Annexin-V positive cell population (53% compared to 32% in PLK4Ctl), confirming that centrosome amplification favors the apoptotic response to Carboplatin (Fig. 3A-C). To determine if the mitochondria outer membrane permeabilization

(MOMP) dependent apoptotic pathway was activated in response to Carboplatin, we stained cells for Cytochrome C in order to observe its release from mitochondria (Fig. 3D). In untreated cells, Cytochrome C was detected in punctate structures throughout the cytoplasm, in agreement with its mitochondrial localization. Upon Carboplatin exposure, the Cytochrome C staining remained similar to untreated cells, while we observed dead cell remnants characterized by condensed DNA (Fig. 3D White arrows and 3E). However if release of Cytochrome C occurred, it could lead to immediate apoptosis initiation and detachment of the cells, precluding the observation of cells via immunofluorescence. We therefore use Q-VD-Oph to inhibit apoptosis in response to Carboplatin and observed a population of cells where Cytochrome C is diffuse in the cytoplasm and nucleus (Fig. 3D Pink arrows and 3E). MOMP, Cytochrome C release and caspase activation therefore occurrs in response to Carboplatin, suggesting that mitochondrial apoptosis is the main cell death mechanism at play.

Importantly, we observed 27% of cells releasing Cytochrome C in PLK4OE cells compared to only 12% in PLK4Ctl cells, suggesting that Carboplatin induces a stronger activation of apoptosis in the presence of centrosome amplification (Fig. 3D-E). In agreement with different stresses leading to apoptosis between PLK4Ctl and PLK4OE, we observed that 36% of cells poised to die with fragmented nuclei in PLK4Ctl compared to 5% in PLK4OE (Fig. 3F). These fragmented nuclei are symptomatic of high chromosome mis-segregation during mitosis, supported by PLK4Ctl cells being killed by catastrophic mitosis, while centrosome amplification favors apoptosis independently of catastrophic mitosis in PLK4OE.

The canonical intrinsic apoptosis pathway linking the DNA damage response to MOMP occurs via p53 stabilization which then drives the transcription of pro-apoptotic BCL2 family genes *(36)*. Centrosome amplification has been linked to p53 stabilization via PIDDosome activation, which is dependent on centriole distal appendage grouping. This leads to Caspase-2 cleavage and activation and cleavage of MDM2 - a major p53 regulator – *(33, 34)*. OVCAR8 cells have a mutant TP53 gene which leads to alternative splicing of exon5, and a 6 amino-acid deletion in p53's DNA binding domain *(37)*. We observed that p53 protein is present, phosphorylated, and accumulates in response to Carboplatin (Fig. S2F, quantified in Fig. S3B). Although the deletion in the DNA damage binding domain is suggested to preclude its transcriptional activities *(37)*, we observed that its transcriptional targets p21 and PUMA mildly increase upon Carboplatin exposure (Fig. S3A-B). Using shRNA, we knocked-down TP53 and

showed that p53 was dispensable for cell death in both PLK4Ctl and PLK4OE in response to Carboplatin (Fig. S3C-D). p21 is best characterized for its functions in cell-cycle arrest and apoptosis inhibition, but has also been shown to upregulate apoptosis *(38)*. As we noticed p21 to be upregulated in PLK4OE cells compared to PLK4Ctl (Fig. S3A-B), we tested its contribution to cell death, but observed no effect of knocking down the p21 coding gene CDKN1a (Fig. S3C-D). Despite apoptosis being p53 independent in Carboplatin treated OVCAR8, we tested whether PIDDosome activation may contribute to enhancing intrinsic apoptosis in PLK4OE. Indeed, upon PLK4OE, we observed cleavage of Caspase-2 and MDM2 reflecting PIDDosome activation (Fig. S3E-F). We knocked-down the distal appendage protein required for PIDDosome activation ANKRD26 and observed a strong reduction of Caspase-2 and MDM2 cleavage in PLK4OE, reflecting efficient PIDDosome silencing (Fig. S3G). However, this had no effect on the enhanced cell death observed upon Carboplatin exposure in PLK4OE, suggesting that centrosome amplification favors apoptosis independently of the PIDDosome (Fig. S3H). Altogether, our results show that centrosome amplification leads to enhanced apoptosis in response to Carboplatin independent of previously described centrosome signaling nodes.

Centrosome amplification primes for MOMP and sensitizes cells to a diversity of chemotherapies.

So far we have observed that PLK4OE cells execute apoptosis faster and to a higher proportion, in response to a level of stress (mitotic behaviors, DNA damage levels and DNA damage response) which is no different than in PLK4Ctl. This therefore suggested that these cells may be primed for MOMP, meaning that the balance between pro-apoptotic and anti-apoptotic BCL2 family proteins that determine the activity of the mitochondrial pore forming proteins BAX and BAK is tilted towards their activation in PLK4OE *(39)*. To test this possibility, we performed MTT dose-response assays during 72h to drugs which mimic the activity of specific pro-apoptotic BH3-only BCL2 family proteins. Strikingly, we observed that PLK4OE induces a strong sensitization to WEHI-539 - a specific BCL-XL inhibitor - (Fig. 4A-B), but not to Venetoclax or A1210477 - specific inhibitors of BCL-2 and MCL-1 respectively- (Fig. S4A-B). We confirmed that 72h 300nM WEHI-539 exposure selectively induced apoptosis in PLK4OE cells in a Caspase dependent manner, via Annexin V and PI cytometry (Fig. 4C). We also observed release of Cytochrome C from mitochondria in WEHI-539 treated PLK4OE cells upon pan-caspase inhibition, confirming that BCL-XL inhibition induces MOMP specifically in

PLK4OE (Fig. 4D-E). Counting centrosomes in PLK4OE cells revealed that the 72h 300nM WEHI-539 treatment reduced the proportion of cells with extra centrosomes to the level observed in PLK4Ctl cells (Fig. 4F-G). These results suggest efficient killing of cells with centrosome amplification, which is suppressed upon pan-caspase inhibition. We were also able to count centrosomes in the population of cells that release Cytochrome C from mitochondria and are therefore poised to die, revealing that the majority of these cells have centrosome amplification in WEHI-539 treated PLK4OE cells (Fig. 4G). Interestingly, an extremely small proportion (1%) of PLK4Ctl cells also release Cytochrome C in response to WEHI-539 (Fig. 4E) and counting centrosomes in these cells revealed a higher level of centrosome amplification than the untreated PLK4Ctl population (Fig. 4G). This suggests that independently of induced PLK4 over-expression, centrosome amplification primes for MOMP in OVCAR8 cells. We confirmed this observation in parental OVCAR8 cells devoid of the inducible PLK4OE transgene to exclude the possibility that PLK4OE leakage sensitizes the PLK4Ctl cells to WEHI-539 inhibition (Fig. S4C).

We next tested if similar effects might be observed in other cell lines and established inducible centrosome amplification via PLK4OE in ovarian cancer cell lines COV504 and SKOV3 (Fig. S4D-E). We then tested if MOMP priming identified in OVCAR8 was also observed in these cell lines (Fig. S4F). We used the less specific BH3-mimetic Navitoclax (inhibitor of BCL2, BCL-XL and BCL2), as the dependency on BCL-XL in PLK4OE OVCAR8 might be reflecting OVCAR8 apoptotic wiring rather than a specific effect of centrosome amplification on BCL-XL. We observed that Navitoclax reduced the viability of PLK4OE cells preferentially compared to PLK4Ctl cells in COV504 (EC80 of 400nM and 3,6uM respectively) although to a lesser extent than in OVCAR8 (EC80 of 40nM and 2,2uM respectively). Priming was however not observed in SKOV3. We then established the IC50s for Carboplatin and Paclitaxel, and determined combination concentrations in PLK4Ctl cells (Fig. S4G). We used Trypan blue assays to determine viability in response to chemotherapy and confirmed this approach in OVCAR8 by showing that viability decreases more in PLK4OE compared to PLK4Ctl (Fig. S4H left). Interestingly, we observed a gradation in the enhanced cell death induced by centrosome amplification in the different cell lines, with the strongest effect observed in OVCAR8 (Fig. S4H left), the weakest in SKOV3 (Fig. S4H right), and an intermediate effect in COV504 (Fig. S4H middle), which can be put in perspective with the observed gradation in

MOMP priming. For responses to Paclitaxel however we have to take into account the fact that multipolar divisions are also favored in COV504 PLK4OE cells (Fig. S4I).

Our identification of apoptotic priming in cells with centrosome amplification suggests that it might be associated with enhanced cell death in response to a larger panel of drugs. We therefore tested whether centrosome amplification sensitizes ovarian cancer cells to PARP inhibitors which are now included in standard of care protocols in epithelial ovarian cancer *(40)*, focusing on Olaparib (IC50s determined and presented in Fig. S4G). Trypan Blue viability assays in OVCAR8 and COV504 confirmed that PLK4OE leads to reduced viability compared to PLK4Ctl in response to Olaparib (Fig. S4J). This effect was not observed in SKOV3 in which we have not observed MOMP priming linked to centrosome amplification. Together our results suggest that centrosome amplification enhances cell death in response to chemotherapy differentially depending on the cell line, and that centrosome amplification associated apoptotic priming can sensitize to a diversity of chemotherapies.

Centrosome amplification primes for MOMP independently of chromosome instability or lengthened mitosis

Centrosome amplification induces an increase in chromosome instability and a spindle-assembly checkpoint dependent extension of mitosis duration *(7, 8, 11)*, both of which we observed in PLK4OE OVCAR8 cells (Fig. S1F and S1I). Apoptotic priming and in particular sensitization to BCL-XL inhibition has previously been linked to mitotic defects. In particular chromosome instability, micronuclei formation and cGAS/STING signaling can drive a transcriptional response that drives apoptosis or priming *(41, 42)*. Alternatively, extended mitotic duration can lead to the proteosomal degradation of anti-apoptotic BCL2 family proteins, leading to BCL-XL sensitization *(43–46)*. We were therefore interested in determining if apoptotic priming observed in response to centrosome amplification is caused by cumulated mitotic stress in these cells.

First, we aimed to better characterize the mitotic stress induced by centrosome amplification in the already chromosomally instable OVCAR8 cell line (Fig. S1I). We used single-cell DNA-sequencing to assess karyotype heterogeneity (Supplementary Material and Methods) and observed scores of 0,119 in PLK4Ctl, 0,137 in PLK4OE cells and 0,283 in PLK4Ctl cells treated with 1µM of the MPS1 inhibitor AZ3146 as a positive control of chromosome mis-segregation (Fig. 5A). PLK4OE therefore only mildly increased aneuploidy, in

line with levels of chromosome-mis-segregation observed by time-lapse imaging (Fig. 5B). We also assessed the extent of mitotic lengthening induced in PLK4OE cells (Fig. 5C) and observed it was mild (median=60min in PLK4OE and median=35min in PLK4Ctl) compared to that induced by low doses of the CENP-E inhibitor GSK923295 (median=100min at 30nM and 175min at 35nM), despite levels of chromosome mis-segregation being similar (Fig. 5B).

Mitotic stress is therefore mild in PLK4OE compared to the other perturbations we tested, but we were nevertheless interested in determining if it contributes to apoptotic priming. We were not able to reduce mitotic duration in PLK4OE cells via spindle assembly checkpoint inhibition without inducing a strong increase in multipolar divisions (data not shown), so we used MPS1 and CENP-E inhibition to mimic mitotic stress observed in PLK4OE. We pretreated PLK4Ctl cells with inhibitors during 72h before adding WEHI-539 for an additional 24h. In PLK4OE cells this lead to 33% Annexin V positive cells, whereas it only induces 9% in response to MPS1 inhibition (Fig. S5A), making it unlikely that priming occurs in response to chromosome instability in PLK4OE. In CENP-E inhibition pretreated cells at 30nM and 35nM, WEHI-539 induces 12% and 25% Annexin V cells respectively, in line with mitotic lengthening inducing priming *(46)*. Importantly however, 35nM CENP-E inhibition pretreatment already induces 12% Annexin V positive cells which is considerable compared to the 4% observed in PLK4OE (Fig. S5A), and most likely is explained by the extensive mitotic lengthening observed in response to 35nM CENP-E inhibition (Fig. 5C). This results in the ratio of cell death induced by WEHI-539 relative to the basal observed level of cell death to be comparable in PLK4Ctl cells and CENP-E inhibition pretreated cells (around 2-fold). In contrast, the ratio of cell death was much higher and close to 8 fold increase upon PLK4OE (Fig. 5D). Therefore, the priming induced in PLK4OE stands out from that induced by other sources of mitotic stress in that PLK4OE cells are viable but strongly dependent on BCL-XL. These results also suggest that the combination of chromosome instability and mitotic lengthening is not the major contributor to MOMP priming upon centrosome amplification in OVCAR8 cells.

To identify transcriptomic signatures that may influence cell death responses in cells with extra centrosomes, we used bulk RNAseq comparing PLK4OE and PLK4Ctl OVCAR8 cells. A strong inflammatory signature in PLK4OE (Fig. S5B) was identified, and we also observed STING phosphorylation (Fig. S5C), suggesting that the cGAS/STING pathway may shape the transcriptional response to centrosome amplification. We were therefore interested in directly

testing if cGAS/STING signaling might contribute to priming, although this seemed unlikely as CENP-E and MPS1 inhibition also activate STING (Fig. S5C) but are not associated with priming. We used a bulk LentiCRISPR knock-out approach of STING, but observed no influence on PLK4OE cells sensitivity to WEHI-539 (Fig. S5D-E).

We therefore identify that centrosome amplification in OVCAR8 leads to MOMP priming which is revealed by a selective sensitization to the BCL-XL inhibitor WEHI-539. Comparing with other mitotic perturbations, we conclude that the centrosome amplification associated priming is independent of mitotic lengthening and chromosome instability.

High centrosome numbers are associated with a better response to chemotherapy in a High grade Serous Ovarian Cancer patient cohort.

To assess if centrosome amplification is associated with chemotherapy responses in patients, we turned to the characterization of centrosomes we previously performed *in situ* in treatment-naive epithelial ovarian tumors. Here centrosomes were detected as the colocalization of Pericentrin and CDK5RAP2 in confocal images of methanol-fixed patient tissue sections *(5)*. To assess centrosome numbers in samples we defined the centrosome to nucleus ratio (CNR) as the number of centrosomes detected in a field by the number of nuclei which we averaged over 10 fields per patient (Fig. 6A). In healthy tissues obtained from prophylactic oophorectomy or hysterectomy, the CNR was 1.02±0.02 suggesting cells have on average one centrosome per cell which is expected for a non-proliferative tissue. On average, the CNR in tumor tissues was 1.43±0.04, with the minimum at 0.61 and maximum at 2.55. While only 9% of tumors had a CNR above 2, suggesting that pervasive centrosome amplification - when defined by the presence of more than 2 centrosomes per cell - is infrequent, 89% of the tumors presented a CNR superior to the average CNR found in healthy tissues. Considering that the CNR did not correlate with proliferation as established by the mitotic index (Fig. S6A) and Ki67 staining (Fig. S6B), centrosome amplification could contribute to this increase in CNR in tumors compared to healthy samples.

We next examined if the CNR was associated with chemotherapy responses restricting our analysis to the high-grade serous ovarian cancers (HGSOCs) in our cohort. We dichotomized our population into two groups using the Classification And Regression Trees (CART) method, resulting in the categorization of the cohort into 55 low CNR (<=1.45) tumors and 33 high CNR

(> 1.45) tumors. Importantly, we observed no association between CNR and FIGO stage, with 59% stage III patients in the cohort comprising both High and Low CNR (Fig. S6C). We next plotted HGSOC patient survival curves according to the CNR status. We found that high CNR was associated with better overall survival (Fig. 6B). These results suggest that despite its oncogenic potential *(7, 17–19)*, centrosome amplification might improve patient prognosis at least in ovarian cancer. This puzzling observation could be explained if High CNR promotes chemotherapy responses as overall survival data reflects patients complete clinical course which includes Carboplatin and Paclitaxel therapy in this cohort. To directly assess a link between CNR and chemotherapy responses, we plotted patient time to relapse and found that High CNR was associated with a longer time to relapse (Fig. 6C). Together, this work suggests that centrosome status in ovarian cancer can influence patient outcome, in particular with High CNR favoring response to chemotherapy.

DISCUSSION

Centrosome amplification as a therapeutic target has been mainly explored from the prism of multipolar division, but mitotic drugs that limit centrosome clustering have had limited success in the clinic *(48)*. Our results identify apoptotic priming as a novel cell death susceptibility conferred by centrosome amplification. In particular, we show that centrosome amplification sensitizes cells to BH3-mimetic drugs.

The apoptotic priming seems to be specific to centrosome amplification, rather than a consequence of the associated mitotic stress. Possible causes of this priming could be disruption of mitochondrial networks during mitosis, or in interphase. This may be in link with recent observations of subcellular reorganization in response to centrosome amplification in RPE-1 cells *(49)*, although we observe no striking effect on mitochondria organization in OVCAR8 (data not shown). Centrosomes are also involved in multiple signaling pathways *(31, 50)* and given the pleiotropic effects of centrosome amplification which also favors ROS and inflammation *(15)*, we consider that the best method to identify the source of the priming would be whole-genome screening approaches.

From a clinical perspective, our analysis of a patient cohort shows that high centrosome numbers limit relapse in response to chemotherapy, indicating that centrosome amplification must be considered beyond its malignant potential. Given the toxicity of cytotoxic therapies, the

perspective of better patient stratification and response prediction, considering centrosome amplification as a sensitizing factor offers promising perspectives. Our observation that centrosome amplification enhances cell death independently of multipolar mitosis broadens the therapeutic importance of this cancer cell feature, beyond treatments that target spindle assembly and mitosis

Our identification of apoptotic priming in cells with centrosome amplification also has clinical relevance, and asks whether centrosome numbers could be considered to better direct BH3-mimetic administration whose use in the clinic is hampered by lack of good prognostic markers *(51)*. Alternatively, we also wonder if centrosome amplification might be a contributor to the on-target toxicity of BCL-XL inhibition leading to thrombocytopenia. Indeed, the megakaryocytes that produce platelets are polyploid and present multiple centrosomes *(52)* and this might contribute to their targeting by BCL-XL inhibitors.

There are multiple limitations to our study. We must emphasize that the levels of centrosome amplification in the cohort is low *(5)* and that centrosome loss might also contribute to modulating chemotherapy responses. It nevertheless remains interesting to consider that targeting low levels of centrosome amplification could have an observable clinical effect, and to explain these results we propose that elimination of cells with centrosome amplification might be advantageous given the malignant potential of these cells *(7, 13–15, 19)*. We are also eager to know if centrosome numbers influence responses to chemotherapy in additional epithelial ovarian cancer cohorts and in different cancer types. An important step to facilitate broader studies is the automatization of centrosome detection and counting in patient tissues. Additionally our identification of apoptotic priming in response to centrosome amplification and the associated clinical perspectives justify the need for a better understanding of the priming mechanism induced by centrosome amplification. This would also help identify the contexts in which this priming emerges as we have not observed it in all the cancer cell lines studied.

MATERIAL AND METHODS

Study design:

This work is a study of the influence of centrosome amplification on the response to chemotherapy in epithelial ovarian cancer. The objectives of the cell biology work were to identify if and how centrosome amplification favors cell death in response to chemotherapy,

using a combination of single cell live imaging, and classical cell biology experiments such as cytometry and Western Blot. All the presented data has been replicated in 2 to 5 biological replicates. The objective of the clinical work was to identify if centrosome numbers influence clinical parameters in a patient cohort. All samples were taken before chemotherapy administration and obtained from the Biological Resource Center (BRC) of Institut Curie (certification number: 2009/33837.4; AFNOR NF S 96 900). In compliance with the French regulation, patients were informed of the studies performed on tissue specimens and did not express opposition. The National Commission for Data Processing and Liberties (N° approval: 1487390) approved all analysis, as well as The Institutional Review Board and Ethics committee of the Institut Curie. Centrosomes were previously stained and detected in a HGSOC patient cohort of 100 patients *(5)*. Here we determined an index allowing the quantitative assessment of centrosome numbers in patient tissues, which we then correlated with patient clinical parameters. Data collection for each experiment is detailed in the respective figure legend.

Cell lines and cell culture:

All cell lines were cultured at 37°C with 5% CO2 in DMEM/F12 media (ThermoFisher Scientific #31331028) supplemented with 10% Tetracyclin-free Fetal Bovine Serum (Dutscher #500101L), 100 µg/ml streptomycin and 100U/ml penicillin (ThermoFisher Scientific #15140122). OVCAR8 and COV504 were obtained from the laboratory of F. Mechta-Grigoriou, and SKOV3 were purchased from ATCC (#HTB-77). Cell cultures underwent authentification by short tandem repeat analysis (powerplex16 HS kit, Promega #DC2101) and were routinely checked for mycoplasma (PlasmoTest Mycoplasma detection kit, InvivoGen, #rep-pt1).

Cell line generation:

Inducible PLK4 over-expression, H2B-RFP expression, FUCCI expression, shRNA expression and bulk CRISPR-Cas9 knock-out of STING were stably established by lentiviral infection. Viruses were produced in HEK cells using Lipofectamine 2000 (ThermoFisher Scientific #11668019) to co-transfect lentiviral constructs with pMD2.G and psPAX2 plasmids. Viral particles were collected in the supernatant 48h after transfection, filtered, and used to infect the cell lines during 24h. Cells were then FACS sorted (inducible PLK4 over-expression and H2B-RFP) or selected using Puromycin at 5 µg/ml (shRNA lines and CRISPR-Cas9 knock-out of STING). Efficiency of knock-down and knock-out was assessed by Western Blot. The list of plasmids used is available in Table S1.

Drug treatments:

All chemicals used are listed in Table S2. To induce centrosome amplification, cells were exposed to doxycycline (1 µg/ml) or DMSO (diluent control, 1/10000) for 72h. If cells were subsequently treated with another drug, cells were detached and replated without addition of doxycycline to the PLK4OE population, and left to attach for 8h. Drug treatments were then carried out for 72h at the indicated concentrations. For the experiments comparing centrosome amplification to other mitotic stresses (CENP-E and MPS1 inhibition), cells were exposed to doxycycline (1 µg/ml for centrosome amplification), AZ3146 (1µM, for MPS1 inhibition), GSK923295 (30-35nM, for CENP-E inhibition) or DMSO (diluent control) for 72h. Subsequent treatments (WEHI-539) or analysis (live-imaging of mitotic phenotypes) were then carried out in presence of the same initial concentrations of drug for 24h.

Live-Imaging and analysis:

For live-imaging of chemotherapy responses, cells were plated on Ibidi µ-Slide 8 Well slides (Clinisciences, #80806-G500). Chemotherapy treated and untreated cells from both PLK4Ctl and PLK4OE populations were imaged during the same experiment. Imaging was performed with a 20x objective (CFI Plan Apo LBDA 20x 0,75/1 mm CCo 0,17) via an EMCCD camera (Evolve, Photometrics) on an inverted microscope (Inverted Ti-E Nikon) equipped with a spinning disk (CSU-X1 Yokogawa), a stage-top temperature and CO2 incubator (Tokai Hit) and integrated in Metamorph software. For each well, 4-6 positions were acquired every 10min during 72h, with a single slice in the brightfield channel and 10 slices per z-stack in the H2B-RFP channel or in the mKO2-Cdt1(30-120) and mAzami-Green-Gem1(1-110) channels for the FUCCI cells. Time-lapse movies were then analyzed manually using a custom Fiji macro to record a list of events, and a custom Python script to generate excel data files and single-cell profiles.

For live-imaging of mitotic phenotypes induced by centrosome amplification, MPS1 inhibition and CENP-E inhibition, the same approach was used, acquiring each position every 5min during 24h. Imaging was performed using the equipment described above. .

Immunofluorescence:

Cells were plated on 18mm glass coverslips in 12-well plates. Cells were fixed for 5min in ice-cold methanol (for Fig.s S1A and S4D), or for 10min in 4%PFA at room-temperature (for Fig.s 3D, 4C, 4E) or at 4°C (for Fig. S2H). Cells were washed 3 times in PBST (PBS + 0,1% Triton X-

100) and incubated in PBST + BSA 0,5% for 30min at room temperature. Cells were then incubated for 1h in primary antibodies diluted in PBST + BSA 0,5%, washed 3 times in PBST, incubated for 30min in secondary antibodies diluted in PBST + BSA 0,5%, and washed 3 times in PBST. Cells were then stained for DNA using 3 µg/ml DAPI diluted in PBST + BSA 0,5%, washed 3 times in PBS and mounted with mounting medium (1.25% n-propyl gallate, 75% glycerol, in H2O). Antibodies used are listed in Table S3.

Immunofluorescence imaging and quantifications:

Immunofluorescence images were acquired with a sCMOS camera (Flash 4.0 V2, Hamamatsu) on a widefield microscope (DM6B, Leica systems), with a 63x objective (63x HCX PL APO 1.40-0.60 Oil from Leica), using Metamorph software. Z-stacks were acquired at 0,3 µm intervals.

Centrosome numbers and cytochrome C release were scored manually. DNA damage marker intensity or foci number were determined on z-projections of images, using a custom Python script to run the h_maxima function from the skimage.morphology.extrema module.

Western Blotting:

Cells were lysed in RIPA (150mM sodium chloride, 1% NP-40, 0.5% sodium deoxycholate, 0.1% sodium dodecyl sulfate, 50mM Tris, pH8.0) complemented with protease (Sigma-Aldrich # 11697498001) and phosphatase (Sigma-Aldrich #4906845001) inhibitors. Samples were dosed using a BiCinchoninic acid Assay (Pierce BCA protein assay, ThermoFisher Scientific # 23227). Samples were diluted in RIPA with 4X NuPage LDS sampling buffer (ThermoFisher Scientific # NP0007) and heated at 80°C for 10min. 20µg of protein was loaded in Bolt 4-12% Bis-Tris precast gels (ThermoFisher Scientific #NW04125BOX), and subjected to electrophoresis in Bolt MOPS SDS running buffer (ThermoFisher Scientific # B0001). The gels were transferred to nitrocellulose membranes (Dutscher # 10600001) using transfer buffer (25mM Tris, 192mM Glycine, 20% Methanol) for 90min at 4°C. Membranes were stained in primary or horse-radish peroxidase coupled secondary antibodies diluted in PBS or TBS + 0,5% Tween 20 + 0,5% BSA or non-fat milk according to providers instructions. Membranes were first stained using Ponceau, before saturating for 1h at room temperature in 5% non-fat dry milk or 5% BSA in PBS or TBS + 0,5% Tween20. Membranes were then incubated overnight in primary antibodies, washed 5 times in PBS or TBS + 0,5% Tween 20, then incubated for 1h at room temperature in secondary antibodies. Membranes were then washed again 5 times in PBS or TBS +0,5% Tween 20. Horse-

radish Peroxidase reaction was developed using SuperSignal Plus Chemiluminescent substrates (Thermo Fisher Scientific # 34580 and #34094) and imaged (BioRad ChemiDoc MP). The Image Lab software (BioRad version 6.0.1) was used to measure background-adjusted volume intensity, which was normalized using GAPDH signal. Antibodies used are listed in Table S3.

Transfection:

HT-DNA was transfected as a positive control for cGAS/Sting activation. Trasnfection of 1µg/mL HTDNA was carried out using Lipofectamine 2000 (ThermoFisher Scientific #11668019) for 24h.

Cytometry:

Cells were detached, rinsed in PBS, rinsed in AnnexinV Binding Buffer (BioLegend # 422201), and around 100000 cells were resuspended in 50µL Annexin V Binding Buffer. Cells were stained using Annexin V APC and Propidium Iodide (Biolegend # 640932) at 0,6µg/mL and 10mg/mL respectively. Cells were incubated for 15min, then diluted in 200µL Annexin V Binding Buffer. Cells were analysed using a Bio-Rad ZE5 analyzer, and data was analyzed using FlowJo 10.6.0 software.

MTT viability assays:

For dose-response to drugs, cell viability was assessed using MTT viability assays. Cells were plated in triplicates at 15000cells/well in 96-well plates and left for 2h to adhere prior to drug addition. Cells were left to grow for 72h, and MTT diluted in PBS was added at 5µg/mL. After 4h incubation, medium was removed and replaced by 150uL DMSO. 570nm absorbance was performed on a BMG Labtech ClarioStar plate reader. Triplicates were averaged and normalized by untreated controls.

Trypan Blue Proliferation and Viability assays:

For proliferation and viability assays, cells were plates at 100000 cells/well in 6-well plates. Cells were then detached, resuspended in 500uL medium, and live/dead cells were counted using a Beckman Coulter Vi-Cell cell counter.

RNA sequencing:

Following centrosome amplification with doxycycline for PLKOE vs DMSO for PLK4Ctl, total RNA was extracted with RNeasy Mini kit (Qiagen #74104) following manufacturer's instructions. RNA integrity and quality were checked with Agilent RNA 6000 Nano Kit (Agilent,

5067-1511) and corresponding devices. Samples were processed at Institut Curie NGS platform from cDNA synthesis, amplification, quality assessment and sequencing. Novaseq 6000 system (Illumina) was used for sequencing (read length of 100 bp, paired end) . All the bioinformatic analysis were done by Genosplice (http://www.genosplice.com) including quality control of sequences generated, read mapping and gene differential analysis (R software, Deseq2). Biological interpretation of the identified genes was done using GSEA tool for pathway enrichment analysis between distinct conditions.

Single-cell whole genome sequencing:

Cells were treated with DMSO (1/10000), Doxycycline (1µg/mL) or AZ3146 (1µM) for 72h. Cells were then frozen in freezing medium (10% DMSO, 40% FBS in DMEM-F12).

Nuclei preparation and sorting

Cells were thawed, and single-cell sequencing was performed on cell nuclei isolated from cell lysis, leaving the nucleus intact. Thawed cells were prepared by resuspending in PBS + 1% BSA, washing, and pelleting. To generate nuclei, cells were resuspended and incubated (15 minutes on ice in dark environment) in cell lysis buffer (100 mM Tris-HCl pH 7.4, 154 mM NaCl, 1 mM CaCl2, 500 µM MgCl2, 0.2% BSA, 0.1% NP-40, 10 µg/mL Hoechst 33358, 2 µg/mL propidium iodide in ultra-pure water). Resulting cell nuclei were gated for G1 phase (as determined by Hoechst and propidium iodide staining) and sorted into wells of 96 wells plates on a MoFlo Astrios cell sorter (Beckman Coulter), depositing one cell per well. 96 wells plates containing nuclei and freezing buffer were stored at -80°C until further processing. Automated library preparation was then performed as previously described *(53)*.

AneuFinder analysis

Sequencing was performed using a NextSeq 2000 machine (Illumina; up to 120 cycles; single end or up to 113 and 7 cycles; paired end). The generated data were subsequently demultiplexed using sample-specific barcodes and changed into fastq files using bcl2fastq (Illumina; version 1.8.4). Reads were afterwards aligned to the human reference genome (GRCh38/hg38) using Bowtie2 (version 2.2.4; *(54)*). Duplicate reads were marked with BamUtil (version 1.0.3; *(55)*).
The aligned read data (bam files) were analyzed with a copy number calling algorithm called AneuFinder (version 1.14.0; *(56)*) using an euploid reference *(57)*. Following GC correction (R package: BSgenome.Hsapiens.UCSC.hg38_1.4.1; The Bioconductor Dev Team 2015) and

blacklisting of artefact-prone regions (extreme low or high coverage in control samples), libraries were analyzed using the dnacopy and edivisive copy number calling algorithms with variable width bins (average binsize = 1 Mb; step size = 500 kb) and breakpoint refinement (refine.breakpoints = TRUE). Results were afterwards curated by requiring a minimum concordance of 90 % between the results of the two algorithms. Libraries with on average less than 10 reads per bin and per chromosome copy (~ 55,000 reads for a diploid genome) were discarded.

Aneuploidy score

The aneuploidy score of each bin was calculated as the absolute difference between the observed copy number and the expected copy number when euploid. The score for each library was calculated as the weighted average of all the bins (size of the bin as weight) and the sample scores were calculated as the average of the scores of all libraries.

Heterogeneity score

The heterogeneity score of each bin was calculated as the proportion of pairwise comparisons (cell 1 vs. cell 2, cell 1 vs cell 3, etc.) that showed a difference in copy number (e.g. cell 1: 2-somy and cell 2: 3-somy). The heterogeneity score of each sample was calculated as the weighted average of all the bin scores (size of the bin as weight).

Centrosome numbers in tumors:

For each sample, 10 randomly chosen fields were considered. Using ImageJ software, we visually counted the number of nuclei and the number of centrosomes in a blind manner without taking into account tumor identity. The Centrosome to Nuclei Ratio (CNR) was obtained by dividing the total number of centrosomes by the total number of nuclei in each field.

Proliferation and mitotic index:

For Ki67 proliferation assessment, we performed immunochemistry assays using mouse anti-human ki67 antibody (M7240, DAKO, 1/200 at pH9) in a series of paraffin-embedded tissue blocks of HGSOC. Sections of 3 µm were cut using a microtome from the paraffin-embedded tissue blocks of normal tissue and invasive lesions. Tissue sections were deparaffinized and rehydrated through a series of xylene and ethanol washes. Briefly, the key steps included: (i) antigen retrieval with ER2 pH9, (Leica: AR9640); (ii) blocking of endogenous peroxidase activity with Bond polymer refine detection kit (Leica: DS9800) (iii) incubation with primary

antibodies against the targeted antigen; (iv) immunodetection with Revelation and counter staining Bond polymer refine detection kit (Leica: DS9800). Immunostaining was performed using a Leica Bond RX automated immunostaining device. We performed an immunohistochemical score (frequency x intensity) through analysis of 10 high-power fields (HPF, x 400). All quantifications were performed by 2 pathologists with blinding of patient status.

For mitotic index, paraffin-embedded tissue sections of tumors were stained with hematoxylin and eosin. The mitotic count was determined by the number of mitotic figures found in 10 consecutive high-power fields (HPF), in the most mitotically active part of the tumor (entire section). Only identifiable mitotic figures were counted. Hyperchromatic, karyorrhectic, or apoptotic nuclei were excluded.

Statistical analysis:

Statistical analysis were performed using GraphPad Prism. The tests used are specified in the figure legends. The numbers of cells analyzed and the number of replicates are reported either on the figure or in the respective figure legends.

List of Supplementary Materials

Figs. S1 to S6

Table S1 to S3

Representative cytometry profiles

References

1. P. T. Conduit, A. Wainman, J. W. Raff, Centrosome function and assembly in animal cells. *Nat. Rev. Mol. Cell Biol.* **16**, 611–624 (2015).

2. G. Marteil, A. Guerrero, A. F. Vieira, B. P. De Almeida, P. Machado, S. Mendonça, M. Mesquita, B. Villarreal, I. Fonseca, M. E. Francia, K. Dores, N. P. Martins, S. C. Jana, E. M. Tranfield, N. L. Barbosa-Morais, J. Paredes, D. Pellman, S. A. Godinho, M. Bettencourt-Dias, Over-elongation of centrioles in cancer promotes centriole amplification and chromosome missegregation. *Nat. Commun.* (2018), doi:10.1038/s41467-018-03641-x.

3. O. Goundiam, R. Basto, Centrosomes in disease: how the same music can sound so different? *Curr. Opin. Struct. Biol.* **66**, 74–82 (2021).

4. M. Wang, R. B. Nagle, B. S. Knudsen, A. E. Cress, G. C. Rogers, G. C. Rogers, Centrosome

loss results in an unstable genome and malignant prostate tumors. *Oncogene* (2019), doi:10.1038/s41388-019-0995-z.

5. J. Morretton, A. Simon, A. Herbette, J. Barbazan, C. Pérez-González, C. Cosson, B. Mboup, A. Latouche, T. Popova, Y. Kieffer, A. Macé, P. Gestraud, G. Bataillon, V. Becette, D. Meseure, A. Nicolas, O. Mariani, A. Vincent-Salomon, M. Stern, F. Mechta-Grigoriou, S. Roman Roman, D. M. Vignjevic, R. Rouzier, X. Sastre-Garau, O. Goundiam, R. Basto, A catalog of numerical centrosome defects in epithelial ovarian cancers. *EMBO Mol. Med.* **14**, 1–12 (2022).

6. N. J. Quintyne, J. E. Reing, D. R. Hoffelder, S. M. Gollin, W. S. Saunders, Spindle multipolarity is prevented by centrosomal clustering. *Science (80-.).* **307**, 127–129 (2005).

7. R. Basto, K. Brunk, T. Vinadogrova, N. Peel, A. Franz, A. Khodjakov, J. W. Raff, Centrosome Amplification Can Initiate Tumorigenesis in Flies. *Cell* **133**, 1032–1042 (2008).

8. M. Kwon, S. A. Godinho, N. S. Chandhok, N. J. Ganem, A. Azioune, M. Thery, D. Pellman, Mechanisms to suppress multipolar divisions in cancer cells with extra centrosomes. *Genes Dev.* **22**, 2189–2203 (2008).

9. V. Marthiens, M. Piel, R. Basto, Never tear us apart - the importance of centrosome clustering. *J. Cell Sci.* **125**, 3281–3292 (2012).

10. D. Sabino, D. Gogendeau, D. Gambarotto, M. Nano, C. Pennetier, F. Dingli, G. Arras, D. Loew, R. Basto, Moesin is a major regulator of centrosome behavior in epithelial cells with extra centrosomes. *Curr. Biol.* **25**, 879–889 (2015).

11. N. J. Ganem, S. A. Godinho, D. Pellman, A mechanism linking extra centrosomes to chromosomal instability. *Nature* (2009), doi:10.1038/nature08136.

12. W. T. Silkworth, I. K. Nardi, L. M. Scholl, D. Cimini, Multipolar spindle pole coalescence is a major source of kinetochore mis-attachment and chromosome mis-segregation in cancer cells. *PLoS One* **4** (2009), doi:10.1371/journal.pone.0006564.

13. S. A. Godinho, R. Picone, M. Burute, R. Dagher, Y. Su, C. T. Leung, K. Polyak, J. S. Brugge, M. Théry, D. Pellman, Oncogene-like induction of cellular invasion from centrosome amplification. *Nature* (2014), doi:10.1038/nature13277.

14. S. D. Adams, J. Csere, G. D'angelo, E. P. Carter, M. Romao, T. Arnandis, M. Dodel, H. M. Kocher, R. Grose, G. Raposo, F. Mardakheh, S. A. Godinho, Centrosome amplification mediates small extracellular vesicle secretion via lysosome disruption. *Curr. Biol.* **31**, 1403-1416.e7 (2021).

15. T. Arnandis, P. Monteiro, S. D. Adams, V. L. Bridgeman, V. Rajeeve, E. Gadaleta, J. Marzec, C. Chelala, I. Malanchi, P. R. Cutillas, S. A. Godinho, Oxidative Stress in Cells with Extra Centrosomes Drives Non-Cell-Autonomous Invasion. *Dev. Cell* (2018), doi:10.1016/j.devcel.2018.10.026.

16. T. Boveri, Concerning the Origin of Malignant Tumours by Theodor Boveri. Translated and annotated by Henry Harris. *J. Cell Sci.* **121**, 1 LP – 84 (2008).

17. P. A. Coelho, L. Bury, M. N. Shahbazi, K. Liakath-Ali, P. H. Tate, S. Wormald, C. J. Hindley, M. Huch, J. Archer, W. C. Skarnes, M. Zernicka-Goetz, D. M. Glover, Over-expression of Plk4 induces centrosome amplification, loss of primary cilia and associated tissue hyperplasia in the mouse. *Open Biol.* **5** (2015), doi:10.1098/rsob.150209.

18. Ö. Serçin, J. C. Larsimont, A. E. Karambelas, V. Marthiens, V. Moers, B. Boeckx, M. Le Mercier, D. Lambrechts, R. Basto, C. Blanpain, Transient PLK4 overexpression accelerates tumorigenesis in p53-deficient epidermis. *Nat. Cell Biol.* **18**, 100–110 (2016).

19. M. S. Levine, B. Bakker, B. Boeckx, D. Lambrechts, F. Foijer, A. J. Holland, M. S. Levine, B. Bakker, B. Boeckx, J. Moyett, J. Lu, B. Vitre, D. C. Spierings, P. M. Lansdorp, D. W. Cleveland, D. Lambrechts, F. Foijer, A. J. Holland, Centrosome Amplification Is Sufficient to Promote Spontaneous Tumorigenesis in Mammals. *Dev. Cell* **40**, 313-322.e5 (2017).

20. A. Krämer, B. Maier, J. Bartek, Centrosome clustering and chromosomal (in)stability: A matter of life and death. *Mol. Oncol.* **5**, 324–335 (2011).

21. F. Galimberti, S. L. Thompson, S. Ravi, D. A. Compton, E. Dmitrovsky, Anaphase catastrophe is a target for cancer therapy. *Clin. Cancer Res.* **17**, 1218–1222 (2011).

22. C. A. Watts, F. M. Richards, A. Bender, P. J. Bond, O. Korb, O. Kern, M. Riddick, P. Owen, R. M. Myers, J. Raff, F. Gergely, D. I. Jodrell, S. V. Ley, Design, synthesis, and biological evaluation of an allosteric inhibitor of HSET that targets cancer cells with supernumerary centrosomes. *Chem. Biol.* **20**, 1399–1410 (2013).

23. E. Kawamura, A. B. Fielding, N. Kannan, A. Balgi, J. Eaves, M. Roberge, S. Dedhar, Identification of novel small molecule inhibitors of centrosome clustering in cancer cells. **4** (2013).

24. G. Konotop, E. Bausch, T. Nagai, A. Turchinovich, N. Becker, A. Benner, M. Boutros, K. Mizuno, A. Krämer, M. S. Raab, Pharmacological inhibition of centrosome clustering by slingshot-mediated cofilin activation and actin cortex destabilization. *Cancer Res.* **76**, 6690–6700

(2016).

25. B. Navarro-Serer, E. P. Childers, N. M. Hermance, D. Mercadante, A. L. Manning, Aurora A inhibition limits centrosome clustering and promotes mitotic catastrophe in cells with supernumerary centrosomes. *Oncotarget* **10**, 1649–1659 (2019).

26. I. Vitale, L. Galluzzi, M. Castedo, G. Kroemer, Mitotic catastrophe: a mechanism for avoiding genomic instability. *Nat. Rev. Mol. Cell Biol.* **12**, 385–392 (2011).

27. B. A. Weaver, How Taxol/paclitaxel kills cancer cells. *Mol. Biol. Cell* **25**, 2677–2681 (2014).

28. L. M. Zasadil, K. A. Andersen, D. Yeum, G. B. Rocque, L. G. Wilke, A. J. Tevaarwerk, R. T. Raines, M. E. Burkard, B. A. Weaver, Cytotoxicity of paclitaxel in breast cancer is due to chromosome missegregation on multipolar spindles. *Sci. Transl. Med.* **6** (2014), doi:10.1126/scitranslmed.3007965.

29. C. M. Scribano, J. Wan, K. Esbona, J. B. Tucker, A. Lasek, A. S. Zhou, L. M. Zasadil, R. Molini, J. Fitzgerald, A. M. Lager, J. J. Laffin, K. Correia-Staudt, K. B. Wisinski, A. J. Tevaarwerk, R. O'Regan, S. M. McGregor, A. M. Fowler, R. J. Chappell, T. S. Bugni, M. E. Burkard, B. A. Weaver, Chromosomal instability sensitizes patient breast tumors to multipolar divisions induced by paclitaxel. *Sci. Transl. Med.* **13** (2021), doi:10.1126/scitranslmed.abd4811.

30. A. Krämer, N. Mailand, C. Lukas, R. G. Syljuåsen, C. J. Wilkinson, E. A. Nigg, J. Bartek, J. Lukas, Centrosome-associated Chk1 prevents premature activation of cyclin-B-Cdk1 kinase. *Nat. Cell Biol.* **6**, 884–891 (2004).

31. L. I. Mullee, C. G. Morrison, Centrosomes in the DNA damage response—the hub outside the centre*Chromosom. Res.* (2016), doi:10.1007/s10577-015-9503-7.

32. L. L. Fava, F. Schuler, V. Sladky, M. D. Haschka, C. Soratroi, L. Eiterer, E. Demetz, G. Weiss, S. Geley, E. A. Nigg, A. Villunger, The PIDDosome activates p53 in response to supernumerary centrosomes. *Genes Dev.* (2017), doi:10.1101/gad.289728.116.

33. M. Burigotto, A. Mattivi, D. Migliorati, G. Magnani, C. Valentini, M. Roccuzzo, M. Offterdinger, M. Pizzato, A. Schmidt, A. Villunger, S. Maffini, L. L. Fava, Centriolar distal appendages activate the centrosome-PIDDosome-p53 signalling axis via ANKRD26. *EMBO J.* **40**, 1–22 (2021).

34. L. T. Evans, T. Anglen, P. Scott, K. Lukasik, J. Loncarek, A. J. Holland, ANKRD26 recruits PIDD1 to centriolar distal appendages to activate the PIDDosome following centrosome amplification. *EMBO J.* **40**, 1–18 (2021).

35. D. D. Bowtell, S. Böhm, A. A. Ahmed, P. J. Aspuria, R. C. Bast, V. Beral, J. S. Berek, M. J. Birrer, S. Blagden, M. A. Bookman, J. D. Brenton, K. B. Chiappinelli, F. C. Martins, G. Coukos, R. Drapkin, R. Edmondson, C. Fotopoulou, H. Gabra, J. Galon, C. Gourley, V. Heong, D. G. Huntsman, M. Iwanicki, B. Y. Karlan, A. Kaye, E. Lengyel, D. A. Levine, K. H. Lu, I. A. McNeish, U. Menon, S. A. Narod, B. H. Nelson, K. P. Nephew, P. Pharoah, D. J. Powell, P. Ramos, I. L. Romero, C. L. Scott, A. K. Sood, E. A. Stronach, F. R. Balkwill, Rethinking ovarian cancer II: Reducing mortality from high-grade serous ovarian cancer*Nat. Rev. Cancer* (2015), doi:10.1038/nrc4019.

36. B. J. Aubrey, G. L. Kelly, A. Janic, M. J. Herold, A. Strasser, How does p53 induce apoptosis and how does this relate to p53-mediated tumour suppression? *Cell Death Differ.* **25**, 104–113 (2018).

37. P. M. O'Connor, J. Jackman, I. Bae, T. G. Myers, S. Fan, M. Mutoh, D. A. Scudiero, A. Monks, E. A. Sausville, J. N. Weinstein, S. Friend, A. J. Fornace, K. W. Kohn, Characterization of the p53 tumor suppressor pathway in cell lines of the National Cancer Institute anticancer drug screen and correlations with the growth-inhibitory potency of 123 anticancer agents. *Cancer Res.* **57**, 4285–4300 (1997).

38. T. Abbas, A. Dutta, P21 in cancer: Intricate networks and multiple activities. *Nat. Rev. Cancer* **9**, 400–414 (2009).

39. R. Singh, A. Letai, K. Sarosiek, Regulation of apoptosis in health and disease: the balancing act of BCL-2 family proteins. *Nat. Rev. Mol. Cell Biol.* **20**, 175–193 (2019).

40. S. N. Banerjee, C. J. Lord, First-line PARP inhibition in ovarian cancer — standard of care for all? *Nat. Rev. Clin. Oncol.* **17**, 136–137 (2020).

41. M. F. Gulen, U. Koch, S. M. Haag, F. Schuler, L. Apetoh, F. Radtke, A. Ablasser, A. Villunger, Signalling strength determines proapoptotic functions of STING. *Nat. Commun.* , doi:10.1038/s41467-017-00573-w.

42. S. Lohard, N. Bourgeois, L. Maillet, F. Gautier, A. Fétiveau, H. Lasla, F. Nguyen, C. Vuillier, A. Dumont, A. Moreau-aubry, M. Frapin, L. David, D. Loussouarn, O. Kerdraon, M. Campone, P. Jézéquel, P. P. Juin, S. Barillé-nion, STING-dependent paracriny shapes apoptotic priming of breast tumors in response to anti-mitotic treatment. *Nat. Commun.* , 1–16 (2020).

43. I. E. Wertz, S. Kusam, C. Lam, T. Okamoto, W. Sandoval, D. J. Anderson, E. Helgason, J. A. Ernst, M. Eby, J. Liu, L. D. Belmont, J. S. Kaminker, K. M. O'Rourke, K. Pujara, P. B. Kohli, A.

R. Johnson, M. L. Chiu, J. R. Lill, P. K. Jackson, W. J. Fairbrother, S. Seshagiri, M. J. C. Ludlam, K. G. Leong, E. C. Dueber, H. Maecker, D. C. S. Huang, V. M. Dixit, Sensitivity to antitubulin chemotherapeutics is regulated by MCL1 and FBW7. *Nature* **471**, 110–114 (2011).

44. H. Inuzuka, S. Shaik, I. Onoyama, D. Gao, A. Tseng, R. S. Maser, B. Zhai, L. Wan, A. Gutierrez, A. W. Lau, Y. Xiao, A. L. Christie, J. Aster, J. Settleman, S. P. Gygi, A. L. Kung, T. Look, K. I. Nakayama, R. A. Depinho, W. Wei, SCFFBW7 regulates cellular apoptosis by targeting MCL1 for ubiquitylation and destruction. *Nature* **471**, 104–109 (2011).

45. M. D. Haschka, C. Soratroi, S. Kirschnek, G. Häcker, R. Hilbe, S. Geley, A. Villunger, L. L. Fava, The NOXA-MCL1-BIM axis defines lifespan on extended mitotic arrest. *Nat. Commun.* **6**, 1–13 (2015).

46. A. Bennett, O. Sloss, C. Topham, L. Nelson, A. Tighe, S. S. Taylor, Inhibition of Bcl-xL sensitizes cells to mitotic blockers, but not mitotic drivers. *Open Biol.* **6** (2016), doi:10.1098/rsob.160134.

47. T. Popova, E. Manié, G. Rieunier, V. Caux-Moncoutier, C. Tirapo, T. Dubois, O. Delattre, B. Sigal-Zafrani, M. Bollet, M. Longy, C. Houdayer, X. Sastre-Garau, A. Vincent-Salomon, D. Stoppa-Lyonnet, M. H. Stern, Ploidy and large-scale genomic instability consistently identify basal-like breast carcinomas with BRCA1/2 inactivation. *Cancer Res.* **72**, 5454–5462 (2012).

48. V. C. Yan, H. E. Butterfield, A. H. Poral, M. J. Yan, K. L. Yang, C. D. Pham, F. L. Muller, Why Great Mitotic Inhibitors Make Poor Cancer Drugs. *Trends in Cancer* **6**, 924–941 (2020).

49. P. Monteiro, B. Yeon, S. S. Wallis, S. A. Godinho, Centrosome amplification fine-tunes tubulin acetylation to differentially control intracellular organization. *EMBO J.* **44**, 2022.10.17.512471 (2023).

50. L. L. Fava, F. Schuler, V. Sladky, M. D. Haschka, C. Soratroi, L. Eiterer, E. Demetz, G. Weiss, S. Geley, E. A. Nigg, A. Villunger, The PIDDosome activates p53 in response to supernumerary centrosomes. *Genes Dev.* **31**, 34–45 (2017).

51. J. Montero, R. Haq, Adapted to Survive: Targeting Cancer Cells with BH3 Mimetics. *Cancer Discov.* **12**, 1217–1232 (2022).

52. S. Mazzi, L. Lordier, N. Debili, H. Raslova, W. Vainchenker, Megakaryocyte and polyploidization. *Exp. Hematol.* **57**, 1–13 (2018).

53. H. van den Bos, B. Bakker, A. Taudt, V. Guryev, M. Colomé-Tatché, P. M. Lansdorp, F. Foijer, D. C. J. Spierings, *Quantification of aneuploidy in mammalian systems* (2019).

54. B. Langmead, S. L. Salzberg, Fast gapped-read alignment with Bowtie 2. *Nat. Methods* **9**, 357–359 (2012).

55. G. Jun, M. K. Wing, G. R. Abecasis, H. M. Kang, An efficient and scalable analysis framework for variant extraction and refinement from population-scale DNA sequence data. *Genome Res.* **25**, 918–925 (2015).

56. B. Bakker, A. Taudt, M. E. Belderbos, D. Porubsky, D. C. J. Spierings, T. V. de Jong, N. Halsema, H. G. Kazemier, K. Hoekstra-Wakker, A. Bradley, E. S. J. M. de Bont, A. van den Berg, V. Guryev, P. M. Lansdorp, M. Colomé-Tatché, F. Foijer, Single-cell sequencing reveals karyotype heterogeneity in murine and human malignancies. *Genome Biol.* **17**, 1–15 (2016).

57. H. van den Bos, D. C. J. Spierings, A. S. Taudt, B. Bakker, D. Porubský, E. Falconer, C. Novoa, N. Halsema, H. G. Kazemier, K. Hoekstra-Wakker, V. Guryev, W. F. A. den Dunnen, F. Foijer, M. C. Tatché, H. W. G. M. Boddeke, P. M. Lansdorp, Single-cell whole genome sequencing reveals no evidence for common aneuploidy in normal and Alzheimer's disease neurons. *Genome Biol.* **17**, 1–9 (2016).

Acknowledgments:

We are grateful to the patients who consented to participate in this research and to the medical teams involved in their care. We thank Andrew Holland for the kind gift of the inducible PLK4 over-expression plasmid. We thank the ICGEX platform at Institut Curie (IC) headed by Sylvain Baulade for bulk RNA sequencing and Genosplice (http://www.genosplice.com) and P. Delagrange and W. Zeitouni for performing the analysis. We thank the Tissue Imaging (PICT-IBiSA) and Nikon Imaging Centre at IC, member of the French National Research Infrastructure France-BioImaging (ANR10-INBS-04) and the IC cytometry platform. We thank the Genomics Platform of the translational research department at IC for cell line authentication. We thank Nicolas Manel and Sebastian Montealegre for discussions and the gift of reagents used to characterize cGAS/STING signaling. We thank Stephen Taylor for discussions about this project. We also thank all the members of the Basto team for discussions and comments on the manuscript.

Funding:

Labex CelTisPhyBio post-doctoral fellowship (F.E.)

Agence pour la Recherche contre le Cancer postdoctoral fellowship PDF20190508563 (F.E.)
La Ligue contre le cancer PhD fellowship 17562 (G.F.)
Institut National du Cancer grant 2015-PLBIO15-237
World Wide Cancer research grant 21-0042
The Basto lab is a member of the CelTisPhyBio Labex and is supported by the Institut Curie and the CNRS.

Author contributions:

The project was designed and conceptualized by FE, and RB with significant input from OG and GF. FE, GF, and AYS performed most experiments including time-lapse imaging, image analysis, cytometry, immunofluorescence, western blots and quantifications. FE developed the code used for time-lapse imaging of single-cell responses to chemotherapy. GF prepared cells for single cell whole genome sequencing which were then processed by AET, with data analysis performed by RW under the supervision of DCJS and FF. AYS and OG prepared cells for bulk RNA sequencing, and OG supervised the data analysis. SG helped establish the stable FUCCI cell lines; AH contributed to determine IC50s; SF helped analyze time-lapse imaging experiments. XS-G and AVS provided human samples from the pathology department of IC. OM managed the patient database, and SRR provided advice in methodology. JPM quantified the centrosomes in patient tissue samples and OG supervised their analysis. Figures were prepared by FE with help from GF and AYS. FE wrote the manuscript with input from RB and OG. The work was supervised by FE, OG and RB.

Competing interests:

Authors declare that they have no competing interests.

Data and materials availability:

All data and code are available upon request.

Figures:

Fig. 1

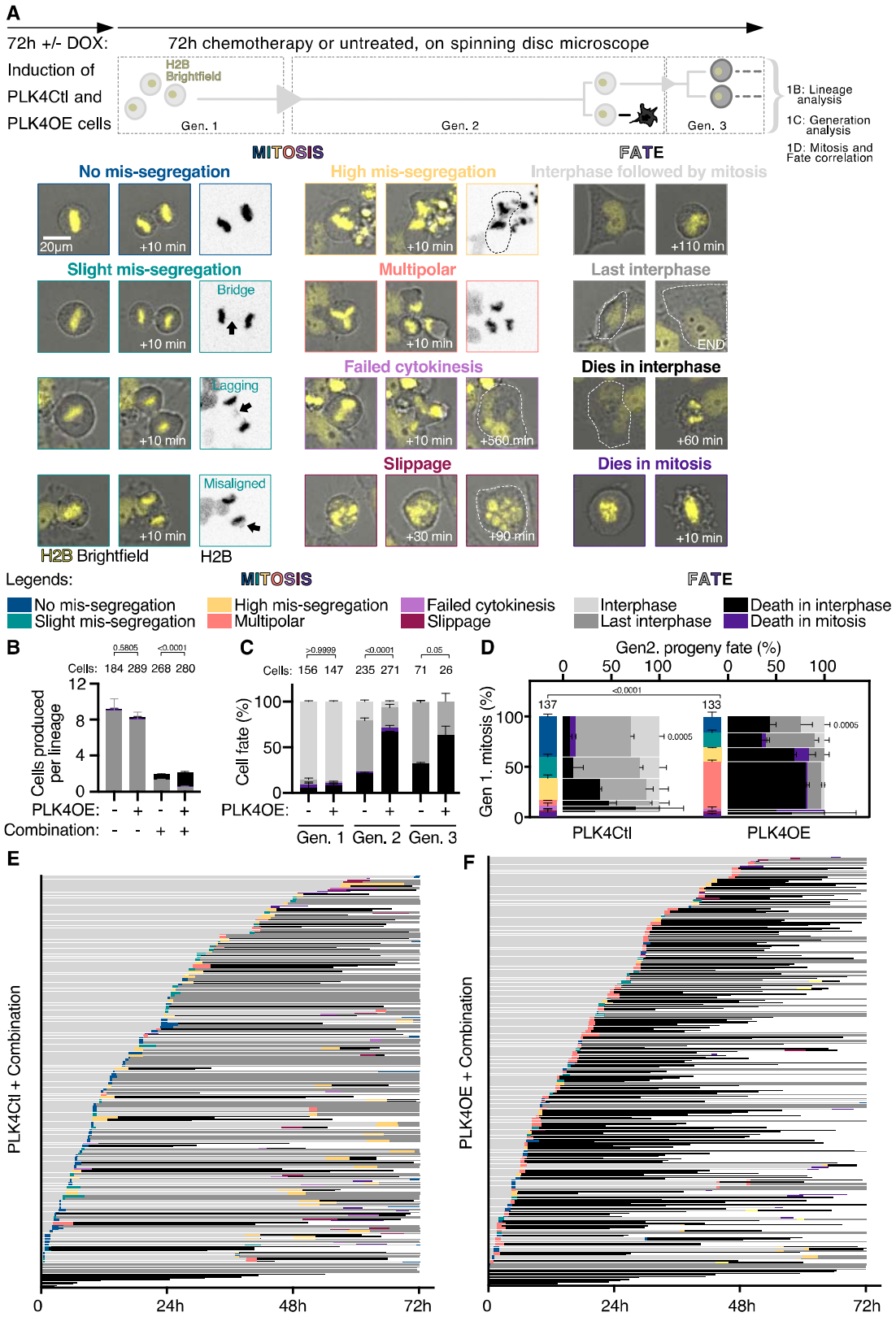

Fig. 1. Centrosome amplification favors cell death in response to combined chemotherapy.

(A) Single-cell live-imaging workflow. OVCAR8 cells expressing H2B-RFP and inducible for PLK4 over-expression are exposed to DMSO or 1µg/ml Doxycycline (DOX) for 72h to induce centrosome amplification. PLK4Ctl and PLK4OE cells are then filmed during 72h of chemotherapy and lineages are tracked over multiple generations. Representative images of mitotic behaviors and cell fates are shown with the color-coded legends used in the subsequent panels. Lineage analysis consists in counting for each starting cell, the number of cells adopting the different fates (See panel B). Generation analysis consists in determining the percentage of a generation that will adopt the different fates (See panel C). Mitosis and fate correlation consists in determining the percentage of cells adopting the different fates, depending on the behavior of the mother cell during mitosis (See panel D). **(B)** Bar graphs showing the averages and SEM of the number of cells per lineage adopting the indicated fates (Legends in panel A). A minimum of 20 lineages were analyzed from two independent experiments, statistical tests: Fisher's exact test on the number of cell death events (pooling death in interphase and in mitosis). Numbers on the top of each graph represent the number of cells analyzed per condition. **(C)** Bar graphs showing the average and SEM of the percentages of cells undergoing indicated fates (Legends in panel A). Two independent experiments, statistical tests: Fisher's exact test on the number of cell death events (pooling death in interphase and death in mitosis). Numbers on the top of each graph represent the number of cells analyzed per condition. **(D)** Vertical axis: Bar graphs showing the average and SEM of the percentages of mitotic phenotypes (Legends in panel A). 137 and 133 cell divisions were analyzed from two independent experiments, statistical test: Fisher's exact test on the number of multipolar divisions. Horizontal axis: Bar graphs showing the average and SEM of the percentages of cells undergoing indicated fates (Legends in panel A) according to the mitotic behavior of mother cells, with bar width depending on the proportion of cells displaying a given mitotic phenotype. Two independent experiments, statistical test: Fisher's exact test on the number of *No mis-segregation* progeny (progeny of blue mitosis) dying in mitosis and interphase. **(E- F)** Single cell profiles of PLK4Ctl (E) and PLK4OE (F) undergoing Carboplatin+ Paclitaxel exposure. Each row corresponds to one cell (Legends in panel A).

Fig. 2

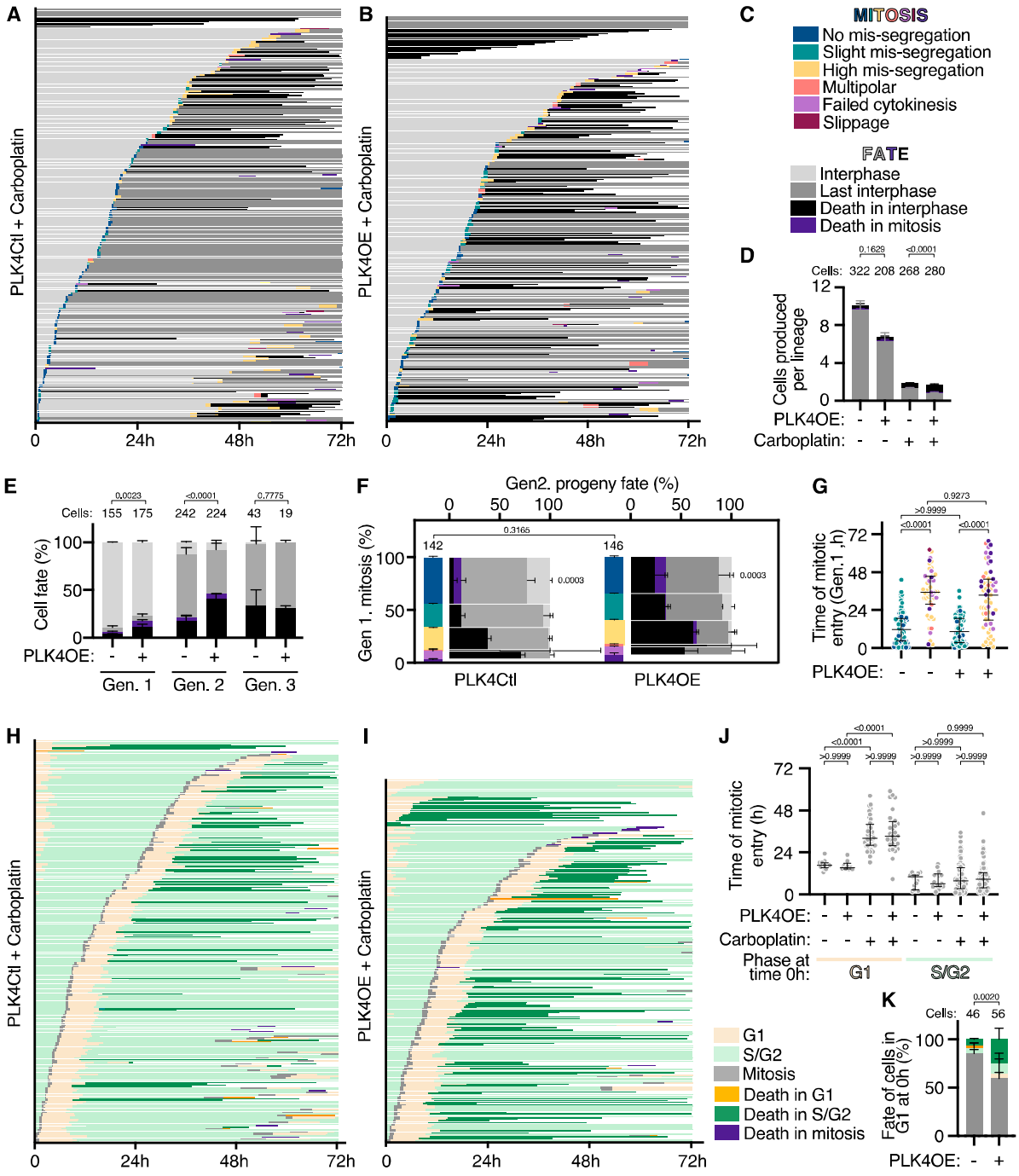

Fig. 2. Centrosome amplification enhances cell death in response to Carboplatin independently of chromosome mis-segregation.

(A- B) Single cell profiles of PLK4Ctl (A) and PLK4OE (B) undergoing Carboplatin exposure. Color coding of mitosis and fates legends in panel C. **(C)** Legends for panels A,B,D,E,F and G, as defined in Figure 1A. **(D)** Bar graphs showing the averages and SEM of the number of cells produced per lineage, adopting the indicated fates (Legends in panel 1A). A minimum of 31 lineages were analyzed from two independent experiments, statistical tests: Fisher's exact test on the number of cell death events (pooling death in interphase and in mitosis). **(E)** Bar graphs showing the average and SEM of the percentages of cells undergoing indicated fates (Legends in Figure 1A and panel C). Two independent experiments, statistical tests: Fisher's exact test on the number of cell death events (pooling death in interphase and death in mitosis). Numbers on the top of each graph represent the number of cells analyzed per condition. **(F)** Vertical axis: Bar graphs showing the average and SEM of the percentages of mitotic phenotypes (Legends in Figure 1A and panel C). 142 and 146 cell divisions analyzed from two independent experiments, statistical test: Chi-square test. Horizontal axis: Bar graphs showing the averages and SEM of the percentages of cells undergoing indicated fates (Legends in Figure 1A and panel C) according to the mitotic behavior of the mother cell, with bar width depending on the proportion of cells according to their the mitotic behavior. Two independent experiments, statistical test: Fisher's exact test on the number of *No mis-segregation* progeny (progeny of blue mitosis) dying in mitosis and interphase. **(G)** Scatter dot plot graphs showing time of mitotic entry, with median and interquartile range. Cells were classified depending on mitotic phenotypes with color-code defined in panel C. Two independent experiments with a minimum of 48 mitosis analyzed per category. Statistical tests: Kruskal-Wallis with Dunn's multiple comparisons tests. **(H- I)** Single cell profiles of FUCCI PLK4Ctl (I) and PLK4OE (I) cells undergoing Carboplatin exposure. Times in G1, S/G2 and mitosis, as well as death in each of these phases are color-coded as indicated. **(J)** Scatter dot plots of the time of mitotic entry depending on cell-cycle phase at movie start, with median and interquartile range. Two independent experiments with a minimum of 10 times analyzed per category. Statistical tests: Kruskal-Wallis with Dunn's multiple comparisons tests. **(K)** Bar graphs showing the average and SEM of the percentage of cells adopting the indicated fates (legends in panel I). Two independent experiments, statistical test: Fischer's exact

test on the number of cells dying (irrespective of the cell-cycle phase). Numbers on the top of each graph represent the number of cells analyzed per condition.

Fig. 3

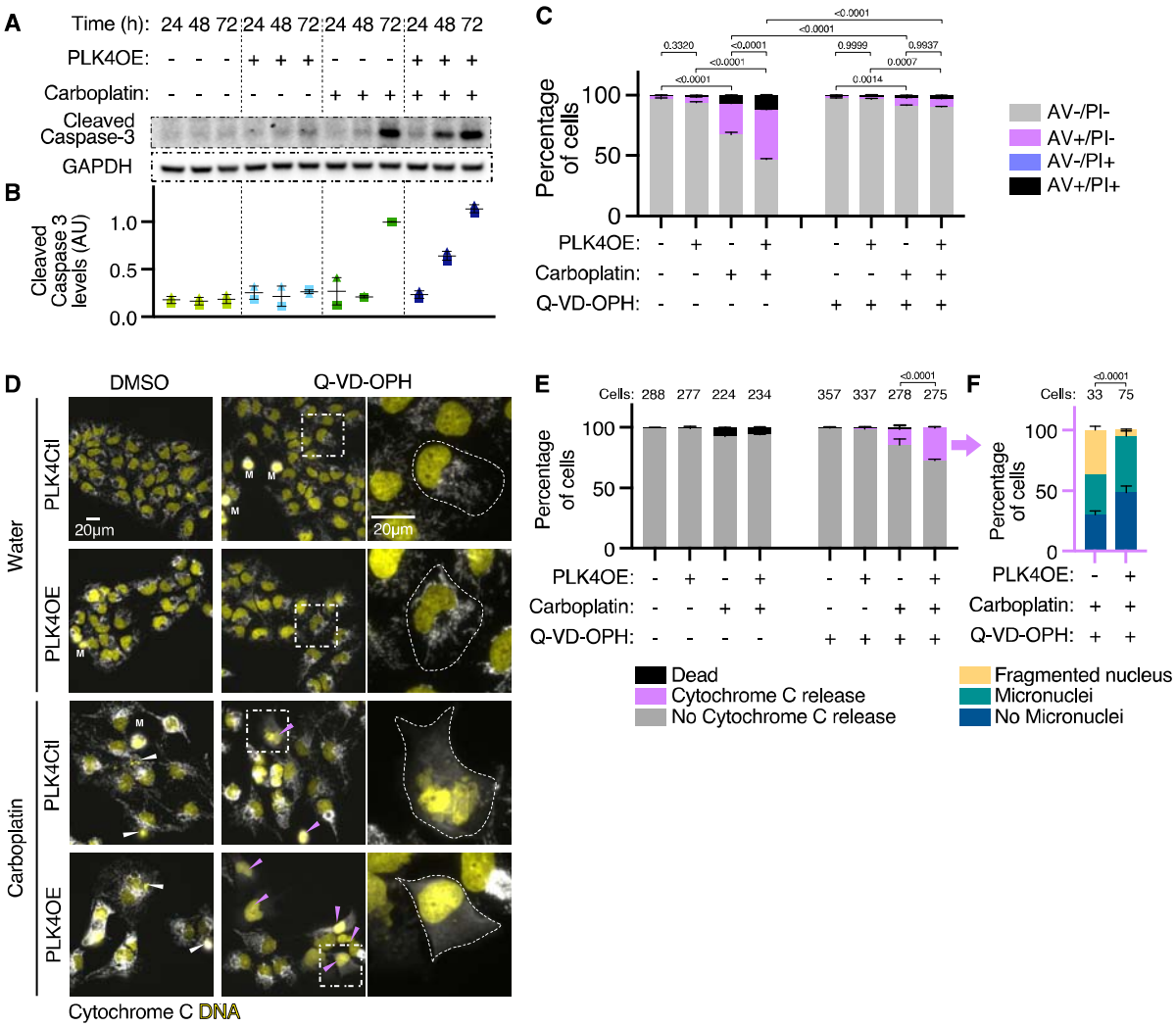

Fig 3. Centrosome amplification favors mitochondrial outer membrane permeabilization in response to Carboplatin.

(A) Representative Western Blot detecting Caspase-3 cleavage. **(B)** Average and SEM of cleaved caspase 3 protein levels from 2 independent experiments, normalized to levels measured in Carboplatin treated PLK4Ctl cells at 72h. **(C)** Bar graphs showing the average and SEM of the percentage of cells in specified Annexin V-APC/PI gates analyzed by flow cytometry. 4 replicates obtained from 2 independent experiments, with a minimum of 60000 cells analyzed per condition and replicate. Statistical test: comparison of the percentage of Annexin V positive cells, using ANOVA with Sidak's multiple comparison test. Representative cytometry profiles can be found in the supplementary materials. **(D)** Representative images of cells labelled with DAPI (yellow) and antibodies against Cytochrome C (gray). White arrows indicate dead cell debris, pink arrows indicate cells that have released Cytochrome C in the cytoplasm, M indicates mitotic cells. Representative insets are shown for individual Q-VD-Oph treated cells. **(E)** Bar graphs showing the average and SEM of the percentages of indicated cell populations. Two independent experiments, statistical test: Fisher's exact test on the number of cells releasing Cytochrome C. Numbers on the top of each graph represent the number of cells analyzed per condition. **(F)** Bar graphs showing the average and SEM of the percentages of cells releasing Cytochrome C with indicated nuclear phenotypes. Two independent experiments, statistical test: Fisher's exact test on the number of cells with fragmented nuclei. Numbers on the top of each graph represent the number of cells analyzed per condition.

Fig. 4

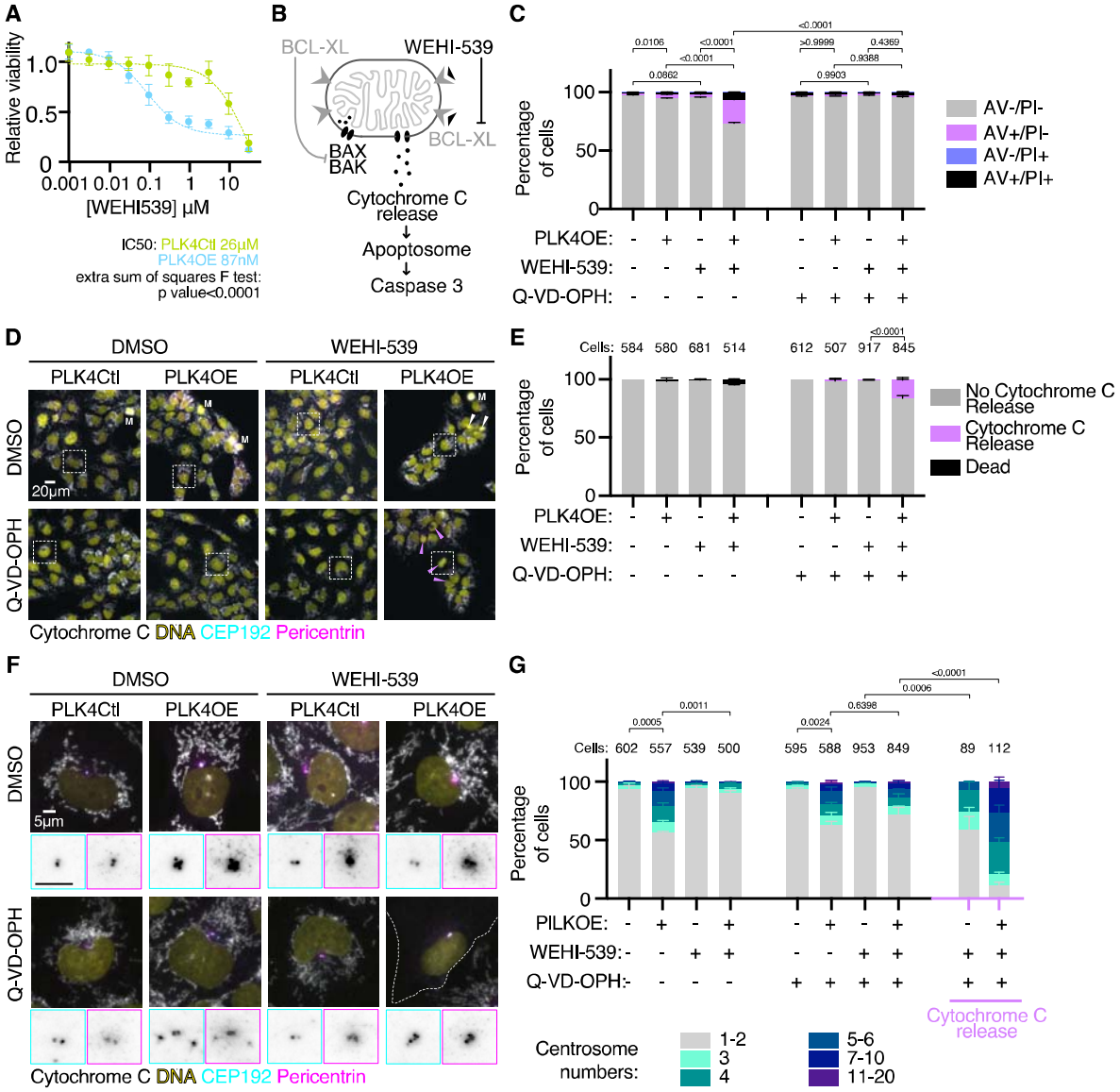

Fig 4. Centrosome amplification primes for mitochondria outer membrane permeabilization

(A) Dose-response of PLK4Ctl and PLK4OE cells to WEHI-539, normalized to their respective untreated conditions, obtained from MTT viability assays. Mean and SEM of 3 independent experiments each obtained from averaging 3 technical replicates. **(B)** Schematic of the induction of apoptosis by WEHI-539. When BAX and BAK channel formation are inhibited by BCL-XL, Cytochrome C is present in the mitochondria intermembrane space (Left). WEHI-539 inhibits BCL-XL which relieves the inhibition of channel formation by BAX and BAK, leading to Cytochrome C release, Apoptosome activation, and cleavage of Caspase 3 (Right). **(C)** Bar graphs showing the average and SEM of the percentage of cells in specified Annexin V-APC/PI gates analyzed by flow cytometry. 4 replicates obtained from 2 independent experiments with a minimum of 15000 cells analyzed per condition and replicate. Statistical test: comparison of the percentage of Annexin V positive cells, using ANOVA with Sidak's multiple comparison test. Representative cytometry profiles can be found in the supplementary materials. **(D)** Representative images of cells labeled with DAPI (yellow) and antibodies against Cytochrome C (gray), CEP192 (Cyan) and Pericentrin (Magenta). White arrows indicate dead cell debris, pink arrows indicate cells that have released Cytochrome C in to the cytoplasm, M indicates mitotic cells. Representative insets are shown in panel (F). **(E)** Bar graphs showing the average and SEM of the percentages of indicated cell populations. Two independent experiments, statistical test: Fisher's exact test on the number of cells releasing Cytochrome C. Numbers on the top of each graph represent the number of cells analyzed per condition. **(F)** Insets from panel (D) with inverted grayscale insets zooming on the centrosomes showing CEP192 (cyan border) and Pericentrin (Magenta border). **(G)** Bar graphs showing the average and SEM of the percentage of cells with the indicated number of centrosomes (determined by the co-localization of CEP192 and Pericentrin). Two independent experiments, statistical test: comparison of the percentage of cells with more than 2 centrosomes, using ANOVA with Sidak's multiple comparison test. Numbers on the top of each graph represent the number of cells analyzed per condition.

Fig. 5

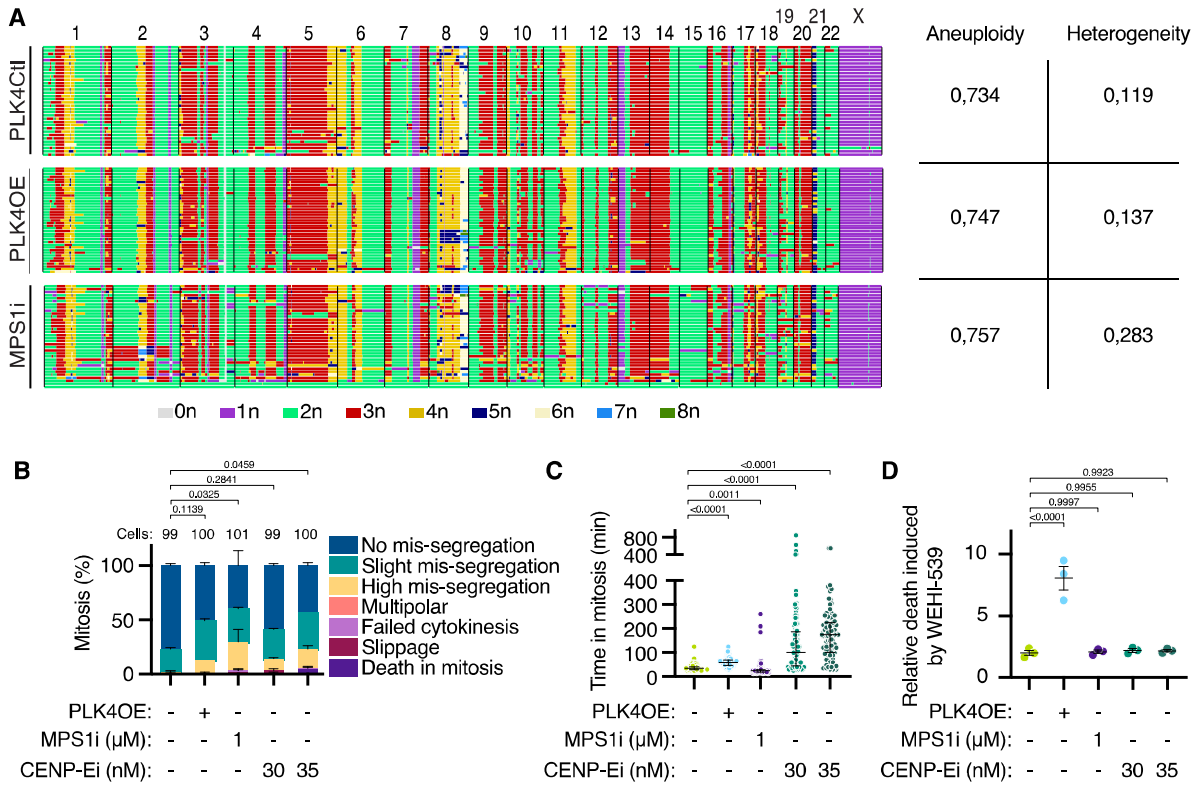

Fig. 5. Centrosome amplification primes for mitochondria outer membrane permeabilization independently of mitotic stress

(A) Genome-wide copy-number plots for G1 OVCAR8 cells. Each row represents a cell. Indicated aneuploidy and heterogeneity scores are calculated as described in material and methods. **(B)** Bar graphs showing the average and SEM of the percentage of mitotic phenotypes as defined in Figure 1A. Two independent experiments, statistical test: comparison of the percentage of cells with no mis-segregation using ANOVA with Dunnett's multiple comparison test. Numbers on the top of each graph represent the number of cells analyzed per condition. **(C)** Scatter dot plot graph of mitosis length with median and interquartile range. At least 96 mitosis analyzed from two independent experiments, statistical test: Kruskall-Wallis with Dunn's multiple comparison test. **(D)** Bar graphs showing the ratio between the percentages of Annexin V positive cells observed in presence and absence of WEHI-539 300nM. Average and SEM of 3 replicates from two independent experiments. Statistical test: ANOVA with Dunnett's multiple comparison test. Numbers on the top of each graph represent the number of cells analyzed per condition.

Fig. 6

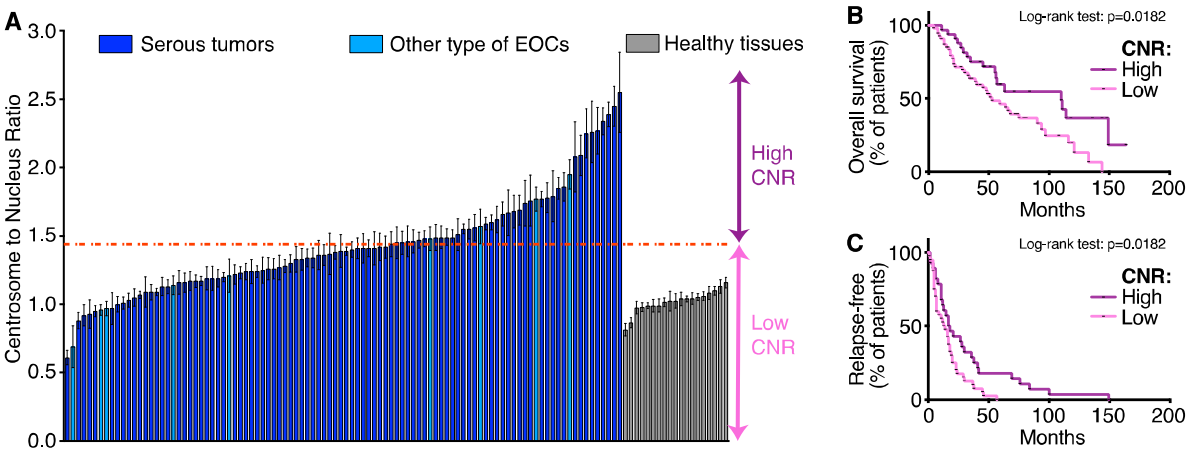

Fig. 6. High centrosome numbers favor the response to chemotherapy in a HGSOC patient cohort.

(A) Average and SEM of the CNR established in 10 fields per tumor or healthy tissue sample. Red dotted line indicates CNR=1,45, the cut-off between High-CNR and Low-CNR patients. **(B-C)** Kaplan-Meier curves for overall survival (B) and relapse-free time after the first line of chemotherapy (C) according to CNR status.

SUPPLEMENTARY MATERIAL

Supplementary Figures:

Fig. S1

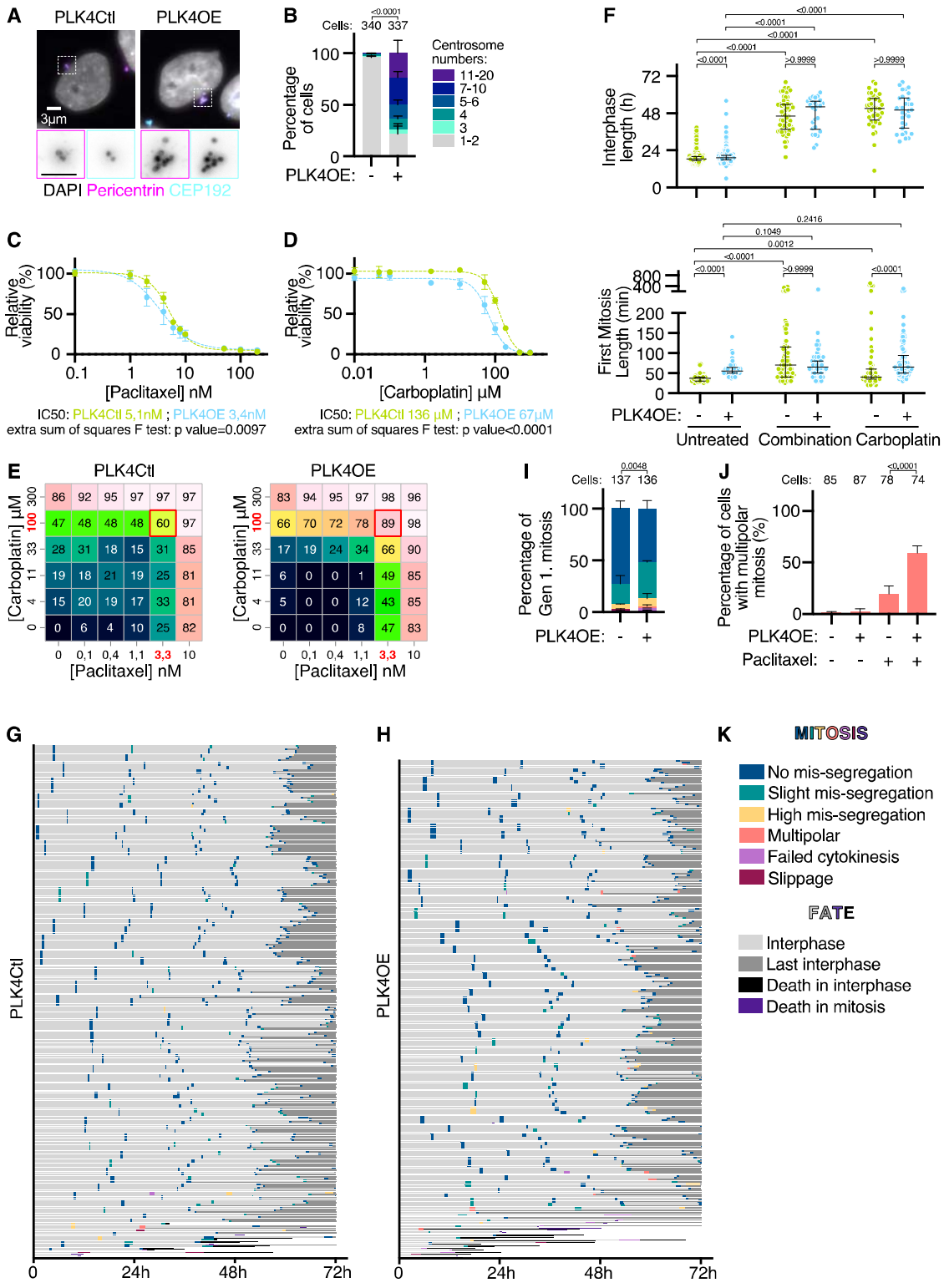

Fig. S1.

(A) Representative images of OVCAR8 cells stained with DAPI (gray) and antibodies against CEP192 (Cyan) and Pericentrin (Magenta). **(B)** Bar graphs showing the averages and SEM of the percentage of cells with the indicated number of centrosomes (CEP192 dots colocalizing with Pericentrin). 3 independent experiments, statistical test: Fisher's exact test comparing the number of cells with more than 2 centrosomes. **(C- D)** Dose-response of PLK4Ctl and PLK4OE cells to Paclitaxel (C) and Carboplatin (D), normalized to their respective control conditions, obtained from MTT viability assays. Mean and SEM of 2 independent experiments each obtained from averaging 3 technical replicates. **(E)** Combination matrixes for Carboplatin and Paclitaxel combined treatment, representing percentage of viability inhibition compared to control cells. Chosen working concentrations are highlighted in red. **(F)** Scatter dot plots of Interphase length (top) and First mitosis length (bottom), with Median and interquartile range. Data from two independent experiments are pooled for Combined treatment and Carboplatin treatment, data from the 4 corresponding control experiments are pooled for Untreated. For interphase length a minimum of 26 cells was analyzed, and for mitosis length a minimum of 133 cells was analyzed. Statistical tests: Kruskal-Wallis with Dunn's multiple comparisons tests. **(G- H)** Single cell profiles of PLK4Ctl (G) and PLK4OE (H) Untreated cells. Color coding of mitosis and fates refers to categories defined in Figure 1A, with legend repeated in panel K. **(I)** Averages and SEM of the percentages of mitotic phenotypes (legends in Fig. 1A and panel K). Two independent experiments, statistical test: Fisher's exact test on the number of *Slight Mis-segregation* events. **(J)** Percentage of multipolar divisions observed in presence or absence of 5nM Paclitaxel. Two independent experiments, statistical test: Fisher's exact test on the number of multipolar divisions. **(K)** Legends for panels G-H and I, as defined in Fig. 1A.

Fig. S2

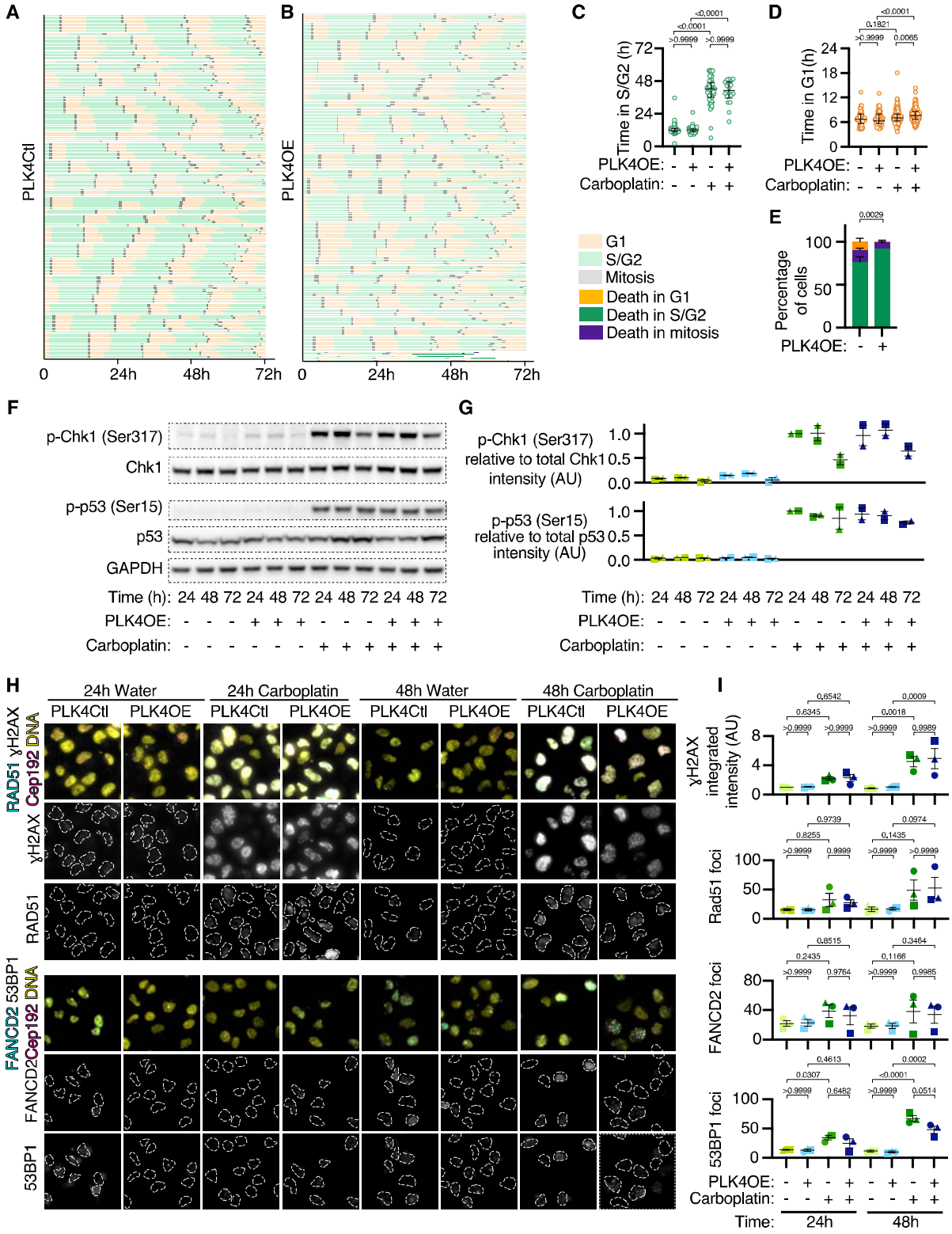

Fig. S2.

(A-B) Single cell profiles of FUCCI PLK4Ctl (A) and PLK4OE (B) untreated cells. See panel B for color-coded legends of cell cycle phase and cell fate. **(C-D)** Scatter dot plot graph of S/G2 (C) and G1 (D) phase lengths in the second generation, with median and interquartile range. Two independent experiments with a minimum of 18 times analyzed per category. Statistical tests: Kruskal-Wallis with Dunn's multiple comparisons tests. **(E)** Bar graphs showing the averages and SEM of the percentages of cell death events occurring in the indicated cell-cycle phases. Two independent experiments, statistical test: Fisher's exact test on number of death events occurring in S/G2. **(F)** Representative images of Western Blot analysis of phosphorylated Chk1 and p53 **(G)** Graph showing the average and SEM of phosphorylated protein relative to total protein levels, normalized to the levels detected in PLK4OE cells treated with Carboplatin for 24h, from 2 independent experiments. **(H)** Representative images of cells stained with DAPI an antibodies against FANCD2 (Cyan), 53BP1 (gray) and CEP192 (Magenta). Grayscale images of RAD51 and γH2AX are shown. **(I)** Dot-plot representing integrated nuclear γH2AX fluorescence intensity per cell, or numbers of Rad51, FANCD2 or 53BP1 foci per cells. Average and SEM of the averages obtained from 3 independent experiments, each quantifying a minimum of 94 cells per condition. Values are normalized to the average of untreated PLK4Ctl cells at 24h. Statistical test: ANOVA with Sidak's multiple comparison tests.

Fig. S3

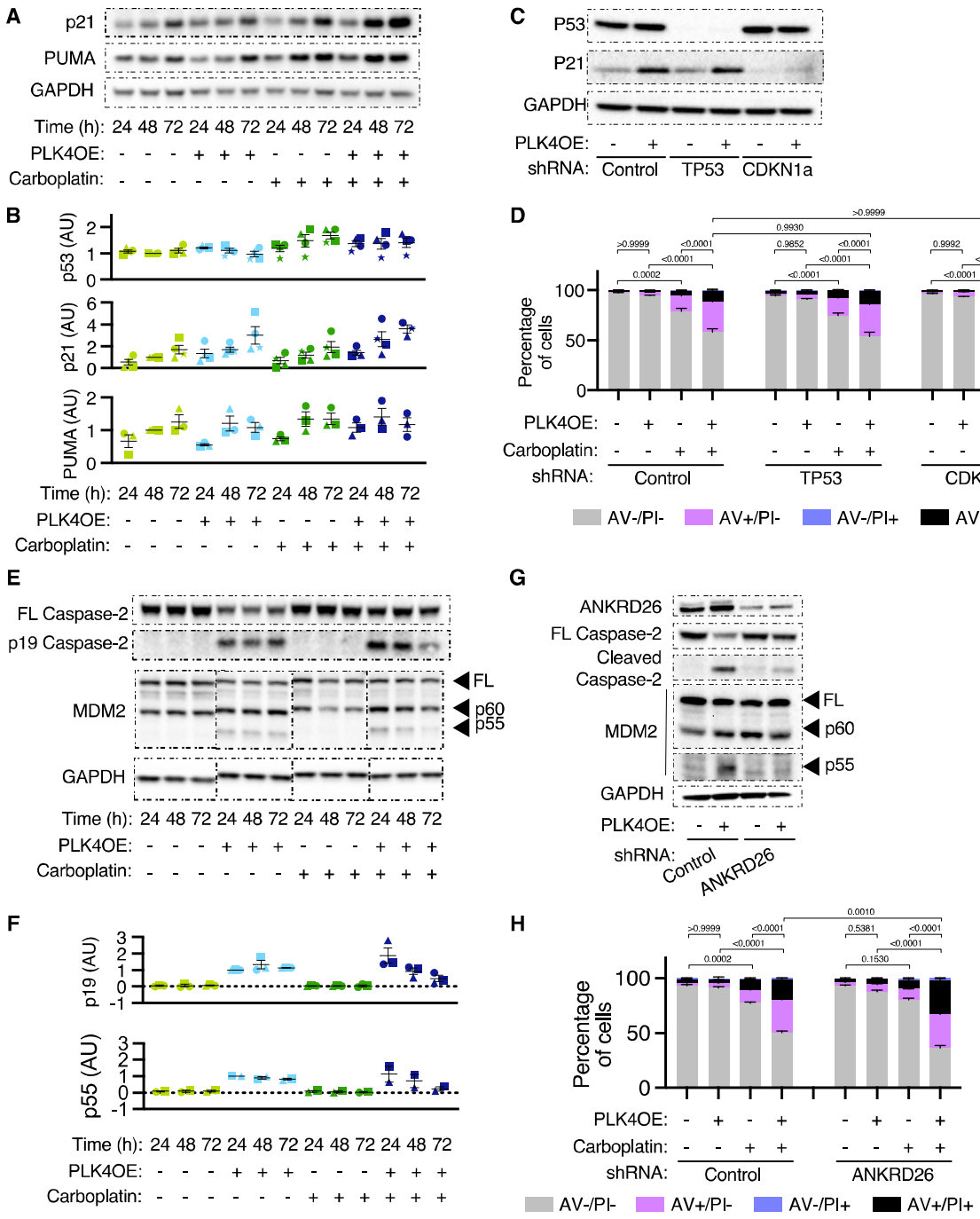

Fig. S3.

(A) Representative images of Western Blot analysis of p21, and PUMA. **(B)** Graph showing the average and SEM of protein levels from 4 (p53 and p21) or 3 (PUMA) independent experiments, normalized to levels measured in untreated PLK4Ctl cells at 48h. **(C and G)** Representative images of Western blot analysis of indicated shRNA cell lines. **(D and H)** Bar graphs showing the average and SEM of the percentage of cells in specified Annexin V-APC/PI gates analyzed by flow cytometry. (D) 6 replicates obtained from 4 independent experiments, with a minimum of 10000 cells analyzed per condition and replicate. (H) 4 replicates obtained from 2 independent experiments, with a minimum of 10000 cells analyzed per condition and replicate. Statistical test: comparison of the percentage of Annexin V positive cells, using ANOVA with Sidak's multiple comparison test. Representative cytometry profiles can be found in the supplementary materials. **(E)** Representative images of Western Blot analysis of Caspase2 and MDM2 cleavage. **(F)** Average and SEM of protein levels from 3 (p19 Caspase2) or 2 (p55 MDM2) independent experiments, normalized to levels measured in untreated PLK4OE cells at 24h.

Fig. S4

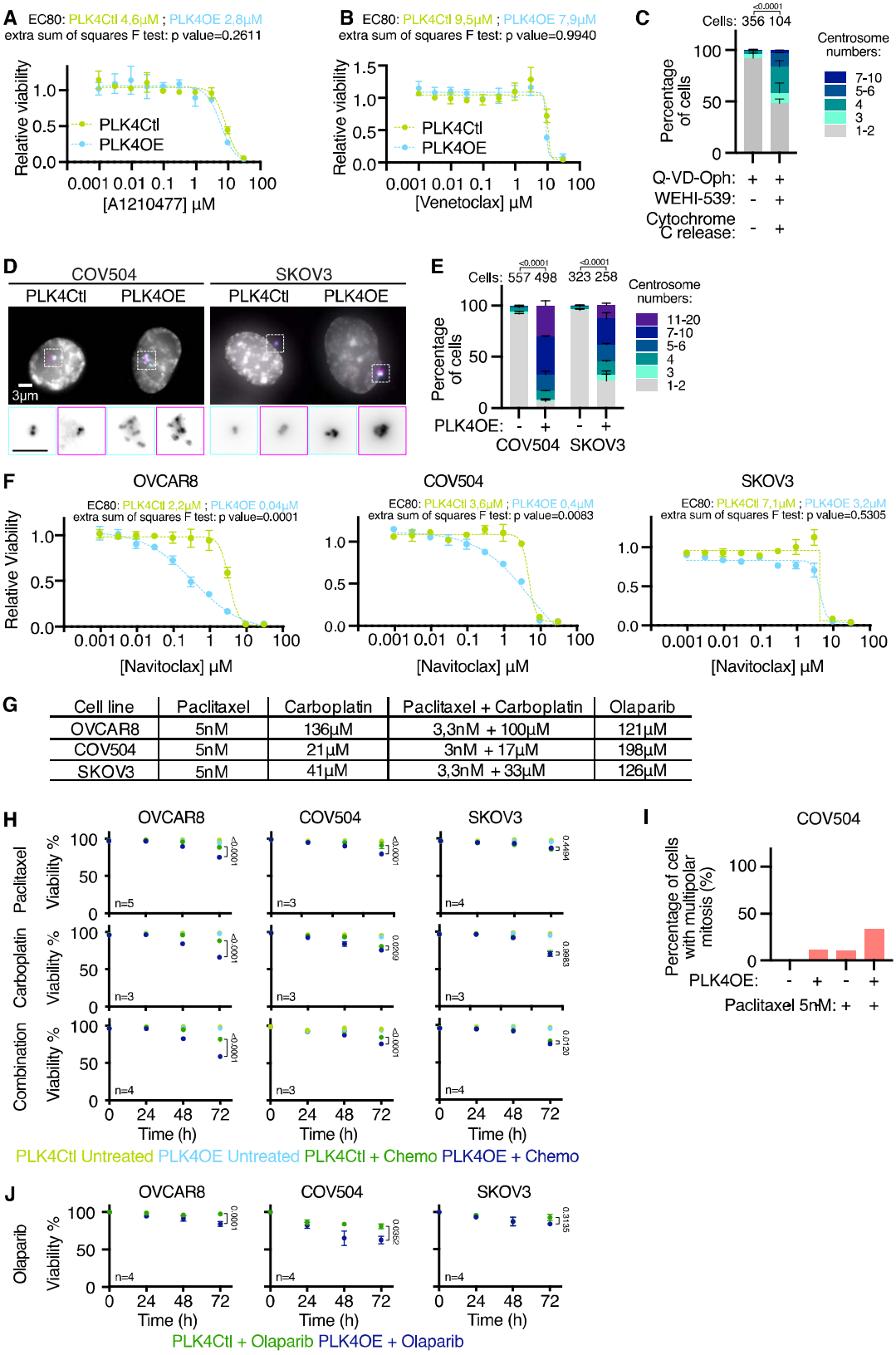

Cell line	Paclitaxel	Carboplatin	Paclitaxel + Carboplatin	Olaparib
OVCAR8	5nM	136µM	3,3nM + 100µM	121µM
COV504	5nM	21µM	3nM + 17µM	198µM
SKOV3	5nM	41µM	3,3nM + 33µM	126µM

Fig. S4.

(A- B) Dose-response of PLK4Ctl and PLK4OE cells to A1210477 **(A)** and Venetoclax **(B)**, normalized to their respective untreated conditions, obtained from MTT viability assays. Mean and SEM of 2 independent experiments each obtained from averaging 3 technical replicates. **(C)** Bar graphs showing the average and SEM of the percentage of cells with the indicated number of centrosomes (CEP192 dots colocalizing with Pericentrin). 2 independent experiments, statistical test: Fisher's exact test comparing the number of cells with more than 2 centrosomes. Numbers on the top of each graph represent the number of cells analyzed per condition. **(D)** Representative images of COV504 and SKOV3 cells stained with DAPI (gray) and antibodies against CEP192 (Cyan) and Pericentrin (Magenta). **(E)** Bar graphs showing the average and SEM of the percentages of cells with the indicated number of centrosomes (CEP192 dots colocalizing with Pericentrin). 3 independent experiments, statistical tests: Fisher's exact tests comparing the number of cells with more than 2 centrosomes. Numbers on the top of each graph represent the number of cells analyzed per condition. **(F)** Dose-response of PLK4Ctl and PLK4OE OVCAR8 (Left), COV504 (Middle) and SKOV3 (Right) to Navitoclax, normalized to their respective untreated conditions, obtained from MTT viability assays. Mean and SEM of 2-3 independent experiments each obtained from averaging 3 technical replicates. **(G)** Table summarizing the IC50s and drug concentrations used in combinations, determined via MTT dose-response viability assays, for PLK4Ctl OVCAR8, COV504 and SKOV3. **(H)** Viability (% of Trypan Blue negative cells) counted for PLK4Ctl and PLK4OE OVCAR8 (Left), COV504 (Middle) and SKOV3 (Right), in response to indicated chemotherapies using concentrations indicated in panel G for 72h. Average and SEM of the number of independent experiments indicated, each obtained from averaging 3 technical replicates. Statistical test: two-way ANOVA with Sidak's multiple comparison test. **(I)** Percentage of multipolar divisions observed in COV504 in response to 5nM

Paclitaxel exposure. **(J)** Viability (% of Trypan Blue negative cells) counted for PLK4Ctl and PLK4OE OVCAR8 (Left), COV504 (Middle) and SKOV3 (Right), in response to Olaparib using concentrations indicated in panel G for 72h. Average and SEM of 4 independent experiments, each obtained from averaging 3 technical replicates. Statistical test: two-way ANOVA with Sidak's multiple comparison test.

Fig. S5

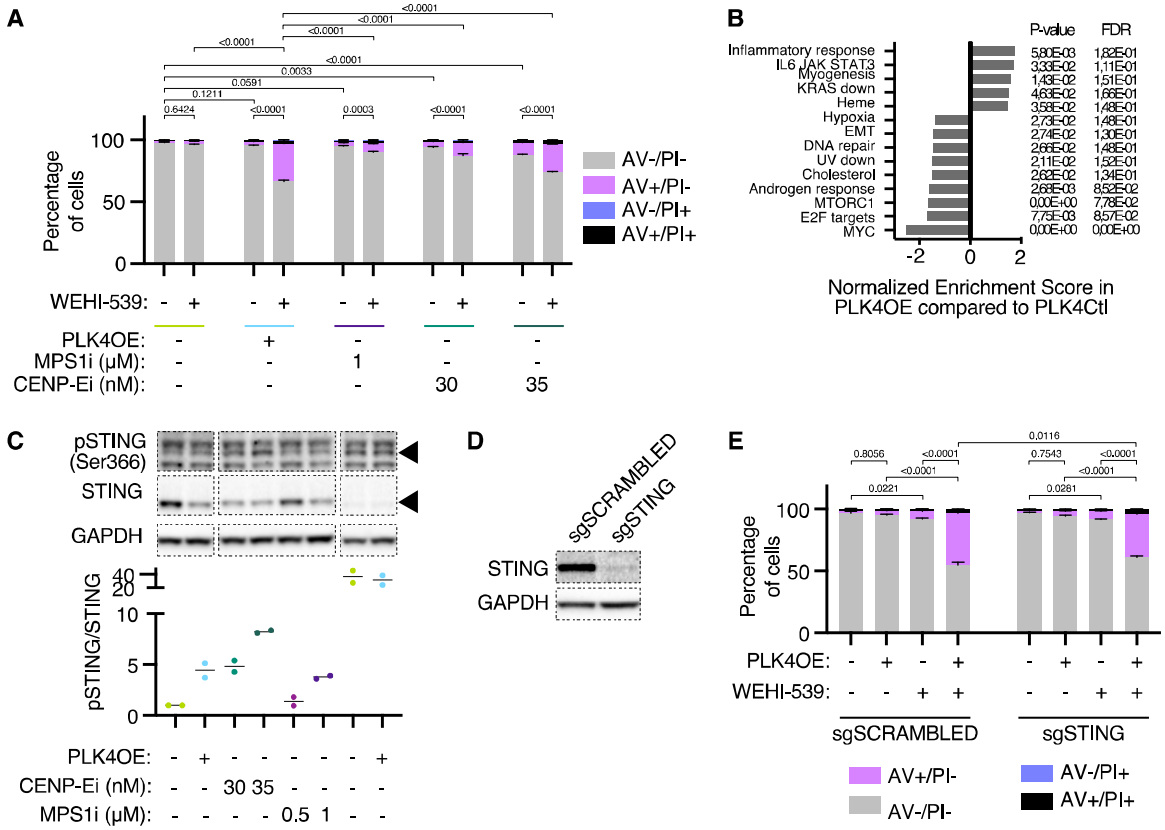

Fig. S5.

(A) Bar graphs showing the average and SEM of the percentage of cells in specified Annexin V-APC/PI gates analyzed by flow cytometry. 3 replicates obtained from 2 independent experiments, with a minimum of 20000 cells analyzed per condition and replicate. Statistical test: comparison of the percentage of Annexin V positive cells, using ANOVA with Sidak's multiple comparison test. Representative cytometry profiles can be found in the supplementary materials. **(B)** GSEA Hallmarks with |normalized enrichment score >1,5 and p-value < 0,05, from differential RNA expression analysis of PLK4OE cells compared to PLK4Ctl. **(C)** Western-Blot analysis of STING phosphorylation after 72hr of indicated drug treatments with quantification of pSTING relative to total STING. Average and SEM of 2 independent experiments, normalized to untreated PLK4Ctl. HT-DNA transfection was performed 24h before cell collection. **(D)** Western blot analysis of indicated bulk LentiCRISPR cell lines. **(E)** Bar graphs showing the average and SEM of the percentage of cells in specified Annexin V-APC/PI gates analyzed by flow cytometry. 4 replicates obtained from 2 independent experiments with a minimum of 15000 cells analyzed per condition and replicate. Statistical test: comparison of the percentage of Annexin V positive cells using ANOVA with Sidak's multiple comparison test. Representative cytometry profiles can be found in the supplementary materials.

Fig. S6

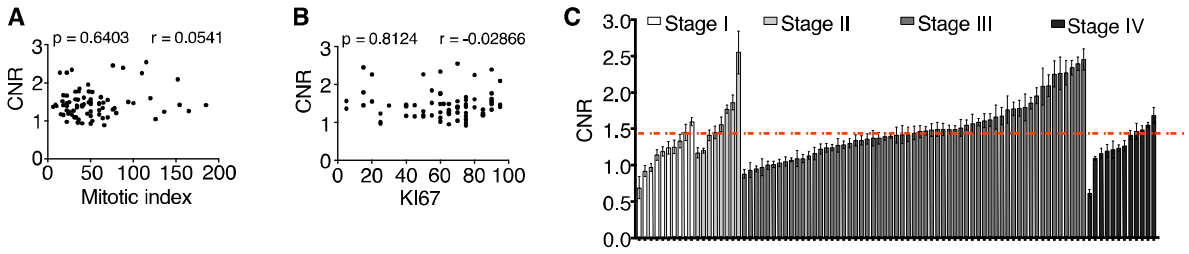

Fig. S6.

(A- B) Distribution of the Mitotic Index (A) and of the percentage of Ki67 positive cells (B) as a function of CNR. Statistical test: Spearman correlation. **(C)** Average and SEM of CNR per patient classified depending on FIGO stage.

Supplementary Tables:

Plasmid	Origin
pMD2.G	Addgene 12259, gift from Dider Trono
psPAX2	Addgene 12260, gift from Didier Trono
Lenti Tet-ON Myc-hPLK4	Gift from Andrew Holland
pSMPUW-IRIS-Neo-H2B-RFP	Gift from Daniele Facchinetti
pBOB-EF1-FastFUCCI-Puro	Addgene 86849, gift from Kevin Brindle and Duncan Jodrell
pLKo.1-puro shRNA Control	Sigma-Aldrich SHC016-1EA
pLKo.1-puro shRNA TP53	Gift from Daniele Facchinetti
pLKo.1-puro shRNA CDKN1a	Horizon Discovery RHS3979- 200795839
pLKo.1-puro shRNA ANKRD26 1	Horizon Discovery RHS3979-201867496
pLKo.1-puro shRNA ANKRD26 2	Horizon Discovery RHS3979- 201865755
sgRNA CRISPR Control	Gift from Nicolas Manel
sgRNA CRISPR STING	Gift from Nicolas Manel

Table S1. List of plasmids

Chemical	Origin	Stock dilution
Doxycyline	Sigma-Aldrich D3447	10 mg/mL in DMSO
Puromycine dichlorhydrate	ThermoFisher Scientific A1113803	10 mg/mL in 20mM HEPES
Carboplatin	Selleck chemicals S1215	10mM in Water
Paclitaxel	Sigma-Aldrich T7402	10mM in DMSO
A1210477	MedChem Express HY-12468	10mM in DMSO
WEHI-539 hydrochloride	MedChem Express HY-15607A	5mM in DMSO
Navitoclax	Selleck chemicals S1001	10mM in DMSO
Venetoclax	MedChem Express HY-15531	10mM in DMSO
AZ3146	Selleck chemicals S2731	10mM in DMSO
GSK923295	Selleck chemicals S7090	10mM in DMSO
Q-VD-Oph	MedChem Express HY-12305	20mM in DMSO
DMSO	ThermoFisher Scientific 022914.M1	

Table S2. List of drugs

Antibody	Origin	Species
CEP192	Home-made	Guinea pig
Pericentrin	Abcam 28144	Mouse
Pericentrin	Abcam 4448	Rabbit
Cytochrome C	ThermoFisher Scientific 15808698	Mouse
gamma-H2AX (S139)	Abcam 22551	Mouse
Rad51	Abcam 133534	Rabbit
53BP1	Millipoare MAB3802	Mouse
FANCD2	Novus Biologicals 100-182	Rabbit
Caspase3	Cell Signaling Technology 14220	Rabbit
Cleaved Caspase 3	Cell Signaling Technology 9661	Rabbit
pChk1 (Ser317)	Cell Signaling Technology 2344	Rabbit
Chk1	Santa Cruz 8408	Mouse
pChk2 (Thr68)	Cell Signaling Technology 2661	Rabbit
Chk2	Cell Signaling Technology 2662	Rabbit
pp53 (Ser15)	Cell Signaling Technology 9284	Rabbit
p53	Santa Cruz 126	Mouse
p21	Millipore OP64-100UG	Mouse
PUMA	Santa Cruz 374223	Mouse
Caspase2	Millipore MAB3507	Rabbit
MDM2	ThermoFisher Scientific MA1-113	Mouse
ANKRD26	GeneTex GTX128255	Rabbit
pSTING	Cell Signaling Technology 19781	Rabbit
STING	Cell Signaling Technology 13647	Rabbit
GAPDH	Sigma-Aldrich G9545-100UL	Rabbit
HRP-coupled anti-rabbit	ThermoFisher G21234	Goat
HRP-coupled anti-mouse	Jackson ImmunoResearch 115-035-003	Goat
anti-mouse IgG (H+L) Highly Cross-Adsorbed Secondary Antibody, Alexa Fluor 647	ThermoFisher Scientific A-21245	Goat
anti-rabbit IgG (H+L) Highly Cross-Adsorbed Secondary Antibody, Alexa Fluor 647	ThermoFisher Scientific A-21245	Goat
anti-guinea pig IgG (H+L) Highly Cross-Adsorbed Secondary Antibody, Alexa Fluor 647	ThermoFisher Scientific A-21450	Goat
anti-mouse IgG (H+L) Cross-Adsorbed Second-ary Antibody, Alexa Fluor 546	ThermoFisher Scientific A-11003	Goat
anti-rabbit IgG (H+L) Highly Cross-Adsorbed	Thermo Fisher Scientific A-11035	Goat

Secondary Antibody, Alexa Fluor 546		
anti-guinea pig IgG (H+L) Highly Cross-Adsorbed Secondary Antibody, Alexa Fluor 568	ThermoFisher Scientific A-11075	Goat
anti-mouse IgG (H+L) Highly Cross-Adsorbed Secondary Antibody, Alexa Fluor 488	ThermoFisher Scientific A-11029	Goat
anti-rabbit IgG (H+L) Highly Cross-Adsorbed Secondary Antibody, Alexa Fluor 488	ThermoFisher Scientific A-11034	Goat
anti-guinea pig IgG (H+L) Highly Cross-Adsorbed Secondary Antibody, Alexa Fluor 488	ThermoFisher Scientific A-11073	Goat

Table S3. List of antibodies.

Representative cytometry profiles:

Representative cytometry profiles

3C

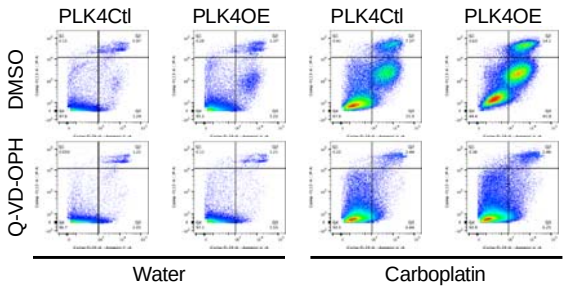

4C

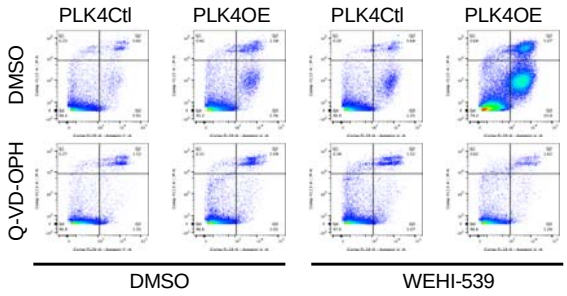

S3D

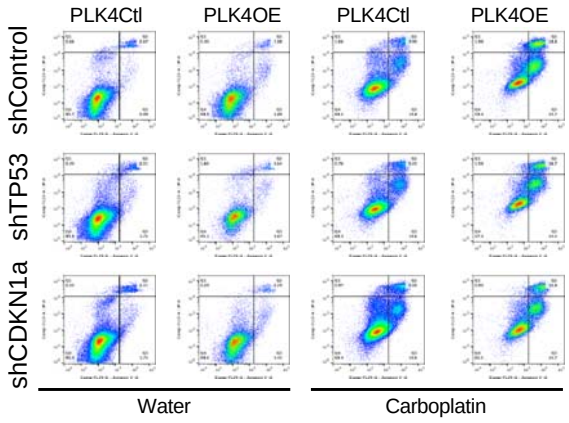

S3H

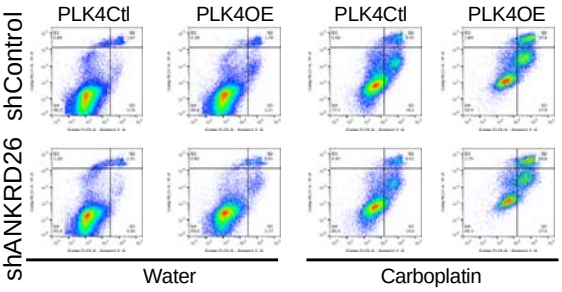

S5A

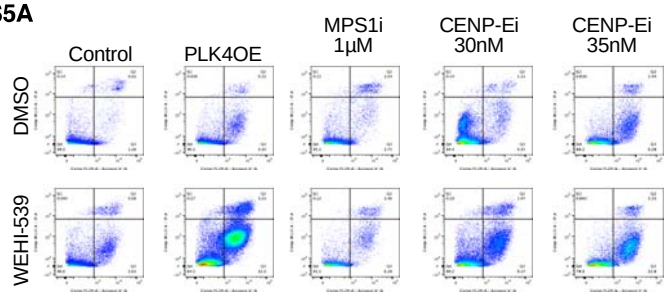

S5E

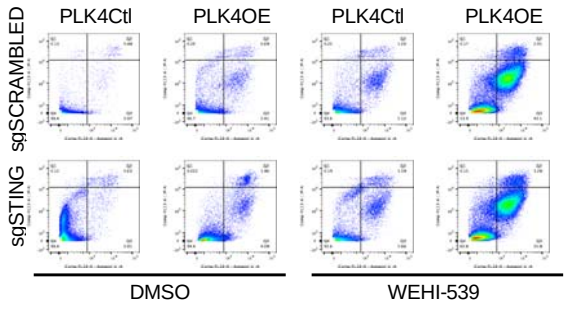

RÉSUMÉ

Le cancer épithélial de l'ovaire (CEO) est l'une des principales causes de décès par cancer chez la femme, en raison d'un diagnostic souvent tardif. Le traitement de première intention consiste en une chirurgie, suivie d'une combinaison de paclitaxel et de carboplatine comme chimiothérapie. Malgré une réponse initiale à ces traitements chez 80 % des patientes, malheureusement 70 % d'entre elles vont présenter une récidive. Le centrosome est le principal centre organisateur des microtubules dans les cellules animales. Il contribue à la division cellulaire, à la migration et à l'invasion. L'amplification des centrosomes, autrement dit la présence de plus de deux centrosomes par cellule, est souvent observée dans les lignées cellulaires cancéreuses, y compris les CEO. Cette anomalie contribue à l'oncogenèse en impactant la ségrégation correcte des chromosomes, qui est source d'aneuploïdie. Afin de vérifier si le statut du centrosome peut influencer la réponse à la chimiothérapie, j'ai utilisé des tests de viabilité et des approches d'imagerie en temps réel dans des lignées cellulaires de CEO inductibles pour le gène Polo Like Kinase 4 (*PLK4)*. En effet la surexpression de *PLK4* génère l'amplification des centrosomes. Mes résultats montrent que l'amplification du centrosome favorise la mort cellulaire en réponse au paclitaxel seul ou en combinaison avec le carboplatine en favorisant les divisions multipolaires. Par ailleurs, j'ai pu observer que la sensibilité accrue au carboplatine en présence d'amplification du centrosome est indépendante de la ségrégation mitotique, des dommages à l'ADN et des mécanismes de réparation des dommages à l'ADN. Aussi, la caractérisation de la réponse au carboplatine a révélé que la mort cellulaire ou l'arrêt du cycle cellulaire arrive en phase S / G2 de la deuxième génération. Enfin, j'ai démontré *via* le séquençage de l'ADN à partir de cellules uniques que l'amplification des centrosomes ne contribue pas significativement à l'instabilité chromosomique, et à l'aneuploïdie dans les cellules de CEO. Ainsi, l'amplification du centrosome semblent modifier la façon dont les cellules réagissent au stress, indépendamment du type de stress induit par la chimiothérapie. Ce travail contribuera à élucider le rôle de l'amplification du centrosome dans les CEO et comment cela peut affecter la réponse au traitement.

MOTS CLÉS

Centrosome/ Cancer ovarien/ Chimiothérapie/ Instabilité chromosomique

ABSTRACT

Epithelial Ovarian Cancer (EOC) remains one leading cause of death from cancer in woman. First-line treatment involves debulking surgery followed by chemotherapy treatment, represented by a combination of paclitaxel and carboplatin. Despite an initial response to these treatments in 80% of patients, unfortunately 70% of them will have recurrence. The centrosome is the major microtubule organizing center in proliferating animal cells and contributes to cell division, migration, and invasion. Centrosome amplification, the presence of more than two centrosomes per cell, is often observed in cancer cell lines, including EOC. Centrosome amplification is suggested to contribute to oncogenesis via chromosome mis-segregation which generates aneuploidy. To test if centrosome status can influence the response to chemotherapy, I have used viability assays and live imaging approaches in EOC cell lines inducible for Polo-like kinase4 (PLK4), to generate centrosome amplification. Surprisingly, I have found that centrosome amplification favors cell death in response to chemotherapy. Centrosome amplification contributes to enhancing cell death in response to combined chemotherapy and paclitaxel by favoring multipolar divisions. Surprisingly, I discovered that increased response to carboplatin is independent from mitotic mis-segregation, DNA damage and DNA damage repair mechanisms. Characterization of carboplatin response revealed a cell cycle arrest and cell death occurring in S/G2 phase in the second generation. Finally, I demonstrated *via* DNA single cell sequencing that centrosome amplification does not significantly contribute to chromosomal instability and aneuploidy in EOC cells. Thus, extra centrosomes seem to alter how cells respond to stress, independently of the type of stress induced by chemotherapy. This work will contribute to elucidate the role of centrosome amplification in EOC and how they can affect chemotherapy treatment.

KEYWORDS

Centrosome/ Ovarian cancer/ Chemotherapy/ Chromosome instability